PROCEEDINGS OF THE 1ST INTERNATIONAL SEMINAR ON DAM PROTECTIONS AGAINST OVERTOPPING AND ACCIDENTAL LEAKAGE, MADRID, SPAIN, 24–26 NOVEMBER 2014

Dam Protections against Overtopping and Accidental Leakage

Editors

Miguel Ángel Toledo & Rafael Morán
Department of Civil Engineering: Hydraulics, Energy and Environment
E.T.S. de Ingenieros de Caminos, Technical University of Madrid, Madrid, Spain

Eugenio Oñate
International Center for Numerical Methods in Engineering, Barcelona, Spain

CRC Press
Taylor & Francis Group
Boca Raton London New York Leiden

CRC Press is an imprint of the
Taylor & Francis Group, an **informa** business

A BALKEMA BOOK

CRC Press/Balkema is an imprint of the Taylor & Francis Group, an informa business

Typeset by MPS Limited, Chennai, India
Printed and bound in Great Britain by CPI Group (UK) Ltd, Croydon, CR0 4YY

Published by: CRC Press/Balkema
P.O. Box 11320, 2301 EH Leiden, The Netherlands
e-mail: Pub.NL@taylorandfrancis.com
www.crcpress.com – www.taylorandfrancis.com

ISBN: 978-1-138-02808-1 (Hardback)
ISBN: 978-1-315-68535-9 (eBook PDF)

Dam Protections against Overtopping and Accidental Leakage – Toledo, Morán & Oñate (Eds)
© 2015 Taylor & Francis Group, London, ISBN: 978-1-138-02808-1

Table of contents

Preface IX
Acknowledgements XI
Scientific and Organizing Committees XIII
Organizing institutions XV
Supporting institutions XVII
Sponsoring company XIX

Keynote lectures

Technical manual: Overtopping protection for dams 3
T.E. Hepler

Review of embankment dam protections and a design methodology for downstream rockfill toes 25
R. Morán

Flood overtopping protection for concrete dams 41
W.R. Fiedler

Failure of embankment dams due to overtopping or accidental leakage

Dam failures of embankment dams caused by overtopping or accidental leakage – New aspects for breach widening and deepening processes 59
A. Vogel, J.-R. Courivaud & K. Jarecka

Failure of dams due to overtopping – A historical prospective 73
M.J. Harris

Overtopping and internal erosion on small dams in Burkina Faso 83
A. Nombré, E.A. Somda, M. Kabore & F. Millogo

Failure of the downstream shoulder of rockfill dams in overtopping or accidental leakage scenario 89
M.Á. Toledo, H. Campos, Á. Lara & R. Cobo

Structural failure of the clay core or the upstream face of rockfill dams in overtopping scenario 101
M.Á. Toledo, R.M. Alves & R. Morán

Simulation of the beginning of failure in rockfill dams caused by overtopping 111
A. Larese, R. Rossi & E. Oñate

CFD study of the time dependent flow pattern around the slope of rockfill dams in overtopping scenario 123
J. San Mauro, M.Á. Toledo & R. Morán

Soft protections for embankment dams

Design of overtopping-resistant rockfill dams 133
M.Á. Toledo & L. Morera

Isoresistant double slope for the optimization of overtopping-resistant rockfill dams 143
M.Á. Toledo & L. Morera

Practical challenges and experience from large-scale overtopping tests with placed riprap 151
P.H. Hiller & L. Lia

Hard protections for embankment dams

Continuously-reinforced concrete slab spillways built over embankment dams in Spain: Molino de la Hoz and Llodio Dams 161
R.M. Alves & R. Morán

Comprehensive literature review on dam overtopping incidents 169
N. Tavakoli

Barriga Dam spillway: a case study of wedge-shaped blocks technology 181
R. Morán & M.Á. Toledo

Physical and numerical modeling for understanding the hydraulic behaviour of Wedge-Shaped-Blocks spillways 193
F.J. Caballero, F. Salazar, J. San Mauro & M.Á. Toledo

Masonry dams failure due to overtopping and its protections

Failures of masonry or concrete dams by overtopping 207
A. Vogel, F. Laugier & E. Bourdarot

Laboratory measurements and numerical simulations of overtopping nappe impingement jets 219
J.M. Carrillo & L.G. Castillo

Characterization of the dynamic actions and scour estimation downstream of a dam 231
L.G. Castillo & J.M. Carrillo

Highly-converging chutes as an overtopping protection for concrete dams: physical and numerical modelling 245
L. Morera, J. San Mauro, F. Salazar & M.Á. Toledo

Miscellaneous

Probabilistic methods for hydrologic dam safety analysis 261
I. Flores, A. Sordo-Ward & L. Garrote

Two-dimensional direct rainfall hydraulic models applied to direct calculation of hydrologic events in dams to prevent overtopping 275
P. Batanero, I. Martínez & E. Martínez

CFD analysis of flow pattern in labyrinth weirs 287
F. Salazar, J. San Mauro, E. Oñate & M.Á. Toledo

Analysis of the design of energy-dissipating structure in spillways 295
I. Robles, A. Palacio & A. Rodríguez

Author index 305

Dam Protections against Overtopping and Accidental Leakage – Toledo, Morán & Oñate (Eds)
© 2015 Taylor & Francis Group, London, ISBN: 978-1-138-02808-1

Preface

During the last decades, and especially in the recent years, the technology of dam protection against overtopping and accidental leakage, mainly due to internal erosion, has undergone major advancement. Although they are different technical problems, frequently the available technology for the solution is the same, so both issues are considered together in this book.

The increasing demand for safety in modern societies, combined with the limited availability of financial resources, has created the need for cost-effective solutions. Different technologies have been successfully applied to a considerable number of dams all over the world, but cases are scattered across the technical publications. Also the increasingly wide scientific work related to this subject is dispersed and disconnected from the professional work. So it was considered convenient to promote an international forum for showing and discussing cases and researches related to dam protection.

The book contains a selection of the proceedings of the 1st International Seminar on Dam Protection against Overtopping and Accidental Leakage held in Madrid (Spain) in 24–26 November 2014. The latest advances on dam protections and a portfolio of applications in representative case studies are included. Topics of the book are: failure analysis of embankment dams; soft and hard protections for embankment dams; failure and protection of concrete dams and additional issues related to dam protections. The book also includes a summary of the technical manual "Overtopping Protection for Dams", published by the US Federal Emergency Management Agency (FEMA) in March 2014, that was presented in Europe during the seminar.

This book can be considered as a comprehensive summary of the background about dam protections including case studies and applied research worldwide.

Dam Protections against Overtopping and Accidental Leakage – Toledo, Morán & Oñate (Eds)
© 2015 Taylor & Francis Group, London, ISBN: 978-1-138-02808-1

Acknowledgements

The editors want to thank the International and the Spanish Commitee on Large Dams (ICOLD and Spancold), CEDEX and IAHR for their support. Thanks to Adama Nombré, president of ICOLD; to Luis Balairón, manager of the Centre of Hydrographic Studies of CEDEX; to Christopher George, from IAHR; and especially to José Polimón, president of Spancold and Vicepresident of ICOLD, who put his strongest interest and effort; to Luis Ruano, president of Prehorquisa, for the sponsoring; thanks to the authorities of the *ETS de Ingenieros de Caminos* of the Technical University of Madrid (UPM), for the material support, and to our colleague Luis Garrote for his wise advises.

The editors want to highlight the unconditional dedication of the members of the Dam Safety Research group (SERPA) of the UPM for the organization of the 1st International Seminar on Dam Protections against Overtopping and Accidental Leakage, and for the publication of this book: León Morera, Javier Caballero, Ricardo M. Alves, Alfonso Roa, Raffaella Pellegrino, Gloria Cachaza and Cristian Ponce; and also thanks to Fernando Salazar and Antonia Larese, from CIMNE, for their disinterested collaboration.

A summary of the information contained in the FEMA Technical Manual: Overtopping Protections for Dams*, is included in this book. The editors thanks the Federal Emergency Management Agency of the U.S. for the permission.

Our deepest gratitude to our friend Bill Fiedler and to Thomas E. Hepler for their invaluable contribution to the success of the seminar and to the high technical level of this book.

Thanks to all the authors because this book is their creation.

Miguel Á. Toledo, Rafael Morán and Eugenio Oñate

*FEMA P-1015, Technical Manual: Overtopping Protection for Dams, Federal Emergency Management Agency, U.S. Department of Homeland Security, Washington D.C., May 2014.

Dam Protections against Overtopping and Accidental Leakage – Toledo, Morán & Oñate (Eds)
© 2015 Taylor & Francis Group, London, ISBN: 978-1-138-02808-1

Scientific and Organizing Committees

Scientific Committee

Luis Balairón, *Centro de Estudios y de Experimentación de Obras Públicas (CEDEX), Spain*
Ignacio Escuder, *Universitat Politècnica de València, Spain*
William Fiedler, *USA*
Kathleen Frizell, *USA*
Warren Frizell, *Bureau of Reclamation, USA*
Luis Garrote, *Technical University of Madrid, Spain*
Alfredo Granados, *Technical University of Madrid, Spain*
Thomas E. Hepler, *Schnabel Engineering, USA*
Antonia Larese, *International Center for Numerical Methods in Engineering (CIMNE), Italy*
Rafael Morán, *SERPA. Technical University of Madrid, Spain*
Eugenio Oñate, *Universidad Politécnica de Cataluña, Spain*
José Polimón, *Spanish National Committee on Large Dams (SPANCOLD), Spain*
Riccardo Rossi, *Universidad Politécnica de Cataluña, Italy*
Benjamín Suárez, *Universidad Politécnica de Cataluña, Spain*
Christopher I. Thornton, *Colorado State University, USA*
Miguel Á. Toledo, *SERPA. Technical University of Madrid, Spain*
Peter Viklander, *Vattenfall, Sweden*
James Yang, *KTH Architecture and the Built Environment, Sweden*

Organizing Committee

Ricardo Alves, *Dam Safety Research Group (SERPA), Portugal*
Javier Caballero, *Dam Safety Research Group (SERPA), Spain*
Gloria Cachaza, *Dam Safety Research Group (SERPA), Spain*
Rafael Morán, *SERPA. Technical University of Madrid, Spain*
León Morera, *Dam Safety Research Group (SERPA), Spain*
Fernando Salazar, *International Center for Numerical Methods in Engineering (CIMNE), Spain*
Eugenio Oñate, *Universidad Politécnica de Cataluña, Spain*
Raffaella Pellegrino, *Dam Safety Research Group (SERPA), Italy*
Cristian Ponce, *Dam Safety Research Group (SERPA), Perú*
Alfonso Roa, *Dam Safety Research Group (SERPA), Spain*
Miguel Á. Toledo, *SERPA. Technical University of Madrid, Spain*

Dam Protections against Overtopping and Accidental Leakage – Toledo, Morán & Oñate (Eds)
© 2015 Taylor & Francis Group, London, ISBN: 978-1-138-02808-1

Organizing institutions

The 1st International Seminar on Dam Protections against Overtopping and Accidental Leakage was organized by the following institutions:

Dam Safety Research Group (SERPA)

International Center for Numerical Methods in Engineering (CIMNE)

Fundación Agustín de Betancourt

Technical University of Madrid (UPM)

Dam Protections against Overtopping and Accidental Leakage – Toledo, Morán & Oñate (Eds)
© 2015 Taylor & Francis Group, London, ISBN: 978-1-138-02808-1

Supporting institutions

The 1st International Seminar on Dam Protections against Overtopping and Accidental Leakage was supported by the following institutions:

International Committee on Large Dams (ICOLD)

Spanish National Committee on Large Dams (SPANCOLD)

Centro de Estudios y de Experimentación de Obras Públicas (CEDEX)

International Association for Hydro-Environment Engineering and Research (IAHR)

Dam Protections against Overtopping and Accidental Leakage – Toledo, Morán & Oñate (Eds)
© 2015 Taylor & Francis Group, London, ISBN: 978-1-138-02808-1

Sponsoring company

The 1st International Seminar on Dam Protections against Overtopping and Accidental Leakage was sponsored by:

PREHORQUI S.A.

This book is dedicated
to Alfonso Álvarez *in memoriam,*
a pioneer and a master.

Keynote lectures

Dam Protections against Overtopping and Accidental Leakage – Toledo, Morán & Oñate (Eds)
© 2015 Taylor & Francis Group, London, ISBN: 978-1-138-02808-1

Technical manual: Overtopping protection for dams

Thomas E. Hepler
Schnabel Engineering Oak Branch Drive Greensboro, North Carolina, USA

ABSTRACT: This paper provides an overview of *Technical Manual: Overtopping Protection for Dams*, which was recently released by the Federal Emergency Management Agency (FEMA) of the United States, to be included in the Proceedings of *International Seminar on Dam Protection against Overtopping and Accidental Leakage*. U.S. customary units have been converted to S.I. metric units for purposes of this international seminar.

Keywords: Dam, Embankment, Overtopping, Protection, Spillway

1 INTRODUCTION

Inadequate spillway capacity is a common problem with many dams. Reservoir inflow that exceeds available storage and/or spillway discharge capacity can lead to dam overtopping, failure, and potential for loss of life and significant downstream damages. The design and construction of overtopping protection for dams is increasingly being viewed as a viable alternative to constructing larger spillways or increasing reservoir storage by raising the dam crest. However, the decision to pursue overtopping protection for a dam must give strong consideration to the risk of failure of the protection system, which could lead to a full breach of the dam. Overtopping protection should generally be reserved for situations with a very low annual probability of operation (typically less than 1 in 100); with physical or environmental constraints on constructing other methods of flood conveyance and with a prohibitive cost of other alternatives; or where downstream consequences of dam failure are demonstrated to be low.

Alternatives for overtopping protection may utilize a variety of different materials, such as roller-compacted concrete and continuously-reinforced concrete slabs (for "hard" protection); or articulated concrete blocks, gabions, grass cover, turf reinforcement mats, flow-through rockfill, reinforced rockfill, riprap, and various types of geosynthetic materials (for "soft" protection). Not all materials are applicable in every situation. In most cases, significant research and hydraulic testing has been conducted on these materials, but since most overtopping protection is designed to function at an infrequent recurrence interval, practical experience on constructed projects that have been subjected to overtopping flows is limited. New materials and methods of analysis are always being developed, so design engineers may need to rely upon manufacturers' design recommendations, always mindful of the limitations of product testing and analysis. Independent analysis should always be considered when appropriate.

It is critically important that when an overtopping protection alternative is considered, the designer must understand all aspects of its design, construction, and long-term maintenance needs. Regulatory agencies should also be consulted to confirm the circumstances for which overtopping protection can be approved. Due to the absence of any single recognized standard for overtopping protection alternatives for dams, there has been some inconsistency in the design and construction rationale to date. The goal of the FEMA technical manual, *Overtopping Protection for Dams* [1] is to provide a source of information on various overtopping protection alternatives for both embankment and concrete dams, to promote greater consistency between similar overtopping project designs, facilitate review, and aid in the design of safer, more reliable facilities. The manual is intended

for use by personnel familiar with dams, such as dam designers, inspectors, construction oversight personnel, dam safety engineers, and decision-makers, but is not intended to provide detailed design procedures for all potential applications. FEMA, as the lead agency for the National Dam Safety Program in the United States, sponsored the development of the technical manual in conjunction with the U.S. Bureau of Reclamation. Part 1 (Chapters 1–10) provides general guidance on the design and construction considerations associated with overtopping protection alternatives for embankment dams, while Part 2 (Chapters 11–16) provides similar guidance for concrete dams. The manual concludes with a selection of case histories demonstrating field applications of the various overtopping protection systems presented. This paper and associated presentation will focus on the design and application of various types of overtopping protection systems for embankment dams. A second paper will present overtopping protection systems for concrete dams.

2 GENERAL CONSIDERATIONS FOR EMBANKMENT DAMS

Many early dams were designed to accommodate floods based on the largest experienced local flood or a standardized probable maximum flood (PMF) considered appropriate at that time. Over the years, significant technological and analytical advances have led to better watershed and rainfall information, improvements in the analysis of extreme floods, and tools for evaluating hydrologic events in a risk-based context, which have resulted in the reclassification of some dams as being hydrologically deficient. Guidance for the evaluation of the hydrologic safety of both new and existing dams in the United States based on flood loading is provided by the FEMA manual, *Selecting and Accommodating Inflow Design Floods for Dams* [2].

The FEMA technical manual, *Overtopping Protection for Dams* [1] assumes that a hydrologic deficiency exists at a dam and that traditional approaches to safely accommodate a larger design flood, such as increasing reservoir storage by raising the dam crest or increasing release capability by increasing the spillway discharge capacity, have first been investigated and found to be cost prohibitive or impractical. Overtopping protection may then be an attractive alternative because of its potential economic advantages and could offer an economical solution to a hydrologic deficiency that would otherwise not be addressed. Maintaining the existing hydraulic conditions at the dam to the extent possible is also increasingly important as downstream river corridors are developed in close proximity to the channel.

Where applicable, overtopping protection may involve all or a portion of the dam crest. This may be more cost effective than constructing an auxiliary spillway on either abutment at dams where increased hydraulic capacity is required. A major concern with overtopping protection for embankment dams is that if the protection fails during a flood event and the underlying embankment is exposed, erosion and headcutting in the embankment materials could progress rapidly. This could lead to a breach of the dam during the flood event, with no potential for preventing the failure. A careful analysis of all potential failure modes for the dam and appurtenant features must be performed for both the existing (baseline) conditions and for the proposed modified conditions.

Understanding the behavior of an embankment dam during an overtopping event provides a basis for the design of protective measures. Flow over an embankment dam, as shown in Figure 1, generally proceeds from a subcritical velocity over the upstream portion of the crest, through critical velocity on the crest and supercritical velocity across the remainder of the crest, to accelerating turbulent flow on the downstream slope until reaching the hydraulic jump. The hydraulics of overtopping flow in terms of unit discharge, depth, and velocity can be estimated by conventional open-channel flow theories. The unit discharge of the overtopping flow, q, in $m^3/s/m$, is a function of the overtopping depth, H, in meters, as follows:

$$q = C\,H^{1.5} \tag{1}$$

where C = a discharge coefficient dependent upon the geometry of the embankment and the depth of flow.

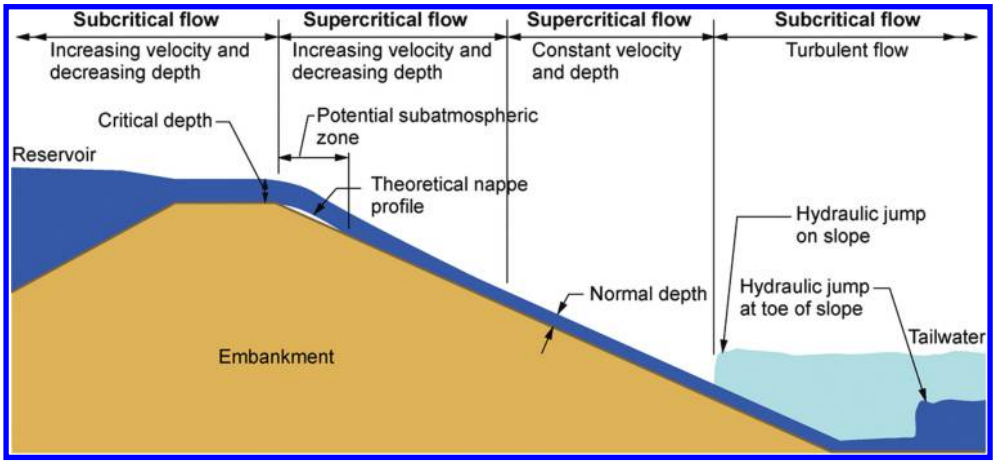

Figure 1. Typical hydraulic conditions during embankment overtopping.

Dam overtopping flow is normally compared to broad-crested weir flow with a sloping approach. The exact location of critical depth on the crest will be dependent upon the crest profile, the ratio of the overtopping depth (H) to the crest length in the direction of flow (L), and the relative roughness of the crest surface. Beyond the critical depth location, flow depth and pressure profiles will decrease from hydrostatic pressure as the flow begins curving toward the slope beyond the downstream edge of the crest, or crest brink, where separation of the nappe occurs. Increasing (or steepening) the downstream embankment slope will increase the pressure gradient and produce a negative pressure. Large pressure gradients at the crest brink could produce erosion of the dam embankment or failure of an overtopping protection system. A change from supercritical to subcritical flow will occur at the location of the hydraulic jump near the downstream toe, with increased turbulence and pressure fluctuations, and changes in vertical profile where flows are no longer parallel to the embankment slope (transition from chute to stilling basin). Embankment erosion or overtopping protection system failure may also occur at this location.

The evaluation of several case histories of embankment dams being overtopped resulted in the following conclusions related to overtopping performance:

- Uniform vegetation can generally provide some protection for shallow overtopping depths (up to about 0.3 m) for short durations of a few hours, especially on clayey, compacted soil surfaces.
- Granular rockfill materials at the embankment toe may be more easily eroded and cause undermining of a more resistant cohesive fill.
- High tailwater reduces the head differential on the embankment and can reduce erosion.
- Interruptions to a smooth downstream slope surface (e.g., a change in slope from steeper to flatter, or from flatter to steeper; or a projecting structure, berm, roadway, or abutment groin) produce turbulence which can initiate erosion.
- Flow concentrations due to elevation changes along the embankment crest (generally caused by camber or by crest settlement) can initiate erosion.
- Flatter embankment slopes have greater resistance to erosion.

Overtopping protection should not be considered as a low-cost substitute for a service spillway, especially where frequent use, high unit discharge, or high head is a design requirement, or where the structure impounds a substantial volume of water and downstream consequences in the event of failure would be significant. Overtopping protection is generally discouraged for use on new embankment dams due to settlement concerns, unless they can be addressed in the design and no other practical alternatives exist. Most embankment dam overtopping protection features serve as

an auxiliary spillway[1], with service spillways provided to pass the more frequent floods. When planning to use embankment dam overtopping protection as an auxiliary spillway, the designer should consider the limitations and risks of conveying spillway flow over an earthen embankment. Important engineering design considerations include:

- Significant quantities of concentrated flowing water may be introduced over erodible materials, such as an earthen embankment or foundation material at the abutment contacts.
- Higher static loading on an embankment dam may result in slope failure.
- Uncontrolled leakage from the overtopping protection may cause embankment erosion and instability.
- Debris carried in the flood flows may damage the overtopping protection.
- Numerous overtopping protection projects have been constructed, but few have seen significant use—and none has been tested for full design flood conditions.
- Overtopping protection typically involves a significant change to the visual appearance of the structure.

The embankment dam overtopping protection should be designed so that the abutment groins and toe of the dam are protected from localized erosion caused by flow concentrations and by high velocity flow. Hydraulic analyses should be performed to determine the characteristics of the overtopping flow, including: flow velocity, depth, and type (laminar or turbulent, supercritical or subcritical); slope changes and discontinuities; and the energy dissipation requirements at the downstream toe. If erosion at the toe of the dam is expected to occur during overtopping, the eroded conditions should be evaluated in both the embankment stability and embankment seepage analyses, and considered in the design of the overtopping protection system.

The construction of overtopping protection on an embankment dam could impact the long-term stability of the embankment, and affect monitoring of its performance. An impermeable structure on the downstream slope of an embankment dam can block existing seepage paths and thereby increase the phreatic surface and decrease embankment stability. Any reductions to the embankment cross-section can decrease the factor of safety for slope stability. Excavation at the toe of the embankment to construct a downstream stilling basin, or for over-steepening of the downstream slope, will change the stability of the overall embankment. Any excavation of the existing dam crest can increase the potential for dam overtopping during construction. An evaluation of the estimated potential risks of dam failure during construction, in addition to long-term impacts, should be performed as part of the design of overtopping protection for an embankment dam.

Before designing overtopping protection for an existing dam, site reconnaissance and subsurface investigations will be needed to fully understand the conditions of the embankment, foundation, and downstream area, and to develop appropriate geotechnical parameters for analyzing embankment slope stability and seepage conditions, estimating the bearing capacity of the foundation, providing analysis of filter compatibility, and predicting settlement or heave. Overtopping protection systems for large, high hazard potential embankment dams require more rigorous and detailed analysis to ensure stability for higher unit discharges, drop heights, and flow velocities. Suitable provisions must be made to protect, modify, or abandon and replace existing instrumentation systems, and to provide new systems as required for monitoring the modified dam embankment. Overtopping protection systems for embankment dams have been constructed using various types of construction materials as described in the following sections.

[1] The term “emergency spillway” is discouraged, to avoid the implication that an emergency exists when its use is required [2].

3 ROLLER-COMPACTED CONCRETE (RCC)

RCC has been used in dam construction since the late 1970s. The concrete mixture has zero-slump consistency and is placed and compacted with equipment typical of earth-moving or paving operations. The development of RCC technology has provided a successful method of overtopping protection of embankment dams, which has proven to be cost effective while affording a number of other advantages. RCC construction is normally very rapid compared to conventional concrete construction, with minimal project disruption. In most cases, construction for overtopping protection is limited to the dam crest and downstream slope, with little to no impact to reservoir operations. Depending upon the site conditions and discharge requirements, the entire length of the embankment dam can be used by armoring the crest and downstream face with RCC, or a portion of the embankment crest can be lowered for use as an RCC-lined auxiliary spillway.

RCC spillways generally consist of non-air-entrained concrete (and therefore potentially susceptible to freeze-thaw damage), without reinforcement, water-stopped joints, or anchorage, but with underdrain systems similar to conventional concrete spillways. RCC overtopping projects completed in the United States typically range in height from 5 to 20 m, with the volume of RCC typically ranging from 800 to 46,000 m^3. A list of 109 completed RCC overtopping protection projects is included in the technical manual [1]. These projects average 13 m high, with an average RCC volume of 7,600 m^3, an average unit discharge of 7.4 m^3/s per meter of crest length, and an average design overflow depth (or head on crest) of 2.4 m. Maximum RCC applications to date have been for dam heights up to about 30 m and for unit discharges up to about 32 $m^3/s/m$, with a maximum overflow depth up to about 6.1 m. The average cementitious materials content is 200 kg/m^3 (including cement and pozzolan) and the maximum size aggregate most commonly used is about 4 cm.

RCC has a wide application for use as overtopping protection since the material is suitable for a wide range of flow depths and velocities. Laboratory studies, full-scale tests, and field experience have all shown that, even at relatively low strengths and cementitious contents, RCC has exceptional resistance to erosion and abrasion damage, even at an early age. RCC has an added advantage as it can generally resist captured debris impacts (such as trees, cobbles, and boulders) without significant damage and without causing severe irregularities in the hydraulic flow due to snagging of debris. Several RCC overtopping protection projects have reportedly performed well with overtopping depths of up to about 3 m, with damage limited to surface abrasion and minor spalling. The Portland Cement Association (PCA) released the *Design Manual for RCC Spillways and Overtopping Protection* in 2002 [3], from which much of the design information in the technical manual was taken.

The sloped chute is the portion of the spillway that conveys water down the face of the dam or abutment, from the crest to the stilling basin. RCC for the sloped chute is typically placed in 0.3 m thick horizontal lifts resulting in a stepped chute, as shown in Figure 2. RCC chute surfaces constructed in typically 2.4 m wide horizontal lifts can be constructed without formwork, or by using vertical forms to create a more pronounced stepped chute surface along the exposed edges. Formed steps may consist of compacted RCC, grout-enriched RCC, or conventional concrete, and are generally 0.3 or 0.6 m high. RCC for the sloped chute can also be placed parallel to the sloped surface (called "plating") and has generally been considered for projects where the depth of overtopping is less than 0.6 m, the duration of overtopping is short, and the slope is 3H:1V or flatter. This method normally requires considerably less material than the stepped RCC overlay method; however, unit costs are generally higher because of the more difficult placing procedure, and the energy dissipation and resistance to uplift pressure would be reduced when compared to RCC placed in horizontal lifts.

The thickness of the sloped RCC chute is commonly measured perpendicular to the slope. The required thickness is based upon the slope of the spillway, constructability requirements for placement of the RCC, and structural requirements to resist potential uplift pressures and other loading conditions. The location of the maximum uplift pressure beneath the slab is often found

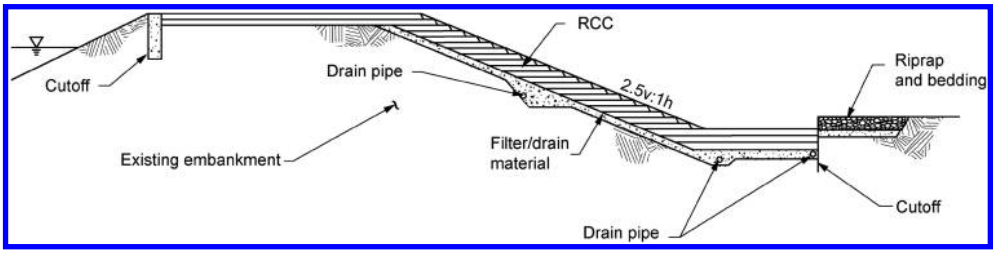

Figure 2. Typical cross-section for RCC overtopping protection.

near the bottom of the slope just above the base of the spillway or adjacent to the downstream apron or basin slab. Most designers have adopted a thickness between 0.6 and 0.9 m for the sloped chute. The slab thickness is generally increased as the overtopping depth increases. Seepage through RCC lifts and at cracks can be safely handled by a properly designed and filtered drainage system beneath the chute.

RCC spillway crests often follow the shape of the embankment crest to simplify construction, but represent a broad-crested weir having a low coefficient of discharge, especially for lower depths of overtopping relative to the crest width. Increasing the efficiency of the spillway crest can reduce the required crest length of the spillway and/or the overtopping depth, which typically reduces material quantities. A narrower spillway chute can also better match the downstream channel geometry. Conventional concrete can be used to provide an ogee-shaped crest or a sharp-crested weir to improve the spillway discharge coefficient. The discharge coefficient of all weirs will vary with the approach channel conditions, approach depth (or crest height), and depth of flow over the weir. The approach apron slab is located upstream of the spillway crest and is designed to reduce channel erosion, establish the crest height for the control section, and reduce seepage from the reservoir beneath the spillway chute by the provision of an upstream cutoff.

The downstream apron or stilling basin is a critical feature of an RCC spillway located over a dam embankment. The designer should have a thorough understanding of the spillway and channel hydraulics, foundation conditions, and erosion control requirements. The type of energy dissipator needed will depend upon the flow depth and incoming velocity, unit discharge, operating frequency, tailwater conditions, and downstream consequences. A simple apron with or without an end sill is generally most applicable to RCC overtopping projects with infrequent use. The length of the downstream apron depends upon energy dissipation and erosion-control features of the design. The U.S. Department of Agriculture (USDA) Agricultural Research Service (ARS) has performed extensive research on stepped spillways for embankment dams [4]. Energy dissipation at any location within the sloped chute was defined as the ratio of head loss to total head, expressed in percent, and was found to vary linearly from near zero at the crest to a maximum of approximately 73 percent entering the basin. Riprap is often placed downstream of the basin to protect the downstream edge of the RCC, and to transition to the downstream channel.

Abutment protection is required for all embankment dam overtopping protection designs. The abutment protection should be designed to safely contain the spillway flow between the embankment groins, and transition to the stream channel. Designs which direct flow in a converging configuration on the downstream face result in three-dimensional concentrated flow channels which increase the velocity and flow concentration from top to bottom. Abutment protection for RCC overtopping projects can be constructed by shaping the RCC to armor the abutments from erosion and to provide a “trough” to channel water from the downstream face of the dam to the natural channel below the dam, or by constructing structural concrete training walls. Generally, it is more economical to use structural concrete training walls if the spillway width is narrow, due to reduced impacts to the RCC placement. The design of abutment groin protection warrants conservative design assumptions and may justify the use of a numerical or physical model.

RCC overtopping protection often changes a grass-covered embankment to a concrete-covered surface having a rough, unfinished appearance. A number of RCC spillways have been covered with soil and grass to provide a more natural appearance and for some freeze-thaw protection. A soil cover is usually only considered for RCC spillways that would operate infrequently, as it can create potential maintenance and environmental impacts at the dam and in the downstream channel when eroded. The minimum thickness of soil cover is usually dependent upon the type of soil and its ability to support vegetation, but has generally ranged from 0.2 to 0.6 m.

4 CONVENTIONAL CONCRETE

Overtopping protection for embankment dams utilizing conventional concrete relies on a continuous layer of concrete to serve as the flow surface for overtopping flows. This normally consists of a smooth, continuously-reinforced concrete slab (CRCS) constructed over a filtered drainage layer. The concrete slab and drainage layer protects the underlying embankment from high velocity flows discharging along the downstream face of the dam. Training walls are normally required at the sides of the overtopping protection to contain the overtopping flows and to protect the abutments. If the abutments consist of competent rock, it may be possible to forego the training walls, as long as the groins are protected and the underlying embankment does not become subjected to high-velocity flow.

There are a number of embankment dams worldwide that have concrete spillways located on the downstream face, rather than on an abutment. Although these installations may not have been originally classified as concrete overtopping protection, their concept is similar—high velocity flow is conveyed along a concrete surface located on the downstream face of an embankment dam. Construction of a CRCS on the downstream face for overtopping protection is similar in many respects to construction of a concrete slab on the upstream face of a concrete-faced rockfill dam for a water barrier. In order for conventional concrete to be effective as overtopping protection, the concrete layer must remain intact and be free of significant defects during a flood event.

Flood frequency studies are generally needed to develop flood hydrographs for various return periods for the site. This information is used in a flood routing study for which magnitudes and durations of spillway flows are determined. Water surface profiles can then be developed to calculate flow depths and velocities along the downstream face of the dam for a suite of spillway discharges and for a range of return periods. This information is used to size training walls at the sides of the overtopping protection to retain the flow depths, or used with the flow velocities to evaluate the impact of overtopping flows on the rock abutments. The conjugate depth (or the flow depth at the downstream end) of the hydraulic jump can also be calculated for sizing the stilling basin. The flow depths and velocities may be used to evaluate the potential for cavitation damage to the concrete surface (for determination of allowable concrete surface tolerances and potential aeration requirements), the potential for stagnation (or uplift) pressures at transverse joints within the concrete overtopping protection, and for the design of drainage features.

The magnitude of potential uplift pressures at open joints or cracks, and the corresponding unit discharge, can be estimated in order to evaluate the potential for uplift failure of concrete overtopping protection, based on model testing performed by the U.S. Bureau of Reclamation [5]. The following defensive design measures (listed in order of decreasing effectiveness) can help prevent this potential failure mode from developing:

- Waterstops (which block paths for water flow through joints in slabs).
- Transverse cutoffs (which prevent vertical offsets at transverse joints and limit path for water from the flow surface to the foundation).
- Longitudinal reinforcement or smooth dowels across joints (which minimize width of cracks and openings at joints and may help prevent offsets).
- Anchor bars into foundation (which provide additional resistance to uplift pressures on concrete slabs; with soil anchors used for earth foundations).

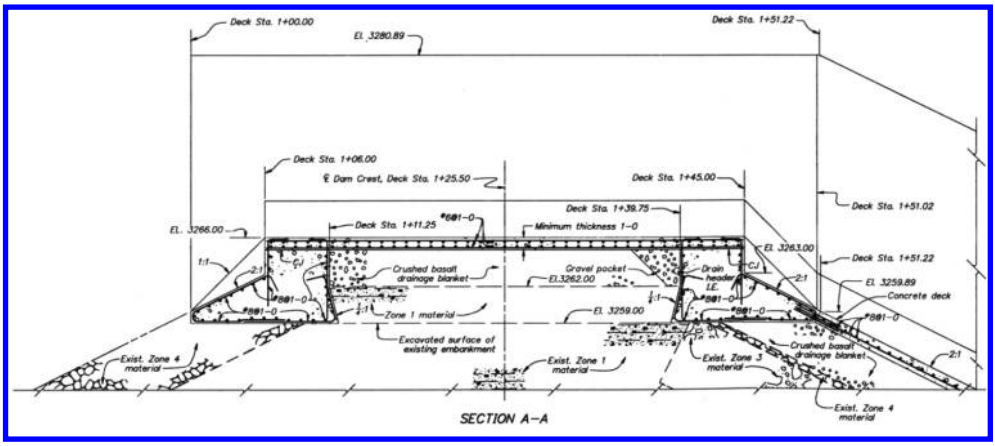

Figure 3. Proposed crest detail for CRCS, A.R. Bowman Dam (U.S customary units).

- Filtered underdrains (which relieve uplift pressures that can be generated beneath slabs and prevent movement of foundation materials into drainage system).
- Rigid plastic foam insulation (which insulates the drainage system and reduces the potential for freezing; and also prevents frost heave locally).

CRCS overtopping protection requires widely-spaced construction joints to control cracking in the concrete slabs, as is commonly done for similar types of construction, such as for concrete-faced rockfill dams and concrete pavements. Appropriate defensive design measures are required to prevent or minimize the passage of water through the joints, including the installation of water-stops and continuous reinforcement. The amount of reinforcement will vary depending on the site conditions, but is usually 0.5 to 0.7 percent of the gross area of the concrete slab cross section. The reinforcement is spliced along the width and length of the concrete slab protection as required and passes through all joints. Properly proportioned reinforcement will keep joints and cracks tightly closed so that they are impervious or allow only minor seepage. The dowelling effect of the reinforcement, in combination with the aggregate interlock of the tightly-closed cracks, will also prevent offsets and help maintain structural integrity. The monolithic behavior of the CRCS should allow for localized distress to occur in the slab, within limits, without compromising the overall integrity of the concrete overtopping protection.

The U.S. Bureau of Reclamation prepared designs for a CRCS system in the 1990s requiring a maximum unit discharge of 26 m^3/s/m, with a corresponding maximum overflow depth of about 5.5 m, for overtopping protection of A. R. Bowman Dam, with a height of about 61 m. The CRCS was designed using the Continuously-Reinforced Concrete Pavement (CRCP) computer program developed by the University of Texas. The program modeled the response of the proposed slab for various loadings based on the properties and dimensions of the concrete, the gradation of the subgrade materials, and on limiting criteria for crack spacing, crack width, and steel stress. Using a design crack width, the seepage volume through the slab during overtopping was estimated to determine the potential uplift loads on the slab and for design of the drainage system. A critical design requirement is the provision of suitable connections at the perimeter of the CRCS, including the dam crest, the toe block, and along the abutments. Hydraulic model studies, along with analyses using the CRCP design techniques, were used in the structural design of these connections. Crest details for the proposed CRCS for A.R. Bowman Dam, which was never built, are shown in Figure 3.

5 PRECAST CONCRETE BLOCKS

Precast concrete blocks can be used over earth materials to provide a hard surface for flow to pass safely without eroding the underlying surface, and are commonly referred to as articulating concrete blocks (ACB) when used for this purpose. An ACB system is comprised of a matrix of individual concrete blocks placed together to form an erosion-resistant revetment with specific hydraulic performance characteristics. The term "articulating" implies the ability of the matrix to conform to minor changes in the subgrade while remaining interconnected with geometric interlock and/or additional system components such as cables or anchors. These systems have also been referred to as cellular concrete mats (CCM).

There are many types of precast concrete blocks, each with its own geometry, useful application based upon hydraulic performance and erosion prevention, installation procedures, aesthetic value, and cost. Most ACBs are either cable-tied, interlocking, or overlapping. Most concrete block products are dry cast at a manufacturing plant near the site using a mold supplied by the manufacturer. Some are wet cast (using a higher water-cement ratio) if uniquely shaped. Most ACBs are from 10 to 23 cm in thickness, and may or may not have an open area equal to anywhere from 2.5 percent for the overlapping (wedge-shaped) blocks, to 18–35 percent for other types of blocks. Some varieties of blocks rely on a vegetative cover grown in soil placed into open areas of the blocks or over the top of the blocks to improve performance. All products require placement over a smooth subgrade with a geotextile and/or a bedding or drainage layer between the subgrade and the block system. Side slopes may be vertical or trapezoidal-shaped. Installation requirements and techniques vary with the product and affect product performance. Of most importance is to select a product or system that has been tested under the flow conditions expected during overtopping. Extensive research in the U.S. on the performance of ACBs has been performed in a 15 m high concrete flume facility at Colorado State University (CSU) in Fort Collins, Colorado. Applications for overtopping protection typically include high velocity flows, steep slopes, and possibly energy dissipation on the flow surface.

Articulating block systems have been defined to fail in performance testing when the blocks lose sustained intimate contact with the subgrade. ASTM D7276 is a standard for analysis and interpretation of ACB revetment system hydraulic test data collected under steep-slope, high-velocity conditions in a rectangular open channel, and this standard is intended to be used in conjunction with ASTM D7277 for performance testing of ACB revetment systems. Methods for computation of discharge, flow depths, friction slope, cross-sectional averaged flow velocity, and boundary shear stress are detailed within ASTM D7276, and guidelines for qualitative assessment of stability are also presented. Overall stability of the embankment under the additional hydraulic loading due to overtopping must be investigated for any ACB system by a competent geotechnical engineer, and is separate from the analysis of the hydraulic performance of the ACBs. Most testing has been performed—and prototype installations constructed—with uniform channel widths and parallel walls. If the spillway walls converge, additional physical or numerical modeling should be performed to assure flow velocities and directions are not exceeding tested design limits.

The design flow from flood routings is used to determine the design unit discharge and design head on the crest for a selected crest length. The revetment should be anchored in accordance with the installation techniques provided by the manufacturer and with ASTM D6884. The transition from the crest to the downstream slope may be graded to minimize the development of subatmospheric pressures, which have been found to produce failures of some block systems under large-scale testing. The crest details must not allow water from the reservoir beneath the system, and the crest must be well anchored. A cutoff wall and suitable connection should be provided at the embankment core. If using a wedge-shaped or individual block system, the first row of blocks should be overlapped and held in place by a cast-in-place, reinforced concrete crest cap.

The blocks on the downstream slope must withstand the hydraulic forces associated with the maximum unit discharge, slope angle, and roughness of the block system. Figure 4 shows a typical force balance on a single unit in a cable-tied ACB system. These forces are similar for an interlocking

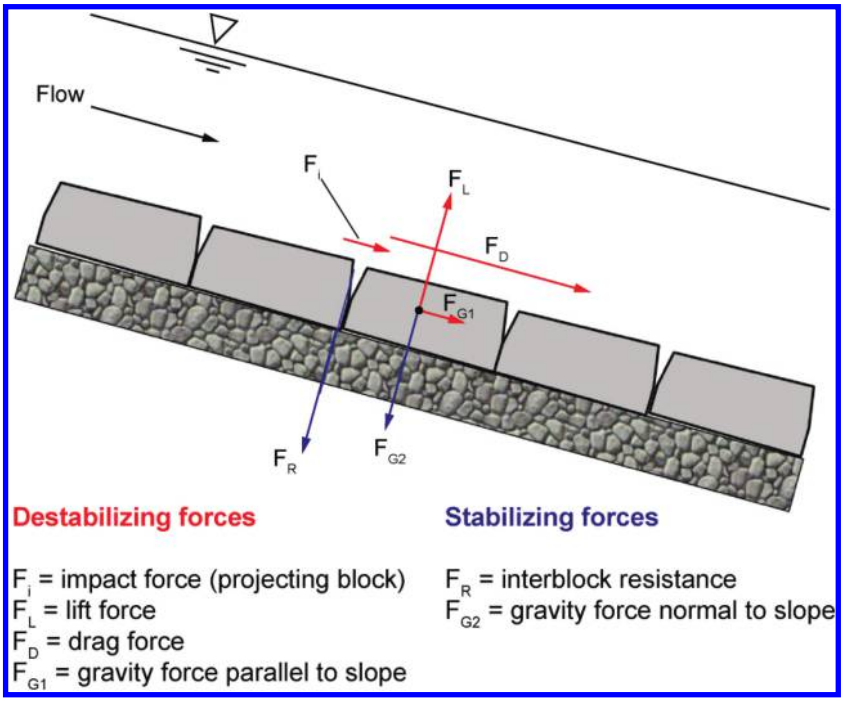

Figure 4. Hydraulic forces on the typical cable-tied ACB system.

block system. The drag force on the blocks should be computed by including both form drag and frictional drag. The destabilizing force from form drag should also include the direct impact of a vertical projection of the upstream face of a block to account for imperfections during installation. These computations lead to shear stresses and safety factors that the project system must meet to ensure no loss of intimate contact with the subgrade. To date, available data for typical cable-tied systems suggest that flow velocities should not exceed 8 m/s on 2H:1V slopes. Manning's "n" values for roughness average between 0.026 and 0.033 for unvegetated systems. Equations for performing stability calculations that are based upon the factor of safety method have been provided by the National Concrete Masonry Association (NCMA) and others. The NCMA documents are used as the current design and installation standards for interlocking and cable-tied ACBs [6].

Tapered wedge block systems are subjected to the hydraulic forces shown in Figure 5. Force balances are similar to the cable-tied equations, but should include an element for aspiration of subgrade pressures.

No tapered wedge block system has failed in laboratory or large-scale flume testing situations up to the capacity of the systems. Velocities up to 14 m/s and critical depths up to 1.1 m have been attained in flume testing on a 2H:1V slope with vertical side walls. The Manning's "n" value that has been computed from several tests is between 0.03 and 0.04. Design guidance for wedge-blocks is being developed by the Bureau of Reclamation, which holds the patent for the product in the U.S.

The toe treatment must be adequate to pass expected seepage and drainage flow, to provide support for the block system, and prevent undermining of the system. The presence of a hydraulic jump must be considered in the design by knowing the project tailwater elevation and performing the hydraulic calculations necessary to determine the location of the jump. All systems have been shown to perform without the formation of the hydraulic jump over the toe. An adequate filter or collector drain must be provided to ensure proper drainage from underneath the block system and through the toe. Cable-tied and interlocking block systems are normally installed with a trench

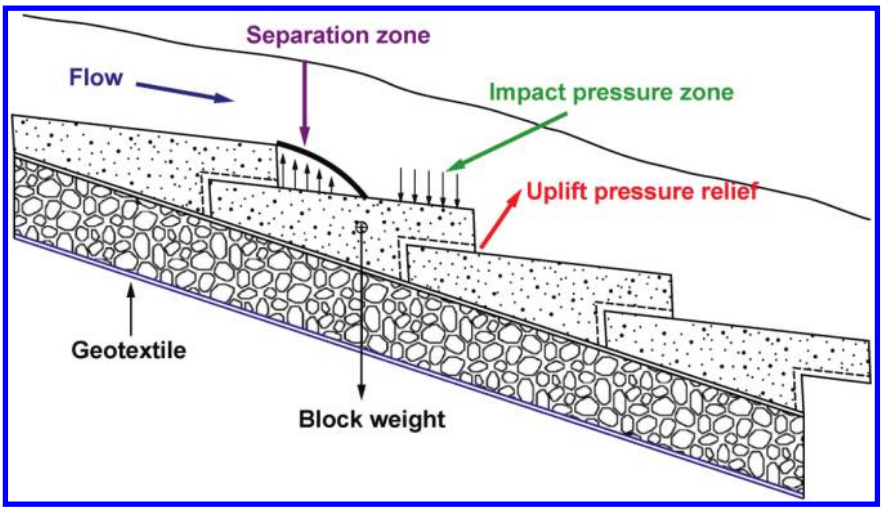

Figure 5. Typical forces on a wedge-block ACB system.

at the toe. Wedge-shaped blocks need a cast-in-place, reinforced concrete toe block or sill that supports the system from sliding while providing free drainage. The toe block or sill is normally placed above the tailwater to prevent the formation of a hydraulic jump on the blocks. The blocks may be cabled or pinned together for additional restraint.

The formation of the hydraulic jump is accompanied by pressure fluctuations that must be accounted for either by the block system, in the design of a terminal structure, or by hard protection at the toe. If the hydraulic jump is to be located on the blocks, the current design practice for a cable-tied block system is to increase the block weight within the hydraulic jump, which may require a heavier product. For a wedge-shaped block system, the blocks may either be cabled or pinned together, or the weight increased. Proprietary testing showed successful performance with the hydraulic jump forced by a gate at the toe of the system up to a unit discharge of 4.0 $m^3/s/m$ without any restraint. The use of an interlocking block system within a hydraulic jump would generally not be recommended.

The layer beneath the block system is normally comprised of one or more layers of free-draining granular material or a combination of granular material and a woven geotextile, which serves as a drainage or bedding layer and a filter layer. This is to assist with relief of uplift pressures below the blocks, protect the subsoil from erosion by drainage flow in the underlayer parallel to the slope, restrain soil particles on the subsoil surface against movement due to seepage exiting the subsoil and aspiration through the aeration vents of the blocks, and provide a smooth foundation for placement of the blocks.

In all systems, there has been no credit given in the hydraulic analyses to the interblock restraint, overlap, cables (if used by the system), or soil anchors. Therefore, it is generally accepted that an inherent conservatism exists in cable-tied and/or interlocking systems. Although soil anchors used to be routinely installed with early cable-tied systems, they are currently used only when determined necessary for an extra measure of conservatism.

6 GABIONS

Gabions are rectangular-shaped baskets or mattresses fabricated from wire mesh, filled with rock, and assembled to form structures such as gravity retaining walls, lined channels, overflow weirs, hydraulic drops, and other erosion control structures. Gabions are also used for spillways and as

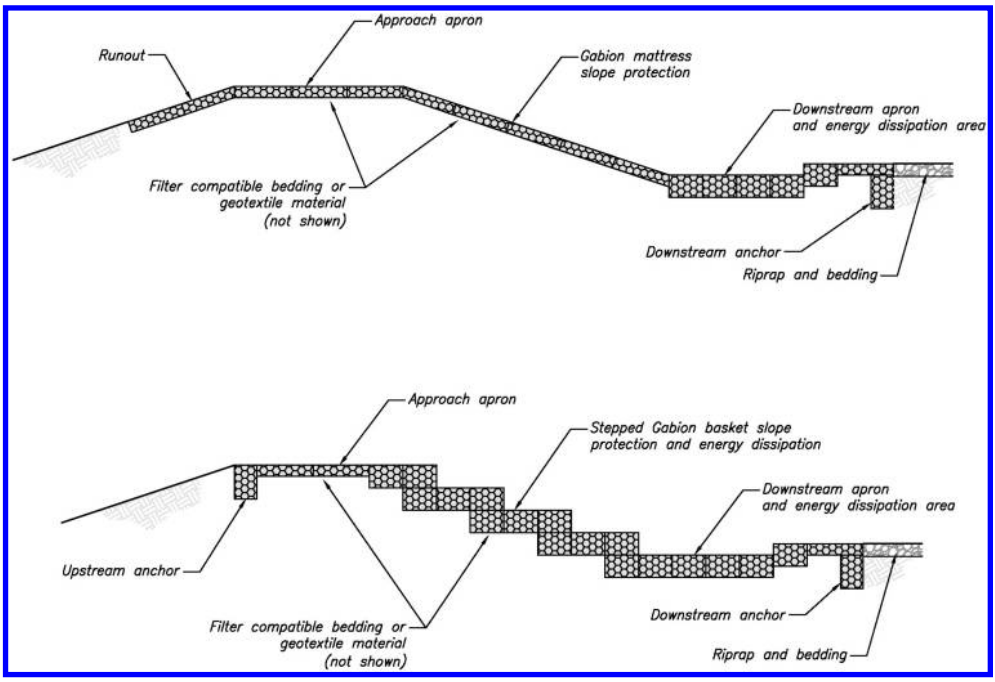

Figure 6. Example gabion sections for overtopping protection and energy dissipation.

overtopping protection for small embankment dams. Gabion baskets are generally stacked in a stair-stepped fashion, while mattresses are generally placed parallel to a slope. Typical sections of both types are shown in Figure 6.

Gabion baskets and mattresses are manufactured in a variety of sizes from hexagonal woven steel wire mesh, as specified in ASTM A975, or from welded wire fabric, conforming to ASTM A974. Hot dip galvanization, zinc treatments, polyvinyl chloride (PVC) coatings, and stainless steel wire products are available to extend design life. The gabions are delivered to the project site with the baskets formed, but collapsed for delivery and handling. At the project site the gabions are expanded to form the baskets and mattresses, and are filled with rock, generally from 5 to 20 cm in size.

Gabion baskets are typically divided into cells by diaphragms (often at 0.9 m centers) to reduce rock movement that can cause deformation. To reinforce the structure, the corners and edges of the baskets are tied and reinforced with heavier gauge wire to prevent unraveling and minimize deformation. Heavier gauge wire and ties are also used to join the adjacent gabions, forming one continuous structure. Once assembled, the gabions form flexible, permeable, rugged, monolithic structures. Gabions depend mainly on the interlocking of the stones and rocks within the wire mesh for internal stability, and the assembled structure's weight to resist hydraulic and earth forces. The wire mesh simply keeps the rockfill in place.

Gabions have advantages over loose riprap because of their modularity and rock confinement properties, thus providing erosion protection with generally less rock volume, within a smaller footprint, and with smaller rock sizes than loose riprap. Gabions also have advantages over more rigid structures as they can conform to ground movement, be easily constructed and repaired, dissipate energy from flowing water, and be designed to drain freely, although permeability may reduce over time as the voids in the rockfill become filled with silt, promoting vegetation growth. Some disadvantages include appearance, since the wire is exposed, and durability, since the wire

mesh may be subject to abrasion and corrosion damage. Gabions are also more susceptible to damage from debris and from vandalism, requiring more frequent maintenance and repair.

The key parameters governing overtopping flow for gabions are slope, drop height, step profile, and unit discharge. Overtopping tests performed on various types of gabion protection systems have indicated satisfactory performance for unit discharges up to 3.7 m^3/s/m and for flow velocities exceeding 9 m/s. Stepped gabion weirs offer greater structural stability and resistance to water loads than sloping mattresses, and provide energy dissipation on the stepped face. Smooth gabion mattresses placed on a slope should probably be limited to a unit discharge of 0.9 m^3/s/m to minimize the potential for damage. Although testing has revealed that stone size and shape do not significantly influence the flow conditions on the stepped gabion slope, tightly packed, angular stones at least 1.5 times larger than the mesh size are normally recommended. Potential debris loads may require the addition of 5 to 10 cm of protective concrete on the step surfaces. For increased stability and energy dissipation, the gabions may be tilted upstream about 10 percent to provide a rising lip. Maccaferri, Inc. provides software for the design of gabion channels and weirs, based upon maximum velocities and shear stresses developed during laboratory studies for mattresses and stepped baskets.

Anchoring the gabion spillway or overflow structure to the crest of the embankment is critical to the performance of the structure, and may be accomplished by constructing a runout extending some distance along the upstream slope (approximately 3 to 4.5 m) or by excavating an anchor trench just upstream of the crest and backfilling the first gabion mattress in the trench. An anchor trench should also be constructed at the downstream end of the stilling basin or downstream apron to prevent headcutting. A scour analysis should be performed to determine the appropriate downstream anchor trench depth where excavation to bedrock is impractical. A riprap blanket over a bedding layer may be provided beyond the end of the gabion structure for additional scour protection.

A filter compatible bedding layer or geotextile material should be designed to serve as a foundation for the gabions and to prevent seepage or overtopping flow from eroding the underlying surface and transporting embankment materials into or through the gabion structure. The most common damage occurring in gabion structures is the rupture of the gabion baskets. This can occur due to continuous abrasion of bedload and debris against the wire, long-term corrosion, excessive settlement, or through vandalism. When wires break or if the basket opens, the stones become loose, and the structure loses its shape and rigidity—and consequently its function. Alternatively, rock inside the gabions can progressively degrade through shaking and abrasion until they are lost through the gabion mesh openings. This can be avoided if rock of high strength and quality is used. Other observed failure modes have included inadequate foundation soil preparation leading to differential settlement, inadequate bedding material or filter material, resulting in migration of foundation materials through the gabions and loss of foundation support, and improper attachment between gabion joints, allowing flow to undermine the structure.

7 VEGETATIVE COVER, TURF REINFORCEMENT, AND SYNTHETIC TURF

Vegetative cover maintained on the downstream faces of embankment dams provides some protection against normal weathering effects and rill development due to rainfall. During small overtopping flows of short duration, vegetation can also provide protection against the initiation of concentrated erosion that can otherwise lead to headcut development and dam breach, and may allow for the planned use of the embankment to convey a portion of a flood hydrograph. For larger flow rates and/or for longer overtopping durations, vegetation alone may not fully protect against failure, but may delay breaching sufficiently to permit evacuation of downstream areas. Vegetative cover is most viable as an overtopping protection method for small dams in humid climates that receive sufficient moisture to establish relatively dense, uniform turf grasses. Good maintenance of the grass cover is essential to achieve significant protective benefits. Grass needs to be cut relatively short on the downstream face of an embankment dam (between 5 to 15 cm) to facilitate visual inspections and to promote uniformity of growth. Vegetative cover is generally not suitable

for very steep embankments because of the difficulty of mowing and other maintenance required to achieve a uniform cover. Installation costs for vegetation are often lower than for other types of overtopping protection, but maintenance costs can be higher. An advantage of vegetative overtopping protection systems, where applicable for use, is the potential for unlimited sustainability via annual growth and renewal, if proper maintenance can be achieved.

Vegetation provides protection of the soil surface by reduction of velocities and shear stresses as a result of the coverage provided by the stems and leaves that blanket the surface, and by reinforcement of the underlying soil due to the presence of plant roots. The reinforcement aspect may be further improved by the use of turf reinforcement mats that can improve root mass continuity following full vegetation establishment. Some types of turf reinforcement may also provide a soil surface protection benefit before grass becomes fully established. Reinforcement can be provided by a variety of materials, broadly classified into the categories of geotextile reinforcement and concrete reinforcement. Geotextile reinforcement may consist of fabrics, meshes, or mats that allow the grass plant to grow through the reinforcement, so that grass roots bind around the geotextile fibers to create an integrated geotextile/soil/root mass. Synthetic turf revetments consist of engineered synthetic (or artificial) turf underlain by a structured geomembrane and infilled with a special blend of cementitious materials for ballast.

Research to determine the limits of vegetation performance in earth spillways led to methods for predicting the thresholds of vegetation failure due to accumulated erosion of the underlying soil through the vegetal cover or due to instantaneous failure of the vegetation itself by stripping of thinly rooted sod or complete destruction of the vegetal material due to gross turbulent hydraulic stress. The USDA's WinDAM B computer model can estimate allowable overtopping discharges for embankment dams protected by unreinforced vegetation or riprap. Considering a range of typical grass properties and embankment dam slopes ranging from 2H:1V to 4H:1V, a practical upper limit on the overtopping unit discharge for unreinforced vegetation is about 0.6 to 2.2 $m^3/s/m$, depending upon the duration of overtopping.

The most complete source of independent information on natural turf reinforcement products and guidance for their design and use has come from the CIRIA research program in the United Kingdom [8]. Two-dimensional fabrics and three-dimensional filled mats improve upon the performance of plain grass during both short- and long-duration flows. The fabrics have been shown to provide protection during establishment, and the three-dimensional open mats provide optimum protection once grass is established. The synthetic HydroTurf™system, a patented product of Watershed Geosynthetics LLC of Alpharetta, Georgia, has been extensively tested at CSU in Fort Collins, Colorado, and has shown good performance under a wide variety of flow conditions, including both sustained flows and wave overtopping. CSU reported stable performance on a silty sand subgrade at a 2H:1V slope for steady-state overtopping depths up to 1.5 m for a total of 12 hours, with a maximum flow velocity of 9 m/s (29 ft/s). Limiting velocities over time (in ft/s) for plain and reinforced grass, from CIRIA, are plotted in Figure 7.

8 FLOW-THROUGH ROCKFILL AND REINFORCED ROCKFILL

The overtopping performance of existing rockfill dams (or massive rockfill placements over existing embankment dams) is much more difficult to predict than for a new flow-through rockfill dam due to the probable non-homogeneity of the existing structure. New rockfill designs will specify the construction materials and placement procedures. Excessive anisotropy between the horizontal lifts can be avoided by specifying a uniform, clean, and durable rockfill. Compactive effort, material properties, and lift thicknesses can be controlled. The erosion protection materials need to remain in place against the forces of flowing water and be filter compatible with the soils that they are meant to protect. These can be competing goals since it takes flat slopes and large rock to resist the forces of the overtopping flow, while it takes smaller particles to be filter compatible with the underlying embankment. Rockfill toe berms may be used to increase mass slope stability and increase the flow-through stability of an embankment dam during a flood event. Rockfill berms

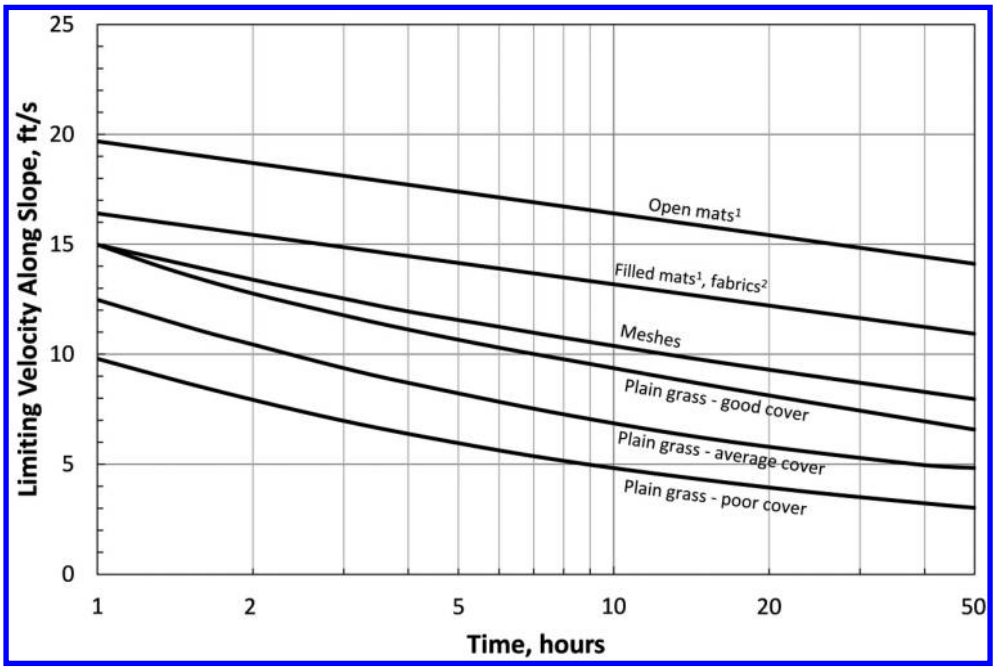

Figure 7. Velocity-duration curves for plain and reinforced grass (U.S. customary units).

placed over the toe of a downstream rockfill shell can be cost effective for moderate overtopping flows when most of the overtopping flow occurs inside the rockfill shell. Rockfill can also be used to slow the erosion rate and delay dam failure, effectively reducing risk. Such an application could provide more time to allow for the safe evacuation of the downstream population and reduce the consequences of dam failure.

There are four essential parts to the analysis and design of a rockfill dam subject to overtopping: flow-over, flow-through, mass stability, and filter compatibility. Knowing when design control shifts from flow-over to flow-through conditions is difficult, so designers are encouraged to select the rock size to accommodate both. However, designs to accommodate flow over a dam are more stringent because overflow velocities can be orders of magnitude higher than flow-through velocities. For flow-through velocities to control a rockfill design, the rockfill would likely have much less than 30 percent of its material sizes smaller than 2.5 cm. Mass slope stability will control the angle of the downstream slope of the outer rockfill zone. Seepage forces need to be included in the static slope stability analysis to accurately compute the stability of a rockfill embankment subject to flow-through conditions. Filter compatibility is required between the outer layers of a rockfill zone, or between the armor protection and the inner zones of an embankment dam. This could require multiple layers of gradually smaller particles from the downstream surface to the center core of the dam.

Because flow through a rockfill is turbulent, Darcy's law for laminar flow does not apply. Equations have been developed to estimate critical parameters of turbulent flow through a clean rockfill. Parameters such as the average velocity of water in the voids, height of seepage exit on the downstream slope, and unit flow rate are solved iteratively beginning with assumed values of rockfill permeability, hydraulic gradient, hydraulic radius of the rockfill voids, void ratio, rock size, and slope of the downstream face. However, these equations do not take into account the non-homogeneous and anisotropic nature of a rockfill placement. Physical model tests have been performed by the Technical University of Madrid in Spain to better understand pore water pressures and permeability within a rockfill for design purposes, and the critical issue of mass slope stability.

Table 1. Maximum permissible flow rates through a downstream rockfill.

Downstream Slope (H:V)	D_{50}, Dominant size of rock in slope (m)	Permissible flow through rockfill ($m^3/s/m$)	
		Loose*	Dense**
1.5:1	0.6	0.4	0.9
1.5:1	1.2	1.4	3.7
1.5:1	1.5	1.9	5.1
5:1	0.3	0.5	1.4
5:1	0.6	1.9	5.1
5:1	0.9	3.3	8.8
5:1	1.2	5.1	13.9
5:1	1.5	7.0	18.6
10:1	0.3	1.4	3.7
10:1	0.6	4.2	11.1
10:1	0.9	7.4	20.4
10:1	1.2	11.1	30.7
10:1	1.5	15.8	43.7

*Dumped rockfill, poorly graded with a relative density less than 50 percent.
**Compacted rockfill (by vibratory compactor) with a relative density near 100 percent.

After the flow rate through an unreinforced rockfill is estimated, it can be compared to the maximum permissible flow rate based on the 50-percent particle size (D_{50}), relative density, and downstream slope of the rockfill, as shown in Table 1. The values shown represent maximum unit discharges without particle movement.

Reinforcement can be incorporated into rockfill to hold the surface rock particles in place during overtopping and flow-through conditions. Improvement to the mass slope stability is also a benefit, but is considered secondary. The reinforcement is a system composed of two essential components: a mesh and anchor bars. The mesh is located on the outside of the rockfill and is intended to hold the rock particles on the outer embankment slope in place, while the anchor bars are attached to the mesh and embedded deep within the rockfill to hold the mesh securely in place. The mesh usually consists of steel reinforcement bars tied together. The mesh is sized relative to the smallest rock that could be dislodged from the downstream face of the embankment slope, and should have sufficient strength to resist the tractive and seepage forces acting on the surface particles, as well as the impact forces of debris carried by the overflow. If the anchor bars are to be used to increase global slope stability, the bars must be embedded beyond the critical shear surface to a depth sufficient to transfer the design loads in the bars to the surrounding rockfill and eliminate the possibility of pullout. To resist through flow, reinforcement should extend above the height of the predicted seepage exit elevation. To resist overtopping flow, the reinforcement should extend over the entire downstream face. The rockfill would be largest and reinforcement would be heaviest at the downstream toe of an embankment dam subject to overtopping.

The reinforcement of rockfill dams is usually designed empirically; that is, by copying designs of older dams performing successfully. Examples of two reinforced dams that have successfully withstood overtopping many times are included in the manual. A 1982 report prepared by the Australian National Committee on Large Dams (ANCOLD) includes information on 50 reinforced rockfill dams and cofferdams [8]. Of these 50 mostly Australian dams, 18 were overtopped by flood flows and 5 of these failed.

9 RIPRAP

A riprap layer on the downstream slope of an embankment dam can generally provide some protection against the initiation of embankment erosion during overtopping flow. Riprap is generally

composed of high quality quarried rock and is dumped or manually placed over a suitable bedding layer. With riprap in place, the overtopping flow is conveyed both through and above the riprap layer, thus preventing erosion by reducing flow velocities and shear stresses along the surface of the erodible embankment materials. Riprap is generally considered to be lower-priced than many other erosion protection alternatives when suitable borrow sources are available nearby. Riprap has always been an attractive option for erosion protection because it is widely available and conceptually simple in function, requiring nonspecialized preparation and installation, and minimal long-term maintenance to achieve apparent effectiveness. However, experience and research have shown that riprap layer and bedding design details and construction quality control can significantly affect performance for protection against overtopping flow. Riprap has been widely used in arid areas and on steeper embankment slopes (up to about 1.5H:1V, or the angle of repose) where vegetative protection is difficult to establish and maintain. The use of riprap for high flow rates and steep slopes generally becomes cost-prohibitive due to the large size of rock required.

There is much uncertainty in the design and analysis of riprap for overtopping protection, and conservative approaches are recommended. Guidance provided in the manual is more applicable to the design of new overtopping protection systems, rather than for the evaluation of existing riprap placements, since it is difficult to accurately assess the in-place gradation and placement uniformity of existing riprap not originally intended to be overtopped. Overtopping performance is very sensitive to the permeability of a riprap placement, primarily governed by the D_{10} size within the riprap layer, which is very difficult to evaluate for an existing dam. The degree of overtopping protection provided by riprap has been the subject of several research efforts in recent years. The primary area of interest in these studies has been determination of the allowable flow rate through and over a specified rock layer or alternately the size and depth of rock needed to protect against a specified flow rate. The secondary area of interest is the energy dissipation produced by the rock, often expressed in terms of the effective hydraulic roughness of the surface. In recent years, riprap has been specified for overtopping protection on mostly small, low hazard dams, although a few high hazard applications are cited in the manual.

Studies have shown that rounded rock can withstand a unit discharge about 40 percent lower than angular rock, and that uniform (or poorly-graded) materials can withstand higher flowrates than non-uniform (or well-graded) rock with the same D_{50}. They also found that uniform materials ($D_{60}/D_{10} = 1.1$) failed more suddenly than non-uniform materials ($D_{60}/D_{10} = 2.2$) when the riprap layer became unstable. Riprap gradations with a wide range of sizes typically experience problems with size segregation during placement. So for best performance under overtopping flow, an angular rock of relatively uniform size is generally desired, while gap-graded materials and mixes with a very large range of sizes ($D_{85}/D_{15} > 7$) are generally avoided. Riprap layer thicknesses are commonly between 2 to 4 times D_{50}, the former being the minimum necessary to protect the bedding material and the latter being a practical upper limit for effective placement. At slopes steeper than 4H:1V, current procedures require the entire computed flow to be conveyed interstitially. For flatter slopes, a portion of the flow can be conveyed above the rock surface, provided the surface flow will not exceed the critical shear stress limit for the rock. The manual provides design guidance for selecting D_{50} for a given unit discharge (in ft^3/s) and slope in Figure 8. These curves are applicable to angular riprap with D_{50} of 0.6 m (2 ft) or less, dumped randomly on appropriate bedding material in a layer at least $2*D_{50}$ thick. Unit discharges above the computed allowable level should be expected to cause riprap failure (defined as exposure of the bedding layer), as no safety factors are included. Several investigators have noted that careful hand placement of riprap to achieve improved armor density and interlocking of individual rocks can significantly increase allowable discharges, but the application of this construction method is not commonplace. Another alternative involves the use of a grout slurry to partially or fully fill the void spaces between the riprap. Until research specifically focused on overtopping flows can be conducted, partially-grouted riprap is not recommended for protection of embankment dams. Fully grouted riprap is also not recommended, since it suffers from the problems that partially-grouted riprap is designed to address, namely the lack of flexibility and inability to relieve high pore-water pressures.

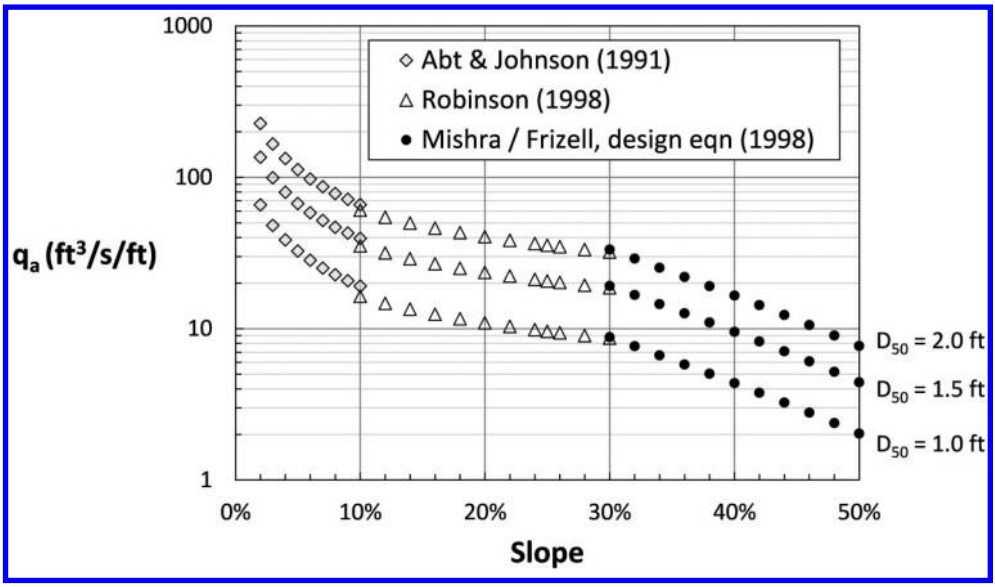

Figure 8. Allowable unit discharge as a function of slope, for a fixed stone size (U.S. customary units).

10 GEOMEMBRANE LINERS, GEOCELLS, AND FABRIC-FORMED CONCRETE

Geomembrane liners, geocells, and fabric-formed concrete have seen limited use for overtopping protection. A geomembrane is an impermeable synthetic liner or barrier made from relatively thin, continuous polymeric sheets. Geomembranes are commonly installed as an impermeable sheet liner with a soil cover. A cellular confinement system (CCS), commonly referred to as a geocell, is normally made from polyethylene strips connected in a honeycomb pattern and filled with earth materials or concrete. Fabric forms, consisting of woven, double-layer synthetic fabric, are normally filled with fine-aggregate concrete. Fabric-formed concrete is also referred to as articulating block (AB) mats.

A geomembrane can be placed over a low embankment dam for overtopping protection, or over an earthen section, swale, dike, or abutment away from the main dam, to provide a non-erodible surface for flow. The geomembrane should be placed over a smooth subgrade with the sides and upstream and downstream ends trenched and/or attached to fixed sills. The liner should then be protected with a granular soil cover that will wash away during flood events. Where feasible, seams between geomembrane rolls should be parallel to the flow. When geomembrane seams cross the flow, the upstream sheet should overlap the downstream sheet by a minimum of 0.9 m. Energy dissipation should not be allowed to occur on the liner. The manual describes a test installation by the Bureau of Reclamation in 1988, which experienced flow velocities up to 8 m/s.

Concrete fill is generally preferred for CCS installations that could be subjected to severe or persistent flows or to hydrodynamic forces from high velocity flows. A geomembrane or geotextile is often placed beneath the CCS for ease of construction or for redundant erosion protection. The woven fabric form consists of a series of compartments linked by an interwoven perimeter. Grout ducts interconnect the compartments, and high-strength cables are normally installed between and through the compartments and grout ducts. Once filled with grout or fine-aggregate concrete, fabric forms can provide concrete linings with deeply patterned surfaces. These patterns create a lining with large hydraulic resistance, which can reduce the overtopping flow velocity over a dam crest and impart stability to the system. Cellular confinement and fabric-formed concrete systems are provided by companies that have proprietary claims on product manufacturing, testing, and

Table 2. Summary of design limits for overtopping protection systems.

Protection system	Chapter	Dam height (m)	Unit discharge ($m^3/s/m$)	Overflow depth (m)	Flow velocity (m/s)	Shear stress (kg/m^2)
RCC	2	30–60	29–32	6	6–9	
CRCS	3	45–60	22–26	6	24	
Cable-tied ACBs	4	12	2.8	1.2	8	93
Wedge blocks	4	15–18	3.9	1.7	14	
Gabions	5	8	2.8–3.7	1.4	7–9	170
Grass	6	8–15	0.6–2.2	0.3–1.2	2.7	66
Reinforced grass	6	12–15	3.0	1.5	6	
Synthetic turf	6	12–15	2.8	1.5	9	44
Reinforced rockfill	7	43	14	3–4		
Rockfill	7	15	0.9–2.2	0.6–1.2		
Riprap	8	15	0.9–2.2	0.6–1.2		
Geo liners	9	8	0.2	0.3	8	
Geocells	9	8			9	78
Fabric-formed conc	9	8				290

application designs. As such, it is difficult to obtain detailed data regarding performance and applicability as an overtopping protection method.

11 SUMMARY OF OVERTOPPING PROTECTION ALTERNATIVES FOR EMBANKMENT DAMS

Part 1 of the manual concludes with a brief assessment of each of the overtopping protection systems presented using physical, hydraulic, and socio-economic factors as a means of comparison. This information is intended to provide a quick reference to identify the various similarities and differences, and potential advantages and limitations, of each of the overtopping protection systems presented in the manual, and can be used to help determine the various systems for further study that may best apply to a given situation.

Table 2 provides a summary of design parameters for various overtopping protection systems for embankment dams that may represent practical upper limits for their applications. The designer must confirm that any particular system selected will perform satisfactorily for the actual conditions of a given project. Most regulatory agencies will only approve applications of overtopping protection technology for embankment dams that are clearly within the established capabilities of the technology proposed.

12 CONCLUSIONS

The performance of most overtopping protection systems in the field under design loads is largely untested due to the remoteness of the design flood events. All systems included in the manual have been tested in the laboratory, or to some degree in the field, and the design parameters of any overtopping protection system should be within the limits tested. Numerous RCC overtopping protection projects have been shown to perform well for long durations and for overtopping depths of up to several meters. Some overtopping performance of both cable-tied and non-cable-tied ACBs has been reported. Some reinforced rockfill dams have also experienced frequent and sustained overtopping. Since embankment dams normally have a downstream slope that is either vegetated or composed of rockfill or riprap, any overtopping of embankment dams can provide information as to their performance up to the maximum conditions sustained, with or without failure. The potential

vulnerabilities and risks of each system should always be carefully evaluated before selection for final design and construction.

Some form of drainage or pressure relief will be required for all overtopping protection systems. Some systems provide natural drainage, such as gabions and rockfill, while others will require special drainage layers, collector pipes, weep holes, and outlets. Drainage systems must protect against the development of uplift pressures and be adequately filtered to prevent internal erosion of fine-grained materials.

Some overtopping protection systems use geotextiles as the primary component, or to provide for filtration, drainage, or added erosion protection of the underlying soils. While the use of geotextiles is gaining acceptance for some dam applications, many regulatory agencies would not permit the use of a geotextile in an embankment dam where its poor performance could lead to failure of the dam or require costly repairs. The filtration function of a geotextile located beneath an overtopping protection system is usually critical to the successful operation of the system. Geotextiles may tear with the placement of the overtopping protection units or displace under the high velocity and turbulent flows of the overtopping event. In some cases, system failure at one small location can cause complete failure of the dam. Overtopping protection systems that rely on a geotextile as an essential line of defense to protect against scouring of the underlying soil materials during overtopping of an embankment dam should be designed with special attention to the durability and longevity of the geotextile or should be avoided.

A terminal structure is normally required at the downstream end of the system to provide energy dissipation for the overtopping flow. Stepped systems, such as RCC placed in horizontal lifts, tapered wedge blocks, and stacked gabions, or systems with high surface roughness, such as rockfill, riprap, and fabric-formed concrete, will provide some energy dissipation before reaching the toe, which can result in the design of a smaller terminal structure. Most systems require some additional strength or capacity to resist the larger hydraulic forces normally associated with a hydraulic jump, such as an increased thickness or additional reinforcement, while other systems must avoid the occurrence of a hydraulic jump on the surface entirely.

Maintenance requirements will also vary with the system. All systems should be inspected regularly to the extent possible for signs of deterioration or damage. Buried systems will still require the maintenance of the vegetative or soil cover. Vegetation must be maintained in good condition. Trees, shrubs, or other woody vegetation should never be permitted on the overtopping protection, to avoid potential damage by roots, allow proper inspection, and avoid flow disturbance during operation. Exposed concrete surfaces should be inspected for cracks and open joints. Drains should be periodically inspected and outlets should be maintained open and free-draining. Systems relying upon steel components, such as gabions and reinforced rockfill, must be periodically inspected for corrosion or abrasion damage. Proprietary systems should be maintained in accordance with the manufacturer's instructions.

The material presented in the manual has been prepared in accordance with recognized engineering practices. The guidance provided in the manual should not be used without first securing competent advice with respect to its suitability for any given application. The publication of this material is not intended as representation or warranty on the part of the individuals or agencies involved that this information is suitable for any general or particular use, or promises freedom from infringement of any patents. Anyone making use of the information presented in the manual assumes all liability from such use. Any use of trade names and trademarks in the manual is for descriptive purposes only and does not constitute endorsement of any product.

ACKNOWLEDGEMENTS

The Federal Emergency Management Agency (FEMA), as the lead agency for the U.S. National Dam Safety Program (NDSP), sponsored the development of this manual in conjunction with the U.S. Bureau of Reclamation. The primary authors of this document were Chuck Cooper, Robert Dewey, Bill Fiedler, Kathy Frizell, Tom Hepler, and Tony Wahl of Reclamation. Additional contributions

were made by Elizabeth Cohen, Christopher Ellis, Dennis Hanneman, and Tracy Vermeyen of Reclamation. Peer review of this manual, in whole or in part, was provided by Dave Gillette and Bill Engemoen of Reclamation; Sal Todaro, U.S. Army Corps of Engineers; Paul Schweiger, Gannett Fleming; and Rafael Morán and Miguel Toledo of the Technical University of Madrid.

REFERENCES

[1] *Technical Manual: Overtopping Protection Alternatives for Dams*. Federal Emergency Management Agency, P-1015 (2014).

[2] *Selecting and Accommodating Inflow Design Floods for Dams*. Federal Emergency Management Agency, P-94 (2013).

[3] *Design Manual for RCC Spillways and Overtopping Protection.* Portland Cement Association (2002).

[4] Hunt, S.L. and K.C. Kadavy, *Energy Dissipation on a 4(H):1(V) Stepped Spillway*. Proceedings of the ASDSO Annual Meeting, Lexington, Kentucky (2008).

[5] *Uplift and Crack Flow Resulting from High Velocity Discharges over Open Offset Joints.* Report No. DSO-07-07, Bureau of Reclamation, Denver, Colorado (2007).

[6] *Design Manual for Articulating Concrete Block (ACB) Revetment Systems*. National Concrete Masonry Association (2010).

[7] Hewlett, H.W.M., L.A. Boorman, and M.E. Bramley, *Design of Reinforced Grass Waterways*. CIRIA Report 116, Construction Industry Research and Information Association, London, England (1987).

[8] *Report on Mesh Protection of Rockfill Dams and Coffer Dams*. Australian National Committee on Large Dams (1982).

Dam Protections against Overtopping and Accidental Leakage – Toledo, Morán & Oñate (Eds)
© 2015 Taylor & Francis Group, London, ISBN: 978-1-138-02808-1

Review of embankment dam protections and a design methodology for downstream rockfill toes

R. Morán
Dam Safety Research Group (SERPA), Technical University of Madrid (UPM), Spain

ABSTRACT: The paper summarizes the most common embankment dam protections as well as some general design considerations. In addition, a brief summary of failure mechanisms is presented. Finally, a new design methodology about rockfill toe protections is introduced. This methodology has been the result of a PhD thesis developed in the Technical University of Madrid. Results of the experimental validation of this methodology are briefly described.

1 INTRODUCTION

During the last decades, there has been a significant increment of the social demand on dam safety standards, especially in the most developed countries. This has yielded to new, and more demanding, dam regulations and guidelines (MOPTMA, 1996). So, the challenge for dam engineers is huge due to the fact that this safety improvement has to be developed over existing dams, mostly designed in accordance to less restrictive technical criteria. Furthermore, the plight of the global economy demands to put it into the practice through cost-effective methods.

There are different possibilities to enhance the safety of the dams. In such a way, during the last years, a great effort has been done in many countries using risk assessment to classify the dams through their potential damages caused by their failure and the probability of occurrence. In addition to this, emergency plans have been developed in some countries to diminish the consequences of dam failures. Also, the improvement in the surveillance of dams through new monitoring technologies and data analysis has induced an increment of dam safety. Such activities have been focused on prevention to reduce damages through early failure detection as well as mitigating its consequences.

However, safety of existing dams can also be improved through adapting their former designs to protect them against foreseeable failure mechanisms. In the particular case of embankment and rockfill dams, it is well known that the most frequent causes of failure are overtopping and leakage due to internal erosion (usually known as "piping") of the materials either of the dam body or its foundation. Having said that, the type of protections considered in this background review will be the ones dedicated to avoid or reduce the effects of the abovementioned causes once they have occurred. Hence, other actions aimed at mitigating the causes of failure such as increment of the capacity of the spillway or flood management, are out of the scope of this paper even though they can be considered as a dam protection as well.

Furthermore, developments on protection technology could be used for functional purposes in new facilities. Thus, in some cases, protections have been used to build cofferdams, auxiliary and service spillways of ponds, small embankment or rockfill dams. In such cases, designers should be aware of the potential risk associated to each type of protection and the high vulnerability of embankment and rockfill dams in case of protection failure of spillways built on the dam body.

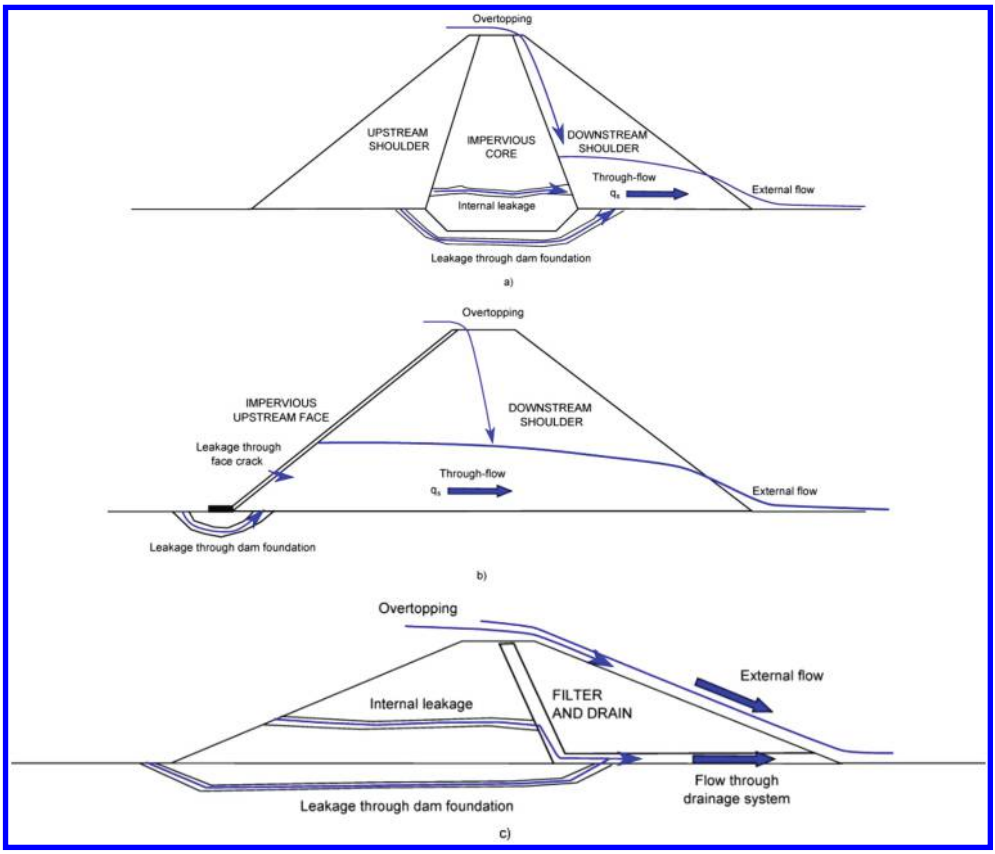

Figure 1. Examples of overtopping and accidental leakage processes in embankment dams: a) impervious core with highly permeable shells; b) upstream face rockfill and c) homogeneous earthfill.

2 FAILURE MECHANISMS OF EMBANKMENT AND ROCKFILL DAMS

Properly design of embankment and rockfill dam protections in overtopping or *piping* scenarios previously requires a conceptual analysis of the failure mechanisms of this type of dams. Both accidental events, when happen, may cause either high unit through-flow or external skimming flow over the downstream surface of the dam body. So, in the very initial phase, these flows could cause damages to the downstream shell because of the loss of the material due to unraveling, erosion or mass slide. Hence, most of the embankment dam protections are focused on reducing the damages in the downstream area of the dam. Therefore, the damages in the impervious element would be avoided or, at least, delayed, as much as the protected downstream shell may withstand.

Apparently, failure mechanisms strongly depend on the type of dam, the materials within the dam body and its foundation. In such a way, Figure 1 shows how overtopping and accidental leakage flows develop, depending on the permeability and cohesion of the different zones of the dam body.

So, in dams with highly permeable downstream shells, typically formed of materials with negligible cohesion (Figures 1a and 1b), the water from overtopping and accidental leakage flows through the material of the downstream shell and exits the dam body at the downstream toe. In most of these cases the failure begins with a significant damage of the downstream shell at the toe of the dam, usually from downstream to upstream.

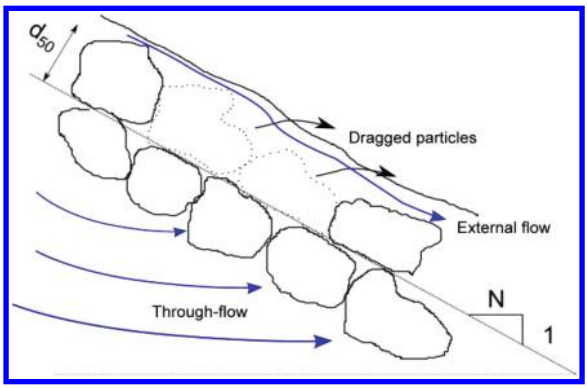

Figure 2. Scheme of particle dragging at the external surface of a rockfill downstream shell.

The main failure mechanisms of the dam body are the following:

- Internal erosion. In highly permeable downstream shells, the turbulent through-flow may develop high seepage velocities. Therefore, the risk of internal erosion due to particle dragging from the inside of the dam body is high. In addition to this, the seepage due to through-flow can cause dynamic pore water pressures with uncertain consequences. Moreover, internal erosion of the material of the impervious core has to be considered due to either a concentrated leakage flow or the overtopping flow over the downstream surface of the central core during the freefall from the crest of the dam.
- Dragging of particles. The particles of the material placed over the downstream surface of the dam shell can be dragged due to the forces caused by the flow pattern at the toe of the dam which is a combination of the exit of the through-flow and the external skimming flow as shown in Figure 2.
- Mass slide. The slope of the downstream shell of earth-rock and rockfill dams is usually designed assuming that it will be free of pore water pressure. Therefore, the presence of pore water pressures developed by the through-flow may cause instability and mass sliding (Toledo, 1997).

On another note, in the case of earthfill dams (Figure 1c) with downstream shell comprising either impervious or semi-permeable material, through-flow seepage turns negligible. So, the principal failure mechanism associated to overtopping will be the scour due to shear stress caused by the skimming flow over the downstream surface of the dam body. In addition, in case of internal leakage, the failure mechanism will be internal erosion of the cohesive material caused by the shear stress between the pressure flow and the soil, when piping has been developed. Granular filters are commonly used to protect internal leakage in this dam type. However, filters and additional protection systems of dam foundation are out of the scope of this technical review.

3 DESIGN CONSIDERATIONS

Once the failure mechanisms of the existing dam have been analyzed, the design of the protection requires additional input to select the suitable technology. This selection strongly depends on the following factors:

- *Design unit-flow*. Most of the protections have a range of suitable unit flows depending of specific tests or previous references in real cases (FEMA, 2014). Every embankment dam is able to withstand certain unit-flow without any protection. Once this discharge is overcome, protections are needed and, as the design unit-flow increases, the number of suitable technologies decreases. However, the estimation of the value of the design unit-flow is still a challenge nowadays. Even

so, in countries like Sweden and Norway there are technical regulations which establish criteria about design unit flows for dam protection against accidental leakage (EBL Kompetanse, 2005; SVENSK ENERGI, 2007). In any case, additional research is necessary to establish uniform criteria about the design unit-flow for dam protections, considering the natural hazards, potential risk and overall environmental and economic benefits.

– *Dam height*. It is also necessary to estimate the maximum velocity and shear stress caused by the flow. The overtopping protection systems have design limits directly related to these values so, a comprehensive analysis of them should be previously done.
– *Structural behavior of the downstream shell*. Most of the embankment protections are placed over the downstream slope of the dam and the new stresses and settlements should be considered in the protection design. This analysis should conclude about possible measures such as drainage systems, anchors to withstand shear forces in the contact surface between the soil and the protection, or the adoption of flexible alternatives, more adaptable to foreseeable dam settlements.

After the protection system has been selected, the design should accomplish the required safety factors. However, the fulfillment of this condition poses a number of difficulties that must be considered:

– As it was already mentioned, the protection system can be subject to different failure mechanisms. Consequently, each one of them should have a correspondent safety factor to be fulfilled. This may cause confusion since there are not standard requirements and it could not be reasonable to demand the same safety factors to the different mechanisms of failure.
– For a particular mechanism of failure there are different alternatives for the safety factor calculation (Cox, Thornton, & Abt, 2014). However, there are significant differences in the obtained results among them. There are also equivalences in the safety factor depending on the action selected to be applied to (Toledo, 1998).
– Nowadays, there is a lack of criteria about the safety factor values to be required depending on the use of the protection system, (e.g. dam body protection, emergency spillway or service spillway) or the potential risk, among others.

On another note, as protection technology is still incipient, there is substantial research to do to properly design additional constructive issues such as joints, inlet transitions, energy dissipation, toe treatments, anchorages between dam and protection, foundation reinforcement, drainage systems, etc. Thus, in many cases, the main problem for dam engineers in a dam protection project is not the selection of the protection system, but solving the construction issues associated to it.

4 GENERAL DESCRIPTION OF EMBANKMENT DAM PROTECTIONS

A possible classification of the protections systems for embankment dams can be done considering how the shear stresses caused by the flow are resisted by them. The key point in this approach is the interaction between the external flow and the dam body.

Thus, **hard protection systems** (Figure 4a) are those in which the flow remains outside the dam body. These kind of overtopping protection systems prevent erosion of the embankment material by keeping the separation between dam body and the main part of the overtopping flow through coverings of highly cohesive materials like reinforced concrete, roller compacted concrete, soil cement, asphaltic mixtures, etc. Most of these hard protections are installed over drainage layers to relief minor flows caused by normal seepage through the dam body and leakages among the protection joints or cracks. Nevertheless, in normal operation of the protection system, this flow should be low and, therefore, no damages should be expected because of it, if drainage systems work properly.

Meanwhile, **soft protection systems** include superficial treatments of the downstream surface of the dam using low cohesive materials or by means of a partial separation between the overtopping

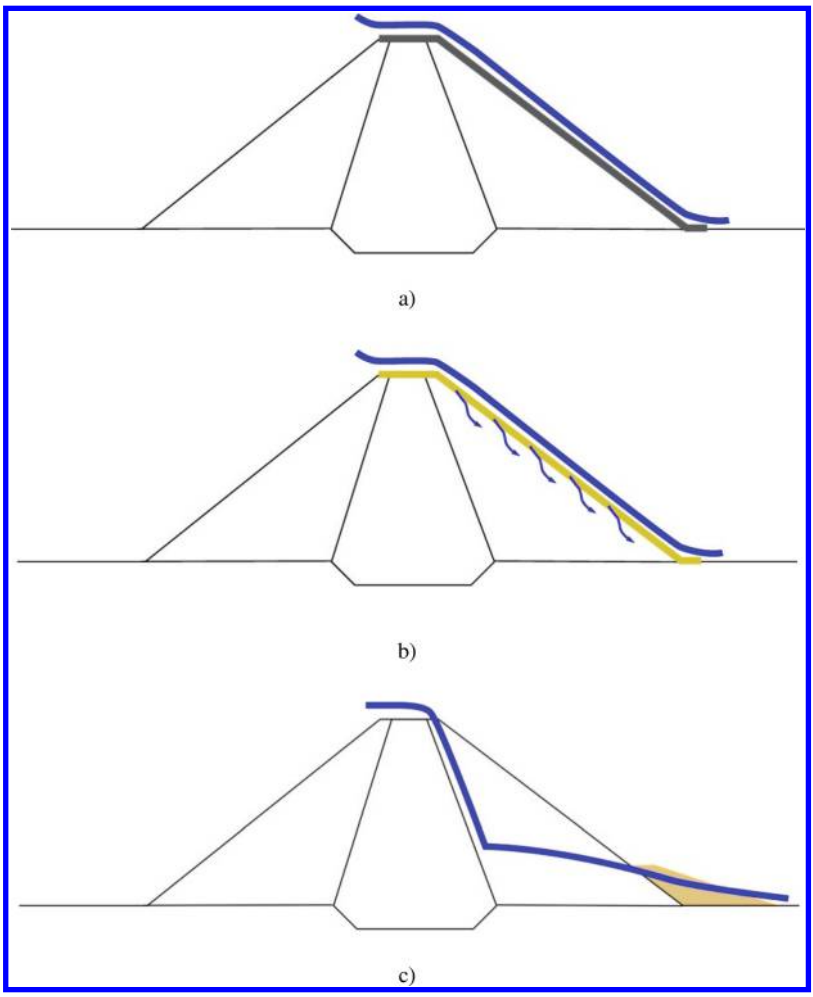

Figure 3. Schemes of embankment dam protection systems: a) hard protections; b) soft protections c) rockfill toe berms.

(or accidental leakage) flow and the erodible material of the downstream shell (Figure 4b). Rockfill toe protections could be included in this category as well (Figure 4c).

4.1 *Hard protections*

The most common types of hard protection systems are:

Rolled Compacted Concrete (RCC). They have been frequently used, especially in the U.S.A. The system usually consists in either overlapped horizontal or parallel lifts of RCC, placed over the downstream slope of the dam. So, the surface of the protection could be stepped or flat depending on the way of the placement of RCC. This technology has been validated in real cases through a high number of successful references (over 130) from approximately 30 to 60 m high with maximum unit discharge around 32 m^2/s. Likewise, soil cement has been used as construction material instead of RCC (Wirtz Dam, USA) although still there are few cases in the bibliography.

Continuously-reinforced concrete slabs (CRCS). The background of this protection system proceeds from non-conventional spillways located on the downstream face of embankment dams

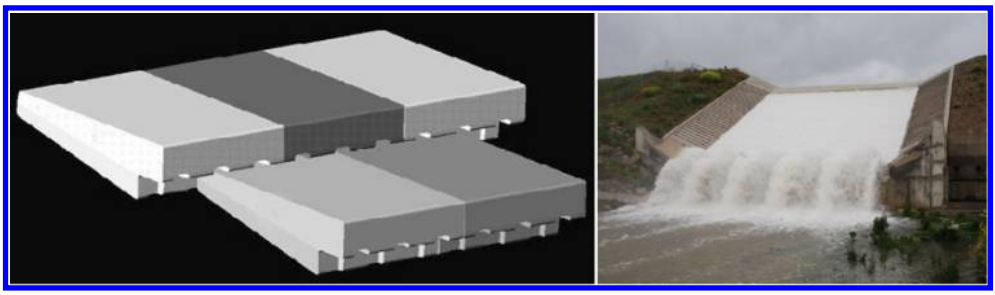

Figure 4. Left: layout of overlapping wedge-shaped blocks. Right: flow discharge of the spillway of Barriga Dam on May 2008.

all over the world. In Spain, this technology was applied at Molino de la Hoz Dam and Llodio Dam with a good behavior as far (Álvarez, Montoya, & Toledo, 1998; Bizcarrondo & Gómez, 1970). The reinforced concrete slabs are structurally divided by joints between them. They are usually placed over a bedding or drainage layer of granular material. The design of this protection system has to consider some key aspects related to stagnation pressures in the transversal joints (W. Frizell, 2007); relief of eventual uplift pressures below the slabs; erosion control at the toe of the dam; and settlements of the downstream shell, especially in the cases of newly constructed embankment dams. Design limits proposed by the Overtopping Technical Manual (FEMA, 2014) for this protection system are a maximum of 60 m high dams and unit flow below 26 m^2/s.

Wedge-shaped blocks (WSB). In a WSB protection system, the downstream shell is covered by a revetment of overlapped precast concrete blocks. As every block overlaps the given downstream one, the revetment works as a stepped spillway for the overtopping flow (Figure 4). This technology can be considered as a transition between hard and soft protection systems due to the fact that a fraction from 0.1 to 0.7 percent of the flow leaks through the joints between adjacent blocks (Relvas & Pinheiro, 2008; Thornton & Robeson, M.D., Varyu, D.R., 2006) and the foreseeable drainage flow is higher than in other hard systems.

The hydraulic stability of each block is assured by the positive pressure of the water on the upper face, the overlapping and the negative pressure of air on its lower face. The vents, located in the lower zone of the step riser, transfer the negative pressure to the surface between the block and the bedding layer, which means that the ensuing suction enhances the stability of the block. There are references (FEMA, 2014) of this protection system in dams below 18 m high, with a maximum unit discharge of 3.9 m^2/s.

Open stone asphalt. It is a self-supporting, coherent and semi-permeable revetment made of crushed sandstone coated with sand mastic (Bieberstein, Quieber, & Wörsching, 2004). This system has been successfully applied in the 4 m high Mönchzell Dam (Germany) and tested in laboratory for a maximum overtopping unit flow of 1 m^2/s. In this case study, the downstream slope of the dam was 8H:1V. Furthermore, the protection system allows vegetation cover on it, reducing the overall environmental impact.

4.2 *Soft protections*

The main typologies of soft protection systems are:

Articulated concrete blocks (ACB). There are different types of articulating concrete blocks: cable-tied, interlocking, overlapping and butt-joined. However, most of dam protection case studies refer to systems formed by cable-tied and overlapping concrete blocks. The last one has been described already in the paragraph of wedge-shaped blocks, into the hard protections chapter. Therefore, only cable-tied blocks are described in this section as a soft protection.

Figure 5. Vegetative cover of Charco Redondo Dam (Spain).

The system consists in a number of concrete block units that are individually formed with or without open areas and laced together with cables into mattresses. They can be easily installed in the dam site by means of cranes.They are usually installed over either granular layers for bedding and drainage purposes or geomembranes. ACB protections have been used successfully in dams with heights under 12 m and maximum unit discharges of 2.8 m^2/s (FEMA, 2014).

Gabions. This protection system has been widely used in civil engineering to reduce erosion and instability of slopes. Gabions are baskets or mattresses fabricated from wire mesh filled with rock that may be assembled together. They may form either a continuous coverage over the downstream slope of the dam, or a stepped spillway, if they are stacked in that way.

The main advantages of this system are the easy installation, the energy dissipation of flowing water and the drainage capacity. However, there are concerns about its durability due to the exposition of the wire mesh to corrosion, abrasion by debris, and vandalism. Gabion protections have been tested for unit discharges of 3.7 m^2/s and maximum dam heights of 7.6 m. There are available design criteria about construction and installation procedures including anchorages, bedding and drainage layers, filters and energy dissipaters (FEMA, 2014).

Vegetative Cover, Turf Reinforcement Mats, and Synthetic Turf Revetments. Vegetative cover over the downstream slope (Figure 5) provides protection against erosion for gentle overtopping unit discharge. The steams of the grass cause an increase of the shear resistance of the soil combining functionality with aesthetic and environmental benefits. Thus, this protection system has worked successfully in certain conditions e.g. velocities below 2.7 m/s and maximum unit discharges of 2.2 m^2/s. In any case, its appliance is always beneficial even for higher flows, due to the probable effect of delay of the dam failure. However, the need of maintenance and the dependence on climate conditions are usual disadvantages of this protection system (FEMA, 2014).

As higher level of erosion protection is required, either artificial reinforce of vegetative cover or synthetic turf revetment turns necessary. Such protections have been successfully tested for a maximum unit discharge of 3 m^2/s in 15 m high dams.

– **Rockfill through-flow protections.** This typology involves every protection system which is applicable to rockfill or earth core dams with a highly permeable downstream shell. In these particular dam types (Figures 1a and 1b) turbulent through-flows can be developed within the dam body due to either overtopping or extremely high leakage flows. Once the through-flow

has been developed, the suitable protection should be able to avoid erosion and mass slide at the toe of the downstream shell as well as assuring the drainage capacity of the extremely high through-flow. The most common flow-through rockfill protections are the following:

- *Reinforced Rockfill*. The system provides a reinforcement of the surface rock particles through steel bars installed as a mesh and also as anchorages to the dam body. There are published design criteria about reinforced rockfill (FEMA, 2014; ICOLD, 1993) and a few case studies, mainly in USA and Australia. The design limits of this technology recommended by FEMA are 14.2 m^2/s and dam heights of approximately 43 m.
- *Through-flow Rockfill Dams*. In this case, the design of the existing dam is adapted to resist through-flows. Wadi Khasab Dam, Oman, is a particular case study of this protection due to the fact that the protection operates as the service spillway. This 17.9 m high dam, with rockfill size of the downstream rock layer from 0.7 m–1.7 m, and a downstream slope of 4H:1V, successfully passed a peak flood discharge of approximately 3500 m^3/s or, in other words, 5.1 m^2/s (Taylor, 1991).
- *Downstream rockfill toes*. This protection system has been applied during the last decades in countries of Northern Europe such as Norway and Sweden. These countries have developed technical guidelines and recommendations about installing this kind of protection in rockfill dams assigned as high hazard potential (Suorva Dam and Seitevare Dam, in Sweden) (A. Nilsson, 2009; Å Nilsson & Rönnqvist, 2004; Å Nilsson, 2004).

Rip-rap protections. Historically, the main use of rip-rap in dam engineering has been limited to wave protection of the surface of the upstream shell. However, this kind of overtopping protection has been thoroughly studied, especially in USA (K. H. Frizell, Ruff, & Mishra, 1998; Mishra, 1998; Robinson, Rice, & Kadavy, 1998). In addition, recent research has been developed basically in Norway, focused on the so-called "layered rip-rap". This particular technology is based on substituting the dumped rip-rap for a stone by stone placement made directly by the machinery operator. The experimental research included laboratory (Norwegian University of Science and Technology and Technical University of Madrid) and full scale tests in 4 m high rockfill for a maximum value of the unit discharge of 8.3 m^2/s, with no apparent damages. A meaningful difference on the resisted unit discharges has been found between dumped and layered rip-rap protection (Lia, Vartdal, Skoglund, & Campos, 2013). The two layered rip-rap protection system has been currently applied in Grøttavatnet Dam and Håen Dam (Norway) according to the national dam regulations.

Geosynthetic systems. This technology has undergone considerable development in the last decades due to the advances of the geosynthetic industry and the growing application of these systems in civil and environmental engineering. Some of manufacturers have developed their own research dedicated to the particular products under patent. So, their conclusions should be limited usually to each particular system. Even though the difficulty to establish general design guidelines due to the high number of involved products and manufacturers, FEMA technical manual recommends not only design limits related to velocity (between 8 and 9 m/s) and dam height (7.6 m) but also another key factors as durability, installation in the dam site, etc.

5 DESIGN METHODOLOGY FOR DOWNSTREAM ROCKFILL TOES

This methodology is one of the results of the research line initiated with the study of the stability of overtopped rockfill dams (Toledo, 1997; Toledo, 1998; Toledo, Lechuga, & Oñate, 2008) and the associated failure mechanisms (Toledo, Morán, & Campos, 2012). Later on, additional studies were developed (Morán, Toledo, Sevilla, & García, 2008; Morán & Toledo, 2009; Morán, Campos, García, & Toledo, 2011; Morán & Toledo, 2011) to establish a design methodology to design rockfill toes in order to protect existing rockfill dams against through-flow, using the available rock near the dam site. In some cases, this material may come from the same quarries opened during the construction of the existing dam, making the solution economically competitive.

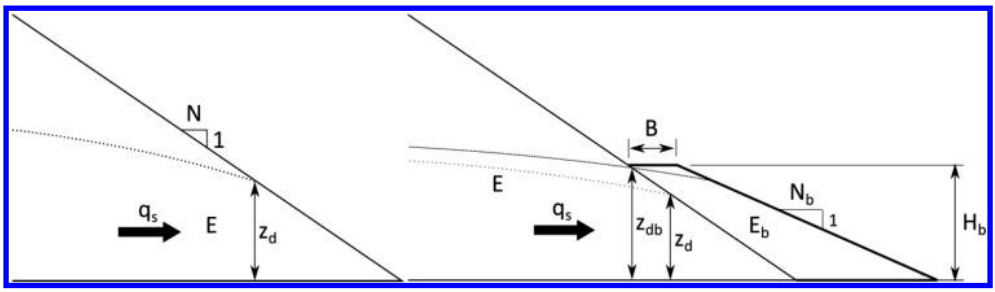

Figure 6. Left: scheme of through-flow exit at the toe of the existing dam. Right: geometrical definition of the rockfill toe protection (Morán, 2013).

5.1 *Overview*

The protection consists (Figure 6) of a dumped rock filling (of material E_b) at the downstream toe of the existing dam (with a downstream shell of material E) in order to achieve the overall mass stability. The rockfill toe can be geometrically defined by three parameters: berm length (B), protection height (H_b) and downstream slope (N_b).

The design parameters are the unit through-flow discharge at the toe of the dam (q_s) and the material properties of both the existing dam and the rockfill toe. The required data of both materials[1], E and E_b are the following:

a, b. Dimensionless coefficients of the parabolic seepage equation (Parkin, 1971) of highly permeable granular soils (Eq. 1):

$$i = a \cdot v + b \cdot v^2 \tag{1}$$

where: i is the hydraulic gradient and v is the average seepage velocity in the porous media, in a continuum approach.

γ_{sat}. Saturated specific weight.

ϕ. Internal friction angle.

5.2 *Design methodology*

5.2.1 *General assumptions*

The proposed methodology has been obtained with the following assumptions:

1. The flow pattern is through-flow seepage with the exit at the downstream toe of the shell.
2. The foundation is considered rigid during the through-flow process.
3. Since methodology is 2D, the design unit flow discharge is referred to a cross section in the bottom of the river valley. Therefore, in case of through-flow caused by overtopping, the unit discharge should consider the width of the valley instead of the length of the dam crest.
4. Rockfill materials (E and E_b) are considered isotropic so that the methodology is suitable for highly permeable rockfill. Therefore, the methodology is not suitable in highly anisotropic rockfill usually caused by the compaction of layers in weak materials.
5. Other failure mechanisms, such as dragging of particles at the downstream surface of the rockfill toe or internal erosion, are out of the scope of this particular research. However, design criteria based on existing references from the state of the art were proposed for external particles sizing and design of the transitions between the dam and protection materials.

[1] Subscripts E and E_b will be used to refer to the material of the existing dam and the rockfill toe, respectively, for each one of the considered parameters.

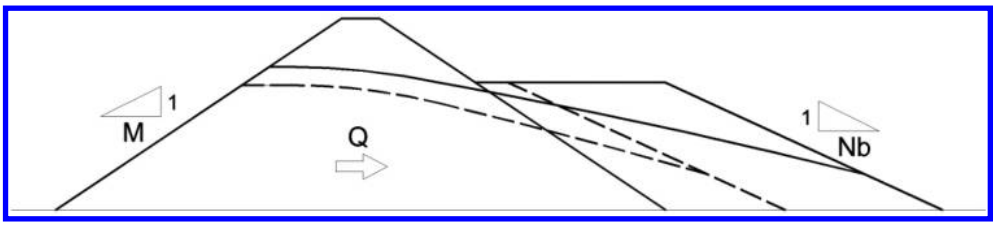

Figure 7. Scheme of the raise of the saturation line due to the increment of the length of the berm of the rockfill protection (Morán & Toledo, 2011).

5.2.2 *Design procedure*

The design procedure allows obtaining the parameters B, N_b and H_b, for a given unit through-flow and the features of the rockfill materials (E and E_b). The procedure starts with the estimation of the *length of the rockfill toe berm* (B). The research studies have shown that the length of the toe berm has to be the necessary minimum for an appropriate compaction of the rockfill layers (Morán & Toledo, 2011). So, for a fixed unit through-flow, as value of B increases, the saturation line raises (from dotted to continuous line in Figure 7) due to the lowering of the overall hydraulic gradient. In such a way, the area affected by the pore water pressures is higher and the protection height should be incremented. Therefore, the length of the rockfill toe berm (B) can be defined previously according constructive issues. This consequence is important due to the fact that as B increases so do the cost of the solution and, however, the stability of the whole dam-protection diminishes.

The slope of the rockfill toe (N_b) can be estimated through the numerically obtained (Toledo, 1997) equations (Eq. 2 and Eq. 3):

$$F = \frac{1}{\gamma_{Eb,sat}} \cdot \left(\gamma_{Eb,sat} - \frac{\beta \cdot \gamma_w}{cos^2\alpha}\right) \cdot \frac{tan\varphi_{Eb}}{tan\alpha} \tag{2}$$

where:

$$\beta = -0{,}32 \cdot N_b + 1{,}52 \cdot N_b - 0{,}77, \text{for } 1{,}5 < N_b < 2;\ \beta = 1 \text{ for } N_b \geq 2 \tag{3}$$

F, mass slide safety factor
N_b, slope (H:V) of the rockfill toe
$\gamma_{Eb,sat}$, saturated specific weight of the rockfill used in the protection
γ_w, specific weight of the water
φ_{Eb}, internal friction angle of the rockfill used in the protection
α, angle between the rockfill slope surface and the horizontal plane, where:

$$\alpha = \arctan\left(\frac{1}{N_b}\right) \tag{4}$$

This formulation (Eq. 2) has been validated experimentally for slope values higher than two, i.e. β equals to one, within this particular research (Morán, 2013). This range of slope values is valid for most of the granular materials used in rockfill construction.

Prior to obtain the height of the protection (H_b), a seepage calculation of the downstream shell of the existing dam for the design through-flow unit discharge (q_d) is needed. The seepage model will be used to find the height of the saturation line at the exit in the surface of the downstream slope of the rockfill, z_d (making q_s equal to q_d in Figure 6). This numerical model must consider the parabolic seepage equation (Eq. 1) of the material of the downstream shell of the existing dam (material E). With regard to this task, the International Center of Numerical Methods in Engineering (CIMNE) has developed specific numerical modeling which allows making these non linear seepage calculations (Larese, Rossi, Oñate, & Idelsohn, 2008; Larese, Rossi, Oñate, & Toledo, 2010;

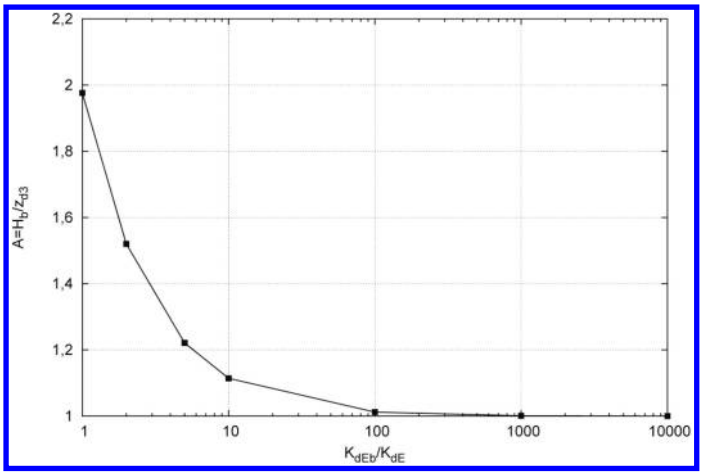

Figure 8. Evolution of coefficient A with the permeability ratio K_{dEb}/K_{dE} (Morán, 2013).

Larese, Rossi, & Oñate, 2011; Larese, Rossi, Oñate, & Toledo, 2011; Larese, Rossi, Oñate, & Idelsohn, 2012).

Once the value of z_d has been obtained, *the protection height* (H_b) can be estimated through the following equation (Eq. 5 and Eq. 6):

$$H_b = A \cdot z_d \tag{5}$$

Coefficient A may be calculated using the transcendent equation (Eq. 6):

$$\frac{K_{dE} \cdot K_{dEb} \cdot (B + z_d \cdot N_b \cdot A)}{K_{dEb} \cdot z_d \cdot N \cdot A + K_{dE} \cdot (B + z_d \cdot (N_b - N) \cdot A)} \cdot A^2 = K_{dE} \cdot \frac{B + z_d \cdot N_b \cdot A}{N \cdot z_d} \tag{6}$$

where: K_{dj}, linear permeability correspondent to the maximum hydraulic gradient at the toe of the slope N_j (N for material E and N_b for material E_b) for a given granular material j (E or E_b) (Eq. 7) with dimensionless coefficients of the parabolic seepage equation a_j and b_j (see Eq. 1):

$$K_{dj} = \frac{N_j \cdot \left(-a_j + \sqrt{a_j^2 + 4 \cdot \frac{b_j}{N_j}} \right)}{2 \cdot b_j} \tag{7}$$

N, downstream slope (H:V) of the dam (Figure 6).

A sensitive study was done to evaluate the effect of the permeability ratios between the dam and protection materials (K_{dEb}/K_{dE}) on the coefficient A or, in other words, the protection height (Figure 8).

Figure 8 shows the benefit of having a highly permeable material in the rockfill protection. So, as the ratio K_{dEb}/K_{dE} increases the coefficient A tends to one, which is a minimum value. Furthermore, the height of the protection exponentially increases as this ratio tends to zero. Therefore, in the practice, lower values of 5 should be avoided in a cost-effective solution.

5.3 *Experimental validation*

The abovementioned design procedure was experimentally validated through a blind test campaign. In such campaign, two different couples of both dam and protection materials were used. So,

Table 1. Main data of the validation tests.

	Test 12_35_10	Test 12_35_16	Test 35_45_25	Test 35_45_35
Dam material, E (D_{50} in mm)	M1 (12.6)	M1 (12.6)	M2 (35.0)	M2 (35.0)
Protection material, E_b (D_{50} in mm)	M2 (35.0)	M2 (35.0)	M3 (45.5)	M3 (45.5)
Dam height, H (cm)	100	100	100	100
Dam slope, N (NH:1V)	1.9	1.9	1.6	1.6
Design unit through-flow, q_d (m^2/s)	0.010	0.016	0.025	0.035
Unit through-flow causing the failure of the unprotected dam, q_r (m^2/s)	0.020	0.020	0.034	0.034
q_d/q_r	0.50	0.80	0.73	1.02

Table 2. Design values of the rockfill toe protections corresponding to the experimental validation.

	Test 12_35_10	Test 12_35_16	Test 35_45_25	Test 35_45_35
Berm length, B (cm)	14	14	18	18
Rockfill toe slope N_b (NH:1V)	2.9	2.9	2.8	2.8
Rockfill toe height, H_b (cm)	28	40	47	59

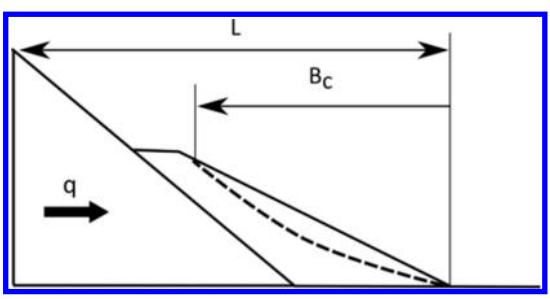

Figure 9. Scheme of measurement of the maximum advance of the breakage (Bc).

homogeneous gravels of sizes (D_{50}) 12.6 mm (M1), 35.0 mm (M2) and 45 mm (M3) were combined to design four cases of rockfill toe protection (Table 1). The tests were posed in advance such that each protection was designed following the proposed methodology. After each protection was dimensioned (Table 2), such case was tested in the laboratory so as to be compared with the theoretical behavior and, accordingly, validate or refute the methodology.

The scope of the validation tests was limited to mass stability. Therefore, even though the damages caused by erosion or dragging were registered, they weren't considered in the analysis of the protection stability. To do so, the research established criteria to distinguish between the mechanisms of failure, either mass slide or particle dragging. This analysis turns especially difficult for unit flows near to the threshold unit-flow when particle dragging initiates.

The effect of the protection was registered through the value of the maximum advance of the breakage (B_c), measured from the downstream toe of the rockfill material. This value was dimensionless expressed by the relation B_c/L, being L the horizontal length between the toe and the crest of the protected dam (Figure 9).

Results of the experimental validation are shown in Figure 10. These graphs represent the *failure paths* (Toledo et al., 2008) of each unprotected dam, as well as the dam with rockfill protections.

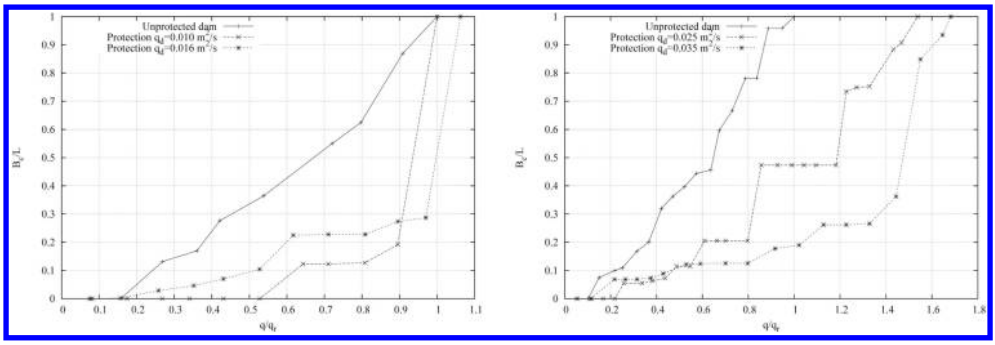

Figure 10. Failure paths obtained from of the validation tests. Left: Cases 12_35_10 and 12_35_16. Right: Tests 35_45_25 and 35_45_35.

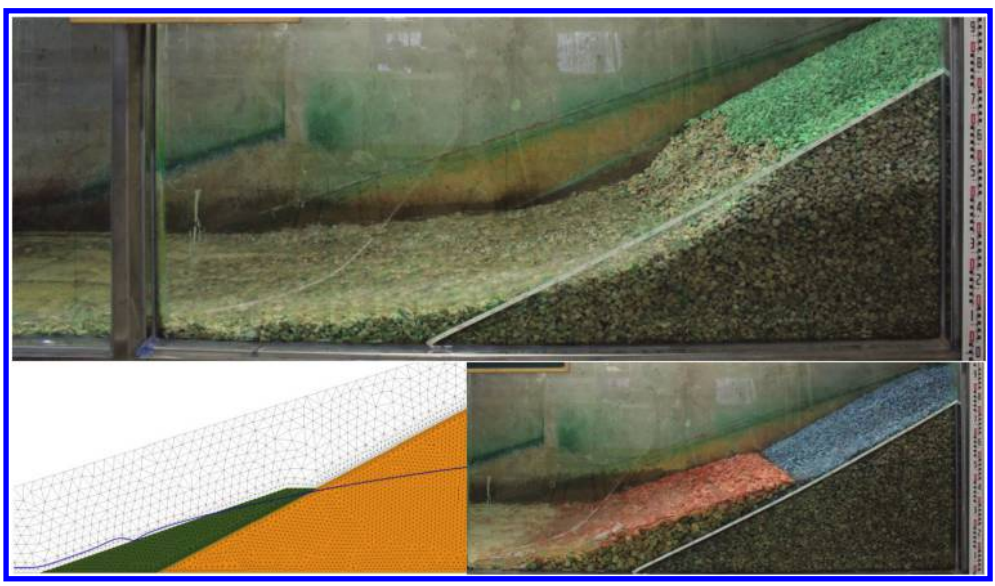

Figure 11. Validation test 12_35_16. Top: Picture showing the damage in the dam without any protection. Bottom-left: numerical model of the through-flow with the proposed protection. Bottom-right: picture of the result of the laboratory blind test (Morán, 2013).

In abscises, unit through flow (q) is represented as a dimensionless parameter referred to the very unit flow which causes the total failure of the unprotected dam (q_r). To do so, the values of q_r were previously obtained through failure tests of the unprotected dams with both materials, M1 and M2.

The results of the validation tests were successful due to, in every case, the posed protection achieved the stability for each design unit-flow (Figure 11). Furthermore, the damages observed for higher unit-flows were caused mainly by dragging of particles and the conclusions of the tests indicated that the effect of the protection remained even for higher unit-flows. In such a way, it was concluded that a promising research line could be focused on a possible adding of external rockfill layers with specific sizing to avoid particle dragging for higher unit flows. This complement could increase the protection levels significantly, with a very low extra cost, as it was noted on the tests where the effect of the dragging of particles was reduced.

6 CONCLUSIONS

The review of the embankment dam protections shows there is a big challenge to achieve in the next future. Even though the technology of protections is still immature, the possibility of increasing the safety of this type of dams with reasonable costs looks like realistic. To do so, additional comprehensive research is needed. These studies should be focused not solely on the particular protection technology but also on the installation procedures and constructive guidelines.

A design methodology for rockfill toe protections has been presented to ensure the mass slide stability of rockfill dams against overtopping and extreme internal leakage. Furthermore, a future research line focused on external reinforcement against particle dragging has been proposed.

ACKNOWLEDGEMENTS

The research on rockfill toe protections was developed with funds from the Spanish National Research and Development Program (2008–2011) with the research project title: "*Rotura del elemento impermeablede presas de materiales sueltos en situacion de sobrevertido y analisis de protecciones combinando modelacion fisica e inteligencia artificial*", with ID code BIA2010-21350-C03-03. The authors also gratefully acknowledge the personal help of Dr. Eugenio Oñate, Dr. Antonia Larese, Dr. Ricardo Rossi, Mr. Fernando Salazar, Mr. Hibber Campos, Mr. Ricardo Alves, Mr. William Fiedler, Mr. Thomas Hepler, Mr. Peter Viklander and Mrs. Kathleen Frizell.

REFERENCES

Álvarez, A., Montoya, F. F., & Toledo, M. A. (1998). Innovaciones en aliviaderos de presas de materiales sueltos. Revista De Obras Públicas, 3378(Julio-Agosto), 19–24.

Bieberstein, J., Quieber, J., & Wörsching, H. (2004). Open stone asphalt. A revetment for dams and embankments designed for overtopping. Oslo, Noruega.

Bizcarrondo, M. A., & Gómez, G. (1970). Presa de escollera con aliviaderos por coronación. Revista De Obras Públicas, 117(Tomo I (3061)), 573–577.

Cox, A., Thornton, C., & Abt, S. (2014). Articulated concrete block stability assessment for embankment-overtopping conditions. Journal of Hydraulic Engineering, 140(5), 06014007. doi:10.1061/(ASCE)HY.1943-7900.0000844

EBL Kompetanse. (2005). Stability and breaching of embankment dams. report on subproject 2: Stability of downstream shell and dam toe during large through-flow. Oslo, Noruega: EBL Kompetanse AS.

FEMA. (2014). Technical manual: Overtopping protection for dams U.S. Department of Homeland Security.

Frizell, K. H., Ruff, J. F., & Mishra, S. (1998). Simplified design guidelines for riprap subjected to overtopping flow. Proceedings of the Annual Conference of the Assoc. of State Dam Safety Officials, 301–312.

Frizell, W. (2007). Uplift and crack flow resulting from high velocity discharges over open offset joints-laboratory studies (Reports DSO-07-07 ed.). Denver, USA: Bureau of Reclamation.

ICOLD. (1993). In Commission Internationale des Grands Barrages (Ed.), Bulletin 89. reinforced rockfill and reinforced fill for dams- state of the art-. Paris, Francia: International Comittee on Large Dams.

Larese, A., Rossi, R., Oñate, E., & Idelsohn, S. (2008). Safety analysis of rockfill dams during overspill phenomena. Proceedings of the 76th Annual Meeting of ICOLD. Sofia, Bulgaria.

Larese, A., Rossi, R., Oñate, E., & Toledo, M. A. (2010). Metodología de análisis de comportamiento de presas de escollera frente a un sobrevertido. Proceedings of the IX Jornadas Españolas De Presas. Valladolid.

Larese, A., Rossi, R., & Oñate, E. (2011). Coupling eulerian and lagrangian models to simulate seepage and evolution of failure in prototype rockfill dams. Proceedings of XI ICOLD Benchmark Workshop on Numerical Analysis of Dams, Valencia, España.

Larese, A., Rossi, R., Oñate, E., & Idelsohn, S. (2012). A coupled PFEM–Eulerian approach for the solution of porous FSI problems. Computational Mechanics, 1–15. doi:10.1007/s00466-012-0768-9

Larese, A., Rossi, R., Oñate, E., & Toledo, M. A. (2011). Physical and numerical modelization of the behavior of rockfi ll dams during overtopping scenarios. Proceedings of XI ICOLD Benchmark Workshop on Numerical Analysis of Dams.

Lia, L., Vartdal, E., Skoglund, M., & Campos, H. (2013). Rip rap protection of downstream slopes of rock fill dams-A measure to increase safety in an unpredictable future climate. 9th ICOLD European Club Symposium, Venice, Italy.

Mishra, S. K. (1998). Riprap design for overtopped embankments (Ph.D.). (9922015).

MOPTMA. (1996). In Centro de Publicaciones Secretaría General Técnica MOP, Transportes y Medio Ambiente. (Ed.), Reglamento técnico sobre seguridad de presas y embalses. Madrid: Centro de Publicaciones Secretaría General Técnica MOP, Transportes y Medio Ambiente.

Morán, R. (2013). Improvement of the safety of rockfill dams during through-flow processes using downstream rockfill toes.

Morán, R., Campos, H., García, J., & Toledo, M. A. (2011). Estudio de protecciones frente al sobrevertido de presas de materiales sueltos mediante repié de escollera. Dam maintenance & rehabilitation II. (). Zaragoza, España: CRC Press. Taylor & Francis Group. Balkema 2010.

Morán, R., & Toledo, M. A. (2009). Protección de presas de materiales sueltos frente al sobrevertido mediante repié de escollera. Actividad Experimental De I+D+ i En Ingeniería Hidráulica En España. Seminarios 2009. 120–121.

Morán, R., Toledo, M. A., Sevilla, J. L., & García, J. (2008). Aliviadero con bloques en forma de cuña sobre la presa de barriga (burgos). VIII Jornadas Españolas De Presas (Córdoba).

Morán, R., & Toledo, M. A. (2011). Research into protection of rockfill dams from overtopping using rockfill downstream toes. Canadian Journal of Civil Engineering, 38(12), 1314–1326. doi:10.1139/l11–091

Nilsson, A. (2009). Maximal credible leakage for large rockfill dams due to internal erosion. International Workshop on Internal Erosion in Dams and Foundations.

Nilsson, Å. (2004). RIDAS tillämpningsvägledning – fyllningsdammar. utvikling av tillämpningsvägledning for fyllingsdammer i sverige. Proceedings of the NNCOLD Fagseminar, Bergen, Noruega.

Nilsson, Å, & Rönnqvist, H. (2004). Measures to strengthening embankment dams in order to stop or control a possible through-flow process. International Seminar. Stability and Breaching of Embankment Dams, Oslo, Noruega.

Parkin, A. K. (1971). Field solutions for turbulent seepage flow. Journal of the Soil Mechanics and Foundations Division, 97(1), 209–218.

Relvas, A. T., & Pinheiro, A. N. (2008). Inception point and air concentration in flows on stepped chutes lined with wedge-shaped concrete blocks.134(8), 1042–1051.

Robinson, K. M., Rice, C. E., & Kadavy, K. C. (1998). Design of rock chutes. Transactions of the ASAE, 41(3), 621–626.

SVENSK ENERGI. (2007). Ridas. directrices de seguridad de presas en suecia. RIDAS – Kraftföretagens Riktlinjer För Dammsäkerhet.

Taylor, E. H. (1991). The khasab self spillway embankment dams. Proceedings of ICOLD Viena Congress, Austria, Q67(R12), 225–239.

Thornton, C. I., & Robeson, M.D., Varyu, D.R. (2006). ArmorwedgeTM data report 2006 testing for armortec erosion control solutions, inc. Unpublished manuscript.

Toledo, M. A. (1997). Presas de escollera sometidas a sobrevertido. estudio del movimiento del agua a través de la escollera y de la estabilidad frente al deslizamiento en masa. tesis doctoral.

Toledo, M. A. (1998). Diseño de presas de escollera resistentes al sobrevertido. Madrid: Comité Nacional Español de Grandes Presas.

Toledo, M. A., Lechuga, C., & Oñate, E. (2008). Análisis del comportamiento de las presas de escollera ante un vertido por coronación. Proceedings of the XXIII Congreso Latinoamericano De Hidráulica, Cartagena de Indias, Colombia.

Toledo, M. A., Morán, R., & Campos, H. (2012). Modelación del movimiento del agua en medios porosos no lineales mediante un esquema de diferencias finitas. aplicación al sobrevertido en presas de escollera. Revista Internacional De Métodos Numéricos Para Cálculo Y Diseño En Ingeniería, 28(4) doi:10.1016/j.rimni.2012.02.002

Dam Protections against Overtopping and Accidental Leakage – Toledo, Morán & Oñate (Eds)

Flood overtopping protection for concrete dams

William R. Fiedler
Civil Engineer, Littleton, Colorado, USA

ABSTRACT: This paper identifies the potential vulnerabilities of concrete dams to flood overtopping and provides an overview of elements that can be used to protect concrete dams against failure during a large flood event.

Keywords: dam, protection, overtopping

1 INTRODUCTION

Concrete dams generally pose less concern regarding failure during an overtopping event than do embankment dams. The dam itself is typically considered non-erodible, and the foundation is generally erosion resistant as most concrete dams are founded on rock. Rock foundations can still be erodible; however, depending on the weathering and fracture profiles in the foundation and the spacing, orientation, opening, and continuity of joints and other discontinuities in the foundation rock. Until fairly recently, there was a reluctance to allow large embankment dams or concrete dams to overtop during a flood, even if it was during a very remote flood, such as the Probable Maximum Flood (PMF). Due to the high cost of preventing flood overtopping for all conceivable floods at a dam and considering the remote probability of floods that would initiate overtopping, in many cases decisions have been made to accept overtopping for remote flood events. In some cases, a mitigating action has been to provide overtopping protection, to reduce the chance of dam failure if overtopping occurs. The Federal Emergency Management Agency of the United States Government recently published a manual on overtopping protection of dams [1]. This paper summarizes some of the key information related to overtopping protection for concrete dams.

2 HISTORICAL PERSPECTIVE

There have been a number of instances where concrete dams have overtopped. Some case histories of concrete dams that overtopped during large floods are briefly described below.

2.1 *Sweetwater Dam—California: 1895*

On January 14, 1916 Sweetwater Dam overtopped for the second time in its history, following 6 days of rain. Another storm drenched the county on January 24 that same year, and the lake rose 0.9 m above the top of the dam, creating a huge waterfall as it spilled over the entire span of the dam. This overtopping initiated erosion of the upper abutments of the dam and created erosion channels around the ends of the dam. This created a torrent of water that rushed down the Sweetwater Valley, causing extensive damage [2].

2.2 *Secondary (Saddle) Dam of Sella Zerbino—Italy: 1935*

The Secondary Dam of Sella Zerbino is one of two dams that were completed in 1925 to form a reservoir on the Orba River, in South Piedmont, Italy, near Liguria. The main dam is a 47-m

high concrete gravity arch dam and the secondary dam was a 14-m high concrete gravity dam. The secondary dam was added late in the design process to close off a low spot in the reservoir rim, when it was decided to increase the capacity of the reservoir. The secondary dam was designed and constructed quickly, without any geologic investigations. The foundation for the secondary dam consisted of highly faulted and fractured schistose rock. A large storm occurred in the drainage basin above the reservoir on August 13, 1935. It was reported that 36 cm of rain fell in the Orba basin in less than 8 hours, equating to about a 1,000-year event. The inflow into the reservoir resulted in both dams being overtopped by about 1.8 m. The Secondary Dam of Sella Zerbino failed as a result of the overtopping, resulting in over 100 fatalities [3].

2.3 *Gibson Dam—Montana, USA: 1964*

Gibson Dam is a concrete arch dam constructed by the Bureau of Reclamation on the Sun River in the state of Montana. The dam was completed in 1929. In June 1964, a major flood developed in the area, producing 30-hour rainfall amounts from 20 to 41 cm. Gibson Dam was overtopped for a duration of 20 hours, with a maximum overtopping depth of 1.0 m. The operators had left two of the spillway gates completely open, two partially open, and two completely closed. The access road was inundated by the overtopping flows, and personnel could not get to the spillway gate controls to operate them. However, even if all gates had been fully open, the dam would have overtopped. The dam survived the overtopping, with some erosional damage to the limestone abutments [4].

3 FAILURE MECHANISMS (POTENTIAL FAILURE MODES)

Overtopping of concrete dams can lead to dam failure and an uncontrolled release of the reservoir through a number of mechanisms. Typical potential failure modes are described below. The specifics of a potential failure mode will depend on the site-specific characteristics of the dam and foundation. It is important to consider potential failure modes when evaluating a concrete dam for overtopping flows. This will help to determine if overtopping protection measures are needed to reduce the probability of dam failure. If it is determined that overtopping protection is needed, the consideration of potential failure modes can help focus the extent of required overtopping protection measures.

3.1 *Scour and undermining*

Rock foundations are generally more resistant to erosion than a soil foundation, but rock foundations can erode extensively, depending on the characteristics of the foundation rock mass, and erosion can lead to undermining and breach of the dam. Overtopping flows can create a scour hole at the downstream toe of the dam, which can lead to headcutting erosion which undermines the downstream portion of the dam. This can lead to either a sliding or overturning failure of dam monoliths.

3.2 *Scour and exposure of sliding planes of foundation blocks*

Dam failure can occur even if the dam is not undermined due to scour and headcutting. If a scour hole develops downstream of the dam, this may allow the sliding plane and side planes for a large foundation block to daylight (with the foundation material removed, the foundation block planes intersect the sides of the scour hole opening). This can initiate sliding of the foundation block which ultimately may lead to loss of foundation support and failure of the concrete dam.

See Figure 1 for a depiction of this potential failure mode.

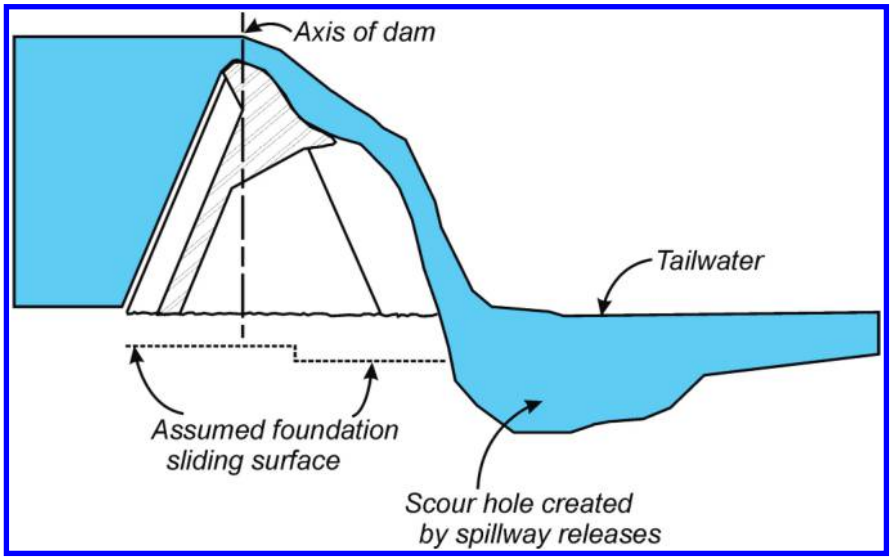

Figure 1. Scour downstream from concrete dam showing potential for daylighting of foundation discontinuities (Reclamation).

4 CONCRETE DAM TYPES

There are three main types of concrete dams: gravity dams, arch dams, and buttress dams. They have different geometries and different abilities to withstand erosion of the foundation downstream and underneath them:

- Gravity dams have a wide base and are massive structures. The crest of a gravity dam is usually straight. Undermining of the dam may have to be extensive to result in dam instability.
- Arch dams have a smaller footprint and can be more easily undermined, but they also have the ability to redistribute loads effectively in the arch and cantilever directions. The crest of an arch dam is curved to match the shape of the top of the arch.
- Buttress dams have a more limited footprint than gravity dams and can be vulnerable if localized erosion occurs at the location of a buttress. The crest of a buttress dam is usually straight.

Each of the three main types of concrete dams has unique stability considerations that can be affected by erosion of the dam foundation.

5 PREDICTING OVERTOPPING JET CHARACETERISTICS

In order to evaluate a concrete dam for overtopping flows or to design overtopping protection for a concrete dam, it is necessary to determine the characteristics of the overtopping jet, so that it's impact on the dam foudnation can be assessed. A first step is to determine the trajectory of the overtopping flows and estimate where the jet will impact on the dam foundation. The key parameters for determining the jet trajectory will be the velocity of flow over the dam crest and the angle of the flow as it leaves the dam crest. Equations for determining the jet trajectory are provided in the FEMA Overtopping Protection Manual [1]. Once the trajectory is determined, the thickness of the jet can be estimated (both of the inner core of the jet and the outer jet spread due to aeration of the flow). The thickness of the jet is a function of the initial depth of flow at the dam crest, the velocity of the jet as it leaves the dam crest, the height of the jet fall at the point of interest and the velocity of the jet at the point of interest. Equations for determining the thickness of the

jet are provided in the FEMA Overtopping Protection Manual [1]. Equations are also provided in the FEMA Overtopping Protection Manual [1] for calculating the spread and dissipation of the overtopping jet as it enters a plunge pool or the downstream tailwater. Figure 2 shows the trajectory of a jet from flows overopping a concrete arch dam. Figure 3 shows a plan view of the impact area of overtopping flows on the foundation for the same arch dam. These plots required calculating the trajecrory of the jet at a number of locations along the dam crest. As can be seen in Figure 3, as the height of the arch dam increases near the center of the dam, the jet impacts at a location further downstream from the downstream edge of the dam crest. Figures 2 and 3 depict the conditions for a single overtopping flow. Ideally, overtopping should be evaluated for a range of overtopping flows, which will require evaluating the jet characteristics and impingement áreas for a number of overtopping flows.

6 ASSESSING POTENTIAL FOR DAMAGE FROM OVERTOPPING

Once the impact area of the overtopping flows has been identified, the potential for the energy from the overtopping flows to erode the dam foundation can be assessed. There are several methods that can be used to evaluate the potential for foundation erosion.

6.1 *Streampower – Erodibility Index method*

The characteristics of the foundation rock will have a major effect on whether or not erosion occurs, and if it does, the extent of the erosion. If the foundation rock is massive with widely spaced discontinuities, erosion will be difficult to iniate due the large foundation block size. If the foundation has closely spaced joints that form removable rock blocks, erosion may initiate easily and proceed rapidly. The characteristics of joints and other discontinuities in the dam foundation will also have an effect on the erodibility of the dam foundation. Joints that are open and oriented into the flow will allow wáter pressures to more easily develop on the surfaces of the foundation blocks.

The potential for rock erosion due to overtopping flows can be evaluated using the Streampower-Erodiblity Index method. This method compares the erosion resistance of the foundation rock to the streampower or energy in the overtopping flows. This method can be used to determine if erosion is likely to occur and also to estimate the vertical extent of the erosion, if it initiates. This information can be used to determine if overtopping protection is necessary and if so to what extent. Erosion from the impingement of overtopping flows on the foundation and from the surface flows that collect and travel down the abutments to the river channel should be considered.

The erodibility index is used to represent the erosion resistance of foundation rock. The rock properties are expressed as a function of the block size, K_b, the material strength or mass strength, M_s, the shear strength of joints, K_d, and the relative ground structure number, J_s and the product of these four parameters represents the erodibility index. Streampower is then calculated for the overtopping jet and also for surface flows that collect and travel down the abutments of the dam. The equations and detailed discussion of calculating the erodibility index and the streampower are provided in the FEMA Overtopping Protection Manual [1].

To predict the potential for foundation erosion, the erodibility index is plotted against the stream power on Figure 4. This figure represents an evaluation of the original data used to develop the streampower erodibility index relationship evaluated using logistic regression by Wibowo et al. [5]. The upper (blue line) represents a 99 percent chance of erosion initiating. The bottom orange line represents a 1 percent chance of erosion initiating, and the red line in the middle represents a 50 percent chance of erosion initiating. The green line just below the middle red line is the initial erosion threshold proposed by Annandale [6]. It can be seen that this represents about a 40 percent chance of erosion initiation based on the regression analysis. The likelihood of erosion initiation can be interpolated between these lines.

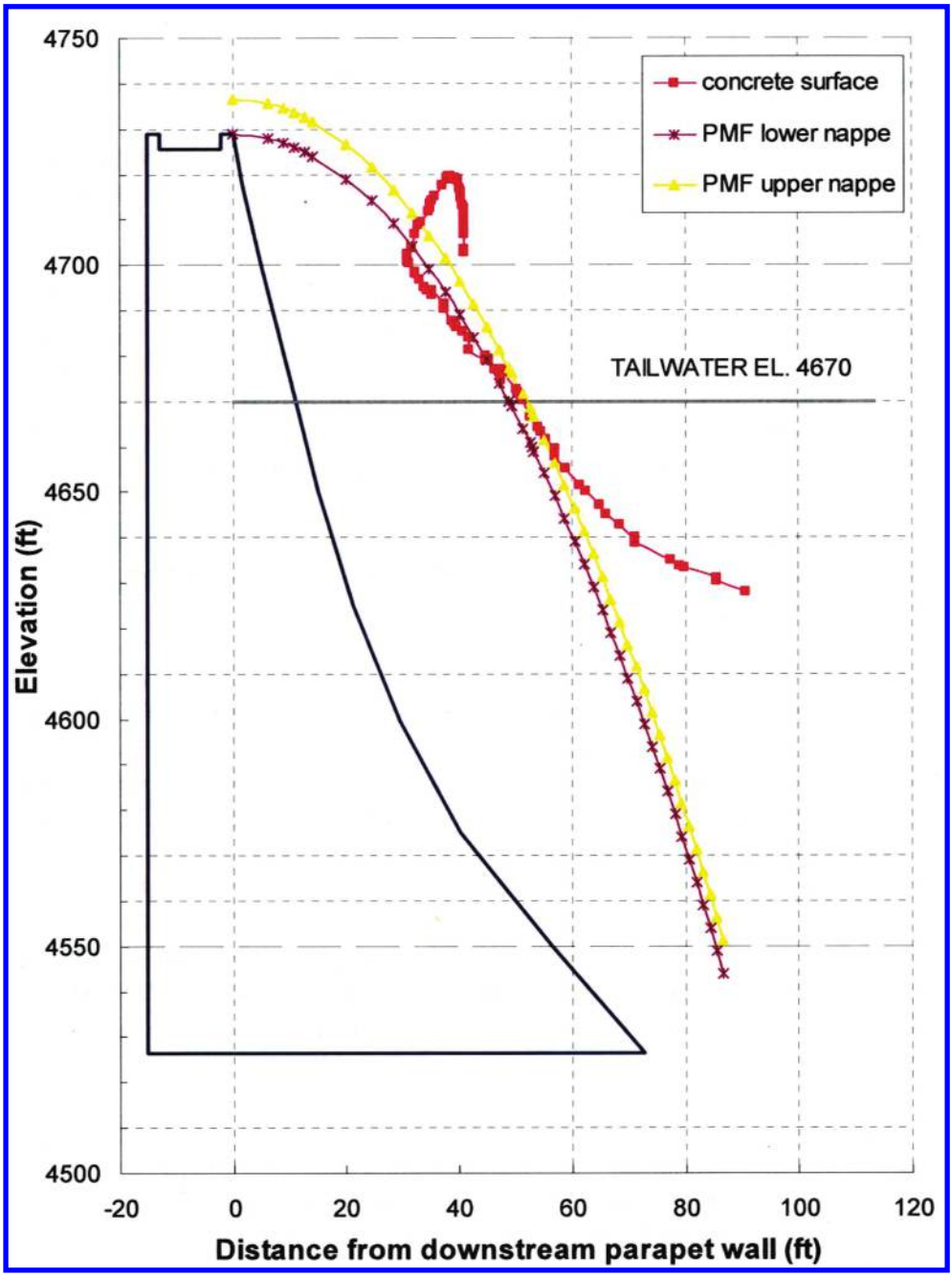

Figure 2. Sectional view of the final trajectory profile for the PMF though a dam section aligned with the river channel (the concrete surface line identifies the downstream edge of the concrete overtopping protection from the upper abutment of the dam down to the maximum section of the dam) [4].

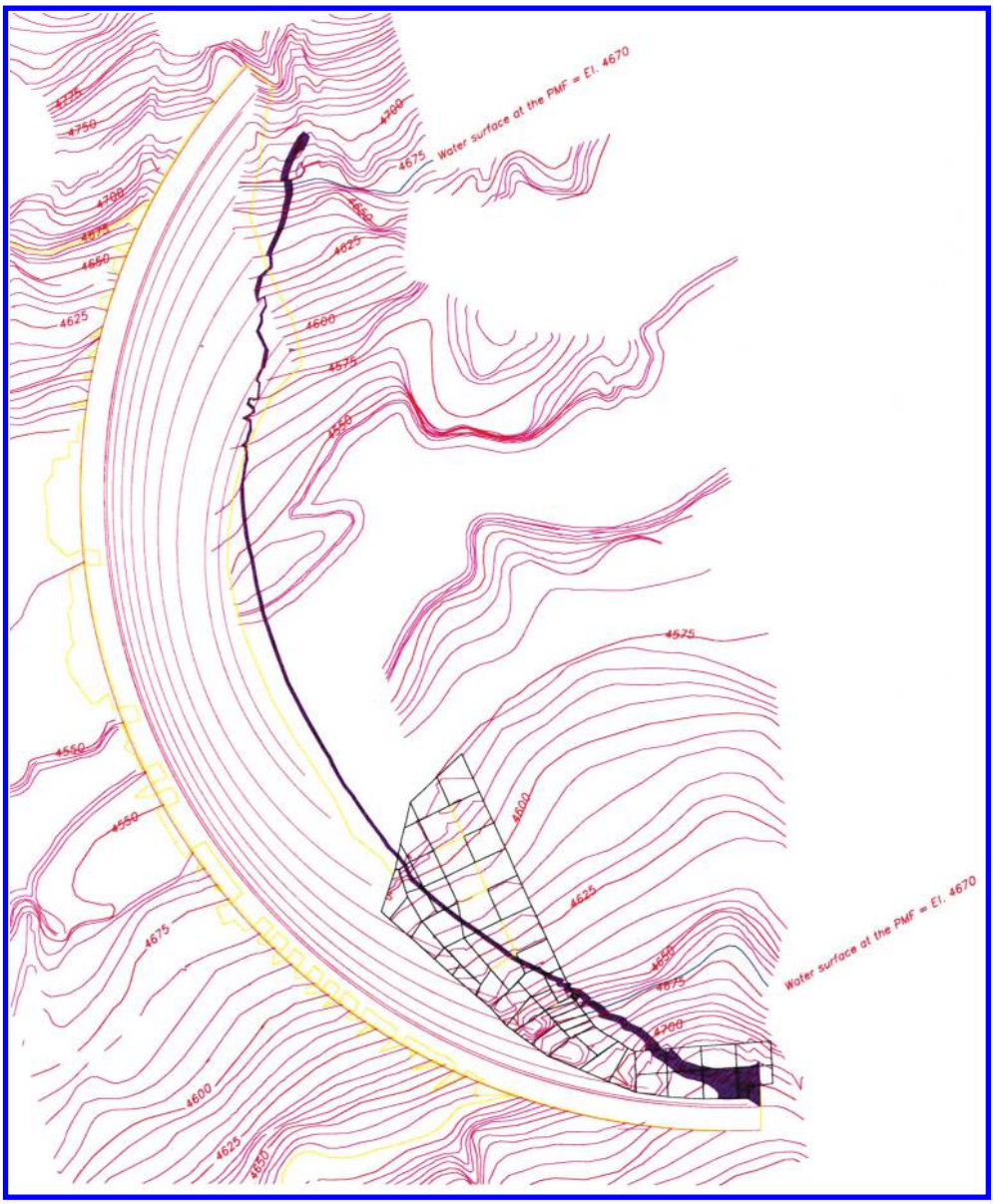

Figure 3. Footprint of the trajectory with no spread of the jet for the PMF overtopping. Note the location of the footprint extends beyond the right abutment protection between contour elevations 4660 and 4710. The tailwater for the PMF is shown on the plan view in blue at elevation 4670 [4].

If erosion is predicted, but the character of the rock or hydraulic characteristics change with depth, then an iterative procedure can be employed whereby the rock is assumed to erode to a certain depth, and then the stream power and erodibility index are recalculated for the new geometry and geologic conditions, and re-plotted on the empirical chart. Due to uncertainties in obtaining input parameters, it is often necessary to look at a range of conditions. In addition, a jet plunging from the crest of a concrete dam will have different stream power values depending on the height of the dam and the distance to the foundation at any given point.

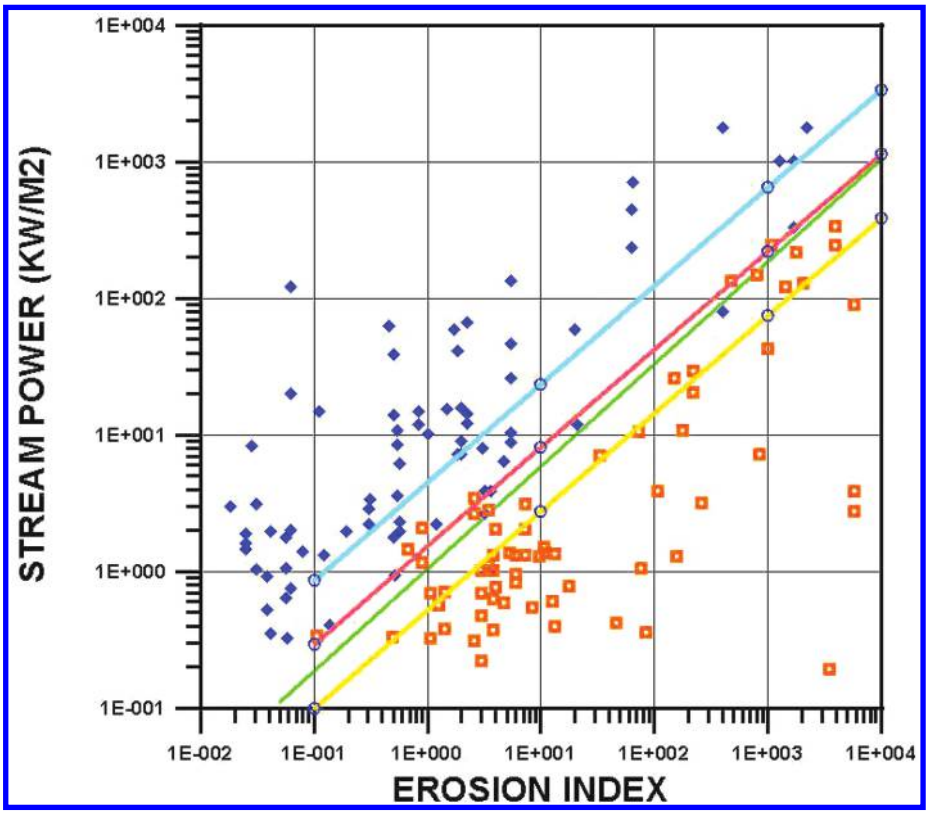

Figure 4. Probability that erosion will occur based upon the available stream power and the characteristics of the rock in terms of the erosion index. Probability of erosion by logistic regression for Annandale's regression line [5].

Some judgment is required when applying this method. The results can be sensitive to K_b, which is somewhat difficult to assess. In addition, materials will be more easily eroded on an abutment slope where there are more degrees of freedom for movement than in the bottom of a plunge pool where only the top of rock blocks are exposed. Cross jointing, if not present, can also increase the erosion resistance of the rock. These issues are not directly accounted for in this method. Unless there are very weak rocks, it takes at least three discontinuities to form a removable block. If removable foundation blocks do not exist, then erosion of the foundation becomes more difficult as fracturing of the rock will be required. A rigorous theorem for identifying removable blocks is given by Goodman and Shi [7].

6.2 *Alternative methods for scour from a plunging jet*

An alternative method that predicts scour from a plunging jet into a tailwater pool is the Comprehensive Scour Model (Bollaert and Schleiss [8] and [9] and Boellaert [10]). This model is more rigorous than the streampower-erodibility index method. The numerical model was developed to account for the physical-mechanical processes that lead to scour in rock channels exposed to a plunging jet. The comprehensive scour model predicts the fracturing along rock joints due to dynamic water pressures (which completes rock joint networks and allows for the formation of rock blocks) and also models the ejection of individual rock blocks due to uplift pressure. The comprehensive scour model predicts the ultimate scour depth and the scour progression with time in a jointed rock mass.

7 CONCRETE DAM OVERTOPPING PROTECTION

If it is determined that the potential for failure of a concrete dam is significant and that there is justification to pursue actions to mitigate this potential, there are a number of different types of overtopping protection that can be provided. Generally, overtopping protection for concrete dams must be very robust, since the systems must be capable of withstanding the impact of concentrated jets overtopping the dam that may have a significant fall height. Overtopping protection systems that will be discussed for concrete dams include:

- RCC overlays
- Conventional or mass concrete overlays
- Rock reinforcement
- Tailwater

7.1 *General design considerations*

Once it is decided that flood overtopping of a concrete dam must be mitigated, there are some general design considerations that will apply to any type of overtopping protection. These considerations are presented below.

7.1.1 *Current hydrologic loadings*

It is important to have current hydrologic loadings, including flood hydrographs for various return period floods. If outdated information is used, there is a chance that the overtopping protection will be underdesigned (possibly leading to failure of the dam for extreme events) or overdesigned (resulting in an overly costly design that is not efficient).

7.1.2 *Flood routing results*

Flood routings will be necessary to evaluate the depths and durations of dam overtopping during floods of interest. A range of return period floods, up to and including the design flood should be evaluated, since different floods will impact different portions of the dam foundation. The depth and duration of overtopping flows will help determine the level of protection needed. This information will be useful in assessing the potential for significant scour depths to develop and the potential for headcutting, once scour initiates.

7.1.3 *Trajectory of overtopping flows*

This will be needed to determine which portions of the foundation will be impacted directly from overtopping flows. Predictions of the flow paths, depths, and lateral extent will also be needed for the overtopping flows that collect along the downstream abutment and flow to the river channel. The extent of the direct impact flows and the surface flows will need to be defined to determine which foundation discontinuities and potential foundation blocks will be subjected to pressures and possible erosion from these flows. Splitter piers may be needed on the crest of the dam to aerate overtopping flows and prevent negative pressures from pulling the jet toward the dam, when the dam crest lengths are long. Estimating the hydraulic characteristics of an overtopping jet are discussed in more detail in Section 5 of this paper.

7.1.4 *Tailwater depths*

Tailwater depths will be important to determine for a range of overtopping flows. Tailwater will serve to dissipate the energy of overtopping flows and a determination of the depths and extent of tailwater will be needed to determine if and where overtopping protection may be needed.

7.1.5 *Hydraulic model studies*

Hydraulic model studies can be very useful in designing overtopping protection systems for concrete dams. The models can be either physical models or numerical models. The models have

the ability to capture three-dimensional effects which may be critical to successfully designing the overtopping protection. A two dimensional study will be able to predict the jet trajectory and impact area of overtopping flows at various locations along the dam axis, but the effect of flows impacting and then collecting and flowing down the downstream groin cannot be easily captured. A three dimensional model study will allow this behavior to be evaluated.

7.1.6 *Foundation erosion evaluation*

The Streampower-Erodibility Index method can be used to evaluate if erosion is likely to occur and also to estimate the vertical extent of the erosion, if it initiates. This information can be used to determine if overtopping protection is necessary and if so to what extent. Erosion from the impingement of overtopping flows on the foundation and from the surface flows that collect and travel down the abutments to the river channel should be considered. Methods of evaluating the potential for foundation erosion due to overtopping flows are discussed in more detail in Section 6 of this paper.

7.2 *Roller compacted concrete overtopping protection*

Potential concerns for overtopping of concrete or masonry dams generally involve blocky or erodible abutments or foundations, rather than concerns for the structure itself. In these cases, overtopping protection may be required for the exposed abutments and foundation within the impact zone of the overtopping flow, to prevent the loss of materials and undermining of the dam which could otherwise result in instability and failure. Alternatively, higher hydrostatic loads on concrete or masonry dams resulting from the passage of a flood event could produce lower factors of safety for sliding at a lift line within the body of the dam, at the dam-foundation contact, or along a potential slide plane within the foundation. The most common use of RCC for overtopping protection of a concrete or masonry dam is to provide a massive buttress for the structure to improve sliding stability. RCC may also be used to protect the dam foundation from erosion and headcutting from an impinging jet, but would not lend itself to the protection of steep abutments.

7.2.1 *Santa Cruz Dam modifications*

Santa Cruz Dam is a cyclopean concrete arch dam located about 40 km north of Santa Fe, New Mexico on the Santa Cruz River. The dam was completed in 1929 with a height of 46 m, a crest length of 152 m, and a radius of 91 m. The dam had safety concerns related to the maximum credible earthquake (MCE) and the PMF, and was experiencing severe concrete deterioration due to freeze-thaw. An RCC buttress was constructed on the downstream face of the dam to address the seismic concerns related to the MCE, and the entire dam crest was designed for overtopping to address the hydrologic concerns related to the PMF (see Figure 5). Completed in 1990, the Santa Cruz Dam modification was the first RCC project to use an air-entraining admixture to improve freeze-thaw durability. Details of this modification can be found in Metcalf et al. [11].

7.3 *Conventional or mass concrete overtopping protection*

Conventional or mass concrete can be used to provide overtopping protection in the form of concrete overlays that protect the underlying rock foundation at the downstream toe of the dam and along the downstream abutments. The overlays protect the rock from overtopping flows that could pluck rock blocks from the rock foundation or that could scour and remove material along shears or faults within the dam foundation. Splitter piers are often used in conjunction with concrete overlay overtopping protection to aerate the overtopping flow jet and prevent it from being pulled close to the toe of the dam (see Figure 6). Concrete overlays can protect the foundation from impinging flows or from overtopping flows that collect and flow down the groin of the dam to the river channel (see Figure 7). In addition to providing concrete overlays to protect the foundation, concrete walls are often constructed to contain overtopping flows and direct them to the downstream river channel. Concrete

Figure 5. Concrete overtopping protection for Santa Cruz Dam in New Mexico. Splitter piers were provided for overtopping of the entire dam crest (Reclamation).

overlays can be constructed of either conventional or mass concrete. Conventional concrete overlays are thinner (60 to 75 cm thick), are continuously reinforced to ensure structural integrity, generally have MSA of 4 cm or less, and typically have a 28-day compressive strength of at least 28 MPa. Mass concrete may not be reinforced (and if so, the reinforcement may only be temperature steel to control concrete cracking); maximum aggregate size may approach 15 cm or more; and thicker placements would typically be used (greater than 0.9 m). A typical mass concrete mix may have a design strength of 21 MPa at one year.

7.3.1 *Gibson Dam modifications*

Gibson Dam is a thick concrete arch dam on the North Fork of the Sun River near Augusta, Montana. Modifications to Gibson Dam were completed in 1981 to provide protection for overtopping flows that would result in up to 3.7 m of overtopping over the parapet walls on the dam crest. The overtopping protection consisted of groutable rock bolts to reinforce and stabilize jointed rock in the abutments and placement of concrete caps on both abutments. The overtopping protection on the right abutment was more extensive than on the left abutment, because the rock was judged to be more erodible on the right side. The reinforced concrete overlays had a minimum thickness of 0.8 m [4]. Figures 6 and 7 are of Gibson Dam.

7.4 *Foundation and abutment reinforcing overtopping protection*

Foundation and abutment reinforcing can be an effective means of stabilizing rock masses against overtopping flow. In many cases, this reinforcing will be most effective if combined with concrete overlays. Without overlays, the joints and discontinuities that form wedges in the rock mass will be subjected to potentially large dynamic pressures and impact loads from the overtopping flows.

Figure 6. Splitter piers designed to aerate overtopping flows (Reclamation).

7.4.1 *Gibson dam modifications*

Gibson Dam is a thick concrete arch dam on the North Fork of the Sun River near Augusta, Montana. Modifications to Gibson Dam were completed in 1981 to provide overtopping protection for overtopping flows that would result in up to 3.7 m of overtopping over the parapet walls on the dam crest. The overtopping protection consisted of groutable rock bolts to reinforce and stabilize jointed rock in the abutments and placement of concrete caps on both abutments. The overtopping protection on the right abutment was more extensive than on the left abutment, because the rock was judged to be more erodible on the right side. Rock bolt spacings and rock bolt lengths were not well documented, but Figure 8 indicates that the rock bolting was extensive. The rock on the left abutment of the dam was not judged to be erodible, except for two weaker beds. Pairs of anchor bars at 1.5-m spacings were provided on each side of the beds. The anchor bars extended 1.5 m into rock and were grouted in place [4].

7.5 *Tailwater effects related to overtopping protection*

Tailwater effects consider the hydraulics of a free-falling jet from concrete dam overtopping into a plunge pool of rock material. The jet will either impinge into the pool below the dam and disperse before impinging on the rock surface or it will not disperse. If the jet will disperse because of adequate tailwater pool depth, then no energy remains to erode the rock material on the sides or base of the pool. If not, then scour may occur, depending upon the rock materials. If scour is predicted and is determined by the designer to be unacceptable, a protective measure, such as a downstream weir may be constructed to artificially raise the tailwater pool depth and prevent scour at the toe of the dam.

Tailwater effects should be a consideration when evaluating a concrete dam for overtopping flows. Even without any special design measures in place, tailwater will help dissipate the energy of

Figure 7. Concrete overtopping protection at downstream toe of dam (Reclamation).

overtopping flows and may reduce the need for or eliminate the need for other forms of overtopping protection. The downstream dam foundation areas protected by tailwater will be limited, however. An additional limitation on the protection provided by tailwater is that tailwater levels can be reduced for a given discharge if downstream channel degradation occurs. If tailwater by itself is not effective in reducing the energy of overtopping flows, the designer must then determine an appropriate protective measure (e.g., adding a reinforced concrete liner to a previously unprotected rock plunge pool or adding a feature to the top of dam or release structure to break up the jet).

7.6 *Vulnerabilities*

Overtopping protection can improve the ability of a dam foundation to withstand overtopping flows but overtopping protection is not foolproof. The protection may not be effective in certain situations.

7.6.1 *Inadequate extent of protection*

To be cost effective, overtopping protection of dam foundations must be targeted to those areas of the foundation likely to experience erosive flows. If the overtopping protection is designed for a specific flood and a related depth of overtopping but a larger flood occurs, the impinging jet from overtopping flows may extend beyond the overtopping protection. It may also be the case that the erosive energy of overtopping flows increases substantially for larger events and that this

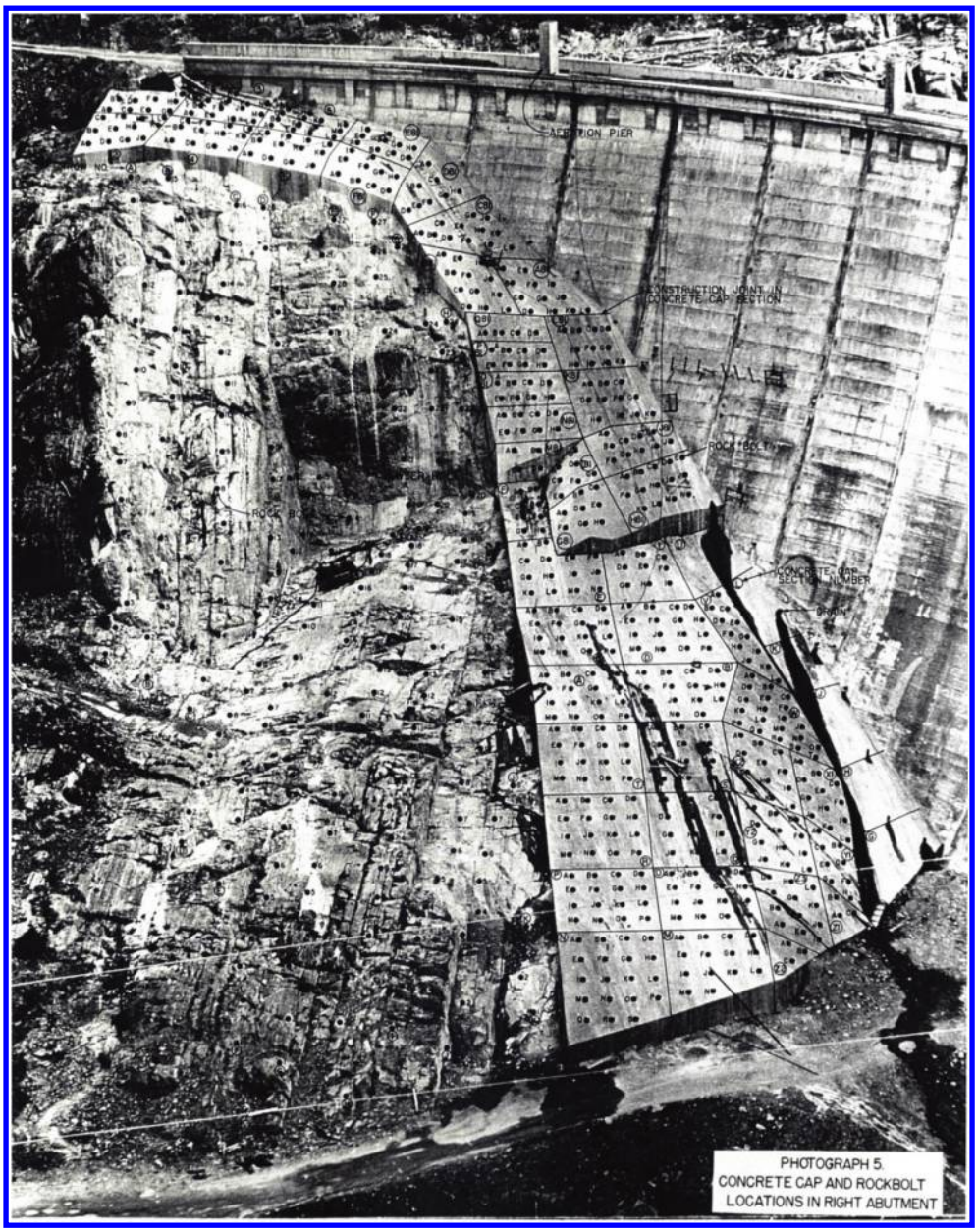

Figure 8. Rock bolt installation on downstream abutment as part of overtopping protection (Reclamation).

is sufficient to cause unacceptable erosion. When evaluating overtopping protection that is already in place, a determination of the design level of the protection should be made and an assessment of the adequacy of the protection for larger flood events should be considered. If a determination is made that the design flood level needs to be updated (possibly because of increased downstream populations and increased risk or if the original design flood has become more frequent due to updated hydrologic studies) and if it is concluded that the existing protection is inadequate for the new design level, an extension of the protection may need to be considered.

7.6.2 *Deterioration of overtopping protection or scheme*

Overtopping protection that is installed may deteriorate over time. If the overtopping protection consists of rock reinforcement, such as rock bolts or rock anchors, the reinforcing steel may corrode if adequate corrosion protection has not been provided. Even if corrosion is very localized, it has the potential to reduce the cross sectional area of the reinforcement and significantly reduce the capacity of the reinforcement. If the overtopping protection consists of concrete or RCC overlays on the dam foundation, the concrete may deteriorate due to alkali-aggregate reaction or freeze-thaw damage. If concrete or RCC overlays are damaged due to deterioration, the protection could fail during a flood overtopping event and expose the foundation to overtopping flows. If overtopping protection does exist at a dam, it is important to review the design considerations for the protection, to determine if it is still adequate. The physical condition of the overtopping protection should also be determined from an inspection and any observed deterioration should be considered when evaluating the design adequacy of the protection.

7.6.3 *Erosion downstream from overtopping protection*

Overtopping protection can be defeated if erosion occurs downstream from the protection and the protection is undermined due to headcutting. It is important to identify the areas of the foundation that will be exposed to erosive flows and determine if erosion of non-protected areas is likely. If there is the potential for erosion downstream from the protected areas, consideration should be given to extending the erosion protection.

7.6.4 *Exceeding design discharge*

If discharges occur that exceed the design discharge for the overtopping protection, the protection may be compromised. This could occur as a result of a change in the hydrologic hazard characterization, the result of plugged or otherwise inoperable spillways or simply from the occurrence of an extremely remote flood event.

7.6.5 *Loss of or miscalculated tailwater*

Tailwater should be a consideration in the design of concrete overlays as overtopping protection. The tailwater may limit the areas that require protection or may reduce the thickness and/or extent of the concrete overlays. If the tailwater depths that were assumed in the design do not develop (due to a change in downstream conditions or from a miscalculation in the tailwater study) the existing overtopping protection may be compromised for larger flows.

8 CONCLUSIONS

Several different types of overtopping protection systems have been considered or used for concrete dams. These systems are often used in combination, such overtopping protection for a concrete arch dam, where the upper abutments are reinforced with rock bolts, conventional concrete overlays are provided on the upper dam abutments in the areas where the overtopping jet will impact the dam foundation and tailwater is relied on in the center section of the dam to dissipate the energy of overtopping flows.

Overtopping protection for concrete dams differs from overtopping protection for embankment dams in that the areas typically protected for concrete dams focus on the foundation. Erosion of the dam itself is typically not a concern. Overtopping protection of the foundation should consider the effects of tailwater in dissipating the energy of overtopping flows and the characteristics of the foundation and the ability of the foundation to resist erosion from overtopping flows. It may be concluded that some areas of the foundation that are exposed to overtopping flows may be erosion resistant and that no protection is required in these areas.

As is the case for embankment dams, overtopping of a concrete dam should only be allowed for remote flood events. There will always be some uncertainty on the reliability of overtopping protection—and if overtopping protection fails, it is unlikely that intervention would be successful

if an overtopping event initiates erosion of the dam foundation. Limiting the overtopping of the dam to remote events will reduce the annualized failure probability for flood overtopping potential failure modes.

REFERENCES

[1] Federal Emergency Management Agency, *Technical Manual: Overtopping Protection for Dams, Best Practices for Design, Construction, Problem Identification and Evaluation, Inspection, Maintenance, Renovation, and Repair*, FEMA P-1015, US. Department of Homeland Security (May 2014).

[2] B. Hansen, Stemming the Flow: The Sweetwater Dam, *Civil Engineering Magazine*, (June 2007).

[3] www.molare.net.

[4] Bureau of Reclamation, *Hydraulic Investigations of the Erosion Potential of Flows Overtopping Gibson Dam. Hydraulic Laboratory Report HL-2006-02*, Technical Service Center Water Resources Research Laboratory (2006).

[5] J.L. Wibowo, D.E. Yule, and E. Villanueva, Earth and Rock Surface Spillway Erosion Risk Assessment, Proceedings, *40th U.S. Symposium on Rock Mechanics*, Anchorage Alaska (2005).

[6] G.W. Annandale, *Scour Technology—Mechanics and Engineering Practice*, McGraw-Hill Civil Engineering Series, First Edition, (2006).

[7] R.E. Goodman and G.H.Shi, *Block Theory and Its Application to Rock Engineering,* Prentice-Hall: Englewood Cliffs, New Jersey (1985).

[8] E.A. Bollaert and A. Schlesiss, Scour of rock due to the impact of plunging high velocity jets Part I: A State-of-the-Art Review, *International Association of Hydraulic Engineering and Research, Journal of Hydraulic Research*, Vol. 41, No. 5, pp. 451–464 (2003).

[9] E.A. Bollaert and A. Schlesiss, Scour of Rock due to the Impact of Plunging High Velocity Jets Part II: Experimental Results of Dynamic Pressures at Pool Bottoms and in One-And Two-Dimensional Closed End Rock Joints, *International Association of Hydraulic Engineering and Research, Journal of Hydraulic Research*, Vol. 41, No. 5, pp. 465–480 (2003).

[10] E.F.R. Bollaert, A Comprehensive Model to Evaluate Scour Formation in Plunge Pools, *International Journal of Hydropower & Dams*, pp. 94–101 (2004).

[11] M. Metcalf, T.P. Dolen, and P.A. Hendricks, Santa Cruz Dam Modification, *ASCE Third Conference on Roller Compacted Concrete* (February, 1992).

Failure of embankment dams due to overtopping or accidental leakage

Dam Protections against Overtopping and Accidental Leakage – Toledo, Morán & Oñate (Eds)
© 2015 Taylor & Francis Group, London, ISBN: 978-1-138-02808-1

Dam failures of embankment dams caused by overtopping or accidental leakage – New aspects for breach widening and deepening processes

A. Vogel
Risk Assessment International (RAI), Vienna, Austria

J.-R. Courivaud
EDF-Centre d'Ingénierie Hydraulique (CIH), Service Géotechnique et Ouvrages Souterrains, Savoie Technolac, Le Bourget du Lac Cédex, France

K. Jarecka
Risk Assessment International (RAI), Vienna, Austria

ABSTRACT: The study of embankment dam failures shows that the erodibility of soils constituting the embankments and their foundation plays a major role in the breach widening and deepening processes. Breach widening celerities deduced from several case studies are provided. Different approaches for modeling breach widening developed by the USDA/ARS/HERU laboratory are then presented. They are relevant approaches for engineering practice and they include a simple physically-based formula and a physically-based numerical model. These approaches all need to determine firstly the parameters of resistance to the soils to erosion with the Jet Erosion Test. The principles and limits of use of the Jet Erosion Test are described. Finally, recommendations to gather data in order to validate modeling of breach widening celerities are proposed.

Studies of failure modes of real-time cases of embankments which failed by overtopping or internal erosion show clearly the fact of different breach widening and deepening processes. Also breaches as consequences of failures of spillways in embankment dams show quite other dimensions as breaches caused by internal erosion. Also obviously is the impact of the kind of downstream protection and the material of the impervious core of an embankment in cases of overtopping and internal erosion.

Keywords: embankment, failure, overtopping, internal erosion

1 EMBANKMENT DAM FAILURES

In spring and in summer 2010 a series of devastating rain events hit Central Europa with extraordinary impacts to the countryside of the border region of Germany and Poland. The catchment area of the River Neisse, a border river between Poland and Germany, was particularly affected by heavy rains on 7 and 8 August. The rain triggered off extensive flooding of a magnitude that last occurred in the Neisse River catchment a century ago. At some gauge stations in this area the 100-year flood levels were exceeded [1].

The Niedow dam was an impervious earthfill embankment dam which was situated at the River Witka in Poland in a short distance before it flows into the River Neisse. The dam 16.7 m in height above lowest foundation level, 269.9 m of crest length and 5 m of thickness at the crest was constructed in 1962 and had a storage capacity of 4.8 Mm^3 [2]. The dam body consisted of sand and mixes of sand and gravel, the upstream shoulder was protected with two layers of reinforced concrete slabs and between the sealing element in form of a bitumen layer, the downstream shoulder was covered with grass (Fig. 1).

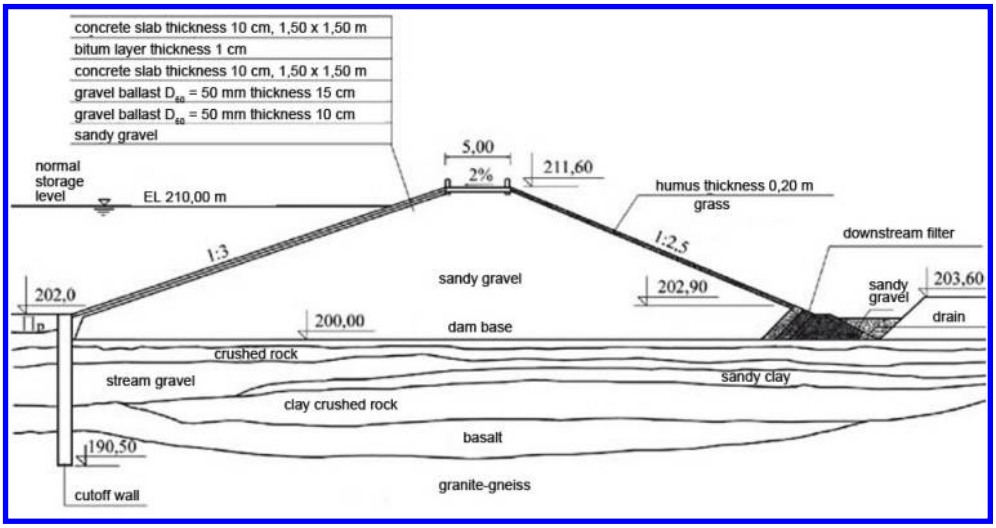

Figure 1. Cross section of Niedow Dam.

Figure 2. Niedow Dam before failure.

Figure 3. Niedow Dam after failure.

In the central part of the dam a 20.7 m long, 3 bay Craeger type concrete spillway section was situated where 3 tainter gates were implemented. Also included were a hydroelectric plant and a pumping station. The foundation at the dam site consisted of sand and loose or medium density sand and gravel mixes in the upper layers to a depths of 4 to 6 metres which were deposited on compacted gravel grounds with a large quantity of rocky scree (Fig. 2) [3].

On August 7, 2010 caused by heavy rains with an intensity never recorded at the rain gauge stations in the River Witka drainage area caused a disastrous flood wave with an extreme volume of 30 Mm^3 passed through the Niedow reservoir. The reservoir was completely filled at that time. The dam was overtopped and failed at 6:00 p.m. (Fig. 3).

Caused by the fact, that an installation for setting of limits for switching the tainter gates allowed the opening of the flood gates to a height of 250 cm only, the inflow significantly exceeded the capacity of the only partly opened gates. The dam was eroded in a very short time and the resultant dam breach wave with a height of 7 m flooded the villages between Bogatyna and Zgorzelec and Zgorcelec itself.

To the left of the spillway section, the dam body was completely eroded and destroyed, leaving only the cutoff wall made of reinforced concrete, embedded into soil down to the impervious ground

Figure 4. Remains of the right wing.

Figure 5. View of the completely eroded left wing.

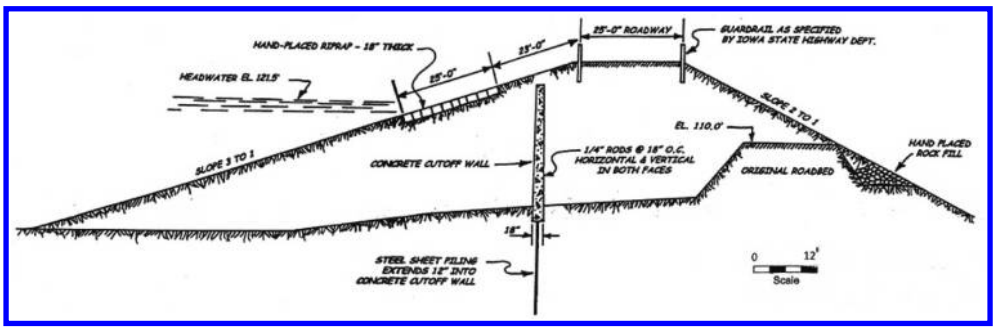

Figure 6. Cross section of Lake Delhi Dam.

layer. Due to a break in the left wing of the dam abutment, an outlet from the reservoir basin for a new river channel was formed along the lateral wall of the block. The new river channel, formed in the location of the former dam axis, had a width of about 28 m. The water flowing through this channel washed away fine-grained soils from the dam foundation down to the saprolite rock layer situated at a depth of four meters. To the right of the spillway block, a section of the embankment dam was preserved, with a length of about 21 m, adjacent to the concrete wings. Significant amounts of clay sediments were deposited upstream of the cutoff on the right bank of the reservoir. Just upstream of the destroyed dam, the depth of newly deposited soft and plastic or liquid sediments reached two meters (Fig. 4, 5).

On July 24th, 2010, after nearly 90 years of operation, the Lake Delhi Dam in Iowa in the USA was hit by a record inflow of water. It was severely overtopped and long dormant design deficiencies and unrepaired maintenance problems led to the destruction of the complete structure.

Lake Delhi Dam was designed as a concrete dam and earthen embankment. The 214.4 m long structure consisted of a 18.5 m long concrete reinforced earthfill section abutting the left limestone abutment, a 18.6 m long conventional reinforced concrete powerhouse, a 26.3 m long gated concrete ogee spillway, with three 7.6 m × 5.2 m vertical lift gates and, a 151 m long embankment section with a concrete core wall. The embankment section was originally constructed with 3:1 upstream slopes and 2:1 downstream slopes, and extended to the right abutment of the dam. The crest of the right embankment section of the dam was 7.6 m wide (Fig. 6).

The maximum section of the concrete portion of the dam has a height of about 18 m and the embankment section has an estimated maximum height of 13.1 m. The Lake Delhi reservoir formed by the dam had a storage volume of about 12.2 Mm^3. The hollow inside of the spillway crest structure was filled with rock.

Figure 7. Lake Delhi Dam before failure.

Figure 8. Lake Delhi Dam after failure.

The concrete reinforced earthfill section of the dam at the left abutment was originally constructed with two parallel concrete retaining walls, founded on rock and spaced 6.1 m apart. Rock fill was placed between the walls. In 1967, a concrete crib wall and additional fill was placed upstream of the original walls.

The spillway gates at Delhi Dam were difficult to open and close. A small crane was used previously to sometimes initiate opening of the gates. A jacking device was installed on the top of the gates to force the gates down to their fully closed position. A factor which also affected the release capacity through the spillway gates was also the potential for debris which plugged the spillway gates. Debris, in the form of woody vegetation, was reported to be a common occurrence at the spillway control structure. Boats on Lake Delhi became sometimes unanchored during previous floods and were passed through the spillway gates. The spillway was the primary waterway for passing flood flows at Delhi Dam. The wicket gates in the old power plant had a discharge capacity of about 14 m^3/s but this flow was relatively small compared to the spillway capacity. With all three gates fully opened at full storage, the estimated spillway capacity was about 906 m^3/s. During the destructive flood, one gate could not be opened more than 1.3 m, which caused a significant reduction of the spillway capacity.

Nothing out of the ordinary was observed related to the dam performance at the beginning of the July 22–24, 2010 flood, until the reservoir water surface exceeded the top of the core wall. Within about 8 hours of this occurrence, vortices in the reservoir and sinkholes on the upper portion of the upstream face of the dam were observed. The first vortex was noticed about 12 to 15 m south of the concrete structure at 3:30 a.m. on July 24. A second one was noticed later and was estimated to be about 30 m south of the concrete structure [4]. Seepage from the downstream slope was first observed around 6:00 a.m. around 12 to 15 m south of the spillway training wall. At the same time, settlement of the dam crest was observed in the areas where the vortices and sinkholes were first observed. Obviously internal erosion occurred in the portion of the embankment above the top of and downstream of the concrete core wall. At 9:00 a.m. dirty flow was observed at toe of downstream slope. At 9:40 a.m. the overtopping process of the dam began and it was observed that 5 cm water was flowing over the road. 20 minutes later a significant erosion of the downstream roadway shoulder began and at 12:00 p.m. heavy flow over the top and underneath the road was noticed. At 12:15 p.m. the roadbed collapsed. The dam breach began to accelerate around 12:30 p.m. The dam breach was initially caused by internal erosion of the embankment, then overtopping of the embankment and finally the structural failure of the thin concrete core wall (Fig. 7, 8).

The full breach of the embankment dam occurred at about 1:00 p.m. As the erosion of the embankment soils continued, some sections of the core wall also toppled (Fig. 9, 10). This effect increased the breach to a maximum width of 71.6 m. It was observed that the concrete core wall slowed down the speed of destruction at which the embankment dam breached.

Figure 9. Breach sequence with core wall still in place.

Figure 10. Breach gap with parts of the core wall.

Figure 11. Homogeneous embankment at the breach.

Figure 12. Foundation conditions at the breach.

The breach of the Gararda Dam in Bundi district of Rajasthan in India on August 15, 2010 led to flooding in at least 12 villages and caused substantial losses to the farmers of the area. It was an earth embankment with a height of 31.76 m, [5] a crest length of 4.271 km [6] and a storage capacity of 48 Mm^3. The enquiry committee report highlighted criminal negligence and corruption leading to substandard work as the main causes for the collapse [7]. The works on the dam were commenced in the years 2003–2004 and were completed in the years 2008–2009. The reservoir filling started on July 26, 2010, as very soon a portion of the dam breached on August 15, 2010 when the water in the reservoir reached a height of 14 m [6,8]. Although the dam was proposed and designed as a zoned earthfill dam, after the failure the breach gap showed clearly the fact, that it was constructed as a homogenous embankment dam, where CL and CI clay material was used (Fig. 11). The dam breached at the deepest point in the area of the former river bed where the foundation rock mass was badly fractured. Many wide, deep and continuous cracks were found, running from upstream to downstream both longitudinal and transverse which covered the whole area of the breach gap. No sealing works for these weak zones were done and the foundation cleanup was obviously also not executed in a proper manner before the earth works started (Fig. 12).

After the end of construction no arrangements were made for controlling the inflow rates during initial filling of the reservoir. The depth of water in the reservoir rose from 0 to 14 m over a period of just 20 days. The maximum rise in any day was of the order of 3.4 m. A day before the reported failure, the reservoir had recorded a rise of 1.8 m. Even at the time of failure, the reservoir was on rising trend. During the filling period a small pool located at about 30 m downstream appeared which was reported always filled to the brim. The water was used by the villages for meeting their water requirements for the many days prior to the dam failure. Some cracks were also reported to have been developed in the breached section prior to failure. At around 4:30 a.m. on August 15,

Figure 13. View of failed Gararda Dam.

Figure 14. Detailed view of breach gap.

Figure 15. Chaq Chaq Dam in May 2005.

Figure 16. Chaq Chaq Dam after failure.

2010 the dam failed on a length of 70 m at its deepest point, obviously by piping. The ruin is still existing (Fig. 13, 14).

On February 4, 2006 at about 10:00 p.m. Chaq-Chaq dam in Iraq failed due to overtopping. Chaq-Chaq dam was a 14.5 m high zoned earth dam with a central clay core and gravelly shell. Its crest width was 9 m, the upstream and downstream slopes had inclinations of 1:3 and 1:2 respectively and the storage volume was 1.4 Mm^3. A recognized design problem and one of the major mistakes was the implementation of the concrete spillway section beside the dam within the dam body and not as a separate structure (Fig. 15). The spillway wall was made vertical and as other similar dam failure cases showed, the compaction of the embankment near this vertical wall was less so that a weak bond at the interface of the wall and the embankment was implemented. In addition, the required compaction for the materials close to the vertical wall was not gained. Therefore this less-compacted portion was weaker compare to the other well-compacted portions of the dam.

The fall of 131.2 mm of rain over a 24-hour period was recorded at Sulaimani meteorological gauge station, which is located about 7.5 km south-east of the dam, which caused an increase of the stored volume to 2.55 Mm^3. As a result, the dam was overtopped. According to the responsible dam operator who was an eyewitness of the failure process, the dam started to erode as the water depth above the dam crest was 50 to 60 cm and finally breached near the spillway at the right abutment after 1 to 1.5 hours. The breach width at the bottom was 29.6 m, the breach top with was measured with 46 m [9]. The concrete spillway section remained after the failure, although the left vertical concrete wall was destroyed and the adjacent embankment was eroded (Fig. 16).

Quite the same circumstances led to the failure of Algodoes Dam which happened on May 27, 2009 in Brazil. Algodoes Dam was an earthfill dam 21.6 m in height and 840 m in length, with a storage volume of 51 Mm^3 which was struck by a flood which did not lead to an overflow of the crest. But caused by the fact that the spillway which was implemented at the right abutment of the dam was destructed after the erosion of the backfill behind the chute walls during the initial phase of the failure (Fig. 17), a 50 m long adjacent section of the embankment was destroyed and the full

Figure 17. Algodoes Dam just before failure.

Figure 18. Algodoes Dam after failure.

storage got lost (Fig. 18). Downstream at the Pirangi River the dam breach flood reached heights up to 5 m [10].

The dynamics of failure processes of embankment dams are obviously different for homogeneous earth dams and embankments which are equipped with central cores. Dams with massive cores made of concrete or steel withstood overtopping loadings for longer times but failed abruptly when the core tipped over after the erosion of downstream shoulders. Typical examples for this fact were the failures of Dells and Hatfield Dams on October 6, 1911 [11] or Lower Otay Dam on January 27, 1916 [12, 13].

Ketner Dam was a 13.7 m high earthfill structure with a concrete core wall and spillways at each end. Its crest length, exclusive of the spillways was 182 m and the width on the crest 4.8 m. The main spillway at the west end of the dam had a length of 21.6 m and was 1.5 m deep. At the east end an auxiliary spillway was installed, 10.7 m long and 1.1 m deep. The core-wall was constructed of concrete. It was 45 cm wide on top, while at the natural ground surface, and to a point within 1.2 m of the foundation, it was 3 m wide, at which point the footing was spread to 4.3 m. The initial work when the dam was constructed was the construction of the core-wall throughout its entire length, and to its final elevation, which was the same as the crest of the embankment. During this time the fill was being placed against the upstream side of this core-wall, but only little fill was deposited against the downstream side. As the core-wall was completed and the fill on the upstream side had been carried up to an elevation 4.6 m below the top of the core-wall, and little filling had been done on the lower side little rain started on the watershed on August 26 and 27. Two already installed outlet pipes, 76 cm in diameter were able to take over the runoff without filling the reservoir more than 2.5 to 3.0 m.

On the following day, August 28th, the rain was exceedingly heavy and a locally cloud-burst occurred, and by 11:00 a.m. the water level had risen behind the dam to a depth of 1.2 m above the outlet pipes. Then the water level remained at this elevation until 2:00 p.m., when it again started to rise slowly. The dam owner then put a force of men at work drilling holes through the core-wall, for the purpose of allowing the water to escape. These holes, 50 in number were drilled 1.5 m apart. By 8:00 or 9:00 p.m. in that night the core-wall was reported to have moved 1.2 to 1.5 m out of alignment of the crest, and drilling was stopped. The water was then within 2.4 m of the crest of the west spillway, and therefore about 0.6 m over the crest of the embankment which had been placed up until that time. Between 10:00 p.m. and 11:00 p.m. the water level increased to 1.2 m over the crest of the embankment, and at 11:00 p.m. the core-wall and the embankment failed abruptly. The core-wall was destroyed throughout almost its entire length, by overturning at a point near the filling line on its downstream side. The entire reservoir, containing approximately 0.3 Mm^3 was practically emptied at once. The breach formed through the dam was 122 m wide at the crest of the

Figure 19. Ketner Dam in the year 1912.

Figure 20. Ketner Dam core-wall today.

core-wall, and 11.6 m in height between the crest of the core-wall and the part of it which remained in place. The core-wall remaining at the west end was 51.8 m long on the crest, and 67 m at the base, and at the east end 4.9 m long on the crest, and 16.2 m long at the base.

Immediately after the failure, the dam was re-built, with however some slight modifications in the design and was put in service again in July 1912 (Fig. 19), [14].

In 1956 as the water of the reservoir was not any longer used for purposes of steam locomotives of a railway organisation owner, the dam was abandoned and the embankment and the core-wall was partly breached with dynamite. A small amount of water still remained behind the remains of the old dam. As in 1978, a boy who was fishing in that area drowned in an apparent attempt to save his dog, the County Commissioners then requested the owner to fully drain the water by removing a valve and demolishing the remainder of the dam. So only the concrete core-wall of Ketner Dam survived up to our times (Fig. 20).

2 BREACH DIMENSIONS – A LITERATURE REVIEW

In the Western World more than 1600 dam failure cases are reported and in addition with non published cases in China and Russia the number will increase to nearly 5000. Initial studies concerning breach parameters, i.e. width, depth, breach time, etc. dated back to the 1980s [15, 16, 17, 18, 19, 20, 21, 22, 23, 24, 25, 26, 27, 28, 29, 30]. A deep research study of experimental and numerical modeling of erosion of embankment dams by overtopping was undertaken in the 1990s and years 2000 by the Hydraulic Engineering Research Unit (HERU) of the Agricultural Research Service (ARS) of the US Department of Agriculture (USDA). This research effort led to a physical description of overtopping erosion processes [33], the development of a laboratory and field test enabling to characterize the erosion resistance of the soil materials (Jet Erosion Test, [31]) and a physically-based numerical modeling of embankment dams' erosion by overtopping (WINDAM B, [32]). This ARS research effort was then followed by a joint research project named "Erosion of Embankment Dams" coordinated by the CEATI Dam Safety Interest Group, where several dam owners and hydraulics laboratories (USBR, USACE, Hydro-Quebec, OPG, EDF, HR Wallingford, ARS/HERU) tested and validated several breach numerical models including WINDAM B [24].

2.1 *Variability of breach widening rates*

Embankment dam failure case studies highlight a large variability in the kinetics of breaching processes. Breach widening rates deduced from several embankment dam failures case studies presented in the table 1 below show that they can vary from 0.2 meter/minute to more than 10 meters/minute.

Table 1. Breach widening rates from several case studies.

Dam Name	Breach Widening Velocity (m/min)	Materials constituting the embankment
Oros	0.28 to 0.50	Central clay core. Satisfactory compaction and clay water content.
Glasshütte	0.52	loam, clay sand and gravels, compaction probably satistactory due to country and date of construction (East Germany, fifties)
Belci	0.94	central clay core, sand gravel filter, gravelly shoulders, reinforced concrete slab on upstream face
Noppikoski	1.11	central moraine core, sandy and gravelly shoulders
South Fork	3.2	center and downstream body made of stones, upstream part made of watertight earth and stones, heavy riprap on u/s and d/s slopes, leak compaction
Castlewood	2.75	earthfill and rockfill with masonry walls on u/s and d/s faces
El Guapo	2.17	central core, sandy gravel shoulders, riprap on d/s slope
Euclides da Cunha	3.33	homogeneous earthfill, riprap on u/s slope, grass on d/s slope
Salles de Oliveira	3.73 to 5.6	homogeneous earthfill with inclined and horizontal filter
Machhu 2	13.5	cohesion-less homogeneous fill, leak compaction

This table shows that breach widening rates in embankment materials that are resistant to erosion are in the range of 0.2 to 0.5 meter/minute while with poor resistant embankment materials, breach widening rates can reach more than 10 meter/minute.

The kinetics of embankment dams breaching process depends mainly on two characteristics: 1) the resistance to erosion of materials constituting the embankment and 2) the reservoir volume. Highly erodible embankment dam materials combined with large reservoirs will lead to the highest kinetics of the breaching process and the highest breach peak outflows. High erodibility of the embankment materials leads to a fast breach widening. In addition, a large reservoir volume leads to a slow lowering of the upstream water level when the breach is opening. Thus, a fast breach widening combined with a nearly constant head upstream leads to the largest breach peak outflows. On the contrary, very resistant embankment dam materials and small reservoirs will lead to the lowest kinetics of the breaching process and the lowest breach peak outflows.

2.2 *How determining erosion resistance characteristics?*

From the observations and the comprehension of physics provided by large laboratory tests, researchers of the USDA-ARS Hydraulic Laboratory in Stillwater, OK, USA, developed the Jet Erosion Test (JET). This test is an erodimeter which can be used either in the field or in a laboratory. This erodimeter reproduces at a small scale the erosion processes observed during overtopping erosion.

This test is normalized by the ASTM norm D5852 (2003). It consists in measuring in time the scouring of a soil under a vertical submerged impinging jet. The apparatus is principally constituted of an adjustable head tank, a jet tube, nozzle, point gage and a jet submergence tank (Fig. 21).

Measurements of the scour versus time are made by the operator by mean of the point gage which is in the axis of the impinging jet. The model of interpretation of the JET developed by the USDA-ARS Hydraulic Laboratory assumes that the erosion occurring during the test is principally due to the shear stress applied to the soil near the jet axis (Fig. 22). This model is based on the theory of an immerged jet impinging a plane surface.

The erosion rate ($\dot{\varepsilon}$, rate of the eroded volume of soil in $m \cdot s^{-1}$) is linked to the shear stress (τ) by the excess stress equation:

$$\dot{\varepsilon} = \begin{cases} 0 \;\; si\, \tau \le \tau_c \\ K_D(\tau - \tau_c) \;\; si\, \tau > \tau_c \end{cases} \quad (1)$$

Figure 21. Jet Erosion Test performed in situ (picture from USDA-ARS).

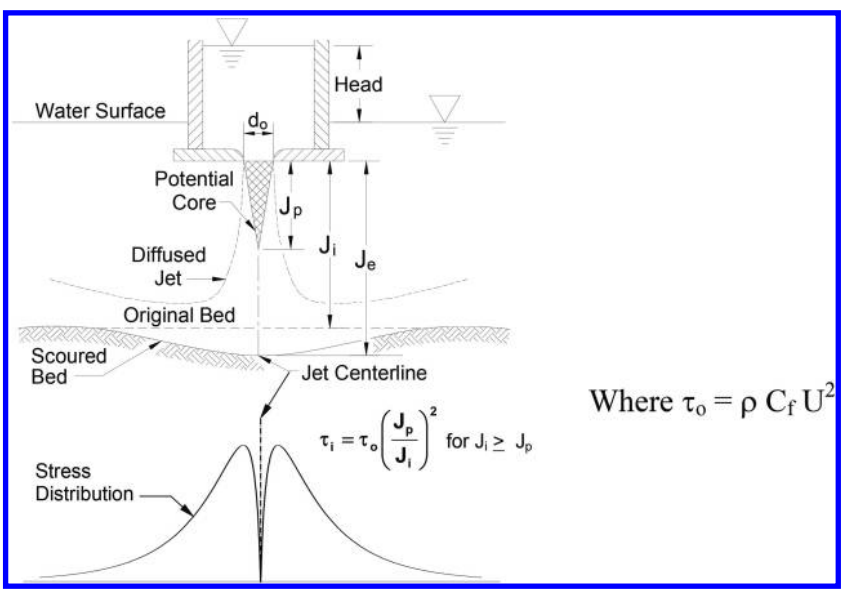

Figure 22. Principal of the Jet Erosion Test developed by USDA-ARS and stress distribution around the jet axis.

where
τ_c is the critical stress;
K_D is the erodibility coefficient.

The model of interpretation of the JET developed by the USDA-ARS Hydraulic Laboratory provides erodibility parameters K_D and τ_c.

The main limit of use of the JET is the maximum grain size of the tested material: 4.5 mm. Therefore, this test is well adapted for fine materials (clay, silts, fine sands) but it is not adapted for coarse materials.

2.3 *Breach widening modeling*

Two different approaches have been developed by the USDA-ARS Hydraulic Laboratory to model breach widening processes. Both approaches rely on the erosion resistance of the soil material constituting the embankment characterized by the erosion parameters provided by the Jet Erosion Test:

- the erosion coefficient K_D (m^3 N h^{-1}),
- the critical shear stress, τ_c (Pa).

The first approach is a simple analytical formula. It was proposed by Hunt in 2005 [34].

The breach widening velocity (dW/dt in meters per hour) is expressed as:

$$dW/dt = 2\ K_D\ (\tau_{ew} - \tau_c) \tag{2}$$

where

τ_{ew} is the hydraulic stress on the breach side walls.

$$\tau_{ew} = 0.7\ \gamma\ g\ ((d_c)^{1/3}\ n)^2 \tag{3}$$

with

γ: the water density,

g: the gravity acceleration,

d_c: the critical water depth in the breach, which can be estimated as 2/3 of the depth of water in the upstream reservoir,

n: the soil material porosity.

This simple expression of the breach widening velocity is very useful to get quickly a reliable order of magnitude when the erosion parameters of the soil constituting the embankment dam could be previously determined by the Jet Erosion Test.

A second approach consists in using the physically-based WINDAM B numerical model. This model provides a time varying evolution of the overtopping erosion process: breach dimensions and breach outflows through time. WINDAM B is a freeware which can be downloaded from the NRCS website: http://www.nrcs.usda.gov.

The main physical hypothesis and limits of use of this numerical model are the following:

- Erosion process by overtopping (piping process not modeled)
- Homogeneous embankment constituted of cohesive soils,
- Regular upstream and downstream slopes (no berms or change of slopes available),
- Foundation not modeled (no erosion of the foundation materials),
- Dam geometry represented by a unique 2D vertical section.

Input data include:

- Dam material characteristics, including erosion parameters,
- Evolution of the upstream water level through time,
- Upstream reservoir capacity curve (reservoir volume versus altitude).

Output data include:

- Breach outflow through time,
- Breach width through time,
- Upstream reservoir level through time.

Further developments still need to be done to meet the needs of the dam profession: similar modeling as WINDAM B for the piping process, taking into account coarse materials, zoned embankment as well as more complex slope geometries, and the erosion of the foundation. But right now, dam engineers can use validated numerical tools to model correctly the overtopping erosion process on homogeneous cohesive embankments.

2.4 *Some recommendations to collect field data to improve validation of breach widening rates modeling*

It is crucial to collect relevant data on new embankment dam failure case studies. Modeling tools designed to represent breach characteristics will always need improved validation using data from real case studies.

Feed-back on dam failure data collection shows that the main shortcomings concern information on times. Times are essential to assess outflows and breach widening rates. Times information is more difficult to gather than breach geometry information because it cannot be measured after the dam failure. Engineers in charge to gather dam failure data should pay a particular attention in searching times information in monitoring records and oral interviews.

REFERENCES

[1] L. Jelonek, L. Wrzeszcz, J. Zawislak, P. Walther, U. Winkler, S. Wortha, J. Srejber and J. Petr. *Gemeinsamer polnisch-deutsch-tschechischer Bericht zum Hochwasser vom 07. bis 10. August 2010 an der Lausitzer Neiße als Bestandteil der vorläufigen Risikobewertung gemäß Artikel 4 der Hochwasserrisikomanagementrichtlinie (2007/60/EG)*, WISE-RTD Water Knowledge Portal (2010).

[2] S. Kostecki and W. Rędowicz and J. Machajski, Wpływ stanu technicznego na katastrofę zapory zbiornika wodnego Niedów. *Przeglad Budowlany,* **83**, 96–99 (2012).

[3] B. Twaróg, Failure of Dam Niedów in Poland – Preliminary Analysis and Conclusions. *Flow-3D Users Conference* (2014).

[4] W. Fiedler, W. King and N. Schwanz, Report on Breach of Delhi Dam. *Independent Panel of Engineers* (2010).

[5] *National Register of Large Dams in India.* The Central Water Commission (2009).

[6] S.K. Sibal, B.R.K. Pillai and Y. Vijay, Safety perspective for dam construction – case study of Gararda Dam failure. *India Water Week 2012 – Water, Energy and Food Security: Call for Solutions* (2012).

[7] Gararda dam collapse in Rajasthan. *Dams, Rivers & People,* **8**, 7–8, 19 (2010).

[8] Breach in dam submerges 12 R'sthan villages, *The Tribune India,* Online edition, August 17 (2010).

[9] K.Z. Abdulrahman, Case Study of Chaq-Chaq Dam Failure: Parameter Estimation and Evaluation of Dam Breach Prediction Models. *International Journal of Engineering Research and Applications,* **4**, 109–116 (2014).

[10] A.W. Lauriano, Estudo de ruptura da barragem de funil: Comparacao entre os modelos FLDWAV e HEC-RAS. *PhD-Thesis, Universidade Federal de Minas Gerais* (2009).

[11] W.D. Pence, Failure of the Dells and Hatfield Dams and the Devastation of Black River Falls, Wis., Oct. 6, 1911. *Engineering News,* **66**, 482–489 (1911).

[12] C.W. Baker, Otay Rock-Fill Dam Failure. *Engineering News,* **75**, 236–239 (1916).

[13] California Floods Wreck Otay Rock-Fill Dam. *Engineering Record*, **73**, 225–228 (1916).

[14] Report of the Water Supply Commission of Pennsylvania, 56–59 (1912).

[15] K.P. Singh and A. Snorrason, Sensitivity of Outflow Peaks and Flood Stages to the Selection of Dam Breach Parameters and Simulation Models. *SWS Contract Report 288, Illinois Department of Energy*

and Natural Resources, State Water Survey Division, Surface Water Section at the University of Illinois (1982).
[16] K.P. Singh and A. Snorrason, Sensitivity of outflow peaks and flood stages to the selection of dam breach parameters and simulation models. *Journal of Hydrology*, **68**, 295–310 (1984).
[17] T.C. MacDonald and J. Langridge-Monopolis, Breaching characteristics of dam failures. *Journal of Hydraulic Engineering*, **110**, 567–586 (1984).
[18] D.C. Froehlich, D.C., Embankment-Dam Breach Parameters. *Proceedings of the ASCE National Conference on Hydraulic Engineering*, 570–575 (1987).
[19] V.P. Singh and P.D. Scarlatos, 1988, Analysis of Gradual Earth-Dam Failure. *Journal of Hydraulic Engineering*, **114**, 21–42 (1988).
[20] D.C. Froehlich, Embankment Dam Breach Parameters Revisited. *Proceedings of the 1st International Conference on Water Resources Engineering*, 887–891 (1995).
[21] D.C. Froehlich, Peak Outflow from Breached Embankment Dam. *Journal of Water Resources Planning and Management*, **121**, 90–97 (1995).
[22] T.L. Wahl, Prediction of embankment dam breach parameters – a literature review and needs assessment. *U.S. Bureau of Reclamation Dam Safety Report DSO-98-004* (1998).
[23] T.L. Wahl, Uncertainty of Predictions for Embankment Dam breach Parameters. *Journal of Hydraulic Engineering*, **130**, 389–397 (2004).
[24] J.-R. Courivaud, Analysis of the dam breaching database. *CEATI International, Dam Safety Interest Group, CEATI Report No. T032700-0207B*, (2007).
[25] T.L. Wahl, G.J. Hanson, J.-R. Courivaud, M.W. Morris, R. Kahawita, J.T. Mc Clenathan and D.M. Gee, Development of Next-Generation Embankment Dam Breach Models. *United States Society on Dams, 28th Annual USSD Conference*, 767–779 (2008).
[26] Y. Xu and L.M. Zhang, Breaching parameters for earth and rockfill dams. *Journal of Geotechnical and Geoenvironmental Engineering*, **135**, 1957–1970 (2009).
[27] T.L. Wahl, Evaluation of Erodibility-Based Embankment Dam Breach Equations. *Hydraulic Laboratory Report HL-2014-02, U.S. Department of the Interior, Bureau of Reclamation* (2014).
[28] G.J. Hanson, K.R. Cook, Procedure to Estimate Soil Erodibility for Water Management Purposes. *ASAE/CSAE International Meeting. Toronto, Ontario Canada. July 19–21, 1999. Paper for Presentation n° 992133* (1999).
[29] D.M. Temple, G.J. Hanson, M.L. Nielsen, WINDAM – Analysis of Overtopped Earth Embankment Dams. *ASABE Annual International Meeting. Portland, Oregon. 9–12 July 2006. Paper for Presentation n° 062105* (2006).
[30] G.J. Hanson, K.R. Cook, S.L. Hunt. Physical Modeling of Overtopping Erosion and Breach Formation of Cohesive Embankments. *Transactions of the ASAE*, **48**, 1783–1794 (2005).
[31] S.L. Hunt, G.J. Hanson, K.R. Cook, K.C. Kadavy. Breach Widening Observations from Earthen Embankment Tests. *Transactions of the ASAE*, **48**, 1115–1120 (2005).

Dam Protections against Overtopping and Accidental Leakage – Toledo, Morán & Oñate (Eds)

Failure of dams due to overtopping – A historical prospective

M. Jonathan Harris
Damwatch Engineering Ltd., Wellington, New Zealand

ABSTRACT: Historically, there has been a high rate of dam failures due to flood overtopping. Inadequate spillway capacity is a common problem with many dams. Failure of dams due to overtopping can lead to a high potential for loss of life and significant downstream damages. This paper provides a historical perspective of international dams that failed due to flood overtopping. Case histories of dams for select failures are also discussed along with lessons learned. Embankment dams have much higher risk of failure due to overtopping than concrete dams. However, concrete dams can be at risk if foundations consist of erodible materials.

Keywords: dam, overtopping, failures

1 INTRODUCTION

For thousands of years mankind has tried to tame the rivers of the earth. Structures built to contain water have experienced varied success throughout history. In the last hundred years dams have been built with increased levels of success. The intent of this paper is to review the history of dams that have failed due to flood overtopping. A general historical overview is given first, followed by case histories of significant dam failures. Case histories include general details, some interesting information and lessons learned.

2 DAM OVERTOPPING HISTORY – GENERAL

Historically, the number one cause of dam failure is flood overtopping. In recent times flood events have been the main natural hazard responsible for human and economic losses and continue to be one of the main reasons for dam failures [1].

A modern dam designer starts first with determining design flood flows for a structure, a practice that was not well understood until the mid-1900's. In the early 1900's design floods were considered for most large dam structures in the most-developed portions of the world. Since the mid-1900's, better tools have been developed to determine the size of floods, including the concept of a Probable Maximum Flood and the development of probabilistic methods for estimating flood frequency. These updated methods have been used to determine the adequacy of a given dam and its ability to retain and pass these flows.

Many dams that were designed with design floods even after the mid-1900's have been reanalyzed using newer techniques and have been shown to be significantly under designed for flood flows. For example, a given dam may have been designed to pass a flood with a recurrence interval of 1,000 years, but recent analysis may show it will only pass a 350 year flood. Owners of such dams must consider both design standards and potential impacts when determining if a structure is to be modified for larger flood flows. Some of these dams have been modified in recent years, especially where potential is high for loss of life and significant downstream damages.

3 HISTORICAL RATES OF FAILURE

ICOLD conducted a study in the 1970's and 1980's to summarize the rate of failure of dams. This database made the attempt to gather existing data and collect new data by requesting owners throughout the world to populate the database with all known failures. One finding of this study was that dams constructed prior to 1950 had a 2.2 percent rate of failure for all causes, and a 0.5 percent rate of failure for those constructed 1951 to 1986 [2].

The ICOLD study [2] showed that dam failure caused by overtopping was not the leading cause of failure of concrete dams, but that poor foundations was one of the leading causes of failures. The database showed dams that overtopped and had poor foundations were at a high risk of failure (the database showed these cases as caused by poor foundation).

The ICOLD study [2] showed that dam failures caused by overtopping was the single highest cause for failure of embankment dams. A more comprehensive study was undertaken by Fell et.al. [3] on the cause of failure of embankment dams in 1988. This study showed that overtopping failures accounted for 48 percent of all embankment dam failures with various types of internal erosion failures at 47 percent.

4 LESSONS LEARNED FROM DAM FAILURES DUE TO OVERTOPPING

Prior to the early-1900's techniques for determining design floods were not sophisticated enough to provide adequate levels of protection for large floods. In the mid part of the 1900's, better tools were developed to account for flood loadings and many dams have operated well since their design. Adequate storage and capacity to pass flood flows is critical to preventing overtopping failures.

This section will provide a few case studies and lessons learned from past failures. The purpose of these summaries is to focus on examples that have occurred since the mid-1970's. It is not the author's intent to provide a comprehensive list of dams that have overtopped and failed but rather to help emphasize common modes of dam failures due to overtopping and ones where clear lessons can be learned. However the first overtopping failure case history is from before 1900, and acts as one of the early dam failures that led to design change within the United States.

4.1 *South Fork Dam, United States – 1889 [4 & 5]*

The South Fork Dam was built between 1838 and 1853 on Little Conemaugh River 23 km upstream of the town of Johnstown, Pennsylvania. The dam was a homogeneous earthfill dam, 22 m high and 284 m long, with a severely undersized spillway. The dam was originally built to support a canal system for transportation routes, but was modified in 1881 after the canal system was no longer used.

When the dam was modified, it was done without thought to flood passage of the structure. Some of the modifications, such as lowering the dam crest to increase the crest width and installing screens above the spillway crest to prevent the loss of stocked fish from the reservoir, actually increased the risk of dam failure due to flood overtopping.

The city of Johnstown was a thriving town with 28,000 residents. The main source of employment was the large steel mill in town which employed between 4,000 and 6,000 workers. Many of the residents lived near the river, which created a relatively high population density.

In late May of 1889, a large storm dropped about 200 mm of rain in 24 hours over the region. Early during the morning of 28 May 1889 debris was reportedly trapped in the spillway and an attempt was made to remove this debris. An attempt to raise the dam and cut a new spillway was made as well. Two separate messages were sent to the City of Johnstown that the dam could collapse but these warnings were not given to the town authorities. Meanwhile, Johnstown was experiencing local flooding which trapped some local residents. In the afternoon of 28 May 1889 the inflow to the lake above the dam continued to increase rapidly and the dam failed due to overtopping and

Figure 1. Johnstown after South Fork Dam failure, 31 May 1889 (Photo Credit: Filson & Son, U.S. LC).

subsequent erosion of the dam embankment which released an estimated peak discharge of 12,000 cubic meters per second.

The sudden release of the lake collected debris of all kinds in its path. One structure that lay in the floods path was a stone railroad bridge that was 24 m high. Debris piled up behind the structure and it failed in less than 10 minutes releasing a new wave of water downstream toward the town and boroughs of Johnstown. The death toll was 2,209 people, which included 99 entire families and 396 children. Most of the town was completely destroyed and major damage occurred at the steel mill which lost a year and a half of production.

Lessons Learned as a result of this failure:

- Dam designers did not understand how to calculate design flood flows to determine adequate spillway capacity
- Dam owners modified the dam and spillway which increased the overtopping risk
- Warning was given but no emergency action was taken
- No emergency action plan
- Embankment dams have a high risk of failure due to overtopping

4.2 *Banqiao Dam, China – 1975 [6]*

Banqiao Dam was originally built in 1952 on the Ruhe River for flood control and power generation. In the late 1950's the dam was raised by about 3 m to a height of 24.5 m. The length of the dam was about 2,000 m. Some reports indicate that the dam was originally designed with 12 sluice gates but only 5 were constructed. The dam was reportedly constructed primarily of poorly compacted clay.

In August 1975, typhoon Nina collided with a cold front which caused 1060 mm of rain in 24 hours, more than the average yearly rainfall of 800 mm. The inflowing flood waters caused the dam to overtop by as much as 0.6 m and for about an hour and a half prior to breach.

One eyewitness report of the failure stated that a line of people were placed on the crest to place sandbags at the crest when the dam started to breach. The dam failed in the early hours of 8 August 1975. A total of 62 dams failed in the region as a result of the storm causing about 171,000 fatalities and destroying homes of 11 million people. Measures to warn downstream areas were attempted after the failure occurred and some areas were purposely flooded to minimize the impacts. The dam failure destroyed the massive power generation facilities and crop lands in the region.

Figure 2. Banqiao Dam failure (photo credit: unknown).

Lessons Learned as a result of this failure:

- Dam designers did not use international design flood standards and/or climatological records were inadequate to determine adequate dam storage and spillway capacity
- Dam owners modified the dam which increased the risk once overtopping occurred
- Warning was given after failure occurred rather than hours prior
- The failure of one structure can cause a catastrophic cascading effect and result in other dam failures and compounded damage
- Embankment dams constructed of clay are resistant to erosion but are still at risk of failure

4.3 *Machhu Dam II, India – 1979 [7]*

Construction of Machhu Dam II was completed in 1972. Considerable discussion occurred during the final approval stages because it was thought to not have enough spillway capacity. Instead of increasing the spillway capacity, the designers simply adjusted their calculations and showed that 20 percent greater capacity was available.

The dam was 25 m high and 3,905 m long and consisted of a central concrete gravity section with zoned earthfill embankments at both abutments. The dam was constructed using modern construction techniques and the embankments had a central clay core, transition zones and gravel upstream and downstream shells. The central concrete gravity section included masonry work on the exterior as well as 18 massive radial arm gates, two of which failed to open during the flood.

The largest cities downstream of the dam were Morbi and Maliya at a distance of 5 km and 25 km from the dam, respectively. Just downstream of the town, there were several smaller towns near the city of Morbi. Four months into the monsoon season, heavy rains fell for 12 days straight prior to the failure on 1 August 1979.

The dam operators had very detailed instructions for dam operations. Much of the operations relied on information on upstream flood inflows and rainfall forecasting. However, very poor communication prevented them from operating effectively. Just after midnight on 1 August 1979 the Deputy Engineer travelled to the dam to inform the operators to open the gates fully because communications lines were down. At 8:00 am a city official from downstream arrived at the dam to tell them to close the gates because their town was getting severely flooded. The operators did not close the gates but they wasted time having to deal with the request. It wasn't until noon that All-India Radio announced that "people were to move to higher ground," even though the dam

Figure 3. Machhu Dam II failure (photo credit: Gunvantbhai Sedani).

was close to overtopping and the request had been made hours earlier. The operator and crew were on the concrete gravity spillway section and had been trying to open the two gates that failed to open. At 1:30 pm, after the dam had overtopped for about an hour, the crew were afraid for their lives and tried to leave. They tried to cross the embankment but the dam was eroding away. They thought it safer to return to the concrete section. They walked a few hundred feet before returning. Within a few minutes of returning both the left and right embankment began to wash away. The dam overtopped for about 2 hours before breach at a maximum depth over the crest of 0.45 m.

The embankment sections washed away almost at the same time. The photo of the post-failure dam shows both embankments completely eroded away. The operator and crew watched the whole failure occur over the next few hours and all survived. However, over 2,000 of the downstream population lost their lives. Many of the fatalities could have been avoided if proper emergency plans and communication were in place and operable. It was determined that the flood was large enough that earlier operations of gates would not have stopped the dams from overtopping and failing due to the massive size of the flood.

The dam was reconstructed by 1993 with the new spillway capacity over 4 times larger than the previous design and the reservoir having one-third larger capacity.

Lessons Learned as a result of this failure:

- Dam designers did not use international design flood standards and/or climatological records were inadequate to determine adequate dam storage and spillway capacity
- Dam designers were under pressure to meet schedules for construction and when concerns over the design flood were raised they were not seriously considered
- During the flood there was no communication with the operations staff without traveling out to the site
- Required information regarding upstream river flows and flow predictions were not communicated to the operations staff
- Messages from nearby towns to close the spillway gates increased confusion during flood operations
- Embankment dams constructed of clay are resistant to erosion but are still at risk of failure

4.4 *Taum Sauk Upper Dam, United States – 2005 [8]*

Taum Sauk Upper Dam was constructed in 1960 to 1963. The dam is an off-stream storage dam with the reservoir filled at night when electricity is cheaper and used to generate power during the day when rates are higher. The dam was built on the top of a small mountain and consists of an embankment in a complete circle. The dam was constructed of material excavated from the mountain top, including silt sand and gravel mostly placed by sluicing. The upstream side of the embankment slope had pneumatically-placed concrete with steel reinforcement. The interior base of the reservoir consisted of asphaltic concrete. To increase the reservoir capacity a reinforced concrete parapet wall about 3 m high was constructed on the crest of the dam. There was no spillway installed because the largest storms would only result in a few cm increases in the reservoir level. All operations of the dam were remotely controlled.

On 14 December 2005 Taum Sauk Upper Dam failed. This was thought to be impossible due to it being an off-stream reservoir. A study conducted by the Federal Energy Regulatory Commission (FERC) of the United States provides detail of the causes of the failure. This report states that the reservoir was overfilled for up to 24 hours with a peak overtopping of about 0.15 m at the location of the main breach. The overtopping of the embankment eroded the embankment away and eventually failed the upstream concrete liner. Once the liner was undermined the dam breached completely in about 30 minutes. The cause of the overtopping was due to the fact that the dam was remotely operated and the water level sensors had come loose. The operators thought the dam was still not quite full when in fact it was overtopping.

The FERC report indicates that, "The breach was entirely avoidable in that the company knew for over two months that the water level sensors were unreliable, as they had broken free from their anchoring system, but unaccountably failed to make repairs." Since there was no spillway there was no way to handle even small flows overtopping the dam without incurring damage to the embankment.

It was extremely fortunate that no fatalities occurred as a result of the failure. Downstream of the dam is a remote area, but during summer months could have up to thousands of people using the recreational area. The home of the caretaker and his family (wife and three children) along with its residents were swept away in the flood. The family suffered injuries and exposure to the cold and were treated for hypothermia.

The dam was reconstructed from 2007 to 2010. The new design consisted of a Roller Compacted Concrete (RCC) dam in place of the embankment which is more resistant to erosion if overtopped. A spillway structure was also added to the design in case of overtopping.

Lessons Learned as a result of this failure:

- Dam designers did not think that overtopping was possible on this structure
- Little onsite observation was conducted at the site during operations – no regular onsite inspections conducted
- Water level sensors were never fixed to provide reliable operations information
- It is very fortunate that there were no fatalities

5 DAM FAILURE DURING CONSTRUCTION

Failures of dams have occurred during construction causing massive damages to construction works, downstream facilities and fatalities. These failures have occurred throughout the world. In many cases, these overtopping events "catch" the dam at the time it's most vulnerable, during construction. In the past, many dams have been designed without much thought to passing flood flows during construction.

One such dam that was under construction at the time of its failure was Oros Dam (Brazil) in 1960. In the second year of construction, the dam was about half finished, when the reservoir behind it rose about 29 m over a 9 day period due to flood flows. The dam was about 33 m tall at the time of the failure. The dam overtopped by as much as 0.8 m. The dam overtopped for about

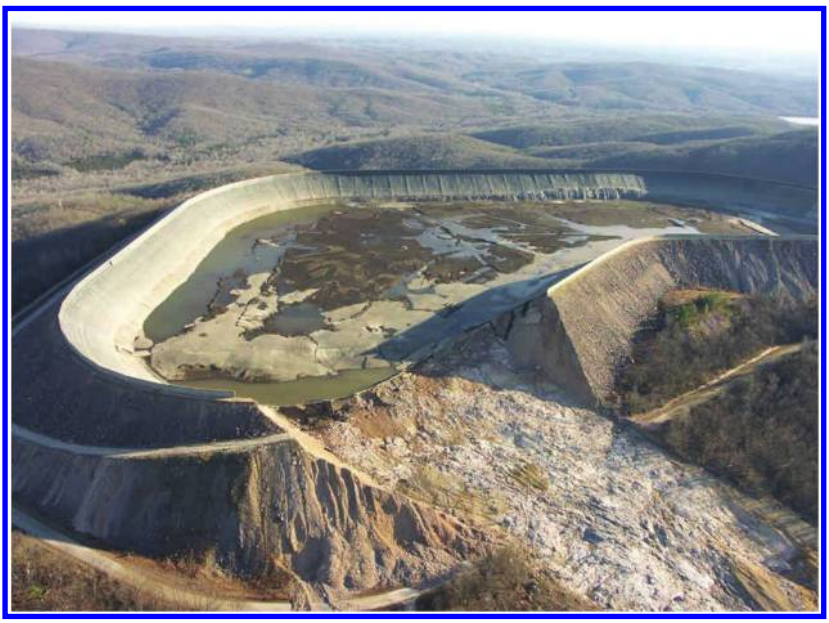

Figure 4. Taum Sauk Upper Dam failure (photo credit: FERC [8]).

8 and a half hours prior to breach with a majority of the overtopping depth much less than 0.8 m. The dam core was constructed of moderately plastic clayey sand and was densely compacted. As a result of the dam failure about 100 people died.

During the planning of the construction phase of work, the passage of flood flows should be considered. A design level for flood passage during construction should be established prior to the initiation of dam construction. In some parts of the world the risk of overtopping failure is very high during rainy seasons. Plans for how to pass these floods and how to stage construction are required to reduce the risk of potential failure.

6 OVERTOPPING PROTECTION OF DAMS

Many smaller dams and some larger dams are overtopped throughout the world every year. Many of these are dams designed with no proper understanding of design flood loadings. Some of these have been constructed in areas of very low population and as a result pose little risk to life loss. However, in some cases development can occur after the dam has been constructed, increasing the downstream population at risk.

As existing dams are assessed for their capacity to pass floods there are several options for design to protect them from failure. These options are discussed below.

6.1 *Concrete dam overtopping protection*

Concrete dams have historically shown to be more resistant to overtopping failure. Generally, this is due to being built of stronger materials that are less susceptible to erosion. Even though concrete dams are stronger they may not be stable due to the increased forces on the structure. Stability of a concrete dam should be assessed when larger design flood flows are calculated. This is in addition to evaluating the potential for foundation erosion should overtopping occur. Increased ability to pass the design flood should be the first option considered if plans are made for modification.

Historically, most concrete dams do not fail due to overtopping unless the foundation is weak. It is not difficult to envision water flowing over a dam not designed to be overtopped and a weak foundation slowly eroding away. In the case of Sweetwater Dam in Southern California (1916), it overtopped and minor damage was caused to the dam itself but the overtopping abutments eroded down and breached the dam. This was not the first time that this had happed to this structure. However, the previous event occurred during a smaller flood and erosion was much less. Consideration of abutment erosion should be considered in addition to erosion of the dam foundation.

6.2 *Embankment dam overtopping protection*

Embankment dams are historically shown to be susceptible to overtopping failure. Generally, this is due to being built of weaker materials that can be very susceptible to erosion. Since embankment dams are not designed to resist overtopping, the risk of failure is high compared to a similar dam made of concrete. Designers of embankment dams that are meeting deterministic design standards should realize that the conditional probabilities of dam failure given an overtopping flood event are typically not similar between concrete and embankment dams. Therefore, preventing overtopping or providing overtopping protection will typically be more critical for an embankment dam.

An increased ability to pass the design flood should be the first option considered and plans made for modifications. This is the highest level of risk reduction of the structure by removing the likelihood of water flowing down its face. Increasingly, engineers have been asked to develop ways to reduce the risk of overtopping failure of dams by construction of downstream facing or other means. These construction techniques vary from construction of RCC facing on the downstream face of the dam and abutments to unique systems for erosion protection. Each of these systems attempt to reduce risk of failure while reducing costs of construction compared to increased spillway and reservoir capacity.

6.3 *Reducing dam overtopping risk by reduction of operational failures [9]*

Operational failures have been known to cause dam overtopping and failure. Operational failures is part of a wide ranging category. The Bureau of Reclamation and U.S. Army Corps of Engineers Dam Safety Risk Analysis Best Practices Training Manual [9] states, “These can result from equipment, instrumentation, control systems (including both hardware and software), or processes failing to do what they were intended to do.” These types of failures can occur very easily and yet can result in spillway gates becoming inoperable during floods as one example. Another example is a log boom that is tied off at a low level so that during high reservoir levels during a flood trapped debris will be released and increase the risk of spillway blockage. Each facility should be evaluated to determine if there are high risks of operational failure during flooding. Many of these will lead to increased risk of overtopping failure even when the dam is properly designed to pass large floods. For some dams, the risk of overtopping during normal operations can be a viable failure scenario if there is a failure of operational equipment and systems like what occurred at Taum Sauk Upper Dam.

7 CONCLUSIONS

- A high percentage of embankment dams that have failed have failed due to flood overtopping
- Case studies show that inadequate ability to pass floods is the leading cause of overtopping failure, therefore, using internationally accepted design methods is critical to reducing the risk of overtopping failure
- Embankment dams are constructed of generally erodible materials, and given enough time, all types of embankment fill dams will fail due to overtopping
- Embankment dams should typically be designed for higher design floods to have the same risk reduction as an equivalent concrete dam

– Concrete dams are generally less susceptible to dam failure from flood overtopping, except when foundations and abutments consist of erodible materials
– Concrete dams are generally resistant to overtopping failures, but erosion of foundation and abutments should be checked along with increased loads on the dam due to higher reservoir levels
– Operational failures can cause a dam with adequate flood passage capacity to fail due to flood overtopping and should be evaluated comprehensively

REFERENCES

[1] ICOLD Bulletin 142, Bulletin on Safe Passage of Extreme Floods (2012).
[2] ICOLD Bulletin 99, *Dam Failure Statistical Analysis* (1995).
[3] M. A. Foster, R. Fell, and M. Spanngle. *Analysis of Embankment Dam Incidents*, The University of New South Wales, UNICIV Report No. R374 (1998).
[4] D. McCullough, *The Johnstown Flood*, Simon & Schuster (1968).
[5] W. F. Johnson, History of Johnstown Flood, Edgewood Publishing Co. (1889).
[6] Yi Si, "*The World's Most Catastrophic Dam Failures: The August 1975 Collapse of the Banqiao and Shimantan Dams*," within M.E. Sharpe, *Dai Qing, The River Dragon Has Come!*, New York (1998).
[7] T. Wooten and U. Sandesara, *No One Had a Tongue to Speak: The Untold Story of One of History's Deadliest Floods*, Prometheus Books (2011).
[8] A. J. Hedron Jr., J.L. Ehasz and K. Paul, FERC Independent Panel of Consultants, Taum Sauk Upper Dam Breach, FERC No. P-2277, Technical Reasons for the Breach of December 14, 2005, FERC (2006).
[9] Dam Safety Risk Analysis – Best Practices Training Manual, Bureau of Reclamation and US Corp of Engineers, April 2011 Version.

Dam Protections against Overtopping and Accidental Leakage – Toledo, Morán & Oñate (Eds)
© 2015 Taylor & Francis Group, London, ISBN: 978-1-138-02808-1

Overtopping and internal erosion on small dams in Burkina Faso

Adama Nombré
ICOLD, Burkina Faso

Eloi A. Somda & Moussa Kabore
IFEC Consulting Firm, Burkina Faso

Founémé Millogo
BCOD, Burkina Faso

ABSTRACT: Burkina Faso is a landlocked country located within the Niger River bend in the Sahel area of West Africa. The total population of the country is around 18 million inhabitants and the main activity is agriculture occupying 80% of the population. The country is located in a semi-arid zone of Africa. The rainfall season is between April and October in the South and June to September in the northern part of the country. Only three rivers are permanent, one with a long duration of very low flow during the year. The country is characterized by a high seasonal and inter-annual variation of rainfall and river flows. Water storage in Burkina Faso is a prerequisite for any human live and activity. Since the 1920's more than one thousand small dams and around 20 large dams have been built to store water (5.5 billion m^3 storage capacity) for multipurpose uses. Due to some weaknesses in the studies and construction and considering the impact of very large floods around 10 dams per year are experiencing overtopping or internal erosion leading to some cases of failures. The profession is trying to address the situation with the improvement of design criteria, construction techniques and the promotion of some low cost technologies to increase the resilience of these structures to resist to large floods.

The paper will present the recent developments in design criteria and low cost technologies.

Keywords: dams, internal erosion, failure, foundation, embankment, recent development, design criteria, low cost technologies

1 INTRODUCTION

The failure of dams by internal erosion and piping is one of the most common causes of dams' failure according Icold. It is the second cause of dams' failure after overtopping by floods.

In Burkina Faso, the assessments place the internal erosion in the third leading cause of failure of small earthfill dams after the flooding and backward erosion downstream lateral spillways channels.

Despite the apparent great experience of Burkina Faso in designing, building and managing small dams, structures failure still occur for various reasons including internal erosion. The dams' professionals are challenged to find solutions to ensure sustainability of these critical infrastructures for millions of peoples living in Rural or small urban areas. In 2007, we have noted the failure of about ten small dams including two by internal erosion in the embankment and in the foundation. These two cases are presented below after the presentation of the general approach of the phenomenon.

2 INTERNAL EROSION – TYPOLOGY AND DEVELOPMENT

2.1 *Typology of internal erosion*

The internal erosion can be defined as the phenomenon of tearing off and transport downstream of the particles of an embankment or foundation as a result of the action of the flow from the

reservoir or groundwater. It develops when the two following conditions are fulfilled: the tearing off of particles and their transport.

The detachment off of particles of the embankment can be done by several ways: backward erosion, blowout, buoyancy, dissolution or defloculation.

The transport can be done by filtration through a conduit created by the removal of particles which can quickly lead to the piping phenomenon and the failure of the dam if not stopped.

The transport can be done by suffusion (external or internal), diffusing in the space between particles and at the contact of the embankment with the foundation. The suffusion modifies slowly the permeability of the material and can, after a long period, lead to the failure of the dam.

For small dams, routine visual inspection made by a trained technician can usually detect internal erosion because of the changing of the permeability of the material and the changes in the leakages rates and the pore presure. The routine visual inspection can help to detect the following phenomenon which can be the signs of internal erosion:

- Emergence of moisture (seepage, development of vegetation, change in color of the water);
- Signs of erosion (materials deposits, suspended particles).

For large dams, in addition to visual inspection, there are many methods of investigations that can detect signs of internal erosion.

2.2 *Failure modes*

If internal erosion is not detected early and stopped, it can lead to the development of piping or suffusion and finally lead to the failure of the dam. So in internal erosion, failure occurs by piping or suffusion, piping is the most common and the most dangerous mode. On dams the piping phenomenon usually develops in the following situations:

- Missing or bad design or construction of downstream filter in the embankment or at the contact with the foundation;
- The presence of animals borrows: in Burkina, crocodiles are the animals that cause the most threat to the dams;
- The poor contact with the underground structures in the embankment: steel or concrete pipes;
- Leakage following the failure of an underground pipe;
- The poor compaction or lack of appropriate wetting of fines silty clay materials.

The suffusion is a phenomenon with can slowly lead to the failure of a dam by collapse of the slope material and the embankment by:

- settlement of dam crest and overtopping of the dam may occur;
- Removal of materials can otherwise induce sinkholes which can lead to a breach in the dam;

Finally, transport and removal of materials can lead to the piping phenomenon; one of the main cause of the high occurrence of internal erosion failures during the last decade in Burkina Faso is due to weak design and construction of the embankment dams (selection of earth material, dispersivity, bad compaction and insufficient wetting associated to the high speed of the reservoir filling due to heavy rainfall and large floods.

2.3 *Causes*

Failure causes were found after the assessment of documents of design, works and monitoring and also the results of field investigations. The main causal elements are presented below:

- The foundation of dams is poorly investigated and the works in the foundation and the central part of the dam are often inappropriate (a tick layer of weathered sandy rock was let under the spillway foundations),

Figure 1. Left: Bampéla dam a hole in the embankment. Right: Gazandouré dam-spillway and leak at the contact with the embankment on right side.

Figure 2. Left: Koumbri dam – stratification and thick compacted layers. Right: Guitti dam – foliation of the embankment is due to overcompaction insufficiently moistened fine materials.

- No test on the fill material in the trench of the foundation of the dam,
- The number of tests in the embankment itself is not enough for the size of dams; moreover they haven't found the results of the tests of several layers,
- Moisture content has not been considered in testing the materials,
- The choice of clay material borrow zone very closed to the dam and spillway axis,
- Lack of well design protection and filters downstream of the stilling basin of the spillway
- Utilization of dispersive and poor quality materials,
- Bad compaction of materials at the interfaces between embankment and concrete structures,
- Compacting layers of material too tick (up to 70 cm).

2.4 *Repair modes*

The techniques to repair or correct problems created by internal erosion are numerous and depend on the type of the dam, the type of problems and the environment of the dam (condition, sizes and hydraulic load). The most common problems due to internal erosion on a dam can be loss of impounded water, instability, failure of the dam by overtopping or piping. The commons repairs techniques are the following: the diaphragm wall, grouting, downstream filter and berm, upstream sealing membrane, and of course building a new dam when the damages are too important. The grouting and the diaphragm wall techniques are generally used for large dams because of the technical requirements and their high costs. For small dams the commons methods are the placing of filter on the downstream face with weighting and the reconstruction in case of failure. The placing of filter on the downstream face with weighting is suitable for situations with low leakage flow rate. It is relatively easy to perform and inexpensive. It consists of:

- Stripping the downstream face and incorporating the filter to stop the transport of the materials. The filter is chosen so that filtering conditions are ensured between the fill, the filter and the weighting materials.
- Placing weighting materials with drainage properties to ensure the stability of the dam.

The works can be performed during any period and do not need to empty the reservoir.

3 OVERTOPPING: CAUSES AND SOLUTIONS

3.1 *Causes*

3.1.1 *Lack of reglementation*

There are no reglementation for the choice of design criteria.

3.1.2 *Lack of sound hydrological studies*

Commonly hydrological studies for dam's project are based on ORSTOM and CIEH empirical and regressions methods.

These methods have been implemented with series of rainfall prior to the 70s. With the climate change these methods are not appropriate to allow protection of structures against flooding. In addition, the parameters of the watershed are often underestimated.

3.1.3 *Lack of hydraulic studies*

Hydraulic studies, including flow conditions of the river downstream of the dam are not determined in many cases.

3.2 *Solutions for overtopping problems*

3.2.1 *Improvement of design criteria*

It is necessary to take into account the effects of climate change which are realized in recent years by exceptional rainfall events (rain Ouagadougou on September 1st, 2009). There is on the one hand, economic necessity and secondly, the need to ensure adequate safety to work to reduce the risks. This approach leads to define a design flood for sizing the spillway and a check flood (with water level at the crest of dam) which is taken as the maximum flood that will not cause the destruction of the dam. This one must also be evacuated by the spillway without the failure even some damages can result downstream. One of the current practices is now to use the safety check floods to assess the real safety of the dam. The check flood is determined by the methods of envelope curves of maximum daily rainfall.

3.2.2 *Utilization of low cost technologies*

Some techniques have been developed in these last years to improve flood discharge capacity by dams. These are Piano Keys Weirs (PKW). The labyrinth weir is characterized by a high capacity discharge rate at a relatively low load unlike straight weirs. This benefit includes the low cost of implementation and maintenance in comparison with straight weirs and more reliable operation compared to weirs winnowed.

3.2.3 *Combination of hydraulic structures*

For the sake of rationality, economy and according to the new trends in the profession for flood management, it is important to consider the possibility of combining a service spillway and an

Figure 3. Liptougou dam protected against extreme floods by two spillways.

emergency spillway. This is to implement an efficient and robust structure to evacuate the design flood and safety spillway to help evacuate extreme flood. The safety spillway which is often placed at the lateral side of dam where the dam height is smallcan be constructed using RCC, Cemented materials etc.

The use of Parapet well is also important and is adopted today by the profession to improve the safety at a very low cost for small dams.

The fuse plugs developed also by Hydro coop France have been used in Vietnam and Burkina Faso to improve storage and floods protection capacity of small dams.

4 CONCLUSION

Engineers must seriously consider these problems in the design and the construction of dams. In the two cases presented, internal erosion occurs generally at the first impoundment of the reservoirs which mean that it linked with bad design and construction reservoir; the fast filling and subsequently the violent load on the dam may have deepened the phenomenon. The overtopping of dams is another problem which can provoke dam lost.

These problems show what efforts have to be undertaken:

- By the implementation of dams legislation,
- By taking into account climate change and extreme floods for the protection of dams against floods,
- By the construction companies to master the techniques to build earth fill dams especially when the earth contains dispersive clay.
- By the Project Implementation unit, Engineers to apply the best practice to follow-up the design, the construction and the first filling of the dam.

REFERENCES

[1] Internal Erosion, typology, detection, repair Barrages et réservoirs Spécial congrès de Florence Mai 1997.
[2] La sécurité des petits barrages au Burkina A. NOMBRE 1994.
[3] Rapport diagnostic de la rupture du barrage de Bampela IFEC 2010.
[4] Rapport diagnostic de la rupture du barrage de Gazandouré IFEC/GERTEC 2010.
[5] Lempérière, F., Ouamane, A. 2003. The piano keys weir: a new cost-effective solution for spillways. The international journal on Hydropower and Dams volume ten, issue Five.
[6] Ouamane, A., Lempérière, F. 2006. Nouvelle conception de déversoir pour l'accroissement de la capacité des retenues des barrages. Colloque International sur la Protection et la préservation des ressources en eau. Blida. Algérie

Dam Protections against Overtopping and Accidental Leakage – Toledo, Morán & Oñate (Eds)
© 2015 Taylor & Francis Group, London, ISBN: 978-1-138-02808-1

Failure of the downstream shoulder of rockfill dams in overtopping or accidental leakage scenario

Miguel Á. Toledo & Hibber Campos
Technical University of Madrid (UPM), Madrid, Spain

Ángel Lara & Rafael Cobo
Center of Hydrographic Studies of CEDEX, Madrid, Spain

ABSTRACT: The failure of a rockfill dam begins with damage to the downstream shoulder prior to the failure of the clay core or upstream face. Accepting that the vertical permeability is enough for allowing water to flow down through the rockfill, damage initiates at the dam toe and progress upward to the crest. So, the complete failure of the shoulder is a process that takes time and require overtopping flow to overcome a threshold value. This process was experimentally analyzed in several testing facilities, one of them specially design for testing rockfill dam failures. Failure patterns for steep and gentle slopes are here described. The failure process is conceptualized through the concepts of *failure path* and *incubation flow*, and the influence of the main parameters on the failure process are analyzed.

Keywords: dam, protection, overtopping, rockfill, failure, shoulder, shell

1 INTRODUCTION

The effect of overtopping or an important accidental leakage on the downstream shoulder of a rockfill dam is similar: the shoulder, designed to be dry, is subjected to water flow through the interstitial pores, suffers water pressure and mass sliding may occur. In addition, water flowing over the shoulder surface, combined with the seepage flowing out of the shoulder, may cause the dragging of rockfill stones. If the overtopping or accidental leakage discharge is high enough, a partial or total failure of the shoulder may occur.

Several questions arise about it: a) which is the minimum overtopping discharge to initiate the failure?; b) where does the failure begins and how does the failure progress?; c) which is the overtopping discharge necessary for the impervious element of the dam, internal core or upstream face, be affected. Answers to this questions are needed to properly assess the safety level of a particular rockfill dam against overtopping or accidental leakage, and to develop realistic emergency plans for managing a probable failure situation.

2 EXPERIMENTAL TESTS

2.1 *Experimental setup*

An extensive test program was developed for that purpose. A facility specially designed for testing embankment dams failure was performed at the Hydraulic Laboratory of the *ETS de Ingenieros de Caminos, Canales y Puertos* of the UPM. It is a 13 m long, 2.5 m width and 1.4 m high channel, provided with a $5 \times 1\,m^2$ glass window for observation and video recording purposes. The test

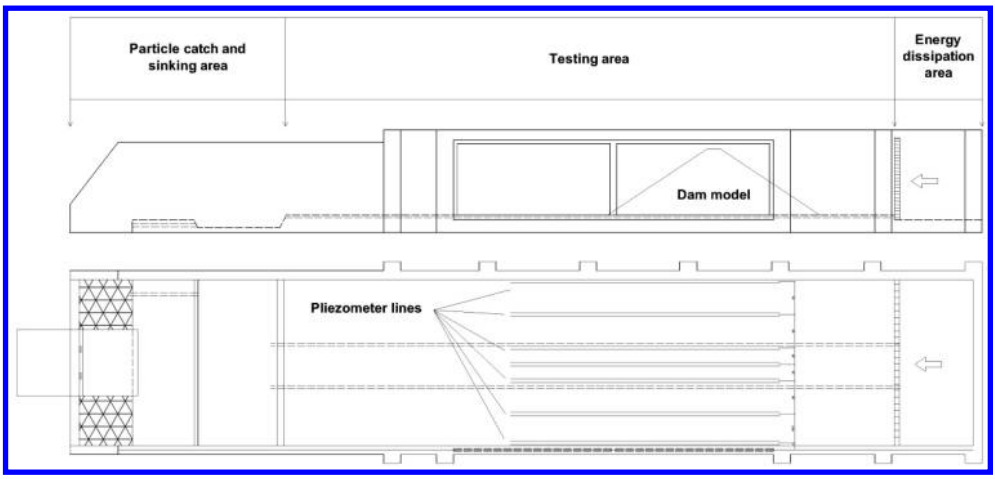

Figure 1. Experimental set up.

channel is divided into four zones (Fig. 1): a) inlet and disipation; b) test zone; c) decantation; and d) return to the tank zone (close circuit). The monitoring instrumentation evolved along time. Nowadays the channel is equipped with a robotized laser profile meter that allows to obtain a Digital Terrain Model (DTM) of the tested rockfill dam at any moment of the failure process. It is also equipped with 85 hydraulic piezometers installed at the base of the testing zone, three ultrasonic limnimeters at the intake zone, downstream of the test zone, and at a triangular wire flow meter located downstream of the test channel, in the return channel. A computer controlled valve and a magnetic flow meter at the intake zone allows to control the discharge entering the test channel.

In addition, two conventional testing channels of the Center of Hydrographic Studies of the CEDEX were used, 0.4 and 1.0 m wide.

2.2 *Materials and test procedure*

Uniform crashed aggregates of different size were chosen. The sieve size passing 50% of the particles of the tested materials was, in mm: 8, 13, 16, 35. The size of the particles was selected so that a non linear relation between hydraulic gradient and seepage velocity was assured.

The rockfill dam was built without compaction and the resulting dam body can be considered homogeneous. Every rockfill dam model was tested for a set of discharges. The test was initiated with the smallest discharge and it was increased step by step to an increasingly higher discharge. The highest tested discharge was that with a degree of failure affecting the crest of the dam. Every discharge value was kept until the steady state was reached, that is, until no additional damage was observed on the shoulder nor change in the water levels and pressures. Then all the variables involved where registered and a DTM of the tested rockfill dam was obtained. So, there is a complete set of registers and a DTM of every overtopping discharge step for every rockfill dam tested.

2.3 *Test program*

The test program was conceived in three phases: I) repeatibility analysis; II) scale effect; III) parametric study.

The aim of the *phase I: repeatibility analysis* was to evaluate the repeatibility of the tests, taking into consideration that apparently equal tests were different in the detail: arrangement of particles

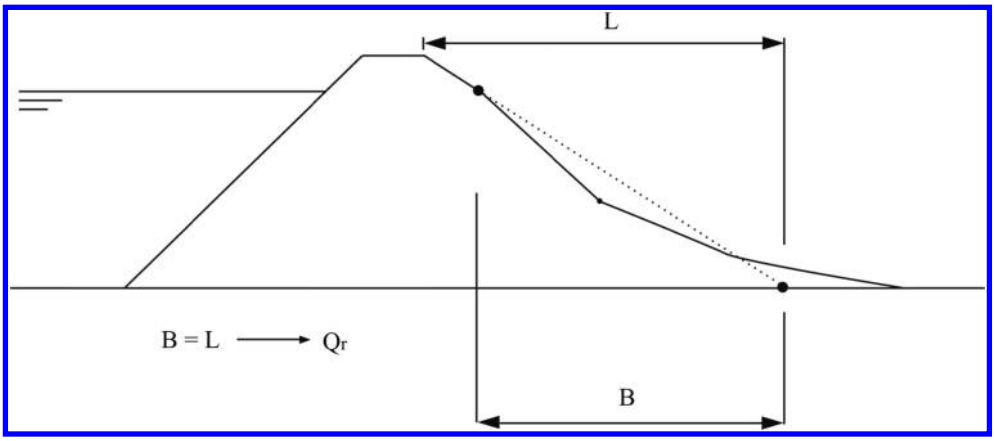

Figure 2. Advance degree of failure. ADF = B; dimensionless ADF = B/L; the overtopping flow that causes B = L is considered the failure flow for the shoulder.

in the dam body is different, although the height, shoulder slope and material were the same. A certain variability in the results of several tests with the same value of the relevant parameters was expected, so it was necessary to asses if it was acceptable.

Scale effect is a critical issue when performing scaled physical tests, specially complex when different physical phenomena are involved in the test, as happens in this research. A simple approach was adopted in phase II, a first attempt to understand the scale effect in the physical modeling of the failure of the downstream rockfill dam shoulder due to overtopping: two scaled geometries were tested.

Phase III was conceived as a parametric study to assess the effect of the main parameters involved in the failure: shoulder slope, material and type of impervious element. Given the limited knowledge about the scale effect, tested rockfill dam models should be considered as prototypes (scale 1:1), admitting the hypothesis that the involved physical phenomena are the same that in a full size rockfill dam. In that case, the conclusions obtained from the experimental tests would be valid for rockfill dams of any size.

More than one hundred tests were performed.

3 CONCEPTUALIZATION OF THE FAILUIRE PROCESS

In view of the results obtained from the tests, several new concepts were defined to properly characterize the process and facilitate the analysis of the influence of the different parameters involved:

Advance degree of failure (ADF): It was observed that the failure was initiated at the dam toe and progressed upstream towards the crest of the dam. For a certain overtopping discharge an *advance degree of failure* may be defined as the horizontal distance from the original toe of the dam before failure to the most upstream point of the dam body affected by the failure. It may be expressed in non dimensional way dividing it by the horizontal projection of the hole downstream dam slope (Fig. 2). So, the non dimensional ADF varies from cero, when failure has not been initiated, to one when the damage affects the crest of the dam. Unless specified the contrary, the non dimensional ADF will be considered.

Path of failure (FP): For every overtopping discharge (Q) there is a related ADF. The evolution of the failure process for increasingly higher overtopping discharge may be defined through the

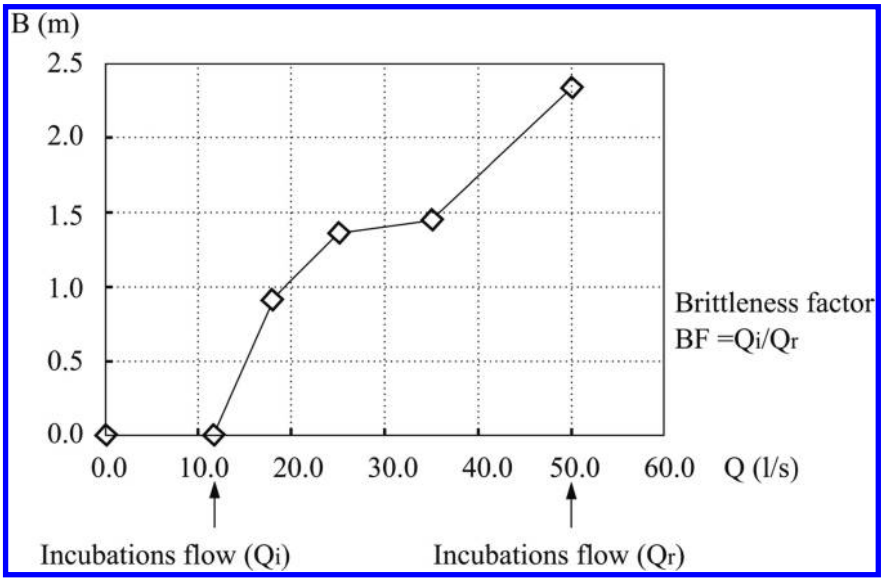

Figure 3. Failure path (FP).

ordered set of pairs (Q, ADF), which was termed *failure path* and can be represented as a line in a cartesian system (x, y) (Fig. 3).

Incubation discharge (Q_i): It was observed that an overtopping discharge threshold should be overcome for the failure to initiate. That threshold was termed *incubation discharge.* No damage happens until overtopping discharge is greater than the incubation discharge. For a practical purpose the first step of overtopping discharge that produced damage to the dam was considered the incubation discharge. Notice that an error arise from the discrete nature of the overtopping discharge set of values tested.

Failure discharge (Q_r): The first step of overtopping discharge that produces a damage that affects the crest of the dam (ADF = 1) was considered the *failure discharge*. It should be overcome for the damage to reach the impervious element of the dam, which is the critical issue for the stored water be released. When the failure discharge is reached, it will be considered that the shoulder has completely failed, although some of the rockfill material is still in place.

A non dimensional path of failure may be defined considering Q/Q_r instead of just Q, that is, expressing the overtopping discharge (Q) as a portion of the failure discharge (Q_r). It allows to put together in the same graphic the path of failure of very different rockfill dams.

Fragility factor (*BF*): If the incubation discharge is high related to the failure discharge, although obviously smaller, we will say that the failure is brittle, in the sense that when damage in initiated a relatively small increment of the overtopping discharge will cause the complete failure of the shoulder. The *brittleness factor* is then defined as the relation Q_i/Q_r and takes values greater than cero and lower than one. A low value of BF indicates low failure fragility and a high value of BF is a sign of high fragility.

4 FAILURE PATTERNS

The observation of the tests allowed to conceive a conceptual model of the shoulder failure process. Two clearly different failure patterns were identified for steep and gentle slopes, around 1.5:1 the former and around 3:1 the latter.

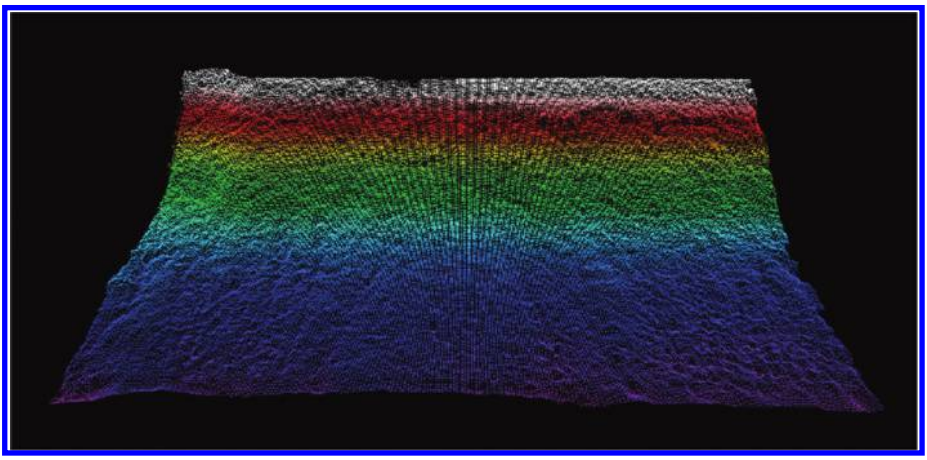

Figure 4. Failure pattern for the shoulder of a rockfill dam with steep slope (around 1.5:1). View from downstream.

Steep slope (around 1.5): This is the case of most existing rockfill dams (Fig. 4). For low overtopping discharge, under the incubation discharge, there is no damage. Then failure is initiated at the dam toe mainly in the form of simultaneous movement of several nearby stones located at the slope surface, like a very shallow sliding affecting a small group of stones. Then, the same happens in different zones of the shoulder toe until all the toe stones are moved. With increasingly higher discharges the level of water inside the dam body increases and the very shallow successive slidings progress upward, affecting the whole width of the dam, as a consequence of the increase of the pore pressure. Dragging of stones is too observed, but the prevalent failure mechanism is mass sliding and for that reason the whole width of the dam is almost equally affected by the damage. It is easy to observe two types of mass slidings: a) the described shallow slidings due to interstitial pore pressure and: b) mass slides due to the mismatch of the stones located upstream of the group of stones moved by the first type of mass sliding formerly described. This way a compound slope is formed, different for every step of discharge: a downstream stretch with slope gentler than the initial, formed by the moved stones, and an upstream stretch with stones that keep in place without movement and slope steeper than the initial. Water flows out of the dam body from around the point of slope change downward.

Gentle slope (around 3:0): This would be the case of a rockfill dam designed for avoiding mass sliding in overtopping scenario. The dam body formed with rockfill is stable and the only failure mechanism is the dragging of stones, admitting that additional possible failure mechanisms are not present, like internal instability or damage to the crest due to suction. The incubation discharge should be overcome to initiate the dragging of stones from the dam toe. Some movement of individual stones is then observed in different places of the dam toe. The movement of one single stone facilitate the dragging of the nearby stones, so the damage tend to concentrate in some of the places where it was initiated. When a significant number of stones are dragged from an area, a hole is formed in the dam body. It has the effect of a drain and flow towards that area is increased and the process of stones dragging is accelerated. This is the mechanism for the formation of several erosion channels. The mismatch of stones located upstream of the dragged particles induces a mass sliding. The material fallen inside the erosion channel reduces the amount of water flowing out throw that channel and temporarily stop or decrease the loss of stones. The damage evolves upstream in every erosion channel by successive phases of dragging of stones and mass sliding due to the mismatch. The different erosion channels compete in the race for reaching the crest as the overtopping discharge step up, but finally one of them is big enough to concentrate most of the

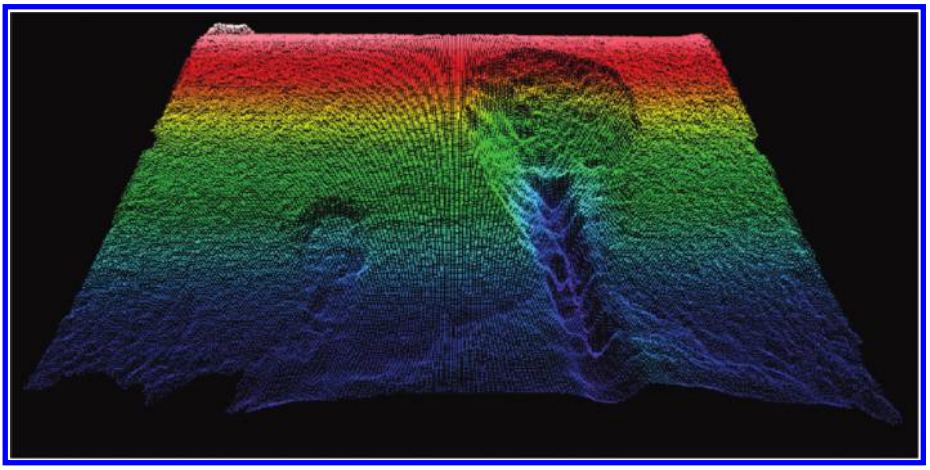

Figure 5. Failure pattern for the shoulder of a rockfill dam with gentle slope (around 3:1). View from downstream.

flow and that erosion channel is the responsible for the complete failure of the shoulder by reaching the dam crest (Fig. 5).

In summary, when the slope is steep the prevalent failure mechanism is mass sliding and damage affect to the hole width of the shoulder; successive shallow mass sliding progress upstream until the crest is affected; and when the slope is gentle the only failure mechanism is the dragging of stones (and mass sliding induced by mismatch), several erosion channels are formed and finally one of them reaches the crest. For intermediate slopes a mixed failure pattern between those two described was observed.

5 REPEATIBILITY OF THE TESTS AND SCALE EFFECT

These two phases were previous to the more extensive experimental parametric study.

5.1 *Repeatibility of the tests*

Tests with different slopes were repeated several times with the same value of the parameters involved in order to assess the repeatibility of this type of tests. The process of failure for every test with the same parameter values was defined by the *failure path* and all of them were put together in a graph (Fig. 6).

From the analysis of the test results we can conclude: a) there is an appreciable variability in the first half of the failure path which is just due to chance, depending on the detailed particles arrangement and probably other uncontrolled factors; b) variability is more remarkable for intermediate slopes, when a mixed failure pattern occurs; c) it is more remarkable too if there is the possibility that several erosion channels to develop, that is, if the rockfill dam is wider related to its height; and most important, d) failure paths of different tests with the same parameter values converge with increasing overtopping discharge so that the *failure discharge* is quite similar for all of them; it happens independently of the width/height relation. Therefore, a reasonable accuracy can be obtained in the *failure discharge* assessment, which is an important issue from the practical

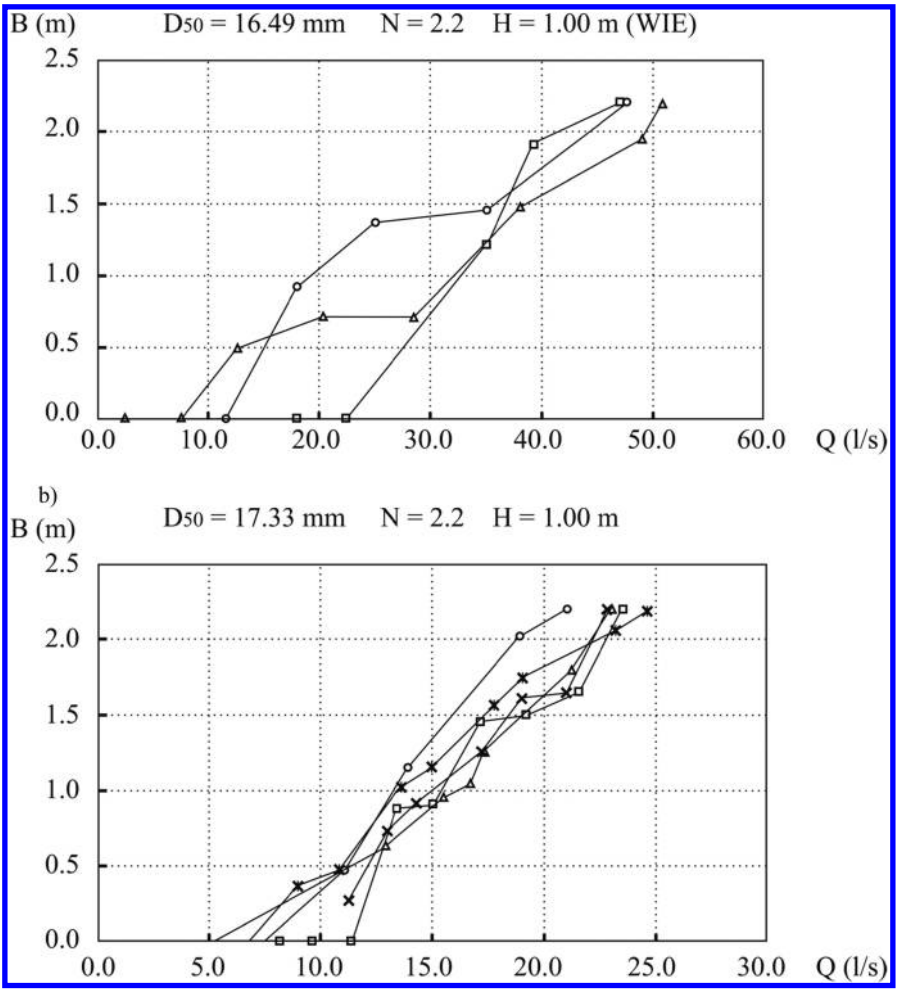

Figure 6. Failure path from the repeatibility tests, for slope N = 2.2; a) D_{50} = 16.49 mm; channel test 2.5 m wide; b) D_{50} = 17.33 mm; channel test 1.0 m wide.

point of view, although an appreciable variability should be expected for the first half of the failure path, and then for the *incubation discharge*.

5.2 *Scale effect*

As mentioned before, physical models tested should be considered as prototypes and are not intended to be a scaled model of any particular rockfill dam. Although not necessary for this research, scale effect still remains an important issue for physical modeling of rockfill dams failure, so a first simple experimental approach to scale effect analysis was done. For three different slopes: 1.5, 2.5 and 3.5, two scaled rockfill dams were tested; scale 1:3.5 for both, the height of the dam and the size of the material (D_{50}). The higher dam was considered the prototype and the lower dam was considered the model. Experimental results are shown in table 1, as well as the *failure discharge* inferred for the prototype from the experimental value registered for the model. Inferred and experimental registered values are pretty close for slopes 1.5 and 3.5. For slope 2.5 a discrepancy

Table 1. Results from scale effect tests.

Scale efect	Slope 1.5	Slope 2.5	Slope 3.5
Model (measured values)			
Failure hydraulic head (cm)	2.04	1.80	2.30
Failure unit flow (l/s/m)	5.3	9.5	6.5
Prototype (measured values)			
Failure hydraulic head (cm)	7.40	6.45	8.20
Failure unit flow (l/s/m)	36.0	46.0	45.0
Prototype (measured values)			
Failure hydraulic head (cm)	7.15	6.30	8.40
Failure unit flow (l/s/m)	35.0	62.0	43.0

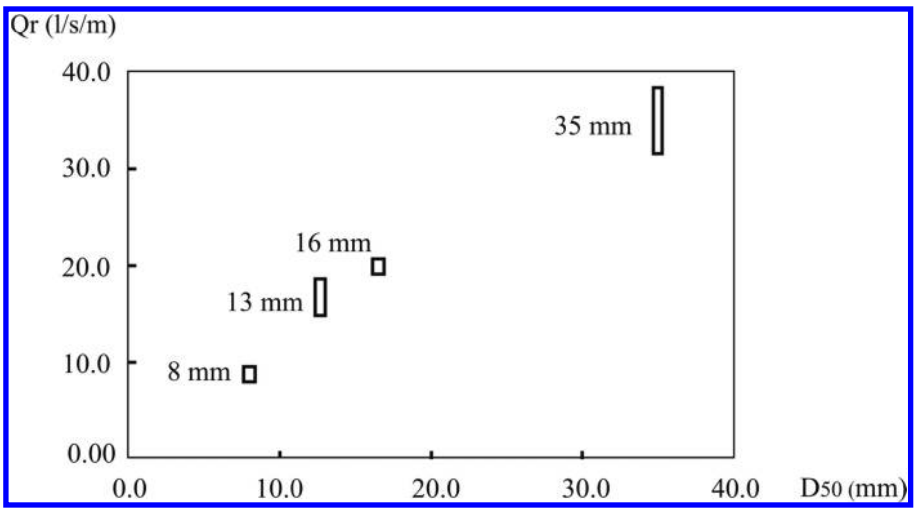

Figure 7. Relationship between uniform material size (D_{50}) and failure discharge (Q_r).

can be observed between failure hydraulic head and discharge, thus an experimental error is a plausible explanation. Of course, the results obtained have not a general validity, but still allow an interesting analysis.

6 FAILURE DISCHARGE

Failure discharge of the downstream shoulder is a relevant parameter because it marks a border between values of the overtopping discharge that cause damage only to the dam shoulder, and those that may be able to break the impervious element and thus are potentially dangerous for people and properties downstream of the dam.

From the result of the experimental tests, it can be concluded that shoulder slope and the type of impervious element have a minor effect on the value of the failure discharge; in return, a remarkable relation between the rockfill size (D_{50}) and the failure discharge is observed (Fig. 7). It should be emphasized that the relation should not necessarily be causal.

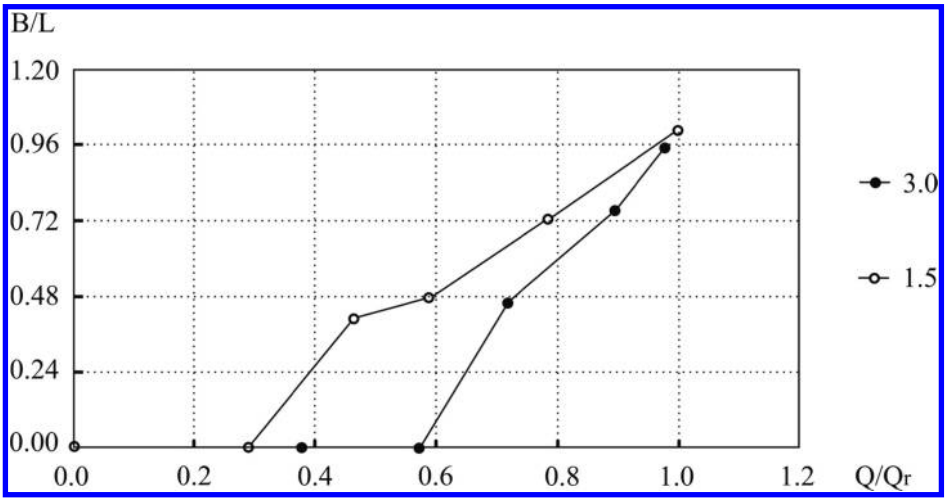

Figure 8. Failure path for $D_{50} = 35$ mm and slopes 1.5:1 and 3:1.

At a first appearance is somehow surprising that the shoulder of rockfill dams exhibiting completely different failure patterns, corresponding to steep to rather gentle slopes, fail with a quite similar overtopping discharge if the D_{50} of the material is the same. Independently of the failure pattern, mass sliding or erosion channels, the level of the water inside the dam body appears to be a key factor in the *advance degree of failure* (ADF), and thus in the *failure discharge*. Of course, the position of the phreatic surface is not independent of the failure pattern, but differences could be slight. Given that all the materials tested are uniform, a plausible hypothesis is that the value of D_{50} influences permeability of the material and so the failure discharge: for a given discharge, as D_{50} decreases, the permeability of the material also is reduced, thus the position of the phreatic surface raises and as a consequence also the ADF heightens. Therefore, a lower D_{50} would imply a lower failure discharge too.

Given that materials with the same D_{50} may have a quite different permeability, if the proposed hypothesis was true, the key factor would be the rockfill permeability, and not the D_{50}. Additional research is necessary for confirming or refuting the hypothesis.

7 EFFECT OF SLOPE AND IMPERVIOUS ELEMENT

As mentioned before, the effect of the slope and the type and position of the impervious element on the failure discharge is not relevant. The phreatic line inside the downstream shoulder is quite similar for rockfill dams with central core, upstream face or even without impervious element. The most evident effect of the slope is on the brittleness factor. Rockfill dams with a gentler slope show a more brittle behavior (Fig. 8). Although rather variable, brittleness factor takes a value around 0.25 for a 1.5:1 slope, while around 0.5 for a 3:1 slope, as shown in Fig. 9. In is remarkable that the failure path can be approximately defined by a straight line on average.

8 CONCLUSIONS

The main conclusions drawn from the extensive experimental research are:

– The failure process can be defined by the dimensionless failure path (FP) that gives the advance degree of failure (ADF) as overtopping discharge increases.

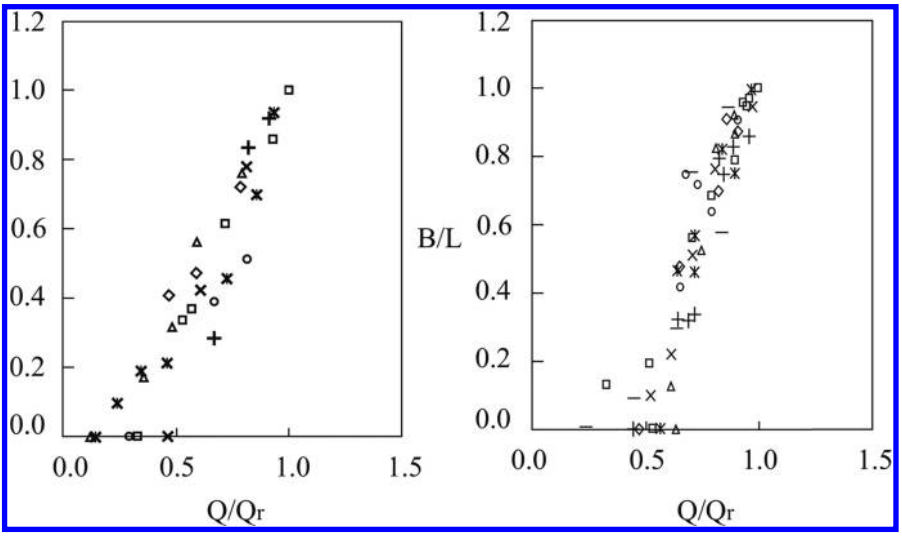

Figure 9. Failure path for: Left) slope 1.5:1; Right) slope 3:1. Every symbol corresponds to a particular test.

- The failure path can be approximated by a straight line.
- Initiation of damage requires a certain incubation overtopping discharge to be overcome.
- The incubation discharge, expressed as a fraction of the failure discharge, is greater for gentler slopes, that is, the rockfill dams behavior is more brittle for gentles slopes.
- The failure discharge mainly depends on the size (D_{50}) of the rockfill for the uniform materials tested, and the slope and type of impervious element plays a minor role regarding failure discharge. The authors opinion is that there is correlation, but not a causal relationship between D_{50} and the failure discharge. It is a plausible hypothesis that failure discharge mainly depends on the permeability of the rockfill, that induces the phreatic surface elevation and so the water pressures and hydraulic gradients that cause the failure.
- There are two clearly different failure patterns: mass sliding is the prevalent failure mechanism for slopes around 1.5, and particle dragging is the only failure mechanism for gentler slopes around 3:1. It is remarkable that prevalent failure mechanism, which depends on the slope, is not relevant for the failure discharge nor for the failure process given by the failure path.

Data from the experimental program are still under analysis for the development of a criterion for the assessment of the failure discharge based on the specific characteristics of a rockfill dam.

REFERENCES

W. Hahn, GJ. Hanson and KR. Cook, Breach Morphology Observations of Embankment Overtopping Tests. Building Partnerships. Proceedings of the 2000 joint conference on water resources engineering and water resources planning and management, Minneapolis, 2000.

GJ. Hanson, KM. Robinson and KR. Cook, Prediction of Headcut Migration Using a Deterministic Approach. Transactions of the ASAE, American Society of Agricultural Engineers, 44 (3), 525–531, 2001.

GJ. Hanson, KR. Cook and SL. Hunt, Physical Modeling of Overtopping Erosion and Breach Formation of Cohesive Embankments. Transactions of the ASAE, American Society of Agricultural Engineers, 48 (5), 1783–1794, 2005.

SL. Hunt, GJ. Hanson, HR. Cook and KC. Kadavy, Breach Widening Observations from Earthen Embankment Tests. Transactions of the ASAE, American Society of Agricultural Engineers, 48 (3), 1115–1120, 2005.

ICOLD. (1995). *Bulletin 99. dam failures statistical analysis*. Paris, Francia: International Comittee on Large Dams.

L. Jenssen, & A. Soreide, (2004). Models tests on the stability of rockfill dams during through flow. *International Seminar. Stability and Breaching of Embankment Dams,* Oslo, Noruega. 1–9.

MW. Morris, MAAM. Hassan and KA. Vaskinn, Conclusions and Recommendations from the IMPACT Project WP2: Breach Formation, http://www.impact-project.net/AnnexII_DetailedTechnicalReports/AnnexII_PartA_WP2/WP2_10Summary_v3_0.pdf, 2005.

MÁ. Toledo, Embankment dams slip failure due to overtopping (Q75 R.24). XIX International Congress on Large Dams, ICOLD. Florence, 1997.

MÁ. Toledo, (1997). *Rockfill dams subject to overtopping. Study of flow through the rockfill and stability against mass sliding*. (in Spanish). Universidad Politécnica de Madrid. PhD Thesis.

MÁ. Toledo, (1998). Design of overtopping-resistant rockfill dams (in Spanish). Madrid: Spanish National Committee on Large Dams.

MÁ. Toledo, C. Lechuga, & E. Oñate. (2008). Analysis of the behavior of rockfill dams in overtopping scenario (in Spanish). *Proceedings of the XXIII Congreso Latinoamericano De Hidráulica,* Cartagena de Indias, Colombia.

TL. Wahl, DJ. Lentz and BD. Feinberg, Physical Hydraulic Modeling of Canal Breaches. Dam Safety Conference, Washington D.C., September 2011.

JY. Zhang, Y. Li, GX. Xuan, XG. Wang and J. Li, Overtopping breaching of cohesive homogeneous earth dam with different cohesive strength. Science in China Series E: Technological Sciences, 52(10), 3024–3029, 2009.

Dam Protections against Overtopping and Accidental Leakage – Toledo, Morán & Oñate (Eds)

Structural failure of the clay core or the upstream face of rockfill dams in overtopping scenario

M.Á. Toledo, R.M. Alves & R. Morán
Dam Safety Research Group (SERPA), Technical University of Madrid (UPM), Spain

ABSTRACT: Three tests of failure of rockfill dams with upstream face (1 test) and central clay core (2 tests) were performed to explore its failure mechanism. The conclusion is that the structural properties of the upstream face or clay core dominates the reservoir water release, and so the failure hydrograph. Failure was more brittle for the more resistant impervious element: the rockfill dam with the widest clay core of the two cores tested. The rockfill dam with upstream face showed a step by step failure, not so sudden as the failure of the rockfill dams with central core. Further research may establish criteria about how to assess the failure hydrograph from the particular properties of the dam.

1 INTRODUCTION AND BACKGROUND

Failure hydrograph due to overtopping at embankment dams is usually determined through the consideration of a breach that widens and deepens in a specified time frame. That is the approach of regulations of different countries adopted to determine the correspondent flooded areas used to develop emergency plans (Escatín, 1996). Most of the research about embankment dam failures due to overtopping has been focused on the analysis of the evolution of that breach during the failure process (Hahn, Hanson, & Cook, 2000; Hanson, Robinson, & Cook, 2001; Hanson, Cook, & Hunt, 2005; Hunt, Hanson, Cook, & Kadavy, 2005; Morris & Wallingford, 2005; Wahl, Lentz, & Feinberg, 2011; Zhang, Li, Xuan, Wang, & Li). This approach assumes that erosion is the failure mechanism that controls the breaking process. That is the case of homogeneous earth fill dams, constructed with cohesive material, but the failure process is quite different for rockfill dams. The subject is important in practice because rockfill dams are abundant among the highest and most risky embankment dams.

The high permeability of the downstream rockfill shell allows the percolation of water inside the dam body in the duration of a flood. As a consequence, pore pressure may cause failure of the shell, while at the same time stones are dragged by the water flow (Toledo, 1997a; Toledo, 1997b). So failure of rockfill dams due to overtopping is initiated at the downstream rockfill shell that protects the impervious element: a clay core or an upstream face.

Once the downstream shell has been partially or completely destroyed, the impervious element is left without adequate structural support and structural failure may control the breakage process, and so determine the reservoir water release and the failure hydrograph. That was the hypothesis of this research: structural failure of the impervious element of a rockfill dam dominates the release of reservoir water and determines the failure hydrograph. Three physical tests were performed for analysing the failure process of rockfill dams and qualitatively verify or refute the above hypothesis.

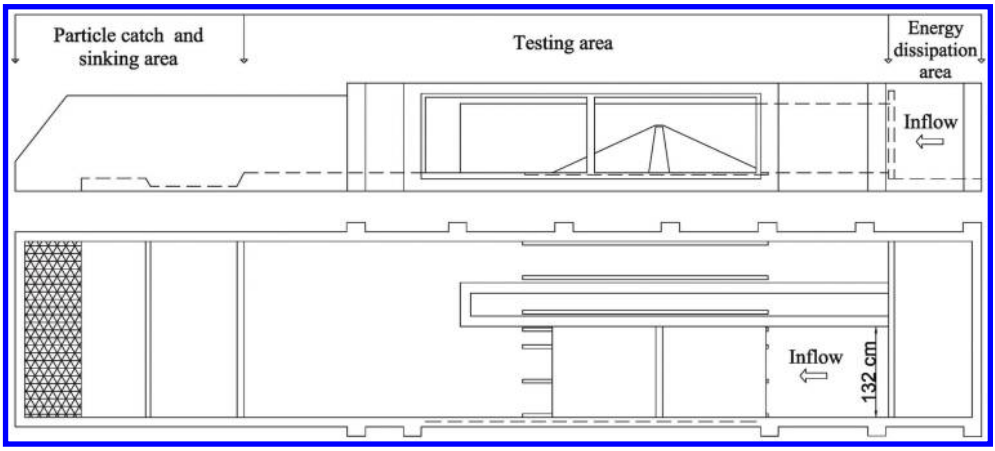

Figure 1. Schematic drawing of the test flume. Side (top) and plan (below) views.

2 TESTING FACILITIES, MATERIALS, SET UP AND PROCESS

2.1 *Testing facilities*

Tests were conducted in a channel type facility located in the hydraulics laboratory of the *E.T.S.I. de Caminos, Canales y Puertos* of the Technical University of Madrid. This facility is 2.4 m wide, 1.4 m high and 13.7 m long subdivided in three functional zones. From upstream to downstream, there is a zone for water supply and energy dissipation delimited by a hollow brick wall. Just after this wall begins the test zone that have in one of its sides an inspection window 2.3 m long and 1.1 m high. This zone ends in a 1.35 m long and 10 cm deep particle catch and sinking area. All the tests were performed in a longitudinal subdivision of this flume 1.32 m wide. Figure 1 shows a schematic drawing of the channel.

Flow rates were measured upstream using an ultrasonic flowmeter, located in the upstream supply pipe, and downstream using a contracted rectangular sharp-crested weir, located in the flume sewer that returns water to the main tank of the laboratory. Measurements of the water level upstream the weir were performed by means of an ultrasonic level sensor.

2.2 *Impervious elements and materials*

Two different types of impervious elements were tested: an upstream face of mortar (Test 1) and a central clay core (Tests 2 and 3). The criterion for the upstream impervious face was that it was fragile enough to simulate what was expect to happen in a real case, *i.e.*, that failure of the upstream impervious face should follow up failure of the downstream rockfill shoulder. In order to do so, a mortar with a low resistance capacity, specially a low bending strength, was designed using a recipe of one volume unit of cement, two of lime, nine of sand and four of water (1C:2L:9S:4W).

The strength was evaluated using squared cross section prismatic samples with 16 cm^2 of area and 16 cm long. Three samples were used for the bending tests. The six halves resulting from these tests were used for the compression tests. Compression and bending strengths after 28 days were 663.64 ± 16.59 kPa and 717.38 ± 19.40 kPa, respectively. The tests with central core were performed using clayey material of the Loteta dam in Zaragoza. A gravel (M1) with diameter 12.5 mm (D_{50}) was used for the shoulders. This diameter correspond to fifty percent, by weight, of the grains smaller than 12.5 mm. The main properties of these materials are summarized in Table 1 and Table 2 and in FFF is showed the grain-size curve of the gravel.

Table 1. Main properties of the central core material.

Specific gravity of solid constituents (γ_s/γ_w)	2.71
Modified mini-Proctor maximum density (g/cm^3)	1.92 ± 0.02
Plasticity index (%)	10.2 ± 3.7
Fine fraction (%)	94.3 ± 0.9
Coefficient of permeability (cm/s)	$<10^{-6}$

Table 2. Main properties of the gravel type material used for the shoulders.

Fine fraction (%)	–
Median grain size D_{50} (mm)	12.5
Dry unit weight (kN/m^3)	14.3
Unit weight in saturated state (kN/m^3)	18.3
Void ratio	0.69
Porosity	0.41

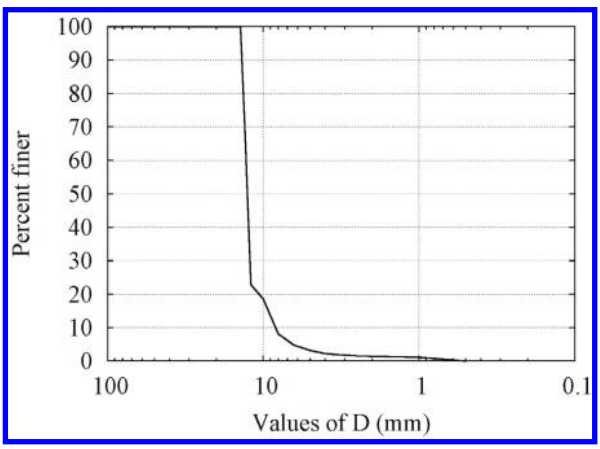

Figure 2. Grain-size curve of the gravel used for the dam shoulders.

2.3 *Test set up and construction*

Dams with upstream and downstream slopes (N) of 1.5:1 where built, similar to that of real rockfill dams. Mass sliding is the dominant mechanism of failure for the downstream shoulder with that value of slope. The height and crest width were 0.67 m and 0.14 m, respectively.

For the dam with upstream face (Test 1), the face was built after the completion of the dam body, with thickness half of D_{50}. A thin paper layer was placed between the body and the face to prevent adhesiveness. Figure 3 (above) shows the building progress of the upstream face. For the central core tests (Tests 2 and 3), the clay core was built by compacting layers 4 cm thick. Every layer was compacted with a mass of 7 kg vertically dropped from a height of 20 cm. Figure 3 (down) shows the typical building progress for the rockfill dam with central core tests.

For Test 2, the central core was 62 cm height. Crest and base widths were 10 cm and 30 cm, respectively. The number of hits per square meter varied between 243 and 403, with average and standard deviation of 319 ± 41 hits/m^2. For Test 3, the central core was also 62 cm height, the crest

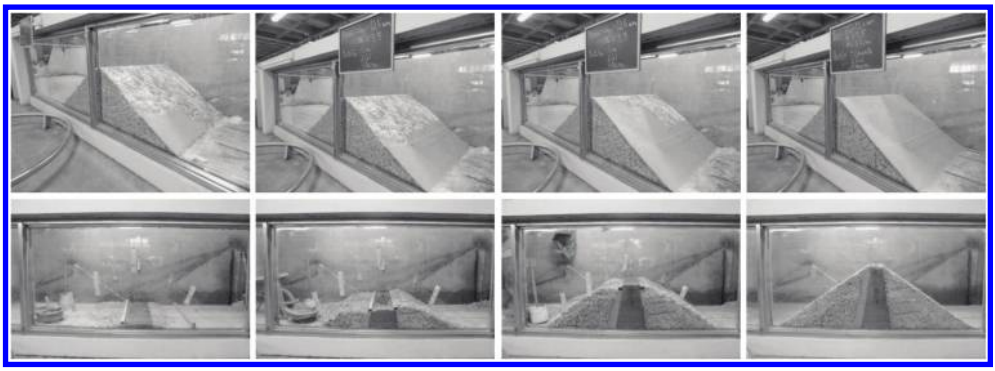

Figure 3. Building progress of the upstream face in Test 1 (above) and internal core in Test 2 (down).

Table 3. Basic characteristics of the experimental campaign.

Test	Test 1	Test 2	Test 3
Height of dam (m)	0.67	0.67	0.67
Width of crest (m)	0.14	0.14	0.14
Upstream slope (H/V)	1.5	1.5	1.5
Downstream slope (H/V)	1.5	1.5	1.5
Thickness of the upstream face (mm)	≈6.3	–	–
Height of the internal core (m)	–	0.62	0.62
Width of the core crest (m)	–	0.10	0.10
Width of the core base (m)	–	0.30	0.20

and a base width were respectively 10 cm and 20 cm and the number of hits per square meter varied from 111 to 209 with average and standard deviation of 159 ± 30 hits/m^2.

Water was spread over the cohesive material before compaction of each layer. Water content was controlled after compaction, measuring the weight of a sample before and after drying it. Before dry, the sample was weighted measuring thus the mixture weight of soil and water. This procedure was repeated until the weight of the sample was constant. The difference of weights refers to the water content of the sample. The water contents for Tests 2 and 3 were around 30% and 34%, respectively. The modified mini-Proctor test performed using four samples of the same cohesive material gave an optimum water content of 12.88 ± 0.25%, so material was compacted well on the wet zone. Basic characteristics of each test are summarized in Table 3.

2.4 *Test description*

Tests were based on a stepwise flow rate increments making for each step all measurements described previously, until failure of the impervious element occurred. For all tests, the downstream shoulder front of failure progressively grew upwards as the flow rate step was increased until it reaches the crest of the dam. Once the crest is reached, the next flow rates will cause washing of the downstream shoulder leaving the impervious element unsupported. In all three tests, failure of the impervious element occurred when imposed a flow rate higher to the flow that caused total failure of the downstream slope. For Tests 1, 2 and 3, the flow rates that caused total failure of the downstream shoulders were, respectively, 18.5 l/s/m, 10.3 l/s/m and 12.4 l/s/m, being the average value of the flow rates 13.73 ± 4.26 l/s/m.

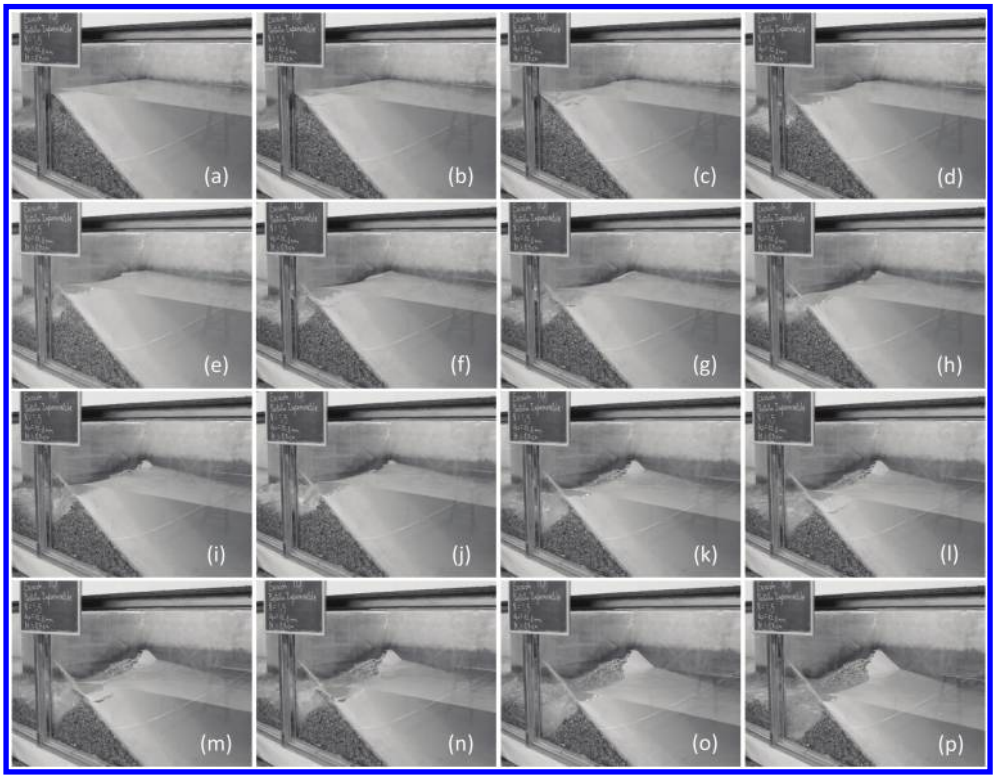

Figure 4. Gradual failure of the upstream face (Test 1).

In Test 1, total failure of the upstream face occurred progressively and for the same flow rate step, *i.e.*, the flow rate that initiated failure was the same that cause the entire failure of the upstream shoulder. Failure of the upstream face starts when a certain quantity of the supporting rockfill material is washed as a consequence of the flow rate imposed to the model, leaving the mortar face in overhang conditions that lead to the first breakage and consequent flood. When this volume of water is released, a part of the downstream slope is again washed leaving another zone of the face more and more unsupported and subjected to bending forces. The next breakage occurs when the bending strength of the upstream face is insufficient to balance the external forces leading to another flood. This failure mechanism is repeated until total failure of the upstream face is reached. Figure 4 (a) shows the overhang conditions that led the upstream face to the first breakage. Is possible to observe that a certain volume of the supporting rockfill material was washed previously to failure. From Figure 4 (b) to (e) is showed a sequence of the washing of rockfill material, consequence of the first flood, that led to the next breakage. From Figure 4 (f) to (k) and from (l) to (p) is showed the second and third breakages. Total failure of the upstream face occurred in four steps, each step for overhang lengths of approximately 8.7 cm, 13.4 cm, 11.8 cm and 13.0 cm, being the average value 11.73 ± 2.13 cm.

In Test 2 total failure of the internal core resulted to occur at once. The flow rate imposed to the model (10.3 l/s/m) washed the rockfill material approximately to half the height of the dam as can be seen in Figure 5 from (a) to (c). The central core, once unsupported by the eroded downstream shoulder, was left alone to resist to hydrostatic pressure. After some time, the central core overturned over an horizontal axis placed approximately half height, washing out the entire

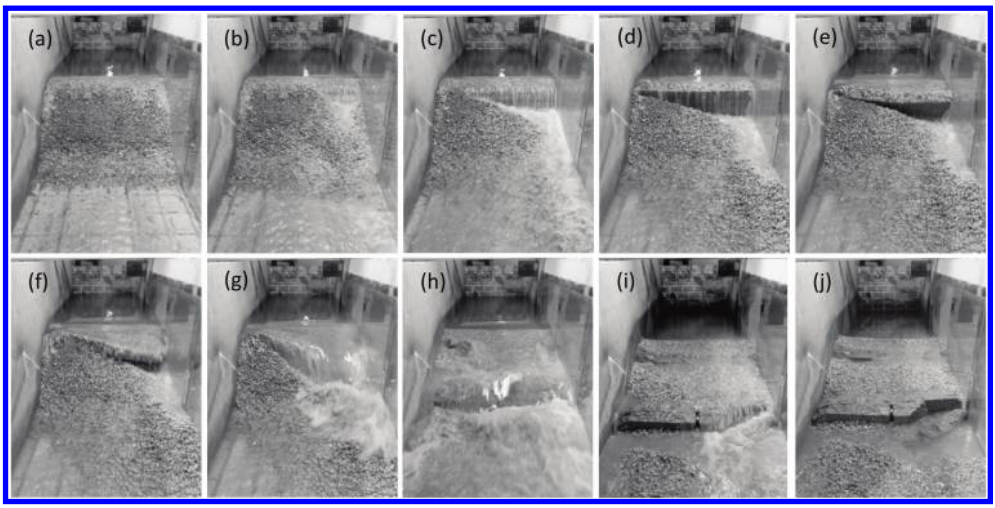

Figure 5. Failure of the cohesive internal core (Test 2).

upstream and downstream rockfill slopes, as can be seen in Figure 5 from (d) to (j). Failure was observed to happen for all width of the clay core.

In Test 3 failure of the internal core occurred in two steps. The erosion of the downstream shoulder consequence of the flow rate imposed to the model (12.4 l/s/m), left a part of the central core unsupported (Figure 6 (a) and (b)). For certain overhang conditions, the external actions forced the unsupported zone of the core to fail. Instead of overturn as in Test 2, this central core opened by means of a vertical crack leading to a flood that washed a considerable part of the downstream shoulder, as can be seen in Figure 6 from (c) to (j). As consequence of the flood, another zone of the cohesive core, once supported, was now unsupported withstanding by its one to the hydrostatic pressure. The flow rate imposed to the physical model was increased to 13.9 l/s/m after observing that the first hydrograph of failure stabilized and caused no more damage in the dam. After some time, the new unprotected zone of the central core failed by means of the same mechanism previously described, i.e., by means of a vertical crack that produced, this time, total failure of the core and dam. Figure 6 from (k) to (o) shows the sequence of the second breakage.

3 DISCUSSION AND CONCLUSIONS

The main conclusion is that, for rockfill dams, the structural failure of the central core or upstream face dominates the release of the water, and so it is the key issue to determine the failure hydrograph. Therefore, and given that the process of erosion is slow compared with the loss of rockfill and the structural failure, the hypothesis of progressive breach opening usually assumed in national regulations is not valid for rockfill dams. Further, given that structural failure may be rather sudden, that hypothesis may be on the unsafe side.

If duration of the flood and peak overtopping flow are high enough, the process of downstream shoulder failure will affect the central core or the upstream face. The failure of these two types of impervious element is quite different and gives rise to a rather different failure hydrograph.

For rockfill dams with upstream face the structural resistance of the concrete or asphalt face governs the failure process. The height of non-supported face that fail suddenly increases with the face structural resistance. Therefore, thinner faces with lower resistances cause a failure process with more but less severe breakage episodes than thicker faces with higher resistances. A failure

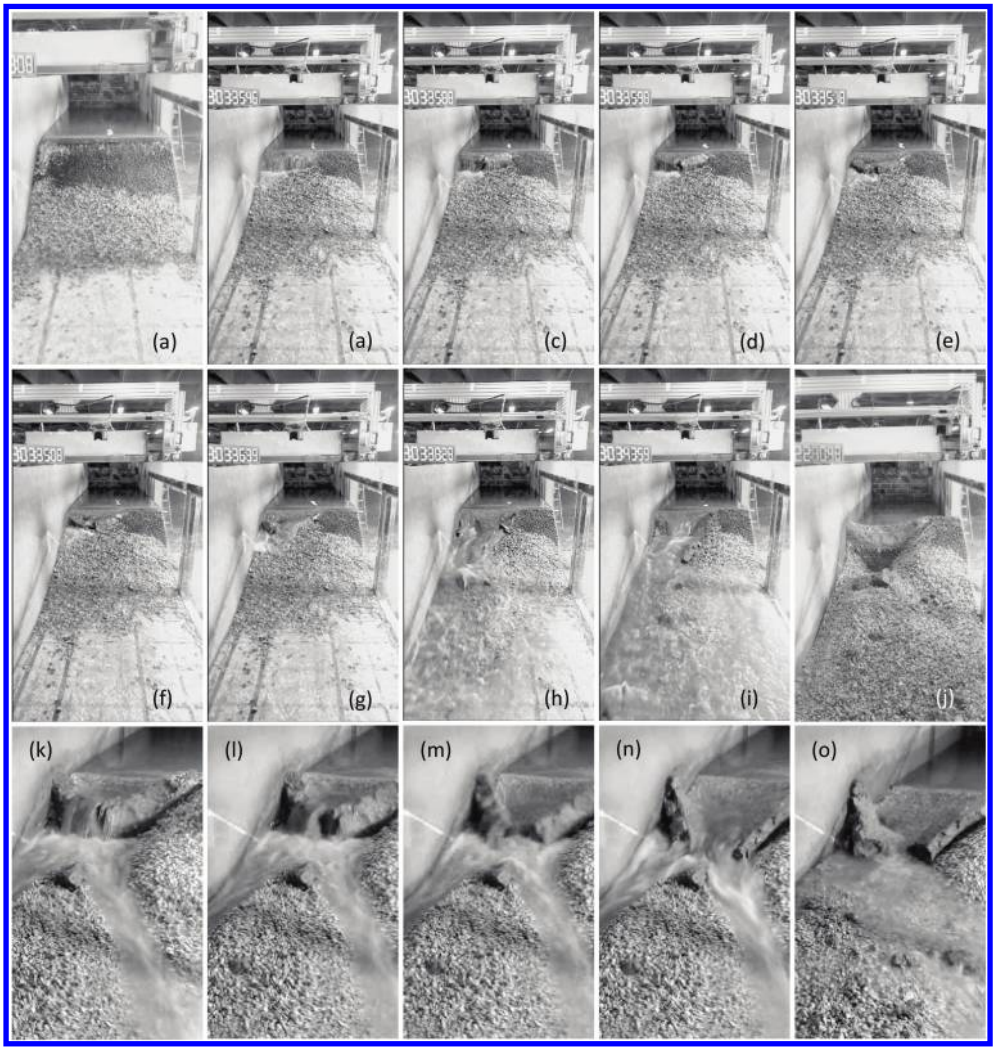

Figure 6. Failure of the cohesive internal core (Test 3).

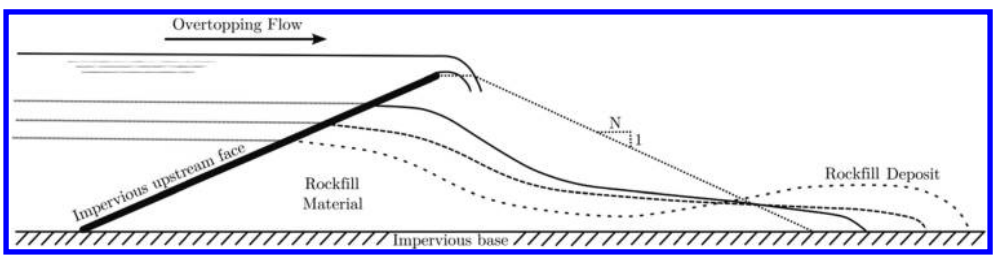

Figure 7. Failure mechanism observed in Test 1.

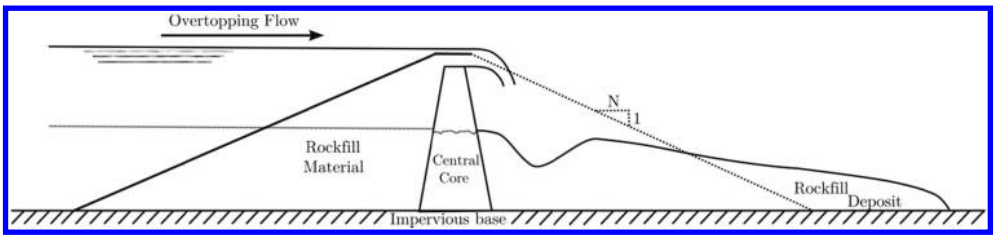

Figure 8. Failure mechanism observed in Test 2.

hydrograph can be expected to be the sum of the failure hydrographs correspondent to the successive breakage episodes. In Figure 7 is schematically drawn the failure mechanism observed for Test 1.

The structural resistance of the central core dominates the failure process of rockfill dams with that type of impervious element. Given that the central core is vertical and much wider than the upstream face, it stands without support better than an upstream face, although the resistance of the clayey material is clearly lower than the resistance of the reinforced concrete of the face. As a consequence, the central clay core accepts an important loss of rockfill of the downstream shoulder without failure and, when failure occur, it gives rise to a more violent failure hydrograph than that due to the failure of a concrete or asphalt face. One or several failure episodes may happen along the overtopping event. The most dramatic failure hydrograph corresponds to a sudden complete structural failure of the core when the rockfill of the downstream shoulder has been completely removed (Figure 8). This scenario is possible for a rockfill dam with a wide central core. It is usually assumed that the worst failure hydrographs are caused by concrete dams, but the scenario of a sudden complete failure is much more credible for a rockfill dam with central core.

Given that the structural failure of the clay core or upstream face dominates the release of water stored in the reservoir, the failure hydrograph may be determined by means of the structural analysis of the impervious element. This way, a more realistic failure hydrograph can be obtained from the own characteristics of the dam under study.

It should be noted that this approach can be useful for the analysis of the effect of an accidental leakage as well as for the analysis of an overtopping scenario. If applicable, the effect of rockfill anisotropy should be considered.

ACKNOWLEDGEMENTS

To Education and Science Ministry of Spain, for financing the investigation project "*Failure of the impervious element of embankment dams under overtopping events and analysis of protections combining physical models with artificial intelligence*" (Rotura del elemento impermeable de presas de materiales sueltos en situación de sobrevertido y análisis de protecciones combinando modelación física e inteligencia artificial) with the code BIA2010-21350-C03-03, corresponding to the Research, Development and Innovation (RDI) Plan of 2007–2011, in the subprogram of Basic non-Oriented Research Projects. It was the performance framework of this research.

REFERENCES

Escatín, C. (1996). In Ministry for the Environment: General Directorate for Hydrayulic Works and Water Quality (Ed.), Technical guide for dam classification as a function of its potential risk (in spanish).

Hahn, W., Hanson, G., & Cook, K. (2000). Breach morphology observations of embankment overtopping tests.

Hanson, G., Cook, K., & Hunt, S. (2005). Physical modeling of overtopping erosion and breach formation of cohesive embankments. Transactions of the ASAE, 48(5), 1783–1794.

Hanson, G., Robinson, K., & Cook, K. (2001). Prediction of headcut migration using a deterministic approach. Transactions of the ASAE, 44(3), 525–531.

Hunt, S., Hanson, G., Cook, K., & Kadavy, K. (2005). Breach widening observations from earthen embankment tests. Transactions of the ASAE, 48(3), 1115–1120.

Morris, M., & Wallingford, H. R. (2005). IMPACT – investigation of extreme flood processes and uncertainty. final technical report.

Toledo, M. A. (1997a). Rockfill dams under overtopping scenario. Study of the water through-flow in gravel type materials and slope stability to mass sliding (in spanish). Technical University of Madrid. ETS de Ingenieros de Caminos, Canales y Puertos. Department of Civil Engineering: Hydraulics and Energy). I(3)

Toledo, M. A. (1997b). Embankment dams slip failure due to overtopping (Q75 R.24). XIX International Congress on Large Dams, Florence. 317–330.

Wahl, T. L., Lentz, D. J., & Feinberg, B. (2011). Physical hydraulic modeling of canal breaches. Hydraulic Laboratory Report HL-2011-09, Bureau of Reclamation, US Department of the Interior, Denver,

Zhang, J., Li, Y., Xuan, G., Wang, X., & Li, J. Overtopping breaching of cohesive homogeneous earth dam with different cohesive strength. Science in China Series E: Technological Sciences, 52(10), 3024–3029. doi: 10.1007/s11431-009-0275-1

Dam Protections against Overtopping and Accidental Leakage – Toledo, Morán & Oñate (Eds)
© 2015 Taylor & Francis Group, London, ISBN: 978-1-138-02808-1

Simulation of the beginning of failure in rockfill dams caused by overtopping

A. Larese, R. Rossi & E. Oñate
International Center for Numerical Methods in Engineering (CIMNE), Barcelona, Spain,
Universitat Politècnica de Catalunya (UPC – BarcelonaTECH), Barcelona, Spain

ABSTRACT: This paper presents the work carried out during the last years for the creation of a numerical model to simulate transient seepage phenomena in rockfill dams when overtopping occurs. The objective is to analyze the trigger of failure mechanism in the downstream slope due to hydrodynamic forces. The current work aims to give a contribution to this field proposing a new computational method of general applicability for simulating, with a unique formulation, the flow throughout and over the dam while failure occurs together with the dam structural response. The numerical results are validated with experiments on scale models rockfill dams.

1 INTRODUCTION

In recent years technology on rockfill dams has developed sensibly due to the advances in soil mechanics knowledge and in all related sciences. Nevertheless the vulnerability of rockfill dams to overtopping still remains their weakest point. In fact, according to the ICOLD bulletin, this is the principal or secondary cause of failure in 31% and 18% of cases respectively. In concrete dams, on the contrary, an overflow does not usually compromise the structure integrity and the causes of failure should be found elsewhere, often in problems in the foundations.

According to the new regulations many dams and dikes exhibit a potential to experience overtopping during high flood events. Climate change induced by global warming is, for instance, one of the main causes that might lead to more devastating flooding than ever. In the case of a dam failure, loss of life and economic damage are the direct cost of such event. Therefore the possibility of predicting the effect of an exceptional flooding is a crucial point to reduce its devastating consequences. Unfortunately this is currently limited by the lack of a precise knowledge of the phenomenon and by the absence of a suitable computational method which can simulate the sudden dynamic change in seepage and flow conditions and predict accurately the subsequent onset and evolution of breaching.

Several examples of dam failures as a consequence of overtopping can be found in the literature. By far the most catastrophic dam disaster ever happened was the failure of the Banqiao dam in 1975 (Figure 1). A Spanish dramatic failure occurs in 1982 at the Tous dam in Valencia (Figure 1), just to mention a pair of them.

These and many other similar historical events demonstrate that when the water exceeds the crest of the dam, the consequences can be catastrophic. An exceptional flooding compromises seriously the structure, leading, in almost all cases, to its failure.

Nevertheless the breaching formation is a relatively slow process. It is never a sudden failure. Chanson in (Chanson, 2009) for example, reported that in the case of the Glashütte dam the complete failure of the structure occurs 4 hours later the beginning of the overtopping. In the case of the Teton dam the reservoir was drained after approximately 12 hours.

Figure 1. Image of Banqiao dam after the failure taken from (Banqiao 2010).

Figure 2. Image of the Tous dam after failure.

This means that when water overpasses the crest of the dam, a seepage process begins leading to the progressive saturation of the downstream rockfill slope. Only after a certain time the first breach usually appears at the toe of the dam due to hydrodynamic forces.

Very little is known on this process that leads to the initiation of failure. A better understanding of how seepage evolves inside the rockfill slopes during the extreme event is therefore of paramount importance to correctly define the structural resistance of the dam. A quantification of the hydrodynamic forces acting during the overtopping may improve significantly the prediction of dam failure.

2 SEEPAGE IN ROCKFILL

It is generally accepted to consider the flow in the pores of rock particles essentially similar to flow in a pipe network but with a more complicated configuration (Toledo, 1997, Taylor, 1948). This analogy is used for the derivation of the resistance law employed for the calculation of the hydraulic gradient due to seepage.

In fact while a linear resistance law (Darcy law) can be adopted in laminar regime, a non-linear one is needed when a turbulent regime is present.

In spite of the unclear definition of the range of validity of Darcy law (i.e. laminar regime) in porous materials (Zeng & Grigg, 2006, Larese et al., 2014), it is generally accepted that the seepage

flow during overtopping phenomena should be considered as turbulent. Therefore a non-linear form of the resistance law must be adopted to correctly evaluate the hydraulic gradient.

Several authors proposed different empirical forms of the resistance equation after the initial work of Forchheimer in 1901 (Li, 1995, Toledo 1997). In this work a quadratic law is chosen to be implemented in the model. The gradient of pressure *i* is given by

$$\boldsymbol{i} = \alpha \boldsymbol{u} + \beta \boldsymbol{u}^2 \tag{1}$$

where **u** is the fluid Darcy velocity and α and β are coefficients that depends on the characteristics of the rockfill materials (Ergun, 1952, Wilkins, 1956, McCorquodale et al., 1978, Stephenson, 1969, Martins et al., 1990).

3 FLUID MODEL

A key point for the complete simulation of the hydrodynamic effect of an overtopping is the capability of the code for simulating at once, not only the seepage evolution, but also the fluid flow in the clear fluid region around the dam. For this purpose the resistance law that governs the seepage evolution is inserted in the balance of linear momentum. This is done providing that the classical Navier-Stokes equations are recovered when porosity is equal to one, that is when no porous medium is present.

Therefore the fluid problem to be solved in a domain Ω for a time instant $t \in (0, T)$ is given by:

$$\begin{aligned} \partial_t \mathbf{u} + \bar{\boldsymbol{u}} \cdot \nabla \boldsymbol{u} + n \nabla p - 2\nabla \cdot \nu \nabla^s \boldsymbol{u} - \boldsymbol{b} n + \alpha \boldsymbol{u} + \beta \boldsymbol{u} \cdot \boldsymbol{u} = \mathbf{0} \; in \; \Omega, t \in (0, T); \\ \nabla \cdot \boldsymbol{u} = 0 \; in \; \Omega, t \in (0, T); \end{aligned} \tag{2}$$

where **u** is the fluid Darcy velocity, $\bar{u}$ is the fluid velocity, p is the fluid pressure, n is the porosity, ρ is the fluid density and ν is the fluid kinematic viscosity, **b** represents the volumetric force and the resistance law is $\mathbf{D} = \alpha y + \beta u \cdot u$. α and β can be arbitrary chosen by the user depending on the characteristics of rockfill and of the flow. All the details of the derivation of equations 2 can be found in Larese et al. (2014).

The weak form of the problem is obtained using a Galerkin formulation. A mixed finite element formulation is used. An Eulerian framework is chosen for the fluid problem and an edge-based approach is used in order to optimize the calculation of the fluid evolution. A semi-explicit fractional step procedure is implemented for the solution of the weak form of the problem and an Orthogonal Sub-grid Scale (OSS) technique is adopted for the stabilization of the pressure and convective term since equal order P1/P1 elements are used. The adoption of a fixed mesh approach for the fluid problem leads to the need of adopting a level set technique for tracking the evolution of the free surface. Additional details on the implementation of the whole algorithm can be found in Larese et al. (2014) and Rossi et al. (2013).

3.1 *Validation*

A series of validation test is carried out to verify the validity of the proposed technique in the simulation of variable seepage inside rockfill.

3.1.1 *Permeameter*

In order to check the correctness in the calculation of the pressure drop due to seepage, the simulations of some empirical tests on a big permeameter are reproduced.

The models mimics the experiments carried out in the Centre for Hydrographic Studies of CEDEX on a permeameter with the following dimensions.

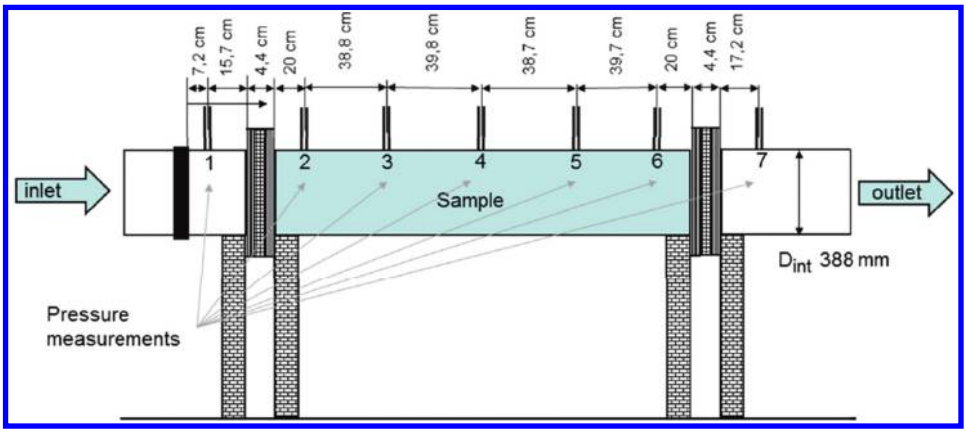

Figure 3. Schematic geometry of the permeameter built in CEDEX. Image curtesy of CEDEX.

Table 1. Characteristics of the different material used in the experiment.

Material	Porosity	Diameter D_{50}
Mat1	0.4133	35 mm
Mat2	0.4074	10 mm
Mat3	0.3983	20 mm

A series of incoming discharges are imposed and the pressure drop is evaluated once a stationary regime was achieved, obtaining the relation between the hydraulic gradient and the imposed velocity.

The variation of the hydraulic gradient was evaluated for three different gravel materials. The characteristics of the material can be seen in Table 1.

Both a 2 and a 3D simulation are carried out leading to good results and confirming that the proposed CFD model correctly reproduces the dissipation induced by seepage.

In Figure 4 a comparison between the experimental data and the numerical results is shown for the three materials.

3.1.2 *Seepage in small scale models of rockfill dams*

An extensive validation of the seepage model has been carried out during the last years taking advanced of the large amount of experiments carried out by UPM and CEDEX in the framework of the XPRES and EDAMS national projects.

All the details of the complete work may be found in Larese et al. (2013), Larese (2012), Larese et al. (2011a), Larese et al. (2011b); here just a brief overview of the main results will be reported.

Figure 5 shows the comparison between experimental data from UPM and numerical results in the case of a small scale homogeneous dam made of gravel with average diameter $D_{50} = 35$ mm and porosity $n = 0.41$. The results are plotted for four different discharges $Q_1 = 25.26$ l/s, $Q_2 = 51{,}75$ l/s, $Q_3 = 69.07$ l/s and $Q_4 = 90.68$ l/s once the stationary regime is achieved. An Ergun resistance law is used in the analysis. For the higher porosities (Q_2, Q_3, Q_4) a progressive failure of the downstream shoulder was observed during the experiment. For that reason the seepage tool was coupled with a code for the evaluation of the structural deformation and the pressure heads are measured once a stable configuration is achieved. The coupled code will be presented in section 4.1.

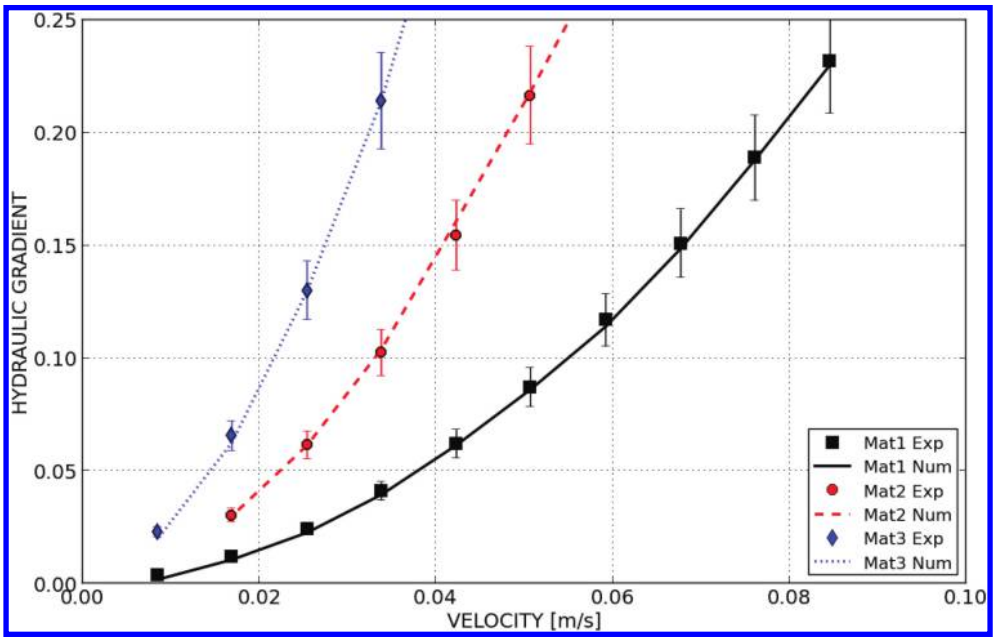

Figure 4. Comparison between experimental data and numerical results for the three different materials.

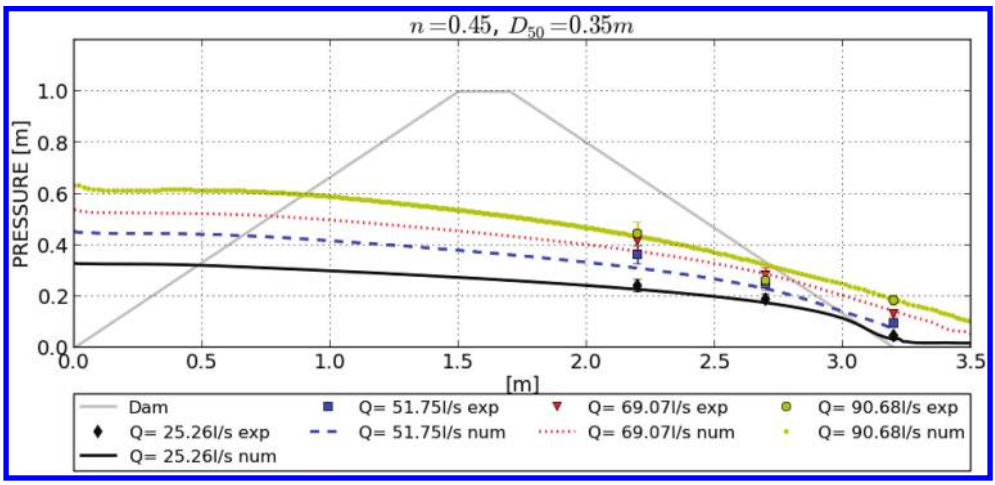

Figure 5. Numerical and experimental comparison of pressure head distribution in a homogeneous dam with four different incoming discharges. Image taken from Larese et al. (2012).

One of the positive feature of the present technique is the possibility of managing **multiple layer porous materials** such as, for example, the small scale dam of Figure 1, Figure 6 which has the body made of gravel with $D_{50} = 1.26$ cm and the protection of the toe made of coarser material ($D_{50\_protection} = 3.5$ mm). The experimental data are taken from Larese et al. (2012). Three incoming discharge have been considered ($Q_1 = 9.2$ l/s, $Q_2 = 11.2$ l/s and $Q_3 = 15.9$ l/s).

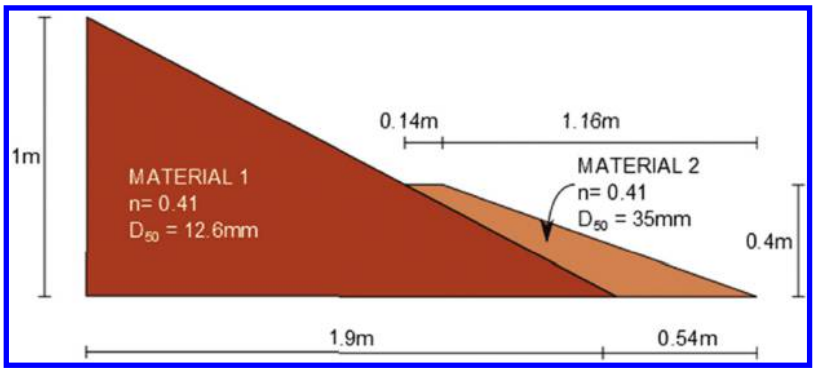

Figure 6. Geometry of the dam with protection on the downstream toe and characteristics of the materials.

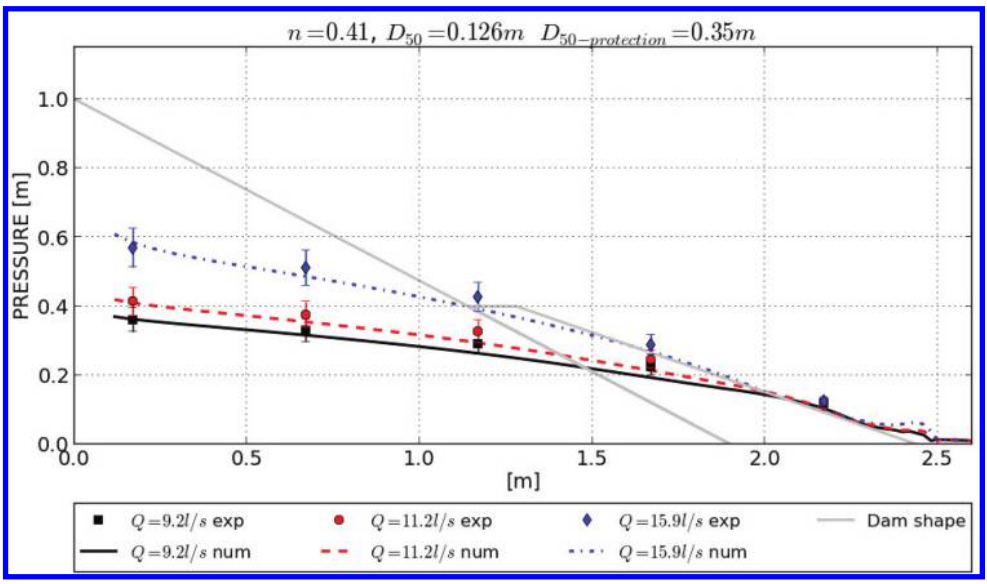

Figure 7. Numerical and experimental comparison of pressure heads distribution at the bottom of the multi-layer dam. Three different incoming discharge have been considered: 9.2 l/s (continuous line), 11.2 l/s (dotted line), 15.9 l/s (pointed line). Image taken from Larese et al. (2014).

In Figure 7 the comparison between the numerical results and the experimental data is shown. The error is always lower than 10% which is the intrinsic error of the data provided during the experiment. The α and β coefficients adopted for the resistance laws of the two materials are those provided in Morán (2013).

All the previous numerical results are compared with the stationary solution; nevertheless one of the important features of the presented tool is the capability to analyze the **transient solution** for any incoming discharge possibly varying in time as well.

Finally it is worth mentioning that the use of a rigorous numerical simulation overcomes by definition the scale effects problems since the simulation is always made in scale 1:1 both in the case of a small scale dam, like those shown in the previous models, and in cases of real dams, such as the one shown in Figure 9.

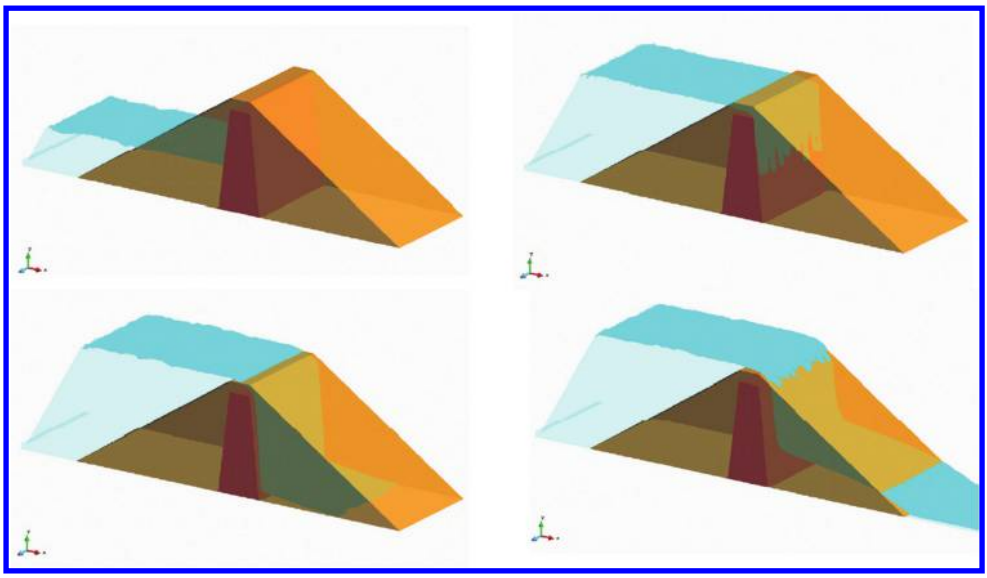

Figure 8. Sequence of seepage evolution in a homogeneous small scale dam with impervious core.

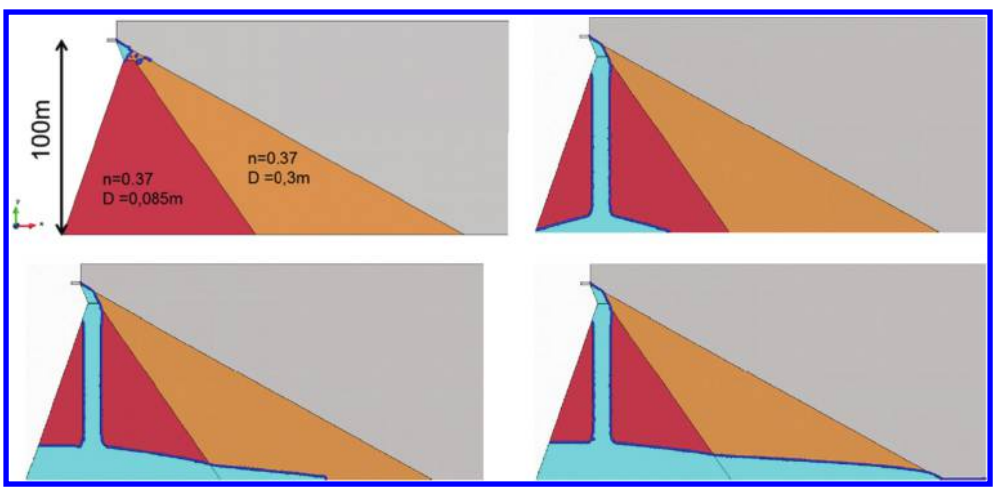

Figure 9. Evolution of seepage in a 100 m height dam composed of two different materials: an internal material with $D_{50} = 8.5$ cm and an exterior (lighter) one of $D_{50} = 30$ cm. Porosity is the same for both materials $n = 0.37$.

4 COUPLED MODEL

The previous seepage tool is coupled with a code to evaluate the structural response with the aim of identifying under which conditions the effects of seepage cause the formation of a breach.

Given that the time scale of the exceptional flooding can be of the order of minutes to hours, the dam material is not suffering from any elastic deformation in the unyielded region (i.e. it is considered as rigid), and its compressibility is neglected. In fact, the volume of the porous matrix is not significantly modified during an exceptional flooding, and the compressibility of a single particle is negligible in comparison with the large deformations to which it may be subjected due to the flooding.

The simulation of the structural response of a slope made of granular material has been faced using a continuous approach despite the intrinsic incoherent nature of the rockfill. This is an acceptable choice under the assumption that the rockfill size is small with respect to the overall size of the structure.

A non-Newtonian constitutive law is adopted for the rockfill. This implies that the material stiffness is controlled by very high values of the viscosity. Only when the yield threshold is exceeded, the viscosity dramatically decreases and the material starts flowing. When the material stops its motion, the viscosity recovers its initial value for which the stress level does not exceed the yield limit. The model developed in this work has its origin in the traditional Bingham plastics using the regularization proposed by Papanastasiou to overcome numerical problems induced by the bilinear stress-strain curve.

In order to include a **Mohr-Coulomb failure criteria** (without cohesion), the possibility of considering a variable yield level is introduced. The structural problem is therefore the following:

$$\begin{aligned} &\rho_s \partial_t \boldsymbol{u}_s + \rho_s \boldsymbol{u}_s \cdot \nabla^s \boldsymbol{u}_s + \nabla p'_s \\ &\quad - 2\nabla \cdot \tilde{\mu} \nabla \boldsymbol{u}_s - \rho_s \boldsymbol{b} + (1-n)\nabla p - \boldsymbol{D} = \boldsymbol{0} \;\; in\; \Omega_s, t\epsilon\,(0,T) \\ &\nabla \cdot \boldsymbol{u_s} = 0 \; in\; \Omega_s, t\epsilon\,(0,T) \end{aligned} \tag{3}$$

where $\mathbf{u}_s$ is the rockfill velocity, p'_s is the effective pressure, and p is the fluid pressure, ρ_s is the rockfill density, $\mathbf{b}_s$ represents the volumetric forces and the apparent viscosity is defined as $\tilde{\mu}_s = \mu_s + \frac{p'_s tg\phi}{\dot{\gamma}}(1 - e^{-m\dot{\gamma}})$ where ϕ is the internal friction angle, $\dot{\gamma}$ is the rate of strain and m is a smoothing coefficient. The equations governing the structural problem are studied in their weak form arriving to the algebraic solution system which is solved with a fully implicit approach. A stabilized, equal-order, mixed velocity-pressure element technology is chosen so to guarantee a locking free behavior.

Since the structural domain is expected to undergo severe deformations as the failure progresses, the kinematic model has to adapt dynamically to such deformations. The Particle Finite Element Method (PFEM) provides the necessary flexibility with a powerful remeshing mechanism (Larese et al., 2012).

4.1 *Validation*

The experiments carried on at the UPM on small scale rockfill dams are used for the validation of the coupled tool.

For each experiment a sequence of incremental discharges is imposed. Every step (characterized by a value of incoming discharge) is analyzed when the stationary regime is reached. When partial failure of the downstream slope or movement of the rockfill appears, a stabilization of the failure mechanism is achieved before calculating the bottom pressure distribution and the advance of failure with the help of a photogrammetric analysis of the new downstream slope stable configuration. The experiment ends when the failure of the dam reaches the crest of the same (Larese et al., 2013).

The advance of failure (B) is defined as the horizontal projection of the distance from the downstream toe of the higher particle that moves. This parameter is given for any incoming discharge and it is compared with the experimental value obtained from the simulation (B_{exp}). The comparison for three different incoming discharges is shown in Figure 10(a–c). For each incoming discharge ($Q_2 = 51.75$ l/s, $Q_3 = 69.07$ l/s and $Q_4 = 90.68$ l/s) the numerical contour fill of displacement is plotted above the experimental digital model of the deformed slope where the line of advance of failure is indicated.

Satisfactory results are achieved with the proposed non-Newtonian model coupled to the free surface/seepage tool presented in the previous sections.

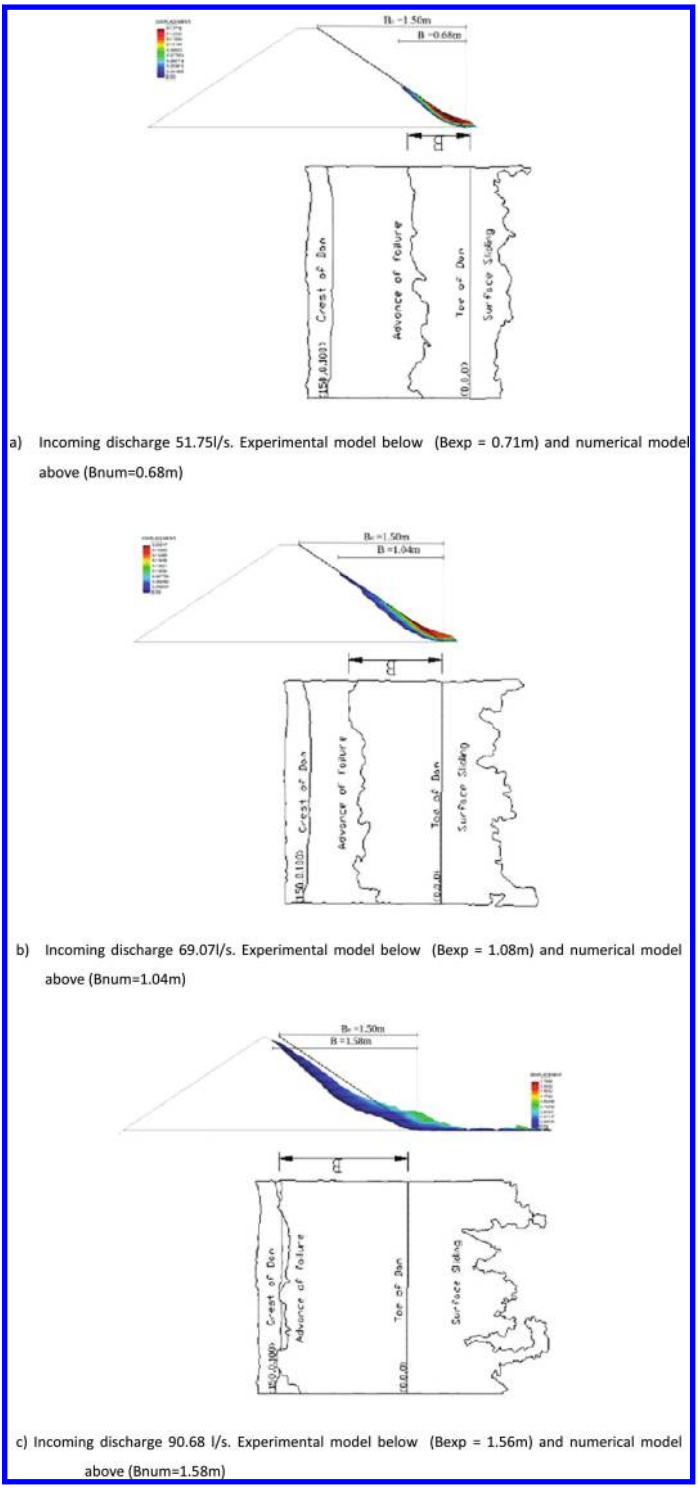

a) Incoming discharge 51.75l/s. Experimental model below (Bexp = 0.71m) and numerical model above (Bnum=0.68m)

b) Incoming discharge 69.07l/s. Experimental model below (Bexp = 1.08m) and numerical model above (Bnum=1.04m)

c) Incoming discharge 90.68 l/s. Experimental model below (Bexp = 1.56m) and numerical model above (Bnum=1.58m)

Figure 10. Numerical and Exmperimental comparison of the advance of failure in a homogeneous small scale rockfill dam with different incoming discharges. Images taken from Larese et al. (2013).

5 CONCLUSIONS

The main achievements of the present work are represented by the creation of a coupled code able to simulate the free surface flow over and throughout the rockfill and to follow the formation of the breach.

In the present work a model for the simulation of the seepage evolution in porous materials and free surface flow is presented. The model is conceived to represent seepage problems that fall outside of the range of validity of the Darcy laws, like rockfill. For this purpose a non-linear resistance law is added as dissipation term in the linear momentum equation. The key aspect of the model is that the governing equations reduce to the classical Navier Stokes equations in the clear fluid region.

The free surface/seepage code is coupled with an algorithm to evaluate the structural response of the dam and the deformation process in case of mass sliding failure mode.

The model is validated using the results of an experimental campaign on small-scale dams, proving that the algorithm accurately reproduces both the fluid and coupled problem.

ACKNOWLEDGEMENTS

The research was supported by the FP7-Capacities ULITES project GA-314891 and ERC Advance Grant SAFECON project AdG-267521.

The authors wants to acknowledge Prof. Miguel Angel Toledo, Dr. Rafa Moran and Mr. Hibber Campos of the Technical University of Madrid (UPM), Mr. Angel Lara and Mrs. Pilar Viña of CEDEX for the experimental results provided for this work.

REFERENCES

Banqiao Dam (2010) *http://worldphotocollections.blogspot.com/2010/01/worlds-worst-ten-deadliest-natural.html*

Chanson, H.; Hayes, W. & Barnes, M. (Eds.) (2009) *Embankments overflow protection system and earth dam spillways.* Chapter 4 of *Dams: Impacts, stability and design* Nova Science Publishers, Inc., NY, USA 101–132.

Ergun, S. (1952) *Fluid flow through packed columns* Chemical Engineering Progress, 48, 89–94.

Larese A. (2012) *A coupled Eulerian-PFEM model for the simulation of overtopping in rockfill dams*. PhD Univeritat Politècnica de Catalunya UPC BarcelonaTech http://hdl.handle.net/10803/108502

Larese, A.; Rossi, R.; Idelsohn, S.R. & Oñate, E. (2012) *A coupled PFEM-Eulerian approach for the solution of porous FSI problems*. Computational mechanics. 50-6, pp. 805–819. ISSN 0178–7675.

Larese, A.; Rossi, R.; Oñate, E.; Toledo, M.A.; Moran, R. & Campos, H. (2013) *Numerical and experimental study of overtopping and failure of rockfill dams*. International Journal of Geomechanics (ASCE) http://dx.doi.org/10.1061/(ASCE)GM.1943-5622.0000345, ISSN 1532–3641.

Larese, A.; Rossi, R. & Oñate, E. (2014) *Finite Element Modelling of free surface flow in variable porosity media.* Archives for Numerical Methods in Engineering DOI: 10.1007/s11831-014-9140-x.

Larese, A.; Rossi, R. & Oñate, E. (2011) *Coupling Eulerian and Lagrangian models to simulate seepage and evolution of failure in prototype rockfill dams* Proceeding of the XI ICOLD Benchmark Workshop on Numerical Analysis of Dams, SpanCOLD, Madrid, Spain, ISBN: 978-84-695-1816-8

Larese, A.; Rossi, R. & Oñate, E. (2011) *Theme B: simulation of the behavior of prototypes of rockfill dams during overtopping scenarios: seepage evolution and beginning of failure* Proceeding of the XI ICOLD Benchmark Workshop on Numerical Analysis of Dams, SpanCOLD Madrid, Spain, ISBN: 978-84-695-1816-8

Li, B. (1995) *Flowthrough and overtopped rockfill dams* Phd thesis: Universty of Ottawa ISBN: 0-612-15734-2

Martins, J. P.; Milton-Taylor, D. & Leung, H. K. (1990) *The effects of non-Darcy flow in propped hydraulic fractures* Proceedings of the SPE Annual Technical Conference.

McCorquodale, J.; Hannoura, A. & Nasser, M. (1978) *Hydraulic conductivity of rockfill* Journal of Hydraulic Research, 16 (2), 123–137.

Morán, R. (2013) *Mejora de la seguridad de las presas de escollera frente a percolación accidental mediante protecciones tipo rapié* PhD Thesis: Universidad Politécnica de Madrid, Madrid, Spain.

Rossi, R.; Larese, A.; Dadvand, P. & Oñate, E. (2013) *An efficient edge-based level set finite element method for free surface flow problems* International Journal for Numerical Methods in Fluids, DOI: 10.1002/fld.3680, 71 (6), 687–716.

Stephenson, D. (1969) *Rockfill in hydraulic engineering* Elsevier Scientific, Amsterdam.

Taylor, D. (1948) *Fundamentals of soil mechanics* John Wiley and Sons, New York.

Toledo, M. (1997) *Presas De Escollera Sometidas a Sobrevertido. Estudio del Movimientos dal Agua a Través de la Escollera e de la Estabilidad Frente al Deslizamiento en Masa* PhD thesis: Universidad Politécnica de Madrid.

Wilkins, J. (1956) *Flow of Water through Rockfill and its Aplication to the Desing of Dams* Proc. 2nd Australia – New Zealand Conference on Soil Mechanics and Foundation Engineering.

Zeng, Z. & Grigg, R. (2006) *A Criterion for Non-Darcy Flow in Porous Media* Transport in Porous Media, 63, 57–69.

Dam Protections against Overtopping and Accidental Leakage – Toledo, Morán & Oñate (Eds)
© 2015 Taylor & Francis Group, London, ISBN: 978-1-138-02808-1

CFD study of the time dependent flow pattern around the slope of rockfill dams in overtopping scenario

J. San Mauro
International Center for Numerical Methods in Engineering (CIMNE), Technical University of Cataluña, Barcelona, Spain

M.Á. Toledo & R. Morán
Technical University of Madrid (UPM), Madrid, Spain

ABSTRACT: The main cause of rockfill and embankment dams failure is overtopping. The dam failure mechanisms are complex and some of the involved parameters are difficult to obtain by physical testing, such as the seepage flow net into the shell. In recent years several numerical models were developed to better understand these failure processes. The main objective of this research was to study the flow pattern around the slope by means of numerical models, in order to simulate rockfill dams behavior in overtopping scenario. A time dependent flow pattern with vorticity was observed around the downstream slope.

1 INTRODUCTION

The safety requirements have always recommended avoiding overtopping spills above the rockfill dams because it could lead to the complete failure of the downstream shell, and to the failure of the impervious element and the release of the stored water. Figure 1 shows the theorical distribution of the inflow, outflow and external flows around the slope, due to overtopping scenarios (Toledo, 1997). These flows are related with the two rockfill dam failure mechanisms which are particle dragging (erosion) and mass sliding (Toledo, 2002). Therefore the detailed study of these flows and their interactions could improve the knowledge about the dam failure mechanisms.

The main objective of the research was to analyze the time dependent flow pattern around the slope of rockfill dams in overtopping scenario by means of numerical methods.

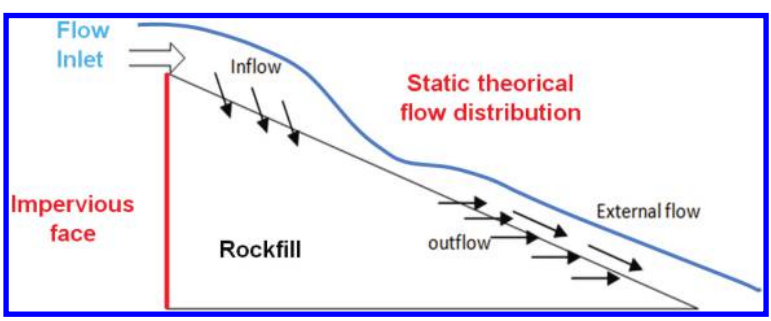

Figure 1. Simplified distribution of inflow, outflow and external flow.

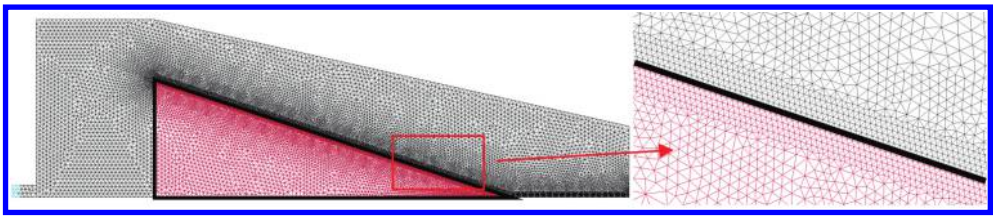

Figure 2. Mesh used in numerical tests, the bold line shows the contour of the dam. Left: complete domain. Right: detail view.

2 THE NUMERICAL MODELS

The research was divided into two phases and for both the numerical simulations were carried out using the specific computational model developed by Larese (Larese *et al*., 2013). This model uses an Eulerian scheme and a level set technique for tracking the evolution of the free surface and the seepage flow. The seepage flow through rockfill dams is reproduced by this computational model by a flow resistance parabolic equation, which the user must calibrate for each tested material. The computational model has been implemented in the open-source object oriented multi-physical analysis platform KRATOS, available at http://kratos.cimne.upc.edu (Dadvand *et al.,* 2010). The mesh used in all numerical tests in the research was triangular and unstructured with the same spatial distribution of maximum element size. The element size around the downstream slope was 0.6 cm and in the remaining calculation domain was 3.5 cm (Fig. 2). All the numerical tests were 2D.

3 THE FLOW RESISTANCE FORMULA

The objective of the first phase of the research was to calibrate the flow resistance parabolic expression for the two rockfill materials studied in this research. The seepage flow through rockfill dams is non laminar and governed by a nonlinear equation represented by a flow resistance parabolic expression (1).

$$i = a \cdot v + b \cdot v^2 \tag{1}$$

where i is the hydraulic gradient, a and b are coefficients which depend on the characteristics of the rockfills, and v is the seepage velocity (Volker, 1969).

Parameters a and b must be obtained to be implemented in the numerical model in order to reproduce the behavior of real rockfill materials (gravels at the model scale). In this phase physical tests and numerical models were performed.

The physical tests were performed at the Hydraulic Laboratory of the ETS de Ingenieros de Caminos, Canales y Puertos of the Technical University of Madrid. Two rockfill dams were built 1 m high; upstream slope 1:1 and downstream slope was 3:1 (N:1). The downstream slope was reinforced by a wire mesh in order to avoid the failure process and geometric deformations; so the seepage domain was kept unaltered. A different material was used for building the dam at each test (M_1:D_{50} = 12.6 mm; and M_2:D_{50} = 35.04 mm; Fig. 3 (Morán & Toledo, 2011)). Both physical tests reproduced an overtopping scenario for three different flow stages; two of them were used to calibrate the numerical model, determining a and b values, and the other flow stage was used for validation.

Next, several numerical models were performed and were also divided into two groups: calibration and validation models.

Figure 3. Rockfill dams built for each physical test. Left: test 1, material M_1. Right: test 2, material M_2.

Table 1. Numerical models simulating overtopping scenarios.

Test	Material	Slope (N)	Flow (q) (l/s/m)
1	M_1	1.5	50
2	M_1	1.5	100
3	M_1	3	50
4	M_1	3	100
5	M_2	1.5	50
6	M_2	1.5	100
7	M_2	3	50
8	M_2	3	100

Calibration models allowed the assessment of the parameters a and b of the flow resistance parabolic equation, by means of an iterative process. The fitting parameter was the height of the free water surface at the reservoir, that was measured at the physical tests.

Validation tests were performed to check the approximation achieved by the flow resistance parabolic equation obtained from the calibration tests.

The resistance formula finally adopted is:

Material M_1: $i = 1.29 \cdot v + 93.65 \cdot v^2$
Material M_2: $i = 0.19 \cdot v + 50.22 \cdot v^2$

4 SEEPAGE FLOW PATTERN

From the previously defined and experimentally verified quadratic resistance formula for the two materials M_1 and M_2, a set of eight numerical models of rockfill dams with vertical impervious element was developed to simulate overtopping scenarios. The main characteristics of the models are summarized in Table 1.

From the results of the different simulation models, it was observed that instantaneous and averaged flow nets were rather different. Streamlines around the slope were markedly curved at any instant in the vicinity of the slope, and specially near the dam toe, and however they were quasi-horizontal at that zone in the averaged flow net (Fig. 4 and 5). This behavior was observed in all the simulated cases.

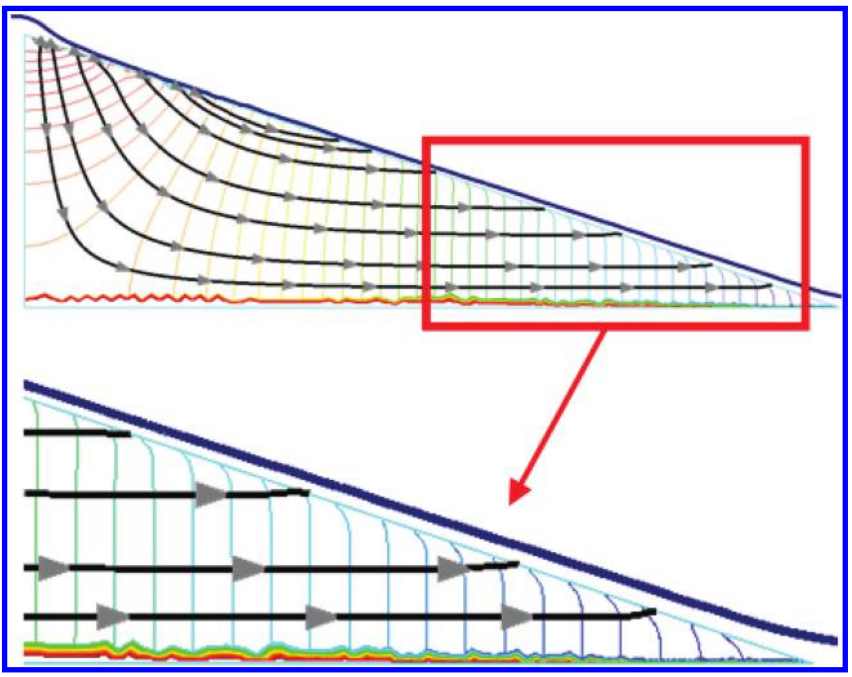

Figure 4. Averaged flow net.

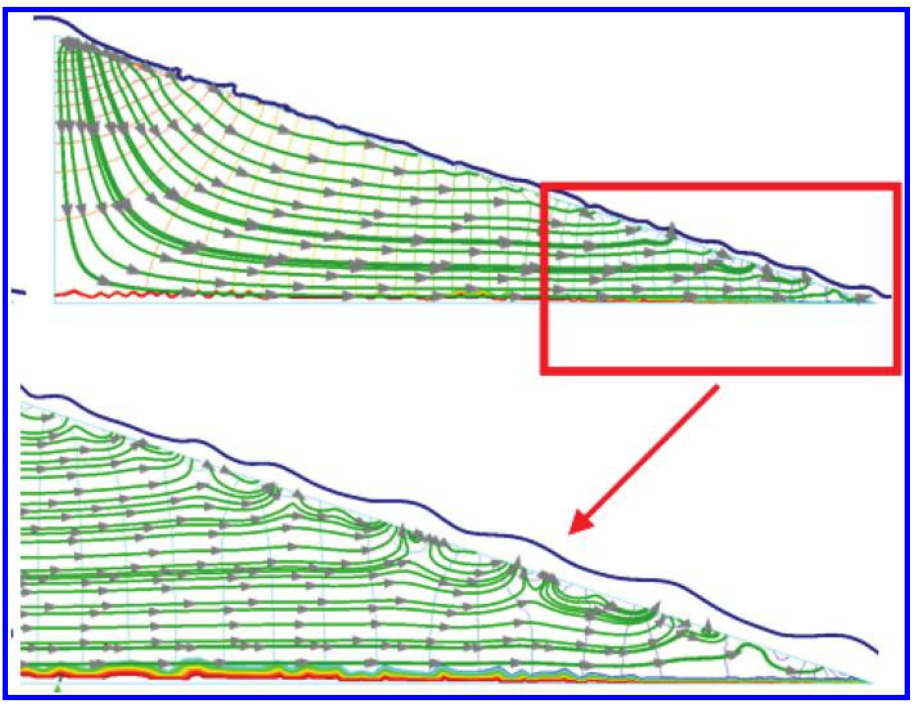

Figure 5. Instantaneous flow net.

5 VELOCITY DISTRIBUTION AROUND THE SLOPE

Velocity distribution around the slope showed the same different patter depending on the consideration of the instantaneous or averaged velocities (Fig. 6). The analysis of instantaneous velocities allows to observe the formation of vortexes in the vicinity of the slope. These vortexes move along the slope.

The flow that emerges through the slope (outflow) changes its direction in order to follow the slope surface and mixes with the high velocity external flow. When these two flows with quite different velocities mix, vortexes are generated. These vortexes cause local instantaneous infiltration at different zones of the slope. Therefore inflow and outflow are observed in the emergency area of the slope at any instant, although the averaged flow is an outflow.

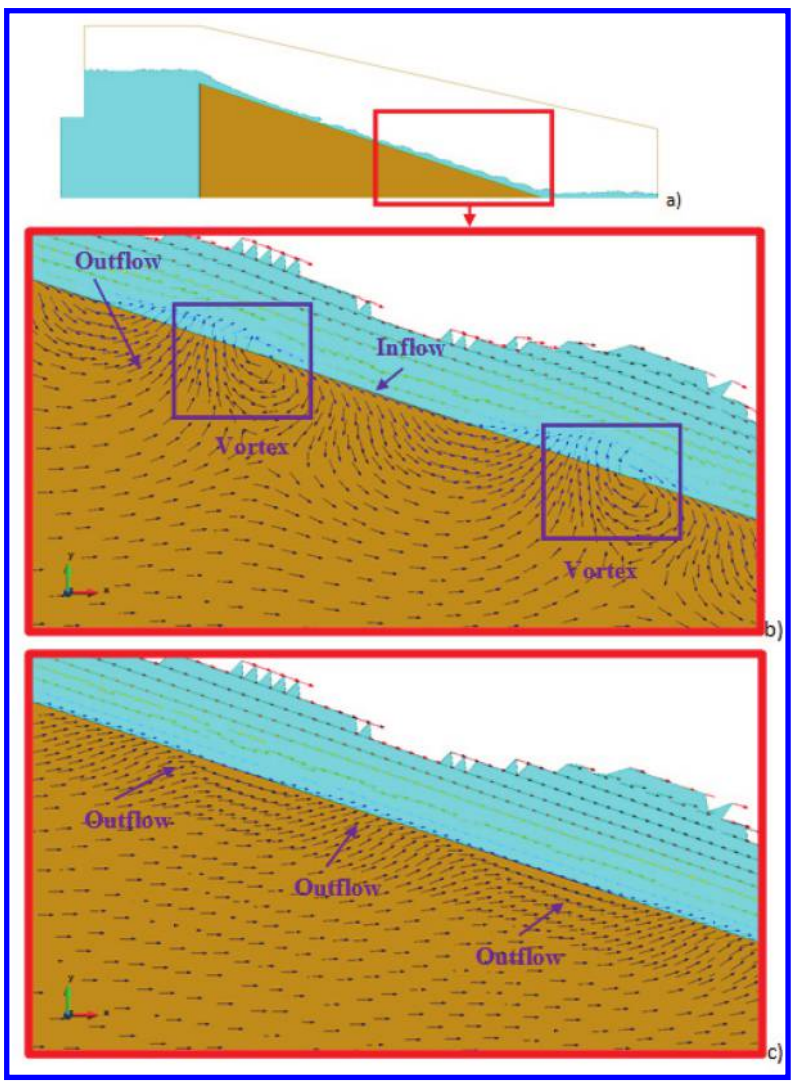

Figure 6. Velocity distribution. a) Overview of the model (Test 8); b) Instantaneous velocity pattern near the toe of the dam; c) Averaged velocity pattern near the toe of the dam.

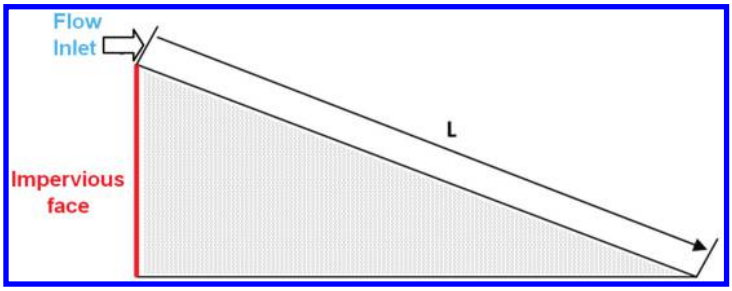

Figure 7. Scheme showing the meaning of parameter L of Figure 8 and 9.

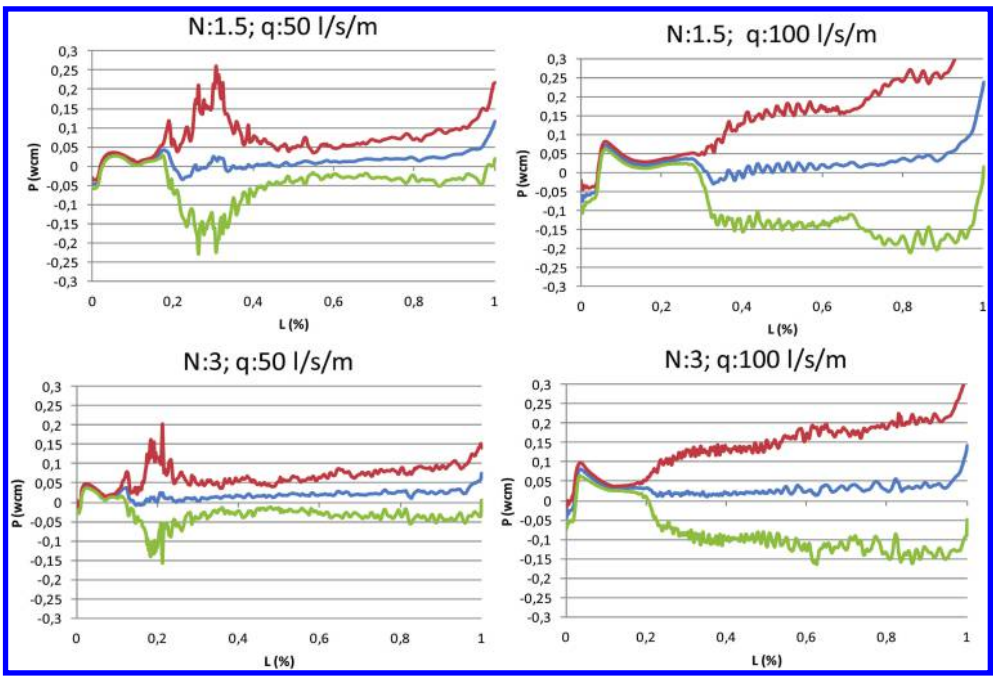

Figure 8. Material M_1. Water pressure on the slope surface. Pressure in water column meters.

The vorticity observed in the numerical models could be incompatible with the size of the stones and the voids between them. In that case, vorticity could be taken just as a tendency. Further experimental work is necessary.

6 PRESSURE FLUCTUATION AROUND THE SLOPE

From the numerical models, a highly fluctuating pressure is observed in the vicinity of the slope. Fluctuation amplitude increases for higher values of the overtopping flow. The water pressure registered at the slope surface is shown in Figure 8 and Figure 9 for the eight simulated cases. Figure 7 shows the parameter L used to define the position on the slope.

The average water pressure obtained was small, but the amplitude between the maximum values and the minimum values of water pressure is remarkable. The alternation between positive and

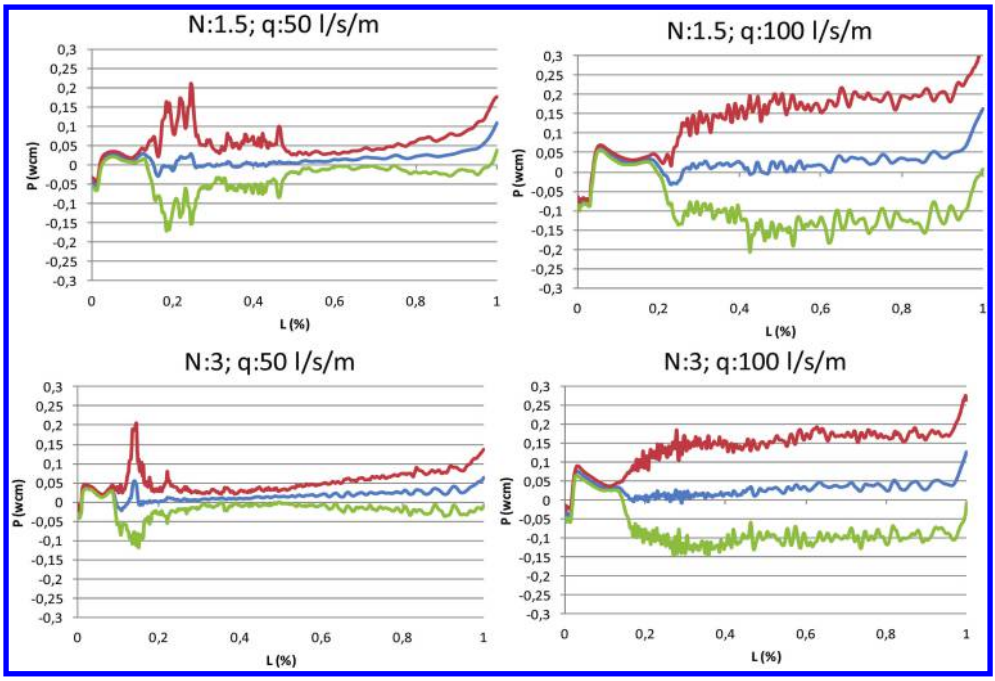

Figure 9. Material M_2. Water pressure on the slope surface. Pressure in water column meters.

negative pressure values could induce significant vibrations in the stones located at the slope surface.

7 CONCLUSIONS

Instantaneous and averaged flow nets and velocity distribution observed were rather different. The analysis of instantaneous velocities allows to observe vortexes which move along the slope. These vortexes cause local instantaneous infiltration in the emergency area of the slope, although the averaged flow is an outflow. This vorticity have to be compatible with the size of the stones and the voids between them, otherwise vorticity should be taken just as a tendency. The remarkable amplitude between the maximum values and the minimum values of water pressure observed could induce vibrations in the stones located at the slope surface.

The numerical models carried out were useful to study the time dependent flow pattern around the slope which would be quite difficult by means of physical tests. The first calibration and validation phase allowed to reproduce the behavior of real materials, so the results obtained could be reproduce by physical tests.

Future research must be orientated to obtain physical evidence of the flow pattern observed by numerical modeling. In addition, the effect of the observed flow pattern on the failure mechanism of a rockfill dam due to overtopping should be analyzed.

ACKNOWLEDGEMENTS

The research was supported by the E-DAM project of the National R+D Plan of the Spanish Ministry of Science and Innovation (BIA2010-21350-C03-00).

REFERENCES

Dadvand, P., Rossi, R. & Oñate, E. (2010) An object-oriented environment for developing finite element codes for multidisciplinary applications. *Archives of Computational Methods in Engineering*, 17, 253–297.

Larese, A., Rossi, R., Oñate, E., Toledo, M. A., Morán, R., & Campos, H. (2013) Numerical and experimental study of overtopping and failure of rockfill dams. *International Journal of Geomechanics, ASCE*.

Morán, R., & Toledo, M. A. (2011) Research into protection of rockfill dams from overtopping using rockfill dowmstream toes. *Canadian Journal of Civil Engineering.* 38, 1314–1326.

Toledo, M. A. (1997) Embankment dams slip failure due to overtopping. *XIX International Congress on Large Dams, ICOLD, 26–30 May 1997, Florence, Italy.*

Toledo, M. A. (2002) Overtopping and Embankment Dams. *Workshop on Stability and Breaching of Rockfill Dams, April 2002, Trondheim, Norway.*

Volker, R. E. (1969) Nonlinear flow in porous media by finite elements. *Journal of Hydraulics Division. Proceedings of the American Society of Civil Engineers*. 4 (9), 2093–2114.

Soft protections for embankment dams

Dam Protections against Overtopping and Accidental Leakage – Toledo, Morán & Oñate (Eds)

Design of overtopping-resistant rockfill dams

M.Á. Toledo & L. Morera
Dam Safety Research Group (SERPA), Technical University of Madrid (UPM), Spain

ABSTRACT: When rockfill dams are subject to overtopping, the mechanisms of mass sliding or particle dragging could appear leading to the complete failure of the infrastructure. In this proceeding, we first study the causes of both mechanisms, gathering specific formulae for assuring both stability conditions. Then we propose a design procedure for making the dam capable of resisting the overtopping situations. This methodology can be eased by the use of the design abacus propounded here.

1 INTRODUCTION

ICOLD statistics (ICOLD, 1995) show that overtopping is the main cause of failure on earth dams, appearing as the main factor in the 31% of the total number of failures, and it is also involved in another 18% of failures as a secondary agent.

A constant trend in the society comprises an increase in the safety requirements for all the critical infrastructures. This increase can be categorized in two conceptual stages: first of all, it is necessary to reach a more accurate specification of the rate of safety-compliance for all the constructions (new projects and existing ones) using quantitative approaches. Going into the second level, safety criteria are being continuously updated, providing more strict conditions that should be also verified for the existing constructions and this can turn some of the current infrastructures into unsafe. Regarding this, as dams are one of the principal subjects of social concern, the flood considerations taken for design have been strongly enhanced. As an immediate consequence, some of the existing dams have insufficient capacity in their outlet works and this could lead to an overtopping situation when considering the updated flood characteristics. Hence, it is necessary to define solutions for adapting the existing dams making them capable of resisting new flood scenarios. For rockfill dams, one possibility could be the design of a rip-rap protection that gives the dam the ability to withstand the updated design-overtopping flow. This type of design can be used, of course, for new projects. There are some project features for which this procedure could be more attractive, such as cofferdam projects, low height dams, or dams with low potential risk in case of failure and also dams with low design discharges.

For the study of overtopping situations affecting rockfill dams, we must first consider two important characteristics of this specific dam typology: 1) the high permeability of the rockfill forming the downstream shoulder (or the whole dam body in the case of a faced rockfill dam) and 2) the rockfill has no cohesion. Therefore, the pore pressure may apply to an important part or the whole rockfill during a flood event, with the corresponding destabilizing effect. No cohesive forces oppose an eventual failure. Considering all the forces involved in the phenomenon, there are two essential mechanisms of failure, which are the mass sliding and particle dragging or erosion (Toledo, 1998; Toledo, Lechuga, & Oñate, 2008). Internal erosion is a third failure mechanism, that will not be treated here, so it should be verified if materials are internally stable.

The two main mechanisms of failure of rockfill dams subject to overtopping are firstly described in this proceeding. Then, a design procedure for overtopping-resistant rockfill dams is proposed together with an example of application.

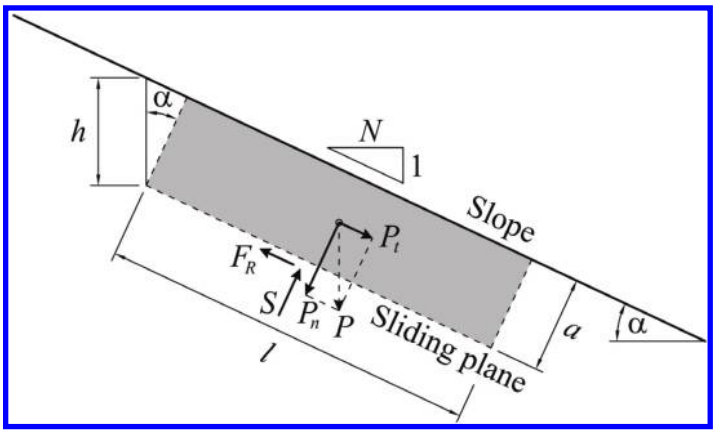

Figure 1. Forces and parameters involved in the calculation of the equilibrium of a shoulder slice (Toledo, 1998).

2 MASS SLIDING

Mass sliding is a common failure mechanism in rockfill dams subject to overtopping. It is characterized by the displacement of groups of stones located near the surface of the downstream shoulder. The main factor which explains this kind of failure in rockfill dams is the development of pore pressures as a consequence of the progressive saturation of the shoulder.

Stability analysis concerning the mass sliding failure (due to an overtopping situation) can be divided into two stages: a) The first one consist in calculating the water pressure field admitting that the shoulder is completely saturated, which is the worse design scenario. This can be done by the application of different numerical methods; b) The second stage comprises the calculation of the safety factor against mass sliding using a limit equilibrium approach.

The main parameters affecting the stability against mass sliding are the following: shoulder slope, angle of internal friction of the rockfill and saturated specific weight of the rockfill. The worst sliding surfaces are shallow and located near the toe of dam.

When analyzing the forces acting on a shallow slice of rockfill parallel to the surface of the shoulder (Fig. 1) (and formulae (1)), is easy to notice that key of the stability problem is the uplift pressure.

$$\left.\begin{aligned} P_n &= \gamma_{e,sat} \cdot a \cdot l \cdot \cos\alpha \\ P_t &= \gamma_{e,sat} \cdot a \cdot l \cdot \sin\alpha \end{aligned}\right\}$$
$$F_R = \frac{\tan\varphi}{F}\left(P_n - S\right) \qquad (1)$$

In which,

- F: safety factor against mass sliding
- $\gamma_{e,sat}$: saturated-specific weight of the dam body rockfill
- φ: internal friction angle of the rockfill
- a: thickness of the slice
- l: length of the slice
- α: angle between the shoulder surface and the horizontal plane
- P: weight of the slice
- F_R: friction force
- S: uplift force

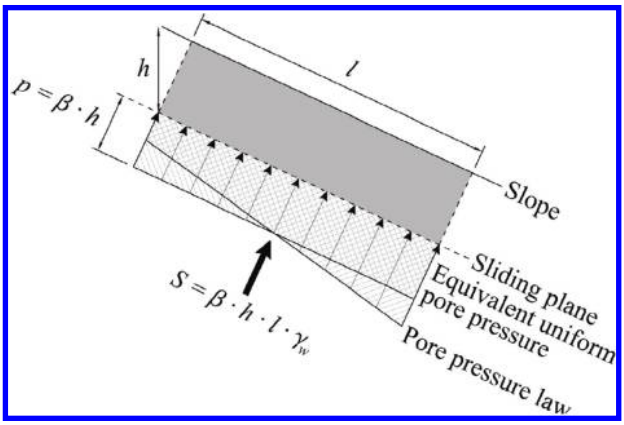

Figure 2. Explanation of the uplift factor, β.

The variable law of uplift pressures acting along the base of the slice can replaced by an equivalent uniform uplift. For that, a new parameter was defined: the uplift factor, β, which represents the uniform uplift pressure expressed as a fraction of the vertical height of the slice. This vertical height has a hydraulic meaning: it may be seen as the hydrostatic pressure at the base of the slide, in the assumption of no water flowing on the slope, outside the shoulder (Fig. 2).

The introduction of the uplift factor allows the deduction of a simple formula for the mass sliding safety factor in overtopping scenario.

$$F = \frac{1}{\gamma_{e,sat}} \left(\gamma_{e,sat} - \frac{\beta \cdot \gamma_w}{\cos^2 \alpha} \right) \frac{\tan \varphi}{\tan \alpha} \tag{2}$$

In which,

– γ_w : specific weight of water

The value of β is 1.0 for values of N > 2.0, and:

$$\beta = -0.32N^2 + 1.52N - 0.77, \text{ for } N < 2.0 \tag{3}$$

The formula for calculating the safety factor against the mass sliding has been experimentally validated (Morán, 2013). For this objective, a set of tests were performed for values of the slope lower than the critical one, defining the critical slope as the minimum slope required for resisting mass sliding, this is, the slope corresponding to a safety factor of 1.0. For the interpretation of the results, Morán introduced the concept of "degree of advance of the breakage" which represents the fraction of the horizontal length between the toe and the crest of the dam that is occupied by the breakage, considering the length at the section in which it takes the maximum value. In the tests, the degree of advance of the breakage obtained due to mass sliding was compared with the value of the slope for different flows and type of materials. The trend in the results confirmed that the degree of advance of the breakage tend to zero when the slope reaches the critical value.

3 PARTICLE DRAGGING

Particle dragging is a general phenomenon widely studied in hydraulics that also is a focus of interest when studying the overtopping situation in rockfill dams. The flow over the downstream slope of a rockfill dam is supercritical, turbulent, spatially non uniform and has high air entrainment.

The bottom has high roughness and this has also high influence on the energy dissipation. Different authors have developed formulas for the design of a stable rip-rap to place on the surface of downstream slope (Abt, Thornton, & Johnson, 1998; Abt, Thornton, Gallegos, & Ullmann, 2008; Jenssen & Soreide, 2004; Lövoll, 2004; Robinson, Rice, & Kadavy, 1998; Skoglund & Solvik, 1995; Solvik, 1991; Stephenson, 1979). Hartung and Scheuerlein (Hartung & Scheuerlein, 1970) provided, based on empirical testing, a procedure that permits the assessment of the necessary equivalent diameter of the rip-rap and downstream slope given the overtopping flow and other rockfill and geometrical conditions. Knauss (Knauss, 1979) introduced some simplifications to the Hartung & Scheuerlein procedure, and proposed a simple formula that can be used for obtaining the rip-rap size necessary for withstanding a given overtopping flow:

$$q_c(m^3/s \cdot m) = 0.84 \cdot \sqrt{G_s(KN)} \cdot (1.9 + 0.8 \cdot \phi - 3 \cdot \sin\alpha) \quad (4)$$

In which,

- q_c: critical flow, in $m^3/s \cdot m$
- G_s: weight of the average rip-rap stone, in kN
- ϕ: compactness coefficient, whose values oscillates between 0.625 (for simply dropped rip-rap) and 1.125 (for manually placed rip-rap)
- α: angle between the shoulder surface and the horizontal plane

There is an interesting case of study in which Hartung, Scheuerlein & Knauss method (HSK method, in advance) was verified: This is the case of Wadi Khasab dam, located in Oman. This dam was designed to withstand an overtopping flow of 3,500 m^3/s, as it does not count with any other outlet work. The HSK method was used and tested in the dam scale model leading to very satisfactory results. The resulting design counts with a 4:1 downstream slope, in which the limiting condition was the particle dragging, not the mass sliding.

Knauss formulation present two main advantages: first, its simplicity, using less and simpler parameters than other formulae, and, second, the fact that it has been tested for the design of an existing dam. Despite these considerations, any other formulation suited for this situations can be used as well.

4 DESIGN PROCEDURE

Designing an overtopping-resistant rockfill dam consist on the assessment of the downstream slope of the dam and the size of the rip-rap, given a previously chosen design-overtopping flow. The downstream slope should be determined taking into consideration the mass sliding mechanism of failure, but also the particle dragging mechanism, given that the stability of a rip-rap stone depends on the slope of the bed where it is placed. However, the size of the rip-rap only depends on the dragging mechanism, admitting a negligible effect of the rip-rap on the overall mass sliding of the rockfill shoulder. It is an assumption on the safe side.

A key issue introduced in the design procedure is the safety factor. It is a well established concept for mass sliding stability using limit equilibrium methods. However, for particle dragging several different approaches are possible.

Regarding mass sliding failure mechanism, with the introduction of the safety factor in the formulae, the stability condition becomes strictly satisfied. At this point, an essential question arises: which value should be chosen for the safety factor? Although the answer is not clear, this value depends on the probability of reaching the overtopping situation. For those cases in which overtopping can be considered an anomalous, a very unlikely situation, a reduced safety factor can be used, and its value could be slightly above 1. However, when the overtopping situation is expected to be reached during normal operation, a common value for the safety factor may be around 1.4.

On the other hand, the particle dragging safety factor can be defined as a reduction factor of the rip-rap rockfill size, but also can be posed as a reduction factor of the critical overtopping flow. This critical value is the overtopping discharge that causes the failure. Rockfill size can be characterized by the weight or the equivalent diameter of the stone corresponding to D_{50} (size of the sieve passing 50% of the rockfill, in weight).

The relation between safety factors associated to weight and to equivalent diameter is easy to draw. Through the Knauss formula, it is possible to find a relationship between the critical-flow safety factor F_q and the other two posed safety factors:

$$F_q = F_d^{1.5} = \sqrt{F_G} \tag{5}$$

The choice of the critical-flow safety factor should be done taking into account the probability of overtopping and the definition of critical flow corresponding to the formula selected for the particle dragging analysis. Hartung and Scheuerlein, and hereinafter, Knauss, defined the critical flow as that causing a generalized failure of the rip-rap, although some stone movements were observed for much lower flows, whose values round 50% of the critical flow (Toledo, 1997). Choosing a value of 2 for the critical-flow safety factor when using the Knauss formula implies accepting some minor stone movements for the foreseen overtopping flow, although a nearly double overtopping flow would be necessary for a generalized failure of the rip-rap.

Safety criteria corresponding to mass sliding and particle dragging should be considered together in order to assess the downstream slope and the rip-rap size. Safety against mass sliding demands a certain slope or gentler, while safety against particle dragging demands a different value for the slope, or gentler, that depends on the stone size. A design step by step is posed. It can be developed using the proposed formula for mass sliding stability and the Knauss formula, or another one, for particle stability. Both formulas can be put together in a double Y axes, assuming a usual saturated unit weight for the rockfill (Fig. 3).

The design procedure can be divided into two conceptually different stages: first, it is necessary to find the values of the slope and the stone size which depends exclusively on the mass sliding and particle dragging considerations combined with the feasibility of the stone size. The first pair of values obtained at this stage could be named as ($d_{\max,ec}, N_{\min,ec}$), which means, respectively, the maximum stone size that can be considered for the economic optimization and the minimum slope that can be considered for the economic optimization. Once this first stage has been reached, is possible to analyze the economical optimization, this is, the result of introducing more gentler slopes that also may permit the utilization of smaller stones. Steps of the design process:

a) Determine or estimate the relevant parameters for mass sliding stability: angle of internal friction, and saturated unit weight of the dam body rockfill.
b) Choose the value of the mass sliding safety factor, depending on the probability of overtopping.
c) Determine the minimum slope (N_c:1) necessary for mass sliding stability using the proposed formula (2).
d) Determine or estimate the design overtopping flow.
e) Choose the value of the critical-flow safety factor, depending on the probability of overtopping and the formula used for particle dragging consideration.
f) Determine, using the Knauss formula or another one, the stone size of the rip-rap necessary from the design overtopping flow (multiplied by the safety factor) and the minimum slope (N_c) previously determined for mass sliding safety.
g) Determine or estimate, from construction and material availability considerations, the biggest feasible stone size, d_f, and then the biggest stone size to be considered, $d_{\max,ec}$.
   For that, if the biggest feasible stone size is bigger than the stone size determined in the previous step *f*, then that previously determined stone size will become the biggest stone size to be considered ($d_{\max,ec}$). Therefore, the slope determined in step *c* (N_c) would be the steepest or the minimum slope to be considered ($N_{\min,ec} = N_c$).

If the biggest feasible stone size is smaller than that determined in step f, then the biggest feasible stone size is the biggest stone size to be considered ($d_{max,ec} = d_f$), and a slope gentler than that determined in step c will be required. In this case, the mass sliding stability does not condition the design process.

h) Only if the biggest stone size to be considered is the biggest feasible stone size ($d_{max,ec} = d_f$), determine, using the Knauss formula or another one, the slope necessary for particle stability from the design overtopping flow multiplied by the safety factor and from the biggest stone size to be considered. The slope so determined would replace the value of the minimum slope (N_c:1) determined in step c.

At this point of the design process, the stage 1 has been completed, the biggest stone size and the minimum slope have been identified, this is, the pair of values ($d_{max,ec}, N_{min,ec}$) has been selected. The following steps only add economical considerations, as the bounds for the values of the slope and the stone size have been just determined:

i) Determine the smaller stone size of the rip-rap to be considered from a practical perspective.
j) Choose a set of stone size values ranging from the smallest to the biggest stone size to be considered.
k) Determine, for every stone size of the chosen set, the necessary slope.
l) Compute the cost of the rockfill shoulder, body rockfill and rip-rap, for every pair of values (stone size, slope).
m) Select for the final design the pair (stone size, slope) with a minimum overall cost.

5 EXAMPLE OF DESIGN

An existing dam counts with the following characteristics:

- Dam height: 30 m.
- Friction angle of the rockfill: 45°.
- Slope: 1.4.
- Length of dam crest: 300 m.
- Spillway capacity: 400 m^3/s.
- New maximum expected flow: 700 m^3/s.
- Biggest feasible stone size: 1 m.

In this example, it is necessary to protect the dam for resisting the new expected flow. According to the procedure above described is possible to design a protection following the next steps:

a) Mass sliding main parameters applied to this problem are the friction angle of the dam body rockfill, $\varphi = 45°$, and its saturated unit weight, that we can assume that has a common value of $\gamma_{e,sat} = 2.2\,T/m^3$.
b) The value chosen for the mass sliding safety factor in this case has been $F = 1.2$, under the consideration of the overtopping situation as extraordinary.
c) Using the formula (2) (or reading the abacus shown on Fig. 3, instead) the minimum necessary slope obtained is $N_c = 2.65$, so it is clearly necessary to adapt the dam to the new overtopping scenario.
d) The design overtopping flow is obtained simply by subtracting the spillway capacity to the total expected flow. Hence, the resulting design overtopping flow is 300 m^3/s, and this implies a flow rate of 1 m^3/s/m.
e) The critical-flow safety factor considering that the overtopping situation has been described as extraordinary, can be set at $F_q = 1.5$ for the Knauss formula (4).
f) Introducing the problem parameters in the Knauss formula (4) (multiplying the flow rate by the safety factor chosen), and considering that the rip-rap is simply dropped, the value obtained for the stone weight is 1.89 kN, which is equivalent to 0.19 T. The corresponding required stone diameter is 0.50 m.

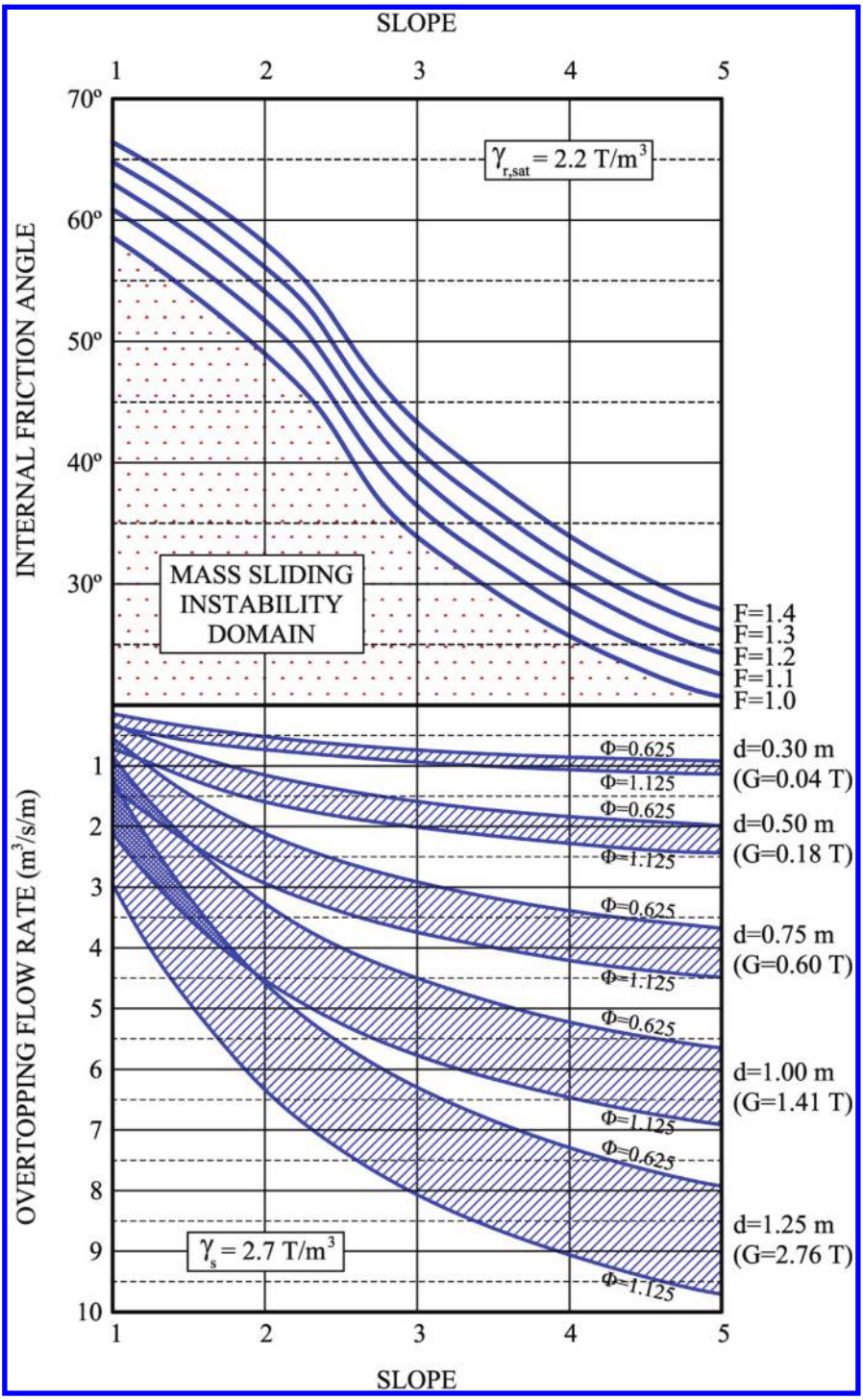

Figure 3. Design abacus, which depends on the problem's essential parameters (Toledo, 1998).

Table 1. Overtopping flow rates obtained for combinations of common values of slope and stone diameter when the overtopping situation is considered unusual.

	q_c (m^3/s/m)	
N	$d_s = 1.0$ m	$d_s = 0.7$ m
2.2	4.9	2.9
2.9	5.7	3.3

Table 2. Overtopping flow rates obtained for combinations of common values of slope and stone diameter when the overtopping situation is considered normal.

	q_c (m^3/s/m)	
N	$d_s = 1.0$ m	$d_s = 0.7$ m
2.85	2.8	1.7
3.80	3.2	1.9

g) Comparing the size just obtained with the feasible stone size of the problem, the biggest stone size to be considered must be the size just obtained, this is, $d_{\max,ec} = 0.50$ m.
h) The problem is out of the assumption made for this step, so the stage 1 of the design process is finished. The preselected pair of values for the minimum slope and the maximum stone size are (0.50 m, 2.65) respectively.

In the remaining steps, economical considerations should be introduced, and the designer may evaluate the total costs of different combinations of gentler slopes with their corresponding smaller stone sizes.

6 REFERENCE VALUES

Depending on the project characteristics, one of the two posed stability conditions will be the most restrictive one. In the following lines, we try to define general ranges of variation in the involved parameters that lead to each limiting condition, considering two safety scenarios:

a) Unusual overtopping situation/Very low potential risk in case of failure ($F = F_q = 1$):

The angle of friction of the rockfill, is commonly located into the range of 35° to 45°. For these values, the necessary slope (with $F = 1$) is about 2.9 and 2.2 respectively. Considering stone diameters of 1.0 m and 0.7 m as two possible limits for the feasible stone size, the previously obtained slopes lead to the overtopping flow rates shown on Table 1.

b) Normal overtopping situation/High potential risk in case of failure ($F = 1.4$, $F_q = 2.0$ or $F_G = 4.0$ or $F_d = 1.6$):

Considering internal friction angles for the rockfill of 35° and 45°, the required slope values (using $F = 1.4$) are 3.80 and 2.85 respectively. On the other hand, reading the design abacus with the value of $F_q = 2.0$, the flow rates shown on Table 2 are obtained.

7 CONCLUSION

When rockfill dams are subject to overtopping flow, two main possible mechanisms of failure may be developed, namely, mass sliding and particle dragging. A design procedure which links together the safety conditions required to withstand both failure causes has been proposed. This methodology can be eased using a design abacus as the one shown on Fig. 3.

Other conclusions of the study are the following:

1) The essential parameters of this phenomenon are the overtopping flow rate, the slope of the rockfill shoulder, the size of the rip-rap and the internal friction angle of the rockfill.
2) In the most part of the situations, the limiting condition is the mass sliding stability, and the sliding associated to this mechanism is always likely to occur in the zone near the toe of the dam.
3) Any system that introduce a reduction in the saturation rate of the downstream shoulder may lead to a reduction in the slope necessary. This idea could be subject of future investigations.

REFERENCES

Abt, S. R., Thornton, C. I., Gallegos, H. A., & Ullmann, C. M. (2008). Round-shaped riprap stabilization in overtopping flow. *Journal of Hydraulic Engineering*, *134*, 1035.

Abt, S. R., Thornton, C. I., & Johnson, T. L. (1998). Riprap sizing at toe of embankment slopes. *Journal of Hydraulic Engineering*, *124*(7), 672–676. doi:10.1061/(ASCE)0733-9429(1998)124:7(672)

Hartung, F., & Scheuerlein, H. (1970). Design of overflow rockfill dams. *Proceedings of ICOLD Montreal Congress, Q36*(R35).

ICOLD. (1995). *Bulletin 99. dam failures statistical analysis*. Paris, France: International Committee on Large Dams.

Jenssen, L., & Soreide, A. (2004). Models tests on the stability of rockfill dams during through flow. *International Seminar. Stability and Breaching of Embankment Dams,* Oslo, Norway. 1–9.

Knauss, J. (1979). Computation of maximum discharge at overflow rockfill dams. (A comparison of different model test results). *Proceedings of ICOLD New Delhi Congress, India, Q50*(R9), 143–160.

Lövoll, A. (2004). Breach formation in embankment dams. results from norwegian field tests. *International Seminar. Stability and Breaching of Embankment Dams,* Oslo, Norway.

Morán, R. (2013). *Mejora de la seguridad de las presas de escollera frente a percolación accidental mediante protecciones tipo repié.* Technical University of Madrid.

Robinson, K. M., Rice, C. E., & Kadavy, K. C. (1998). Design of rock chutes. *Transactions of the ASAE*, *41*(3), 621–626.

Skoglund, M., & Solvik, O. (1995). External and internal erosion in rockfill dams. *International Journal on Hydropower & Dams, 2*(3), 44–47.

Solvik, O. (1991). Throughflow and stability problems in rockfill dams exposed to exceptional loads. *Proceedings of ICOLD Vienna Congress, Austria, Q67*(R20), 333–343.

Stephenson, D. (1979). Rockfill and gabions for erosion control. *Rockfill in hydraulic engineering* (pp. 203–208). Amsterdam, Netherlands: Elsevier Publishing Company.

Toledo, M. A. (1997). *Presas de escollera sometidas a sobrevertido. estudio del movimiento del agua a través de la escollera y de la estabilidad frente al deslizamiento en masa.* PhD Thesis. Technical University of Madrid.

Toledo, M. A. (1998). *Diseño de presas de escollera resistentes al sobrevertido*. Spanish Committee on Large Dams (SPANCOLD).

Toledo, M. A., Lechuga, C., & Oñate, E. (2008). Análisis del comportamiento de las presas de escollera ante un vertido por coronación. *Proceedings of the XXIII Congreso Latinoamericano De Hidráulica,* Cartagena de Indias, Colombia.

Dam Protections against Overtopping and Accidental Leakage – Toledo, Morán & Oñate (Eds)

Isoresistant double slope for the optimization of overtopping-resistant rockfill dams

M.Á. Toledo & L. Morera
Dam Safety Research Group (SERPA), Technical University of Madrid (UPM), Spain

ABSTRACT: Rockfill dams resistant to overtopping require a downstream slope gentler than the critical value for mass sliding failure, that can be determined by means of simple formula. A reduction of the rockfill volume is possible, and a procedure for that purpose is here proposed. It consists on the lowering of the downstream slope value in the upper part of the dam. This change leads to a double-sloped shoulder. The value of the slope and the position of the breakpoint is calculated in such a way that the amount of material used is minimized without decreasing the safety factors against mass sliding and particle dragging.

1 INTRODUCTION

The authors proposed a procedure for designing the downstream shoulder of rockfill dams so that a design overtopping flow could be safely resisted (Toledo, 1998). The main parameters to be determined are the slope of the rockfill shoulder and the stone size of the rip-rap protection. The proposed method assumed a single slope for the whole dam height. However, the worst design conditions occur in the vicinity of the dam toe. Therefore, the chosen single slope, which is critical near the dam toe, is gentler than strictly necessary in the upper region, and a compound slope could be beneficial for lessening the cost of the rockfill shoulder. The option of a continuously-decreasing slope involves an important construction complexity and additional problems, so a compound double slope was considered.

The challenge is to resist overtopping with the same stability safety factor than that obtained with a single slope, but reducing the overall volume by specifying a steeper slope for the upper region. Many pairs of slope values defining a double slope could satisfy this condition. Here, an optimization method is described to obtain the solution with the lowest volume of rockfill given an specified safety factor.

2 PROBLEM SETTING

We first pay attention to the mass sliding issue. The single slope with a safety factor F against mass sliding can be obtained by the formula (Toledo, 1997):

$$F = \frac{1}{\gamma_{e,sat}} \left(\gamma_{e,sat} - \frac{\beta \cdot \gamma_w}{\cos^2 \alpha} \right) \frac{\tan \varphi}{\tan \alpha} \tag{1}$$

In which,

- F: safety factor against mass sliding
- $\gamma_{e,sat}$: saturated-specific weight of the dam body rockfill
- γ_w: specific weight of water

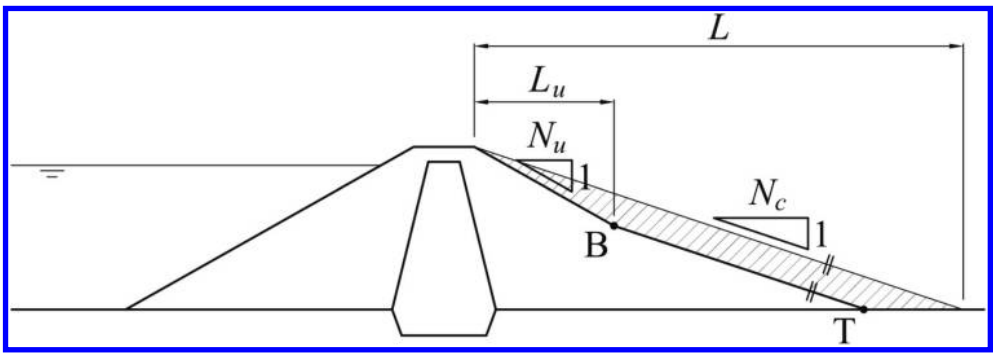

Figure 1. Parameters for the definition of a double-sloped shoulder.

– α: angle between the shoulder surface and the horizontal plane
– φ: internal friction angle of the rockfill

The value of β is 1.0 for slopes (N) gentler than 2:1, and:

$$\beta = -0.32N^2 + 1.52N - 0.77, \text{ for } N < 2.0 \tag{2}$$

The *critical slope* obtained will be denoted as N_c. An isoresistant-double-sloped shoulder may be formed by a lower part with slope $N_l = N_c$, given that no possible reduction in the slope can be posed there, and an upper part with a stepper slope $N_u < N_c$ (Fig. 1). It is also necessary to locate the breakpoint **B**. Any isoresistant-double-sloped shoulder can be defined by only two parameters: the upper slope, N_u, and a position parameter for allocating the breakpoint B. For that purpose, the L_u parameter is defined as the horizontal projection of the distance between the downstream crest vertex and the breakpoint.

The optimization process should allow to determine the pair of values (N_u, L_u) that results in the minimum area of the dam shoulder cross section, keeping the same safety factor as that obtained for the single slope solution.

The parameters affecting the mass sliding problem are: a) geometrical dimensions: the slope of the shoulder, the dam height and the location of the impervious element; b) rockfill properties: the internal friction angle, the saturated specific weight and the coefficients of the resistance formula for the flow inside the rockfill. Some considerations about it:

a) Dam height has no influence in the dimensionless water pressure field, being water pressure expressed as a fraction of the hydrostatic pressure. Hence, it has no influence on the mass sliding safety factor.
b) The location of the impervious element, on the upstream slope or in the middle of the cross section, has no significant influence on the water pressure field near the shoulder surface, where the critical sliding surfaces may be located.
c) The resistance formula for the flow through coarse porous media is not linear, but in practice, the use of a linear model (Darcy's law) implies negligible error when assessing the safety factor against mass sliding.
d) A saturated specific weight of 2.0 T/m^3 was assumed for a practical reason. Given the low influence of this parameter in the usual range of values, the generality of the results is not significantly affected.

These considerations allowed the reduction in the number of parameters involved in the mass sliding problem. Shoulder slope prevailed as the most important geometrical parameter. Regarding material characteristics, it is clear that internal friction angle of the rockfill also plays an essential

role, but it is possible to set it away from the safety factor expression by performing the following operation:

$$F_{\varphi} = \frac{1}{\gamma_{e,sat}} \left(\gamma_{e,sat} - \frac{\beta \cdot \gamma_w}{\cos^2 \alpha} \right) \frac{\tan \varphi}{\tan \alpha}$$

$$F_{38} = \frac{1}{\gamma_{e,sat}} \left(\gamma_{e,sat} - \frac{\beta \cdot \gamma_w}{\cos^2 \alpha} \right) \frac{\tan 38}{\tan \alpha} \tag{3}$$

$$\frac{F_{\varphi}}{F_{38}} = \frac{\tan \varphi}{\tan 38}$$

This means that any variation in the friction angle of the rockfill is equivalent to the corresponding variation of the safety factor performed by using the previous formula.

A friction angle of 38° was arbitrarily chosen for the systematic calculations. The results can be easily applied to any different friction angle by simply using the conversion formula previously shown. The range of safety factor values considered for the calculations was extended to the corresponding range obtained by the application of the previous formula to a reasonable range of rockfill friction angles. If we consider a common range of variation for the friction angle from 35° to 45°, and convert the usual range of safety factors (1.0 to 1.4) to the extremes of the angle range, we obtain the adapted safety factor values of 0.78 and 1.09, for the angle of 35°, and 1.12 and 1.56, for the angle of 45°. Rounding the values obtained to the outer unit, the range resulting range covers from 0.70 to 1.60, and this is the range studied here.

3 OPTIMIZATION ABACUS: THE CONCEPT

For greater generality, it is convenient to use dimensionless parameters. The slope is dimensionless by itself, and the horizontal projection of the distance between the crest downstream vertex of the dam and the breakpoint, L_u, can be divided by the total length of the base of the single slope shoulder, L. The optimization abacus should have three axes:

- X axis: safety factor corresponding to a friction angle of 38° (F_{38}).
- Y axis: slope of the upper part of the double-sloped shoulder (N_u).
- Z axis: the dimensionless projected length of the upper slope (L_u/L).

The use of such abacus would result quite easy:

a) Determine the critical slope value N_c by the mass sliding stability formula (1, 2) with the original friction angle of the dam body rockfill.
b) Convert the value of the desired safety factor to the corresponding safety factor for a friction angle of 38° (F_{38}) by means of the formula (3).
c) Put the F_{38} value on the X axis of the abacus, and obtain N_u and L_u/L from Y and Z axis through the curves. The values of N_u and L_u/L define the position of the breakpoint **B**, and so the double sloped shoulder of minimum volume.

Let see how to obtain the curves of the abacus.

4 ISOSAFETY FUNCTION

An infinite number of breakpoints defining double-sloped shoulders may allow to keep the same safety factor against mass sliding. The optimization process requires the introduction of some additional condition to reduce the amount of points to be considered.

There are two zones which concentrate the local minimums of the safety factor, namely, the toe of the dam (point **T**), and the proximities of the breakpoint **B**. The absolute minimum will be located in one of those regions. If we move the location of the breakpoint **B** by increasing the value of the upper slope, N_u, we will find that the local safety factor against mass sliding, in the vicinity of the breakpoint (F_B), decreases towards the value of the local safety at the dam toe (F_T). This F_T value was previously identified as the global mass sliding safety factor. At this stage, we are interested in finding all the possible breakpoints that satisfy the condition of having a local safety factor F_B with the same value as the safety factor at the dam toe F_T and so, the same value as the overall safety factor against mass sliding. The set of breakpoints that verify this condition can be directly converted into pairs of values of (N_u, L_u/L). We define the *isosafety function* associated to any given safety factor F, as the function giving the relation between the pairs (N_u, L_u/L) which define a double-sloped shoulder in which the safety factors in the proximities of the breakpoint and the toe of the dam have the same value, F.

Then the set of all the possible solutions is limited to those with the same safety factor against mass sliding in both critical zones, the breakpoint and the dam toe. We say that the shoulders that comply with this condition are isoresistant-double-sloped shoulders, regarding the specified safety factor F.

The determination of the isosafety function for an specified safety factor can be performed following these steps:

1) Choose a value for any of the two variables of the function. For example, $N_u = N_{u,1} < N_c$.
2) Choose a value for the other variable involved: L_u/L. This way, a double-sloped shoulder is defined.
3) Determine the seepage network in the downstream shoulder in overtopping scenario.
4) With the pressure field so obtained, determine the safety factor against mass sliding by any limit-equilibrium method. As a result, the corresponding local minima for the safety factors (F_B, F_T) can be associated with the values of $N_{u,1}$ and L_u/L. Two new functions can be represented: $F_B = F_B\ (L_u/L)$ and $F_T = F_T\ (L_u/L)$ corresponding to the specified value $N_{u,1}$.
5) Go back to point 2, but considering another values for L_u/L. By repeating this cycle several times, the functions $F_B = F_B\ (L_u/L)$ and $F_T = F_T\ (L_u/L)$ can be defined. As expected, the values of $F_T = F_T\ (L_u/L)$ remain approximately constant.
6) The intersection between both functions $F_B = F_B\ (L_u/L)$ and $F_T = F_T\ (L_u/L)$, with coordinates ($N_{u,1}$, $L_u/L_{,1}$) defines one point of the isosafety function associated to the safety factor F.
7) Repeat the steps 1 to 6 in order to obtain a set of points ($N_{u,1}$, $L_u/L_{,1}$), ($N_{u,2}$, $L_u/L_{,2}$), . . . , ($N_{u,n}$, $L_u/L_{,n}$), which define the *isosafety function regarding the safety factor F*.

The points that define the isosafety function can be converted into the corresponding coordinates of the breakpoint in the cross section of the dam. Setting the origin in the upper vertex of the shoulder, the 'x' coordinate equals L_u/L and the 'y' coordinate equals $-(L_u/L)/N_u$. The curve obtained applying this transformation to the isosafety function defines the locus of the positions of the breakpoint **B** such that $F_B = F_T = F$, and will be called the *isoresistant path of the breakpoint **B** regarding the safety factor F*. It can be accurately approximated by a linear relationship and the dam toe is one of its points.

5 THE OPTIMUM ISORESISTANT-DOUBLE-SLOPED SHOULDER

Given that the isoresistant path is a straight line, if the breakpoint (**B**) moves from the dam toe (**T**) following up the *isoresistant path of the breakpoint **B** regarding the safety factor F*, the volume of the shoulder will progressively decrease. But, as the upper slope cannot be as steep as we want, there must be a limit in that ascending travel of the breakpoint beyond which the upper slope will become unstable. That upper limit corresponds to the optimum position of the breakpoint ($\mathbf{B}_{opt}$) (Fig. 2).

The exact location of the optimum breakpoint can be determined by successive approximations. It was done and results are shown in table 1.

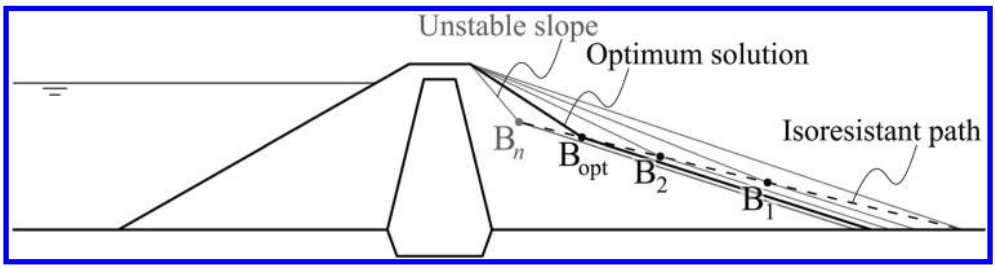

Figure 2. Concept of the isoresistant path of the breakpoints regarding a given safety factor.

Table 1. Position of the optimum breakpoint corresponding to different values of the safety factor.

F	N_u	L_u/L (%)
0.700	1.25	22.55
1.000	1.75	10.82
1.338	2.40	6.56
1.630	3.00	5.10

It is now possible, using the data from table 1, to draw an optimization abacus such as described before in paragraph 3, where the use of the abacus for determining the optimum isoresistant-double-sloped shoulder is explained (Fig. 3).

The optimization process seeks to reduce the rockfill needed for the downstream shoulder while maintaining an specified safety factor. Therefore, it is interesting to estimate the reduction achieved by the isoresistant-double-sloped shoulder compared with the single slope solution. It may be expressed as a function of the main parameters, and it is convenient to express that reduction in relative terms, as a percentage of the total volume of the original single-sloped shoulder. This calculation requires the consideration of another slope value, N_0, that may represent the slope of the internal face of the rockfill shoulder, e.g., the slope of the impervious core on which the rockfill is lying, or, alternatively in case of dam conditioning, the slope of the pre-existent rockfill shoulder. The results are shown in the *volume reduction abacus* (Fig. 4).

6 THE COMPLETE METHOD OF THE ISORESISTANT-DOUBLE-SLOPED SHOULDER

In order to complete the method for optimizing the design of a overtopping resistant rockfill dam, the condition of particle dragging must be considered too. That can be done following the following steps:

a) Categorize the likelihood for the overtopping situation: Normal, exceptional or extreme.
b) According to this categorization, specify the values for the safety factors regarding mass sliding (F), and particle dragging (F_q, when the factor acts on the overtopping flow). It is a designer decision, taking into account the regulations that could be applicable. In the absence of a different criterion the following values could be specified, and if the Knauss formula (Knauss, 1979) is used for the particle dragging analysis, the values for safety factors shown on table 2 could be used.
c) Determine the slope for satisfying mass sliding condition (N_{cs}), by means of the formula (1). It is admitted that the dam body rockfill is chosen according to the availability in the vicinity of the dam site, and therefore its resistant characteristics are not involved in the optimization process.

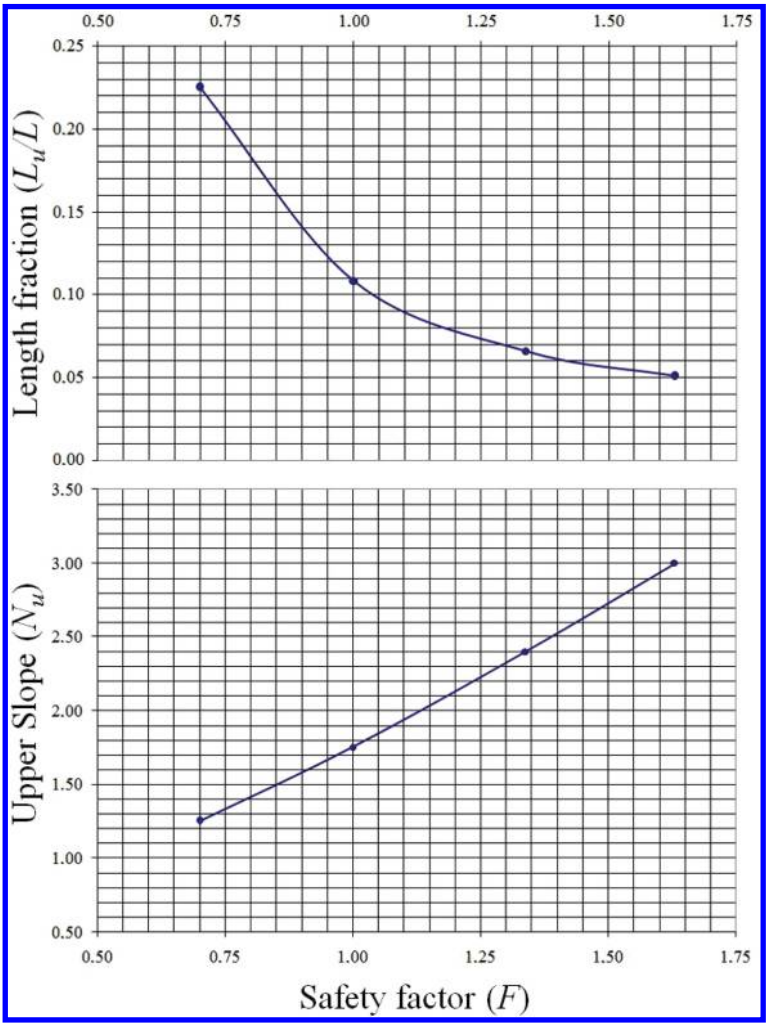

Figure 3. Optimization abacus (Toledo, 1998).

Table 2. Reference values for the safety factors considering different likelihoods for the overtopping event.

Situation	F	F_q
Normal	1.4	2.0
Exceptional	1.2	1.5
Extreme	1.1	1.2

d) Determine or specify the maximum overtopping flow that the dam should be able to withstand, the *critical overtopping flow* (q_c).
e) Determine the maximum stone size (equivalent diameter, d_{max}) to be considered for the rip-rap. It depends on the availability of rockfill and machinery for moving and placing the rockfill. It may often be the size above which a significant increase in costs happens due to the managing difficulty. The chosen size might be changed after the evaluation of the partial results of the method.

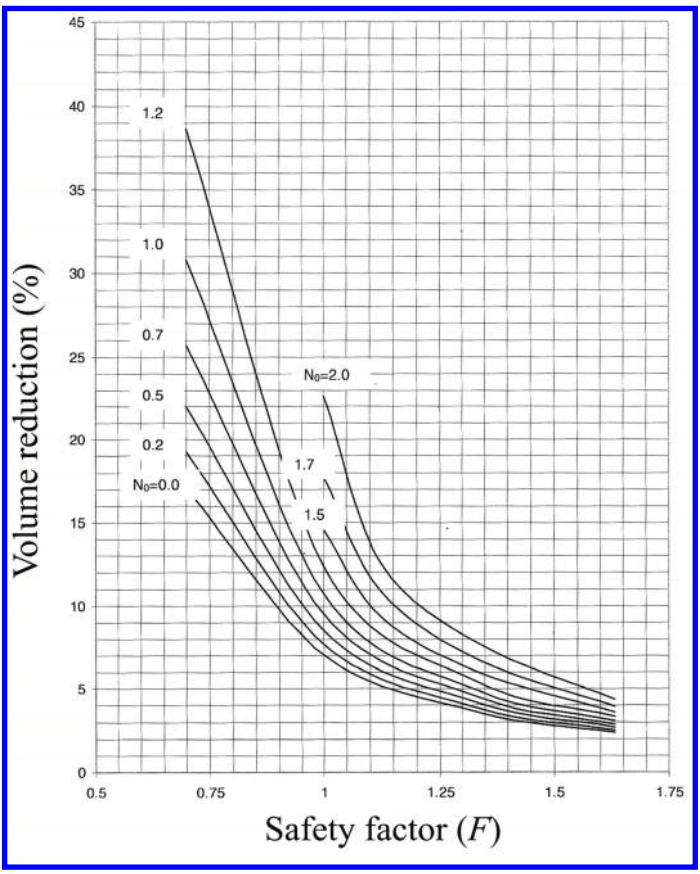

Figure 4. Volume reduction abacus (Toledo, 1998).

f) Select a method for placing the rip-rap. This significantly affects the particle dragging resistance. If the stones are placed thoroughly, one by one, it is preferable to put their largest dimension parallel to the flow direction and the smallest face as the base on the slope.

g) Determine the minimum slope (N_{cd}) for avoiding the particle dragging failure with the specified safety factor (F_q). This can be done using the Knauss formula or any other one (Hartung & Scheuerlein, 1970; Solvik, 1991):

$$q_c(m^3/s \cdot m) = 0.84 \cdot \sqrt{G_s(KN)} \cdot (1.9 + 0.8 \cdot \phi - 3 \cdot \sin\alpha) \quad (4)$$

In which:

- q_c: critical flow, in $m^3/s \cdot m$
- G_s: weight of the average rip-rap stone, in kN
- ϕ: compactness coefficient, whose values oscillates between 0.625 (for simply dropped rip-rap) and 1.125 (for manually placed rip-rap)
- α: angle between the shoulder surface and the horizontal plane

h) At this stage, the comparison between both calculated slopes should be made.
If $N_{cd} > N_{cs}$, that means that the particle dragging condition is more restrictive than the mass sliding one. Therefore, the only possibility for optimizing the design is to try with smaller stone sizes and their correspondent gentler slopes.

If $N_{cd} < N_{cs}$, means that mass sliding condition is more restrictive. In consequence, the optimization process through a double slope can go on.

i) Estimate the volume reduction that could be obtained due to the design of a double-sloped shoulder. This operation can be easily performed by means of the *volume reduction abacus* (Fig. 4).

j) If the expected volume reduction is interesting, then the optimum isoresistant double slope ($N_{u,\min}$ and L_u/L) should be determined with the *optimization abacus* (Fig. 3).

k) The particle dragging phenomenon must be considered again. Compare $N_{u,\min}$ with N_{cd}.
If $N_{u,\min} > N_{cd}$, the value for the slope on the upper section of the slope also satisfies the particle dragging condition for stone stability. In fact, smaller stone sizes for the rip-rap can be specified while still satisfying the particle dragging condition. The minimum stone size should be determined for both, the upper and lower sections of the slope.
If $N_{u,\min} < N_{cd}$, the particle dragging condition is limiting the slope of the upper section. Therefore, a slope $N_u = N_{cd}$ should be specified. Then we must determine the corresponding new breakpoint **B** in the isoresistant pathway. In the lower section of the slope, a reduction of the rip-rap size is possible to strictly verify the particle dragging condition.

Following these steps, an optimum design is achieved with the optimum distribution of slopes between upper and lower sections and minimum stone size in each section of the slope.

7 SUMMARY AND CONCLUSIONS

The study of rockfill dams subject to overtopping revealed that worst conditions for mass sliding occur in the vicinity of the dam toe. So a steeper slope can be specified for the upper section while still satisfying the condition of safety against mass sliding, allowing a reduction of rockfill volume to form the downstream shoulder of an overtopping resistant rockfill dam. The condition of stability of stones against particle dragging was also considered for the complete method of optimization.

For the practical application of the proposed method a question arises about the particular stability condition of the stones located in the vicinity of the breakpoint where the slope changes. It is clear that an abrupt change of the slope would be dramatic for the stability of stones in that area. So, a progressive change of the slope, limited to that area of the breakpoint, through a curve with adequate radius of curvature is required. Anyway, the designer should pay special attention to the area where the slope changes and provide a solution for avoiding the failure to initiate at that critical zone.

REFERENCES

Hartung, F., & Scheuerlein, H. (1970). Design of overflow rockfill dams. *Proceedings of ICOLD Montreal Congress*, Q36(R35).

Knauss, J. (1979). Computation of maximum discharge at overflow rockfill dams. (A comparison of different model test results). *Proceedings of ICOLD New Delhi Congress, India*, Q50(R9), 143–160.

Solvik, O. (1991). Throughflow and stability problems in rockfill dams exposed to exceptional loads. *Proceedings of ICOLD Viena Congress, Austria*, Q67(R20), 333–343.

Toledo, M. A. (1997). *Presas de escollera sometidas a sobrevertido. estudio del movimiento del agua a través de la escollera y de la estabilidad frente al deslizamiento en masa*. PhD Thesis. Technical University of Madrid.

Toledo, M. A. (1998). *Diseño de presas de escollera resistentes al sobrevertido*. Spanish Committee on Large Dams (SPANCOLD).

Dam Protections against Overtopping and Accidental Leakage – Toledo, Morán & Oñate (Eds)

Practical challenges and experience from large-scale overtopping tests with placed riprap

P.H. Hiller & L. Lia
Department of Hydraulic and Environmental Engineering, Norwegian University of Science and Technology, NTNU Trondheim, Norway

ABSTRACT: Downstream slopes of rockfill dams in Norway are protected with placed riprap against considerable leakages through the dam or overtopping. For this purpose, oblong stones are placed one by one in an interlocking pattern. Six large-scale field tests were run to increase the knowledge about placed riprap on steep slopes. The 3.5 m high and 10 m wide test dams withstood unit discharges of over 8 m^3/s/m. There is a presentation of the facilities, test set-up and measuring equipment with focus on practical issues and challenges connected with large-scale tests in order to share useful experience about such uncommon experiments.

1 INTRODUCTION

Hydropower generates 99% of the electricity in Norway which means that there are a large number of dams and reservoirs in the country. There are 182 rockfill dams exceeding 15 m in height (NVE, 2014) and most of them have a downstream slope of 1:1.5 (vertical: horizontal, corresponding to an inclination of 67%). The main advantages of rockfill dams in Norway are that rock is a suitable construction material in cold climate conditions and rock is widely available, even in remote areas. Furthermore, rockfill dams are constructed with low cost construction methods, they are durable and hard to destroy.

In order to protect the downstream slope of rockfill dams against accidental loads caused by substantial leakage through the dam or by overtopping, the Norwegian dam safety regulation (OED, 2009) requires a placed riprap on the downstream slope. The stones forming the riprap have to be placed one by one in an interlocking pattern with their longest axis inclined towards the dam axis as shown in Figure 1. An updated dam safety regulation (OED, 2009) was implemented in 2010 and has a fully retroactive effect (see Midttømme et al. (2010) for details). Most of Norwegian rockfill dams (87%) were finished before 1990. As a consequence, many rockfill dams have to be upgraded after regular reassessment according to the updated regulation to meet the requirements such as freeboard, width of the dam crest and spillway capacity in combination with updated calculations of the design flood. It might be necessary to reconstruct the placed riprap on the downstream slope if the upgrading requires widening or heightening of the dam. An example of such an upgrading and possible challenges is described on the basis of the 129 m high Svartevatn dam in Hiller et al. (2014).

Reconstruction of the placed riprap is time consuming and expensive. Furthermore, a brief literature review revealed that data for placed riprap on slopes similar to the downstream slopes of Norwegian rockfill dams are rare. Peirson et al. (2008) investigated placed rock as erosion protection on slopes of up to 1:2.5 and mention interlocking as a stabilizing factor not previously incorporated in riprap design methods. Design relationships for riprap without any placement pattern are summarized by Abt et al. (2013). Dornack (2001) carried out physical model tests with placed riprap mainly on slopes with an inclination of 1:2 and a few with 1:1.5. Large-scale field tests with rockfill dams but without placed riprap on the downstream slope were conducted in

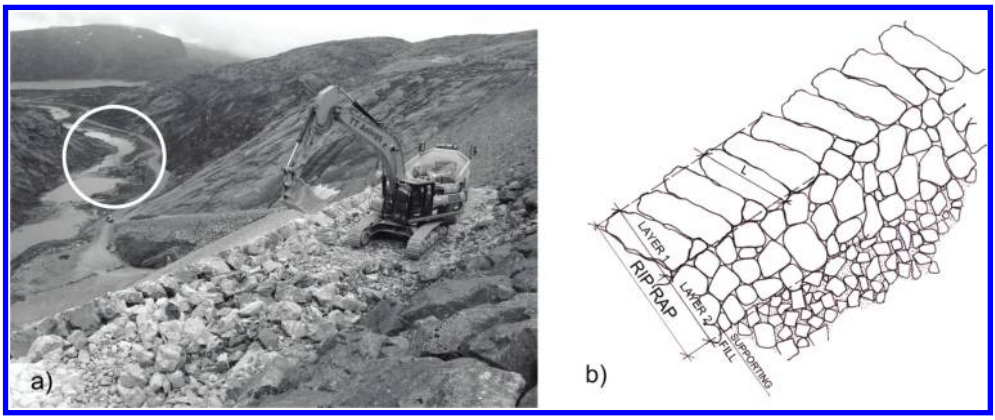

Figure 1. a) Construction of placed riprap on the Svartevatn dam. The research site at the spillway outlet is located within the circle. The placed riprap as well as the layer below and the supporting fill are visible in a) and b). b) Section through layer 1 and 2 of the placed riprap and parts of the supporting fill (from Lia et al., 2013). The inclination angle of the riprap stones is the angle between the longest axis and the surface of the dam.

northern Norway to investigate the breach formation (Løvoll, 2006). A Norwegian research project was initiated in 2011 to increase the knowledge of the stability of placed riprap on steep slopes. In this framework, a PhD study will develop design tools for optimal riprap protection of rockfill dams. The objectives are (i) an in-depth literature study of riprap design and practical solutions for steep slopes; (ii) to identify the hydrodynamic forcing due to the flow over steep slopes and through flow; (iii) execution and analysis of laboratory and large-scale field tests; and (iv) the identification of the relevant parameters of the riprap material and the effect of placement patterns.

This article focuses on practical challenges associated with large-scale tests based on the experience from six overtopping field tests in Norway conducted in 2012 and 2013.

2 METHOD

The Norwegian University of Science and Technology (NTNU) has the opportunity to run large-scale field tests close to the Svartevatn dam in south-western Norway, i.e. at a different site than the tests in Løvoll (2006). Two test series were run in 2012 and 2013. The test site is situated in the outlet channel of the spillway tunnel as shown in Figure 1 and Figure 2.

Water from the reservoir is discharged through a gated outlet which is located 44 m below the full supply water level. Consequently, the discharge is controlled by the gate opening and the water level in the reservoir. In addition, a limnograph registers the discharge 300 m downstream of the test site. Approximately 3.5 m high and 10 m wide permeable test dams were built in the outlet channel. The upstream slope of the test dams was 1:1 and the downstream slope 1:1.5. A section of a test dam is shown in Figure 3. For the tests in 2012 full-scale riprap stones with a median diameter $d_{50} = 650$ mm were used. The riprap stone size was reduced to $d_{50} = 550$ mm for the tests in 2013. However, full-scale riprap stones were used in the bottom, along the sides and for the dam crest. The grain distribution curves for the riprap stones and for the supporting fill are presented in Figure 4.

In 2012, Lia et al. (2013) investigated the influence of different inclination angles of the longest axis of the riprap stones on the stability of the placed riprap. The test set-up as well as the results are summarized in Table 1. An experienced operator constructed the placed riprap with an excavator with a gripper from downstream of the dam. The stone axes were measured with a yardstick and

Figure 2. Test site in the outlet channel of the spillway of the Svartevatn dam in Norway. Test dam 3 in 2012 which did not fail completely in the front and the 129 m high Svartevatn dam in the background.

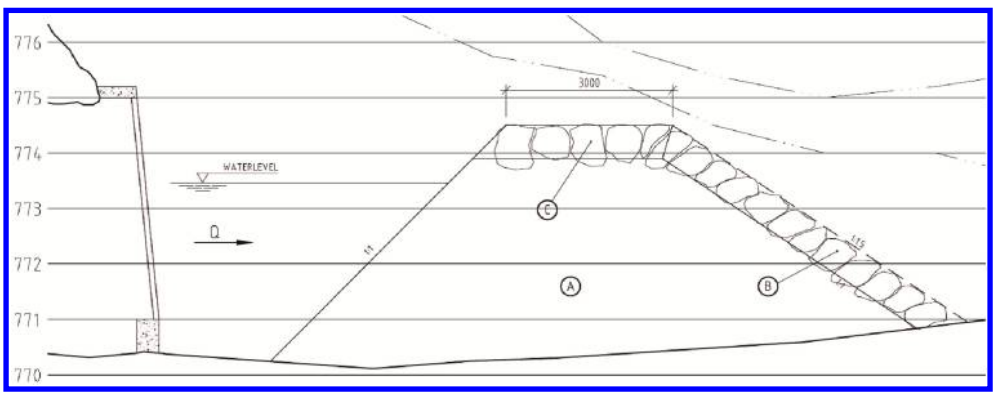

Figure 3. Section through the channel with a test dam. A: supporting fill, B, C: placed riprap.

the inclination angle of the stones with an inclinometer. Two video cameras recorded all the tests. The gate for the discharge was operated manually using mobile communication.

In 2013, two test dams with congeneric composition were tested. An operator with limited experience in placing riprap constructed the test dams with an excavator with a bucket in the beginning and later with a gripper from downstream of the dam. The stone axes were measured with a yardstick and the stone inclination with a laser distance meter with embedded inclinometer. A pressure cell (WL 16 from GlobalWater) and two ultrasonic sensors (microsonic, mic + 340/IU/TC) measured the water level upstream of the test dams every 30 seconds and with a frequency of 10 Hz, respectively. Three video cameras recorded the tests from different places. To measure the pressure in the bottom of the dam, four hoses were inserted with an interval of 1 m and led through the dam to the right downstream abutment of the test dam for reading. One camera focused on these hoses to register the changes. A laser scanner (Topcon GLS-1500) was available to scan the test dams before the running experiments. The discharge was planned to be measured with an acoustic Doppler current profiler (ADCP, Teledyne StreamPro). Dry bread served as tracer to measure the velocity on the water surface by observing the displacement of the bread on the video. Two riprap

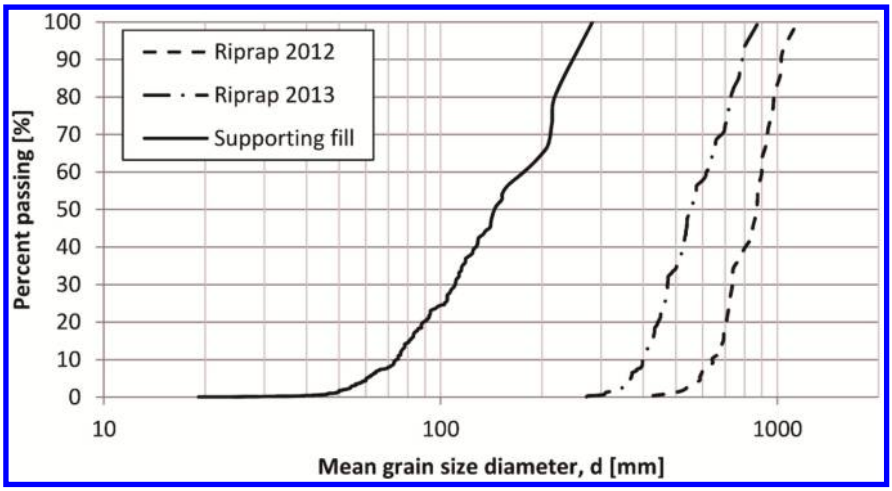

Figure 4. Grain size distribution curves of the supporting fill and the stones used for placed riprap.

Table 1. Test set-up and results.

Test no.	Riprap size d_{50} [mm]	Target angle α_t [°]	Achieved angle α [°]	Unit failure discharge q [m^3/s/m]
1, 2012	650	random	–	2.1
2, 2012	650	33.7	37	5.1
3, 2012	650	$33.7 < \alpha < 90$	63	6.3–8.3*
4, 2012	650	90	71	>8.3*
1, 2013	550	60	61	6.5
2, 2013	550	60	60	2

*indicates no complete breach.

stones in test dam 2 were equipped with accelerometers which were connected to a power supply and a computer by cable.

3 RESULTS AND DISCUSSION

Table 1 summarizes the test results from 2012 and 2013. Those from 2012 are further described in Lia et al. (2013). The results reveal that the riprap stability increases with the increasing inclination angle of the riprap stones. Test dams 3 and 4 in 2012 did not breach completely. They sustained a maximum unit discharge of 8.3 m^3/s/m for 2 minutes before the tests were aborted. This indicates that the failure discharge might be higher. Some riprap stones were eroded from the dam crest in test 3 as presented in Figure 2. In test 4, only two riprap stones were eroded from the dam toe close to the right abutment.

Figure 5 presents test dams 1 and 2 in 2013 before and during the test at maximum discharge. Despite congeneric composition, test dam 1 sustained more than three times the unit discharge of test dam 2. The breach in test dam 1 started with the erosion of single stones at the top of the dam, whereas test dam 2 failed due to instability in the dam toe which caused sliding of the placed riprap layer. The results of the two test series will not be discussed further as the focus of this article is practical challenges with large-scale field tests.

Finding a suitable test facility for doing large-scale field tests is not easy. NTNU is pleased to have the opportunity to use an appropriate site close to the Svartevatn dam. The channel at the outlet

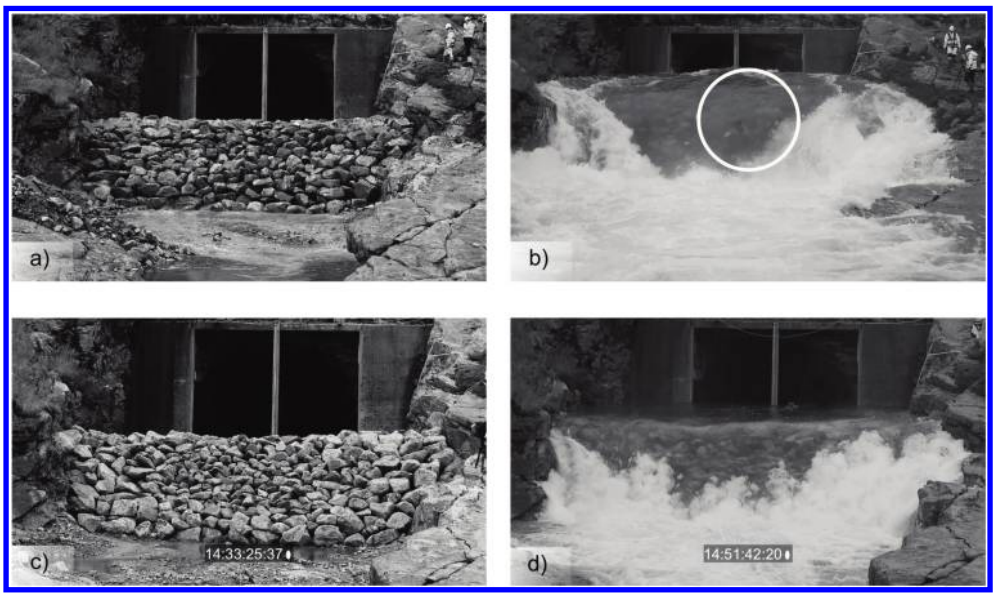

Figure 5. Test dams 1 (a, b) and 2 (c, d) in 2013. a) and c) show the dams at the start of the tests, b) and d) at the start of breaching. A moving stone is marked with a circle in b). (Photos: S. R. Skilnand).

serves as a flume though with irregularities along the sides and on the bottom. The discharge can be regulated and measured indirectly by the gate opening. However, the distance between the gate and the test site causes some delay in the discharge. Important information is consequently given by measuring the water level directly upstream of the test dams. The pressure cell monitored the water level every 30 seconds and delivered data of adequate quality although it was inconvenient to read the water level in real time. Apart from that, the device is designed for outdoor use and suitable. The ultrasonic sensors have a small display where the distance to the water surface can be read. As they are designed for indoor use, they have to be connected to a power supply and a computer to save the data. Direct contact with water should be avoided. The sensors were packed in plastic bags to protect them from rain. A tent sheltered the electronics and the computer. A mobile power unit supplied all the equipment with electricity. The attempt to measure the discharge in the same section as the water level measurement failed, because dam 2 collapsed in 2013 just before the ADCP was ready for use.

The stones had to be placed on the dam slope with an excavator due to the stone size of the riprap in the full- and large-scale. Good collaboration between the operator and the researchers is important. Construction in 2012 by an experienced operator in the excavator and suitable equipment to place the riprap was without major difficulties. For the tests in 2013 a different operator built the test dams. As the stones were smaller compared to 2012 and usually used for placed riprap, it was more complex and time consuming to construct the riprap. Using a grab instead of a bucket facilitated the work. However, these challenges combined with an inexperienced driver influenced the quality of the riprap significantly.

Large-scale tests with overtopping means dealing with relatively high discharges, for these tests over 8 $m^3/s/m$. Consequently, intrusive measurements become very challenging or impossible due to high velocities. The buried hoses were protected with a wooden structure bolted into the rock along the channel wall, but during the first overtopping test the construction was destroyed. The accelerometers did not deliver useful measurements because the cables were destroyed during the test. A predetermined breaking point in the cable prevented the computer and the power supply from being dragged along with the riprap. As a consequence, intrusive measurements in large discharges

should be avoided or equipment designed for such conditions is to be used. Video is a convenient and suitable method to document the tests and to enable analysis of the breach process frame by frame.

The test site, as many rockfill dams, is located in a remote and mountainous area. This means that it is time consuming to get spare parts or additional equipment. Consequently, the tests have to be planned in detail. In addition, weather conditions may vary during the tests. Weather is a non-controllable factor. Test dam 1 in 2013 could not be scanned with the laser scanner because rain-wet surfaces made the optical measurement impossible. During test 2 in 2013, heavy rainfall started directly after starting the test. The lenses of the cameras had consequently to be cleaned for drops and dew regularly. In an optimal way one should postpone a test if weather conditions suddenly turn unfavorable. However, as the tests involve many people and access to the site is limited, only a small time window is available. Apart from the weather when running tests, long-term weather conditions and hence available discharge can also become a limiting factor for the site.

Many parties are involved in running large-scale tests in the field and to operate different measuring equipment as well as the gate for the discharge. Hence, one person in charge has to coordinate all the parties. Altogether seven people ran the tests in 2013. Communication was complicated because of distance between the operating places and the noise of running water. Appropriate safety measures are necessary depending on where people stay during the tests.

4 CONCLUSIONS

Field tests with full- and large-scale riprap stones on an overtopped dam give valuable additional information and enable verifying results from physical model tests in the laboratory. As the tests are demanding, the test set-up has to be chosen and planned carefully. Close collaboration with the operator at the site is essential. The coordination of both people and equipment is challenging and must not be underestimated. Measuring equipment should be tested under similar conditions to check if it is working, as well as to train the operator especially if devices will be used under different conditions than they are designed for. Water velocities on an overtopped downstream slope are high and intrusive measurements are not appropriate in this area. Uncontrollable factors such as sudden rain may cause some extra challenges. The experience from the previous tests will be used to plan the upcoming field tests in 2015.

ACKNOWLEDGEMENTS

The financial support from the Research Council of Norway and Energy Norway is gratefully acknowledged. Sira-Kvina Power Company provided access and water supply from the Svartevatn dam. Without this kind collaboration the field tests would not have been possible.

REFERENCES

Abt, S. R., Thornton, C. I., Scholl, B. A. & Bender, T. R. (2013) Evaluation of overtopping riprap design relationships. *Journal of the American Water Resources Association*, 49 (4), 923–937.

Dornack, S. (2001) *Überströmbare Dämme – Beitrag zur Bemessung von Deckwerken aus Bruchsteinen*. PhD thesis, Technische Universität Dresden. Dresdener Wasserbauliche Mitteilungen, 20.

Hiller, P. H., Lia, L., Johansen, P. M. & Guddal, R. (2014) Dam Svartevatn – An example of challenging upgrading of a large rockfill dam. In: Indonesian Committee on Large Dams (eds.): *Electronic Proceedings of the International Symposium on Dams in Global Environmental Challenges, ICOLD Bali 2014, 1–6 June 2014, Bali, Indonesia.* 11–40.

Lia, L., Vartdal, E. A., Skoglund, M. & Campos, H. E. (2013) Rip rap protection of downstream slopes of rock fill dams – a measure to increase safety in an unpredictable future climate. In: Italian Committee on Large Dams (eds.): *Sharing Experience for Safe and Sustainable Water Storage: Electronic Proceedings of the 9th ICOLD European Club Symposium. 10–12 April 2013, Venice, Italy*. B.55.

Løvoll, A. (2006) Breach formation in rockfill dams – results from Norwegian field tests. In: International Commission on Large Dams (eds.): *Transactions of the 22nd International Congress on Large Dams, 18–23 June 2006, Barcelona, Spain.* Volume III, Question 86, pp. 35–51.

Midttømme, G. H., Grøttå, L. & Hyllestad, E. (2010) New Norwegian Dam Safety Regulations. In: Austrian National Committee on Large Dams (eds.): *Dam Safety – Sustainability in a Changing Environment: Proceedings of the 8th ICOLD European Club Symposium, Innsbruck, Austria*. Graz, Verlag der Technischen Universität Graz. pp. 351–355.

NVE, Norwegian Water Resources and Energy Directorate (2014) Damdatabase SIV. [Accessed 4 February 2014].

OED, Ministry of Petroleum and Energy (2009) FOR 2009-12-18-1600. *Forskrift om sikkerhet ved vassdragsanlegg (Regulation on dam safety)*. [Online] Available from: http://www.lovdata.no [Accessed 24 January 2011].

Peirson, W. L., Figlus, J., Pells, S. E. & Cox, R. J. (2008) Placed rock as protection against erosion by flow down steep slopes. *Journal of Hydraulic Engineering*, 134 (9), 1370–1375.

Hard protections for embankment dams

Dam Protections against Overtopping and Accidental Leakage – Toledo, Morán & Oñate (Eds)

Continuously-reinforced concrete slab spillways built over embankment dams in Spain: Molino de la Hoz and Llodio Dams

R.M. Alves & R. Morán
Dam Safety Research Group (SERPA), Technical University of Madrid (UPM), Spain

ABSTRACT: When projecting and designing an embankment dam usually the cost of the spillway constructed as an independent body is high in comparison to the global cost of the dam. In some situations, special constraints forced to find innovative solutions to discharge floods maintaining the safety level of the dam. Molino de la Hoz and Llodio Dams are two examples of embankment dams with innovative solutions in this field. They were constructed in Spain in the seventies of the 20th century. This article describes these two case studies that were successfully implemented and have been operating correctly for the past forty years.

1 INTRODUCTION AND BACKGROUND

In embankment dam projects the cost of the spillway in proportion with the cost of the dam is usually high. Consequently spill over the crest and downstream shoulders of embankment dams generally implies a great reduction of the global cost of the dam, mainly for small exploitations where the cost relationship is normally higher. It is an issue that has been developed for the past seventy years (Bizcarrondo & Gomez, 1970) and embraces different techniques as, for example, the continuously-reinforced concrete slabs (CRCS) as those used in Molino de la Hoz and Llodio dams Dams (Bizcarrondo & Gomez, 1970; Martínez & Toledo, 2000; Martínez, Montoya, & Toledo, 1998), or, more recently, wedge-shaped concrete blocks spillways (WSB), a specific case of the articulating concrete blocks (ACB) (Baker & Gardiner, 1994; Couto, Pinto, Toledo, & Morán, 2007; Pravdivets & Slissky, 1981).

The CRCS system consists on utilizing a continuous layer of reinforced concrete to serve as the flow surface for overtopping flows, constructed over a drainage layer aiming to protect the underlying embankment from high velocity flows discharging along the face of the downstream shoulder (FEMA, 2014). This spillway typology has been applied worldwide and some examples were summarized by Sherard (1972). In the United States of America exist two embankment dams constructed with concrete service spillways over the downstream face, the Meeks Cabin Dam in the state of Wyoming and the Currant Creek Dam in the state of Utah (FEMA, 2014). The first one is a 54 m high dam constructed between 1966 and 1971 with a spillway consisting of an uncontrolled ogee crest structure on the upstream face of the dam, with a concrete box conduit/chute and a downstream stilling basin. The second one is a dam 50 m high constructed between 1974 and 1977 with a spillway conceptually similar to the one of the Meeks Cabin Dam.

CRCS are mainly vulnerable to harsh climates where large temperature fluctuations are observed and to potential settlements of the embankment dams. Large temperature fluctuations may cause damage to the concrete slab due to the freeze-thaw cycles and thermal expansion-contraction of the concrete. Settlement of the embankment dam is more likely to occur in newly constructed dams than in dams operating for a large period of time. Settlements could lead to differential movements of the slab causing the arising of cracks. Other problem associated with CRCS is the occurrence of erosion underneath the concrete slab without being initially detected (FEMA, 2014) producing undermining that could lead to a dangerous situation, as failure, without any apparent warning.

2 DESCRIPTION

2.1 *Molino de la Hoz Dam*

The Molino de la Hoz Dam, located on the Guadarrama River in Madrid (Spain) was planned for recreational uses. It aimed to create an artificial lake to improve the environmental conditions of that area assigned for urban development (Martínez & Toledo, 2000). An embankment dam was found to be the best solution based on technical issues such as availability of construction materials on site and poor mechanical properties of the foundations, as well as aesthetic constraints set by the owner.

The reservoir capacity was not a decisive item so that a small dam fulfilled the conditions for the water level set by the dam owner. This limited the flood routing capacity of the reservoir and resulted in design flood discharge of 600 m^3/s. A conventional spillway with gates was planned to be constructed separately from the dam in the left abutment of the river valley. The cost of conventional spillway construction meant at the time a significant investment comparing with the whole project, what led the owner to almost abandon the idea of creating the artificial lake. This forced the technical team to seek a more cost-efficient solution to discharge safely that amount of water. Finally, it was decided to place the spillway over the embankment (Figure 1), resulting in a cost saving of 20% comparing to the cost of the initial solution.

The dam was constructed between 1973 and 1975 and has been operating since then. It is approximately 12 m high and 60 m wide being the elevation level of the foundation and crest roughly 613 m and 625 m (Figure 1). The upstream and downstream slopes of the dam are approximately 3.5 (H:V) and 2.0 (H:V), respectively. The reservoir has 0.40 hm^3 of storage capacity. The spillway consists of an uncontrolled curved ogee weir structure over the upstream face and crest of the dam, with a reinforced concrete chute and a downstream stilling basin. It covers all width of the dam overlaying from the upstream shoulder, under the impact of the wind waves, to the toe of the downstream slope (Martínez & Toledo, 2000), indicated in Figure 1 (top) with a thickest line. This layout enables to discharge the abovementioned design flood with a hydraulic head of approximately 4 m.

The spillway chute was made by a 0.30 m slab of reinforced concrete with the steel mesh reinforcement placed at half its thickness. It was constructed taking into account the necessary drainage and anchorage systems to avoid uplift pore water pressures under the slab. The anchorage system consisted of horizontal steel bars placed inside gutters over each compacted soil layer. These anchorages were connected to massive concrete blocks (1 m^3) installed inside the dam body. Before the next soil layer was compacted, the gutters were filled with concrete to protect the steel bars against corrosion. Both abutments and the stilling basin were also protected by concrete slabs. Areas 1 and 2 marked in the Figure 1 (top) refers to the impervious and permeable zones, respectively. The detail of the anchoring system is showed in the same figure. Figure 2 shows two perspectives of the dam.

2.2 *Llodio Dam*

Llodio Dam, located on the Olarte stream in the province of Álava (Basque Country, Spain) was planned to supply water to the village of Llodio. The river basin at the dam site was 4 km^2. The geology of the dam site was composed by marls and sandstones of the lower cretaceous (Gomez, Franco, & Romero, 1976). The topography is steep and various landslides were observed in the dam site and surrounding area. Thus, taking into account the characteristics of the foundation, it was decided to construct an embankment dam using the soils of the nearby landslides. The dashed area marked in Figure 3 shows the landslide found in the dam site.

The material from the landslides had low permeability coefficients (10^{-7} cm/s), proper natural water content, ideal to achieve the optimum compaction levels (natural water content roughly equal to 16% of its weight close to the 14% optimum Proctor water content), and also good resistance properties (maximum Proctor density of 1.78 g/cm^3, cohesion of 157 kPa and angle of friction of 25°C).

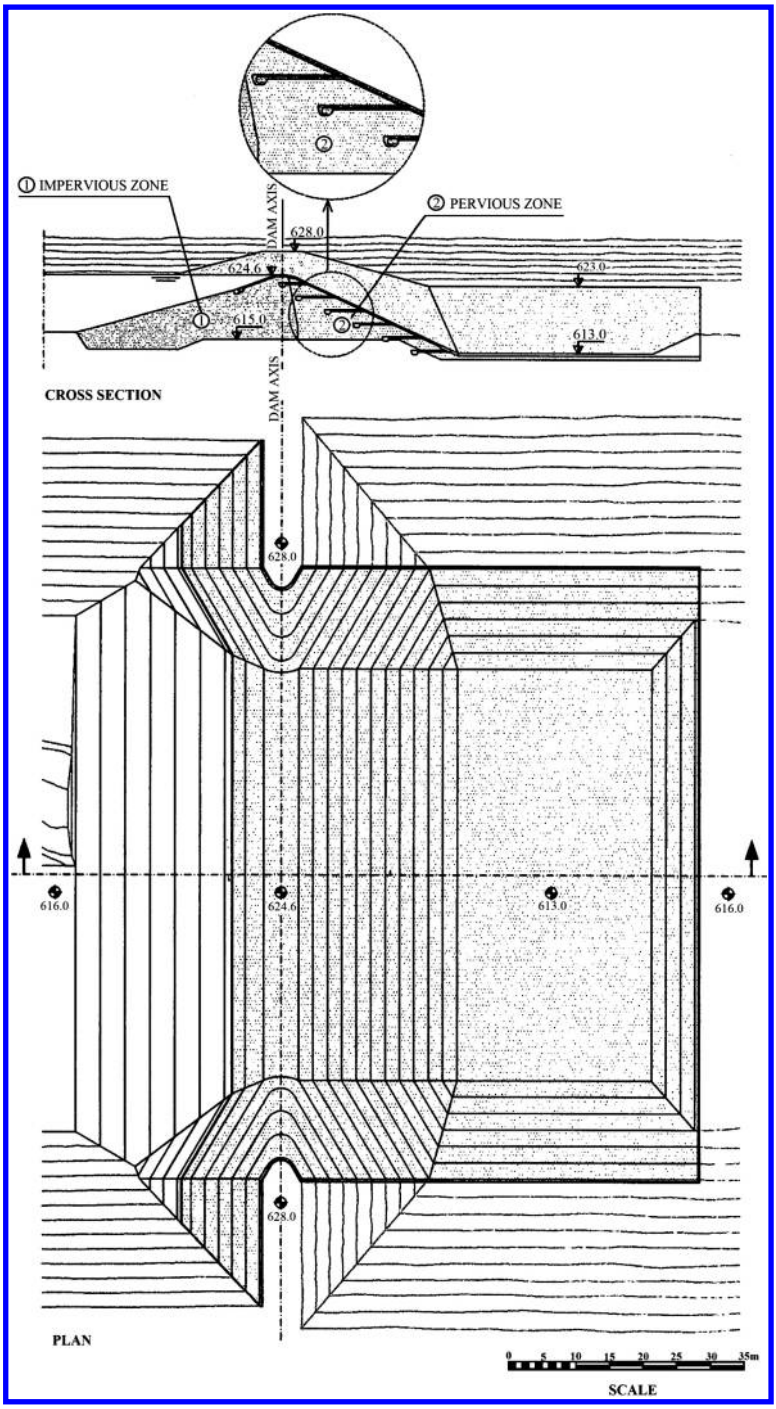

Figure 1. Cross section (top) and plan (bottom) of Molino de la Hoz Dam (Martínez et al., 1998).

Figure 2. Molino de la Hoz Dam. Left: picture from the right abutment (with Mr. Alfonso Álvarez, designer of the dam, walking on the spillway). Right: picture from the downstream river bank.

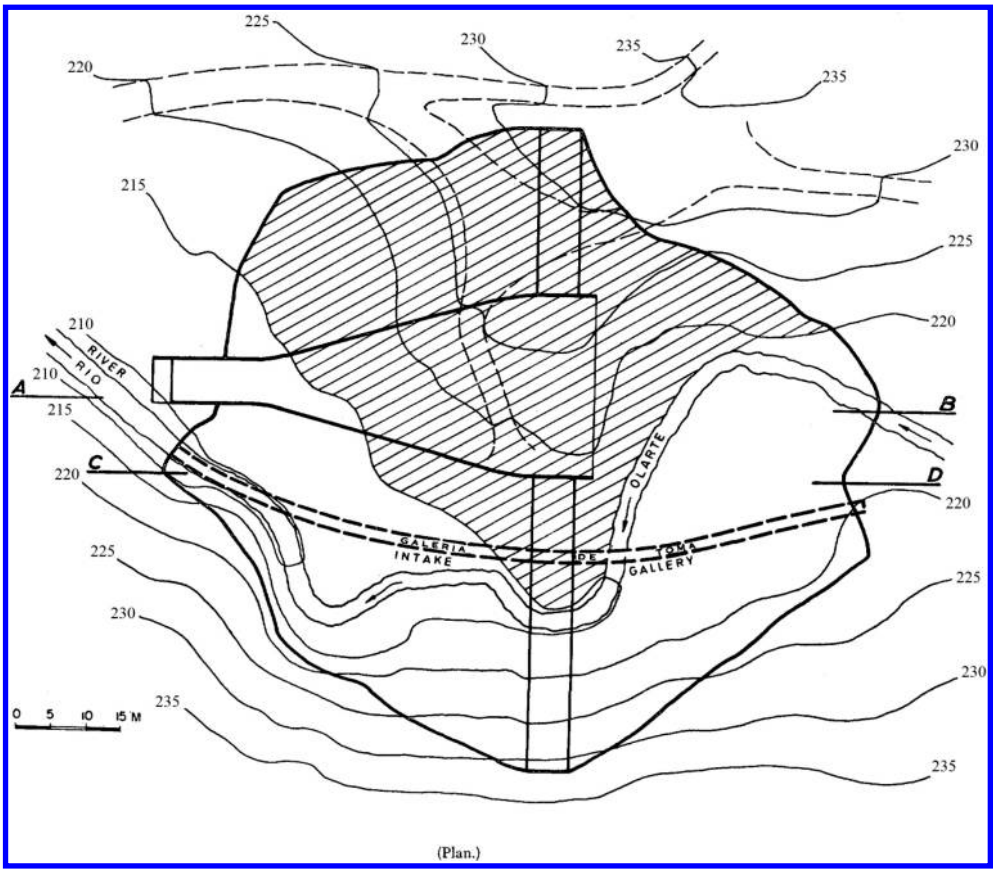

Figure 3. Plan view of Llodio Dam (Bizcarrondo & Gomez, 1970).

Figure 4. Llodio Dam. Left: upstream view. Right: downstream view.

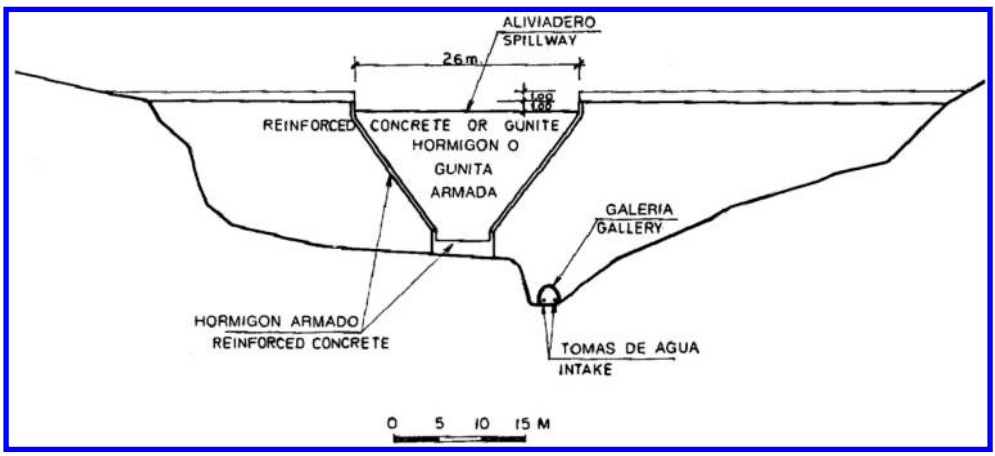

Figure 5. Front view of Llodio Dam (Bizcarrondo & Gomez, 1970).

The dam, constructed in 1972, is approximately 23 m high, from foundation to crest, and 95 m long. The reservoir has a storage capacity of approximately 0.10 hm^3. The upstream and downstream slopes of the dam are 3.0 (H:V) and 2.5 (H:V), respectively. To avoid erosion of the embankment upstream shoulder, a rip-rap coating layer was applied all over the upstream surface of the dam body, as can be seen in Figure 4 (left).

As said before, the dam site was very susceptible to landslides so that locating the spillway in one of the abutments would seriously compromise its stability. Finally, the spillway was constructed over the embankment dam. Besides the spillway, floods were planned to be discharged also using the bottom outlets.

The adopted solution in this case was a spillway consisting of an uncontrolled curved ogee structure over the upstream face of the dam, with a reinforced concrete converging chute with lateral training walls and a flip bucket. The spillway ogee and flip bucket are 26 m and 6 m wide, respectively (Figure 5). This layout allows discharging a maximum hydraulic head of 0.80 m for a total discharge of 40 m^3/s. The entire spillway, from the crest to the flip bucket is approximately 65 m long. Figure 6 and Figure 7 show transversal cross sections A-B and C-D showed in Figure 3.

To avoid undermining underneath the concrete slab, was applied a highly permeable reinforced rockfill layer to allow free circulation of leakage flow through the slab cracks avoiding uplift pressures. A filter layer was placed between the rockfill and the embankment material. Figure 4 (right) shows a picture of the finished spillway in 1972.

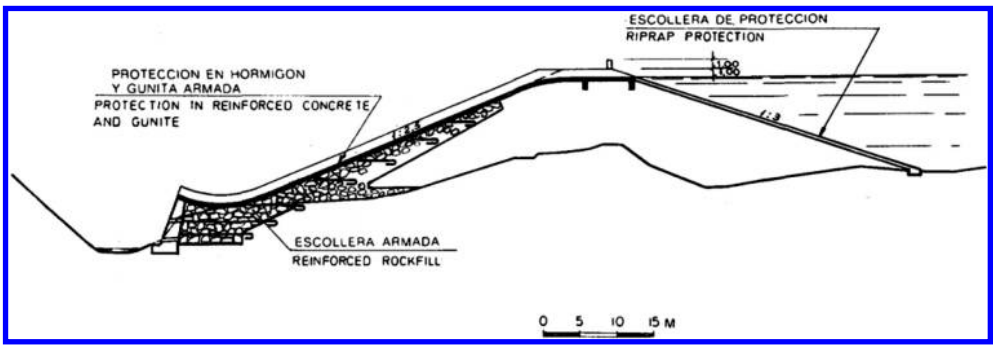

Figure 6. Cross section A-B (Bizcarrondo & Gomez, 1970).

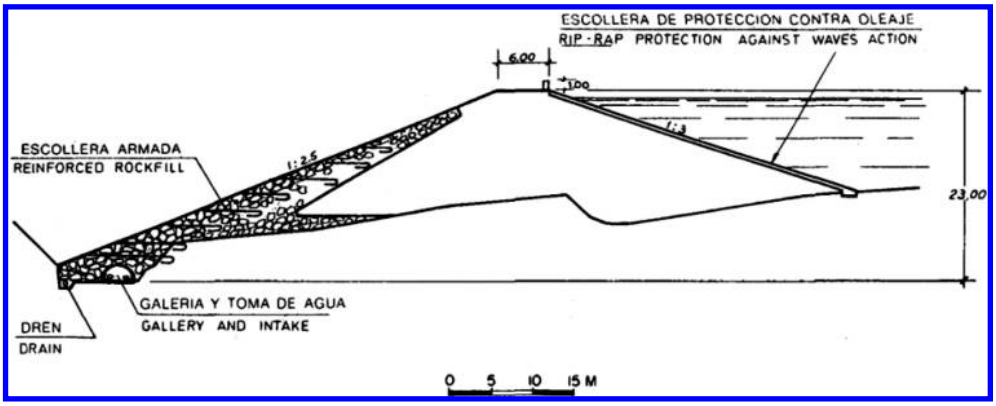

Figure 7. Cross section C-D (Bizcarrondo & Gomez, 1970).

3 CONCLUSIONS

This article briefly describes the main two references of service spillways over embankment dams with CRCS chutes constructed in Spain. In both cases, the CRCS slab spillway resulted in a significant reduction of the global cost of the dams. In Molino de la Hoz Dam, the final cost was reduced 20% mainly due to the cost saving of the construction of a separate gate-controlled spillway. In the Llodio Dam case study, the construction of a separate spillway would imply additional measures to stabilize the abutments, very prone to landslides. Another advantage can be assigned by the historical observation of its behavior. If well designed, this kind of solutions can be very robust. Both dams still work properly and have been operational for the past forty years resisting both to various floods (Martínez et al., 1998), specially the Llodio Dam that resisted to the floods of 1983.

As disadvantages, it must be said that a reinforced concrete slab placed over embankments must be designed taking into account the inevitable settlements, trying to avoid or minimize cracking. Additionally, appearance of offsets between consecutive slabs may cause flow impingement and dynamic pressures (Frizell, 2007). This could cause serious damages to the spillway chute and, consequently, to the dam body. In addition, this kind of spillways is more sensitive to harsh climates.

REFERENCES

Baker, R., & Gardiner, K. (1994). The construction and performance of a wedge block spillway at brushes clough reservoir. *Proceedings of the 8th Conference of the British Dam Society on Reservoir Safety and the Environment,* 214–223.

Bizcarrondo, A., & Gomez, G. (1970). Presa de escollera con aliviadero por coronación. [Rockfill dam with spillway over the crest] *Revista De Obras Públicas, 117*(3061), 573–577.

Couto, L., Pinto, A., Toledo, M. Á., & Morán, R. (2007). A new solution for a concrete spillway over a rockfill dam. hydraulic model study of barriga dam in spain. In: Pina, C., Portela, E. and Pereira, J. (eds) *Proceedings of the 5th International Conference on Dam Engineering,* Lisbon, Portugal: LNEC. 139–146.

FEMA. (2014). *Technical manual: Overtopping protection for dams. best practices for design, construction, problem identification and evaluation, inspection, maintenance, renovations and repair.* Department of Homeland Security.

Frizell, W. (2007). *Uplift and crack flow resulting from high velocity discharges over open offset joints – laboratory studies.* (No. DSO-07-07). Denver, Colorado: U.S. Department of the Interior. Bureau of Reclamation. Technical Service Center. Water Resources Research Laboratory Group.

Gomez, G., Franco, M. A., & Romero, J. L. (1976). Utilización de materiales pliocuaternarios en presas de "materiales sueltos". algunos ejemplos españoles. [Plio-quaternary materials used in embankment dams. Some cases in Spain] *Revista De Obras Públicas, 123*(3131), 253–276.

Martínez, A. Á., & Toledo, M. Á. (2000). Aliviadero de presas de labio fijo o compuertas. [Dam spillways with fixed weir crest or gates] *Revista De Obras Públicas, 147*(3396), 21–30.

Martínez, A. Á., Montoya, F. F., & Toledo, M. Á. (1998). Innovaciones en aliviaderos de presas de materiales sueltos. [Innovations in embankment dam spillways] *Revista De Obras Públicas, 145*(3378), 19–24.

Pravdivets, Y. P., & Slissky, S. M. (1981). Passing floodwaters over embankment dams. *International Water Power and Dam Construction, 33*(7), 30–32.

Sherard, J. L. (1972). Guaremal dam design review, appendix. *Spillways constructed on top of earth dams: Some information on recent projects: Statistics and photographs*.

Dam Protections against Overtopping and Accidental Leakage – Toledo, Morán & Oñate (Eds)

Comprehensive literature review on dam overtopping incidents

Nima Tavakoli
Department of Civil Engineering, International Campus of University of Sistan and Baluchestan, Chabahar, Iran

ABSTRACT: Roller-Compacted Concrete (RCC) has become a popular method for providing spillway and overtopping protection for earthen dams. Over recent years, RCC has been used as a spillway or overtopping protection for hundreds of dams. In addition to providing protection from erosive forces of flowing water, several of these projects are located in areas exposed to numerous freeze-thaw cycles. The operating frequencies of RCC spillways and overtopping protection projects range from serving as principal spillways to frequencies less than that of 500-year flood events. However, most RCC overtopping protection structures are emergency spillways designed to operate at a frequency not exceeding that of a 100-year storm. There are several reasons for the popularity of RCC with designers and owners, the primary ones being its simplicity and speed of construction, strength and durability, and economic advantages over alternative methods. Because RCC emergency spillway and overtopping protection projects are designed to operate infrequently during major flood events, limited information is available on the actual performance of these types of structures. However, the few that have operated performed satisfactorily with no evidence of excessive wear or structural distress. In this paper, a comprehensive literature review on dam overtopping incidents is presented.

Keywords: Dam, Protection, Overtopping

1 INTRODUCTION

Several research projects have confirmed the excellent abrasion resistance and durability of RCC. Comparative tests on soil-cement, RCC and conventional concrete showed RCC to have a greater abrasion resistance than conventional concrete of higher strength. This was primarily due to the presence of a larger percentage of aggregate in the mixture and less paste. In underwater abrasion tests using ASTM C 1138, it was determined that abrasion resistance was a function of both the aggregate hardness and the strength of the paste.

Despite the research findings, there is still a need to evaluate the reliability and performance of RCC under actual field conditions when subjected to debris laden flows and hydraulic forces. The following examples describe a few projects that have experienced multiple flows during their service life.

2 OCOEE DAM No. 2, TENNESSEE

In 1980, Ocoee Dam No. 2 saw the first known use of RCC for overtopping protection. The dam is located in Ocoee (east of Cleveland), Tennessee. It was constructed in 1912–1913 and was operating almost continuously until 1976. The dam is a 30 foot (9.1 m) high, 450 foot (137 m) long rock-filled timber crib structure. Water from the reservoir is transported via a 4.6 mile (7.4 km) long wooden flume and two steel penstocks to a power plant. Deterioration of the dam and the wooden flume forced the owner, Tennessee Valley Authority (TVA), to temporarily cease power

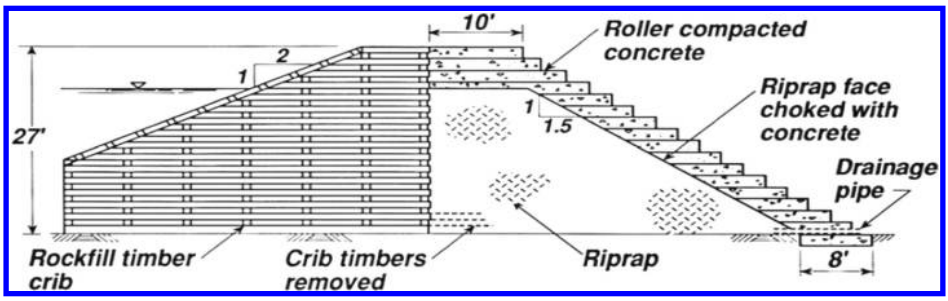

Figure 1. Typical cross-section of Ocoee Dam No. 2.

Figure 2. Ocoee Dam No. 2 without white-water rafting overflow (provided by TVA).

generation operations at Ocoee No. 2. The downstream face of the rock-filled timber dam was severely damaged. Several rehabilitation alternatives were considered and the owner elected to restore the flume using similar materials as per the original design and to buttress the dam with RCC (Figure 1).

The dam rehabilitation was completed in 1980 with approximately 4,550 yd^3 (3479 m^3) of RCC being placed. The RCC mix used ¾ inch (19 mm) maximum size aggregate (MSA) and the specified compressive strength was 3,750 psi (25.9 MPa) at 28 days.

Since completion, the dam has been subjected to more than 80 days per year of regularly planned overtoppings to accommodate the popular white-water rafting business downstream. The river site was also the 1996 Olympics site for canoe and kayak competitions, which required overtopping the dam 160 times that year. In addition, on 16 February, 1990, a major flood overtopped the dam by approximately 12 feet (3.7 m).

Where energy dissipation is minimal near the top of the dam, the RCC experienced very minor erosion. Further downstream, where energy dissipation is greater, the water has eroded the uncompacted lift edges and in some areas several inches (millimetres) of the compacted RCC. The RCC surface appears rough and uneven, but the dam continues to perform well (Figures 2–5).

3 BROWNWOOD COUNTRY CLUB DAM, TEXAS

In 1984, RCC was used as overtopping protection for an earthen dam in central Texas. This 19 foot (5.8 m) high earth embankment was constructed in 1938. It is owned by Brownwood Country Club

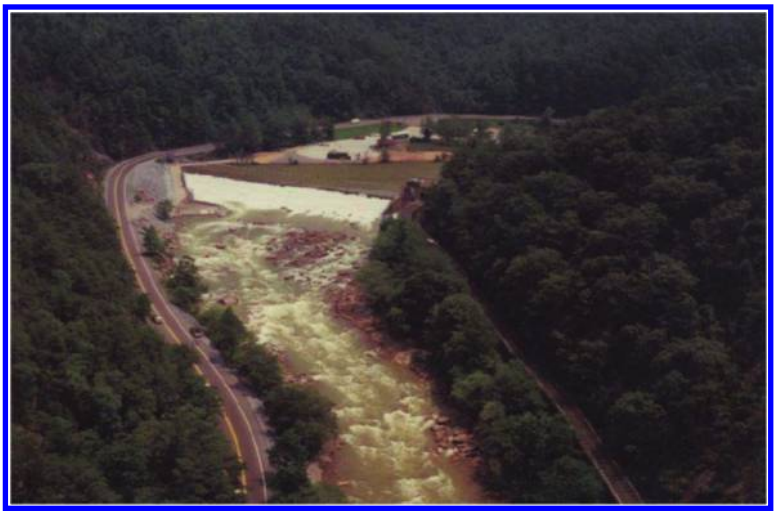

Figure 3. Ocoee Dam No. 2 with white-water rafting overflow (provided by TVA).

Figure 4. Close-up of Ocoee Dam No. 2 operating with rafters downstream.

in Brownwood, Texas. In 1972, the dam was classified as a high hazard dam, and subsequently the dam was determined to be lacking adequate spillway capacity. The dam spillway capacity was rated at 2,600 cfs (74 cms), far below the required Probable Maximum Flood (PMF) of 11,600 cfs (329 cms).

To provide adequate spillway capability, the spillway length was increased to 300 feet (91.4 m) and RCC armour was constructed on the downstream face of the spillway. Figure 6 shows a typical cross-section of the RCC overtopping protection which was designed by Freese and Nichols. The new spillway was designed to withstand a maximum overflow depth of 5.5 feet (1.7 m).

The RCC mixture contained 310 lb/yd^3 (184 kg/m^3) type IP blended cement consisting of 247 lb/yd^3 (147 kg/m^3) Portland cement and 63 lb/yd^3 (37 kg/m^3) fly ash. Aggregate for the RCC was dolomitic crushed limestone with 1-1/2 inch (38 mm) MSA. The project required 1,400 yd^3 (1,070 m^3) of RCC to be placed in just two days.

The dam has been overtopped at least once every one to two years. Overtopping events are estimated to be up to 2 feet (0.6 m) deep. Similar to Ocoee No. 2 dam, erosion of the uncompacted RCC at the lift edges has taken place. However, the compacted RCC a few inches (millimetres)

Figure 5. Ocoee Dam No. 2 after 27 years of service (provided by TVA).

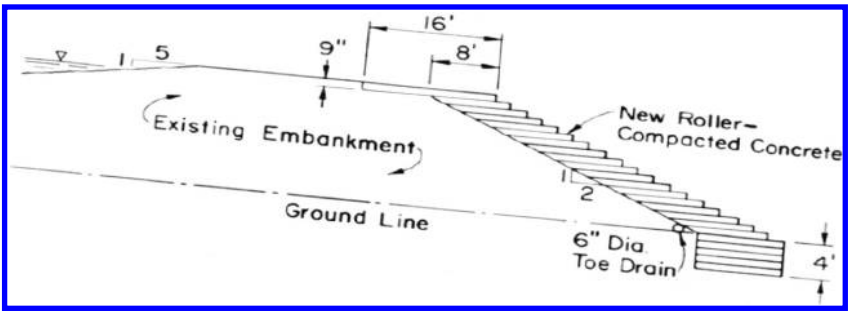

Figure 6. Overtopping protection method at Brownwood Country Club Dam.

away from the original uncompacted edge remains durable and the spillway continues to function properly. Figure 7 is a photo of the dam taken a few years after construction.

4 KERRVILLE DAM, TEXAS

"The performance of an incomplete roller-compacted concrete (RCC) dam during a massive flood in Texas last October has demonstrated that the product of the relatively new technique can take a dosing and come out smelling like a rose." This quote from *Engineering News Record*'s 24 April, 1986 issue, referred to Kerrville Dam located in Kerrville, Texas and owned by the Upper Guadalupe River Authority.

Completed in 1980, the original dam is a water supply and recreation clay fill embankment with 8 inch (200 mm) thick reinforced concrete facing. The dam had two spillways with one crest elevation lower than the other. The dam suffered some damage during a storm event in 1981 that sent 4 feet (1.2 m) of water over the dam.

Additional and more severe damage took place when the dam was overtopped by 4.5 feet (1.4 m) during another storm in 1982. The damage consisted of concrete cracking and displacement, loss of filter materials, and undermining of the concrete facing in spillway sections. Subsequent repairs included replacement of slab sections and grouting.

On New Year's Eve, 1984, about 40 percent of the service (lower crest) spillway concrete facing was lost and the clay core was eroded to bedrock when heavy rains overtopped the structure by

Figure 7. Brownwood Country Club Dam.

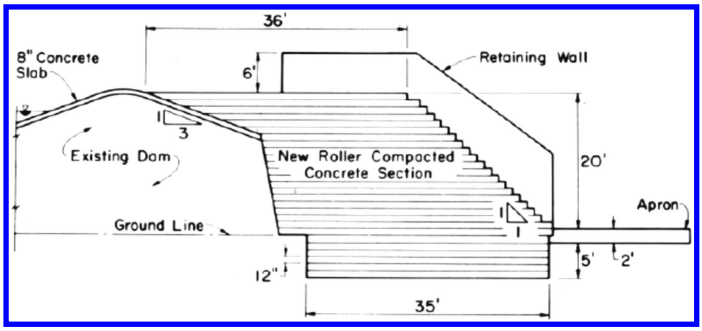

Figure 8. Repair solution for damaged Kerrville Dam.

10 feet (3.0 m). The emergency (higher crest) spillway was also damaged and loss of filter materials took place at the spillways and near the abutments

After considering several alternatives, the design team of Espey, Huston & Associates, Inc. (design engineer and project manager) and Rone Engineers (geotechnical consultant) decided to construct an RCC structure immediately below the existing structure. Figure 8 is a typical cross-section of the selected rehabilitation alternative.

The project required approximately 23,000 yd^3 (17,600 m^3) of RCC to complete. The mixture contained 200 lb/yd^3 (119 kg/m^3) Portland cement for the majority of the dam and 400 lb/yd^3 (237 kg/m^3) for the upper seven lifts. Bedding mortar was also used to improve bonding strength at the lift joints of several upper lifts. The RCC aggregate was pit-run river deposit with 3–1/2 inch (89 mm) MSA. Compressive strength test results of RCC cores were in the order of 1,600 psi (11 MPa) at 90 days for RCC containing 200 lb/yd^3 (119 kg/m^3) cement and 3,000 psi (20.7 MPa) at 90 days for RCC containing 400 lb/yd^3 (237 kg/m^3) cement. Normal water flow at this dam is continuously passed over the RCC spillway area. Significant flood events causing overtopping of the entire dam are listed below:

1. On 19 October, 1985, 30 days after completion of RCC placement and before final completion of the project, up to 11 inches (28 mm) of rain fell upstream of the dam. At peak flow, the water overtopped the main portion of the dam by 14.5 feet (4.4 m) and the lower spillway section by 15.5 feet (4.7 m). This event was estimated to be a 50-year flood with a maximum flow of

Figure 9. Kerrville Dam after major overtopping events.

125,000 cfs (3540 cms). The flow from the storm lasted five days over the entire dam and three weeks over the spillway.

2. The dam was overtopped again on 17 July, 1987. This time the flow peaked at 162,000 cfs (4587 cms) and the maximum depth of the flow at the dam was estimated at 16.2 feet (4.9 m), which is close to the 100-year storm.
3. Additional significant events reported by the owner include one in 1988 and another in 1990 causing the water to overtop the dam by 10 feet (3.0 m) and 8 feet (2.4 m), respectively.

Observation after the flood events listed above and subsequent inspections, including an inspection fairly recently done in 2007, revealed that the RCC performed and continues to perform remarkably. No significant damage was observed. RCC damage was limited to surface erosion exposing large aggregates and, at isolated locations, minor spalling took place during the July 1987 event. Figure 9 shows Kerrville Dam after several overtopping events.

5 LOWER LAKE ROYER DAM, MARYLAND

Lower Lake Royer Dam is a water supply dam owned by the U.S. Army and located at Fort Ritchie, Maryland. The purpose of using RCC at this facility was to upgrade the dam and increase spillway capacity. USACE Baltimore District designed the dam modifications that included (1) replacing existing concrete spillway with a new RCC gravity section, and (2) constructing an RCC overtopping protection over the left abutment.

Both the gravity section and the armoured left abutment formed the service spillway for the dam. The spillway was designed with a sloped collection channel directing the flow toward a discharge culvert located downstream from the RCC gravity section. The dam upgrades also included a new reinforced concrete water intake and conduit. The downstream slope of the RCC spillway was 1.5H:1V (Figures 10–11).

The RCC mix proportions per cubic yard consisted of 200 lb (90.7 kg) cement; 100 lb (45.4 kg) fly ash; 205 lb (93 kg) water; 3,530 lb (1601 kg) aggregates; 18 oz (532 ml) water reducing admixture; and 30 oz (887 ml) air entrainment admixture. The MSA was 1-1/2 inches (38 mm). It took 16 days to place a total of 10,000 yd^3 (7645 m^3) of RCC in June 1995.

The RCC steps were unformed and hand compaction equipment was used to compact the sloped edge of each lift. This method sometimes produces zones of lower density RCC as compared to the

Figure 10. RCC construction at Lower Lake Royer Dam (provided by Maryland Department of the Environment).

Figure 11. Lower Lake Royer Dam after 10 years of service.

density of formed RCC compacted with vibratory rollers. After 12 years of service, this service spillway has shown only minor erosion, a few inches (millimetres) deep, mainly at the exposed lift edges. Considering the frequency of operation and the harsh freeze-thaw environment at this facility, the spillway has been performing as expected with no excessive wear.

6 LAKE THOLOCCO DAM, ALABAMA

Constructed in the 1930s, Lake Tholocco Dam is an earth embankment owned by the U.S. Army and located on Clay Bank Creek in Fort Rucker, Alabama. The lake encompasses 680 acres (275 hectares) and has been used for training of military personnel at Fort Rucker and for recreational activities for the fort personnel as well as surrounding civilians.

The dam is an earth embankment 2,400 feet (732 m) long with a maximum height of 45 feet (13.7 m). The service spillway is a 50 foot (15.2 m) long reinforced concrete structure with a

Figure 12. A view of principal and auxiliary spillways at Lake Tholocco Dam.

Figure 13. March 2005 overtopping event at Tholocco Lake Dam (provided by U.S. Army).

fixed ogee crest. A 1979 Phase I Inspection Report under the National Dam Safety Program showed that the dam did not meet current standards due to insufficient spillway capacity. Since it was constructed, the dam's earthen emergency spillway was regularly overtopped causing severe erosion.

Major storms in the 1990s breached the emergency spillway twice. The first breach was the result of a huge 1990 storm that dumped 14.5 inches (368 mm) of rain in five hours. The USACE Mobile District recommended raising the dam and increasing spillway capacity. However, due to lack of funds, these recommendations were not implemented. Instead, repairs were made to restore the earthen emergency spillway to pre-1990 storm condition. Four years later, during 1–4 July, 1994, the tropical Storm Alberto caused the earthen spillway to fail a second time. Then the reservoir remained dry for six years.

Figure 14. Excellent condition of RCC steps at Tholocco Lake Dam (May 2007).

Figure 15. Red Rock RCC inflow spillway (January 2005). Note pile of sediment in stilling basin.

USACE Mobile District explored several upgrade alternatives and determined that the most cost-effective solution was to install an RCC auxiliary spillway with a collection channel in the embankment adjacent to the reinforced concrete service spillway. The design called for a 1,550-foot (472 m) long, 36 foot (11 m) high spillway constructed with 12 inch (300 mm) thick RCC steps. The crest elevation was set to discharge water from rainfall events once every one to two years and the design maximum overflow height was 6.5 feet (2.0 m). The RCC lifts varied in width from 8 to 12 feet (2.4–3.7 m).

The slope of the spillway chute was 6H:1V whereas a slope of 3H:1V was selected for the downstream side of the collection channel. The design also included large riprap placed immediately downstream of the collection channel to prevent damage to the backside of the collection channel should the estimated tail water levels not be realized during storm events.

Figure 16. 2004 storm overflow at Red Rock Detention Basin Spillway (provided by Clark County Regional Flood Control District).

Figure 17. Red Rock RCC inflow spillway (February 2006).

Approximately 26,000 yd^3 (19,878 m^3) of RCC were placed in the spring of 2000. The RCC mixture contained 275 lb/yd^3 (163 kg/m^3) Portland cement and 50 lb/yd^3 (30 kg/m^3) fly ash. The MSA for the RCC was 1-1/2 inches (38 mm). Figure 12 shows the spillway shortly after completion.

On-site USACE personnel report that the spillway has been overtopped at least twice. The first was during hurricane Ivan on 16 September, 2004. At peak flow, overflow height was determined to be 3 feet (0.9 m). The second storm took place on 27–28 March, 2005. Maximum overflow depth during this storm was 1.5 feet (0.45 m). Figure 13 was taken during this overtopping event. Figure 14 was taken in May 2007 and shows the excellent condition of the RCC steps.

Figure 18. Boulders deposited on the RCC steps during 2005 storm. Photo taken in February 2006. Note limited wear of RCC steps.

7 RED ROCK DETENTION BASIN INLET SPILLWAY, NEVADA

Red Rock Detention Basin (RRDB) in the south-western portion of Las Vegas Valley, Nevada, is one of five detention basins on the USACE Tropicana and Flamingo Washes Project. The detention basins are part of a master plan for providing flood protection and erosion control in Las Vegas Valley. USACE completed the construction on RRDB in 2001. The facility included an RCC inflow spillway (or drop structure), a holding reservoir, and three outflow spillways: the principal, auxiliary, and emergency spillways.

The RCC inflow spillway as it appeared in January 2005 is shown in Figure 15. The purpose of the spillway is to handle inflow floodwater carrying heavy sediment loads without eroding or lowering the streambed, which would undermine the stability of the bridge upstream.

The RCC structure consists of an approach apron, stair-stepped chute, stilling basin and training walls. The spillway is 42-feet (12.6 m) high and the slope of the chute is 3H:1V. The steps are 2 feet (0.6 m) high compacted in two lifts, and the individual lifts are 10 feet (3.0 m) wide. The RCC mixture contained 364 lb/yd^3 (216 kg/m^3) cement and 74 lb/yd^3 (44 kg/m^3) fly ash.

The RCC spillway operates during every rain event generating a flow in the wash, normally occurring a few times a year. Figure 16 shows the inflow water during a 2004 storm. The storm carried heavy sediment loads evidenced by the presence of a large sediment pile in the basin of the RCC structure (Figure 15). In 2005, a stronger storm deposited boulders up to 200 lb (90.7 kg) each on the RCC steps, distributing the sediment pile throughout the detention basin (Figures 17–18).

Observations in 2005 and in 2006 show the effect of flow (carrying abrasive sediments) on the RCC to be limited to surface erosion or polishing. Loss of surface materials ranged from none at the tread interior corner to 2 inches (50 mm) or less at the tread (step) nosing. Spalling was also observed at isolated areas; however, almost all of the spalling was confined to where localized segregation had occurred.

8 CONCLUSIONS AND RECOMMENDATIONS

Although RCC is still a relatively new method of construction and performance data are limited, structures that have been overtopped show strong evidence that the material is performing

satisfactorily when subjected to the elements, hydrostatic pressures, and flows containing very abrasive sediments.

In addition to proper structural design, the primary factors contributing to the successful performance of these structures are related to the RCC mix design and construction methods. These factors include:

- Proper mix proportioning, including use of a well-graded aggregate so that the volume of coarse aggregate in the mixture is maximized without segregation while still providing an adequate amount of paste.
- Use of the hardest aggregate available.
- Sufficient cementation content in the RCC mixture and proper compaction to achieve adequate strength and high density, especially where the RCC is subjected to repeated freeze-thaw cycles and/or frequent overtopping.
- To limit erosion at the exposed lift edges, the steps should be formed and compacted to a high density.
- Proper bonding of RCC lifts, especially at the upper few lifts and where energy dissipation occurs in the vicinity of the stilling basin.

REFERENCES

U.S. Army Corps of Engineers, "Erosion Test of Roller-Compacted Concrete (RCC)", *Design Memorandum*, No. 3 – Exhibit 15. Zintel Canyon Dam, Walla Walla District, September 1980(a).

U.S. Army Corps of Engineers, "Summary of Erosion Study at Detroit Dam for Zintel Canyon Dam," *Design Memorandum*, No. 3 – Exhibit 16. Zintel Canyon Dam, Walla District, September 1980(b).

"Test Results of Roller-Compacted Concrete Mixtures; Rio Salado Project:" U.S. Army Corps of Engineers, Los Angeles District (unpublished), October 1999.

Omoregie, F. A., Gutshow, R. A., and Russell, M. L., "Cement-Hardened Materials for Abrasion-Erosion in Hydraulic Structures", *Concrete International*, July 1994.

Laboratory Tests and Field Studies on Erosion and Abrasion Resistance of Soil-Cement and Roller-Compacted Concrete – Results of a Literature Review, R&D Serial, No. 2436, Portland Cement Association, 2001.

USCOLD News, July 1980, p. 12 and p. 15.

Engineering News Record, 24 April, 1986, pp. 28–29.

McKown, M. A., *Public Works Digest*, January/February 2001, pp. 14–15.

Hudson, S., *Dixie Contractor*, 19 June, 2000, pp. 20–27.

Dam Protections against Overtopping and Accidental Leakage – Toledo, Morán & Oñate (Eds)

Barriga Dam spillway: a case study of wedge-shaped blocks technology

R. Morán & M.Á. Toledo
Dam Safety Research Group (SERPA), Technical University of Madrid (UPM), Spain

ABSTRACT: The spillway of Barriga Dam (Burgos, Spain) may be considered a singular case study in dam engineering. The spillway has been working successfully during 7 years with seasonal discharges in winter and spring time. Its distinguishing features are its location, on the rockfill dam body, and the chute, composed of wedge-shaped concrete blocks (WSB). In such a way, the design and construction of the spillway involved two years of applied research and international collaboration. As a result of that, two scaled physical models were developed at Colorado State University (Fort Collins, Colorado) and the Laboratório Nacional de Engenharia Civil (Lisbon, Portugal). This technical paper summarizes the main features of the studies, the key aspects of the final design of the block units and relevant details of the spillway design and construction. The conclusion of this experience is that WSB technology is cost-effective, easy to install, and may be suitable for appliance as auxiliary spillways, or service spillways of small dams, cofferdams or ponds. However, the technology is still immature and engineers have to be cautious about its risks. Therefore, more experience and additional research is needed in the future to consolidate the practical application of this technology.

1 INTRODUCTION

Barriga Dam was constructed to irrigate an area of 1000 ha in the north of the province of Burgos (Spain). The project was funded by the Regional Authority of Castilla y León. The dam is located in the Nabón Creek and the drainage basin area is 20 km^2. The Nabón Creek behaves as a torrent with large differences between summer and winter flows, which are influenced by the state of the aquifer head and the snowmelt in the upper basin. In order to design the spillway, a discharge capacity of 161 m^3/s (8.0 m^2/s) was considered, whereas an extreme flood discharge of 229 m^3/s (11.4 m^2/s) was estimated as the limit scenario. The reservoir capacity is roughly 0.5 hm^3 and the maximum height of the dam 17 m. The geology of the dam site and reservoir area is composed of highly-permeable karstic limestone. For such reason, it was necessary to install a high-density polyethylene membrane over the entire surface of the reservoir to avoid unacceptable water leakage. This membrane was also used as the impervious element on the upstream face of the rockfill dam.

A feasibility study of the spillway was conducted to compare a typical reinforced concrete approach in the right abutment of the valley with other alternatives, including technologies of protection for a non-conventional alternative, constructed on the downstream slope of the dam body. This study considered several key factors (including environmental protection, economy, and innovation) to implement new technologies in future projects that will be undertaken by the dam owner. The study concluded that the most suitable alternative in this case was a spillway placed upon the dam body, including a WSB revetment of the chute. The project was concluded in 2006 and, so far, the spillway successfully passed several floods with a peak unit discharge of approximately 0.5 m^2/s.

2 BACKGROUND

In a WSB spillway, the usual reinforced concrete slab is replaced by a revetment that consists of overlapped precast concrete blocks. As every block overlaps the next downstream one, the revetment constitutes a stepped spillway. The stability of each block is assured by the positive pressure of the water on the upper face, the overlapping from adjacent blocks and the negative pressure of air on its lower face. A set of vents, located in the lower zone of the step riser, transfer the negative pressure to the surface between the block and the bedding layer, so that the ensuing suction enhances the stability of the block (Morán & Toledo, 2014).

2.1 *Development of the WSB technology*

The WSB technology was originally developed in the late 1960s by Professor Yuri Pravdivets at the Moscow Civil Engineering Institute. In the first stage, scale models (scales 1:100, 1:50, 1:6) were developed to analyze the suitability of the approach. In addition, prototypes with extremely unfavorable operating conditions were tested at the Dnieper River (Pravdivets & Slissky, 1981); a maximum unit flow of 60 m^2/s was successfully discharged.

Later on, Professor Baker, from Salford University (United Kingdom), carried out further studies and the construction of a new prototype (Baker & Gardiner, 1994) at the Brushes Clough Reservoir in Greater Manchester (UK). These studies were summarized in a Design Manual (Hewlett, Baker, May, & Pravdivets, 1997) published by the Construction Industry Research and Information Association (CIRIA). The maximum unit flow tested at the Brushes Clough Reservoir was 2.2 m^2/s. The chute slope was 3H:1V.

In addition, the Bureau of Reclamation (USA) also performed WSB spillway tests at Colorado State University (CSU) laboratory facility in Fort Collins, Colorado (Frizell, 1997). This facility is approximately 15 m high with a chute slope of 2H:1V. In such facility, tests of WSB were developed with a maximum unit flow higher than 4 m^2/s, with successful results. Such research was the basis for the Armorwedge™ U.S. patent, which at the time of Barriga Dam construction was owned by Armortec, Inc.

The most recent research has been performed in Portugal by the Instituto Superior Técnico (Relvas & Pinheiro, 2008), the Laboratório Nacional de Engenharia Civil (LNEC) (Portugal), the Technical University of Madrid and International Center for Numerical Methods in Engineering (Spain) (Salazar et al., 2013) and remains ongoing.

2.2 *WSB spillways around the world*

Most of the cases of WSB spillways prior to the Barriga Dam project were prototype facilities. The most important were Bolshevik, Klinbeldin, Maslovo, Sosnovski, the Dnieper Hydropower Dam, Dneister, Kolyma, Transbaikal, and Jelyevski in Russia; Jiangshe Wanan in China; and Wadi Sahalnawt in Oman (Hewlett et al., 1997). In Spain, there are some cases of spillways located on the downstream slope of embankment dams such as Molino de la Hoz Dam and Llodio Dam, though both were constructed using a continuously reinforced concrete slab (CRCS) protection. After construction of the Barriga Dam, Bruton Dam WSB spillway was built in Somerset, United Kingdom (Pether, Marsh, & Cartwright, 2009) as well as Friendship Village auxiliary spillway in Missouri, USA (FEMA, 2014).

3 DESIGN OF THE BARRIGA WSB UNIT

The design and manufacture of the block units took place during the construction of the dam. The final design was based on the standard Armorwedge™ unit, though significant changes were

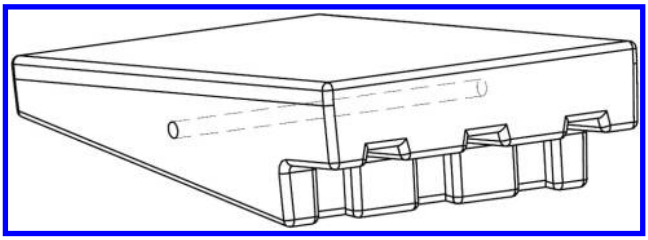

Figure 1. 3D view of the Barriga Dam WSB unit.

made by the project team to improve the safety of the spillway. Accordingly, the Armorwedge™ block was the unit that was tested in the physical models performed at CSU for the Barriga Dam spillway (Thornton & Robeson, M.D., Varyu, D.R., 2006). The scale factor used to size the blocks of Barriga Dam was based on the CSU and LNEC flume tests and took into account the following aspects:

- Strict hydraulic Froude scaling using the brink depths in the models.
- Discussions over the ideal block weight, focusing on potential vandalism; durability, associated with use on a service spillway; and the construction process.

The two-dimensional flume tests performed at CSU were developed in a rectangular cross-section chute, instead of the trapezoidal section of the prototype. However, approach conditions of the flow were not the same in the model as in the prototype. For such a reason, an additional three-dimensional model was performed at the LNEC. So, the measured maximum discharge into the CSU flume and the measured brink depth at the break in the slope were used to compare the CSU flume results with the ones from the LNEC study (LNEC, 2006) and the computed values for the prototype.

The standard block size was tested in the flume up to the flume discharge capacity (4.7 m^2/s). Consequently, the block sizes were then scaled up to produce a block with the geometry, thickness, weight and strength to meet the flow requirements for the Barriga Dam spillway and the safety level needed with regard to vandalism, durability, impact resistance, and constructability issues, which are not scalable.

The hydraulic forces that act on the block are due to the impingement of the flow on the upper face of the block and the aspiration in the step offset. Such aspiration is transferred to the inner face making possible the suction between the block and the bedding layer. In addition to those forces, the overlapping of the blocks allow the stability of every unit. Although the stability of the block is not due entirely to its weight or thickness, its durability and resistance to vandalism may be enhanced by adding mass. The scaling criterion was examined first by analyzing the hydraulic test results; it was then determined whether the results of the selected scale factor met the other less tangible concerns with regard to the size and weight of the blocks. A scale factor of 1.6 was finally adopted to ensure good hydraulic behavior, as determined by the rate of the head over the spillway on the prototype and the model. The final dimensions with this scale factor were considered adequate in order to avoid vandalism and enhance the durability and impact resistance.

An interior hole was added transversely to the block (Figure 1) to allow a cable to be introduced into it, to join each WSB with the others in the same row. This made it more difficult for the blocks to be pulled out of the revetment due to unforeseen causes. In addition, this hole was useful in the transportation and placement of the blocks in the spillway site. The convergence of the lateral surfaces were adopted to improve the demolding of the units.

The concrete compressive strength was increased up to 50 N/mm^2 to improve the impact resistance. The main differences between the standard Armorwedge™ and the Barriga Dam units are summarized in Table 1.

Table 1. Comparison between the Armorwedge and the Barriga Dam WSB.

	Armorwedge^{TM} unit	Barriga Dam unit
Maximum dimensions (cm)	45.7 × 30.4 × 13.0	73.0 × 50.0 × 20.0
Weight (kN)	0.22	1.09
Aeration vents	3 of 3.8 × 1.3 cm^2	3 of 5.0 × 2.0 cm^2
Type of concrete	Dry cast concrete with a 20 N/mm^2 compressive strength	Wet cast concrete with a 50 N/mm^2 compressive strength
Transverse hole	No	Yes. 22 mm diameter.
Lateral surfaces	Vertical	Small convergence for easy demolding

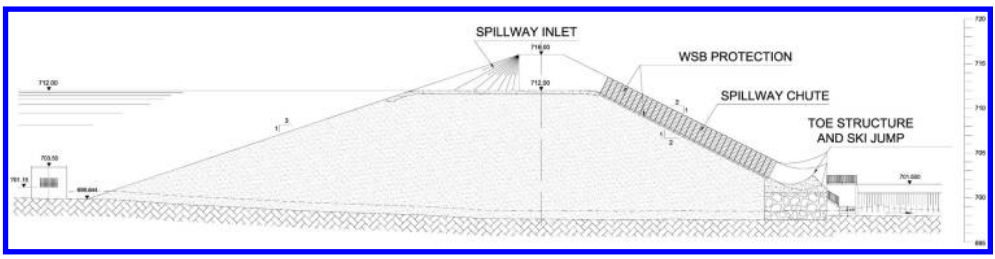

Figure 2. Cross section of Barriga Dam spillway.

4 SPILLWAY SETUP

The spillway description is divided in three parts: the inlet structure; the chute protected with WSB; and the toe structure, which includes the flip bucket with the ski jump (Figure 2).

4.1 *Inlet structure*

The spillway inlet comprises a smooth, curved transition between the reservoir and the trapezoidal chute (Figure 3). A 0.40 m thick reinforced concrete slab is part of the horizontal trapezoidal channel necessary to pass the flow discharge through the dam crest toward the WSB chute.

The inlet structure was tested in the LNEC scaled model to select the final design. After conducting tests with alternative transitions between the reservoir and the trapezoidal channel, the final selection was a curved surface with elliptical horizontal sections. The slab and slopes of the trapezoidal channel and transition were made of 0.4 m thick reinforced concrete that was anchored to the dam body with a grid of one-meter bolts. Moreover, the upstream end of the inlet transition was used to anchor the impervious polyethylene membrane by extending it approximately 10 m beneath the reinforced concrete structure.

The LNEC model showed difficulties in controlling shockwaves with the original design and especially in avoiding flow concentration in the middle of the chute. However, the selected solution distributed the flow quite uniformly along the whole width of the trapezoidal channel so that the hydraulic conditions upstream of the WSB chute were considered appropriate. Furthermore, the discharge capacity of the spillway was also experimentally determined (Figure 4).

4.2 *WSB chute*

As it was already mentioned, the spillway chute is located on the downstream shell of the dam. The construction process started with the filling of the theoretical slope of the dam to then excavate the bottom and side slopes of the trapezoidal channel. Afterwards, the bottom of the excavation of the chute was then filled again with both the transition and bedding layers. Finally, the WSB were

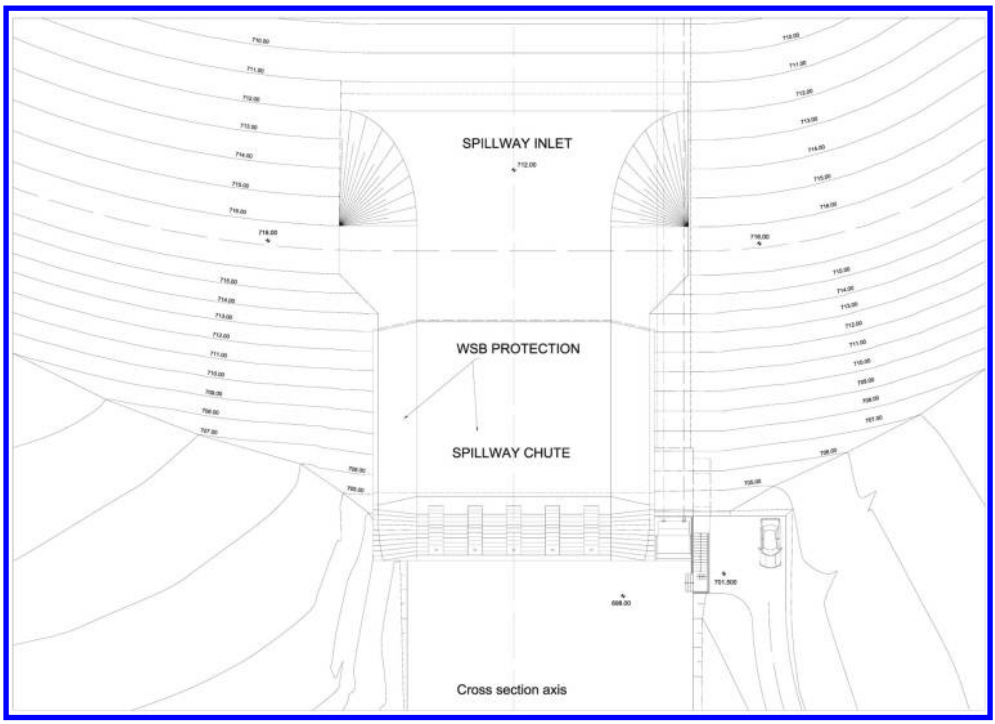

Figure 3. Plan view of the spillway of Barriga Dam.

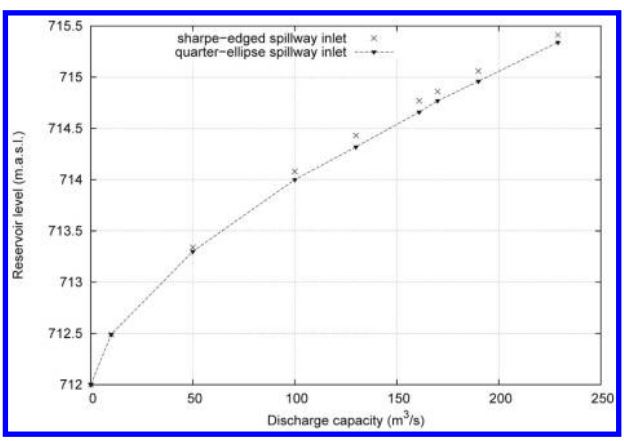

Figure 4. Discharge capacity of the weir of Barriga Dam.

placed manually over the bedding layer. In this way, the material in the dam body below the chute could be suitably compacted before the spillway construction. The distance between the bottom of the chute, which is considered the upside plane of the WSB, and the theoretical slope of the dam body was approximately 2 m. The transversal slopes of the chute (2H:1V) were also protected with WSB.

The WSB chute starts at the end of the inlet horizontal channel, which is rounded off with a vertical transition to join it to the longitudinal chute slope (2H:1V), the same as the downstream slope of the dam. From this point, the WSB chute maintains constant the slope until its end at the

Figure 5. View of the spillway from downstream.

Table 2. Gradation curve of the dam body material.

Sieve UNE (mm)	% finer
150.00	95.45
125.00	81.30
100.00	72.30
80.00	57.75
63.00	49.65
50.00	42.00
40.00	33.75
25.00	26.10
20.00	22.80
12.50	16.60
10.00	14.75
6.30	12.15
5.00	10.65
2.00	8.15
1.25	7.05
0.40	5.50
0.16	4.80
0.08	4.40

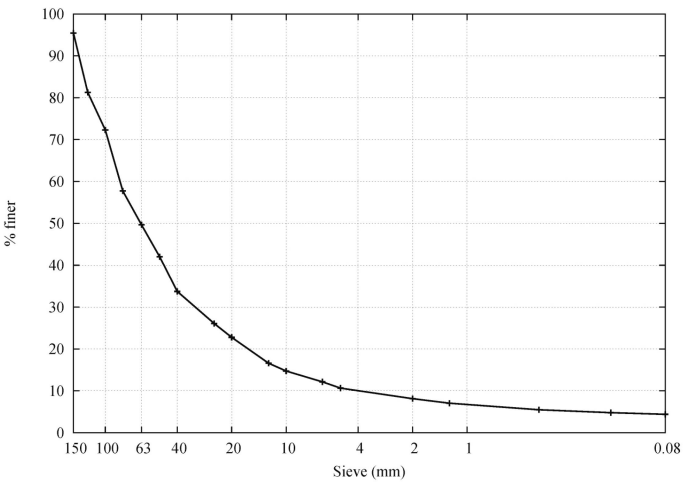

toe structure (Figure 5). In the chute, the flow is highly aerated due to the steps formed by the rows of WSB.

The sizing of the bedding and drainage layers was made considering the features of the material of the dam body. Such material was a compacted limestone rockfill (Table 2) with percentage of fines of 4.4%. Therefore, the ability of the dam body to drain the seepage flows coming from the spillway leakage was ensured.

Thus, an additional important issue was to achieve the internal stability of the materials beneath the blocks. To do so, two layers of gravel were placed between the blocks and the dam body (Table 3). Immediately below the blocks, a 20 cm bedding layer of crushed limestone was extended upon another 20 cm crushed limestone layer of transition material, which simultaneously fulfilled the filter condition with respect to the dam body material and served as the drainage layer as well. Both materials were designed to be internally stable, as defined by Sherard through the instability ratio (IR) criteria.

The aim of the bedding layer was supporting the blocks and avoiding the uplift pressure on the bottom side of the WSB chute. The material had to be large enough so as not to pass through the vents of the blocks, while at the same time small enough so that the WSB can be placed easily

Table 3. Requirements for the drainage and transition layers (d_i indicates the sieve size that allows a percentage i of granular material, measured by weight, to pass through).

	d_{15} (mm)	d_{50} (mm)	d_{85} (mm)	d_{60}/d_{10}	Size limits
Bedding layer	27.7	38.1	55.0		<2% over 65 mm <5% under 15 mm
Transition layer	14.0	—	55.0	<4	<2% over 65 mm

Figure 6. Bedding layer material and cable endings in longitudinal joint.

in a uniform alignment of rows in the chute. The transition layer had the objective of maintaining internal stability by avoiding migration of the drainage material through the voids in the dam body material. Both bedding and transition layers were manufactured by considering the gradation curve (Table 2) of the dam body material as well as the WSB size of the vents. In addition, the feasibility of placing the rows of WSB over the bedding layer was tested in site during construction.

Issues regarding certain construction details arose during the project, for which no specific design criteria were availabe to the authors' knowledge, such as:

- The upstream joint between the inlet reinforced concrete channel and the most upstream row of WSB;
- the downstream joint between the most downstream row of WSB and the ski jump structure;
- the longitudinal joints between the slopes and the bottom of the WSB trapezoidal chute (Figure 6).

Nevertheless, the right and left borders of the WSB chute were considered less critical because they were not affected by the discharge flow depth due to the freeboard criteria.

The upstream joint was located in a section of the chute where the water velocity was still low. Therefore, there were concerns about the presence of the stabilization forces due to the negative pressures developed in the steps. In addition, this could cause higher leakage flow also due to the higher depth of the flow in such area of the spillway. Thus, the adopted solution was an extension of the reinforced concrete of the inlet channel which overlapped the first row of WSB, as a theoretical upstream row of blocks would do (Figure 7).

On another note, the downstream joint was located at the border between the first row of WSB, downstream from the chute, and the flip bucket at the toe of the dam. Given that this row of WSB is the one from which the rest of the revetment is installed, its correct positioning was considered a

Figure 7. Detailed view of the upstream joint between the chute and the spillway inlet.

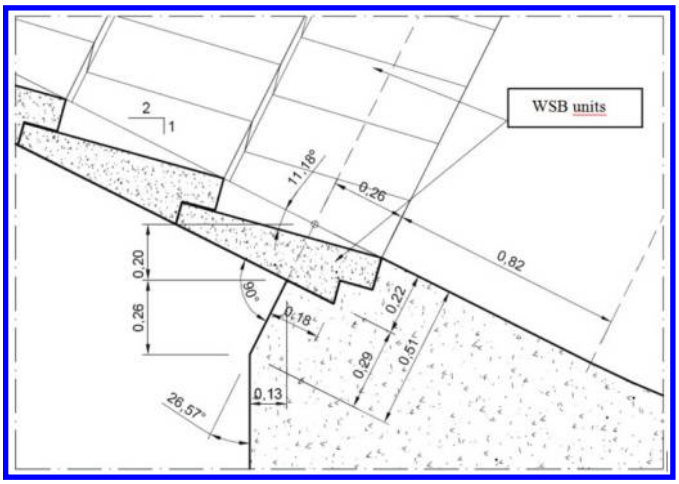

Figure 8. Downstream joint. Cross section of the first row of WSB next to the flip bucket.

key factor for the spillway construction. In addition, the downstream WSB row was also important because the next upstream rows rest over the first one. Therefore, an incorrect installation of such row would have serious consequences for the rest of the spillway chute. The adopted solution was placing the first row resting on a notch at the edge of the toe structure to be filled with cement mortar (Figure 8) so as to achieve an appropriate support. Thus, at the downstream row of the chute, the aeration vents were blocked by the mortar filling so aeration at that point was not allowed.

Finally, the longitudinal joints, i.e., the unions between the slopes and the bottom of the trapezoidal WSB chute, were studied. After considering several alternatives, the engineering team decided to adopt a joint that kept the geometry of the converging rows, so that also resulted in a stepped joint at that point. The joints were built after the construction of the converging rows and were useful as well for placing the anchors of the cable lines (Figure 6, Figure 9 and Figure 10). The gap between WSB was filled with mass concrete. In addition, this filling was reinforced with steel bars longitudinally with 3 m spaced transversal joints along the whole length of the chute.

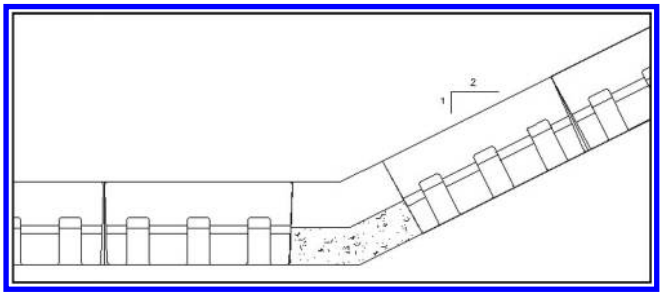

Figure 9. Cross-section view of the intermediate joint.

Figure 10. Detail of the intermediate joint.

4.3 *Toe structure and flip bucket*

The solution selected to restore the spillway discharge to the river bed was a flip bucket. The former idea of this type of toe structure was originally devised by Alfonso Álvarez (Álvarez, Montoya, & Toledo, 1998) for overtopped embankments. The flip bucket was located at the end of the chute. It was composed of two lateral structures on both sides of the spillway, and four parallelepiped blocks with dimensions of 1.8 m (width) × 7.0 m (length) × 4.0 m (height) founded in the river bedrock (Figure 5). The gaps between these blocks (2 m wide and 4 m high) were filled with large stones (minimum size of 0.8 m) to allow the drainage of spillway leakage flow. Besides, the ski jump was constructed above this toe structure (Figure 11) in order throw the flow discharge downstream the dam. The radius of the ski jump was 4.45 m, and the exit angle 30°. Additionally, five baffle blocks were added with a radius of 3.68 m and an exit angle of 45°. These baffle blocks was provided with aerators on the downstream face.

The main reasons behind the choice of this alternative were the following:

– The good quality of the river bedrock. Indeed, the limestone of the downstream river bed was considered appropriate for a plunge pool. In addition to this, an erosion study was conducted using the LNEC model to analyze the potential erosion damage that would be caused by the jet.

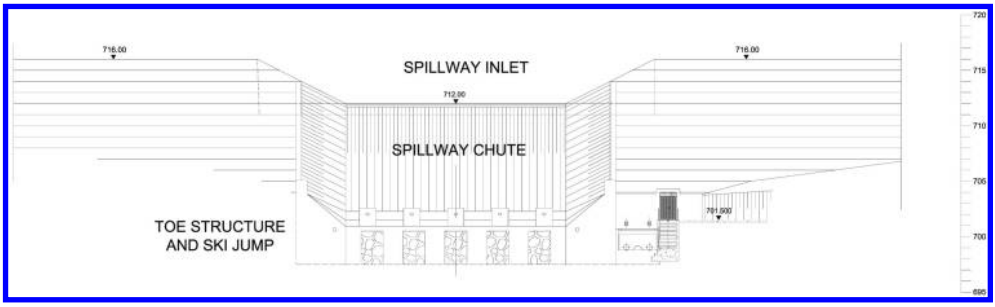

Figure 11. Drawing of the spillway from downstream.

Figure 12. Erosion in the mobile bed model of the plunge pool performed at the LNEC.

– The flip bucket achieved a complete hydraulic regime separation between the WSB chute and the downstream water level. Thus, the WSB did not have to be subjected to the highly turbulent flows developed in the plunge pool.
– The drainage of possible through-flows within the dam body material due to eventual leakages in the spillway was ensured by means of the gaps between concrete mass blocks, even for extreme floods. In such a way, the LNEC model showed that the downstream water level was lower than the upper level of the gap, even in the case of having a partial blocking of the spans of the new bridge downstream the dam, due to the deposits of the eroded material. Therefore, uplift pressures below the WSB chute were prevented.

Abovementioned new bridge was not affected by the jet discharge. Besides, the five baffle blocks allowed a significant reduction in the maximum depth of the erosion in the river bed, approximately 38%, from a 4.4 m erosion depth without baffle blocks to 2.7 m (Figure 12).

The lateral convergence of the sides of the flip bucket avoided erosion of both riverbanks. This was verified with the results from the LNEC model. In addition, some large stones were placed at the toe of the ski jump structure to avoid erosion with low discharges.

5 CONCLUSIONS AND FUTURE RESEARCH

The work performed in the project of the Barriga Dam spillway has enabled to learn lessons about some engineering problems associated to this type of technology. Hence, it was necessary to examine the manufacturing process of the WSB, materials, quality control, commissioning work, design of the block supporting layers and joints between parts of the spillway.

The overall conclusion is that WSB technology offers a suitable and cost-effective solution for erosion protection with relative high unit flows. Although this technology is necessarily limited in the scope of application at the time of writing, an expansion of this non-conventional spillway can be expected in the future. Possible applications of the WSB protection system includes overtopping protection for dams and cofferdams; auxiliary spillways to increase the hydraulic capacity of existing spillways; spillways of ponds with controlled inflows; and service spillways in small dams, such Barriga Dam case study. Likewise, it can be especially suitable in cases where the cost of a conventional concrete spillway could be out of the budget limits due to the low cost, easy installation and the possibility of transport of the WSB units directly to the dam site.

However, additional research on this type of technology is still necessary for further expansion. Possible future research lines could be summarized in:

- A deeper understanding of the hydraulic behavior and the dependence of the shape and dimensions of WSB blocks;
- The hydraulic optimization of the WSB shapes;
- Studies of new materials or concrete additives to improve the mechanical behavior of the blocks, especially for impact resistance against flow debris.
- Additional design criteria about compatible energy dissipation structures and a portfolio of construction details.

ACKNOWLEDGEMENTS

The authors of this article would like to thank all of the institutions involved in this project for their support and dedication in making it come to fruition. In particular, they seek to highlight the exquisite care and treatment received during their technical visits to the United States and Portugal, specifically from Kathleen Frizell's team at the U.S. Bureau of Reclamation; Clayton Fawcett and Robert McDonald from CONTECH, Inc.; Christopher Thornton from Colorado State University; Michael Messaros from Applied Design Corporation; Pinto Magalhaes, Lucia Couto, Teresa Viseu, and Jose Falcao de Melo from the Labóratorio Nacional de Engenharia Civil; and Antonio Pinheiro from the Instituto Superior Técnico in Lisbon. Finally, we especially thank to José L. Sevilla, from Junta de Castilla y León, for his personal effort and support to make Barriga Dam project possible.

This research line is partially supported by the ACUÑA project (ref. IPT-2011-0997-020000) funded by the Spanish Ministry of Economy and Competitiveness (MINECO) and the European Regional Development Fund (ERDF).

REFERENCES

Álvarez, A., Montoya, F. F., & Toledo, M. A. (1998). Innovaciones en aliviaderos de presas de materiales sueltos. Revista De Obras Públicas, 3378 (Julio–Agosto), 19–24.

Baker, R., & Gardiner, K. (1994). Construction and performance of a wedge block spillway at brushes clough reservoir. Proceedings of the 8th Conference of the British Dam Society on Reservoir Safety and the Environment, 214.

FEMA. (2014). Technical manual: Overtopping protection for dams U.S. Department of Homeland Security.

Frizell, K. H. (1997, September). Protecting embankment dams with concrete stepped overlays. Hydro Review, 16, 36–45.

Hewlett, H., Baker, R., May, R., & Pravdivets, Y. P. (1997). Design of stepped-block spillways. London, U.K.: Construction Industry Research and Information Association.

LNEC. (2006). Presa de barriga. estudo hidráulico em modelo reduzido do descarregador de cheias. Unpublished manuscript.

Morán, R., & Toledo, M. A. (2014). Design and construction of the barriga dam spillway through an improved wedge-shaped block technology. Canadian Journal of Civil Engineering, 41(10), 924–927.

Pether, R., Marsh, P., & Cartwright, P. (2009). An innovative new spillway for bruton flood storage reservoir. Dams and Reservoirs, 19, 67–72.

Pravdivets, Y. P., & Slissky, S. M. (1981). Passing floodwaters over embankment dams. International Water Power and Dam Construction, 33(7), 30–32.

Relvas, A. T., & Pinheiro, A. N. (2008). Inception point and air concentration in flows on stepped chutes lined with wedge-shaped concrete blocks. 134(8), 1042–1051.

Salazar, F., San Mauro, J., Irazábal, J., Larese De Tetto, A., Rossi, R., Oñate Ibáñez de Navarra, Eugenio, Toledo, M. Á. (2013). El papel de los modelos numéricos en la investigación y el diseño de aliviaderos de presas.

Thornton, C. I., & Robeson, M.D., Varyu, D.R. (2006). ArmorwedgeTM data report 2006 testing for armortec erosion control solutions, inc. Unpublished manuscript.

Dam Protections against Overtopping and Accidental Leakage – Toledo, Morán & Oñate (Eds)
© 2015 Taylor & Francis Group, London, ISBN: 978-1-138-02808-1

Physical and numerical modeling for understanding the hydraulic behaviour of Wedge-Shaped-Blocks spillways

Francisco J. Caballero
Dam Safety Research Group (SERPA), Technical University of Madrid (UPM), Madrid, Spain

Fernando Salazar & Javier San Mauro
International Center for Numerical Methods in Engineering (CIMNE), Universitat Politècnica de Catalunya, Barcelona, Spain

Miguel Á. Toledo
Dam Safety Research Group (SERPA), Technical University of Madrid (UPM), Madrid, Spain

ABSTRACT: The technology of Wedge Shaped Blocks (WSB) for spillways had a slow development through decades but has proven its practical reliability. Ongoing additional research aims to complete the theoretical knowledge, improve current design criteria and make this technology available to practitioners as one more solution to consider when designing an embankment dam spillway. Here a summary is provided about recent physical and numerical modelling of WSB spillways performed by UPM and CIMNE.

Keywords: Wedge shaped blocks, WSB protections, overtopping, Dam research

1 INTRODUCTION AND OBJETIVES

The increasing demand for safety in modern societies has resulted in the drafting of new regulations and technical manuals to protect critical infrastructures in several countries around the world, such as dams. As a result, it will be necessary in the forthcoming years to act on plenty of existing dams, some of them still underway, all over the world. So there is a need of cost-effective measures.

Although different protection techniques for embankment dams have already been successfully applied all over the world, some of them have not yet been properly tested and the technology is still in progress. This results in a lack of credibility for potential users that prefer more conventional and expensive solutions. Given that the budget availability for every dam owner is limited, the overall resultant situation is that plenty of dams are waiting for the necessary amount of money while suffering an unsatisfactory situation regarding the safety. A proper understanding of the problem, and a suitable modeling technique could sometimes solve the safety problem with a moderate investment by means of an unconventional solution.

Therefore, additional research is still necessary to improve current design criteria for this unconventional spillways. It is the case of wedge-shapped blocks protections (WSB). Being aware of that, and after the design and construction of a WSB solution for Barriga dam (2007) in Spain [1], the R+D project ACUÑA arose. Executed by the consortium of the companies PREHORQUISA and ALATEC and research organizations: Dam Safety Research Group (SERPA) of the Technical University of Madrid (UPM) and the International Center for Numerical Methods in Engineering (CIMNE). The project aims to properly characterize the behavior of this type of spillway for the placement on the downstream shoulder of embankment dams.

The technology for design and construction of a WSB spillway has a long history and has proven its practical reliability, but had a slow development through decades. The final objective of ACUÑA

project is to complete the body of knowledge needed to dissipate the theoretical uncertainties and improve on the design of the WSB.

2 BACKGROUND

The stability of wedge shaped blocks is based on the positive pressure of the water impacting on the upper face of each block, the overlapping, and the development of negative pressures at the base due to the air vents when a suction occur in the step. WSB have proven to be highly stables even in very unfavorable conditions.

Professor Y. Pravdivets (1981) [2] carried out in Russia his pioneer works in this field, followed along the next decades by Baker, Hewlett et al. (1994–1997) [3], [4] and [5] in United Kingdom and by Frizell (2000–2007) [6] and [7] in United States.

The US Bureau of Reclamation conducted physical tests in the test channel available at Colorado State University, in Fort Collins, with a slope of 2:1 and maximum unit flows above 4 m^2/s [7], [8] and [9]. From these experiences a US Patent arose for the tested WSB (Armorwedge^{TM}) held by the company Armortec, Inc. However, there are still few WSB spillways in the world, most of them in Russia and the United States, prototypes and minor works. In 2007 the first dam having a service spillway of wedge shaped blocks was built in Spain: the Barriga Dam.

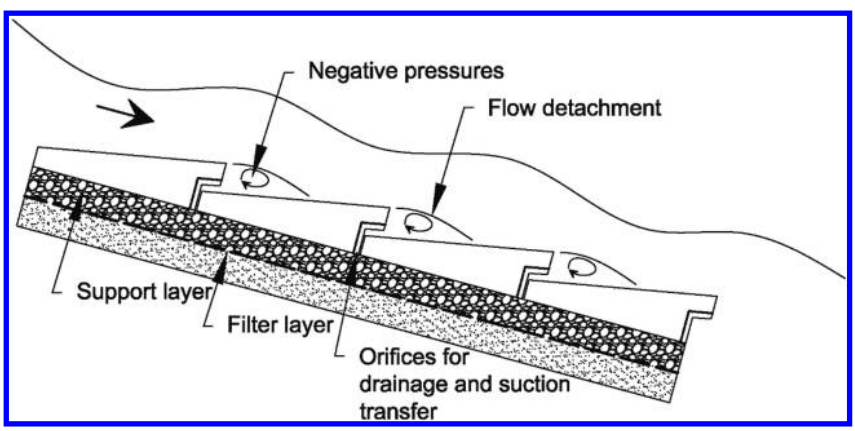

Figure 1. Sketch of the hydraulic performance of a wedge-shaped blocks spillway.

Figure 2. Left: Aerial view of Barriga dam (Source: Regional Authority of Castilla y León). Right: Spillway dicharge (Source: José Manuel Ruiz, May 2008)

After construction of the Barriga Dam, Bruton Dam WSB spillway was built in Somerset, United Kingdom (Pether, Marsh, & Cartwright, 2009) [10] as well as Friendship Village auxiliary spillway in Missouri, USA (FEMA, 2014) [11].

3 PHYSICAL MODELING

Physical models are needed for the calibration and validation of numerical models. and allow the understanding of the hydraulic behavior of the WSB spillway, including the effect of aeration.

3.1 *Previous tests*

Firstly a series of tasks were performed to determine the instrumentation to be used in the final model. Two types of instrumentation for recording water pressures were testes at the Hydraulic Laboratory of the *E.T.S. Ingenieros de Caminos* of the *Technical University of Madrid*: scanivalve sensors (Figure 3a) and pressure transducers (Figure 3b).

The tests were performed in a channel 0.30 m wide and 7 m long. A methacrylate wedge shaped block was installed inside the channel, with dimensions scaled to 1/3 of the Barriga Dam block unit. Water pressures were recorded at several points of the block for discharges between 3 l/s and 15 l/s.

Several trial tests were performed, with and without step, with shorter and longer plastic tubes, with different diameters of the same plastic tubes and so on. From the tests it was concluded that both types of instrumentation (Figure 3) for measuring the water pressure were equally valid for the purpose of the physical modeling.

3.2 *Test set up*

3.2.1 *Testing facilities*

Testing facilities are located at the Hydrographic Studies Center of CEDEX. The main features of the test channel are: a) level difference between extremes: 470 cm; b) slope 2:1; c) width: 50 cm; d) height: 85 cm (perpendicular to the base); e) maximum discharge: 170 l/s.

A 6 m high tank with a section 2.5 × 2.5 m^2 feed the test channel. At its top a window of 0.5 m wide and 0.7 m high in the vessel wall at 4.7 m above the ground was run. For a better control the point where critical depth occurs and to ensure water adequately entering the test channel, a horizontal channel section 0.5 m wide, 0.75 m high and 1.5 m long joins the tank and the test channel.

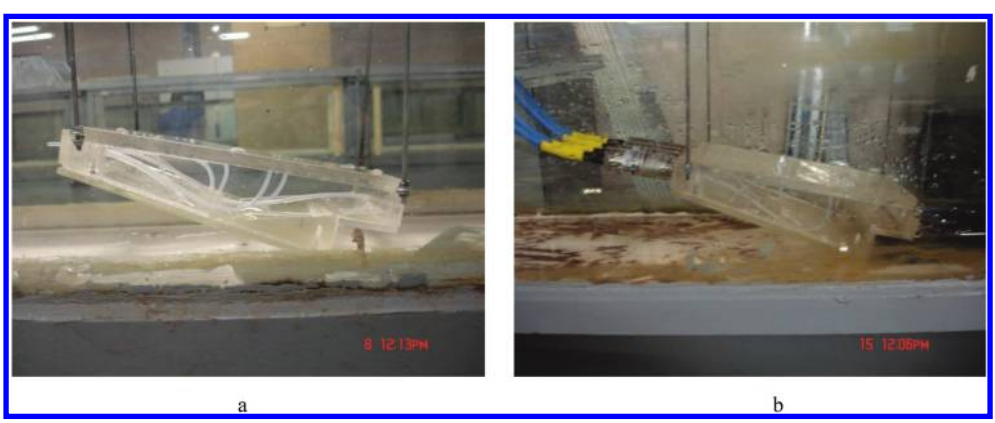

Figure 3. a) WSB of methacrylate with scanivalve device; b) WSB with pressure transducers.

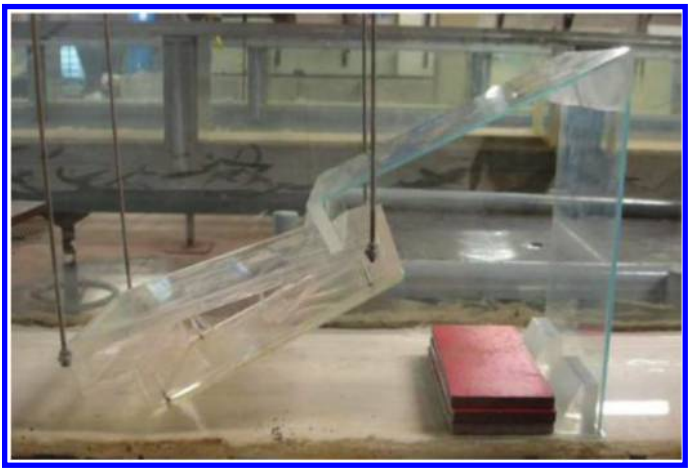

Figure 4. Step and WSB prepared for testing.

A non-slip metallic grill allows the WSBs to stand 0.2 m over the channel bottom (Figure 5b). The purpose of this grill is to drain, and then measure, the flow that seeps down between the lateral faces of the WSBs. This flow is collected at the end of the chute through a tube that drains into a triangular weir and then returns to the lower tank.

At the end of the test channel the flow enters into a stilling basin (Figures 5c and 5d) that reduces water velocity and allows the control of the water discharge through a rectangular weir before returning to the lower tank to be pumped again.

3.2.2 *Measuring devices and data acquisition*

The test set up includes measuring devices that can be grouped into four main categories:

- Measuring devices for water levels and flows:
  - Electromagnetic flowmeter for pumped flow measurement.
  - Triangular sharp crested weir to measure the flow that seeps through the open joints between blocks.
  - Electromagnetic limnimeters (4), for measuring the water level in the upper feeding tank, at the beginning of the test channel, on the above mentioned sharp crested wire, and on the final rectangular weir.
- Pressure measurement system, formed by a set of 12 Messtech submersible pressure transducers XA-700, installed in the methacrylate measuring block (Figure 6c and 6d), and a Scanivalve DSA3207 Corp. model sockets 16 with measuring tubes (Figure 6b) installed on another measuring block. Both types of measuring devices are used to register the water pressures at several points on the footprint, base and the rise step of the WSBs (Figure 6a).
- Fiberglass probe and equipment for two-phase flow local measurements (Figure 7). It registers the concentration of air bubbles in the water-air two-phase flow, and so allow to determine the depth of the flow according to a specified criterion.

The data acquisition is performed by means of a data collection equipment (cDAQ) of National Instruments. A conventional video camera is used for recording the tests.

3.3 *Measuring blocks and methodology*

Two methacrylate wedge shaped blocks were designed as measuring blocks. Pressure sensors were placed on the block faces (Figures 6 and 8). Data acquisition occurs in a time interval of 3 minutes per tested flow.

Figure 5. Testing facilities.

As expected, pressure records are negative (suction) at the bock base and quasi vertical face. Sensors 3, 4 and 5 show positive pressure; pressure sign is variable at sensor 6, sometimes negative and sometimes positive, and sensors 7 and 8 show negative pressure. Air concentration was considered for defining water depth along the test channel. Water surface was set where air concentration is 90% [12].

Air concentration data were acquired over a time interval of 60 seconds in each position of the air meter. Discharges was tested from 40 to 150 l/s with a discharge step of 10 l/s.

4 NUMERICAL MODELING

4.1 *Methodology*

Two different numerical tools have been used to model the flow over the wedge-shaped blocks. They reproduce both the overall behaviour and the specific phenomena near the block surface, such as air-water interaction or vorticity.

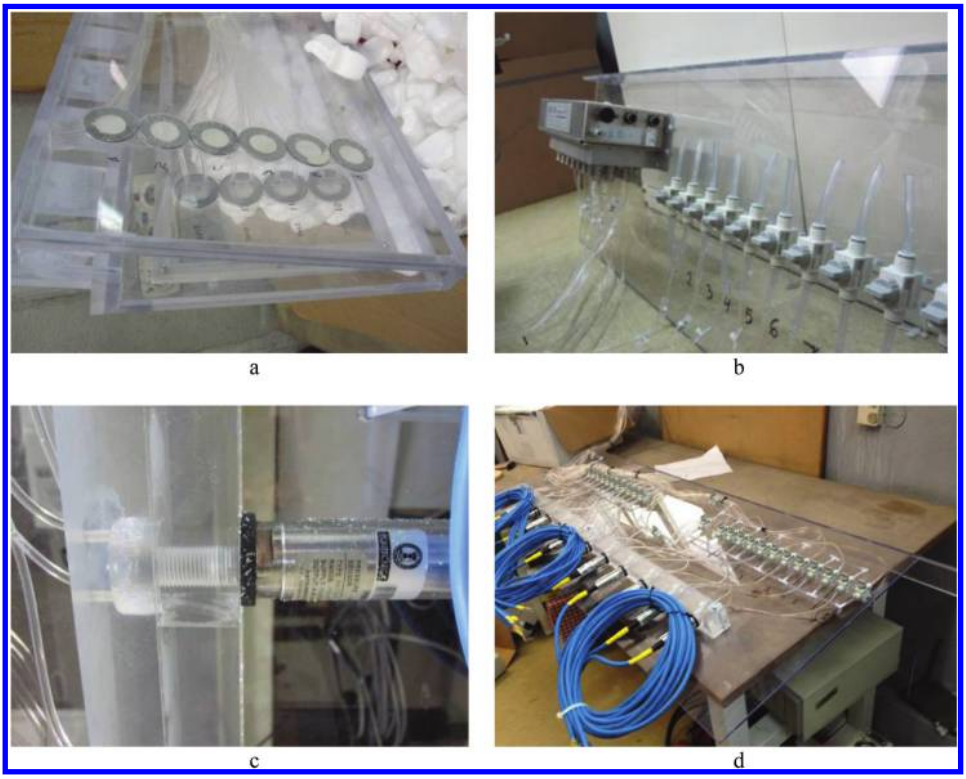

Figure 6. a) Methacrylate wedge shaped block pressure measurement device, b) Installing sensors in laboratory with scanivalve device, c) and d) Installing sensors in laboratory with pressure transducers.

Figure 7. Installation of equipment for two-phase flow local measurements in testing channel.

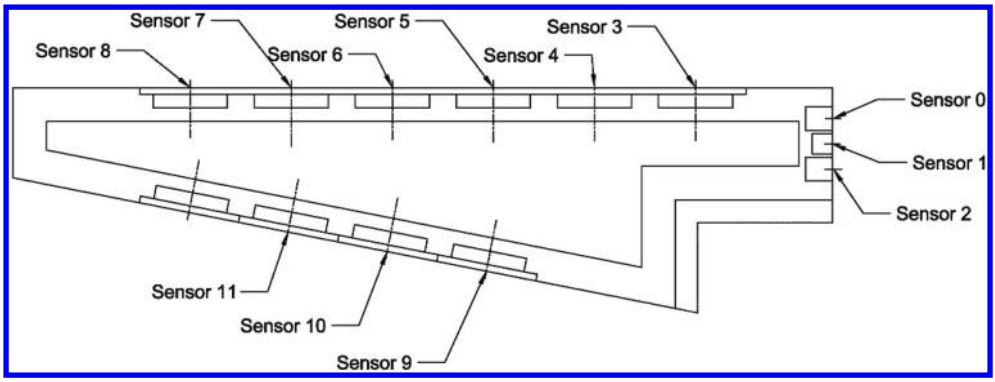

Figure 8. Location of pressure sensors in a measuring wedge shaped block.

Both are based on the finite element method (FEM) and solve the Navier-Stokes equations in 3D. However, one of them is based on a lagrangian formulation (the particle finite element method, PFEM) whereas the other uses an eulerian formulation.

The eulerian code is an application of the open source software Kratos Multi-physics. It has been previously applied in spillway hydraulics [13], among other engineering problems. The details on the numerical implementation can be found in [14] and [15].

The lagrangian one is based on the PFEM method developed by CIMNE [16]. PFEM allows considering the interaction between several fluids and structures [17], so it was used to model the air-water interaction phenomenon. PFEM has been validated for the simulation of various hydraulic problems in the field of dam hydraulics [18].

In summary, two numerical campaigns were performed:

1. The eulerian code was used for reproducing the whole experimental facility, with the aim of measuring the flow depth and the dynamic pressure. The preliminary results presented correspond to the validation of the numerical tool: flow depth and pressure measurements in step 25 (Figure 9) were compared to those registered in laboratory for 100 l/s of incoming flow.
2. The PFEM was applied to small 2D models, representing the vicinity of one step. Air-water interaction was considered in order to qualitatively assess the efficiency of the orifices.

4.2 *Results*

4.2.1 *Flow depth and pressure. Eulerian code*

The laboratory facility was numerically reproduced in 3D. Figure 9 shows a side view of the numerical model, as well as a detail of step 25, where the pressure and air concentration sensors were installed.

Air entrainment in stepped spillways leads to the formation of an air-water mixture flow without a steady free surface. Given that the flow depth is a useful parameter for the design of the chute walls, the concept of 'characteristic depth' was developed and is often used instead [12]. It corresponds to the depth where the air concentration reaches 90%.

This is in contrast with the numerical scheme of the eulerian code, which computes the 'exact' position of the free surface at each time-step. However, it is reasonable to think that the free surface in the numerical results may be representative of a certain value of the air-concentration.

Figure 10 shows the comparison between numerical results and the experimental records of the characteristic depth in three locations above step 25. It turns out that the position of the free surface in the numerical model oscillates significantly for a quasi-steady state. Hence, the maximum, minimum and average flow depth have been computed and plotted in Figure 10. It can be noted that the maximum flow depth in the numerical model corresponds to the characteristic depth recorded in the experiments.

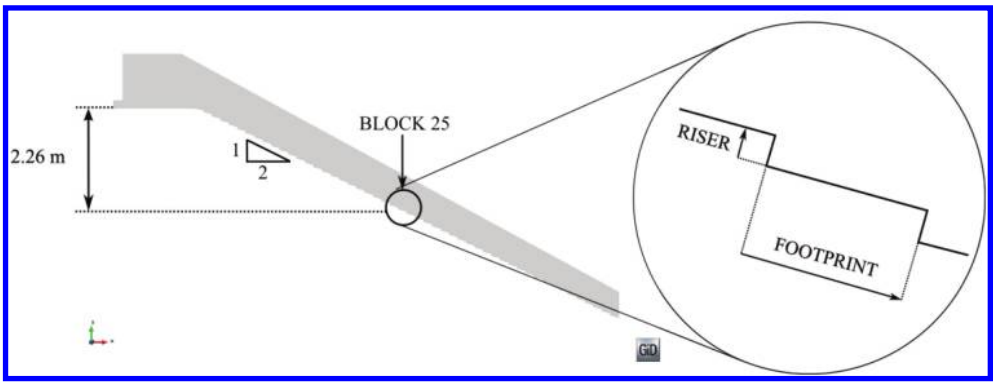

Figure 9. Left: Numerical model (side view). Right: detail of the instrumented block.

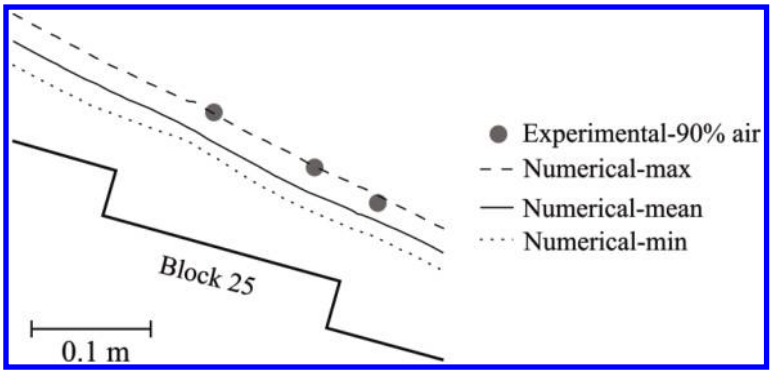

Figure 10. Numerical and experimental location of the free surface location in block 25.

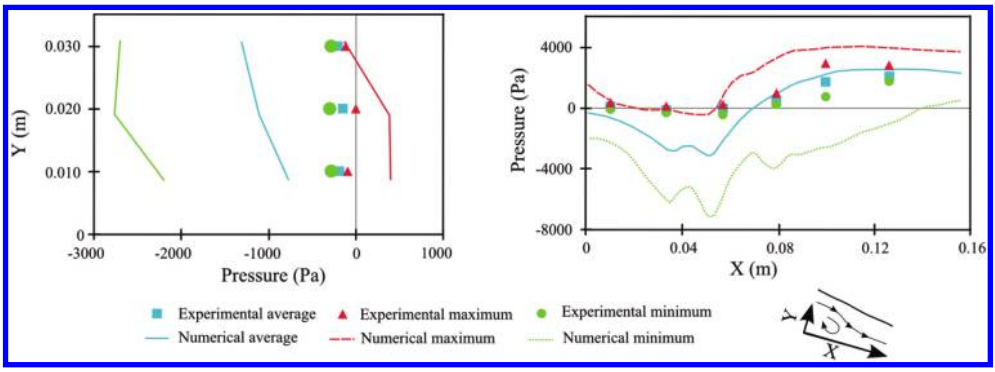

Figure 11. Numerical and experimental pressure recorded along the riser (left) and the footprint (right) in the numerical and the experimental models.

Dynamic pressure has been extracted from the numerical model output at different locations along the riser and the footprint of step 25. Again, the values fluctuate, so the maximum, the minimum and the average are considered. Figure 11 shows the comparison with the experimental results.

It can be noted that the pressure fluctuations are higher for the numerical model. The comparative analysis of the average values results in two well-identifiable areas: a) the riser and the upstream

Table 1. Cases analysed.

Flow depth (m)	Velocity (m/s)	Flow depth (m)	Velocity (m/s)
0.1	1.0	0.33	5.0
0.1	3.0	0.33	7.0
0.1	5.0	0.33	15.0
0.1	7.0	1.0	7.0
0.33	3.0	1.0	15.0

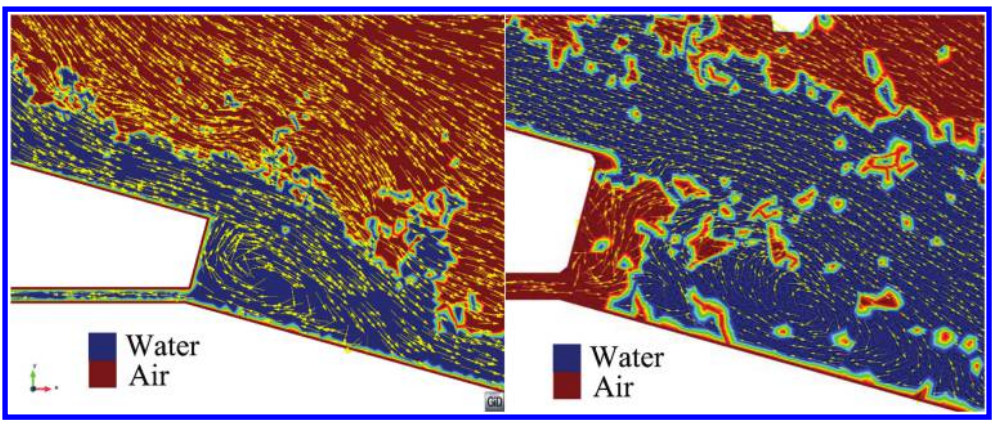

Figure 12. Examples of different performance of the bottom orifice. Left: Flow depth = 0.1 m; Inflow velocity = 3 m/s. The eddy generates water exit through the conduit. Right: Flow depth = 0.1 m; Inflow velocity = 7 m/s. The higher velocity results in more negative pressure and air entrainment. The eddy moves downstream.

half of the footprint, where experimental pressure is close to zero, whereas negative values are registered in the numerical model, and b) the downstream half of the footprint, where results are similar, both quantitatively and qualitatively.

This discrepancy is due to the simplification assumed in the numerical model: the orifices located in the internal edge of the block are not considered. The flow over the external edge generates negative pressures, as registered. In the experimental tests, the blocks feature bottom holes which transmit the negative pressure to the base, thus reducing it close to zero.

4.2.2 *Aeration. PFEM*

The orifices are meant to transmit the negative pressure generated by the flow toward the base of the block, increasing stability. As aforementioned, a more accurate representation of the actual performance requires consideration of air-water interaction, for which PFEM was considered more suitable. The tool has been already applied to the simulation of similar phenomena, such as the aeration in bottom outlets [19].

Two simplifications of the problem were assumed: a) it was modelled in 2D, and b) the geometry of the orifice was modelled as a straight conduit of the same width. The objective was to study the influence of the fluid parameters (depth and initial velocity) on the hydraulic performance.

Different combinations of flow depth and velocity and were tested, as listed in Table 1.

The results show that the orifices at the bottom of the block can operate in two ways: a) if the flow generates enough negative pressure, air flows towards the spillway surface, and b) if the air-water mixture flow results in positive pressure, water exits the block surface through the conduit. Examples of the aforementioned behaviours are depicted in Figure 12.

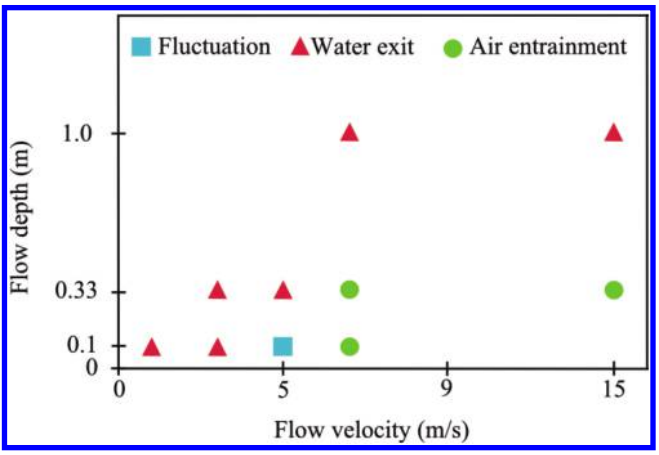

Figure 13. Aeration conduit performance.

The qualitative analysis of the results (Figure 13) show that an increase in flow depth leads to higher positive pressure for a given velocity. This favours water exit through the conduit. On the contrary, for a given flow depth, a higher velocity results in lower pressure in the riser, what stimulates air entrainment.

5 CONCLUSIONS

Preliminary results of the numerical simulation of flow over wedge-shaped blocks showed good agreement between the maximum flow depth in the numerical model and the characteristic depth recorded in the experiments. These results need to be confirmed for other flow conditions and spillway configurations.

The numerical eulerian code reproduced the dynamic pressure in the downstream reach of the block. On the contrary, it provided negative values in the riser and the upstream half of the footprint, while experimental measures were close to zero. This discrepancy was attributed to the non-consideration of the orifices located in the internal edge of the block, which dissipate the negative pressure generated by the flow.

The effect of the orifices and the air-water interaction were modelled with the PFEM in a simplified manner for various flow conditions (depth and velocity). The results obtained are reasonable, although need to be validated with experimental measurements.

Numerical modelling offered useful information for better understanding the complex phenomena involved, which will be used for developing and testing improved designs.

ACKNOWLEDGEMENT

The research was founded by the Spanish Ministry of Economy and Competitiveness (Ministerio de Economía y Competitividad, MINECO) through the projects ACUÑA (IPT-2011-0997-020000) and DIABLO (RTC-2014-2081-5).

REFERENCES

[1] Morán, R., & Toledo, M. A. (2014). Design and construction of the Barriga dam spillway through an improved wedge-shaped block technology. Canadian Journal of Civil Engineering, 41(10), 924–927.

[2] Pravdivets, Y. P., & Slissky, S. M. (1981). Passing floodwaters over embankment dams. International Water Power and Dam Construction, 33(7), 30–32.

[3] Baker, R., & Gardiner, K. (1994). Construction and performance of a wedge block spillway at brushes clough reservoir. Proceedings of the 8th Conference of the British Dam Society on Reservoir Safety and the Environment, 214.
[4] Baker, R. & Gardiner, K.D. (1995). Building blocks., International Water Power and Dam Construction, vol. 47, no. 11, pp. 2.
[5] Hewlett, H., Baker, R., May, R., & Pravdivets, Y. P. (1997). Design of stepped-block spillways. London, U.K.: Construction Industry Research and Information Association.
[6] Frizell, K. H. (1997, September). Protecting embankment dams with concrete stepped overlays. Hydro Review, 16, 36–45.
[7] Frizell, K.H. (2007). ArmorwedgeTM analysis report: block size scaling and bedding information. (Confidencial).
[8] Armortec Erosion Control Solutions (2006). Pre-cast concrete units. Barriga dam project. Burgos. Spain., Submittal documents edn. (Confidencial).
[9] Thornton, C.I. & Robeson, M.D., Varyu, D.R. (2006). ArmorwedgeTM Data
[10] Pether, R., Marsh, P., & Cartwright, P. (2009). An innovative new spillway for bruton flood storage reservoir. Dams and Reservoirs, 19, 67–72.
[11] FEMA. (2014). Technical manual: Overtopping protection for dams U.S. Department of Homeland Security.
[12] I.R. Wood (1983). Uniform region of self-aerated flow. *Journal of Hydraulic Engineering* 109.3: 447–461.
[13] F. Salazar, R. Morán, R. Rossi and E. Oñate (2013). Analysis of the discharge capacity of radial-gated spillways using CFD and ANN–Oliana Dam case study. *Journal of Hydraulic Research*, 51(3), 244–252.
[14] P. Dadvand, R. Rossi, and E. Oñate (2010). An object-oriented environment for developing finite element codes for multi-disciplinary applications. *Archives of Computational Methods in Engineering*, 17, 253–297.
[15] R. Rossi, et al (2013). An efficient edge-based level set finite element method for free surface flow problems. *International Journal for Numerical Methods in Fluids* 71.6: 687–716.
[16] E. Oñate, S.R. Idelsohn, F. Del Pin, and R. Aubry (2004). The particle finite element method: an overview. *International Journal on Computational Methods*. 1:267–307.
[17] E. Oñate, M.A. Celigueta, S. R. Idelsohn, F. Salazar, and B. Suárez (2011).. Possibilities of the particle finite element method for fluid–soil–structure interaction problems. *Computational Mechanics*, 48(3), 307–318.
[18] A. Larese, R. Rossi, E. Oñate, S.R. Idelsohn (2008). Validation of the particle finite element method (PFEM) for simulation of free surface flows. *Engineering Computations* 25.4: 385–425.
[19] D. Pozo, F. Salazar, and M.Á. Toledo (2014). Modelación del funcionamiento hidráulico de los dispositivos de aireación de desagües de fondo de presas mediante el método de partículas y elementos finitos. *Revista Internacional de Métodos Numéricos para Cálculo y Diseño en Ingeniería*, 30(1), 51–59. [In Spanish]

Masonry dams failure due to overtopping and its protections

Dam Protections against Overtopping and Accidental Leakage – Toledo, Morán & Oñate (Eds)
© 2015 Taylor & Francis Group, London, ISBN: 978-1-138-02808-1

Failures of masonry or concrete dams by overtopping

A. Vogel
Risk Assessment International (RAI), Vienna, Austria

F. Laugier & E. Bourdarot
EDF-Division Production Ingénierie Hydraulique, Centre d'Ingéniérie Hydraulique – Département Génie Civil, Savoie Technolac, Le Bourget du Lac Cédex, France

ABSTRACT: Dam resistance of concrete or masonry dams in overtopping condition has to be considered regarding the possible failure mechanisms. From this point of view indications provided by the analysis of the recorded failure (complete or partial) of dam cases appears very useful. In this paper available cases of gravity, buttresses and arch dam failures will be reviewed, pointing out the possible consequences in flood conditions of overtopping effects on dam or foundation stability conditions or the behaviour of mechanical components. Some cases will be examined and an attempt to draw some general features will be performed.

Keywords: Dam, Failure, Overtopping

1 INTRODUCTION

At the beginning of the 20th century failures of masonry or concrete dams were common events. Overtopping conditions as a result from underestimated flood events were always connected with additional uplift forces which often led to sliding effects of complete dam bodies or static overburdens at destinguished points within the dam construction. Well known are the failures of Lynx Creek Dam (Fig. 1) in 1891 [1], Mc. Donald Dam (Fig. 2) in 1900 [2, 3], Fergus Falls Dam (Fig. 3, 4) in 1909 [4] and Bayless Dam (Fig. 5, 6) in 1911 [5, 6, 7]. An extraordinary tragedy was the life span of Habra Dam in Algeria which failed three times in 1872, 1881 and 1927 [8, 9, 10] always under flood conditions (Fig. 7, 8). Today events which led to overtopping processes of dams are most times based on natural catastrophes but sometimes the causes are also manmade.

Figure 1. Lynx Creek Dam after failure.

Figure 2. Mc. Donald Dam after failure.

Figure 3. Fergus Falls Dam before failure.

Figure 4. Fergus Falls Dam after failure.

Figure 5. Bayless Dam before failure.

Figure 6. Bayless Dam after failure.

Figure 7. Habra Dam in the 1920s.

Figure 8. Habra Dam after its third failure.

2 DAM FAILURE CASES CAUSED BY OVERTOPPING

Nowadays the main reasons for overtopping of dams are underestimations of natural flood events, siltation of reservoirs, unfavorable maintenance of gates and spillways, and flood situations after failures of large dams, which led to cascade failures of other dams situated downstream in the path of the initial dam break flood wave.

2.1 *Dam failures caused by underestimation of natural flood events*

Obviously the intensities of typhoons and hurricanes but also of local storm events increased in the last decades. A gap between weather forecasts and rain intensities in the reality seems to exist,

Figure 9. Gillespie Dam with cars on its apron crossing the Gila River.

Figure 10. Gillespie Dam today.

because otherwise the high numbers of failed dams after flood events must be explained as results of construction faults or too late human reactions. But the fact that many of the affected dams stand in operation for many years lets crumble the theory of faulty constructions.

The Gillespie Dam in Arizona, a concrete multiple arch dam was constructed in 1921. It is a free overflow construction with an ogee crest with 6,1 m in height and about 520 m in length. There is a small concrete stilling basin beneath the dam, and gates exist on each side of the river to release water to irrigation canals. The Gila River drains 128.540 km^2 above Gillespie dam [11]. As the dam was located at an important river crossing that would later become US Route 80, the former Arizona Highway Department constructed a concrete apron at the foot of the dam to allow for vehicular crossings.

As the dam was a simple spillover construction, during times of heavy runoff cars would have to be pulled through the flow by trucks, and during floods could not cross at all (Fig. 9). Today this fact is history because 1926, the Highway Department commissioned the construction of a steel truss bridge just downstream from the dam. The bridge was completed and opened to traffic on August 1, 1927.

Unusually intense and prolonged rains in January 1993 caused the most widespread and severe flooding in the State of Arizona since ever, in the entire state the precipitation received an excess of 300% of normal. The Gila River basin was confronted with the largest volume of runoff since record keeping began since 1888. The precise size of the flood at the Gillespie Dam site was not recorded due to an equipment failure, but an estimate value based upon a high water mark recorded on U. S. Geological Service equipment yielded a peak flow of approximately 5.700 m^3/s which correspond to a predicted 65-year flood. In the morning of January 9, 1993 the dam failed when a segment with 37 m in length collapsed into the river (Fig. 10). While the precise cause of the failure is officially still unknown, the extreme flooding was almost certainly a contributing factor [12]. Another goal for the disaster was the fact that the reservoir was filled with sediments as a result of abundant upstream sediment supply within the first decade after its construction. In the 1980s, the county Flood Control District initiated projects near the dam to clear a 300 m wide channel to the dam. The district signed an indemnity agreement with the then-dam owners, under the condition that the district would pay for liability or losses that may result from the clearing projects. At the time of failure the elevation of the deposits in the reservoir immediately upstream of the dam have exceeded the elevation of the top of the dam by 60 cm. Therefore as a result of the flooding after the dam break 26.0 to 27.5 Mm^3 of sediments were caused to settle on downstream properties. Two years after the failure more than a dozen landowners along the Gila River sued the then-owners of the Gillespie Dam and the County Flood Control District to refund costs for damages to a height of 23.7 M$. They alleged the dam owners were negligent in operating the dam, and the district contributed to the dam breaching because of its clearing project. Nine years later in 2004, a jury found the district was responsible for 10 percent of the farmer's damages, and the dam owners were responsible for 80 percent, because they were negligent in maintaining the dam and caused the breach [13].

Figure 11. Sella Zerbino Dam before failure.

Figure 12. Sella Zerbino Dam after failure.

In opposite to Gillespie Dam a main fact for the unsafe overtopping of masonry or concrete dams is the lack of safeguards against dam toe erosion. Erodibility of the downstream foundation or the absence of works of effective energy dissipation often led quickly to the total loss of the construction. Well known is the catastrophic failure of Sella Zerbino Dam in Italy at 1935. The Ortiglietto Reservoir built from 1923 to 1925 was stored by two gravity dams with a capacity of 18 Mm^3. It was situated on the Orba River, near the city of Molare in northern Italy. Both dams were founded on serpentine of good quality with some fissures only at the dam site of Sella Zerbino [14, 15].

The larger of both constructions Bric Zerbino Dam was a curved gravity dam with a maximum height of 49.8 m, a crest length of 160 m and a crest thickness of 6 m. A bottom gate, a discharge tunnel with an automatic valve, a free overflow spillway with a length of 68 m at the right abutment and 12 automatic siphons built into the dam crest had a total discharge capacity of 855 m^3/s, which corresponded to the known 20-year flood.

The smaller Sella Zerbino Dam was a straight gravity dam with a maximum height of only 16.8 m, a crest length of 80 m and a crest thickness of 3.3 m (Fig. 11). On August 13, 1935 a heavy cloudburst caused an inflow of 1.350 m^3/s into the reservoir and overtopping of both dams to a height of 3 m. The smaller Sella Zerbino Dam which was constructed as a saddle dam failed completely. After the erosion of the unprotected dam toe also the rock of the foundation was eroded. As the dam tipped over the complete storage volume was lost (Fig. 12). Despite warnings downstream the flood wave caused more than 100 victims in the nearby city of Ovada [16, 17].

In 1969 for the water supply of Choma in Zambia a 15 m high gravity dam was constructed on Muzuma River. The dam included a free overflow section which was nearly as long as the full crest length (Fig. 13). Therefore the stilling basin was not only situated in the river bed but also on both sides of the abutments. The used concrete was of bad quality with less compaction. During the construction a flood less than the design flood was the cause for overtopping the dam along its full crest length. The absence of works for effective energy dissipation led to the erosion and destruction of the stilling basin and finally to the destruction of the dam (Fig. 14). After the failure it was found that the stilling basin and the dam itself was founded directly on the river alluvilas and not on rock which was situated 2 m below the alluvials [18].

On March 17, 1979 the Poquim Dam with a height of 10 m and a crest length of 110 m failed in Brazil. It had a free overflow section which could be gated by flashboards during draught periods to increase the water level in the reservoir about 1 m (Fig. 15). During rainy seasons the gates could be removed to allow a free passing of floods. Due to negligence of operation in February 1979 a flood occurred while the flashboards were still in place at the dam crest. It was the reason that the dam was overtopped with massive erosion effects downstream at both sides on the right and left abutments (Fig. 16). After this incident the operation personal was instructed to maintain the dam under half load why the bottom outlet kept open. Before any repair works were started in March 1979 an even larger flood occurred, which caused the failure of the dam (Fig. 17). Downstream in the city of Itambacuri 158 houses were destroyed why 1.700 persons left homeless, but fortunately the flood caused no fatalities [19].

Figure 13. Muzuma Dam just before failure.

Figure 14. Muzuma Dam after failure.

Figure 15. Poquim Dam in the 1950s.

Figure 16. Erosion damage at the left abutment of Poquim Dam after the flood event in February 1979.

Figure 17. Poquim Dam after failure.

Figure 18. Detail of breach formation.

It is of interest that the dam was not overtopped during the second flood event and the failure occurred at the right side of the dam, where the dam was founded only on natural soils onsite and not on rock as along its middle part. Obviously the failure was caused by piping through the abutment, because parts of the structure toppled upstream instead of downstream, as it would be expected if water had passed over the dam (Fig. 18) [20].

In 1996, major flooding occurred along a number or rivers in British Columbia, Alberta, Saskatchewan, and Manitoba in Canada. The most disastrous flooding however occurred in the Saguenay – Lac-Saint-Jean area, in southern Quebec, due to heavy rain that fell at July 18 to 21, 1996. The Seguenay floods caused severe inundation and extensive erosion along some rivers reaches, resulting in major channel widening and bank erosion, the breaching of dams and dykes, and damage to other infrastructural facilities. Also at this event at the Lake Ha!Ha! Reservoir,

Figure 19. Ville de Jonquière Dam after failure.

Figure 20. Chute-Garneau Dam after failure.

inadequate available capacity to spill during the storm at the outlet dam resulted in the overtopping and erosion of a nearby earthfill saddle dyke. A new outlet formed at the site of the dyke and drained the reservoir over a period of many hours [21].

In the same area floodwaters overtopped four dams and eroded deeply into unconsolidated sediments adjacent to the dams, forming new channels that captured the flow of the river. These extreme geomorphic effects happened along the Rivière aux Sables and Rivière Chicoutimi and they occurred locally at the affected dam sites. At the Jonquière and Chute-à-Besy dams on the Rivière aux Sables and the Chute-Garneau and Pont-Arnaud dams on the Rivière Chicoutimi, floodwaters overtopped and incised an area immediately adjacent to each dam, breaching the impoundment, and diverting the entire river flow into a newly-eroded channel course. The new channels rejoined the river downstream of the dams over distances ranging from several 10s of metres (Chute-Garneau dam) to about 500 m (Chute-à-Besy dam). Following the flood, all four dams were intact, but non-functional, as the level of the diverted flow was below the base of the dams [22].

At the Ville de Jonquière Dam a breach occurred within the concrete wing of the dam, lowering the reservoir level by several metres (Fig. 19). At the dam site of Chute-Garneau dam on the Chicoutimi River, a newly eroded channel carried the entire flood beside the dam, bypassing the penstocks and sluice gates. The dam remained intact, but was non-functional (Fig. 20).

The cascade failures of Canadian dams in the Seguenay area and the failure case of Gillespie Dam are impressive examples for the fact that siltation of reservoirs obviously increase the risk of dam failures in situations of additional flood loadings. Dams holding back silted up environments and keep the risk to fail by overtopping are endangered to release not only stored water but also sediments and need therefore special treatments, sometimes with the same effect as dams, which have failed.

2.2 *Dam failures caused by siltation of reservoirs or deterioration*

To retard the sediment transport and its effect on the Shimen reservoir in Taiwan, large check dams were built in the main channels of the reservoir watershed. In 1977 the Baling Dam was built as one of the largest in this area. The concrete dam had a height of 38 m and a crest length of 80 m and was designed to hold back sediments materials to an amount of 10 Mm^3 (Fig. 21). 2005 after the typhoon Matsa the reservoir of Baling Dam was covered with debris [23] and during the typhoon Wipha on 17 to 19 September 2007 the dam was overtopped and its foundation was undermined that it breached on a length of 60 m (Fig. 22). As a result of the outburst of 10 Mm^3 of sediments significant geomorphic impacts along the Dahan River could be observed and downstream the nearby city of Baling was destroyed [24].

To avoid catastrophic outbursts of sediments from silted reservoirs or the overtopping of old dams out of operation, affected constructions also often get breached.

The Lake Leigh Dam was built in 1906 by the Ambursen Hydraulic Construction Company as a hollow reinforced concrete dam with a height of 9.8 m and a crest length of 97.5 m, exclusive of

Figure 21. Baling Dam in November 2005.

Figure 22. Baling Dam in December 2008.

Figure 23. Lake Leigh Dam today.

Figure 24. Breached Lake Leigh Dam.

earthen embankments at each end. The earth embankments at the ends, 62.2 m and 51.2 m long, respectively were provided with concrete core-walls and the slopes were protected with riprap. The spillway 7.3 m long and 0.6 m deep was at about the middle of the concrete section. No apron was provided on the downstream side of the spillway [25].

In 1909 and again in 1911 the dam suffered an icipient failure by the development of copious leaks beneath the cut-off wall of the concrete section. The dam was successful repaired and was integrated in a new state park opened to the public on August 1, 1943. On April 20, 1958 in the concrete section developed a hole, which caused the Pennsylvania State Police to evacuate up to 2.000 people from the park. Engineers from the state inspected the dam and made a second breach in the dam near ground level to drain the lake. In the resulting flood some of the hiking paths in Glen Leigh Park were destroyed. The Lake Leigh Dam is still existing but since that date it will never store water again (Fig. 23, 24).

A quite similar example was for many years the Des Plats Dam in France which was constructed in 1958. It is a concrete arch dam 21.2 m in height and 140 m in length. The dam always stored water and was never emptied until autumn 2005. After a period of extreme low temperatures in November 2005 during the period where the reservoir was emptied, the dam cracked. To avoid any risk the responsible authorities decided to breach the dam and a hole of 10 m^2 was cut into the construction to allow the pass of the design flood without loading the vault. After the decision to rehabilitate the dam with RCC, the hole was closed, the existing vault was reinforced and injected and also the free overflow section was strengthened with RCC and massive concrete steps were integrated to use it as energy dissipaters. The works were finished in this year, but now the surrounding population is engaged that the dam should not come back into operation (Fig. 25, 26)

In the USA in the last 2 to 3 decades, dam decommissioning has become an option for dam owners to consider when the dam no longer meets its original purpose, or the benefits of dam removal outweigh the benefits and costs to maintain the dam's operations. For example, the decision to

Figure 25. Des Plats Dam before reconstruction.

Figure 26. Des Plats Dam after rehabilitation.

Figure 27. Matilija Dam today.

Figure 28. Silted up Matilija reservoir.

remove a dam may be focused on eliminating risk associated with the dam's structural integrity, or may be geared toward ecological restoration of river processes and aquatic habitat. When a decision has been made to decommission a dam, structural alternatives range from leaving the dam in place, partial dam removal, complete dam removal, or staged breaching. Partial dam removal could mean leaving a lower portion of the dam in place to retain coarse sediments or leaving portions of the dam near the abutments to retain sediments along the reservoir margins.

Since many years the removal of Matilija Dam in California is discussed. Matilija Dam was designed as a 58 m high constant angle arch dam with a crest 189 m long. In 1965 a 9 m notch was cut in the dam and approximately 3.2 Mm^3 of the storage volume was lost. The upper part of the dam had alkali-aggregate reaction that caused the concrete in the upper section of the dam to be weakened. The Matilija reservoir originally stored approximately 8.6 Mm^3 of water, but is now approximately 90% filled with 4.6 Mm^3 of sediment (Fig. 27, 28). The reservoir now is filled with sediments, effectively eliminating its water storage capacity and any incidental flood control function.

Obviously a major challenge to the removal of the Matilija Dam will be the management of the sediment impounded in the reservoir. Mechanical removal of the impounded sediments will entail large economic and societal costs because of restricted access, distance to disposal sites, and the length of time to excavate and transport material. Natural flushing of sediments through the river system could adversely impact aquatic habitat, including their estuaries, as well as cause potential impacts to water supply systems and flooding of floodplain situated properties [26, 27, 28]. Faced with this problems it seems it will need additional years until a final decision will be settled.

Figure 29. Cascade Dam failure sequence.

Figure 30. Cascade Dam failure sequence.

2.3 *Cascade failures of dams*

In some watersheds the dam breach flow after the collapse of a single dam may cause also failures of dams which are situated downstream in form of cascades. Well known are the embankment failures of Banqiao, Shimantan, Tian Gang, Zhu Gou, Bai Guo Chong Dams and other 55 dams in China on August 8, 1975 [29], the failures of Euclides da Cunha and Salles de Oliveira Dams in Brazil on January 19, 1977 [30], but also the failures of Upper and Lower Shelton Dams in the USA on February 22, 1903, where the Lower Shelton Dam was a masonry dam with 7.6 m in height [31]. The most recent known cascade failures happened on September 12, 2013 as 5 small embankments failed at the Little Thompson River Flooding [32].

On July 15, 1982, Lawn Lake Dam, a 7.9 m high earthfill irrigation dam built in 1903 in Rocky Mountain National Park, Colorado, failed, due to piping, releasing 0.8 Mm^3 of water with a peak discharge of 510 m^3/sec down the Roaring River. Three people were killed, and damages were estimated at $31 million. Cascade Lake Dam, downstream from Lawn Lake Dam, a concrete dam 5.2 m in height and 43.6 m in length, subsequently failed as a result of the flood, increasing the peak flow at this point from 204 m^3/sec to 453 m^3/sec (Fig. 29, 30). The channel of the Roaring River was scoured as much as 15 m and widened 90 m. An alluvial fan of 172.000 m^2, containing 0.3 Mm^3 of material, was deposited at the mouth of the Roaring River, damming the Fall River and forming a 70.000 m^2 lake [33].

On July 12, 1961 the 32.6 m high and 1.470 m long Khadakwasla Dam in India was overtopped and failed. It was completed in 1875 and was located a few miles downstream of the Panshet dam, a 51 m high zoned earthfill dam which was under construction at that time. Khadakwasla Dam was of conventional design constructed in rubble masonry and "surki" mortar (burnt clay and lime) with no allowance for uplift in its original design. After the failure of Panshet Dam the ensued breach flood which had a volume of 198 Mm^3 impinged on the already full Khadakwasla reservoir which had a storage capacity of 113 Mm^3. The impact was so intensive that the dam was immediately overtopped along its whole crest length. The water height rose 2.7 m above the top of the dam and the overflow scoured most of the earth at its downstream toe. After 4 hours of overload the dam failed on a length of 92 m (Fig. 31, 32), but not at the place of maximum height, but at a place, where there is a step in the foundation and when the overflow was decreased to about 0.9 m above the crest [34, 35, 36].

2.4 *Dam failures caused by gate failures*

Malfunctions of spillways or spillway gate failures are also factors which increase the risk of dams to get overtopped during time of operation. On August 7, 1978 debris and timber completely blocked the spillway at Palagnedra Dam in Switzerland (Fig. 33). Water spilled over the main concrete arch dam and through a low spot upstream on the right bank. Flood waters washed out 50.000 m^3 of glacial moraine material from the downstream side of a 40 m high diaphragm wall upstream on

Figure 31. Khadakwasla Dam after failure.

Figure 32. Kahadakwasla Dam after failure.

Figure 33. Palagnedra Dam.

Figure 34. Kerckhoff Dam.

the right side of the reservoir which led to the near failure of the wall [37]. On January 1, 1997, a similar case was noticed at the Kerckhoff Dam in California (Fig. 34). The spillway became plugged due to a massive amount of debris, consisting of fallen trees from the drainage area. The trees became knitted together in a large mass and were pushed against the dam ant the spillway by incoming flows. The dam was overtopped, but the rock abutments of the concrete arch dam did not erode and the dam did not fail.

The performance of dam gates and associated operating systems has important impacts regarding the safety of dams. On July 17, 1995, the Folsom Dam spillway radial gate number 3 failed during its raise (Fig. 35), resulting in an uncontrolled release of 1.133 m^3/s. The radial gate, 13 m wide by 15.2 m high, was one of five normally used for flood control. There were three additional gates on the dam crest which had the same width, but they were 16.2 m high and were used only in the case of an emergency. An uncontrolled drawdown with a height of 11 m of the reservoir occurred before the breach was closed with stoplogs [38].

Since the 1995 failure of a gate at Folsom Dam, dam safety professionals have been increasingly aware of the vulnerability of gates and other hydraulic control systems at dams. While the event at Folsom Dam raised awareness of gate system reliability, this event was not unique.

On July 2, 1967 the gate arms of one of four radial gates of Wachi Dam in Japan buckled and failed towards the inside on a vertical plane. As a whole the gate arms did not have sufficient rigidity, and particularly at the joints of the gate arms and main beams of the gate the bending moment got too great, which was the main cause of the failure. The gate along with the bridge over the gate was swept at least 136 m downstream of the gate bay, leaving a giant hole in the gate bay (Fig. 36). The four gates were replaced with new gates which are operating safely and satisfactory till today [39].

On November 30, 1934 as a result of the Latrobe River flood in Australia all radial gates of the Yallourn Weir were washed away (Fig. 37) and only the concrete basement of the weir survived the flood overloading [40].

Figure 35. Folsom Dam after gate failure.

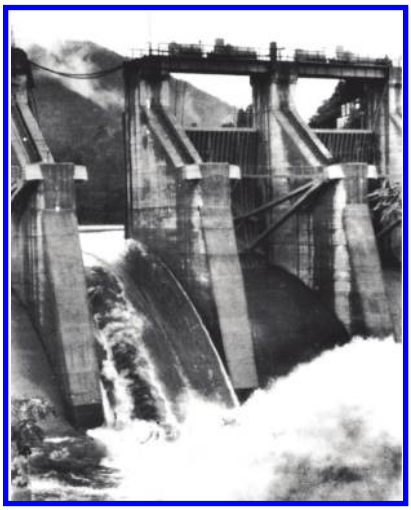

Figure 36. Wachi Dam after gate failure.

Figure 37. Yallourn Weir after failure.

Figure 38. Tuilieres Dam after gate failure.

During the night of January 29, 2006, one of eight Stoney gates broke at the Tuilieres Dam in France and the reservoir emptied relatively quickly without control. A maximum flow of about 350 m^3/s was measured in the main city downstream which lead to an increase of the water level by approximately 1.5 m. Fortunately there were no human and material casualties [41].

REFERENCES

[1] J.D. Schuyler, The Failure of the Lynx Creek Masonry Dam near Prescott, Arizona. *Engineering News*, **39**, 362 (1898).

[2] Failure of the great masonry dam across the Colorado River at Austin, Tex. *Engineering News*, **43**, 244–246 (1900).

[3] *The Austin Dam.* Water Supply and Irrigation Papers of the United Geological Survey, Paper No. 40, (1900).

[4] F. McMillan, The Failure of the Fergus Falls, Minn., City Dam. *Engineering News*, **62**, 393–395 (1909).

[5] The Destruction of the Austin Dam, *Engineering Record*, **64**, 429–436 (1911).

[6] The Destruction of the Austin Dam – Additional Facts, *Engineering Record*, **64**, 442–444 (1911).

[7] P. Leger, R. Tinawi, S.S. Bhattacharjee and M. Leclerc, Failure Mechanisms of Gravity Dams Subjected to Hydrostatic Overload: Influence of Weak Lift Joints. *Proceedings 19th International Congress on Large Dams ICOLD*, Vol. 4, 11–37 (1997).

[8] La rupture du barrage de l'Habra, prés de Perrégaux (Algérie). Les barrages á chute fractionée, *Le Genie Civil*, **92**, 256–259 (1928).

[9] La rupture du barrage de l'Habra, près de Perrégaux (Algérie). Le rapport de la Commission technique d'enquete, *Le Genie Civil*, **92**, 283–285 (1928).
[10] Rupture du barrage de l'Qued Fergoug, *La Houille Blanche*, **27**, 121–125 (1928).
[11] B.J. Doeing and D.T. Williams, Gas pipeline erosion failures: January 1993 floods, Gila River Basin, Arizona; Storm-Induced Geologic Hazards. *Geological Society of America, Reviews in Engineering Geology*, **11**, 25–38 (1997).
[12] Some Dam – Hydro News. *National Performance of Dams Program*, 1–3 (June 7, 2012).
[13] Some Dam – Hydro News. *National Performance of Dams Program*, 3–5 (January 2, 2013).
[14] L'utilizzazione del torrente Orba in Comune di Molare da parte della Societá Officine Elettriche Genovesi. *L'Energia Elettrica*, **2**, 1178–1219 (1925).
[15] L'utilizzazione del torrente Orba in Comune di Molare da parte della Societá Officine Elettriche Genovesi. *L'Energia Elettrica*, **3**, 8–48 (1926).
[16] E. Probst, Der Einsturz der Talsperre bei Molare. *Der Bauingenieur*, **16**, 425–428 (1935).
[17] E. Probst, Overtopping of Small Dam Causes Flood in Italy. *Engineering News-Record*, **115**, 607–610 (1935).
[18] G. Grabrecht, Die Muzuma-Talsperre (Sambia), Zerstörung, Neuplanung, Wiederher-stellung. *Mitteilungen des Instituts für Wasserbau und Wasserwirtschaft, RWTH Aachen*, **9**, 71–85 (1975).
[19] Com as enchentes: Tragedia. *Esteio, Uma Publicação do Centro Mineiro de Cultura Popular*,**2**, No. 4 (1979).
[20] C.B. Viotti, The Poquim Dam. *Annual Meeting on Large Dams ICOLD* (2014).
[21] G.R. Brooks and D.E. Lawrence, The drainage of the Lake Ha!Ha! reservoir and downstream geomorphic impacts along Ha!Ha! River, Saguenay area, Quebec, Canada. *Geomorphology*, **28**, 141–168 (1999).
[22] G.R. Brooks and D.E. Lawrence, Geomorphic effects of flooding along reaches of selected rivers in the Saguenay region, Quebec, July 1996. *Géographie physique et Quaternaire*, **54**, 281–299 (2000).
[23] C.Y. Chen, L.K. Chen, F.C. Yu, S.C. Lin, Y.C. Lin, C.L. Lee and Y.T. Wang, Landslides affecting sedimentary characteristics of reservoir basin. *Environmental Earth Sciences*, **59**, 1693–1702 (2010).
[24] Y.L. Kao, W.H. Tseng, S.C. Chou and C.L. Shieh, Study on the River Bed Variation after the Baling Check-Dam Failure. *Journal of Chinese Soil and Water Conservation*, **44**, 255–264 (2013).
[25] Report of the Water Supply Commission of Pennsylvania, 61–62 (1912).
[26] M.H. Capelli, San Clemente and Matilija Dam removal: Alternative sediment management scenarios. *Proc.of the 27th Annual USSD Conference*, 607–620 (2007).
[27] *Environmental Impact Report for the Matilija Dam Ecosystem Restoration Project*. U.S. Army Corps of Engineers, Los Angeles (2004).
[28] *Sediment Considerations for Potential Dam Removal Projects.* Technical Report No. SRH-2009-39, U.S. Department of the Interior Bureau of Reclamation (2009).
[29] J. Guo and C. Shen, Some Experiences on Safe Passage of Extreme Flood in China. *Proc.of the Workshop on Dam Safety Problems and Solutions-Sharing Experience, 72nd Annual Meeting ICOLD*, 486–495 (2004).
[30] Brazilian dam failures: a preliminary report. *Water Power & Dam Construction*, **30**, 51–53 (1977).
[31] Two Dams Failed at Shelton. *Engineering News*, **49**, 185 (1903).
[32] *Report of September 2013 Little Thompson River Flooding and Big Elk Meadows Dam Failures.* Colorado Division of Water Resources, Dam Safety Branch (2014).
[33] R.D. Jarrett and J.E. Costa, Hydrology, geomorphology, and dam-break modelling of the July 15, 1982, Lawn Lake Dam and Cascade Lake Dam failures, Larimer County, Colorado. *Geological Survey professional paper no. 1369* (1986).
[34] N.G.K. Murti, Khadakwasla, the oldest masonry dam in India. *Proc. 9th Int. Congr. on Large Dams ICOLD*, Vol. 3, 895–915 (1967).
[35] J.K. Hunter, Failure of Khadakwasla and Panshet Dams, Bombay. *Water Power & Dam Construction*, **16**, 251–252 (1964).
[36] N.S.G. Rao, Failure of Khadakwasla and Panshet Dams. *Journal of the Institution of Engineers India*, **47**, 1123–1144 (1967).
[37] J. Bruschin, S. Bauer, P. Delley and G. Trucco, The overtopping of the Palagnedra dam. *Water Power & Dam Construction*, **34**, 13–19 (1982).
[38] R.V. Todd, Failure of Spillway Radial Gate at Folsom Dam, California. *Proceedings 19th International Congress on Large Dams ICOLD*, Vol. 4, 113–126 (1997).
[39] *Deterioration cases collected and their preliminary assessment.* ICOLD, **2**, II–7 (1979)
[40] A.L. Galbraith, The Latrobe River Flood of December, 1934 And Its Effects at the Yallourn Works. *Transactions of the Institution of Engineers Australia*, 16, 377–386 (1935).
[41] E. Robbe, Rehabilitation of Tuilières Dam: Behaviour under seismic load. *Dam Maintenance and Rehabilitation II* (2010).

Dam Protections against Overtopping and Accidental Leakage – Toledo, Morán & Oñate (Eds)

Laboratory measurements and numerical simulations of overtopping nappe impingement jets

José M. Carrillo & Luis G. Castillo
Universidad Politécnica de Cartagena (UPCT), Cartagena, Spain

ABSTRACT: Rectangular jets constitute one of the energy dissipation methods in the overtopping of dams. The high turbulence and aeration phenomena that appear in falling jets and dissipation basins make it difficult to carry out studies based only on classical methodologies. There are studies modeling spillways with Computational Fluid Dynamics (CFD) which produces accurate results. However, the study of overflow nappe impingement jets has not been sufficiently examined. Simulations of free air-water overflow weirs are scarce, and require small mesh sizes and a high computational effort. This work seeks to address such simulation. Results obtained with ANSYS CFX are compared with laboratory measurements and empirical formulae. Good agreement is obtained with experimental and theoretical data. Knowing the parameters analyzed, designers will be able to estimate the scour effects and the stability of the dam with a higher certainty.

Keywords: Impingement Jets, Laboratory, Numerical Simulations, Overtopping

1 INTRODUCTION

In recent years, the increasing magnitude of design floods has prompted re-evaluations of spillway capacity and operational scenarios for large dams throughout the world. Current capacity of many spillways is inadequate, raising the possibility that dams might be overtopped during extreme events. This creates new loading scenarios for the dam and raises questions about erosion and scour downstream from the dam (Wahl *et al.* [47]).

Nappe flow constitutes one of the types of plunge pool operation in the overtopping of dams. In turbulent flow, pressure fluctuations are the main mechanism affecting the incipient movement of the particles. The erodibility index relates the relative magnitude of the erosive capacity of water and relative resistance of the material (natural or artificial) to resist erosion (Annandale [3]). In order to obtain the right pool depth, the designer needs to know the magnitude, frequency and extent of the dynamic pressures on the pool floor as a function of the jet characteristics.

Different empirical formulae may be used to characterize the pressures in plunge pools. Due to the great difficulty of instrumenting prototypes, all of the formulae have been obtained by using diverse experimental facilities and reduced scale models. Research in plunge pools has been published by many authors including Moore [38], Albertson *et al.* [1], Horeni [29], Lencastre [31], Cola [20], Hartung and Häusler [27], Ervine and Falvey [21], Franzetti and Tanda [24], Castillo ([9], [10], [11]), Withers [50], Puertas [40], Ervine *et al.* [22], Puertas and Dolz [41], Castillo *et al.* ([12], [13], [18], [19]), Bollaert [5], Bollaert and Schleiss ([6], [7]), Manso *et al.* ([33], [34]), Melo *et al.* [37], Federspiel [23], Castillo and Carrillo ([14], [15], [16], [17]), and Carrillo [8]. Recent studies in this field have been focused on scour formation. These include the studies carried out by Annandale ([2], [3]), Hoffmans [28], Asadollahi *et al.* [4] and Mehraein *et al.* [36]. Modeling of falling jets is difficult because the break-up and air entrainment characteristics of the jet are influenced by both surface tension and turbulence effects. In addition to this, the pressure fluctuation spectrum is also affected by the turbulence scale. In a physical model scale effects will

appear. However, their effects may be minimized or accounted for through careful choice of the model size and careful interpretation of the results.

In falling jets and dissipation basins it is difficult to carry out studies based only on classical methodologies. The computational fluid dynamics (CFD) programs allow researchers and designers to evaluate different effects with a smaller cost than that incurred building scale models. There are studies modeling spillways with which produces accurate results. However, the study of overflow nappe impingement jets has not been sufficiently examined. Simulations of free air-water overflow weirs are scarce, and require small mesh sizes and a high computational effort.

In this paper, previous studies have been revised and complemented with new laboratory data obtained in a new installation of nappe flow. Pressure data at the bottom of the plunge pool have been obtained and compared using three different experimental facilities (i.e., data from Castillo [9] and Puertas [40], and data obtained in a new experimental facility).

Turbulence in the falling jet has been analyzed using computational fluid dynamics (CFD) techniques. Results obtained with ANSYS CFX are compared with laboratory measurements and empirical formulae. To identify the level of reliability of computed parameters, validation of air entrainment and velocity along free falling jets, thickness and break-up of jets, and pressures on the bottom of the plunge pool, are carried out by using a two-fluid model, turbulence models and mesh-size analysis.

2 EXPERIMENTAL FACILITY

2.1 *Turbulent jet experimental facility*

The hydraulics laboratory at the Universidad Politécnica de Cartagena in Spain has a turbulent jet experimental facility in which the energy dissipation of turbulent rectangular jets is being studied (Figure 1). The mobile mechanism allows researchers to vary the discharge heights between 1.70 and 4.00 m and flows from 10 to 150 l/s. It has an inlet channel with a length of 4 m and width of

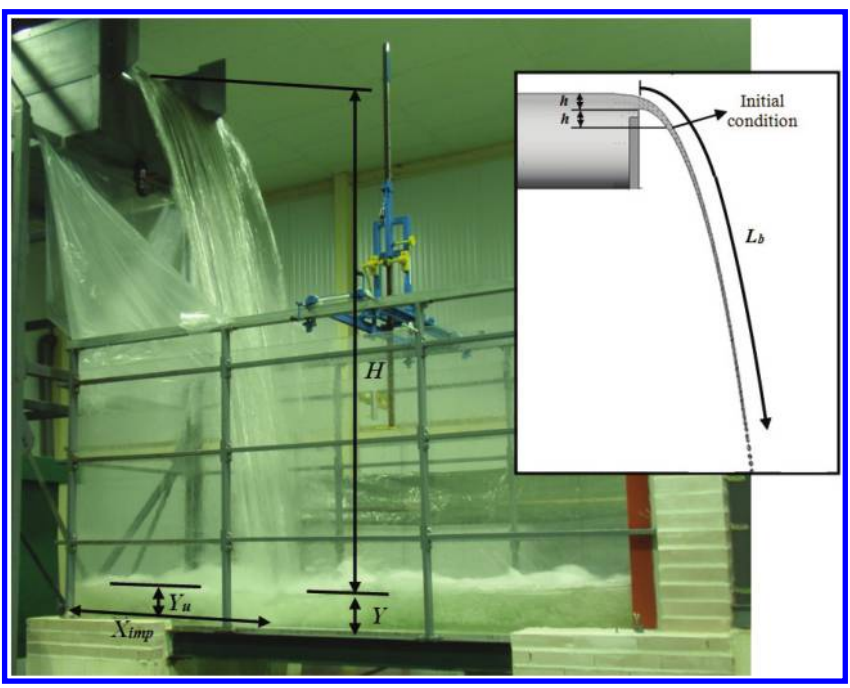

Figure 1. Device of turbulent jets.

0.95 m, in which different dissipation systems have been located. The weir is a sharp crest with a width of 0.85 m and height of 0.37 m.

The plunge pool, in which different water cushions may be regulated, is a 1.60 m high and 1.05 m wide box made of methacrylate. Instantaneous pressure measurements were registered with piezoresistive transducers located on the plunge pool bottom, kinetic energy at the inlet channel with Acoustic Doppler Velocimeter (ADV) equipment, mean velocities and air entrainment rate in different sections of the falling jet with optical fibre instrumentation.

The flow was measured with a V-notch weir, located downstream from the plunge pool. The discharge rate of the V-notch was tested with a velocity-area method using ADV equipment upstream from the weir. Differences between V-notch results and the velocity-area method were smaller than 5% of the current flow.

Experiments carried out in this study correspond to different falling heights H between 1.70 m and 3.00 m, seven water cushion heights Y (from direct impact to 0.60 m) and seven specific flows q (from 0.020 to 0.064 m^2/s). Laboratory data cover a range of $0.60 \leq H/L_b \leq 2.02$, with L_b being the break-up length. Almost 190 registers were obtained, with each one being of 7200 points and with an acquisition rate of 20 samples per second.

2.2 *Pressure transducers*

With the aim of obtaining the instantaneous pressures, GE Druck model UNIK 5000 pressure transducers were used. The sensors were located on the bottom of the plunge pool, at the symmetry plane of the turbulent jet device and equally spaced at 5 cm intervals. These sensors have a pressure range between -200 and $+800$ mbar and a precision of $\pm 0.04\%$ of the full scale output. After carrying out a static calibration, the pressure precision of the transducers was ± 0.01 water column meters. Instantaneous pressures were obtained by considering a frequency rate of 20 Hz and measurements of 360 s. In each measurement, seven sensors were used at the same time (one at the stagnation point, three upstream from the stagnation point, and three downstream). Each measurement was repeated three times.

2.3 *Optical fibre equipment*

To measure the mean velocity and the air entrainment at the falling jet, an RBI-instrumentation dual-tip probe optical phase-detection instrument was used. This equipment enables measurement in water up to 20 m/s flow velocity and the relative uncertainty concerning the void fraction is estimated at about 15% (Stutz and Reboud [45], [46]). The rise and fall of the probe signal corresponds, respectively, to the arrival and the departure of the gas phase at the tip of the sensor.

The void fraction was defined as the ratio of the total time the probe is in gas (Σt_{Gi}) to the experiment duration time t. The mean velocity of the fluid was estimated by using a cross correlation technique between the signals obtained for the two tips. The accuracy of the velocity measurements performed under steady flow conditions was estimated at about $\pm 10\%$ for the velocity range analyzed (Stutz and Reboud [45], [46]).

2.4 *The Acoustic Doppler Velocimeter (ADV)*

ADVs have become highly useful in fluid dynamics and are applied to the study of three-dimensional flow and turbulence in both the laboratory and field (rivers, channels and hydraulic structures, amongst others).

The setting characteristics were selected considering that the main objective is to measure the mean velocity and macroscopic turbulence. In this way, the velocity range was selected as ± 0.30 m/s with a frequency of 10 Hz, avoiding the noise generated by the equipment when higher frequencies are used. With this setting, the ADV equipment was able to measure the time-averaged flow field with an accuracy of better than ± 0.002 m/s. The kinetic turbulence measured 0.50 m upstream the weir in the experimental facility was used as the inlet condition in the numerical simulations.

3 NUMERICAL MODELING

3.1 *Considerations*

For the turbulent flow, CFD codes solve the differential Reynolds-Averaged Navier-Stokes (RANS) equations of the phenomenon in the fluid domain, retaining the reference quantity in the three directions for each control volume identified. The equations for conservation of mass and momentum may be written as:

$$\frac{\partial \rho}{\partial t} + \frac{\partial}{\partial x_j}(\rho U_j) = 0 \tag{1}$$

$$\frac{\partial \rho U_i}{\partial t} + \frac{\partial}{\partial x_j}(\rho U_i U_j) = -\frac{\partial p}{\partial x_i} + \frac{\partial}{\partial x_j}\left(2\mu S_{ij} - \rho\overline{u_i' u_j'}\right) \tag{2}$$

where i and j are indices, x_i represents the coordinate directions ($i = 1$ to 3 for x, y, z directions, respectively), ρ the flow density, t the time, U the velocity vector, p the pressure, u_i' presents the turbulent velocity in each direction ($i = 1$ to 3 for x, y, z directions, respectively), μ is the molecular viscosity, S_{ij} is the mean strain-rate tensor and $-\rho\overline{u_i' u_j'}$ is the Reynolds stress.

Eddy-viscosity turbulence models consider that such turbulence consists of small eddies which are continuously forming and dissipating, and in which the Reynolds stresses are assumed to be proportional to mean velocity gradients. The Reynolds stresses may be related to the mean velocity gradients and eddy viscosity by the gradient diffusion hypothesis:

$$-\rho\overline{u_i' u_j'} = \mu_t\left(\frac{\partial U_i}{\partial x_j} + \frac{\partial U_j}{\partial x_i}\right) - \frac{2}{3}\delta_{ij}\left(\rho k + \mu_t \frac{\partial U_k}{\partial x_k}\right) \tag{3}$$

with μ_t being the eddy viscosity or turbulent viscosity, $k = 1/2\overline{u_i' u_i'}$ the turbulent kinetic energy and δ the Kronecker delta function.

In preparing this study, an extensive literature review of hydraulic dams was carried out. However, given that the CFD methodology is relatively recent there are few well documented references for free overflow spillways. For this reason, it is necessary to review CFD accuracy in similar typologies.

3.2 *Numerical simulations*

For the numerical modeling, the CFD volume finite scheme program ANSYS CFX has been used.

The fluid domain is divided into control volumes, which must satisfy the balance of the governing equations. The code allows different types of elements to be solved. The main difference between the types of elements is the number of nodes used to solve the equations within each control volume. A larger number of nodes per element obtains a more accurate solution in their internal resolution. Following Castillo *et al.* [19] and Carrillo [8], the mesh size was 0.01 m based on hexahedral elements, approximately the half of the impingement jet thickness for the tests carried out.

All scenarios were obtained by a transient calculation time of 60 seconds, using 20 Hz frequency, the same as used in the laboratory pressure measurements. The transient statistics were obtained by considering that permanent conditions are reached after 20 seconds of simulation.

In order to reach the closure of the Navier-Stoke equations, turbulence models can be used. There are different approximations, from one-equation turbulence models to the direct simulation.

As a compromise between accuracy and computational effort, the RANS turbulence models are widely used. Eddy-viscosity turbulence models consider that such turbulence consists of small eddies which are continuously forming and dissipating, and in which the Reynolds stresses are assumed to be proportional to mean velocity gradients.

Castillo *et al.* [19] and Carrillo [8] tested different turbulence models in the falling jet case. In this work, the SST turbulence model has been selected. The SST model takes into account the

accuracy of the k-ω model in the near-wall region and the free stream independence of the k-ε model in the outer part of the boundary layer. To do this, the original k-ω model (Wilcox [49]) is multiplied by a blending function F_1, while the k-ε model (Launder & Sharma [30]) is transformed to a k-ω formulation and multiplied by a function 1-F_1 (Menter [35]). F_1 is designed to be one inside the boundary layer and decreases to a value of zero away from the surface.

In judging the convergence of a solution in a finite-volume scheme, a widely used method entails monitoring the residuals (Wasewar and Vijay Sarathi [48]). Residuals are defined as the imbalance in each conservation equation following each iteration. The solution is said to have converged if the scaled residuals are smaller than prefixed values ranging between 10^{-3} and 10^{-6}. In this work, the residual values were set to 10^{-4} for all the variables.

To solve the air-water two-phase flow, the Eulerian-Eulerian multiphase flow homogeneous model was selected. In each control volume, the sum of the volume fraction of all phases is the unit.

In general, it may be assumed that the free surface is on the 0.5 air volume fraction. However, due to the high air entrainment in the nappe, the jet thickness and the break-up length were calculated using a 0.8 air volume fraction.

The model boundary conditions corresponded to the flow, the turbulence at the inlet condition obtained with ADV (located 0.50 m upstream of the weir), the upstream and downstream levels and their hydrostatic pressures distributions (Figure 2).

The inlet condition considers the mass flow rate with a normal direction to the boundary condition ($q = 0.058\ m^2/s$, $q = 0.037\ m^2/s$, $q = 0.023\ m^2/s$), the turbulent kinetic energy ($0.00036\ m^2/s^2$ for $q = 0.058\ m^2/s$, $0.00019\ m^2/s^2$ for $q = 0.037\ m^2/s$, $0.00011\ m^2/s^2$ for $q = 0.023\ m^2/s$), and the water level height at upstream deposit (2.445 m for $q = 0.058\ m^2/s$, 2.423 m for $q = 0.037\ m^2/s$, 2.397 m for $q = 0.023\ m^2/s$). For simplicity, the symmetry condition in the longitudinal plane of the plunge pool was used.

The outlet condition has been considered as an opening condition with flow normal to the boundary condition and hydrostatic pressure. The water level height at outlet has been modified according to the water cushion depth, Y, in the laboratory device.

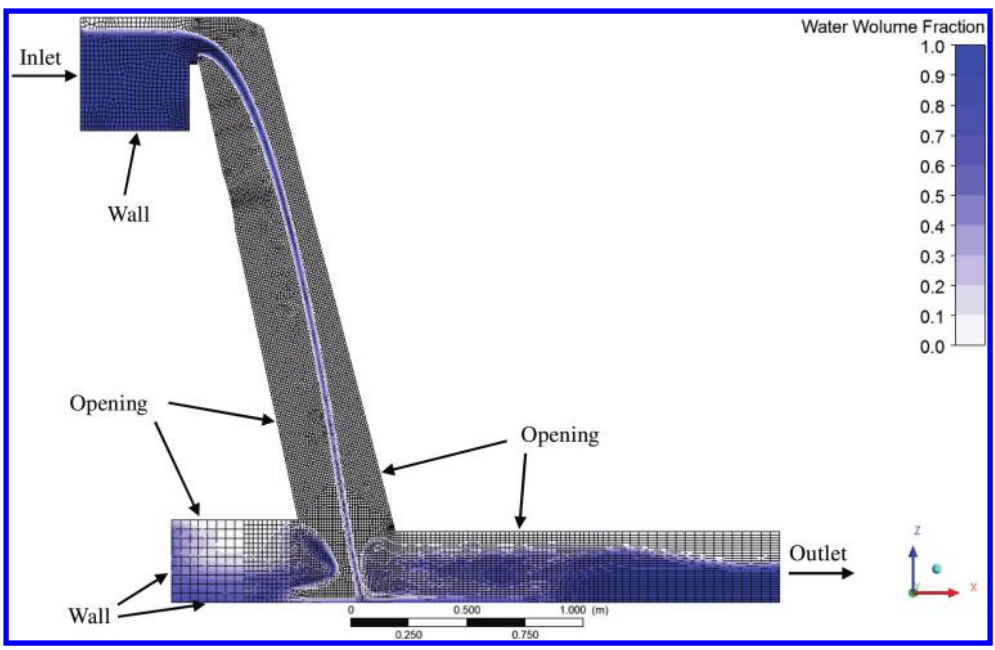

Figure 2. Scheme of boundary conditions.

For the walls of the upper deposit, the weir and the dissipation bowl, no slip wall conditions and smooth walls have been considered.

The atmosphere condition has been simulated as an opening condition with a relative pressure of 0 Pa, air volume fraction of 1 and water volume fraction of 0.

4 EMPIRICAL FORMULAE

Using instantaneous pressure registers obtained at the bottom of plunge pools, Castillo ([10], [11]) proposed estimators for the nappe flow case: the turbulence intensity at issuance conditions T_u, the jet break-up length L_b, the lateral spread distance ξ, the impingement thickness B_j, and the mean dynamic pressure coefficient C_p.

The turbulence intensity at issuance conditions for laboratory specific flow ($q < 0.25\ \mathrm{m^2/s}$) may be estimated as:

$$T_u^* = q^{0.43}/IC \tag{4}$$

with IC being the initial conditions with dimensions $[L^{0.86}T^{-0.43}]$:

$$IC = 14.95g^{0.50}/(K^{1.22}C_d^{0.19}) \tag{5}$$

where g is the gravity acceleration, K is a non-dimensional fit coefficient (≈ 0.85) and C_d is the discharge coefficient $[L^{0.5}T^{-1}]$.

However, for prototype specific flows ($q >> 0.25\ \mathrm{m^2/s}$) a mean turbulence index is $T_u \sim 1.2\%$ (Castillo [10]).

The designers need to know the height between the upstream water level and the downstream water level H, the impingement jet thickness B_j, the water cushion depth Y, and the jet break-up length L_b. In this way, the head mean may be calculated at the stagnation point of the plunge pool bottom H_m.

Following the results obtained by Ervine *et al.* [22] in circular jets, the jet break-up length in the rectangular jet case is calculated as (Castillo [10]):

$$\frac{L_b}{B_i F_i^2} = \frac{K}{\left(K_\varphi T_u F_i^2\right)^{0.82}} \tag{6}$$

with B_i, F_i and $T_u = \overline{V}_i'/V_i$ being the jet thickness, the Froude number and the turbulent intensity at issuance conditions, while K is a non-dimensional fit coefficient (≈ 0.85). $K_\varphi = \overline{V}_i'/w'$ is the turbulent parameter coefficient, where $\overline{V}_i'$ and w' are the root mean square (RMS) and the streamwise turbulent velocity component.

The impingement jet thickness is obtained with the following:

$$B_j = B_g + 2\xi = \frac{q}{\sqrt{2gH}} + 4\varphi\sqrt{h}\left[\sqrt{2H} - 2\sqrt{h}\right] \tag{7}$$

where H is the height between the upstream water level and the downstream water and $\varphi = K_\varphi T_u$ is the turbulence parameter in the nappe flow case.

The trajectory of the central nappe may be obtained with the Scimeni [44] formulation:

$$x^* = 2.155(z^* + 1)^{\frac{1}{2.33}} - 1 \tag{8}$$

where $x^* = x/h$ and $z^* = z/h$, with x and z being the coordinate axes considering the origin in the weir crest.

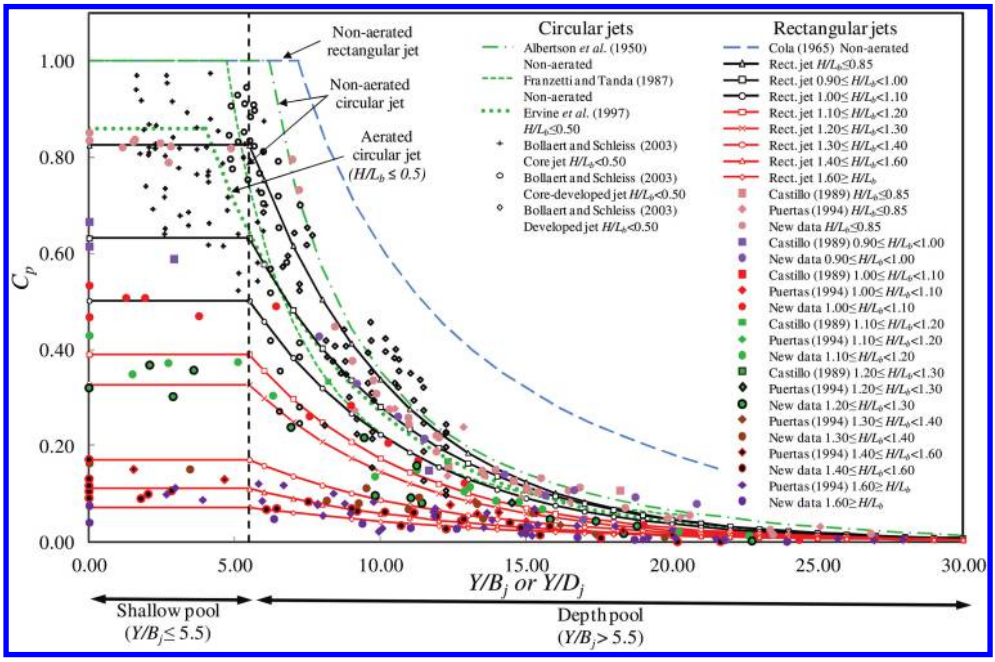

Figure 3. Mean dynamic pressure coefficient for different jet shapes and air entrainment.

5 RESULTS AND DISCUSION

5.1 *Mean dynamic pressure coefficient*

The mean dynamic pressure coefficient C_p may be obtained as a function of Y/B_j and H/L_b rates. In this way, the instantaneous pressures signals obtained on the bottom of the plunge pools may be adjusted in curves for different ranges. Two cases were considered for the mean dynamic pressure coefficient.

For the non-effective water cushion ($Y \leq 5.5B_j$):

when $H/L_b \leq 1.00$:

$$C_p = 1 - 0.0014e^{5.755(H/L_b)} \tag{9}$$

when $H/L_b > 1.00$:

$$C_p = 14.643e^{-3.244(H/L_b)} \tag{10}$$

The energy dissipation is due to the air entraining into the falling jet and the depth of water standing upstream from the jet, while downstream from the stagnation point the cushion does not influence the energy dissipation. Exponential adjustments have been obtained, with regression coefficients R^2 of 0.97 and 0.91 for $H/L_b < 1.00$ and $H/L_b \geq 1.00$, respectively.

For the effective water cushion ($Y > 5.5B_j$), in Figure 3 data are compared with the formula obtained by Cola [20] for non-aerated rectangular jets. As the Cola formula considers the mean pressure instead of the mean dynamic pressure, the curve has been modified to consider the relation $C_p = f(Y/B_j)$ without the water cushion.

Figure 3 also shows the fit of the aerated circular jets obtained by Ervine *et al.* [22] and Bollaert and Schleiss [7], and non-aerated circular jets obtained by Albertson *et al.* [1] and those by Franzetti and Tanda [24]. In the same way as the Cola formula, the Albertson curve has been modified to consider the relation $C_p = f(Y/D_j)$ without the water cushion, being D_j the impingement diameter jet.

Table 1. Parameters of the mean dynamic pressure coefficient for $Y > 5.5B_j$.

H/L_b	a	b	R^2
≤0.85	2.5	0.2	0.93
0.90–1.00	1.7	0.18	0.7
1.00–1.10	1.35	0.18	0.85
1.10–1.20	1.05	0.18	0.95
1.20–1.30	0.88	0.18	0.85
1.30–1.40	0.39	0.15	0.76
1.40–1.60	0.24	0.14	0.68
≥1.60	0.14	0.12	0.56

Table 2. Results obtained at the stagnation point.

			CFD		LAB		PARAM.	
q (m^2/s)	Y (m)	H (m)	H_m (m)	C_p (–)	H_m (m)	C_p (–)	H_m (m)	C_p (–)
0.023	0.02	2.377	0.36	0.14	0.41	0.16	0.45	0.18
0.023	0.11	2.277	0.35	0.10	0.34	0.10	0.35	0.11
0.023	0.22	2.177	0.22	0.00	0.29	0.03	0.29	0.03
0.023	0.3	2.097	0.30	0.00	0.31	0.00	0.32	0.01
0.037	0.02	2.397	1.06	0.45	0.97	0.39	0.70	0.28
0.037	0.12	2.297	0.71	0.26	0.81	0.30	0.79	0.29
0.037	0.24	2.177	0.44	0.09	0.43	0.08	0.44	0.09
0.037	0.33	2.087	0.32	0.00	0.39	0.03	0.41	0.04
0.058	0.03	2.411	1.23	0.46	1.26	0.51	1.24	0.50
0.058	0.17	2.276	1.07	0.40	1.15	0.43	1.17	0.44
0.058	0.25	2.191	0.88	0.29	0.73	0.22	0.78	0.24
0.058	0.35	2.091	0.56	0.10	0.55	0.10	0.57	0.11

For $Y/B_j > 5.5$, it was obtained that $C_p = f(Y/B_j, H/L_b)$. The C_p reduction is similar to a comparable circular jet.

For the effective water cushion ($Y > 5.5B_j$), eight cases have been considered as a function of the H/L_b ratio:

$$C_p = \frac{H_m - Y}{V_j^2/2g} = ae^{-b(Y/B_j)} \tag{11}$$

where H_m is the head mean registered at plunge pool bottom (stagnation point), Y the depth of the plunge pool and V_j the impingement velocity. The parameters a and b of the Eq. 11, and their regression adjustments R^2, are obtained from Table 1.

A study with the CFD code was also carried out. Three different specific flows (0.023, 0.037 and 0.058 m^2/s) and four water cushions (one non-effective and three effective water cushion depths) were analyzed. Results were compared with laboratory measurements and Parametric Methodology. Great similitude was obtained in the velocity of the free falling jet and the jet thickness. The distance from the weir to the stagnation point differed less than 2% from the observed in laboratory and calculated with the Scimeni [44] formula.

Table 2 collects the pressure results obtained at the stagnation point with the weir crest located 2.35 m above the bottom of the plunge pool. In general, good agreement was obtained for the mean pressure coefficieants and the head mean with the three methodologies. Maximum differences among laboratory, Parametric Methodology and numerical results corresponded with direct

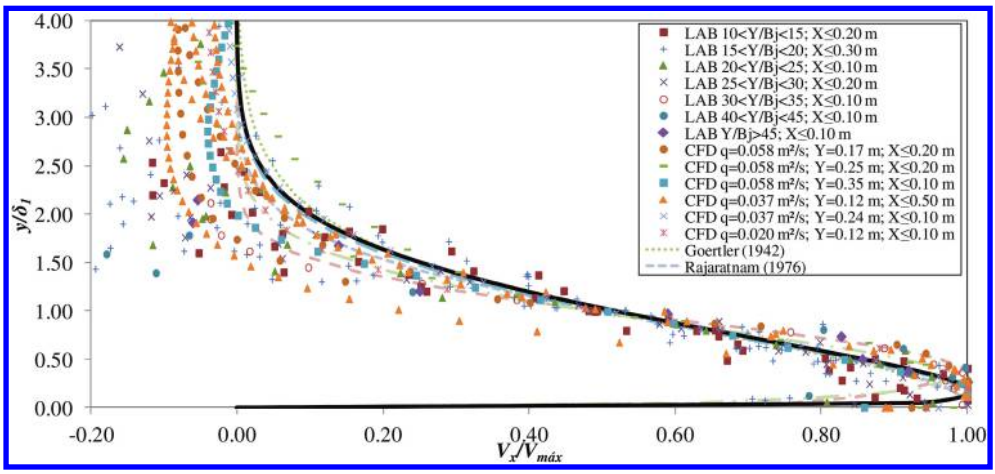

Figure 4. Distribution of the mean velocity downstream the stagnation point with laboratory data and numerical simulations. Profiles with negative flow.

impacts. In these cases, the pass from kinetic energy to potential energy is very abrupt, with significant pressure gradients appearing in reduced areas.

Considering the height between upstream water level and downstream water level, H, of each test, differences between simulations and laboratory data show a maximum error from -4% to 7%.

In these cases of direct impact, laboratory results revealed that the C_p is very sensitive to the H/L_b rate when H/L_b is between 0.70 and 1.30.

5.2 *Velocity profiles in the plunge pool*

To obtain the non-dimensional mean velocity profile in the hydraulic jump case (free and submerged), diverse authors (e.g. Görtler [25], Rajaratnam [42], [43], Hager [26], Ohtsu *et al.* [39], Wu and Rajaratnam [51], Liu *et al.* [32]) have obtained adjustment equations.

Supposing that V_j is the impingement velocity of the jet, B_j the jet thickness, and β the angle of the jet with the horizontal plane, Rajaratnam [43] carried out the dimensional analysis of the Reynolds-averaged Navier–Stokes equations and obtained the basic characteristics of the flow in a stilling basin.

Figures 4 and 5 show the horizontal mean velocity obtained in both, laboratory and numerical simulations, for a weir crest height of 2.35 m, diverse specific flows and water cushion depths together with the formulae proposed by some authors. Data have been divided by considering if the profile shows negative recirculation flow or if the entire velocity profile has direction to downstream.

The threshold between both behavior seems to be around 0.20–0.30 m of the stagnation point for the range of specific flows and water cushion depth analyzed. Data collapse for ratios $V_x/V_{max} \geq 0.40$. Under these value, results do not follow a single law. This is due to the jet enters into the plunge pool with an angle almost vertical, while the jet enters horizontally in the submerged hydraulic jumps downstream gates or spillways. The maximum differences among both behavior appear for the bigger water cushion (ratios $Y/B_j > 20$).

With these data, an adjustment has been proposed to define the non-dimensional velocity profile and the recirculation region of the inverse flow:

$$\frac{V}{V_{máx}} = 1.48\left(\frac{y}{\delta_l}\right)^{1/7}\left(1 - erf\left(0.66\frac{y}{\delta_l}\right)\right) \tag{12}$$

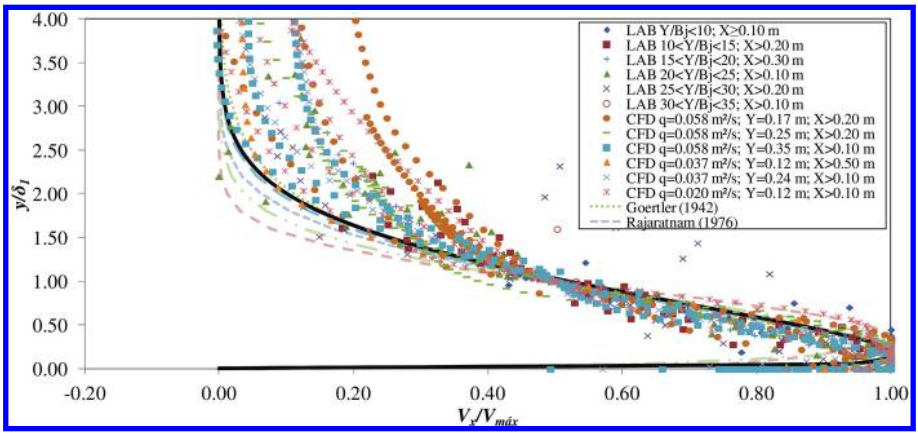

Figure 5. Distribution of the mean velocity downstream the stagnation point with laboratory data and numerical simulations. Profiles with positive flow.

where *erf* is the error function, δ_l the characteristic length of the velocity distribution in the hydraulic jump (depth where $V_x = V_{max}/2$).

6 CONCLUSIONS

In the circular jet case, a transition region is considered between shallow and deep pool for ratios $4 < Y/B_j < 6$. In the nappe flow case, an effective water cushion is obtained when $Y/B_j > 5.5$. The maximum mean dynamic pressure coefficient is $C_p = 0.86$ in the case of circular jets, while it is reduced to $C_p = 0.83$ for the rectangular jet case. With effective water cushions, tendencies are similar for both types of jets.

In the rectangular jet case, eight groups of C_p were obtained as a function of the H/L_b ratio, with ratios $0.8 \leq H/L_b \leq 1.60$. The results obtained complement the data of well-documented circular jets obtained from diverse authors.

In general, the results obtained with ANSYS CFX offered good agreement with the laboratory measurements and the Parametric Methodology. However, given that RANS turbulence models were used, the program obtained an average pressure register in contrast to the natural variability of the phenomenon which limited the possible analysis of fluctuant dynamic pressures.

Good agreement was obtained for the mean pressure coefficients and the head mean with laboratory results and Parametric Methodology. Considering the height between the upstream water level and downstream water level of each test, differences between simulations and laboratory data showed a maximum error from −4% to 7%.

The numerical results of the velocity profiles in the plunge pool downstream the stagnation point follow the laboratory data with differences smaller than 10% of the impingement velocity of the jet. However, these differences are significant in the aerated region. It was possible to adjust a velocity distribution for ratios $V_x/V_{max} \geq 0.40$. For smaller ratios it is necessary to consider different families of adjustments.

With the aim of improving the design of overtopping flows and their energy dissipation, it would be necessary to provide advances in the knowledge and characteristics of the hydrodynamic actions. More experimental studies, both in physical models and prototypes, are necessary in characterizing simultaneously the phenomena produced in the jets (aeration and velocity), combined with measurements of pressures, velocities and aeration rates in stilling basins.

In order to develop this work further, the researchers plan to examine use of inhomogeneous models and hence identify results independent from the mesh size. In future activities, comparison with diverse CFD codes (open source and commercial ones) will be considered.

ACKNOWLEDGEMENTS

The researchers express their gratitude for the financial aid received from the Ministerio de Economía y Competitividad and the Fondo Europeo de Desarrollo Regional (FEDER) through the Natural Aeration of Dam Overtopping Free Jet Flows and its Diffusion on Dissipation Energy Basins project (BIA2011-28756-C03-02).

REFERENCES

[1] M.L. Albertson, Y.B. Dai, R.A. Jenson and H. Rouse, Diffusion of submerged jets. *Proc. Int. Conf. ASCE*, **74**, (1950).
[2] G.W. Annandale, Erodibility. *J. Hydraulic Res.* **33**(4), 471–494, (1995).
[3] G.W. Annandale, *Scour Technology*. McGraw-Hill Professional, NY, USA, (2006).
[4] P. Asadollahi, F. Tonon, M.P.E.A. Federspiel and A.J. Schleiss, Prediction of rock block stability and scour depth in plunge pools. *J. Hydraulic Res.* **49**(6), 750–756, (2011).
[5] E.F.R. Bollaert, *Communication 13. Transient water pressures in joints and formation of rock scour due to high-velocity jet impact.* Laboratoire de Constructions Hydrauliques. Ed.: A.J. Schleiss, Ecole Polytechnique Fédérale de Lausanne, (2002).
[6] E.F.R., Bollaert and A.J. Schleiss, Scour of rock due to the impact of plunging high velocity jets Part I: A state-of-the-art review. *J. Hydraulic Res.* **41**(5), 451–464, (2003).
[7] E.F.R., Bollaert and A.J. Schleiss, Scour of rock due to the impact of plunging high velocity jets Part II: Experimental results of dynamic pressures at pool bottoms and in one- and two-dimensional closed end rock joints. *J. Hydraulic Res*. **41**(5), 465–480, (2003).
[8] J.M. Carrillo, *Metodología numérica y experimental para el diseño de los cuencos de disipación en el sobrevertido de presas de fábrica*. PhD Thesis. Departamento de Ingeniería Civil, Universidad Politécnica de Cartagena, Spain, (2014). [in Spanish].
[9] L. Castillo, *Metodología experimental y numérica para la caracterización del campo de presiones en los disipadores de energía hidráulica. Aplicación al vertido libre en presas bóveda.* PhD Thesis. Departamento de Ingeniería Hidráulica, Marítima y Ambiental, Universidad Politécnica de Cataluña, (1989). [in Spanish].
[10] L. Castillo, Aerated jets and pressure fluctuation in plunge pools. *Proc. Int. Conf. The 7th International Conference on Hydroscience and Engineering (ICHE-2006)*, Philadelphia, 1–23, M. Piasecki and College of Engineering, Drexel University, USA, (2006).
[11] L. Castillo, Pressure characterization of undeveloped and developed jets in shallow and deep pool. *Proc. 32nd IAHR Congress*, Venice, 2, 645–655, (2007).
[12] L. Castillo, J. Puertas and J. Dolz, Discussion of "Pressure fluctuations on plunge pool floors" by D.A. Ervine, H.T. Falvey and W.A. Withers. *J. Hydraulic Res.* **37**(2), 272–288, (1999).
[13] L. Castillo, J. Puertas and J. Dolz, Discussion of "Scour of Rock due to the impact of plunging high velocity jets. Part I: A state-of-the-art review" by E.F.R. Bollaert and A.J. Schleiss. *J. Hydraulic Res.* **45**(6), 853–858, (2007).
[14] L. Castillo and J.M. Carrillo, Numerical simulation and validation of hydrodynamics actions in energy dissipation devices. *Proc. 34th IAHR World Congress*, Brisbane, Australia, 1, 4416–4423, (2011).
[15] L. Castillo and J.M. Carrillo, Hydrodynamics characterization in plunge pools. Simulation with CFD methodology and validation with experimental measurements. *Proc. 2nd European IAHR Congress*, Munich, 1, (2012).
[16] L. Castillo and J.M. Carrillo, Analysis of the scale ratio in nappe flow case by means of CFD numerical simulation. *Proc. 35th IAHR World Congress*, Chengdu, China, 1, (2013).
[17] L. Castillo and J.M. Carrillo, Análisis numérico y experimental de velocidades en cuencos de aliviaderos de vertido libre. *Proc. 25 Congreso Latinoamericano de Hidráulica*, IAHR, Santiago, Chile, (2014). [in Spanish].
[18] L. Castillo, J.M. Carrillo and A. Blázquez, Plunge pool dynamic pressures: a temporal analysis in the nappe flow case. *J. Hydraulic Res* (in press), (2014).
[19] L. Castillo, J.M. Carrillo and A. Sordo-Ward, Simulation of overflow nappe impingement jets. *J. Hydroinformatics*, **16**(4), 922–940, (2014).
[20] R. Cola, Energy dissipation of a high-velocity vertical jet entering a basin. Proc. Int. *Conf. 11th International Association for Hydraulic Research Congress*, Leningrado, Ex-USSR, 1, (1965).
[21] D.A. Ervine and H.R. Falvey, Behaviour of turbulent water jets in the atmosphere and plunge pools. *Proc. Int. Conf. Institutions of Civil Engineers*, **83**(2), 295–314, (1987).

[22] D.A. Ervine, H.T. Falvey and W.A. Withers, Pressure fluctuations on plunge pool floors. *J. Hydraulic Res.* **35**(2), 257–279, (1997).
[23] M.P.E.A. Federspiel, *Response of an Embedded Block Impacted by High-Velocity Jets*. PhD Thesis. Faculté environnement naturel, architectural et construit, École Politechnique Fédérale de Lausanne, Suisse, (2011).
[24] S. Franzetti and M.G. Tanda, Analysis of turbulent pressure fluctuation caused by a circular impinging jet. *Proc. Int. Conf. on New Technology in Model Testing in Hydraulic Research*, India, 85–91, (1987).
[25] H. Görtler. Berechnung von Aufgaben der freien Turbulenz auf Grund eines neuen Näherungsansatzes. *Journal of Applied Mathematics and Mechanics / Zeitschrift für Angewandte Mathematik und Mechanik – ZAMM*, **22**(5), 244–254, (1942). [in German].
[26] W. H. Hager, *Energy dissipators and hydraulic jump*. Vol. 8. Dordrecht, The Netherlands: Kluwer Academic Publ. Water Science and Technology Library, (1992).
[27] F. Hartung and E. Häusler, Scours, stilling basins and downstream protection under free overfall jets at dams. *Proc. Int. Conf. 11th Congress on Large Dams*, Madrid, Spain, 39–56, (1973).
[28] G.J.C.M. Hoffmans, Closure problem to jet scour. *J. Hydraulic Res.* **47**(1), 100–109, (2009).
[29] P. Horeni, *Disintegration of a free jet of water in air.* Byzkumny ustav vodohospodarsky prace a studie. Sesit 93, Praha, Pokbaba, (1956). [in Czech].
[30] B.E. Launder and B.I. Sharma, Application of the energy dissipation model of turbulence to the calculation of flow near a spinning disc. *Lett. Heat Mass Transfer* **1**(2), 131–138, (1972).
[31] A. Lencastre, *Descarregadores de lâmina livre: Bases para o seu estudo e dimensionamento*. Memoria Nº 174. Laboratorio Nacional de Engenharia Civil, Lisbon, (1961). [in Portuguese].
[32] P. Liu, J. Gao and Y. Li, Experimental investigation of submerged impinging jets in a plunge pool downstream of large dams. *Science in China*, **41**(4), 357–365, (1998).
[33] P.A. Manso, E.F.R. Bollaert and A.J. Schleiss, Dynamic pressures generated by plunging jets in confined pools under extreme flood discharges. *Proc. XXXI IAHR Congress*, Seoul, **1**, 2848–2860, (2005).
[34] P.A. Manso, E.F.R. Bollaert and A.J. Schleiss, Evaluation of high-velocity plunging jet-issuing characteristics as a basis for plunge pool analysis. *J. Hydraulic Res.* **46**(2), 147–157, (2008).
[35] F.R. Menter, Two-equation eddy-viscosity turbulence models for engineering applications. *AIAA J.* **32**(8), 1598–1605, (1994).
[36] M. Mehraein, M. Ghodsian and A.J. Schleiss, Scour formation due to simultaneous circular impinging jet and wall jet. *J. Hydraulic Res.* **50**(4), 395–399, (2012).
[37] J.F. Melo, A.N. Pinheiro and C.M. Ramos, Forces on Plunge Pool Slabs: Influence of Joints Location and Width. *J. Hydraulic Eng*. **132**(1), 49–60, (2005).
[38] W.L. Moore, Energy loss at the base of a free overall. *Transactions, American Society of Civil Engineering*, **108**(1), 1343–1360, (1943).
[39] F. Ohtsu, Y. Yasuda and S. Awazu, *Free and submerged hydraulic jumps in rectangular channels.* Report of the Research Institute of Science and Technology. Nihon University. No 35, (1990).
[40] J. Puertas, *Criterios hidráulicos para el diseño de cuencos de disipación de energía en presas bóveda con vertido libre por coronación*. PhD Thesis. Departamento de Ingeniería Hidráulica, Marítima y Ambiental, Universidad Politécnica de Cataluña, Spain, (1994). [in Spanish].
[41] J. Puertas and J. Dolz, Plunge pool pressures due to falling rectangular jet. *J. Hydraulic Eng.* **131**(5), 404–407, (2005).
[42] N. Rajaratnam, The hydraulic jump as wall jet. *Proc. ASCE, Journal of Hydraulic Division. 91(HY5)*, 107–132, (1965).
[43] N. Rajaratnam, *Turbulent jets*. Elsevier Scientific, Development in Water Science, 5 New York, USA, (1976).
[44] E. Scimeni, Sulla forma delle vene tracimanti. *L'Energia Elettrica*, **7**(4), 293–305, (1930). (in Italian).
[45] B. Stutz and J.L. Reboud, Experiment on unsteady cavitation. *Exp. Fluids* **22**, 191–198, (1997).
[46] B. Stutz and J.L. Reboud, Two-phase flow structure of sheet cavitation. *Phys. Fluids* **9**(12), 3678–3686, (1997).
[47] T.L. Wahl, K.H. Frisell and E.A. Cohen, Computing the trajectory of free jets. *J. Hydraul. Eng.* **134**(2), 256–260, (2008).
[48] L. Wasewar and J. Vijay Sarathi, CFD modelling and simulation of jet mixed tanks. *Eng. Appl. Comp. Fluid Mech.* **2**(2), 155–171, (2008).
[49] D.C. Wilcox, *Turbulence modeling for CFD*, 3rd edition. DCW Industries, Inc., La Canada, California, (2006).
[50] W. Withers, *Pressure fluctuation in plunge pool of an impinging jet spillway*. PhD Thesis. Department of Civil Engineering, University of Glasgow, United Kingdom, (1991).
[51] S. Wu and N. Rajaratnam, Free jumps, submerged jumps and wall jets, *J. of Hydraulic Research*, **33**(2), 197–212, (1995).

Dam Protections against Overtopping and Accidental Leakage – Toledo, Morán & Oñate (Eds)
© 2015 Taylor & Francis Group, London, ISBN: 978-1-138-02808-1

Characterization of the dynamic actions and scour estimation downstream of a dam

Luis G. Castillo & Jose M. Carrillo
Universidad Politécnica de Cartagena (UPCT), Cartagena, Spain

ABSTRACT: The study analyzes the expected changes in the Paute River, located in Ecuador, as a result of the construction of the Paute-Cardenillo Dam (owned by Celec Ep-Hidropaute). The dam will integrate the National Electric System of Ecuador with a total electricity installed capacity of 600 MW which will produce 13000 GWh per year. To evaluate the stability and safety of the structure, it is necessary to ascertain the shape and dimensions of the scour generated downstream from the dam. The scour, due to the operation of the spillway and outlets, is studied with three complementary procedures: empirical formulae obtained in models and prototypes, semi-empirical methodology based on pressure fluctuations-erodibility index and computational fluid dynamics simulations.

Keywords: Dam, Spillway, Scour, Pressure fluctuations, Erodibility index, CFD

1 DAM CHARACTERISTICS

The Paute-Cardenillo Dam, located in Ecuador, is a double curvature arch dam with a maximum height of 135 m to the foundations. The top level is located at 926 meters above mean sea level (MASL). The reservoir has a length of 2.98 km with normal maximum water level located at 924 MASL. The river bed consists of a layer of 24 m of alluvial, below which there is a layer of 10 m of weathered rock. It has a free surface weir controlled by sluices that spill a flow of $Q_4 = 700\ m^3/s$ (return period TR = 4 years) and a half-height outlet with two almost symmetrical ducts. Considering the maximum normal operating level (924 MASL), the intermediate outlet capacity is $Q_{40} = 1760\ m^3/s$. Hence, the total flow of the weir and half-height outlet is $Q_{100} = 2340\ m^3/s$. If the bottom outlet were considered, the discharge capacity of the dam would be $Q_{10000} = 5520\ m^3/s$.

2 EMPIRICAL FORMULAE

In the study, 29 formulae are examined. The scour hole is estimated for different return periods flows.

Most of the equations were obtained by dimensional and statistic analysis of data obtained in Froude scale reduced models, with few formulae based on prototypes and many obtained for the ski-jump. As discharge is produced by a free surface weir and in pressure conditions by an intermediate outlet, the general expression is modified which provides the following simplified general expression:

$$D_s = h + D = K\frac{q^x H_n^y h^w}{g^v d^z} \quad (1)$$

where D_s is the scour depth below tailwater level, h the tailwater depth, D the scour depth below the original bed, K an experimental coefficient, q the specific flow, H_n the energy net head, and d the characteristic size of bed material. The meaning of the rest variables can be seen in Figure 1.

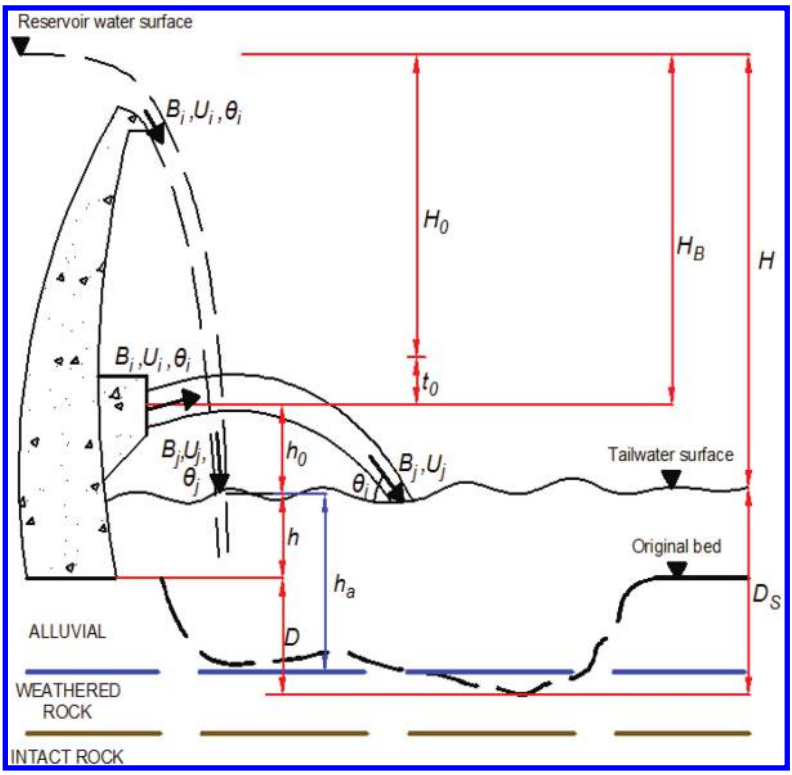

Figure 1. Scheme of scour in Paute-Cardenillo Dam.
x, y, w, v, z. Empirical exponents defined by regression or optimization.
t_0 = energy losses in the duct.
$H_n = H_0 = H_B - t_0$. Net energy head at the exit of the outlet.
$H_n = H$. Falling height from reservoir level to tailwater level (ski-jump and free surface weir).
h_0. Vertical distance between outlet exit and tailwater level.
h_a. Vertical distance between tailwater level and scour bed.
B_i, U_i, θ_i. Thickness, velocity and angle of the jet in initial conditions.
B_j, U_j, θ_j. Total thickness, velocity and angle of the jet in impingement conditions.

Table 1. Coefficients of five scour simplified formulae with values that fall in the mean value +/− 1 standard deviation.

Author	K	x	y	z	d
Hartung [25]	1.400	0.64	0.360	0.32	d_{85}
Chee and Padiyar [17]	2.126	0.67	0.180	0.063	d_m
Bisaz and Tschopp [3]	2.760	0.50	0.250	1.00	d_{90}
Martins-A [29]	1.500	0.60	0.100	0.00	–
Machado [28]	1.350	0.50	0.3145	0.0645	d_{90}

Table 1 shows the coefficients corresponding to five simplified formulae with values that fall in the mean values +/− 1 standard deviation, while Table 2 shows five more general expressions with values in the same range.

Figure 2 shows the results obtained for the free surface weir. The mean value +/− 1 standard deviation is indicated. If the mean value for the design flow (700 m^3/s) were considered, the scour

Table 2. Five scour general formulae with values that fall in the mean value +/− 1 standard deviation.

Author (Year)	Formulae
Jaeger [27]	$D_S = 0.6q^{0.5}H_n^{0.25}(h/d_m)^{0.333}$
Rubinstein [36]	$D_s = h + 0.19\left(\frac{H_n + h}{d_{90}}\right)^{0.75}\left(\frac{q^{1.20}}{H_n^{0.47}h^{0.33}}\right)$
Mirskhulava [34]	$D_s = \left(\frac{0.97}{\sqrt{d_{90}}} - \frac{1.35}{\sqrt{H_n}}\right)\frac{q \cdot \sin\theta_r}{1 - 0.175 \cdot \cot\theta_T} + 0.25h$
Mason-B [30]	$D_s = 3.39\frac{q^{0.60}(1+\beta)^{0.30}h^{0.16}}{g^{0.30}d^{0.06}}$
Bombardelli and Gioia [6]	$D_S = K\frac{q^{0.67}H_n^{0.67}h^{0.15}}{g^{0.33}d^{0.33}}\left(\frac{\rho}{\rho_S - \rho}\right)$

d_m. Average particle size of the bed material.
d_{90}. Bed material size in which 90% is smaller in weight.
θ_T. Impingement jet angle.
g (9.81 m/s^2). Gravity.
β. Air-water relationship.
ρ. Water density.
ρ_s. Density of sediment.

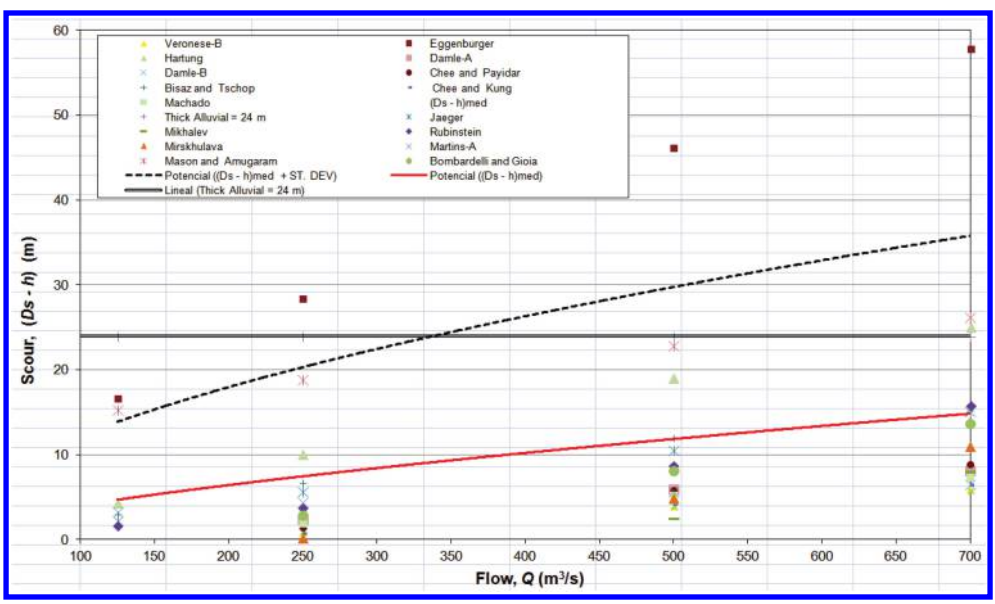

Figure 2. Scour of alluvial and weathered rock for the free surface weir.

could reach a depth of 15 m. However, if the mean value + 1 standard deviation were taken into account, then the flow of 500 m^3/s would penetrate the weathered rock (scour about 30 m).

Figure 3 shows the results obtained for the half-height outlet. The mean value +/− 1 standard deviation is indicated. The jet would scour the alluvial layer (24 m) with a return period flow $Q_{22} = 1320$ m^3/s. The design flow ($Q_{40} = 1760$ m^3/s) would not reach the intact rock. However, if the mean value + 1 standard deviation were taken into account, then the flow of 1250 m^3/s would erode the weathered rock layer (scour about 34 m).

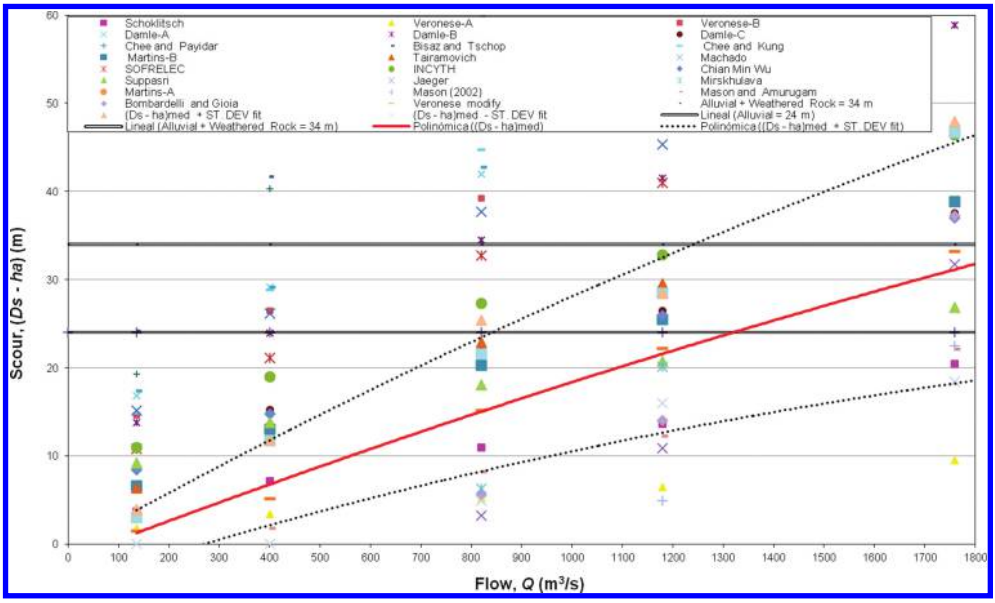

Figure 3. Scour of alluvial and weathered rock for the half-height outlet.

3 SEMI-EMPIRICAL METHODOLOGY

The erodibility index is based on an erosive threshold that relates the magnitude of relative erosion capacity of water and the relative capacity of a material (natural or artificial) to resisting scour. There is a correlation between the stream power or magnitude of the erosive capacity of water (P) and a mathematical function [$f(K)$] that represents the relative capacity of the material to resisting erosion. On the erosion threshold, this may be expressed by the relationship $P = f(K)$. If $P > f(K)$, the erosion threshold is being exceeded and the material is eroded.

Scour in turbulent flow is not a shear process. It is caused by turbulent, fluctuating pressures (Annandale [2]). Quantification of pressure fluctuations of incident jets in stilling basins has been studied mainly by Ervine and Falvey [20], Ervine et al. [21], Castillo [9, 11, 12, 14], Castillo et al. [10, 13], Puertas [35], Bollaert [4], Bollaert and Schleiss [5], Melo et al. [33], Felderspiel [22], and Carrillo [8].

The dynamic pressures of jets are a function of the turbulence intensity at the discharge conditions, length of the jet flight, diameter (circular jet) or thickness (rectangular jet) in impingement jet conditions and water cushion depth. Annandale [1, 2] summarized and established a relationship between the stream power and the erodibility index for a wide variety of materials and flow conditions. The stream power per unit of area available of an impingement jet is:

$$P_{jet} = \frac{\gamma Q H}{A} \tag{2}$$

where γ is the specific weight of water, Q the flow, H the drop height or the upstream energy head, and A the jet area on the impact surface. The erodibility index is defined as:

$$K = M_s \cdot K_b . K_d \cdot J_s \tag{3}$$

where M_s is the number of resistance of the mass, K_b the number of the block size, K_d the number of resistance to shear strength on the discontinuity contour, and J_s the number of structure relative of the grain. Table 3 shows the formulae of the parameters.

Table 3. Erodibility index parameters (Adapted from Annandale [2]).

Material	Formulae	Parameters
Rock	$M_s = 0.78 C_r UCS^{1.05}$ when $UCS \leq 10$ MPa $M_s = C_r UCS$ when $UCS > 10$ MPa $C_r = \frac{g\rho_r}{\gamma_r}$	C_r. Relative density ratio. ρ_r. Rock density. g (9.81 m/s^2). Gravity. γ_r ($27 \cdot 10^3$ N/m^3). Specific weight of the intact rock.
Non-cohesive granular	The relative magnitude is obtained from the SPT results. When this value exceeds 80, the non-cohesive granular material is considered equivalent to rock.	
Rock	$K_b = \frac{RQD}{J_n}$	RQD values are between 5 and 100, J_n between 1 and 5, and K_b between 1 and 100.
Non-cohesive granular	$K_b = 1000 D^3$	D. Diameter of the average block.
Rock	$K_d = \frac{J_r}{J_a}$	
Non-cohesive granular	$k_d = \tan\phi$	Φ. Angle of residual or internal friction of the granular material.

The threshold of rock strength to the stream power, expressed in kW/m^2, is calculated and based on the erodibility index K:

$$\begin{aligned} P_{rock} &= 0.48K^{0.44} \quad if \quad K \leq 0.1 \\ P_{rock} &= K^{0.75} \quad if \quad K > 0.1 \end{aligned} \tag{4}$$

The dynamic pressure in the bottom of the stilling basin is based on two components: the mean dynamic pressure (C_p) and the fluctuating dynamic pressure (C_p'). These dynamic pressure coefficients are used as estimators of the stream power reduction coefficients, by an effect of the jet disintegration in the air and their diffusion in the stilling basin.

Hence, the dynamic pressures are also a function of the fall height to disintegration height ratio (H/L_b) and water cushion to impingement jet thickness (Y/B_j). Thus, the total dynamic pressure is expressed as:

$$P_{total} = C_p(Y/B_j)P_{jet} + FC_p'(Y/B_j)P_{jet} \tag{5}$$

where $C_p(Y/B_j)$ is the mean dynamic pressure coefficient, $C_p'(Y/B_j)$ the fluctuating dynamic pressure coefficient, P_{jet} the stream power per unit of area, and F the reduction factor of the fluctuating dynamic pressure coefficient. In rectangular jet case (nappe flow), Castillo and Carrillo [16] and Carrillo [8] adjusted the formulae by using new laboratory data (Figures 4, 5 and 6).

Table 4 shows the values of the different variables considered and their respective calculus in the semi-empirical methodology.

Table 5 shows the results obtained in the three types of material existent in the place of the dam and the concrete slab proposed. In Figure 7 the stream power of the free surface weir jet is indicated, together with the power threshold of alluvial, weathered and intact rock.

Considering a water cushion depth of 24 m, the flow rate of 500 m^3/s would have the power to erode weathered rock, although the design flow of 700 m^3/s would not have enough power to erode the intact rock. These results confirm that the maximum scour of the free surface weir could be near to 34 m.

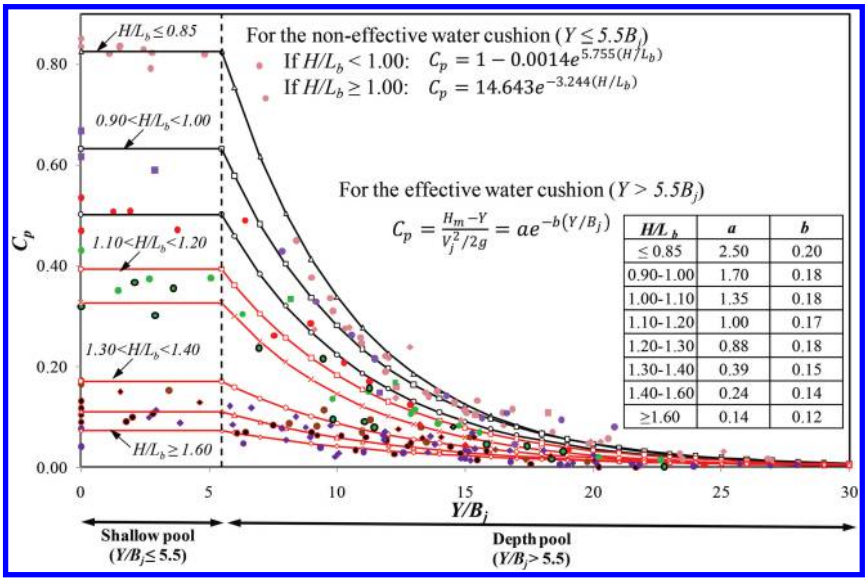

Figure 4. Mean dynamic pressure coefficient, C_p, for the nappe flow case.

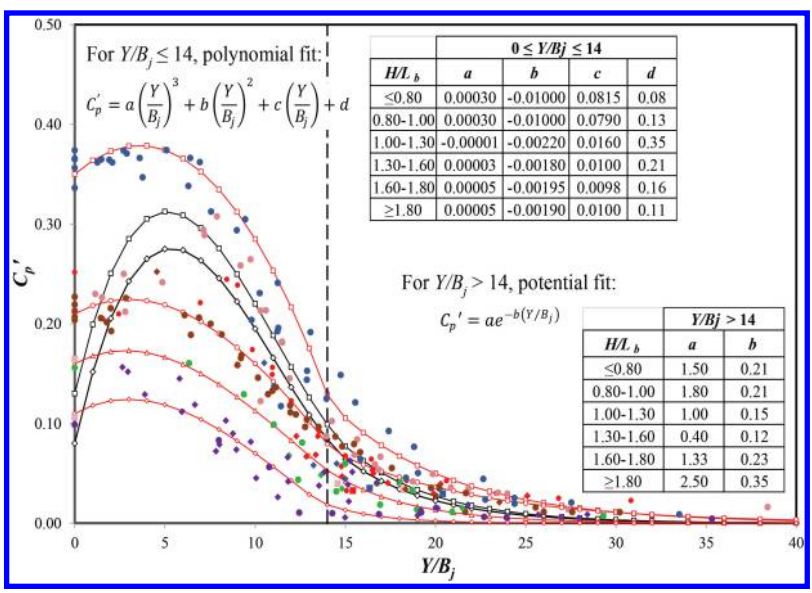

Figure 5. Fluctuant dynamic pressure coefficient, C_p', for the nappe flow case.

We can observe that the half-height outlet case does not correspond strictly with circular neither rectangular (nappe flow) jet case. For circular jets, the C_p and C_p' are valid for $H/L_b \le 0.50$ (Ervine et al., [21]). However, for the design flow ($Q_{40} = 1760\,\mathrm{m^3/s}$) the $H/L_b = 1.67$. For this reason the calculus were carried out by using the rectangular analogy.

The stream power threshold of weathered rock ($P_{weathered\_rock} = 16\,\mathrm{kW/m^2}$) does not resist the flow of annual return period ($Q_{ma} = 136\,\mathrm{m^3/s}$). The intact rock stream power ($P_{rock} = 408\,\mathrm{kW/m^2}$)

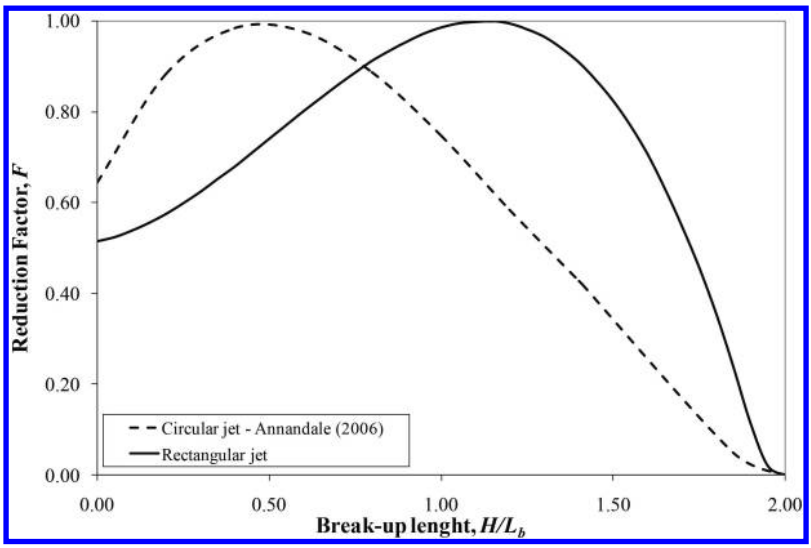

Figure 6. Reduction factor F of fluctuating dynamic pressure coefficient.

Table 4. Semi-empirical methodology. Input and calculated values.

Angle of rock friction, *SPT* (°)	38	Number of join system (calculated), J_n	1.83
Specific weight (kN/m^3)	27.64	Discontinuity spacing, J_x, J_y, J_z (m)	0.50
Unconfined compress. resistant, *UCS* (MPa)	50	Average block diameter (calculated), (m)	0.50
Relative density coefficient, *Cr*	1.02	Roughness degree, J_r	2.00
RQD (calculated)	82.66	Alteration degree, J_a	1.00

Table 5. Stream power of free surface jets for different flows as a function of the erodibility: alluvial, weathered rock, intact rock and concrete slab indexes (water cushion depth 24 m).

	Alluvial	Weathered rock	Intact rock	Concrete
M_s	0.19	0.41	51.19	20.47
K_b	11.39	125	49.18	49.18
K_d	0.78	0.78	2.00	5.33
J_s	1.00	1.00	0.60	1.00
Erodibility index, K	1.69	40.04	3021	7280
Stream power, P_{rock} (kw/m^2)	1.50	16	408	788

could resist up to a flow return period of 5 years ($Q_5 = 820\,\text{m}^3/\text{s}$). The $Q_{10} = 1180\,\text{m}^3/\text{s}$ would exceed the rock strength.

As a solution to the scour, a concrete slab of 20 MPa characteristic strength and thickness of 2 m ($P_{conc} = 788\,\text{kW/m}^2$) is placed directly on the alluvial level (796 MASL). The geometry of the pre-excavated basin should be similar to the geometry of the basin that would be formed with the flow $Q_{40} = 1760\,\text{m}^3/\text{s}$. Figure 8 indicates that the concrete slab would resist the power stream of the design flow ($P_{jet} = 664.95\,\text{kW/m}^2$).

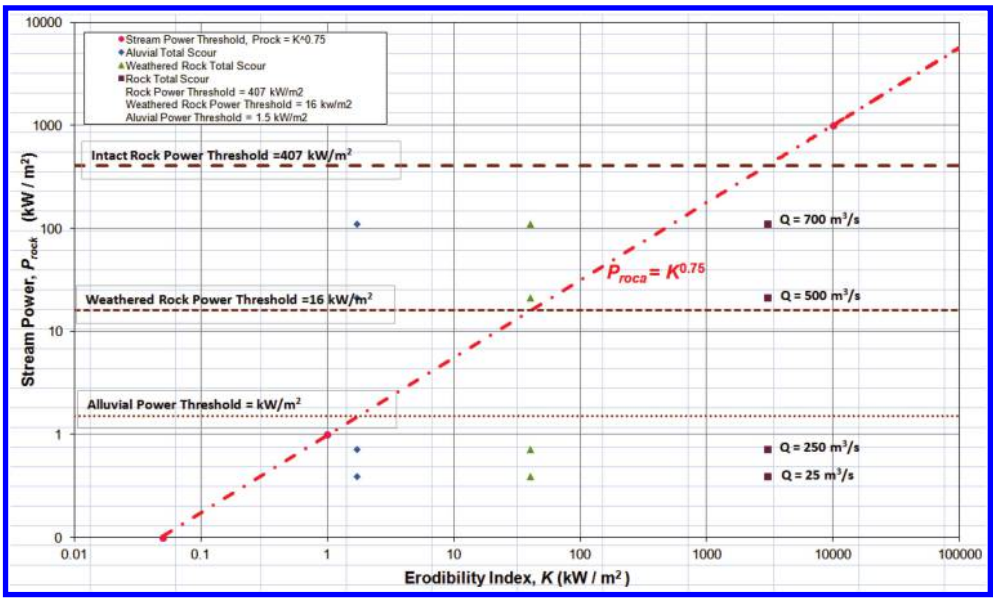

Figure 7. Free surface weir. Stream power of the jet for different flows as a function of the erodibility: alluvial, weathered rock and intact rock indexes (water cushion depth 24 m).

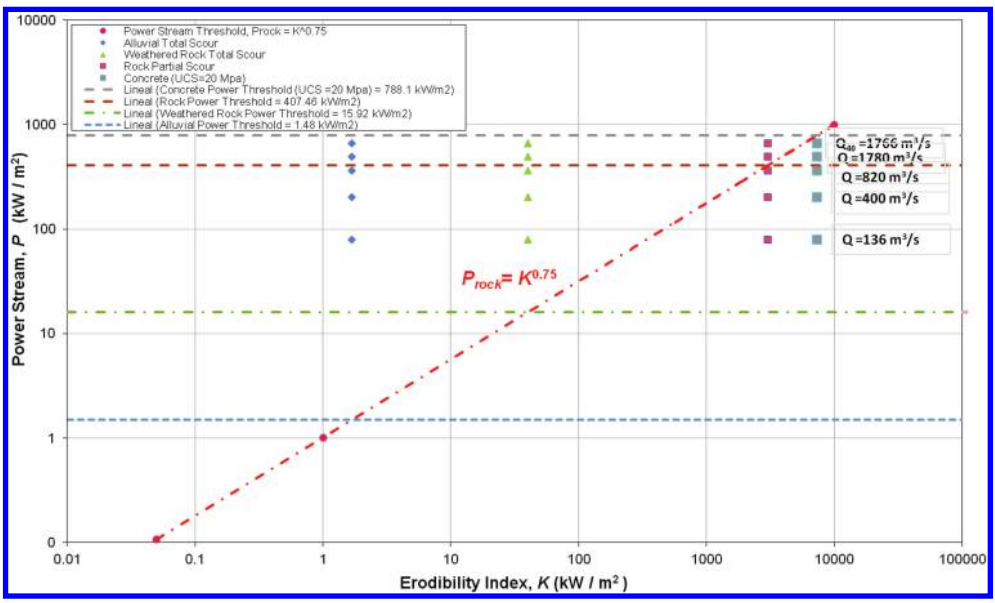

Figure 8. Half-height outlet. Stream power of the jet for different flows as a function of the erodibility: alluvial, weathered rock, intact rock and concrete cases (Water cushion depth 24 m).

4 NUMERICAL SIMULATION

As a complement of the empirical and semi-empirical methodologies, three-dimensional mathematical model simulations were carried out. These programs allow a more detailed characterization than one-dimensional and two-dimensional numerical models and, thus, a detailed study of local

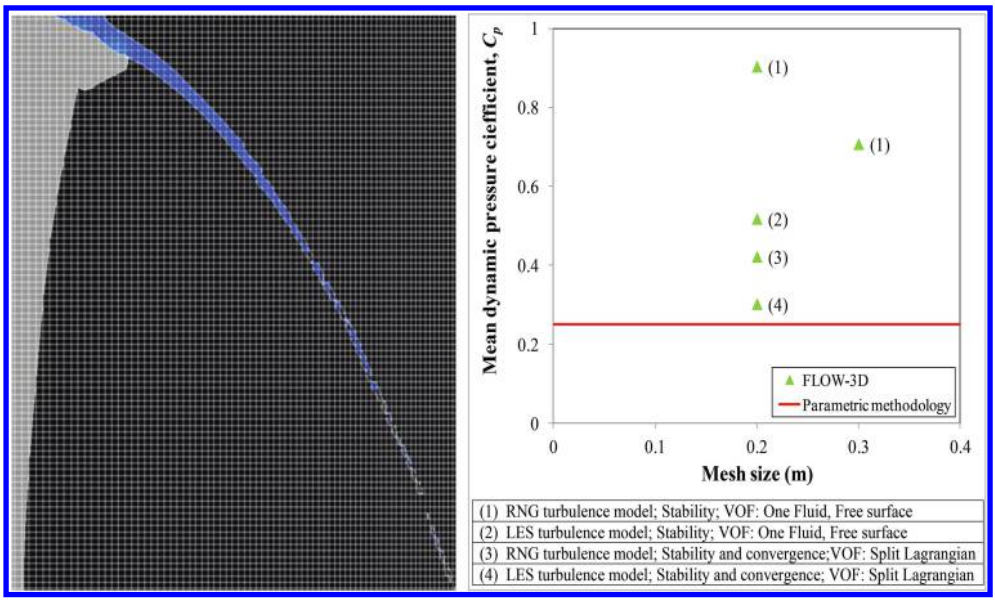

Figure 9. Mesh and sensibility analysis of FLOW-3D.

effects of the sediments transport. The numerical simulation of the hydraulic behavior and scour by the action of the free surface weir, intermediate and bottom outlets were also analyzed.

The computational fluid dynamics (CFD) program FLOW-3D was used. This program solves the Navier-Stokes equations discretized by finite differences. It incorporates various turbulence models, a sediment transport model and an empirical model bed erosion (Guo [24]; Mastbergen and Von den Berg [32]; Brethour and Burnham [7]), together with a method for calculating the free surface of the fluid without solving the air component (Hirt and Nichols [26]). Pressures obtained in the stagnation point and their associated mean dynamic pressure coefficients were compared with the parametric methodology proposed by Castillo [12, 14], actualized by Castillo and Carrillo [16] and Carrillo [8].

In order to simulate the proper functioning of the free surface weir, several simulations were carried out by means of sensibility analysis: air entrainment models, turbulence models, grid size and type of solver, among others (Figure 9).

We can observe that the results are anomalous when RNG k-ε turbulence model and the one fluid free surface method are used. So, if the mesh size is reduced from 0.30 m to 0.20 m, C_p changes from 0.71 to 0.90. However, when the RNG k-ε model is used with the split Lagrangian free surface method, then the results are more similar to the expected value.

The most accurate results were obtained by using a mesh size of 0.2 m, and large eddy simulation (LES) turbulence model. In the solver options, the stability and convergence method was selected and the free surface solved with the split Lagrangian method.

Table 6 compares the mean pressure and the mean dynamic pressure coefficient obtained by the non-effective water cushion case. Results were similar to the parametric methodology. It may be observed that the mean dynamic pressure and C_p coefficient obtained with FLOW-3D are somewhat greater than parametric methodology values, which is due to the air entrainment model not resolving the two-phase flow in an appropriate way.

As far as scour is concerned, free surface weir jets tended to impact on a small area. The upstream face of the scour bowl occurred approximately 29 m downstream from the dam. The plant scour was near 24 m long and 53 m wide (Figure 10). Erosion generated a scour depth of 22 m, which

Table 6. Comparison of pressures and C_p, considering a water cushion depth of 2 m.

	Parametric methodology	FLOW-3D
Drop height (m)	102.0	102.0
Mean dynamic pressure (m)	30.56	33.44
Mean dynamic pressure coefficient, C_p	0.28	0.31

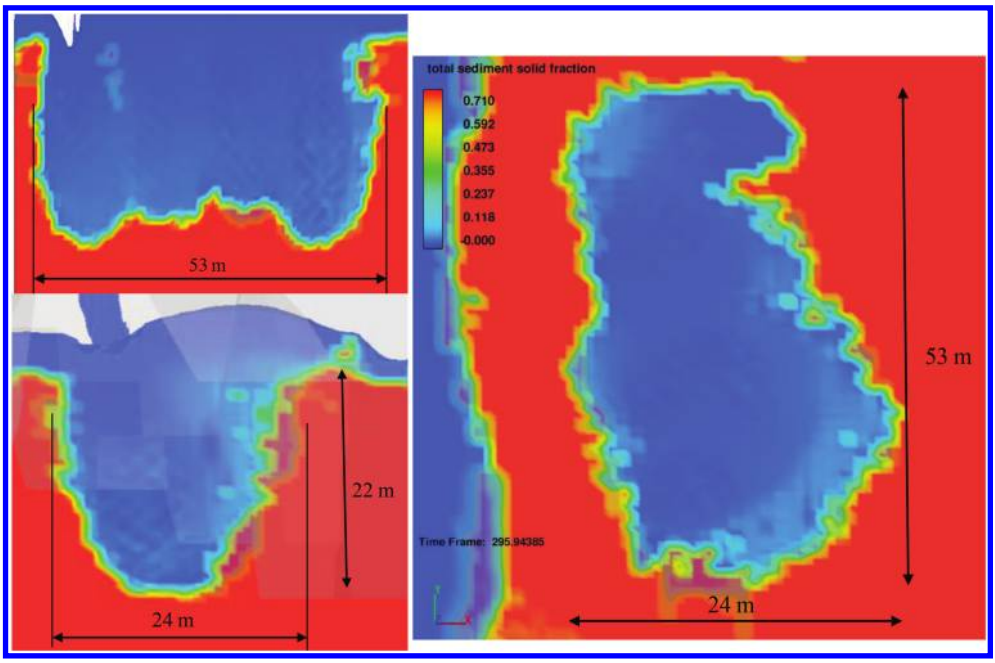

Figure 10. Front, lateral, and top view of the scour due to the free surface weir.

was a little greater than that calculated with the mean value of the empirical formulae and similar to that obtained with semi-empirical methodology.

For the simulation of half-height outlet ducts (5.00 × 5.80 m), the selection of the mesh size is function of their dimensions and of the thickness of the falling jets. The mesh consisted in hexahedral elements of 1 m. The Re-Normalization Group (RNG) k-ε turbulence model was selected. The volume-of-fluid advection was solved with the Split Lagrangian method. The time-step size was controlled by stability and convergence criteria.

Pressures obtained in the stagnation point and their associated mean dynamic pressure coefficients were compared with the parametric methodology [12, 14, 16, 8].

As far as the numerical simulation is concerned, the scour shape considering the concrete slab was analyzed. In this way, the level 798 m was considered as a non erodible. For the design flow, the half-height outlet jets tend to impact on a small area.

The upstream face of the scour occurred approximately 85 m downstream from the dam. The plant scour was near 108 m long and 50 m wide (Figure 11). Scour would reach the left natural slope and could cause landslides. The pre-excavated stilling basin shape should be adjusted to the geometry and the space available. Figure 12 shows the velocities vectors in lateral and top views of the pre-excavated basin.

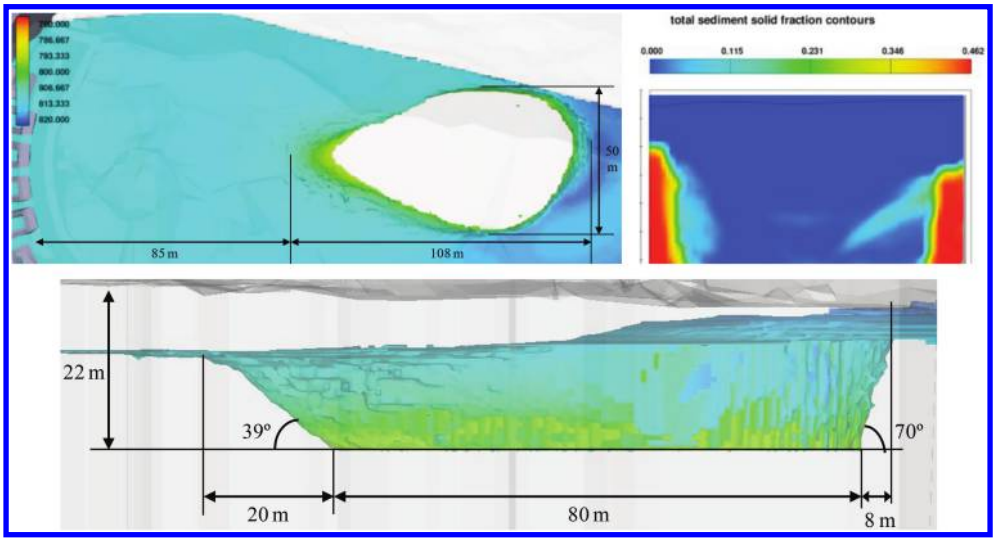

Figure 11. Top, front and lateral views of the scour due to the half-height outlet.

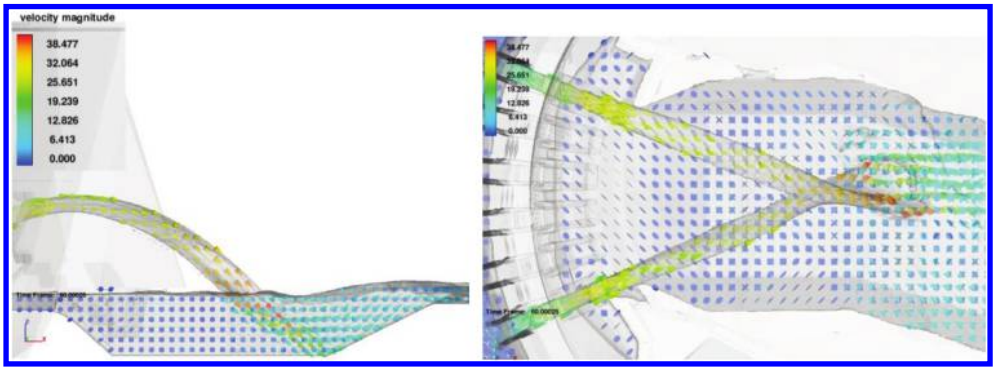

Figure 12. Lateral and top views of the velocity vectors in the pre-excavated stilling basin.

5 CONCLUSION

In this paper, similar results have been obtained by solving the problem from three different perspectives: empirical formulations, erosion potential semi-empirical formulation and CFD simulations.

The results demonstrate the suitability of crossing methodologies to solve complex phenomena. Thus, numerical simulations were used to complement the classical formulations, allowing a better understanding of the physical phenomena in order to obtain an adequate solution. Methodology leads us to propose a pre-excavated stilling basin.

The basin would allow to generate an effective water cushion. Besides this, it would reduce the sedimentation due to the excavation and the material transported by the river, especially during the flushing operations of the reservoir. The pre-excavated basin also would help to have a symmetric and regular flow, reducing the risk of potential landslides.

ACKNOWLEDGMENTS

The authors are grateful to CELEC EP – Hidropaute and the Consorcio POYRY-Caminosca Asociados for the data provided.

REFERENCES

[1] G.W. Annandale, Erodibility. *Journal of Hydraulic Research*, 33 (4), 471–494 (1995).
[2] G.W. Annandale, *Scour Technology. Mechanics and Engineering Practice*. McGraw-Hill, (2006).
[3] E. Bisaz and J. Tschopp, Profundidad de erosion al pie de un vertedero para la aplicación de correccion de arroyos en quebradas empinadas. *Proceedings of the Fifth Congreso Latinoamericano de Hidraulica (IAHR)*, Lima, Peru, 447–456, (1972).
[4] E. Bollaert, *Transient Water Pressures in Joint and Formations of Rock Scour due to High-Velocity Jet Impact, Communication Nº. 13*. Laboratory of Hydraulic Constructions, École Polytechnique Fédérale de Lausanne, Switzerland, (2002).
[5] E.F. Bollaert and A. Schleiss, Scour of rock due to the impact of plunging high velocity jets. Part 1: A state-of-the-art review. *Journal of Hydraulic Research*, 41(5), 451–464, (2003).
[6] F.A. Bombardelli and G. Gioia. Scouring of granular beds by jet-driven axisymmetric turbulent cauldrons. *Phys. Fluids*, 18(8), 088–101, (2006).
[7] J. Brethour and J. Burnham, Modeling Sediment Erosion and Deposition with the FLOW-3D Sedimentation & Scour Model. *Flow Science Technical Note, FSI-10-TN85*, 1–22, (2010).
[8] J. M. Carrillo, *Metodología numérica y experimental para el diseño de los cuencos de disipación en el sobrevertido de presas de fábrica*. PhD Thesis. Universidad Politécnica de Cartagena, Spain, (2014).
[9] L. Castillo, *Metodología experimental y numérica para la caracterización del campo de presiones en los disipadores de energía hidráulica. Aplicación al vertido en presas bóveda*. PhD Thesis. Universitat Politécnica de Catalunya, Spain, (1989).
[10] L. Castillo, J. Dolz and J. Polo, Acquisition and analysis of data to characterize dynamic Actions in Hydraulic Energy Dissipators. *XXIV IAHR Congress*. D, 273–280. Madrid, (1991).
[11] L. Castillo, Parametrical Analysis of the Ultimate Scour and Mean Dynamic Pressures at Plunge Pools. *Workshop on Rock Scour due to High Velocity Jets*. École Polytechnique Fédérale de Lausanne, (2002).
[12] L. Castillo, Areated jets and pressure fluctuation in plunge pools. *The 7th International Conference on Hydroscience and Engineering* (ICHE-2006), IAHR, ASCE, Drexel University. College of Engineering. DSpace Digital Library. DU Haggerty Library, Philadelphia, USA, (2006).
[13] L. Castillo, J. Puertas and J. Dolz, Discussion about Scour of rock due to the impact of plunging high velocity jets Part I: A state-of-the-art review. *Journal of Hydraulic Research*, 45 (6), 853–858, (2007).
[14] L. Castillo, Pressure characterization of undeveloped and developed jets in shallow and deep pool. *32nd Congress of IAHR*, the International Association of Hydraulic Engineering & Research, Vol. 2, 645–655, Venice, Italy, (2007).
[15] L.G. Castillo and J.M. Carrillo, Hydrodynamics characterization in plunge pool. Simulation with CFD methodology and validation with experimental measurements. *2nd IAHR Europe Congress*, Munich (2012).
[16] L.G. Castillo and J.M. Carrillo, Analysis of the ratio scale in nappe flow case by means of CFD numerical simulations. *Proceedings of 2013 IAHR Congress*, Chengdu, China, (2013).
[17] S.P. Chee and P.V. Padiyar, Erosion at the base of flip buckets. *Enginering Journal, Inst. of Canada*, 52(111), 22–24, (1969).
[18] CONSORCIO PCA. *FASE B: Informe de Factibilidad, Anexo 2, Meteorología, Hidrología y Sedimentología*, (2012).
[19] CONSORCIO PCA. *FASE B: Informe de Factibilidad, Anexo 6, Hidráulica*, (2012).
[20] D.A. Ervine and H.R. Falvey, Behavior of turbulent jets in the atmosphere and plunge pools. *Proceedings of the Institutions of Civil Engineers*, 83 (2), 295–314, (1987).
[21] D.A. Ervine, H.R. Falvey and W. Whiters, Pressure Fluctuations on Plunge Pool Floors. *Journal of Hydraulic Research*, 35 (2), (1997).
[22] M.P. Felderspiel, *Response of an embedded block impacted by high-velocity jets*. PhD Thesis. École Polytechnique Fédérale de Lausanne, Suisse, (2011).
[23] Flow Sciences Incorporated. *FLOW-3D Users Manual Version 10.0*. Santa Fe, New Mexico, (2011).

[24] J. Guo, Hunter Rouse and Shields diagram. *Proc 1th IAHR-APD Congress*, Singapore, 2, 1069–1098, (2002).
[25] W. Hartung, Die Kolkbildung hinter Uberstromen wehren im Hinblick auf eine beweglich Sturzbettgestaltung. *Die Wasser Wirtschaft*, 49(1), 309–313, (1959).
[26] C.W. Hirt and B.D. Nichols, Volume of Fluid (VOF) Method for the Dynamics of Free Boundaries. *Journal of Computational Physics*, 39 (201), (1981).
[27] C. Jaeger, Uber die Aehnlichkeit bei flussaulichen Modellversuchen. *Wasserkraft und Wasserwirtschaft*, 34(23/24), 269, (1939).
[28] L.I. Machado, Formulas to calculate the scour limit on granular or rock beds. *XIII National workshop on large dams*, Subject 1, Rio de Janeiro, Brazil, 35–52, (1980).
[29] R. Martins, Scouring of rocky riverbeds by free-jet spillways. *Water Power & Dam Construction*, April, (1975).
[30] P.J. Mason, Effects of air entrainment on plunge pool scour. *Journal of Hydraulic Engineering*, 115(3), 385–399, (1989).
[31] P.J. Mason and K. Arumugan, Free Jets Scour below Dams and Flip Buckets. *Journal of Hydraulic Engineering, ASCE*, 111(2), 220–235, (1985).
[32] D.R. Mastbergen and J.H. Von den Berg, Breaching in fine sands and the generation of sustained turbidity currents in submarine canyons. *Sedimentology*, 50, 625–637, (2003).
[33] J.F. Melo, A.N. Pinheiro and C.M. Ramos, Forces on plunge pool slabs: influence of joints location and width. *Journal of Hydraulic Engineering*, 132 (1), 49–60, (2006).
[34] T. E. Mirtskhulava, Alguns Problemas da Erosao nos Leitos dos Rios. Moscow. *Trans. No 443do L.N.E.C.*, (1967).
[35] J. Puertas, *Criterios hidráulicos para el diseño de cuencos de disipación de energía en presas bóveda con vertido libre por coronación*. PhD Thesis, Universidad Politécnica de Cataluña, Spain, (1994).
[36] G.L. Rubinstein, Laboratory investigation of local erosion on channel beds below high overflow dams, *Transactions of Coordination Conferences on Hydraulic Engineering. 1ss. VII, Conference on Hydraulics of High Head Water Discharge Structures*. Gosenergoizdat M.L., (1963).
[37] I.I. Taraimovich, Deformation of channels below high head spillways on rock foundations. *Hydrotechnical Construction*, 9, 917–922, (1978).

Dam Protections against Overtopping and Accidental Leakage – Toledo, Morán & Oñate (Eds)
© 2015 Taylor & Francis Group, London, ISBN: 978-1-138-02808-1

Highly-converging chutes as an overtopping protection for concrete dams: physical and numerical modelling

L. Morera
Dam Safety Research Group (SERPA), Technical University of Madrid (UPM), Spain

J. San Mauro & F. Salazar
International Center for Numerical Methods in Engineering (CIMNE), Barcelona, Spain

M.Á. Toledo
Dam Safety Research Group (SERPA), Technical University of Madrid (UPM), Spain

ABSTRACT: Spillways with highly-converging chutes are a non-conventional kind of spillway in which the length of the crest is greater than the width of the stilling basin. A pair of converging chutes leads the water into the stilling basin. This typology has two possible advantages: increase of the discharge capacity or reduction of the hydraulic head for a given discharge flow. The first improves dam safety, whereas the second results in higher storage capacity and power generation. In this proceeding, the authors present the investigation performed in order to study and characterize this kind of spillways. The utilization of this typology as an overtopping protection has emerged as a third possibility, presenting some particularities that are introduced here.

1 INTRODUCTION

There is a non-conventional spillway typology suitable for concrete dams that is characterized for having much more width at the crest of the dam than that at the entrance of the stilling basin. A pair of converging chutes is required, which consequently conduct the water over the dam face towards the stilling basin. An example of the described scheme is represented on fig. 1.

Given that no specific name has been identified in the scientific and technical communities for referring to this uncommon typology, the authors proposed "spillways with highly-converging chutes" (SHCC, in advance). The word "highly" refers to the idea that the converging elements introduce an important change in the flow pattern, in such a way that the water, once has reached the training wall of the chute, makes a quick turn and forms a roller wave. By contrast, in the cases of "low" convergence, shockwaves are observed. The presence of the converging chutes clearly reveals an interesting possibility of usage as an overtopping protection for concrete dams. They are capable of catching any eventual overtopping flow along the dam crest, preventing scour in the toe of the dam and any other damage to the constructions located in the downstream abutments (e.g., a hydroelectric power station).

With the purpose of studying this kind of spillways, a hydraulic model with changeable geometry has been constructed, in which a set of tests has been performed. The information and the data acquired in these tests have been analyzed and compared with a series of numerical models in order to both calibrate and validate the software and also reach a better comprehension of the flow characteristics. One of the final aims of this research is to define design guidelines for this kind of spillways, and to combine them with the particularities of its usage as an overtopping protection.

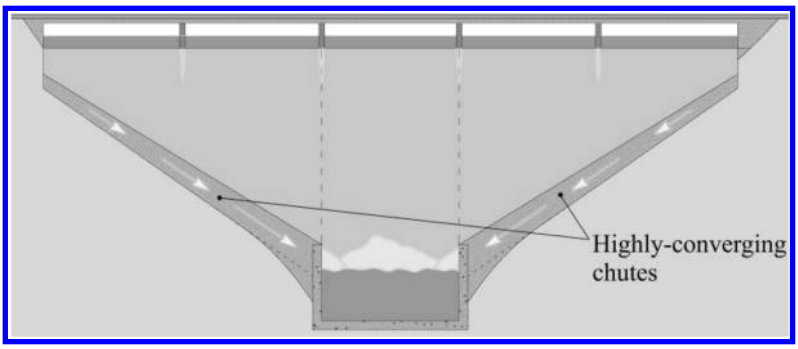

Figure 1. Sketch showing the concept of the spillways with highly-converging chutes. Elevation view.

Figure 2. Three examples of dams with highly-converging chutes. Left: Nunome Dam (Japan), with RCC-stepped chutes. Center: Zapardiel de la Cañada Dam (Spain), with parabolic-floor chutes. Right: Torre Abraham Dam (Spain), in which the converging chutes were added after dam construction to increase the spillway capacity.

2 CHARACTERISTICS AND APPLICATIONS OF THIS SPILLWAY TYPOLOGY

Spillways with highly-converging chutes are a non conventional solution for concrete dams suitable for those cases in which it is necessary to maximize the width of the spillway at the crest of the dam. Although there are many dams around the world including this type of spillway (fig. 2), there is a lack of unified design criteria and almost no scientific literature on the field (Martín Vide, 2005).

The consideration of a wider spillway crest affects significantly to the discharge capacity of the dam and also to the reservoir water level reached in flood events, as follows:

- The spillway capacity is increased, whereas the reservoir flood-routing would be reduced in different magnitude, also depending on the characteristic curve of the reservoir.
- The hydraulic head over the dam crest in flood events is reduced.

These two effects are directly related with two possible advantages or applications of this configuration:

- If the enhancement of dam safety criteria leads to the reconsideration of the freeboard as insufficient (in relation with larger return periods considered for the design flood), the implementation of SHCC could serve as a solution.
- The reduction in the hydraulic head over the dam crest in flood events could be used for increasing the normal operation level, which in turn can be beneficial for the hydroelectric power generation, affecting both to hydraulic head over the turbines and also to reservoir storage capacity (fig. 3)

These previously known advantages, which were deducted in a theoretical way, can be added to other hydraulic benefits that have been revealed after the realisation of the tests.

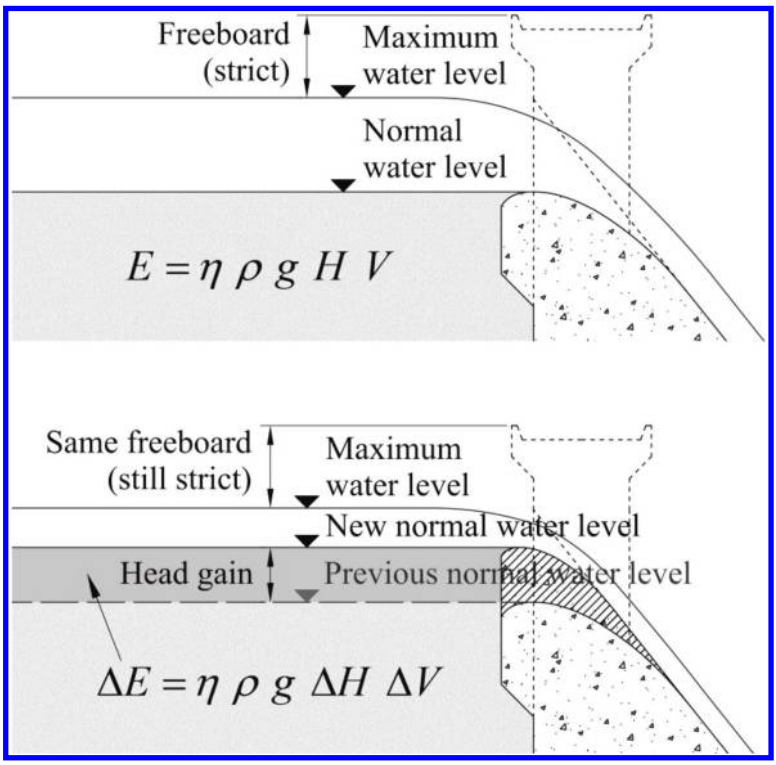

Figure 3. Sketch showing the hydroelectric benefits of the spillway regrowth with highly-converging chutes. Top: Previous situation. Bottom: the increment in the energy (E) is explained by the increments in two terms of the formula: the hydraulic head (H) and the reservoir storage capacity (V).

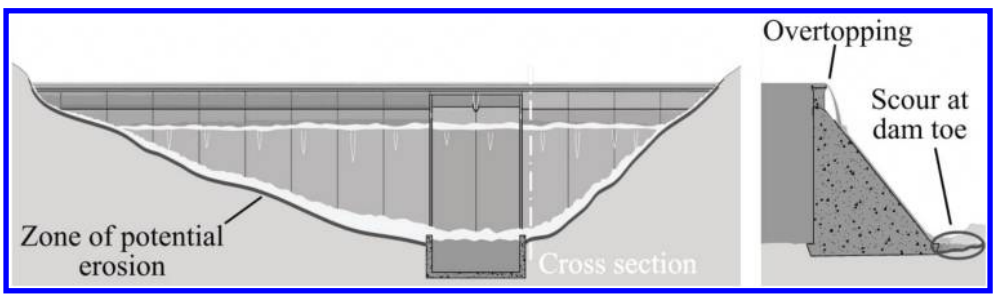

Figure 4. Overtopping situation in a non protected concrete dam (Elevation and cross section views).

As mentioned before, this configuration could be used as an overtopping protection, since the pair of chutes is capable of collecting any eventual overtopping flow, protecting the abutments and the dam-toe from any potential erosion (fig. 4). The protection achieved can be also very useful in case of presence of constructions or buildings immediately downstream the dam.

SHCC can be implemented for the design of new dams, but also for the enlargement and improvement of existing ones. There are several possibilities for this second option:

a) Increase in the spillway length by removing part of the dam crest. This can be combined with a raise of the spillway crest to increase the height of the maximum operation level in relation with the previously mentioned advantages in terms of power generation and storage capacity (fig. 5).

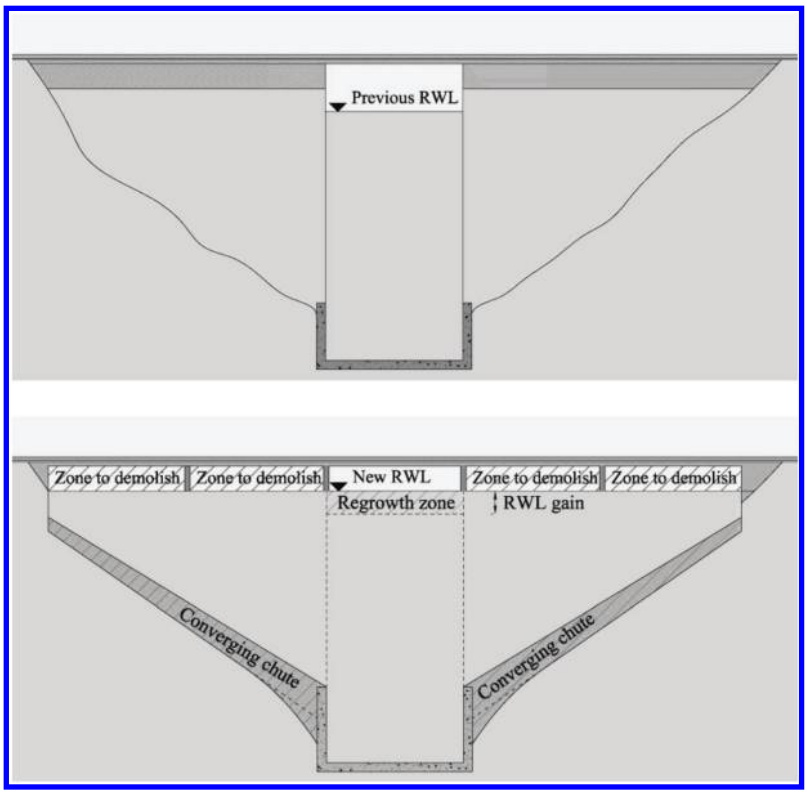

Figure 5. Implementation of a spillway with highly-converging chutes in an existent dam, with partial demolition of the crest. Elevation view. Top: previous situation. Bottom: required modifications.

b) Adaptation of the dam crest and its elements to endure the overtopping flow in new flood scenarios. In this alternative, the main part of the flow would be running through the pre-existing central spillway, and a smaller flow rate would overtop the dam crest and impinge into the downstream face, as shown on fig. 4 (right). Another difference of this option is that the converging chutes would hold smaller flows, what will affect to their size and also to the flow pattern.
c) There is a third possibility that combines aspects from the two previous ones. It consists of a spillway with the crest at two different heights. The central part may be located at a lower height, and serve to conduct regular floods. Side spillways, whose crest is located at a higher point, will be working only over a specific discharge value.

Finally, the implementation of this typology in single-curvature-arch dams has not been studied in this proceeding, but many of the aspects presented here can be considered for this application.

3 STUDIES PERFORMED AND METHODOLOGY

3.1 *Description of the testing facilities*

A physical model has been constructed in the UPM hydraulics laboratory in order to perform series of tests. In fact, the hydraulic model acts as a prototype for the calibration and validation of the numerical models. For that reason, there is no specific scale related to this facility, though, the authors took into account scales ranging from 1:10 to 1:50 as a reference.

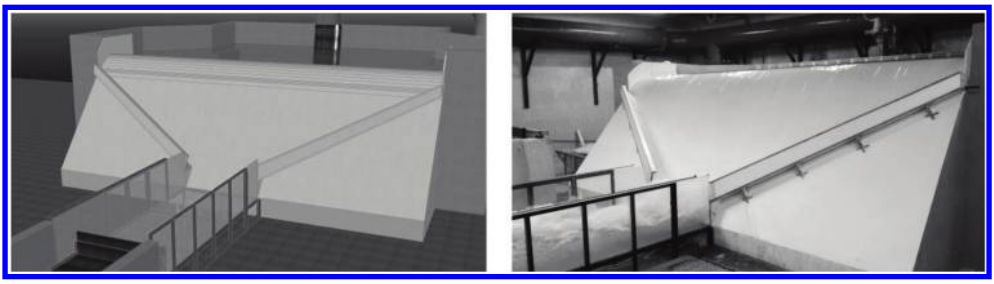

Figure 6. General view of the initial plan (left) and the constructed model (right).

The main parameters of the model are the following:

- Maximum length of the spillway crest: 5.00 m (though this is one of the parameters to be varied in the tests).
- Dam height over the stilling basin: 1.50 m.
- Downstream slope: 0.8
- Width of the stilling basin: 1.00 m.
- Length of the stilling basin: variable (with a maximum size of 4.00 m).
- Height of the end sill (delimiting element for the stilling basin): variable (with a maximum height of 0.15 m).

The model has been sized considering a design flow equal to 0.25 m^3/s. This affected mainly to the Creager profile, the dimensions of the converging chutes and the length and depth of the stilling basin.

The converging chutes were designed accordingly to concrete formwork possibilities. The chosen design is composed of three parts. The floor slab and the training wall have variable width and height, both equal and increasing along the descending direction, from 0.10 m at top (fixed as a constructive minimum considering the range of possible real scales) to 0.15 m at bottom. The chutes feature a deflector at the top of the training wall to prevent spilling and ease the water to flip forming a roll wave. Initial sizing references were obtained considering supercritical-and-uniform flow conditions in a channel with the corresponding trapezoid cross section (although the expected flow characteristics were different). Another important design aspect is related with the point at which the chutes launch the water into the stilling basin. In this model, the water is thrown at the point in which the end of the chute is naturally inserted between the dam face and the vertical wall of the stilling basin. In consequence, a triangular extension of the vertical wall is needed under the chute to contain the water.

Regarding the equipment and instrumentation used, the physical model counts with the following devices:

- A varying-power pump-control system, capable of acting over three pumps with a joint capacity of more than 0.25 m^3/s.
- An electromagnetic flow meter. The measured flow acts as the controlling variable.
- A set of manual level meters, one of them located at the tank of the model and the others attached to a movable truck located over the stilling basin.
- 20 pressure gauges located at the bottom of the stilling basin.
- An electronic level meter located at the outlet weir, downstream the model, to check the measurements of the electromagnetic flow meter.
- A data acquisition system capable of showing real-time measurements.

A general view of the constructed model is shown on fig. 6 (right).

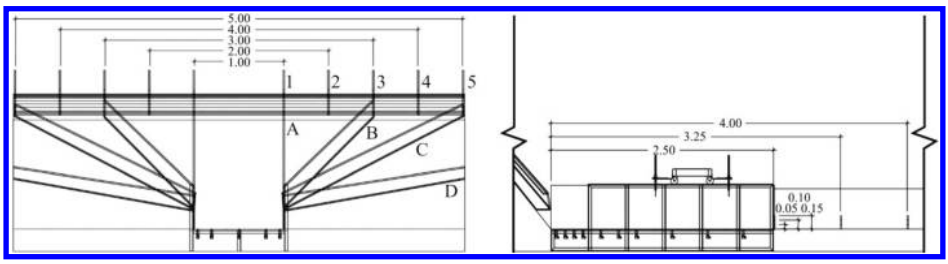

Figure 7. Representation of the parameters to be varied in the test campaign (values are expressed in meters). Left: elevation view. Each letter is associated to certain degree of convergence, and each red number is the value of the length of the spillway. Right: side view.

3.2 *Physical test campaign*

The physical model was designed for allowing the variation in some of the most relevant problem parameters, which are:

- The degree of convergence of the pair of chutes.
- The length of the spillway crest.
- The length of the stilling basin.
- The height of the end-sill.

In consequence, the variations shown on fig. 7 were posed.

The chosen values for the lengths of the stilling basin were 2.50, 3.25 and 4.00 m. Regarding the height of the end sill, the values chosen were: 0.00 (no sill), 0.05, 0.10 and 0.15 m. And the flows finally tested, were: 25, 75, 125 and 175 l/s.

At the first stage of the research project, the configurations tested were the C5 (considered as the referential configuration), the C3, the B3 and the A1 (conventional straight spillway). The dispositions D5, D4, D3, D2, C4, C2 and B2 were not physically tested at this stage.

For each test, a set of pictures and videos were shot. The pressure measurements were registered using the data acquisition system. Also, the water depth was measured in different points: water tank of the model, two points of the spillway and at different points in the stilling basin and over the end sill.

3.3 *Numerical simulations*

The numerical modeling was performed with an eulerian finite element method (FEM) completed in the open-source code Kratos (Dadvand et al, 2005 and Rossi et al, 2013) developed at CIMNE. The solution module was designed for the resolution of the 3D Navier-Stokes equations using the FEM. In this work, a level-set approach was applied for the computation of the free-surface position.

The same tool was previously applied for the analysis of spillway hydraulics (Salazar et al, 2013) among other fluid-dynamics problems. The detailed description of the numerical implementation is beyond the scope of this paper, though can be found in (Rossi et al, 2013).

All the simulations were performed in 3D, in accordance with the highly three-dimensional characteristics of the geometry and the flow pattern.

The results of the numerical modeling of two laboratory tests are presented:

1. A hydraulic jump forced in a horizontal rectangular channel. It consisted on allowing the free flow discharge over a conventional Creager-type weir, while fixing the downstream water level by varying the opening of a sluice gate. The formation and characteristics of the hydraulic jump could thus be controlled (fig. 11).
2. Several configurations of the SHCC previously described (Table 1).

Table 1. Cases analyzed in the numerical models.

Spillway configuration	End-sill height (cm)	Flow (l/s)	Spillway configuration	End-sill height (cm)	Flow (l/s)
A1	15	150	A1	15	250
B3	0	150	A1	35	250
B3	5	150	C3	5	250
B3	10	150	C3	7	250
B3	15	150	C3	10	250
C3	10	150	C3	15	250
C3	15	150	D5	0	250
D5	0	150	D5	15	250

4 RESULTS AND DISCUSSION

4.1 *Physical model results*

4.1.1 *Flow pattern in the converging chutes*

As described before, the converging chutes are composed of three elements: floor slab, training wall and top deflector. This configuration should contribute to the development of a helical flow pattern, as the descending wall jet impinges first with the floor and then with the side wall and top deflector making a quick turn and forming a sort of roller wave. In fact, the tests have revealed that the development of the roller wave depends on:

- The speed of the impinging flow (related to the hydraulic head between the chute and the spillway crest).
- The side-flow rate (this is, the flow rate entering the chutes).
- The degree of convergence.

In this sense, the cases with lower convergence would require higher side-flow rate for the development of the roller wave. Moreover, some tests presented partially developed roller waves, this is, the helical pattern was fully observed only below a certain section of the chute, and this has suggested the influence of the impingement speed.

Another feature observed in the trials is the formation of a descending water cord, which lies above the roller wave and the water jet over the dam face (fig. 8, right). This phenomenon was observed for higher values of the side-flow rate also depending on the degree of convergence.

Finally, the observed air-entrainment at the chutes supports the idea that there is considerable energy dissipation at these elements, especially for higher values of the degree of convergence. Flow pattern has also been studied in the numerical models.

4.1.2 *Jet impingement at the entrance of the stilling basin and stilling basin performance*

Another topic of major importance is the entrance of the converging jets into the stilling basin. This detail affects significantly to the flow pattern developed at the stilling basin and to the formation of the hydraulic jump. The fig. 9 (left) shows the jet collision in three tested configurations (C5, C3 and B3). The fig. 9 (right) depicts the pressures measured in these cases, at 5 sensors located just after the dam toe.

Several influential parameters have been identified:

- The fraction of the total flow that enters through the converging chutes (compared with the central flow).The higher fraction of side flow, the more three-dimensional the flow pattern is (less resemblance with the conventional hydraulic jump) and the bigger the fraction of energy dissipation upstream the jump.

Figure 8. Example of the flow pattern observed in the chutes for the C3 configuration varying the flow rate. Left: 6.7 l/s/m, the roller wave is not yet formed. Centre: 13.3 l/s/m. Helical flow is observed along all the chute. Right: 35.6 l/s/m. A water cord is formed above the roller wave.

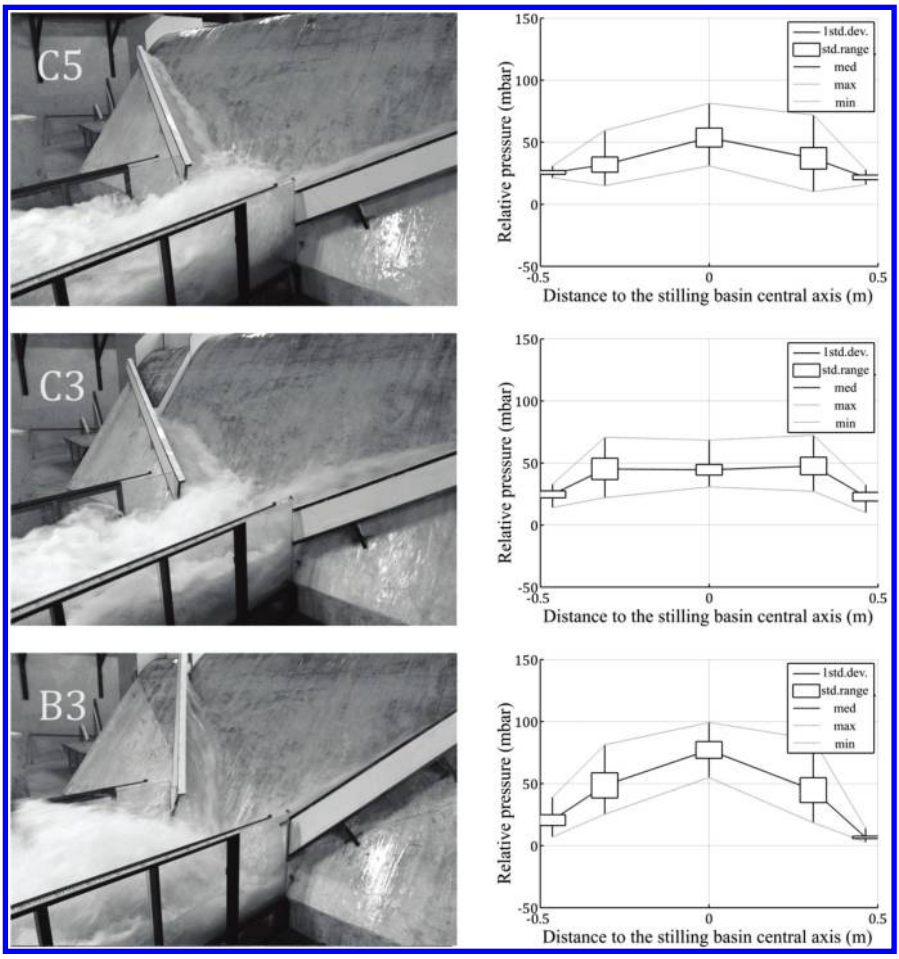

Figure 9. Left column: General view of the jet impingement in three different tests. Right column: Pressure values registered in the stilling-basin-cross section located at a distance of 0.06 m from dam toe, for each test. Top: C5 configuration. Centre: C3 configuration. Right: B3 configuration. Flow: 175 l/s. Length of the basin: 2.50 m. Height of the end sill: 0.15 m.

– The degree of collision between the converging jets, which depends on the chute trajectory, the height at which the jets are thrown and the width of the basin. Achieving a high degree of collision helps to the energy dissipation. Another aspect detected in the tests is that there is considerable water-spilling over the walls of the basin when the jets are more directly launched to the basin floor before colliding (B3 configuration).

There are other aspects regarding jet throwing that may be thoroughly studied in future researches:

– The influence of asymmetry in the converging chutes. As the cases studied are symmetric, the high three-dimensionality of the flow pattern at the stilling basin suggests that asymmetric cases could have important peculiarities. In fact, asymmetry is the most likely situation when using this solution as an overtopping protection, as the most part of the dams have different crest lengths and abutment profiles at each side of the stilling basin (fig. 4, left)
– The degree of submergence of the converging jets. As explained before, in the constructed model the jets are thrown into the basin at a certain height with respect to the basin floor. Tests have revealed that the energy dissipation of the jets mainly occur in their own impingement and also involves only a shallow part of the basin water. This characteristic is more noticeable when the end sill height is increased to 0.10 or 0.15 m. In those cases, an important mass of water near the bottom of the stilling basin remains with no apparent contribution to energy dissipation. The efficiency of the stilling basin could be improved by the reduction of the launching height, (for example, throwing the jets directly at the basin floor) using the basin more as a plunge pool.

The exposed phenomena suggest that the evaluation of the stilling basin performance is somewhat complicated compared with the conventional two-dimensional studies (Hager, 1992). First, the flow pattern is clearly three-dimensional, and it tends to turn into asymmetric. Secondly, the water pressures have important fluctuations near the jet-collision zone (fig. 10). The peaks obtained should be matter of study in order to prevent cavitation at bigger scales. Different modes and shapes of the 3D hydraulic jump have been detected:

a) Jump with the roller over the sloping dam face (with particularities due to the presence of the water crest).
b) Jump with the roller starting under the jet-colliding zone.
c) Partially swept jump, in some cases with an oblique and asymmetric roller.
d) Absence of jump before the end sill (totally swept jump).

The energy dissipation occurred at the chutes and in the converging-jet impingement helps to the formation of the jump. This is revealed when comparing with the referential two-dimensional case studied (also called A1), in which the proper formation of the jump requires much lower values of the flow or, alternatively, increasing the height of the end sill.

Unfortunately, three-dimensionality and, especially, the water collision difficult the study of the hydraulic jump using the Froude's number approach, as it is not always possible to determine the water depths at the toe of the jump.

4.2 *Numerical models results*

4.2.1 *Hydraulic jump in rectangular channel*

Fig. 11 shows an image of the hydraulic jump generated in laboratory (left) with an average downstream water level of 8 cm (fluctuating between 7 and 9 cm). The phenomenon was highly unstable, according to the fluctuations observed and to the fact that small variations of gate opening significantly changed the flow regime. The numerical model reproduced the geometry and flow conditions of the experiment when setting the downstream level to 7.5 cm.

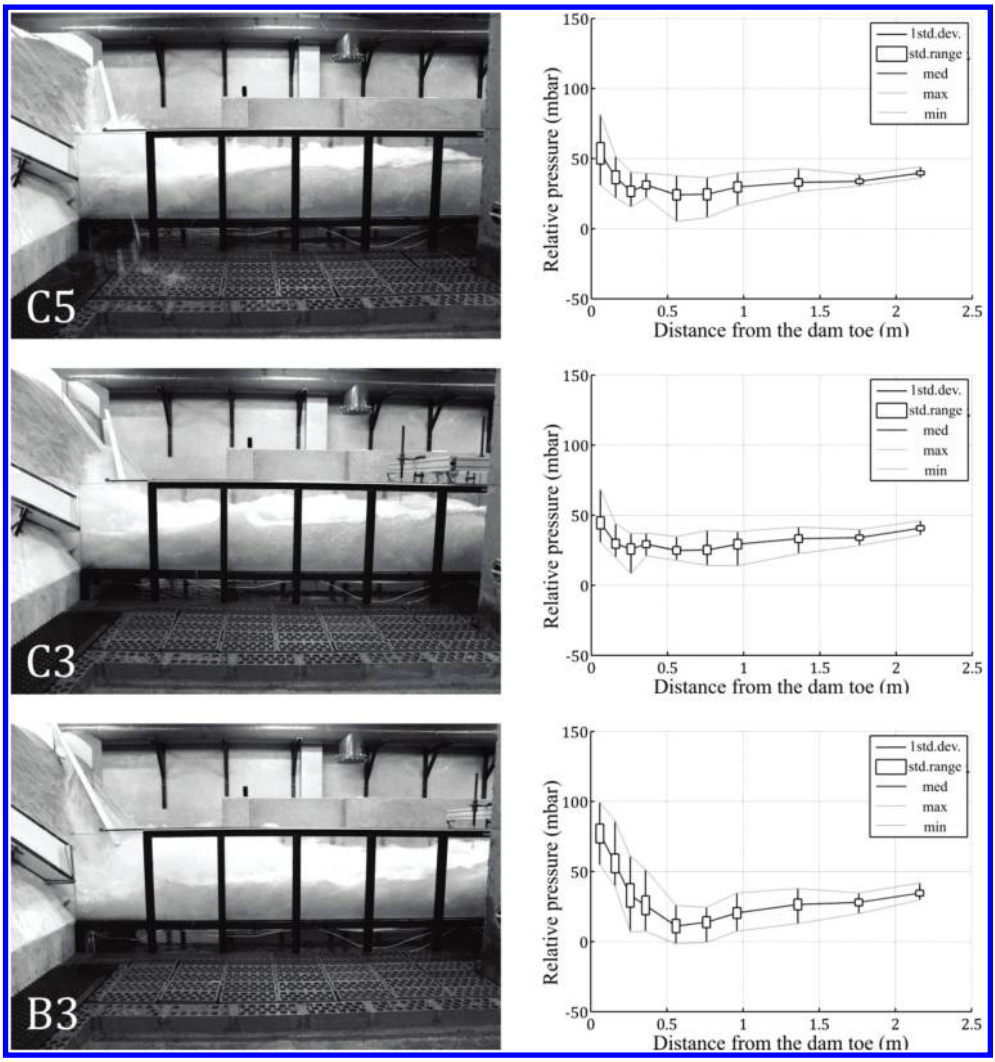

Figure 10. Left column: Side view in three different tests (same as fig. 9) (Vertically-mirrored images). Right column: Pressure values registered in the central axis of the stilling basin for each test. Top: C5 configuration. Centre: C3 configuration. Right: B3 configuration. Flow: 175 l/s. Length of the basin: 2.50 m. Height of the end sill: 0.15 m.

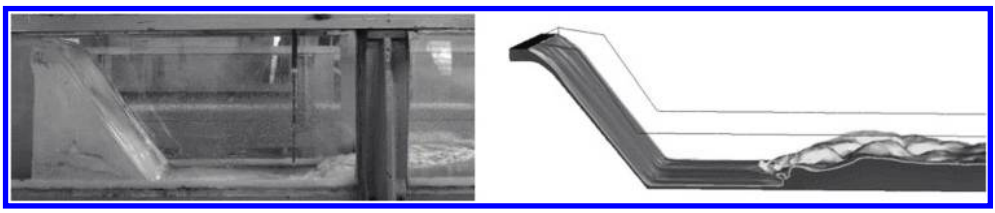

Figure 11. Hydraulic jump generated in laboratory (left) and reproduced numerically (right).

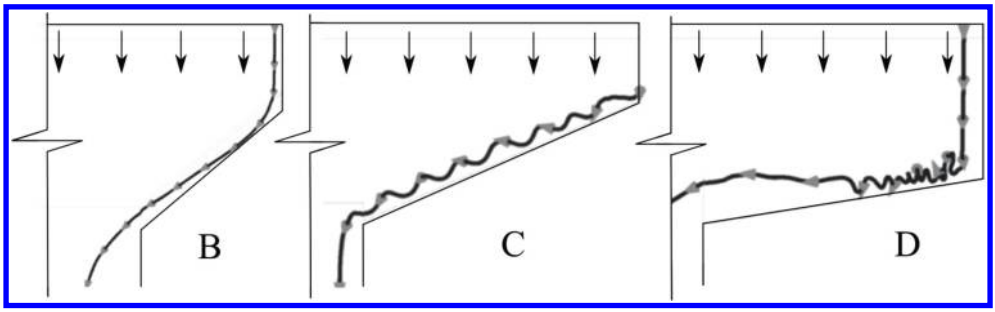

Figure 12. Characteristic stream-lines in the training walls for different geometries. Plan view.

4.2.2 *Flow pattern in the converging chutes*

The appropriate design of the chutes is essential in these spillways, in order to a) avoid flow overtopping, and b) foster energy dissipation. The flow pattern in these elements depends upon several aspects:

- Relative orientation with respect to the spillway crest.
- Discharge flow
- Cross section geometry

Some numerical results are depicted in fig. 12, which displays the characteristic shape of the stream-lines for configurations B, C and D and 150 l/s.

It can be noted that for low-angles (B configuration), the change in flow direction is small, what results in low energy dissipation, high velocity and small flow depth. The higher angle (D) favours energy dissipation in the converging chutes, though at the cost of a high flow depth, what requires large (and costly) walls in order to avoid overtopping.

Configuration C results in a neat helical flow pattern, and a compromise between flow depth and energy dissipation.

4.2.3 *Energy dissipation in the stilling basin*

The performance of the stilling basin is one of the major concerns for this solution to be adopted in an existing dam. It is important to know whether (and which) adaptation works are required to ensure adequate energy dissipation and hydraulic behavior.

The aforementioned dissipation in the training walls reduces the flow energy at the entrance of the stilling basin, as compared to a straight spillway for the same discharge. However, the advantage of implementing this solution is that the design flow can be higher for a given upstream head. Hence, the stilling basin performance needs to be checked for the new design flow.

The results cannot be directly compared to existing literature on straight conventional spillways, given that the flow pattern is highly three-dimensional, and the free surface very irregular. Further checks shall be made in these spillways to assess safety behavior, such as a comprehensive analysis of the pressure field to prevent cavitation. However, two regimes could be neatly identified: a) some sort of hydraulic jump is formed within the stilling basin (referred as a) and b) in section 4.1) and b) it is swept out (referred as d) in section 4.1). It seems reasonable to think that the formation of a hydraulic jump is a necessary (but not sufficient) condition for a design to be effective.

A number of cases were numerically modeled, as described in Table 1, some of which were also tested in laboratory. The flow regimes observed in the experiments agree with those registered numerically. Fig. 13 shows an example of these models, and fig. 14 summarizes all the cases analyzed. It can be seen that the higher the convergence of the side chutes, the lower the height needed for the hydraulic jump to form. It should be recalled, though, that more convergent chutes require greater cross section, and thus more complicated and costly works.

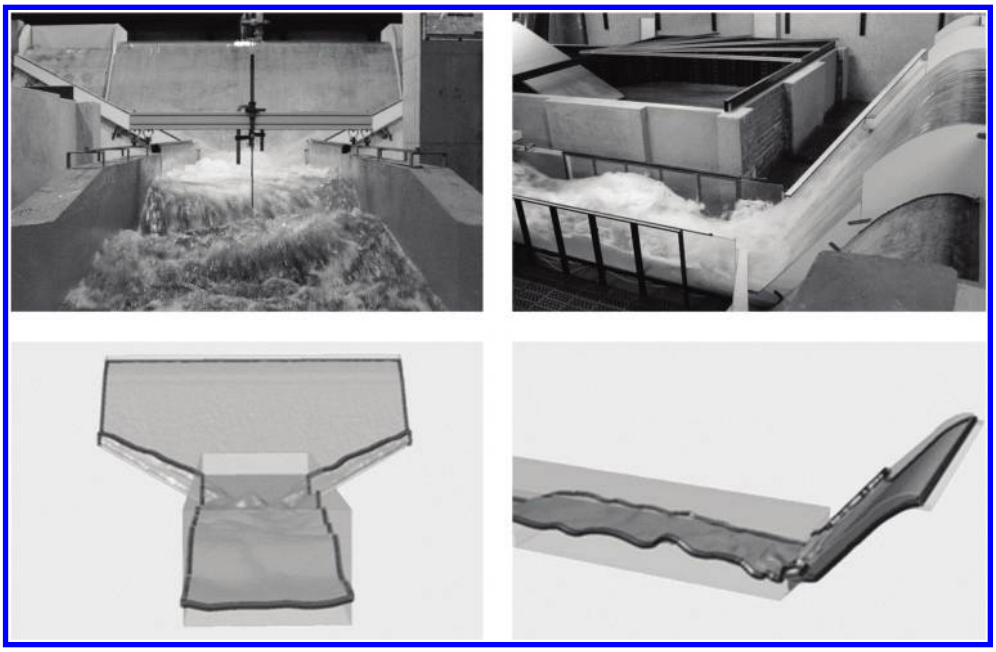

Figure 13. Comparison between experimental (top) and numerical (bottom) model. C3. End sill height = 15 cm.

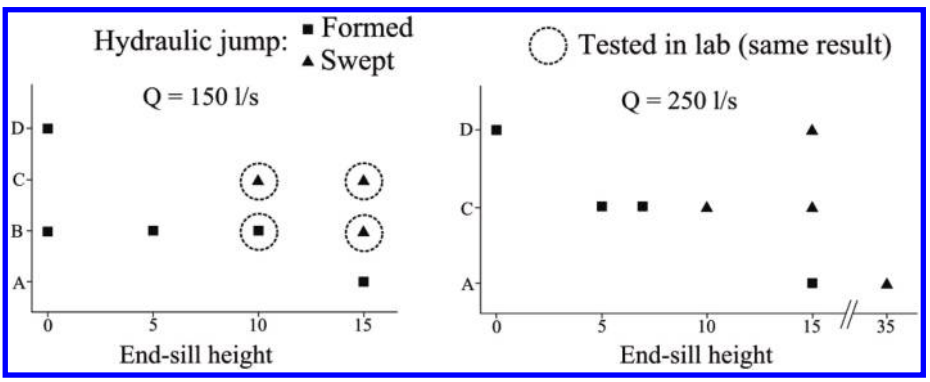

Figure 14. Stilling basin hydraulics in the cases analyzed.

5 CONCLUSION

Spillways with highly-converging chutes can be conceived as an interesting option for increasing the discharge capacity of concrete dams that do not meet hydrological safety requirements. From another point of view, the achieved reduction in the hydraulic head over the dam crest can be converted into hydroelectric and storage benefits. The converging chutes could also act as an overtopping protection for these dams, as they protect the dam toe by catching the overtopped flow.

The ways of energy dissipation are one of the main topics of interest in this spillway typology. A considerable part of the dissipation occurs in the converging chutes, due to the flip and the impingement of the water jet against the walls of the chute and the dam body. Other important fraction of the dissipation happens when the converging jets collide at the basin entrance. These two factors lead to an important reduction in the total amount of energy to be dissipated in the

stilling basin. Thereby, the length of the stilling basin loses importance against its depth and the degree of submergence of the incoming jets. Future research will be made in order to determine better configurations for this kind of basins (e.g. shorter, deeper and with more jet-submergence) also focusing on the approximating trajectory of the jets in the pool.

The utilisation of the highly-converging chutes as an overtopping protection presents certain particularities. The first one is related with the asymmetry of the converging flows, as the length of the dam crest at both sides of the basin axis is likely to be different (symmetry can be forced in those cases in which the protection is not important). Another important difference of this modality of protection compared with the configurations studied in this proceeding, is the fact that the side flow fraction over total flow would be probably lower, since the overtopping may only occur when the original-central spillway is working at full capacity. The authors have settled future research focusing on the usage of this kind of spillways as an overtopping protection.

ACKOWLEDGEMENTS

The research was supported by the "ALCON" project of the National R+D Plan of the Spanish Ministry of Economy and Competitiveness (code number IPT-310000-2010-011). The authors want to thank to the Spanish Government for its support.

REFERENCES

Dadvand, P., Rossi, R. & Oñate. E. (2005) An object-oriented environment for developing finite element codes for multi-disciplinary applications. *Archives of Computational Methods in Engineering*, 17, 253–297.

Hager, W.H. (1992) Energy Dissipators and Hydraulic Jump. *Springer Science & Business Media*.

Martín Vide, J.P. (2005). The design of converging overfall spillways. *Hydropower & Dams*. 9(3), 87–91.

Rossi, R. et al. (2013) An efficient edge-based level set finite element method for free surface flow problems. *International Journal for Numerical Methods in Fluids*, 71.6: 687–716.

Salazar, F., Morán, R., Rossi, R. & Oñate, E. (2013) Analysis of the discharge capacity of radial-gated spillways using CFD and ANN-Oliana Dam case study. *Journal of Hydraulic Research*, 51(3), 244–252.

Miscellaneous

Dam Protections against Overtopping and Accidental Leakage – Toledo, Morán & Oñate (Eds)

Probabilistic methods for hydrologic dam safety analysis

Isabel Flores, Alvaro Sordo-Ward & Luis Garrote
Technical University of Madrid (UPM), Madrid, Spain

ABSTRACT: A group of probabilistic methods for hydrologic dam safety analysis is presented in this paper. The methods were proposed and validated in the MODEX project. The approach proposed in MODEX consisted on the generation of arbitrarily long series of basin response hydrographs in order to characterize the dam hydrologic forcing. Hydrographs can be generated from streamflow gauge observation through multivariate techniques or through use of multivariate stochastic rainfall generation models in conjunction with physically based distributed hydrological models. A pilot basin (Manzanares basin in Spain), where data availability allowed for proper probabilistic calibration of models,was selected. A Monte Carlo probabilistic simulation environment was developed integrating the hydrometeorological modeling chain. A computing platform was used to provide discharge time series that were used in the characterization of hydrographs for high return periods and applied to the hydrological dam safety assessment. Using the probabilistic framework, significant advances by accounting for uncertainties in the precipitation field and in processes governing the rainfall-runoff transformation were achieved. The scientific results of the project were applied to identify methodologies for analyzing hydrological dam safety under a probabilistic approach that can be widely implemented in the professional field. The determination of the real risk associated with existing infrastructure adds an objective criterion to the assessment and prioritization of investment on embankment dam protection.

Keywords: Hydrology, Modelling, Extreme forcing, Dam, Safety, Overtopping

1 INTRODUCTION

One of the main objectives in analyzing the hydrological risk of hydraulic infrastructures is the assessment and prioritization of investment on the actions needed to reduce the risk of infrastructure failure. The risk associated with a structure is related with itsprobability of failure. The failure of a structure occurs when it cannot perform its function. This is evidenced by the exceedance of threshold and may beexamined in terms of return period of certainvariable. The variables that characterize the risk of hydrological failure of a dam are the maximum water level reached inthe reservoir during flood routing (overtopping risk) and the maximum discharge spilled (downstream flood risk). These variables depend on the inflow hydrograph, the dam-reservoir characteristics and the spillway design. (Sordo et al., 2012 [1]; 2013 [2]). Hydrographs with different peak flows and volume can result in a similar maximum water level reached at the reservoir, represent a similar risk and entail an equivalent return period. The peak flow-volume pairs associated to the same return period describe curves in the flow-volume space (Mediero et al., 2010 [3]). The characteristics of hydrographs significant for dam safety vary with the characteristics of the dam-reservoir system as is shown in the changes of the shapes of the equal-risk curves (Requena et al., 2013 [4]).

Dam safety analysis in Spain consists on identifyingone deterministic design flood event. This flood event is obtained from a rainfall event, associated with a return period, through a rainfall-runoff model. The flood event is assumed to correspond to the same return period as the rainfall event. This practice is not advisable according to Adams and Howard (1986) [5], Alfieri et al. (2008) [6] and Viglione and Blöschl (2009) [7], because the probability of the event also depends

on other variables such as the characteristics of the hyetograph and the basin and the initial soil moisture. Moreover, the designer determines the values of the rest of variables that influence the dam safety. This deterministic approach, which is currently used because of its simplicity and low input requirements, hamper the calculation of the real probability of occurrence of the event and its associated uncertainty.

However, scientific and technical developments have produced new hydrological and rainfall models which represent the spatial-temporal processes involvedin the rain generation and the basin response more accurately and take into account a larger number of variables that influence them.Thesedevelopments haveallowed the application of stochastic hydro-meteorological models, which combine stochastic rainfall generators with rainfall-runoff models (Paquet et al., 2013 [8]; Blažkova and Beven, 2002 [9], 2004 [10]).

Rainfall models have evolved from the continuous-time Markov chains used to simulate the occurrence of dry and rainy periods (Gabriel, K. and Neumann, J., 1962 [11]), to those based on the Poisson process (Le Cam 1961 [12], Gupta and Waymire, 1979 [13]) (for example, the Poisson-cluster models), the Neyman-Scott rectangular pulses (NSRP) model (Cowpertwait, 1994 [14], 1995 [15], 2010 [16]; Kilsby et al., 2007 [17]; Leonard et al., 2008 [18]; Burton et al., 2008 [19], 2010 [20]) and Bartlett-Lewis (Rodriguez-Iturbe et al., 1987a [21], b [22]; Verhoest et al., 1997 [23]; Vandenberghe et al., 2011 [24]), which have provided good results in continuous spatial-temporal rainfall simulation.

The hydrological models could be continuous or event-based andlumped or distributed. They may also vary in temporal and spatial precision. High resolution, continuous distributed models need a large amount of input data, present a significant number of parameters to be calibrated and theirsimulations require high computing capacity and computation time. To avoid these drawbacks, continuous lumped or semi-aggregated models can be used, but the spatial precision is reduced, which limits their ability to simulate extreme events. Temporal aggregation of the variables reduces the computation requirements, but preventsthe accurate simulation of reservoir flood routing. For these reasons, a distributed event-based model with a high temporal resolution has been selected in this paper.

Event-based models need to characterize the basin state at the beginning of the storm, which has a significant influence on the results (Castillo et al., 2003 [25]; Zehe et al., 2005 [26]; Noto et al., 2007 [27]; Vivoni et al., 2007 [28]; Berthet et al., 2009 [29]). The basin initial state depends on the soil moisture before the event starts. It is common to use a single initial state for all simulations based on a given criteria (Sordo-Ward et al., 2012 [1]). However, it is possible to treat the initial state as a random variable, characterisedthrough the probability distribution of the initial soil moisture (Cabral et al., 1992 [30]; Garrote and Bras, 1995a [31], 1995b [32]).

This paper presents a new methodology to characterize the long-termbehaviour of the hydrologic basin response to storm events. This methodology combines a stochastic spatial-temporal rainfall generator with a distributed and event-based hydrological model and results ina long series of basin hydrographs. The routing of these hydrographsthrough the dam-reservoir system allowsobtainingthe frequency curves of the maximum water level elevation in the reservoirand the outflow hydrograph which are used to evaluate the hydrological risk of the dam through a multivariate analysis.

2 METHODOLOGY

The objective of the methodology proposed in this paper is to develop dam safety analysis from the hydrologic approach. The procedure consists on the following steps:

1. Stochastic rainfall generation: the synthetic rainfall series are generated by the RainSim V3 model, which is based on a spatial-temporal Neyman-Scott rectangular pulse process (NSRP), developed by the School of Civil Engineering and Geosciences of Newcastle University (Burton et al., 2008 [19]).

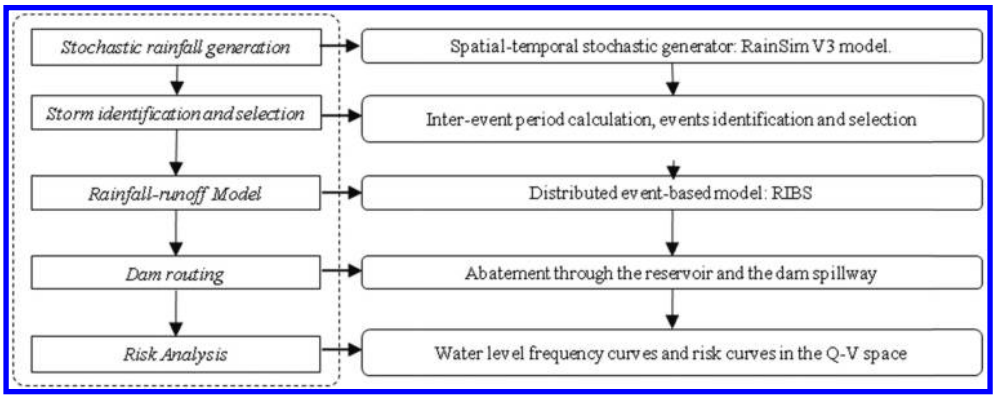

Figure 1. General conceptual framework of the methodology proposed.

2. Identification and selection of rainstorm events: rainstorm events are identified from synthetic rainfall time series following the exponential method (Restrepo and Eagleson, 1982 [33]). The w highest ones of every year according to the maximum accumulated rainfall criteria are chosen.
3. Rainfall-runoff modeling: transformation of selected rainstorm events into flood events is performedby the RIBS model (Garrote and Bras, 1995a [31], 1995b [32]), which is a distributed rainfall-runoff event model. In this way, an ensemble of inflow hydrographs in the reservoir isobtained.
4. Reservoir routing: The peak flow abatement at the reservoir of the generated hydrographsis computed following standard flood control management practices (Girón, 1988 [34]). Outflow hydrograph and the evolution of the water elevation in the reservoir are obtained.
5. Risk analysis: the risk associated with the maximum water level is calculated from the series of water levels. A multi-varied analysis of this risk was carried out to characterize the risk by the input hydrograph and dam-reservoir system characteristics.

2.1 *Stochastic rainfall generation*

The characterization of extremal behavior needs long rainfall or flow time series to be analyzed. Either these records are not available or they are not long enough to characterize high return periods. Stochastic models provide a tool to generate arbitrarily long series of rainfall that can be used as input in the rainfall-runoff model to obtain flow series.

The rainfall stochastic generator used is the Rainfall V3 model which is based on the spatial-temporal NSRP model (Cowpertwait, 1994 [14], 1995 [15]; Burton et al., 2008 [19]). This model allows the simulation of continuous series of rainfall of an N number of years for a set of raingauges in the basin and with an arbitrary time step. The model details are described in Burton et al. (2008) [19].

2.2 *Identification and selection of rainstorm events*

Due to the computational requirements, complex calibration process, computation time and large amount of input data that continuous models require, an event-based model is selected. Consequently, a set of relevant storm events may be identified. In order to reduce the number of simulations a sub-set of w events is selected from each year. The selection criteria is chosen taking into account that the objective is to characterize the basin extremal behavior.

Storm events are identified by fixing a minimum dry period between events (where rainfall is less than a given threshold). The exponential method (Restrepo and Eagleson, 1982 [33]) is used to determine the minimum dry period which ensures that the storm events indentified are independent (Bonta and Rao, 1987 [35]).

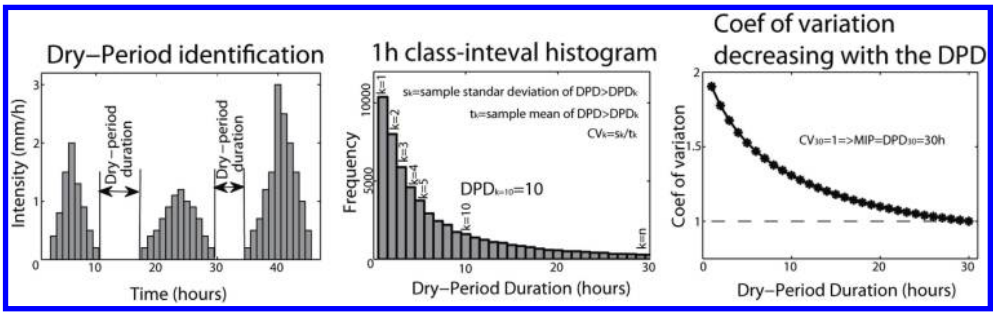

Figure 2. Flow chart that illustrates the steps carried out in storm identification and selection.

The exponential method assumes that dry periods follow an exponential distribution whose mean is equal to its standard deviation ($\mu = \sigma$) and consequently its coefficient of variation is equal to the unit. Dry periods are classified in one-hour class-intervals and the coefficient of variation associated to each one iscalculated. The dry period whose coefficient of variation is closer to the unit will be the minimum inter-event period that ensures independence of the events.

From each year a sub-set of w events is selected. As the objective is to characterize the extremal behavior the event which will generate the maximum volume or peak flow hydrograph has to be among those selected. The selection criteria used is the maximum accumulated rainfall.

2.3 *Rainfall-runoff model*

The RIBS model simulates the basin response to spatially distributed rainfall events and results in flood hydrographs at the basin discharge point.

This model works over a grid of a digital terrain model in a matrix form and the data are stored in layers of raster-type information, which are combined to obtain the model parameters (Garrote and Bras, 1995a [31], 1995b [32]).

The RIBS model consists of two modules. The first is a runoff-generation module and the second simulates the runoff propagation. The runoff generation depends on the soil properties and the parameter f (mm^{-1}). The soil properties are the saturated hydraulic surface conductivities in directions normal K_{0n} and K_{0p} ($\mathrm{mm\,h}^{-1}$) parallel to the surface, the residual soil moisture content θ_r, the satured moisture content θ_s and the index of soil porosity ε and have to be defined for each soil class. The parameter f (mm^{-1}) controls the decrease of saturated hydraulic conductivity with depth and has to be calibrated (Cabral et al., 1992 [30]).

The runoff propagation depends on the hill-slope (v_h) and the riverbed (v_s) velocities. The riverbed velocity is directly proportional to the calibration parameter C_v and related to the hill-slope velocity by the parameter K_v.

Event models need as input the initial state of the basin which depends on the initial recharge value (R_i). A representative set of S initial states are considered. For a given storm, these initial states generate a range of hydrographs uniformly distributed between thoseassociated to totally dry and completely saturated soils.

Sensitivity analyses determine that the most influential parameters are f, C_v, K_v as well as the initial recharge (R_i). The calibration process considered are based on the methodology proposed by Mediero et al. (2011) [36]. The methodology consists on the simultaneous minimization of various objective functions. It results in a set of optimal parameters values characterized by a probability density function.

K representative observed events are selected for calibration. A Monte Carlo simulation of M cases is carried out by using a uniform distribution of the calibration parameter values. Each event is simulated with all the Monte Carlo set of parameter values and a random initial state among the S considered. Through Pareto dominance, the set of parameter values that minimize the objective

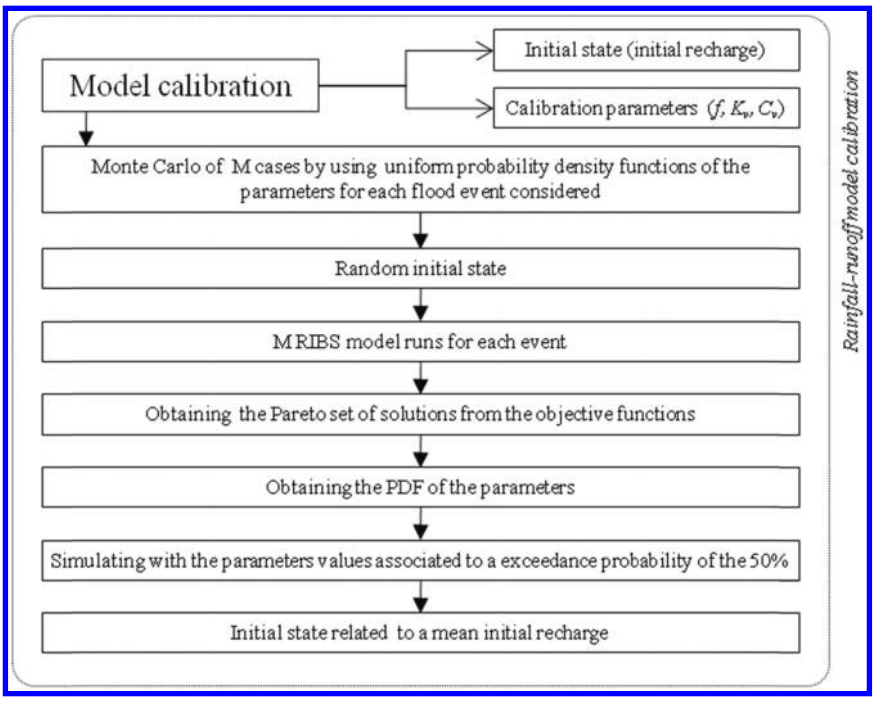

Figure 3. Flow chart that illustrates the steps for the calibration process.

functions are obtained and the probability distribution functions that best represent the variability of each parameterare selected.

The synthetic events are simulated with a deterministic value of the parameters associated with a probability of exceedance of 50% and the initial state corresponding to an average initial recharge.

2.4 *Reservoir routing*

The hydrological risk is related to either overtopping at the crest and the damage suffered downstream. To assess the probability of exceedance of either a water level or flow discharge the routingthrough the dam-reservoir system may be simulated. It consistsof the simulation of reservoir level by the storage indication routing method and the routing through the dam spillway (either fixed crest or controlled by gates). In the fixed crest spillway, the discharge depends only on the water level above the spillway and its length. In gated spillways, the discharge depends also on gate operation and, accordingly, on the managementrules applied. In this case, the Volumetric Evaluation Method (Girón, 1988 [34]) was applied. This method is based on three principles: (i) outflow must be lower than inflow when the flow is increasing; (ii) outflow should increase proportionally to the inflow; (iii) the relative rate between the outflow and the inflow increases with reservoir level.

The results of the abatement simulation are the output hydrograph and the water level variation.

2.5 *Risk analysis*

The risk is defined in terms of the return period of a variable. As explained above, in the case of the hydrological risk of dams, these variables are the water level and the outflow. The frequency curves of them are obtained from the series of variation in water level and output hydrograph. If the

dam is considered to fail either when the water level exceeds the dam crest or the outflow exceeds the downstream capacity, the probability of failure may be obtained from these frequency curves.

The risk variables depend on the inflow hydrograph, the reservoir and spillway characteristics. Hydrograph with different peak-flows and volumes may lead to the same maximum water level and, as consequence, entail equivalent return period. These hydrographs can be represented by a curve in the peak-volume space. The shape of these curves shows the relative influence of the hydrograph characteristics on the dam risk. Moreover, a sensitivity analysis of the shape of these risk curves for different configurations of the dam-reservoir system may be carried out.

3 CASE STUDY

The proposed methodology has been applied at the Manzanares basin in Spain.

The Manzanares River is located in the centre of the Iberian Peninsula, in the Tagus River basin, and crosses the city of Madrid, Spain. The hydrological regime is characterized by a great, both seasonal and year-on-year, irregularitywith extremely low levels in summer and mayor levels in spring due to the thaw. The main stream of the Manzanares River has a length of 80 km and a watershed area of 1248 km^2. The Santillana reservoir is the first one which modifies the river natural regime, has a storage capacity of $91.2 \times 106\ m^3$ and the spillway has a maximum capacity of 300 m^3/s.

The RIBS model calibration in the Manzanares River basin was carried out by Mediero et al. 2011 [38]. Six flooding events were considered in the calibration (Table 1). The probability density function of model parameters obtained as result has been applied in this research.

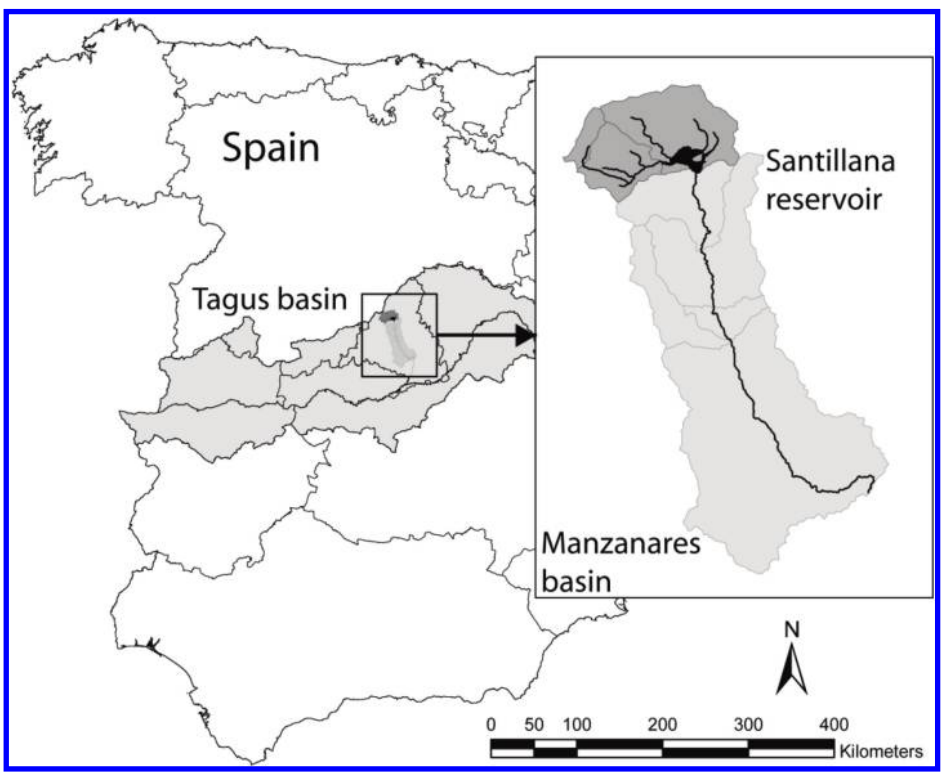

Figure 4. Location of the Manzanares basin.

Rainfall events were characterized by daily data from 15 raingauges supplied by the AgenciaEstatal de Meteorología. These rainfall data wereused to calibrate and validate the RainSimV3 model. Model validation was applied to the daily volume data which were recorded in the reservoir. The data used to validate the methodology consist of 52 years of daily reservoir storage and outflow volumes from which the daily inflow volume was calculated.

In both cases, maps that show drainage areas and slope directions, necessary for the RIBS rainfall-runoff model, were obtained from a digital elevation model.

4 RESULTS AND DISCUSSION

4.1 *Rainfall model calibration*

The RainSim V3 model is calibrated from the series available for the raingauges observed. The rainfall data obtained and correlation between each is characterised by the monthly statistics, calculated for different time intervals. These statistics are used to obtain the model parameters values $\{\lambda, \beta, \eta, \xi, \gamma, \rho$, and $\Phi\}$. 1000 years of hourly rainfall series were simulated. The monthly statistic values of the simulated series are calculated and compared with the observed ones resulting in a good fit for most of the raingauges. The comparison of the maximum 24 h rainfall frequency curves calculated from observed data and by aggregation of the simulated series showed good fitting in most of the raingauges (e.g. raingauge 3196 and PH-0194, Figure 5).

Once the model is calibrated, series of hourly rainfall are generated in all the basins. The series generated in the Manzanares basin has a length of 8.000 years.

The exponential model is applied to the rainfall continuous series generated and the minimum inter-event period obtained is used to identifystorm events. Five events are selected for each year

Table 1. Flood events considered in the RIBS model calibration.

	Event	Duration (h)	Maximum intensity (mm/15 min)	Rainfall volume (hm^3)	Flow volume (hm^3)
1	27–30 March 2003	96	4.2	15.76	3.65
2	14–29 April 2003	144	9.2	20.91	1.71
3	30 September–3 October 2003	96	8.8	27.54	5.45
4	15–28 November 2003	336	7.8	45.95	7.11
5	5–11 December 2003	168	3.6	28.42	4.4
6	28–29 April 2004	48	9.2	16.93	1.75

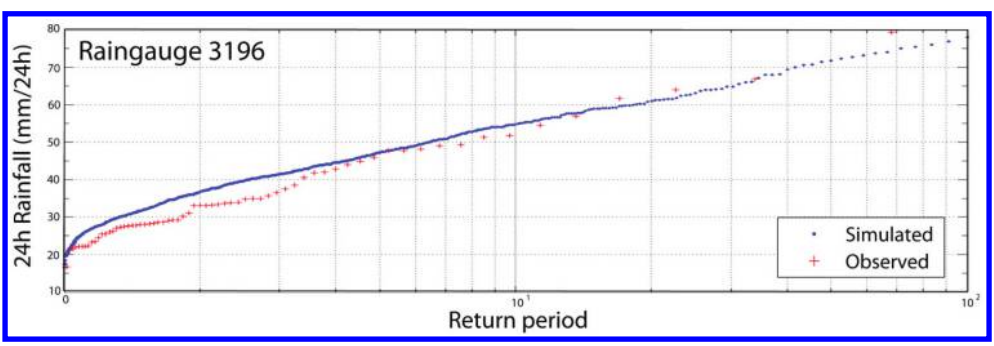

Figure 5. Calibration of RainSim V3 Max. 24 h rainfall frequency curve from observed and simulated data (Raingauge 3196).

according to the criterion of maximum accumulated rainfall. The results are an ensemble of 40.000 hourly rainfall events.

4.2 *RIBS model calibration*

The calibration process is applied to the study case. A Monte Carlo simulation of 1000 cases is performed byusing uniform probability density functions on the calibration parameters (f, C_v and K_v) and defining a set of 13 initial states. 1000 runs of RIBS are carried out for the six events consideredusing as input data the spatial distribution of rainfall, the set of parameters values resulting from the Monte Carlo simulation and a random initial state.

The multi-objective optimization is applied to the results of the events simulation with all the set of parameters considered and the set of optimal solutions are identified. The objective functions used were rootmean square error (RMSE-P); mean absolute error (MAE-B); the coefficient of Nash-Sutcliffe efficiency (NSE) and Time to peak (TP). The set of optimal values for each parameter are adjusted to various probability distribution functions and the one selected is that which best represents the variability of the parameter based on the chi-square and Kolmogorov-Smirnov goodness tests.

4.3 *Synthetic hydrographs generation*

Once, the calibration is finished, the rainfall events are transformed into hydrographs through the RIBS model. In the study case the series of five events of 8.000 years are simulated resulting in one series of 40000 hydrograph.

The nonparametric frequency curves of the annual maximaof the inflow hydrograph characteristics (peak flow and volume) are calculated. The relation between the variables and the return period is obtained through the Gringorten formula.

4.4 *Model validation*

The series of hourly flow data available are not long enough to validate the model. Because of that, the validation data used consist of 52 years of daily reservoir storage and outflow volumes from which the daily inflow volume was calculated.

Two, three and four consecutive days inflow volumes are calculated and their frequency curves obtained by aggregation of daily inflow volume from the observed and simulated data (Figure 6).

The fitting isgood for low and medium return periods, while for the high ones, the uncertainty increases and the simulated curve presents higher deviations from the general tendency, showing sharper slope changes.

Summarising, the frequency curves obtained from observed and simulated dataare significantly similar. Therefore, the models provide good enough information to be applied in risk evaluation.

4.5 *Reservoir routing and risk analysis*

Once the models are validated, the reservoir routingof the series of hydrograph is performed. Here, two studies may be carried out: a risk analysis considering the current characteristics of the dam-reservoir system and a sensitivity analysis of the shape of the risk curves for different configurations of the dam-reservoir system. Depending on the case, the risk analysis may be approached in a different way.

The risk analysis will study the probability of failure of the hydraulic infrastructure and determine whether or not the risk is acceptable. The probability of failure is the probability of the water level exceeding the crest level that is calculated from the water level frequency curve. This is the case of the Santillana reservoir. Figure 7 shows the water level frequency curve obtained and the Figure 8 the peak flow volume pairs classified by maximum water levels (MWL) intervals.

The Santillana spillway is controlled by two gates of 5.5 m wide and 5.10 m tall.

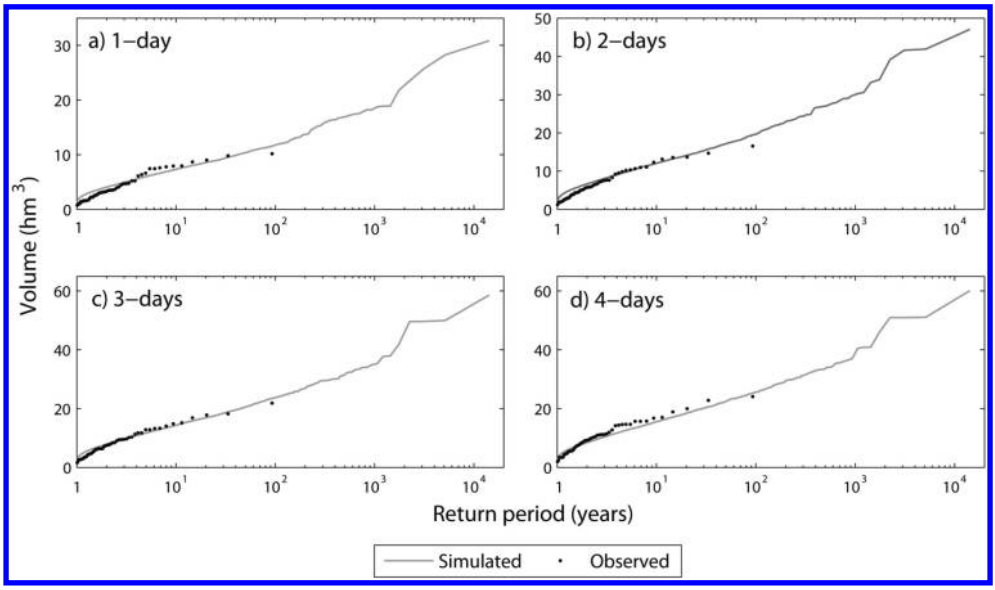

Figure 6. Frequency curves of inflow discharge for a) one day, b) two, c) three and d) four consecutive days obtained from observed and simulated data.

Table 2. Significant levels of the dam to the abatement simulation.

Significant levels	
Spillway crest level	889
Gate top level	894.1
Dam crest level	896.5

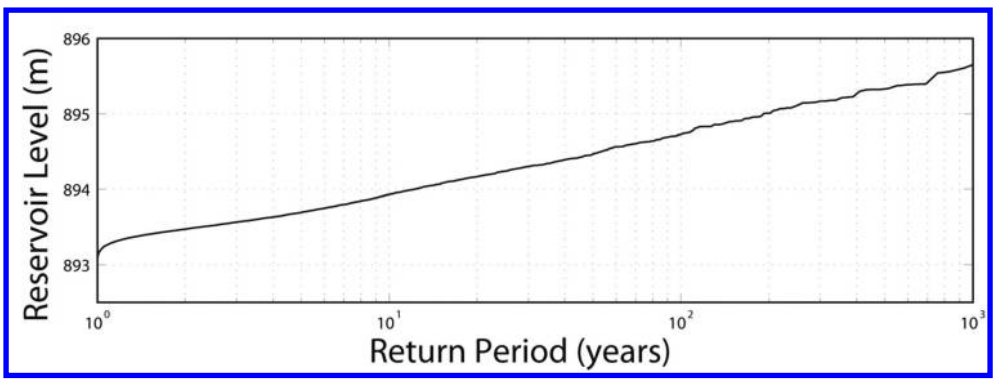

Figure 7. Frequency curve of the maximum water level reached at Santillana reservoir.

Also, peak flow volume pairs classified by maximum water levels (MWL) are obtained from the inflow hydrograph characteristics and the levels reached in the reservoir (Figure 8). No hydrograph generates a water level over the dam crest level (896.5 m) and produces the dam failure, but many hydrographs generate water levels over the gates crest level (894 m) which may jeopardise the dam safety.

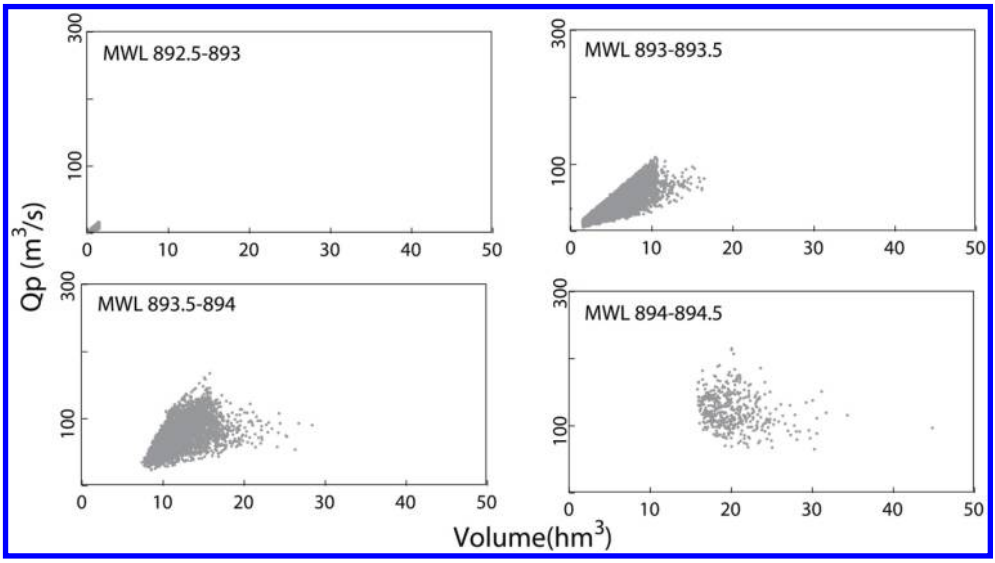

Figure 8. Peak flow volume pairs classified by maximum water levels (MWL) intervals.

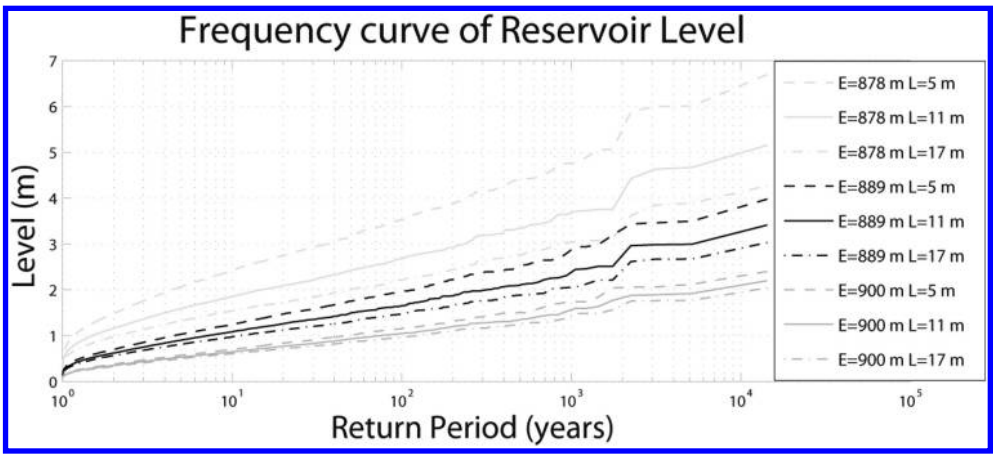

Figure 9. Maximum water level (MWL) over the spillway crest frequency curves for the dam-reservoir configurations.

The Figure 8 shows that different hydrographs with different peak flow and volume lead to similar MWL, therefore they have equal-risk. In addition the Figure 8 shows that there are some hydrographs which lead to different MWL but have similar peak flow and volume. This overlap is due to the shape and duration of the hydrograph. The methodology allows considering hydrographs with more than one peak. Hydrographs with similar maximum peak flow and volume but different number of peaks lead to various MWL in the reservoir. The hydrographs with more than one peak produce higher levels at the reservoir because when the second peak reach the reservoir, the water level is higher than at the beginning of the flood.

The sensitivity analyses (Figure 9) allow examining how the hydrologic dam safety varies across a range of synthetic dams. For these analyses, fixed crest configurations were considered. Nine dam configurations results of the combination of three possible spillway length (5, 11 and 17 m) and three possible spillway crest heights (878, 889, 900 m) and the respective reservoir volumes.

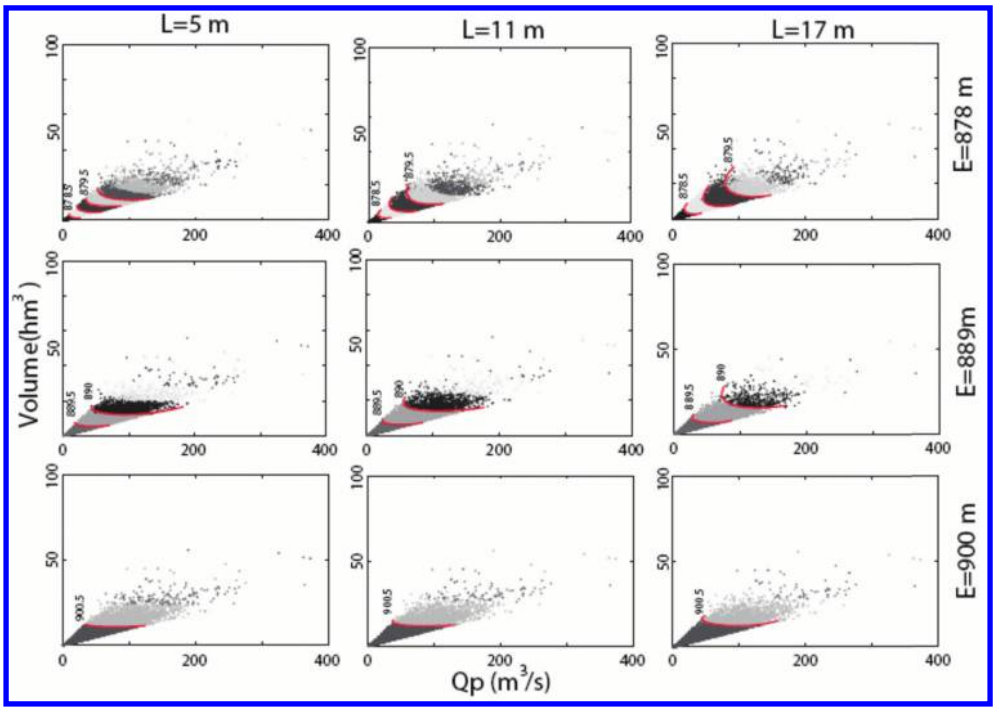

Figure 10. Comparison of risk curves related to the maximum water level (MWL) in the reservoir depending on the reservoir volume or spillway level (E) and spillway length (L).

The frequency curves of the maximum level above the spillway calculated for each dam-reservoir system are different. The risk decreases if the spillway length increase and the volume do not change. If the volume increase and the spillway length remain the same, the risk also decreases (Figure 9).

The risk curves also change with the different configurations. The hydrograph are grouped according to the maximum water level (MWL) reached in half-meter intervals and the resulting risk curves plotted. The differences between the curve shapes reveal what hydrographs represent a greater risk of failure for each configuration. The greater the reservoir volume, the greater the temporary storage capacity is and the greater attenuation of the peak flow results. In these cases, the hydrograph which represent a significant risk are those with a higher volume and the risk curves are more horizontal. Moreover, the shorter the spillway length, the lower discharge capacity is and a greater temporary store capacity is require. So the hydrographs with a greater peak flows represent a greater risk and the curves are also more horizontal (Figure 10).

5 CONCLUSIONS

Analysis of the risk of failure of hydraulic infrastructure is a complex issue due to the number of variables that influence the processes, the long data series required to characterize the extremal behavior and the necessity tosimulate the routingthrough the dam-reservoir system to characterize the variables which determine the hydrological risk. Because of that, simplified models are not advisable.

The methodology proposed combines a stochastic rainfall generator (RainSim V3) with a distributed event-based model (RIBS) to characterize the extremal behavior of the basins. The RainSim

V3 permits extending the rainfall series preserving the main statistics. These series represent adequately the rainfall extremal behavior.

The most extreme events are identified and selected from these series and transformed into runoff through the RIBS model. The rainfall-runoff model calibration and simulation processes take into account the variability of the runoff generation and propagation processes and reproduce accurately the behavior of the basin.

The results of the methodology are discharge hydrograph series which may be routed through the dam-reservoir system to characterize the variables which determine the dam-reservoir risk.

Two studies may be carried out: a risk analysis and a sensitivity analysis of the equal-risk curves. The objective of the study may be to calculate the risk associated to the dam overtopping, and determine if it is needed to improve the security and what are the optimal action plan to reduce the risk.

The sensitivity analysis study focus on determine the risk associated to different options and analyze how the risk vary and what are the more representative hydrographs.

This methodology becomes a useful tool to obtain flood frequency distributions of the risk variables and relate them with the hydrograph characteristics through a multivariate analysis, which are useful to design river structures and evaluate their risk.

ACKNOWLEDGEMENT

The study was made possible by the funds from MODEX project (CGL2011-22868) "Physically-based modelling for characterization of extreme hydrologic response under a probabilistic approach. Application to dam safety analysis and optimization of reservoir operation during floods" funded by the Spanish Ministry of Science and Innovation.

REFERENCES

[1] Sordo-Ward, A., Garrote, L., Martín-Carrasco, F., & Dolores Bejarano, M. (2012). *Extreme flood abatement in large dams with fixed-crest spillways.* Journal of Hydrology, 466, 60–72.

[2] Sordo-Ward, A., Garrote, L., Bejarano, M. D., & Castillo, L. G. (2013). *Extreme flood abatement in large dams with gate-controlled spillways*. Journal of Hydrology, 498, 113–123.

[3] Mediero, L., Jimenez-Olivarez, A., & Garrotte, L.: *Design flood hydrographs from the relationship between flood peak and volume*, Hydro. Earth Syst. Sci., 14, 2495–2505, doi: 10.5194/hess-14- 2495-2010, 2010.

[4] Requena, A. I., Mediero, L., & Garrote, L.: *A bivariate return period based on copulas for hydrologic dam design: accounting for reservoir routing in risk estimation*, Hydrol. Earth Syst. Sci., 17, 3023–3038, doi:10.5194/hess-17-3023-2013, 2013.

[5] Adams, B. & Howard, C.D., 1986. *Design storm pathology*, Can. Water Resour. J., 11(3), 49–55.

[6] Alfieri, L., Laio, F., & Claps, P., 2008. *A simulation experiment for optimal design hyetograph selection*, Hydrol.Process. 22 (6), 813–820.

[7] Viglione, A. & Blöschl, G., 2009. *On the role of storm duration in the mapping of rainfall to flood return periods*, Hydrol. Earth Syst. Sci., 13, 205–216.

[8] Paquet, E., Garavaglia, F., Garçon, R., & Gailhard, J. (2013). *The SCHADEX method: A semi-continuous rainfall–runoff simulation for extreme flood estimation*. Journal of Hydrology, 495, 23–37.

[9] Blažkova, S., & Beven, K., 2002. *Flood frequency estimation by continuous simulation for a catchment treated as ungauged (with uncertainty).* Water Resour.; 38:1–14

[10] Blažkova, S., & Beven, K., 2009. *A limits of acceptability approach to model evaluation and uncertainty estimation in flood frequency estimation by continuous simulation: Skalka catchment, CzechRepublic*. Water Resour; 45.

[11] Gabriel, K.R., & Neumann, J., 1962. *A Markov chain model for daily rainfall occurrence at Tel Aviv*. Quarterly Journal of the Royal Meteorological Society 88, 90–95.

[12] Le Cam, L.M., 1961. *A stochastic description of precipitation*. In: Neyman, J. (Ed.), Proceedings of the Fourth Berkeley Symposium on Mathematical Statistics and Probability, vol. 3. University of California, Berkeley, California, pp. 165–186.

[13] Gupta, V.K., & Waymire, E., 1979. *A stochastic kinematic study of subsynoptic space-time rainfall*. Water Resources Research 15, 637–644.
[14] Cowpertwait, P.S., 1994. *A generalized point process model for rainfall. Proceedings of the Royal Society of London*. Series A: Mathematical and Physical Sciences, 447(1929), 23–37.
[15] Cowpertwait, P.S., 1995. *A generalized spatial-temporal model of rainfall based on a clustered point process*. Proceedings of the Royal Society of London. Series A: Mathematical and Physical Sciences, 450(1938), 163–175.
[16] Cowpertwait, P.S., 2010. *A spatial-temporal point process model with a continuous distribution of storm types*.Water Resources Research, 46(12).
[17] Kilsby, C.G., Jones, P.D., Burton, A., Ford, A.C., Fowler, H.J., Harpham, C., James, P., Smith, A., Wilby, R.L., 2007. *A daily weather generator for use in climate change studies*, Environmental Modelling & Software; 22: 1705–1719.
[18] Leonard, M., Lambert, M.F., Metcalfe, A.V., & Cowpertwait, P.S.P., 2008. *A space-time Neyman–Scott rainfall model with defined storm extent*. Water Resources Research, 44(9).
[19] Burton, A., Kilsby, C.G., Fowler, H.J., Cowpertwait, P.S.P. & O'Connell P.E., 2008. *RainSim: A spatial–temporal stochastic rainfall modelling system*. Environmental Modelling & Software.; 23: 135–1369.
[20] Burton, A., Fowler, H.J., Kilsby, C.G. & O'Connell, P.E., 2010. *A stochastic model for the spatial-temporal simulation of nonhomogeneous rainfall occurrence and amounts.* Water Resour. Res., 46, W11501.
[21] Rodriguez-Iturbe, I; Cox, D. & Isham, V., 1987(a). *Some models for rainfall based on stochastic point processes. Proceedings of the Royal Society of London*. Series A 410. pp. 269–288.
[22] Rodríguez-Iturbe, I; Febres de Power, B. & Valdés, J., 1987(b). *Rectangular pulses point process models for rainfall: analysis of empirical data*. Journal of Geophysical Research. 92. pp. 9645–9656.
[23] Verhoest, N., Troch, P.A. & De Troch, F.P. (1997). *On the applicability of Bartlett–Lewis rectangular pulses models in the modelling of design storms at a point*. Journal of Hydrology, 202(1), 108–120.
[24] Vandenberghe, S., Verhoest, N.E.C., Onof, C. & De Baets, B., 2011. *A comparative copula-based bivariate frequency analysis of observed and simulated storm events: A case study on Bartlett-Lewis modeled rainfall*. Water Resources Research, 47(7).
[25] Castillo, V.M., Gomez-Plaza, A. & Martinez-Mena, M., 2003. *The role of antecedent soil water content in the runoff response of semiarid catchments: a simulation approach*. Journal of Hydrology, 284(1), 114–130.
[26] Zehe, E., Becker, R., Bárdossy, A. & Plate, E., 2005. *Uncertainty of simulated catchment runoff response in the presence of threshold processes: Role of initial soil moisture and precipitation*. Journal of hydrology, 315(1), 183–202.
[27] Noto, L.V., Ivanov, V.Y., Bras, R.L. & Vivoni, E.R., 2008. *Effects of initialization on response of a fully-distributed hydrologic model*. Journal of Hydrology, 352(1), 107–125.
[28] Vivoni, E.R., Entekhabi, D., Bras, R. L. & Ivanov, V.Y., 2007. *Controls on runoff generation and scale-dependence in a distributed hydrologic model*. Hydrology and Earth System Sciences Discussions, 4(3), 983–1029.
[29] Berthet, L., Andréassian, V., Perrin, C. & Javelle, P., 2009. *How crucial is it to account for the antecedent moisture conditions in flood forecasting? Comparison of event-based and continuous approaches on 178 catchments*. Hydrology & Earth System Sciences, 13(6).
[30] Cabral, M.C., Garrote, L., Bras, R.L. & Entekhabi, D., 1992. *A kinematic model of infiltration and runoff generation in layered and sloped soils.* Advances in Water Resources, 15: 311–324.
[31] Garrote, L. & Brass R.L., 1995. *A distributed model for real-time flood forecasting using digital elevation models.* Journal of Hydrol.; 167:279–306.
[32] Garrote, L. & Brass, R.L., 1995. *An integrated software environment for real-time use of a distributed hydrologic model.* Journal of Hydrol.; 167:307–326.
[33] Restrepo-Posada, P.J. & Eagleson, P.S., 1982. *Identification of independent rainstorms.* Journal of Hydrol.; 55:303–319.
[34] Girón, F., 1988. *The evacuation of floods during the operation of reservoirs*. In Trans. Sixteenth International Congress on Large Dams; 4: 1261–1283.
[35] Bonta, J.V. & Rao, A.R., 1988. *Factors affecting the identification of independent storm events*. Journal of Hydrol.; 98: 275–293.
[36] Mediero, L., Garrote, L. & Martín-Carrasco, F.J., 2011. *Probabilistic calibration of a distributed hydrological model for flood forecasting*. Hydrol. Sci. J.; 56: 112–1149.

Dam Protections against Overtopping and Accidental Leakage – Toledo, Morán & Oñate (Eds)
© 2015 Taylor & Francis Group, London, ISBN: 978-1-138-02808-1

Two-dimensional direct rainfall hydraulic models applied to direct calculation of hydrologic events in dams to prevent overtopping

Paloma Batanero
Técnicas del Medio Ambiente y del Agua, S.A., Madrid, Spain

Ignacio Martínez
Ingeniería y Economía del Transporte, Madrid, Spain

Eduardo Martínez
Technical University of Madrid (UPM), Madrid, Spain

ABSTRACT: One of the main concerns when conducting a dam test is the acute determination of the hydrograph for a specific flood event. The use of 2D direct rainfall hydraulic mathematical models on a finite elements mesh, combined with the efficiency of vector calculus that provides CUDA (Compute Unified Device Architecture) technology, enables nowadays the simulation of complex hydrological models without the need for terrain sub-basin and transit splitting (as in HEC-HMS). Both the Spanish PNOA (National Plan of Aereal Orthophotography) Digital Terrain Model GRID with a 5 × 5 m accuracy and the CORINE GIS Land Cover (Coordination of INformation of the Environment) that allows assessment of the ground roughness, provide enough data to easily build these kind of models.

Keywords: Hydrology, 2D Mesh, Dam, Protection, Overtopping

1 INTRODUCTION

Two full river basins were modelled with direct rainfall poured over a 2D elements mesh. This article explains both the method followed and the outflows obtained. Different levels of accuracy (number of elements) and two dams were tested, using the PNOA DTM. Satisfactory results confirm that classical modelling and sub-transit approach (HEC-HMS) can be replaced by simulations of direct rainfall on a 2D mesh, hence reducing the uncertainty inherent in concentration times and transit parameters estimation. When used to accurate calculate a flood event hydrograph, it could prevent dam unexpected overtopping.

Both river 2D watershed examples were computed using an Intel Core i7 CPU @2.67 GHz, equipped with a GeForce GTX TITAN Black GPU card (2880 CUDA cores) on a Windows 7 64 bit OS. Simulations on this machine took between 20 and 70 minutes for the Zapardiel river (1,450 km^2) and form 6 to 17 hours for the Zujar basin (8,500 km^2 & 2 dams).

InfoWorks ICM (Integrated Catchment Model) was the software chosen to perform the 2D hydraulic and hydrologic calculations.

ICM is a state-of-the-art integrated modelling platform that incorporates both urban and river catchments. This software provides full integration of 1D and 2D hydrodynamic simulation techniques, being able to model both the above and below ground elements of catchments to accurately represent all flow paths. It also enables hydraulics and hydrology of natural and man-made environments to be incorporated into a single model. It has total ArcGIS compatibility and uses efficiently hardware developments such as multi-core processors and dedicated Graphics Processing Units (GPUs).

2 SWALLOW WATER FLOW

2.1 *Governing equations*

The Shallow Water Equations (SWE) represent an approximation to the free surface flow of a fluid on a horizontal plane over a prescribed bottom surface given by a bed function $z_B(x;y)$. Denoting the depth of the fluid layer by h and the depth averaged Cartesian velocity components by u and v, the 2D SWE can be written as:

$$\frac{\partial U}{\partial t} + \nabla F = S_b + S_f \tag{1}$$

where the flux vectors U, S_b and S_f are given by:

$$U = \begin{bmatrix} h \\ hu \\ hv \end{bmatrix} \tag{2}$$

$$S_b = -gh \begin{bmatrix} 0 \\ \partial Z_b / \partial x \\ \partial Z_b / \partial y \end{bmatrix}$$

$$S_f = -\frac{g\, n^2 \sqrt{u^2 + v^2}}{h^{1/3}} \begin{bmatrix} 0 \\ u \\ v \end{bmatrix}$$

And F has the expression:

$$F = (E, G) = \begin{bmatrix} hu & hv \\ h\,u^2 + g\,h^2/2 & h\,u\,v \\ h\,u\,v & h\,u^2 + g\,h^2/2 \end{bmatrix} \tag{3}$$

The energy conservation equation is:

$$\frac{\partial H}{\partial t} + v \cdot grad\ H = g\,\frac{\partial h}{\partial t} \tag{4}$$

where $H(x,y)$, energy, is as follows:

$$H = \frac{1}{2}\, V \cdot V + g(Z_B + \mathrm{h}) \tag{5}$$

The discretization of equation (1) on a finite volume V_k can be written (Alcrudo and Mulet-Marti) as:

$$\frac{\partial}{\partial t}\int_{V_k} U + dVV + \oint_{S_k} F \cdot n\, dS = \int_{V_k} (S_b + S_f)\, dV \tag{6}$$

The authors use a classic TVD (Total Variation Diminishing) method made up of Roe's Riemann solver and MUSCL [VLR 79] extrapolation in finite volumes, coupled with two step, second order accurate, explicit time integration. Bottom slope source terms are upwinded and bed friction is computed centrally and implicitly integrated in time. The method has proven robust and accurate in many benchmarks and applications and has been implemented in structured and non-structured grids using triangles and quadrangles.

The finite volume discretization leads to:

$$U_k^{n+1/2} = U_k^n - \frac{\Delta t}{2V_k} \sum_{wk=1}^{wk=nk} \mathbf{F}_{\mathbf{wk}}^{*\mathbf{n}} \cdot n_{wk} \Delta s_{wk} + \frac{\Delta t}{2} \left(\mathbf{S}_{\mathbf{bk}}^{*\mathbf{n}} + S_{fk}^{n+1/2} \right) \tag{7}$$

$$U_k^{n+1} = U_k^n - \frac{\Delta t}{V_k} \sum_{wk=1}^{wk=nk} \mathbf{F}_{\mathbf{wk}}^{*\mathbf{n+1/2}} \cdot n_{wk} \Delta s_{wk} + \Delta t \left(\mathbf{S}_{\mathbf{bk}}^{*\mathbf{n+1/2}} + S_{fk}^{n+1} \right) \tag{8}$$

where U_k stands for the averaged value of the conserved variables over finite volume V_k (actually in 2D it V_k is a surface area) which is enclosed by surface S_k (in 2D this is in fact a line).

S_k is decomposed into plane walls (line segments) with surface areas (lengths) Δs_{wk}. Subindex wk refers to the corresponding plane wall into which S_k has been subdivided. The outward pointing normal vector of wk is n_{wk}.

Superindices $n, n+1 = 2$, and $n+1$, refer to time levels, with Δt time spacing between levels n and $n+1$. **F*** stands for the numerical flux tensor and $\mathbf{S}_b^*$ for the numerical source vector corresponding only to the bed slope.

Friction sources S_f are directly evaluated from expressions (3) and (4). It must be first linearized in order to avoid solving a nonlinear system, as:

$$S_{fk}^{n+1} \approx S_{fk}^n + \left[\frac{\partial S_f}{\partial U} \right]_k^n \left(U_k^{n+1} - U_k^n \right) \tag{9}$$

2.2 *Application to natural catchments*

As natural basins can sometimes have very steep slopes, the SWE equations will be affected by both the vertical component of the depth and the terrain roughness.

Depth values on the SWE model are calculated as the difference between the free water surface and the terrain elevation, therefore measured in the vertical axis, and consequently speed, friction and depth are affected by the slope. Their geometric relationships are expressed as follows:

$$Tag\ a = \frac{1}{p}$$
$$Cos\ a = \frac{L'}{L} \tag{10}$$
$$L' = L \cos a$$

Whilst depth and speed are given by:

$$d = d' \cos a$$
$$V = \frac{V'}{\cos a} \tag{11}$$

Roughness value has a similar problem, so when using Manning's formula, an adjusted value of n is needed to compensate the difference between the real length of the surface and its projection on the horizontal plane, as well as the difference between speeds, so considering the Manning formula, equating energy losses, and assuming that $R_h \cong d$, we have:

$$n = n' \left(\cos a \right)^{13/6} \tag{12}$$

To quantify the error made when hillside slopes are neglected, we analyzed the error in the calculation of depth, speed and n Manning value, at slopes between 1 and 20%.

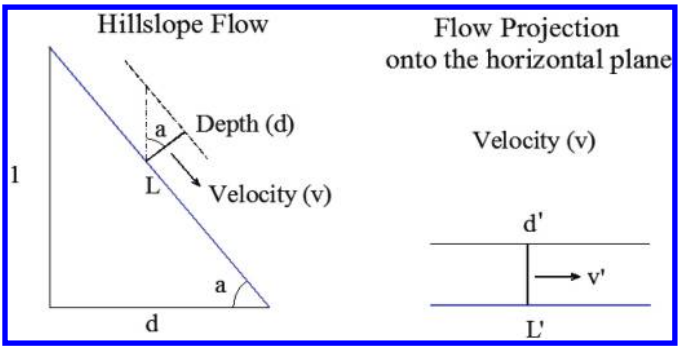

Figure 1. Real depth and velocity on a hill slope and its projections that would be the results given by a SWE mathematical model: The vertical component of depth and the horizontal component of velocity.

Table 1. Committed errors on the estimation of speed, depth and *n* value, depending on the slope.

Slope (%)	Error in depths and speeds (%)	Error in *n* (%)
1.0%	0.005%	0.01%
2.0%	0.020%	0.04%
5.0%	0.125%	0.27%
10.0%	0.496%	1.08%
15.0%	1.106%	2.44%
20.0%	1.942%	4.34%

3 ZAPARDIEL RIVER MODEL

The first model presented is Zapardiel river (Douro basin) with a total area of 1,450 km^2. It is a basin without regulation, but the central section presents some natural storage areas. Two models have been compared: a traditional HEC-HMS model and a direct rainfall 2D mesh InfoWorks ICM model.

3.1 *HEC-HMS model*

The HEC-HMS model consists of 6 subbasins and 4 transits. Basic figures and schemas are given below.

A mean CN of 75 was used, along with the SCS unit hydrograph. Transits were modeled with the 8-point Muskingum Cunge method. Rain poured was 172 mm for one hour, corresponding to a 100 mm effective rainfall in each subcatchment.

3.2 *InfoWorks ICM direct rainfall model*

Simultaneously, a direct 2D mesh rainfall model was built from a PNOA GRID DTM 5 × 5 m. An general 2D mesh with different element sizes (5,000, 10,000 and 20,000 m^2) was set. Along with this, a more precise mesh of 1,000 m^2 size was defined on water sheds.

100 mm of total rainfall during a whole hour was poured over the catchment, as on the HEC-HMS model. Roughness Manning coefficient was 0.040.

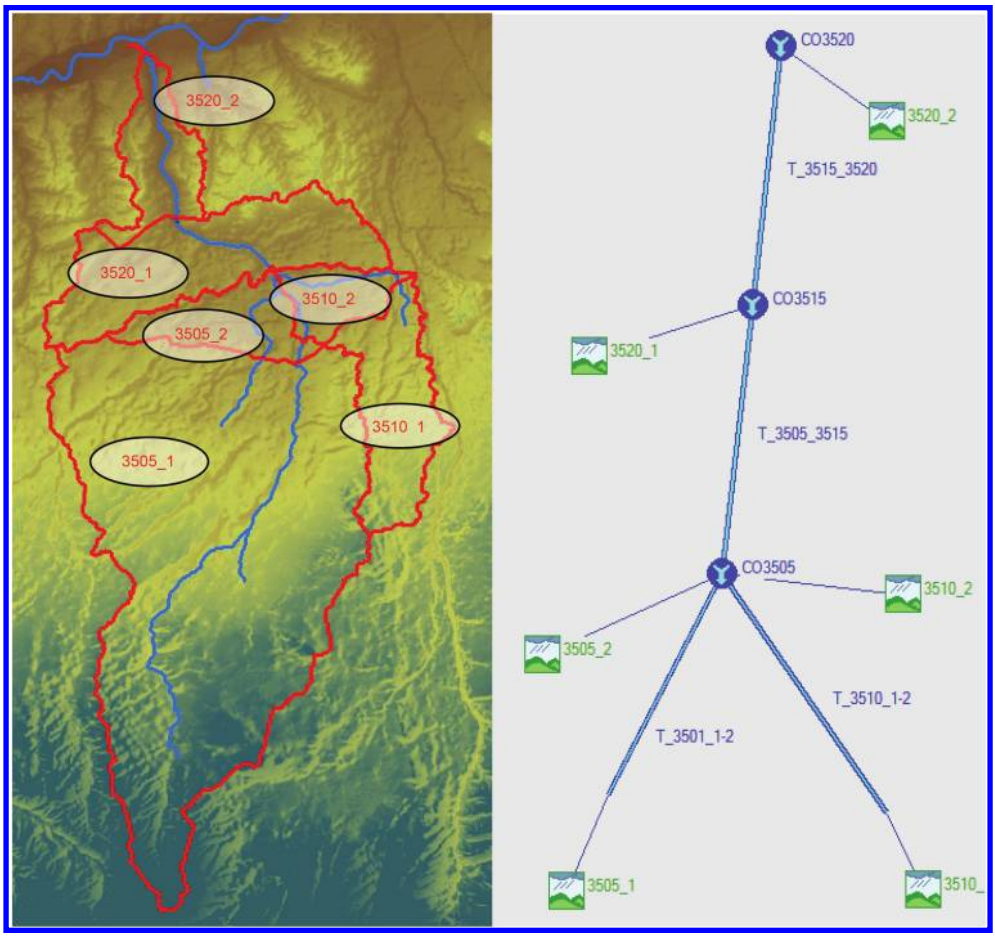

Figure 2. Zapardiel River basin HEC-HMS model.

Table 2. Zapardiel River subbasin model attributes.

Subbasin	Area (km^2)	Length (km)
3505_1	906.1	60.10
3505_2	78.3	9.10
3510_1	128.8	28.50
3510_2	51.7	9.40
3520_1	208.2	16.90
3520_2	81.2	17.12

3.3 *Results comparison*

Outflows are very similar in the three models performed, ranging from 618.4 m^3/s obtained with an element size of 10,000 m^2, to 619.0 m^3/s (5,000 m^2 element size) and 627.5 m^3/s (20,000 m^2 element size). The downward branch of the hydrograph has a smooth slope, due to the expected laminating effect of the basin and transits.

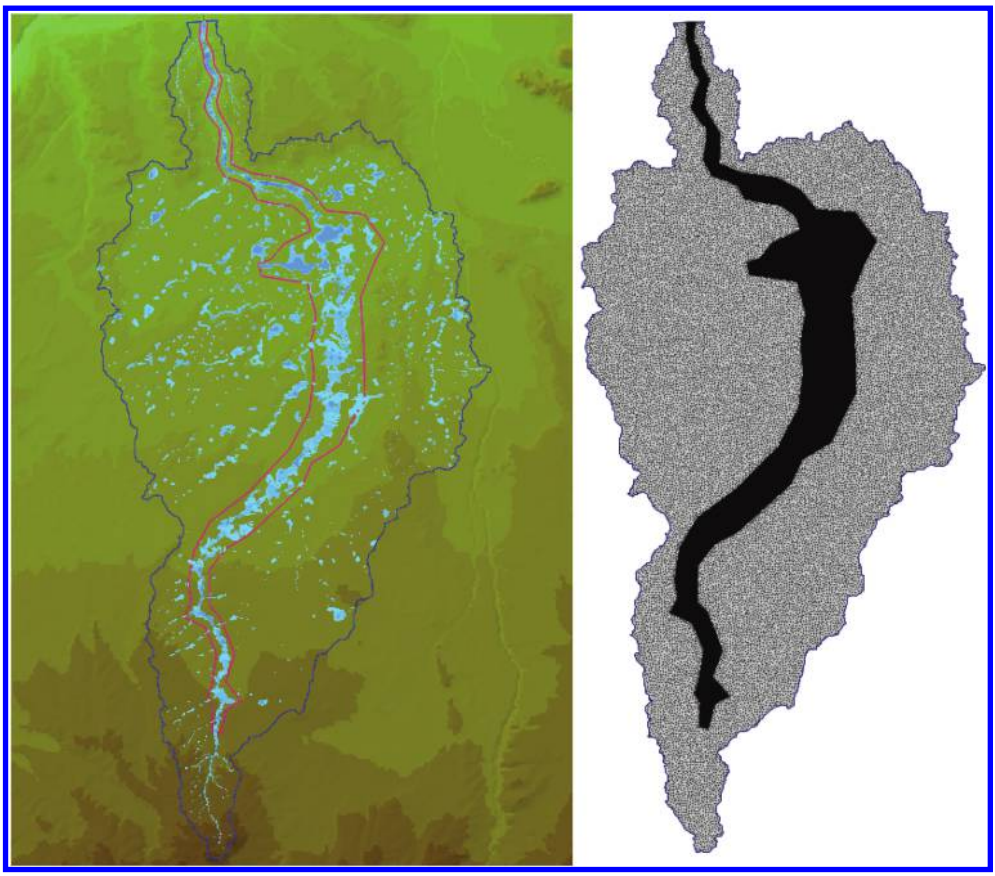

Figure 3. Zapardiel GRID DTM employed and 2D mesh defined on the ICM hydrological model.

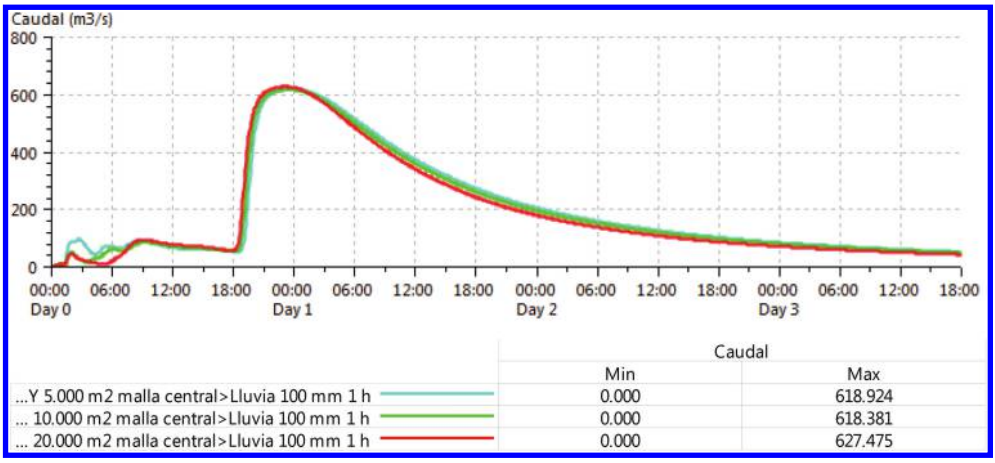

Figure 4. Zapardiel ICM flow model results at the end of the catchment.

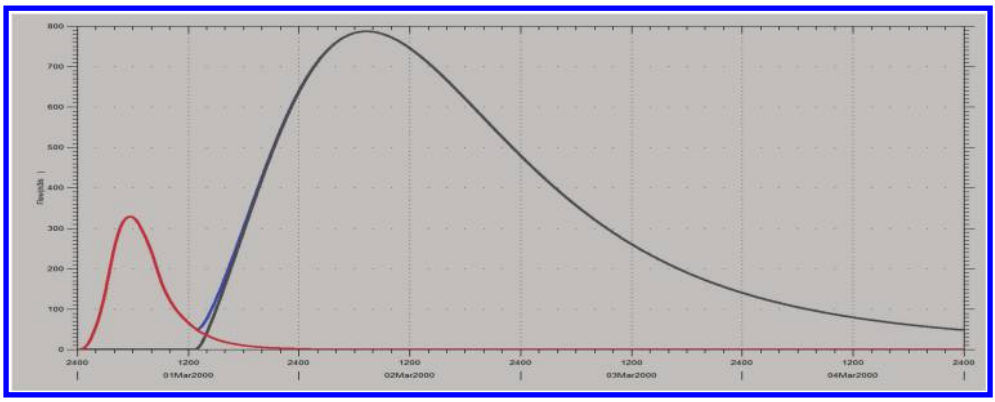

Figure 5. Zapardiel HEC-HMS flow model results at the end of the catchment.

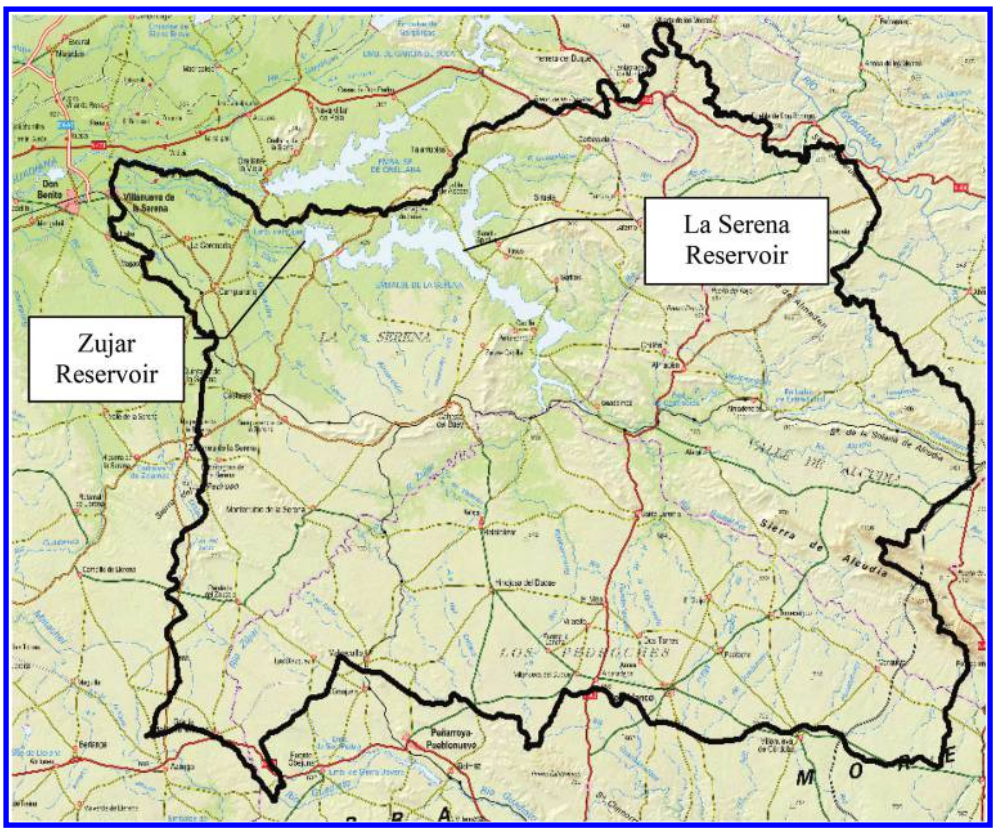

Figure 6. Zujar River Basin.

The outflow hydrograph obtained with the HEC-HMS model was: Both models show similar results, with some differences related mainly to the increased peak flow (787 m^3/s compared to the 619 m^3/s ICM direct rainfall model). The reason for this difference is because the HEC-HMS model is not reproducing the laminating effect on the flat sections of the subbasins, and the downward part of the hydrograph has a steeper slope.

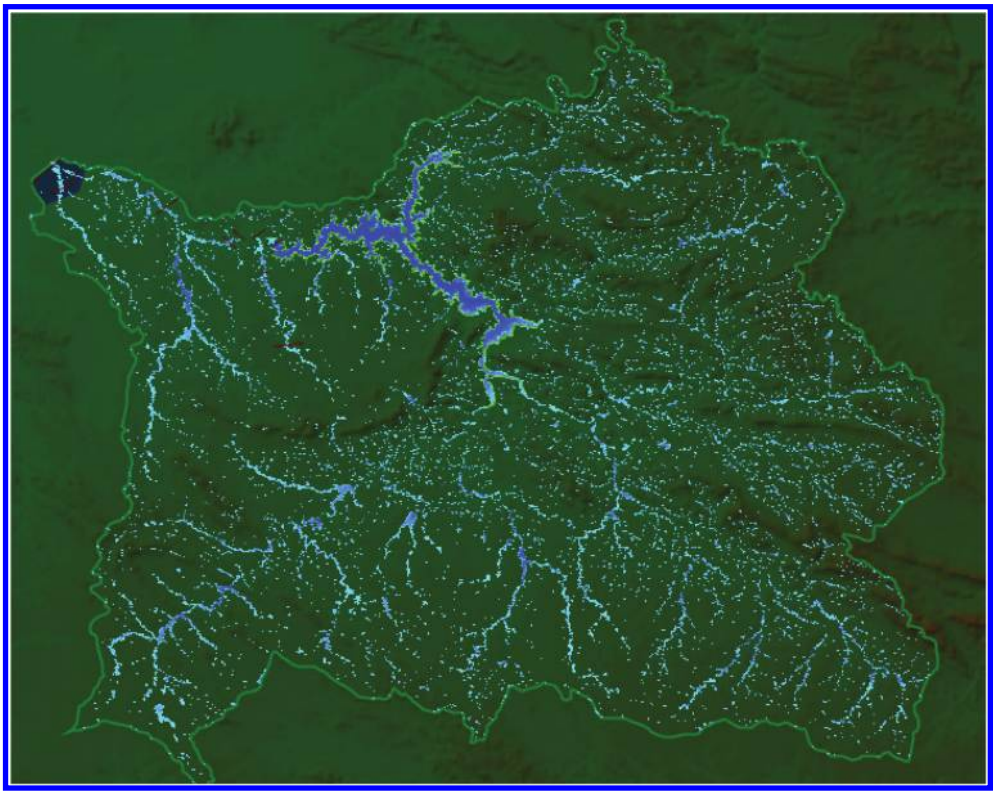

Figure 7. Digital Terrain Model of Zujar River Basin and maximum flood results > 1 m depth.

3.4 *Zujar River*

The second model presented is Zujar River from Guadiana Basin, with a total area of 8,500 km^2, including two large reservoirs: La Serena with a capacity of 3,200 hm^3 and Zujar reservoir, located downstream of the first, with a storage volume of 300 hm^3.

The size of this river can be characterized as medium-high, and poses a good example of the methodology used when there are regulating reservoirs in the basin. In addition to these, there are also some natural basins that drain downstream of these reservoirs and therefore allow the analysis of unregulated rivers behavior.

From PNOA elevation data, a DTM of the whole basin was made. Cell size was 5×5 m, as shown in figure 7.

Two-dimensional hydraulic models define the terrain from surface meshes formed by elements of different sizes and shapes, which locate its vertices on the ground getting the height of the element from these. Therefore, ignoring other constraints of the mesh, the size of the elements defines the terrain precision of the model. Size also influences the total number of elements and this number influences the total computation time. So, there should always be a compromise between the required accuracy and the computing time; and since it is possible to define meshing surfaces with different element sizes, an increase in precision in the areas of higher importance could be used to pursue this equilibrium.

In the case of direct rainfall hydrology, it is necessary to provide sufficient accuracy at river channels, especially in those stretches with narrower sections. This must be done in order to prevent flow obstructions that lead into storage areas that would minimize the total flow downstream.

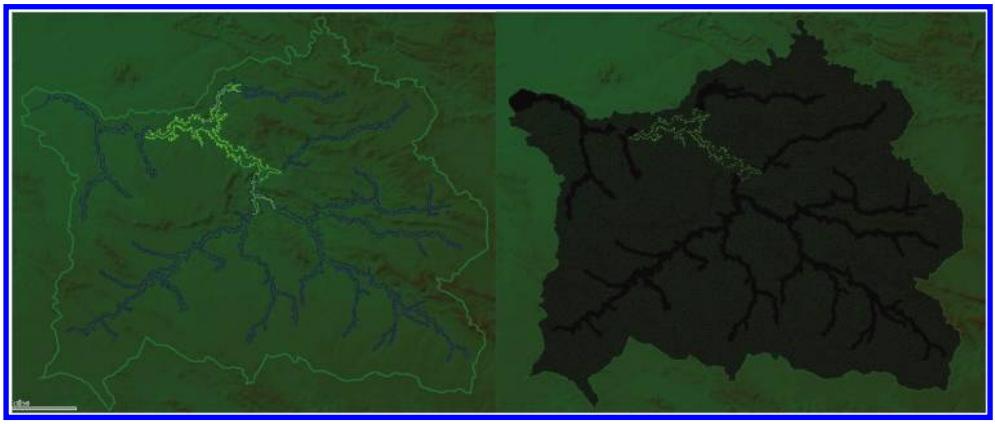

Figure 8. River and streams areas of smaller mesh size obtained with the method described.

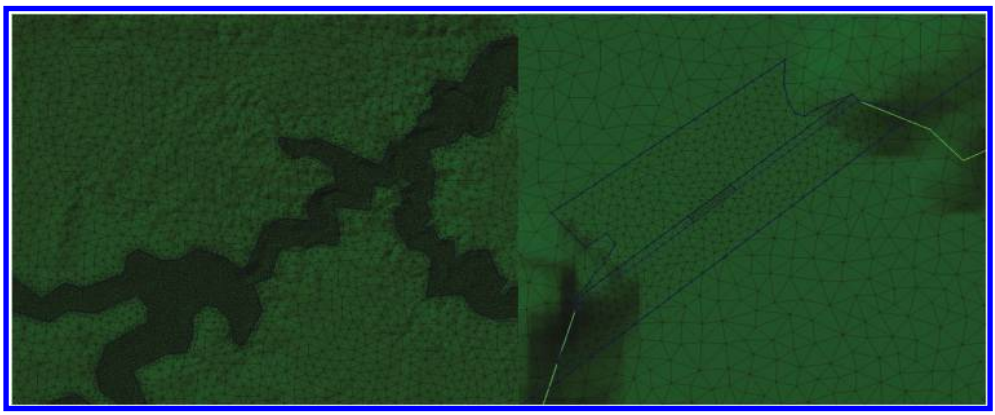

Figure 9. Detailed mesh on river ways and mesh elements defining La Serena Dam.

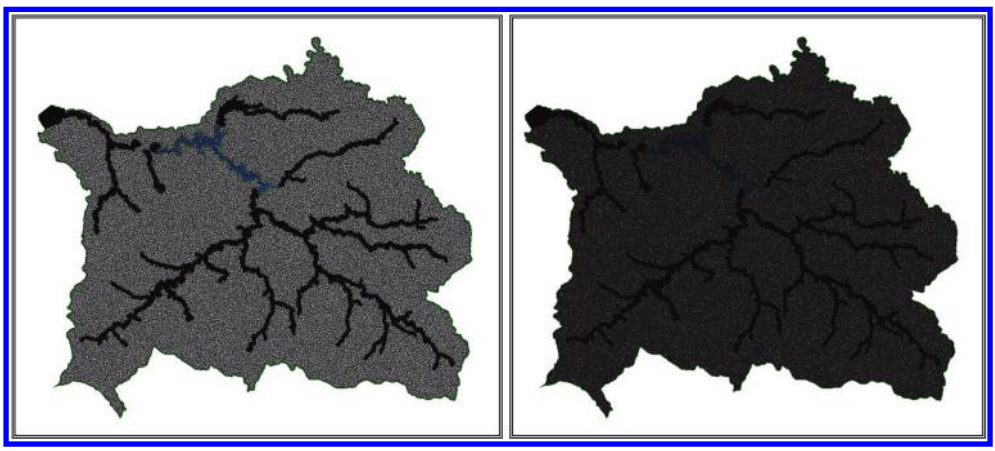

Figure 10. Two mesh element sizes considered.

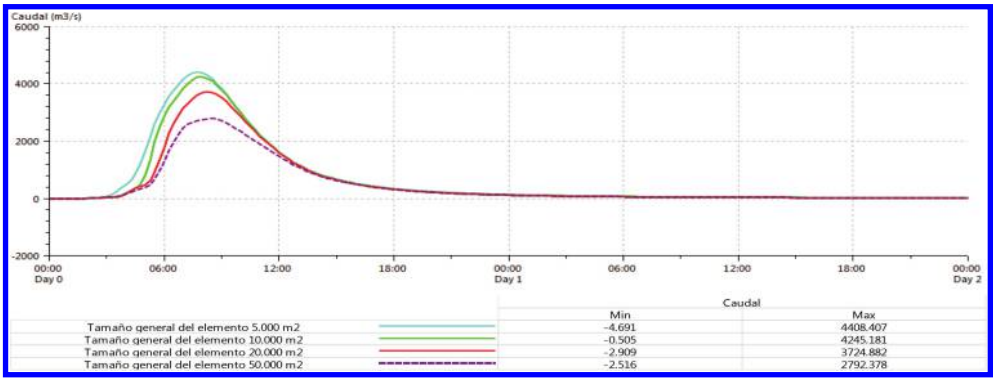

Figure 11. Flow results at river Guadamatilla (Zujar tributary) considering mesh sizes 5,000–50,000 m^2.

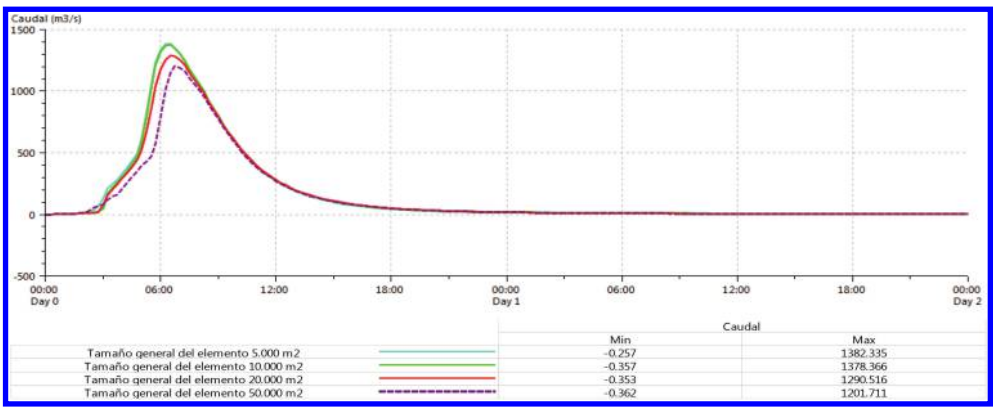

Figure 12. Flow results at river Guadalefra (Zujar tributary) considering mesh sizes 5,000–50,000 m.

A simple method has been developed in order to identify the main channels of the catchment where the accuracy of the model should be higher: first a preliminary model is modeled using an average size of the elements in the mesh. From this initial model, areas that are flooded over a certain depth will determine narrow stretches susceptible to store water.

From these results, a data processing is performed with the aid of GIS to obtain the areas that define the channels that will be meshed with greater precision on the final model. After a few iterations an optimal point should be reached, identifying those main streams that must be treated with increased precision in order to ensure proper accuracy of the model. It is also recommended that those areas should have a mesh size that would include at least 4 or 5 elements inside the riverbed, in order to ensure correct definition.

Furthermore, because of the existence of dams in the basin, it is necessary to fully define them through new areas of smaller mesh size. Those areas will define both the dam and the spillway, as well as their approach areas. The details of the final mesh are shown below.

Several meshes have been tested by varying the element sizes on the general basin extent and in the precision areas (dams and main river ways).

Results present a gradual increase in flow as the element size decreases, up to a certain value at which results are stabilized. The following graphs depict some outflows in tributaries.

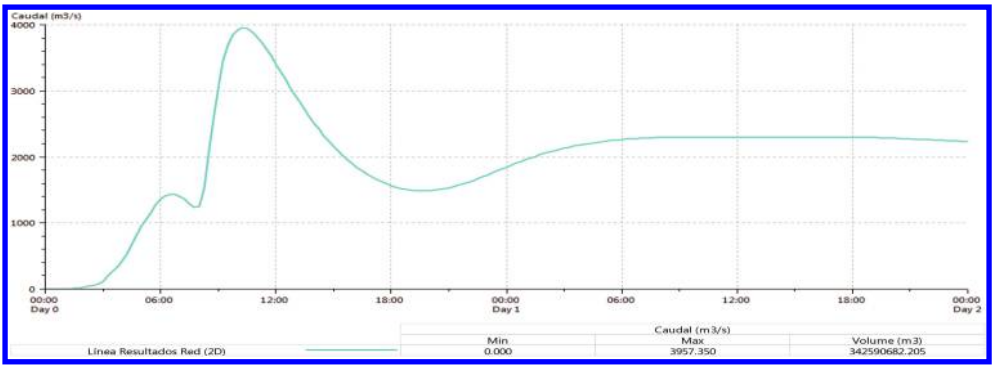

Figure 13. Flows at the final section of the complete Zujar river basin ≈ 4,000 m^3/s.

4 CONCLUSIONS

A new method for determining maximum flood event flows has been presented, giving a valid alternative to the traditional one-dimensional basins transits and reservoir analysis of hydrological models such as HEC-HMS, where results depend on the engineer's skills to define the elements of the basin.

Using PNOA DTM and CORINE public data, it is possible to build 2D mesh models to simulate direct rainfall over catchments. The most important parameter in this type of models is the average size of the 2D elements in main waterways. The proposed method allows better definition of this areas after a few iterations, therefore speeding-up the model without compromising the quality of the results.

With the available hardware in mainstream PCs, a reasonable upper limit for 2D meshes is up to 4 million elements, which allows the correct simulation of direct rainfall on watersheds of around 10,000 km^2. For larger catchments, this process could be applied recursively to several smaller zones or successive sections.

Over the last 5 years, the apparition of multicore processors and graphics cards based on CUDA parallel processing has delivered a fivefold increase in the speed of mathematical calculation. Projecting this trend, it could be assumed that in another five years the modelling of direct rainfall on 2D meshes with over 20,000,000 items, within a reasonable time and on a consumer PC, will be possible.

Based on this, it should be reasonable to think that the proposed method could be a reference tool to obtain flood hydrographs that could be used to prevent undesired dam overtopping events.

REFERENCES

Alcrudo, F. and Mulet-Marti, J., Urban inundation models based on the Shallow Water equations. Numerical and practical issues. *Proceedings of Finite Volumes for Complex Applications IV. Problems and Perspectives*. Pages 1–12. Edited by F. Benkhaldoun, D. Ouazar, S. Raghay. Hermes Science Pub. 2005.

Cleveland, T. G., Garcia, A., He, X., Fang, X., and Thompson, D. B. Comparison of physical characteristics for selected small watersheds in Texas as determined by automated and manual methods. *Proc., Texas ASCE Section Fall Meeting*, El Paso, Tex. 2005.

Fang, Xing, Thompson, David B., Cleveland, Theodore G., Pradhan, P. and Malla Ranjit, Time of Concentration Estimated Using Watershed Parameters Determined by Automated and Manual Methods. *Journal of Irrigation and Drainage Engineering*, ASCE, March/April, 2008.

Gutierrez, J. et al. in prep. Testing and application of a practical new 2D hydrodynamic. *Flood Risk 2008 Conference*, Oxford, 30th September 2nd October 2008.

Hill, J., and Neary, V. S., Factors affecting estimates of average watershed slope. *J. Hydrol. Eng.*, 10(2), 130–140. 2005.

Roussel, M. C., Thompson, D. B., Fang, X., Cleveland, T. G., and Garcia, A. C., Timing parameter estimation for applicable Texas watersheds. *Research Rep. No. 0-4696-2*, Texas Department of Transportation, Austin, Tex. 2005.

Su, D. H., and Fang, X., Estimating traveling time of flat terrain by 2D overland flow model. Shallow flows, G. H. Jirka and W. S. J. Uijttewaal, eds., Balkema, Rotterdam, The Netherlands, 629–635. 2004.

U. S. Army Corps of Engineers. Hydrologic Engineering Center. HEC-HMS, Applications Guide. December 2000.

U. S. Army Corps of Engineers. Hydrologic Engineering Center. HEC-HMS; Hydrologic modelling system user's manual. 2000.

Dam Protections against Overtopping and Accidental Leakage – Toledo, Morán & Oñate (Eds)
© 2015 Taylor & Francis Group, London, ISBN: 978-1-138-02808-1

CFD analysis of flow pattern in labyrinth weirs

F. Salazar, J. San Mauro & E. Oñate
International Center for Numerical Methods in Engineering (CIMNE), Universitat Politècnica de Catalunya, Barcelona, Spain

M.Á. Toledo
Technical University of Madrid (UPM), Madrid, Spain

ABSTRACT: The hydraulic performance of a labyrinth weir was analysed using numerical simulation. The head-discharge relation was compared to the results of an empirical formula, and the flow 3D pattern was studied. The results showed the reliability of the numerical model results, especially for intermediate to high heads. Moreover, they were used to unveil complex phenomena that are difficult to observe in laboratory tests

1 INTRODUCTION

Labyrinth weirs were originally devised with the aim of increasing the spillway discharge capacity for a given channel width. Their main characteristic is their zig-zag shape in plan-view, so that the total length of discharge is larger than that of a straight weir. Their discharge capacity is also higher, especially for low hydraulic heads.

A high number of studies have been performed to analyse the hydraulic capacity of labyrinth weirs, most of which focus on obtaining a mathematical expression to compute the discharge coefficient C_d as a function of the involved parameters (Figure 1). The most common formula for computing the discharge flow over a labyrinth weir is (Crookston & Tullis, 2013):

$$Q = \frac{2}{3} \cdot C_d \cdot L_c \cdot \sqrt{2 \cdot g} \cdot H_t^{1.5} \tag{1}$$

where Q = discharge flow, C_d = discharge coefficient, L_c = total crest length, g = acceleration of gravity, and H_t = upstream hydraulic head.

The most popular formulations are due to Lux III & Hinchcliff (1985), Tullis et al. (1995) and Crookston & Tullis (2013), and were developed on the basis of the results of experimental tests. They are applicable to labyrinth weirs with similar geometry to those tested in each experimental campaign, in terms of inlet geometry, crest shape, flow range, hydraulic head and number of cycles, among other parameters.

Specific features of flow over labyrinth weirs were also studied, such as nappe interference (Crookston & Tullis, 2012a), or aeration (Crookston & Tullis, 2012b). Again, these works are mostly based on experimental results.

More recently, the problem has been faced with numerical modelling (e.g. Paxson & Savage, 2006; Tullis et al., 2007; Crookston et al., 2012c). Some of the advantages of this approach are:

1. They allow extraction of comprehensive information on the hydraulic performance, such as pressure and velocity fields, or stream lines. This information is difficult to obtain from experimental tests.
2. They are free from the restrictions of experimental facilities in terms of space availability or flow capacity, among other aspects.

However, previous studies based on numerical simulation did not take full advantage of the possibilities of numerical models to deeply analyse the problem. They limited to the calculation of the discharge coefficient, as a complement or validation of empirical formulas.

A different approach was followed in the present work: first, the numerical model reliability was checked by comparing the discharge coefficient with empirical formulas. Second, the three-dimensional flow pattern and the free surface shape were deeply analysed for different flows. This information can be useful for a better understanding of the hydraulic phenomenon, as well as to propose design improvements.

2 METHODOLOGY

2.1 *Numerical code*

All the calculations were run using an Eulerian finite element method (FEM) completed in the open-source code Kratos (Davdand et al., 2010; Rossi et al., 2013) developed at CIMNE. The solution module was designed for the resolution of the 3D Navier-Stokes equations using the FEM. In this work, a level-set approach was applied for the simulation of the free-surface problem. The comprehensive description of the numerical implementation can be found in Rossi et al. (2013), while the main ingredients are:

1. Discretisation of the Navier-Stokes equations for incompressible fluid using the standard FEM and an Eulerian approach.
2. Low order (linear) elements 3-noded triangles in 2D and 4-noded tetrahedra in 3D.
3. Time integration with a semi-explicit version of the fractional-step method.
4. Improvement in mass conservation via an "error recovering" technique that allows correcting the solution taking into account the errors made in the previous time steps.
5. Level-Set Method for tracking the free surface.
6. An extrapolation function which allows computing the values of velocity, pressure and pressure gradient on the nodes in the air region area close to the free surface in the fluid.

The algorithm follows the following steps:

1. Extrapolate velocity, pressure and pressure gradient on the analysis domain (including fluid and air subdomains).
2. Convect the level-set function defining the new free surface on the basis of the velocity field both on fluid and air domains.
3. Re-initialise the distance function on the whole domain starting from the zero of the level-set function obtained at step 2.
4. Solve the momentum equations for the fluid flow.
5. Set the pressure boundary condition so that pressure is (approximately) zero at the position indicated by the zero of the level-set function.
6. Solve the pressure equation
7. Solve the correction equation
8. Back to step 1.

The tool has been previously applied for the analysis of hydraulic structures (Salazar et al., 2013).

2.2 *Numerical tests*

A labyrinth weir with four cycles was chosen for this work, installed on a 1-m-width horizontal channel (Figure 1). The values of the geometrical parameters are: $\gamma = 7.45°$, $W = 0.25$ m, $A = 0.032$ m and $P = 0.2$ m.

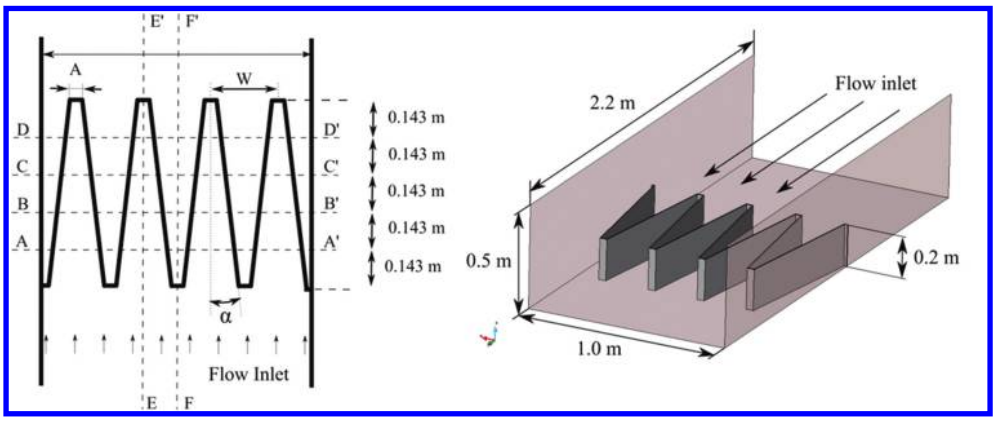

Figure 1. Geometric definition of the numerical model.

Five values of the incoming flow were considered, namely: 100 l/s, 125 l/s, 150 l/s, 200 l/s and 250 l/s. The computational mesh was formed by 5-cm-long-edge tetrahedra, with further refinement in the vicinity of the free surface, where the maximum size of the edges was limited to 1.5 cm.

2.3 *Validation*

As mentioned before, the main purpose of the study was the flow pattern analysis. However, before analysing that issue, the results were checked in terms of a) the shape of the free surface, and b) the discharge coefficient. As for the first case, four cross sections (Figure 1) were observed to check the influence of discharge rate on nappe interference.

As regards the discharge coefficient, it was computed by measuring the upstream hydraulic head and the discharge flow in the numerical results, and introducing them in (1). The results were compared to those obtained with Crookston's formula (Crookston & Tullis, 2013) for quarter-round crest shape. Although the crest was flat in the numerical model, it is actually more similar to a half-round than to a flat crest, due to the way in which the boundary is modelled in the algorithm.

2.4 *Flow pattern analysis*

The flow pattern was analysed for the lowest (100 l/s) and highest (250 l/s) flows, where the differences could be better highlighted. We focused in free surface shape, nappe interference, streamlines and velocity field.

3 RESULTS AND DISCUSSION

3.1 *Validation*

Figure 2 shows the numerical results in comparison with those provided by the Crookston's formula. They are plotted in terms of both the discharge coefficient and the flow depth. It can be observed that results are similar for $H_t/P \geq 0.4$ (discrepancy lower than 3%), whereas they differ for low heads (up to 12% difference in terms of the discharge coefficient). The main reason for this increment is that flow depth decreases as the discharge flow does, so that the error due to the mesh size becomes more relevant. Moreover, H_t is raised to the power of 1.5 in equation (1), so a given discrepancy in terms of H_t implies a greater error in the estimation of C_d. Figure 2 also shows the results in terms of head-discharge relationship. It can be noted that the discrepancy is much lower and homogeneous.

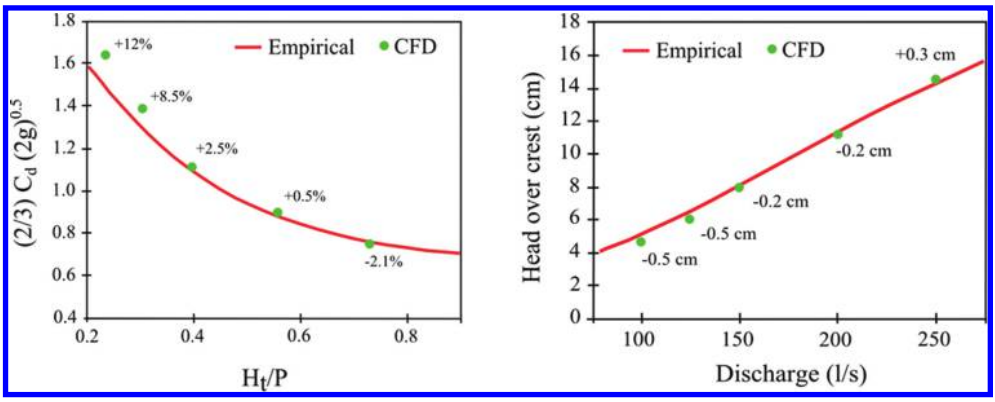

Figure 2. Experimental results as compared to Crookston's empirical formula (Crookston & Tullis, 2013).

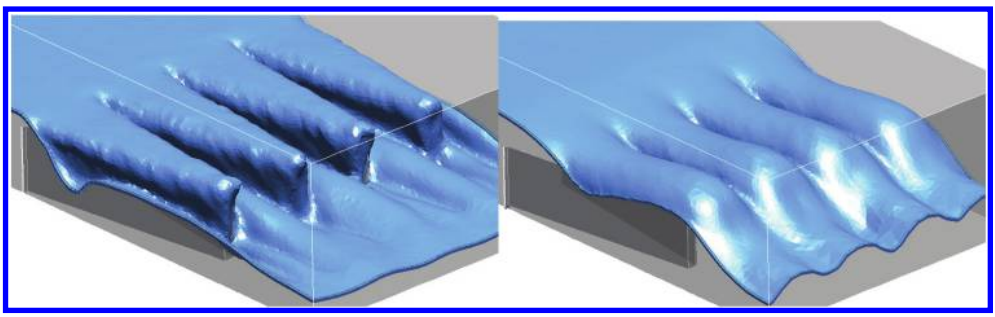

Figure 3. Free surface for 100 l/s (left) and 250 l/s (right).

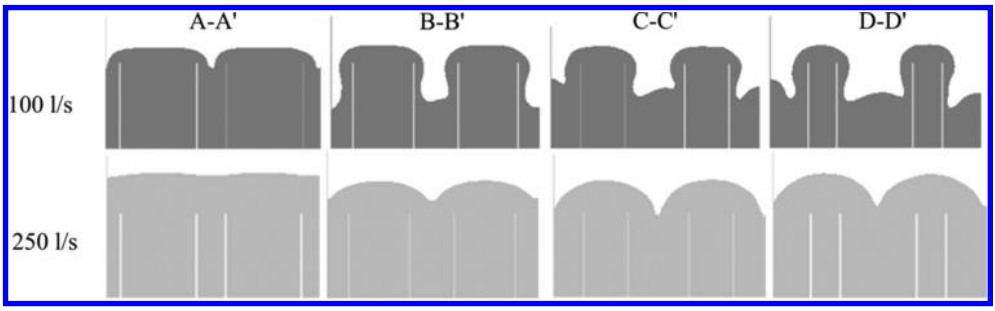

Figure 4. Cross sections of the numerical results (see Figure 1). The influence of the discharge flow on the nappe interference can be observed.

3.2 *Flow pattern analysis*

3.2.1 *Free surface*

Figure 3 shows a general view of the model output for 100 and 250 l/s. The different performance can be observed: whereas the free surface adapts greatly to the weir profile for the low discharge, nappe interference is observed for 250 l/s. This aspect is also highlighted in Figure 4.

The analysis of the free surface along E-E' sections (Figure 5) shows that flow depth is almost constant for 100 l/s, with a small increase in the vicinity of the downstream apex. For 250 l/s,

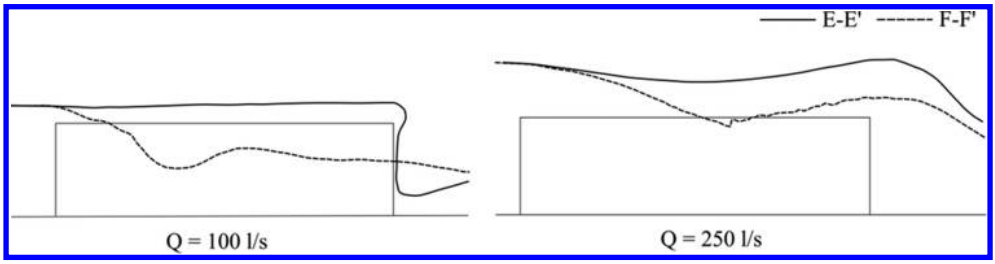

Figure 5. Free surface profiles along longitudinal sections (see Figure 1).

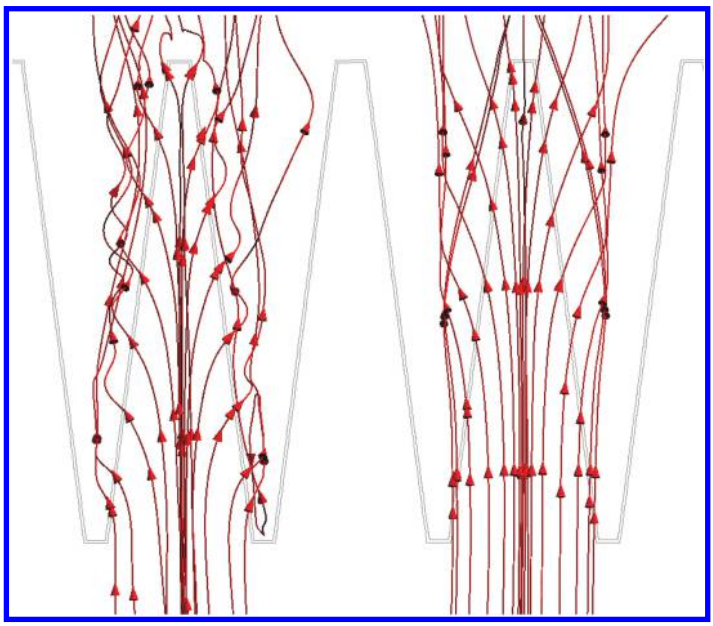

Figure 6. Streamlines on the free surface. Plan view. Left: $Q =$ 100 l/s. Right: $Q =$ 250 l/s.

flow depth is neatly lower in the central third of the cycle, and the increase near the apex is more pronounced.

3.2.2 *Streamlines*

The streamlines in the free surface reveal the different flow pattern in the models analysed. For the lower head, the flow turns sharply from the channel direction, becoming almost perpendicular to the weir crest. On the contrary, the change in direction for 250 l/s is milder (Figure 6), due to the higher incoming velocity.

This effect can contribute to the decrease of efficiency (lower discharge coefficient) of labyrinth weirs for high heads: the effective length is actually lower, provided that the flow is more oblique to the weir crest direction, so that the geometrical length is less exploited.

Streamlines along a vertical line in the upstream boundary of section E-E' were also plotted (Figures 7 and 8). In both cases, the flow approaching along the bottom of the incoming channel is evacuated over the downstream apex. The greater change in direction for low head was also observed in these streamlines.

A low-effective area was registered at the bottom of the downstream apex, greater for 250 l/s (Figure 8).

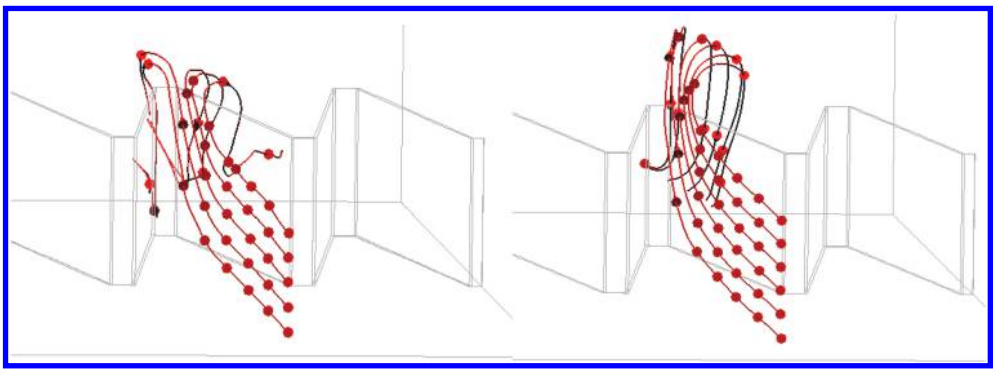

Figure 7. Streamlines along a vertical line in the upstream boundary of E-E' section. Left: 100 l/s. Right: 250 l/s.

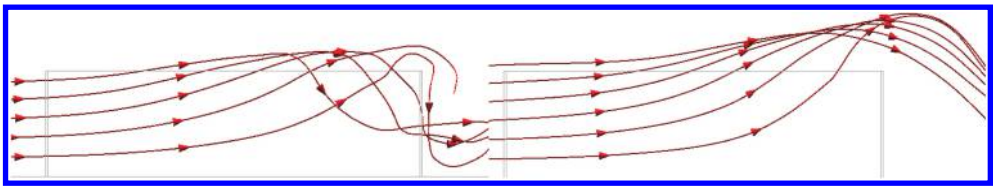

Figure 8. Streamlines along a vertical line in the upstream boundary of E-E' section. Side view. Left: 100 l/s. Right: 250 l/s. Note the ineffective area at the bottom of the downstream apex.

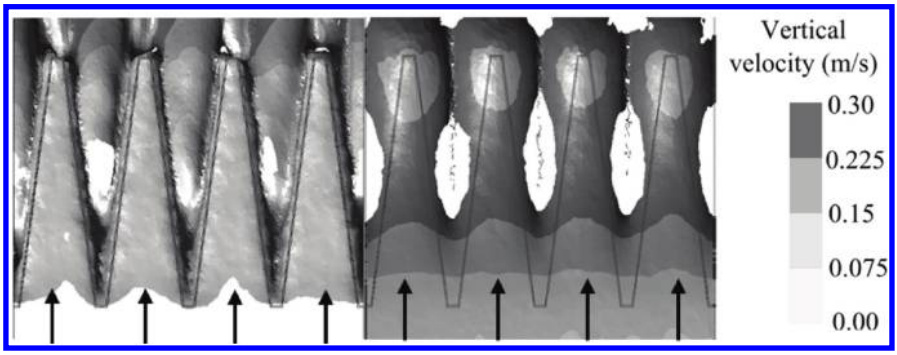

Figure 9. Velocity field in the free surface (plan view). Left: constant value for 100 l/s. Right: flow acceleration in the first reach of each cycle, and deceleration in the vicinity of the downstream apex.

3.2.3 *Velocity field*

The analysis of the velocity on the free surface reveals other aspects of the weir performance. Velocity is almost constant for 100 l/s (Figure 9), in accordance with the sensibly horizontal shape of the fluid surface (Figure 5). For the greater flow, there is acceleration in the first part of the cycle, followed by deceleration before the downstream apex. In this area, the flow near to the surface is forced to "jump" over the portion coming from the bottom, which emerges almost vertically (Figure 10).

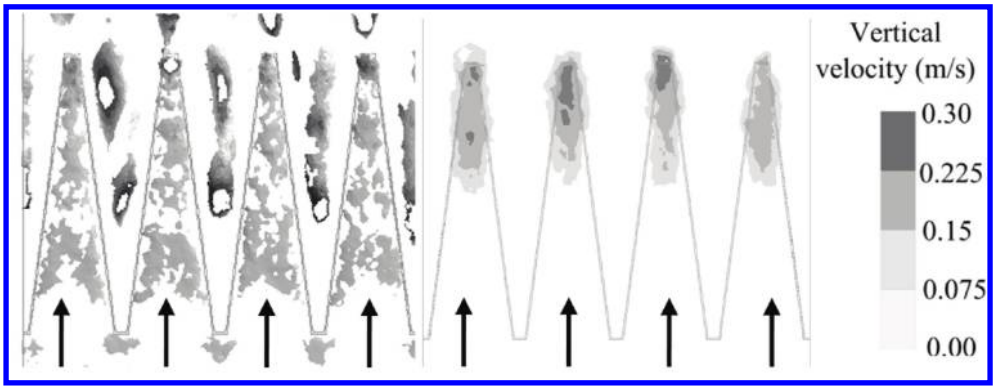

Figure 10. Vertical component of the velocity field in the free surface. Left: for 100 l/s, the value is uniformly distributed and close to zero. Right: for the higher flow, an area with positive value is registered close to the downstream apex.

4 SUMMARY AND CONCLUSIONS

A labyrinth weir was numerically modelled for 5 different discharge flows. The discharge coefficient matched Crookston's empirical formula for $H_t/P \geq 0.4$, with a discrepancy below 2.5%. For lower heads, the error increased as the upstream head decreased, up to 12% for $H_t/P = 0.25$; the numerical error is dependent upon the mesh size, which is constant for all the situations analysed. Hence, the relative importance is higher for low heads. The maximum error in terms of hydraulic head is 0.5 cm.

Numerical model results provided detailed information on the pressure and velocity fields, as well as on the free surface position. Some of the well-known characteristic phenomena of flow over labyrinth spillways were observed, such as the nappe interference.

The analysis of the streamlines and the velocity in the free surface provided insight into the 3D flow pattern, which can be further used to propose and test improved designs.

ACKNOWLEDGEMENT

The research has been founded by the Spanish Ministry of Economy and Competitiveness (Ministerio de Economía y Competitividad, MINECO) through the project POLILAB (IPT-2012-0185-380000).

REFERENCES

Cihan Aydin, M. & Emin Emiroglu, M. (2013). Determination of capacity of labyrinth side weir by CFD. *Flow Measurement and Instrumentation* 29, 1–8.

Crookston, B. M. & Tullis, B.P. (2012a). Labyrinth weirs: Nappe interference and local submergence. *Journal of Irrigation and Drainage Engineering* 138(8), 757–765.

Crookston, B. M. & Tullis, B.P. (2012b). Hydraulic design and analysis of labyrinth weirs. II: Nappe aeration, instability and vibration. *Journal of Irrigation and Drainage Engineering* 139(5), 371–377.

Crookston, B. M., Paxson, G. S. & Savage, B. M. (2012c). Hydraulic performance of labyrinth weirs for high headwater ratios. *4th IAHR International Symposium on Hydraulic Structures, Porto, Portugal, ISBN: 978-989-8509-01-7.*

Crookston, B. M. & Tullis, B.P. (2013). Hydraulic design and analysis of labyrinth weirs. I: Discharge relationships. *Journal of Irrigation and Drainage Engineering*, 139(5), 363–370.

Dadvand, P., Rossi, R. & Oñate, E. (2010). An object-oriented environment for developing finite element codes for multi-disciplinary applications. *Archives of Computational Methods in Engineering*, 17, 253–297.

Lux III, F. L. & Hinchcliff, D. (1985). Design and Construction of Labyrinth Spillways. *Proc. 15th International Congress on Large Dams, Vol. 4, Q. 59, R. 15, pp. 249–274, ICOLD, Paris, France. (1985).*

Paxson, G. & Savage, B. (2006). Labyrinth spillways: comparison of two popular USA design methods and consideration of non-standard approach conditions and geometries. *Proceedings of the international junior researcher and engineer workshop on hydraulic structures, report CH61/06, Division of Civil Engineering, The University of Queensland, Brisbane, Australia*.

Rossi, R., Larese, A., Dadvand, P., & Oñate, E. (2013). An efficient edge-based level set finite element method for free surface flow problems. *International Journal for Numerical Methods in Fluids*, 71(6), 687–716.

Salazar, F., Morán, R., Rossi, R., & Oñate, E. (2013). Analysis of the discharge capacity of radial-gated spillways using CFD and ANN–Oliana Dam case study. *Journal of Hydraulic Research*, 51(3), 244–252.

Tullis, B. P., Amanian, N. & Waldron, D. (1995). Design of labyrinth spillways. *Journal of hydraulic engineering* 121(3), 247–255.

Tullis, B. P., Young, J. C. & Chandler, M. A. (2007). Head-discharge relationships for submerged labyrinth weirs. *Journal of Hydraulic Engineering* 133(3), 248–254.

Dam Protections against Overtopping and Accidental Leakage – Toledo, Morán & Oñate (Eds)
© 2015 Taylor & Francis Group, London, ISBN: 978-1-138-02808-1

Analysis of the design of energy-dissipating structure in spillways

Isidro Robles
Instituto Mexicano de Tecnología del Agua (IMTA), Morelos, México

Arturo Palacio & Alejandro Rodriguez
Instituto de Ingeniería de la UNAM, México, D.F., México

ABSTRACT: In this paper the design of a structure to dissipate energy in the spillways was analyzed as an alternative to reduce the destructive effects of water at high speed. Work on energy dissipation are critical elements in the construction of hydraulic structures, these have been developed based on the experience and wealth of knowledge in the field, however, the design of these structures involves laboratory studies, collection prototype field data, statistics, among others. In order to assist in this effort to collect information useful in the design of structures of energy dissipation information current work is presented with information obtained from laboratory data relevant parameters of structures including willing obstacles especially to achieve this objective. The main objective of the study is to have design elements to build a structure of energy dissipation decreases the undesirable effects present in the spillways flow with a sufficiently quieted to avoid structural damage. This was done with the support of a laboratory physical model provided for this purpose. For testing of the physical model α angle was set in one position and the following dimensionless parameters were varied: *Lh/Lv, d/D*, where *D* is the maximum diameter of the tests performed. Also the velocity profiles of all tests were measured at 0.12 m from the point of supply to the water structure in the physical scale model. There are evidences that the variable that dominates the energy dissipation in these structures is the change in diameter of the cylindrical obstructions.

Keywords: Dam, Spillway, Protection, Overtopping

1 INTRODUCTION

The forces exerted by wind gale and water run-off during storms and floods, have a destructive potential on the built environment that seriously affects communities. As a consequence of global warming, storms are expected to intensify both in frequency and magnitude. In particular, storm run-off will be an increasing challenge to design energy dissipation measures that can mitigate scouring and erosion downstream of dams and irrigation works, e.g. Figure 1. There are various published works of power dissipation where key elements in the construction of hydraulic structures [1], have been developed based on experience and research on the subject. However, the design of these structures involves laboratory studies, field data collection from prototypes, statistical analysis of data, among others endeavors [3]. To assist in this effort to collect information useful in the design of structures for power dissipation, the work herein presents information obtained from laboratory data of relevant parameters of a drop structures with baffle piers obstacles that increase flow resistance and create a tumbling pattern along a mild or steep channel for energy dissipation [4].

Most power generation and irrigation works have elements for power dissipation designed to reduce flow velocities and this study considers the main parameters of a design that has the potential to effectively increase energy dissipation in a sloping channel [5].

The main objective of the study is to demonstrate in a scaled model this effectiveness through a series of tests with various diameters and spacing of the baffle piers.

Figure 1. Unlined spillway erosion (http://www.damsafety.org/).

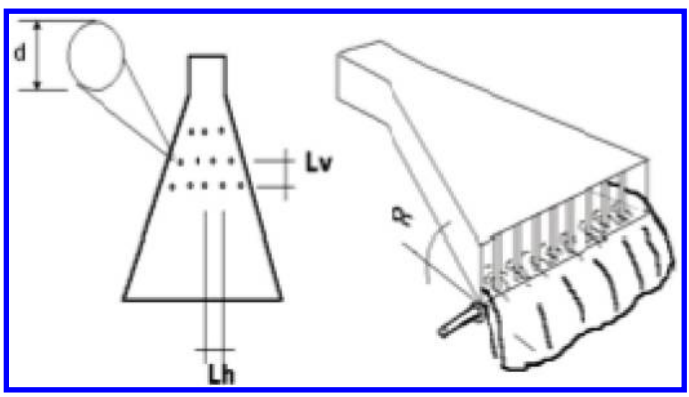

Figure 2. Dissipating flow energy structure and main study parameters.

2 EXPERIMENTAL FACILITY

The structure consists of cylindrical obstructions arranged transversely to the direction of flow that are in a staggered arrangement, with the capability to vary both the diameter and the spatial separation between these cylindrical elements; *d* is the diameter of the cylindrical obstacles; *Lv/Lh* ratio of vertical and horizontal separation between obstacles; α is the slope of the apron of the spillway-like structure (see Figure 2). The model construction and arrangement is shown in Figures 3 and 4, with a schematic of the variables involved (Figures 3 and 4).

Different diameters as cylindrical obstructions were used, allowing changing the general configuration of the dissipative flow structure (Figure 5).

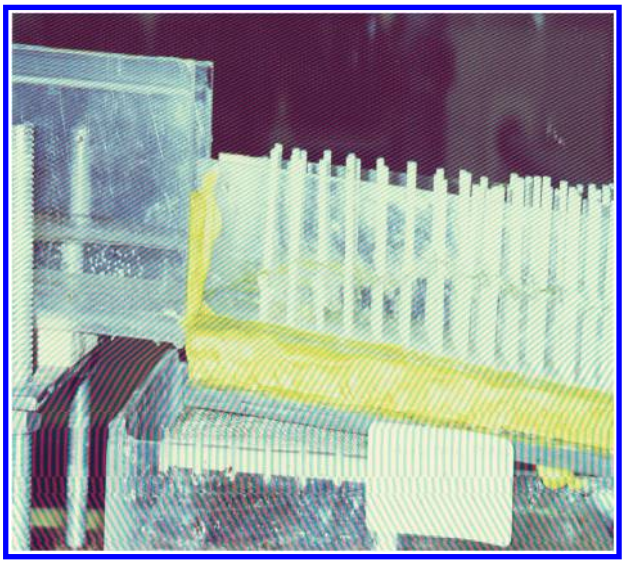

Figure 3. General view of the dissipative structure of energy used for experimental.

Figure 4. Top of dissipating energy structure and flow initial velocity zone.

The equipment used for determining the flow rate at which the discharge end of the device is a high speed camera (Ektacrom). The equipment consists of a data processor, high-resolution monitor and PC (Figures 6 and 7).

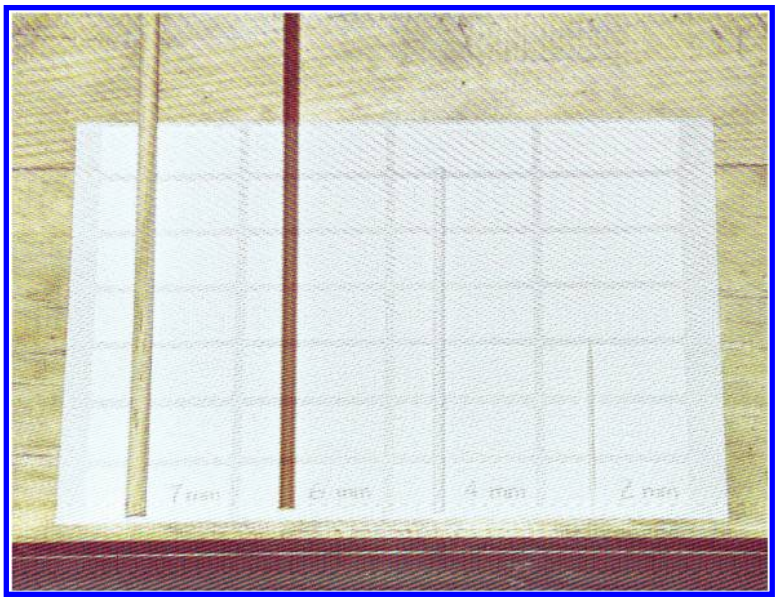

Figure 5. Using elements of different diameter to change the settings in the dissipating structure.

Figure 6. Equipment including high-speed camera for Ektacrom records.

3 ANALYSIS OF THE STRUCTURE

In tests of the physical model, cylindrical elements are placed perpendicularly to the direction of flow in a staggered baffle arrangement as shown in Figure 8 [2]. In Figure 9, the energy dissipation mechanism is assumed as a tumbling flow through a series of horseshoe vortices around each pier.

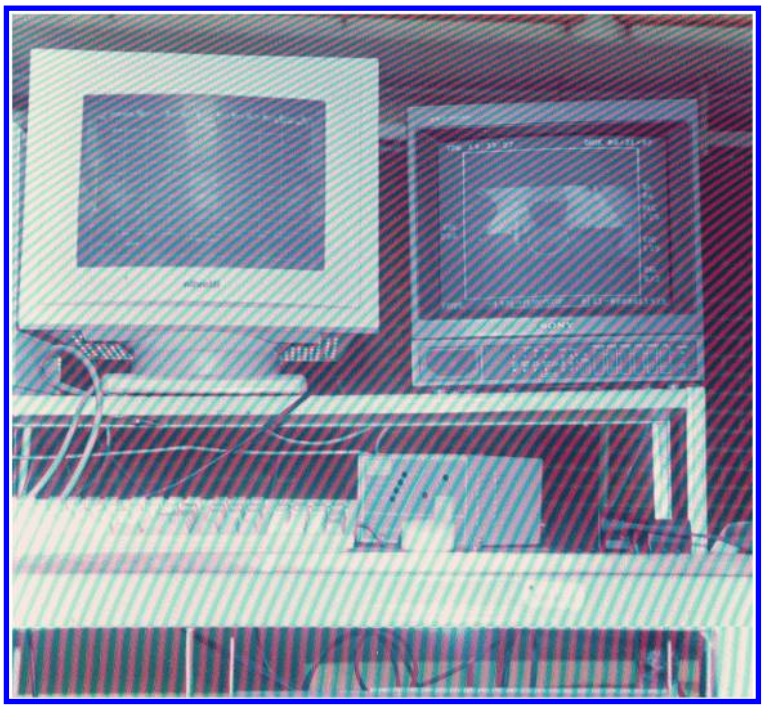

Figure 7. Speed devices for measuring velocities in the dissipative structure.

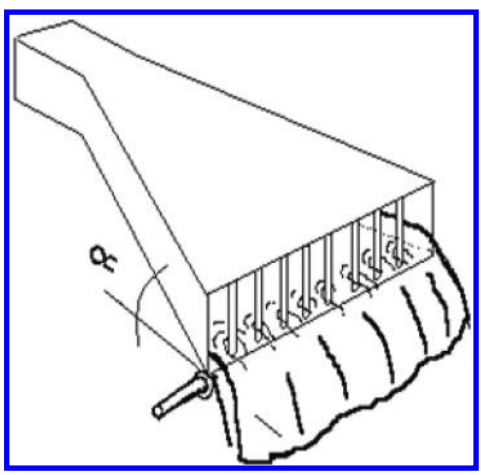

Figure 8. Perspective view of the physical model attacking with flow perpendicular angle α.

The basic premise of the tumbling flow regime is that it will maintain essentially critical flow even on steep slopes.

An important component of the model is an innovative design to aerate the step-like cavity as illustrated in Figure 10. The induced negative pressure drives the air flow, thereby avoiding the cavitating potential on the apron (Figure 10). This system consists of the air inlet at the top of the vertically positioned pipes, which are connected to a general pipe which distributes the air to tiny tubes in a comb arrangement.

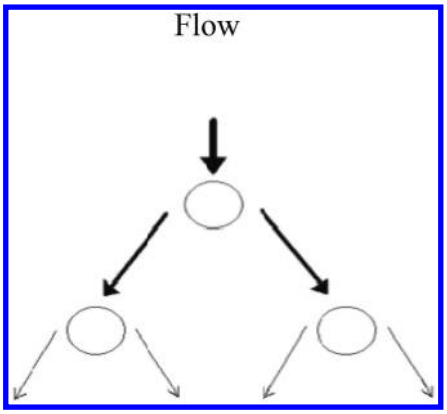

Figure 9. Plan view of the obstacles willing to "staggered" to dissipate the energy flow.

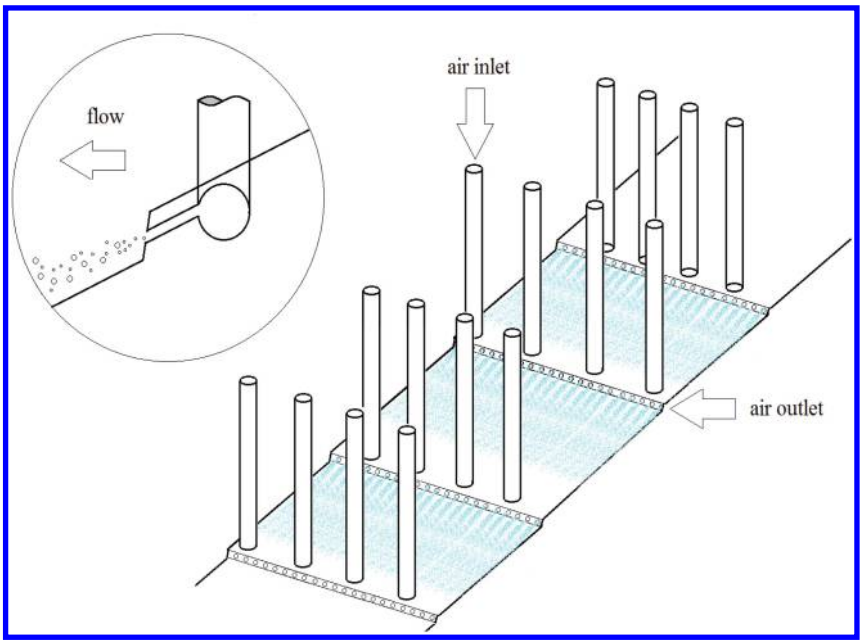

Figure 10. System of negative pressure relief.

4 STUDY VARIABLES

The outlet velocity V_1 of the discharge device is a function of angle α, the diameter d of the cylindrical obstacles, the spacing ratio Lh/Lv, the gravitational acceleration g, and the velocity V_0 of approach at the inlet structure.

For testing of the physical model, angle was set in one position and the following dimensionless parameters were varied: Lh/Lv, d/D, where D is the maximum pier diameter that was implemented during the tests performed. Also the velocity profiles of all tests were measured at 0.12 m from the point of supply to the water structure in the physical scale model.

Table 1. Combinations of tests.

No. de prueba	V_0 (m/s)	V_1 (m/s)	d/D (adim)	Lh/Lv (adim)	$(V_1/V_0)^2$ (adim)
Test 1	0.55	0.549	N/A	N/A	0.996
Test 2	0.55	0.53	0.5	0.667	0.912
Test 3	0.55	0.55	0.5	1	0.987
Test 4	0.55	0.44	0.5	2	0.644
Test 5	0.55	0.50	1	0.667	0.841
Test 6	0.55	0.48	1	1	0.772
Test 7	0.55	0.43	1	2	0.613

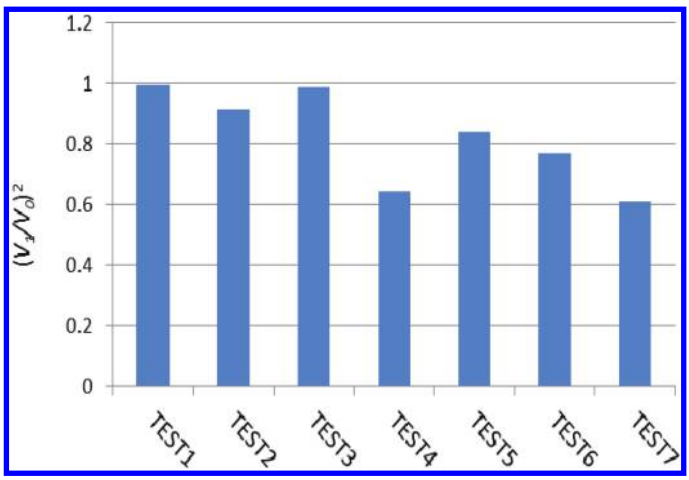

Figure 11. Main test results.

5 DESIGN OF EXPERIMENTAL TESTS

Table 1 shows the possible combinations performed by varying the rate of inflow to the structure, the diameter ratio d/D and the split ratio of blockages in the horizontal direction and vertical Lh/Lv. In these tests the input speed of 0.55 m/s was considered. In the case of the diameter ratio d/D, the value for the largest diameter of 4 mm value was prescribed, and only two other diameters, 2 and 4 mm, were considered, so that the values in Table 1 are obtained as $d/D = 2/4 = 0.50$ & $d/D = 4/4 = 1.0$. Finally, in Table 1 the ratio of cylinders separation is shown Lh/Lv, and the last column corresponds to the ratio of the outlet and inlet velocities. This last ratio is a measure of the amount of kinetic energy dissipated by the structures.

In Figure 11 are the results graphically, where tests 4 and 7 have the lowest values in dissipative energy terms with a reduction with about 35 and 39 percent respectively.

6 MEASUREMENT PROGRAM

Through the combination of the aforementioned parameters, a total of 16 tests were performed on the model. In these tests the slope of the platform, α was varied (5°, 10° and 15°) and the approach velocity was held constant. Then the range for the other dimensionless variables was limited as shown in Table 1 to reduce the number of experimental tests. Preliminary tests were performed to visualize the influence of the cylindrical obstructions on the flow around them, showing as

Figure 12. Flow off the platform without cylindrical obstructions angle α.

Figure 13. The output flow of the angle α platform with cylindrical obstructions.

expected, an elevation of water level on the center of the obstructions. Figures 12 and 13 show very clearly how the extent of the flow reduces with the presence of obstacles.

Given the number of tests in the physical model, only the results of some of them are shown, which represent the extreme values of the flow velocity at the outlet of the platform, which is monitored by a high speed camera and tracers conveniently seeded to be video captured and further processed. The results are shown below.

For a flow velocity of 1.4 m/s at the inlet of the structure with a constant diameter ratio d/D and a split ratio Lh/Lv value of 0.83 values of the Froude number were determined based on the velocity output (V_1) and hydraulic depth ($D_H = A/T$) [m], A being the cross sectional area of the flow, and T the width of the free surface. The Froude numbers obtained with these values are

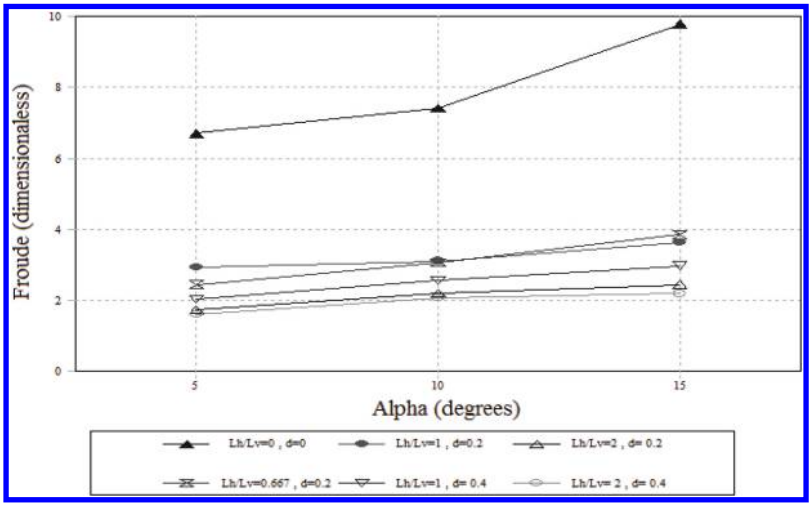

Figure 14. Results of laboratory tests, modifying split ratio *Lh/Lv*, diameter *d*, and tilt angle of the platform.

shown in Figure 14. These results show that the smaller tilt angle, considering a split ratio of 2, and a diameter ratio of 1 gave the best results, as a lower Froude number represents in this case the minimum outlet velocity, and therefore the maximum kinetic energy dissipation [6].

7 CONCLUSIONS

A total of 16 experimental trials were run of which the most representative is shown. In these tests the spacing ratio *Lh/Lv*, the cylinder diameter *d*, and the inclination α of the platform have been considered. After review of the tests of the physical model, it was found that although all variables identified in the phenomenon have an important influence, there is evidence that the diameter ratio of the cylindrical obstructions is the predominant factor for energy dissipation. From the tests performed, the results show that for maximum d/D tried (1) and ratio of cylinders separation of 2, almost 40% of the kinetic energy may be dissipated.

REFERENCES

[1] Aldama, A. A., Levi, E. "Nuevos diseños en obras hidráulicas" Instituto de Ingeniería, Cd. Universitaria, México, D.F. (1978).
[2] A. J. Peterka US Bureau of Reclamation, Denver, Colorado, EU, Hydraulic design of stilling basins and energy dissipators, a water resources technical publication engineering monograph no. 25, may 1984.
[3] García, M. H. "*Hidrodinámica Ambiental*" Universidad Nacional del Litoral, Santa Fe, Argentina, octubre, (1996).
[4] Hydraulic Design of Energy Dissipators for Culverts and Channels, HEC 14, September 1983.
[5] https://www.fhwa.dot.gov, chapter 7: internal (integrated) dissipators. pg 7–1.
[6] 6.36.060 Baffled aprons (USBR Type IX, baffle chute drop).

Dam Protections against Overtopping and Accidental Leakage – Toledo, Morán & Oñate (Eds)
© 2015 Taylor & Francis Group, London, ISBN: 978-1-138-02808-1

Author index

Alves, R.M. 101, 161

Batanero, P. 275
Bourdarot, E. 207

Caballero, F.J. 193
Campos, H. 89
Carrillo, J.M. 219, 231
Castillo, L.G. 219, 231
Cobo, R. 89
Courivaud, J.-R. 59

Fiedler, W.R. 41
Flores, I. 261

Garrote, L. 261

Harris, M.J. 73
Hepler, T.E. 3
Hiller, P.H. 151

Jarecka, K. 59

Kabore, M. 83

Larese, A. 111
Lia, L. 151
Lara, Á. 89
Laugier, F. 207

Martínez, I. 275
Martínez, E. 275
Millogo, F. 83
Morera, L. 133, 143, 245
Morán, R. 25, 101, 123, 161, 181

Nombré, A. 83

Oñate, E. 111, 287

Palacio, A. 295

Robles, I. 295
Rodríguez, A. 295
Rossi, R. 111

Salazar, F. 193, 245, 287
San Mauro, J. 123, 193, 245, 287
Somda, E.A. 83
Sordo-Ward, A. 261

Tavakoli, N. 169
Toledo, M.Á. 89, 101, 123, 133, 143, 181, 193, 245, 287

Vogel, A. 59, 207